

π^0 -HADRON CORRELATIONS IN 200 GeV Au+Au COLLISIONS

by

CHEUK-PING WONG

Under the Direction of Megan Connors, PhD

ABSTRACT

In a newly explored kinematic condition which is extremely hot and dense, the asymptotic freedom feature of Quantum Chromodynamics (QCD) predicts a deconfined phase of nuclear matter, known as quark-gluon plasma (QGP), where quarks and gluons can move freely like a perfect liquid. The QGP can be produced using the Relativistic Heavy-Ion Collider at Brookhaven National Laboratory. During these collisions, high momentum partons are produced. These partons fragment into jets which are collimated sprays of particles. In the case that the QGP is formed, these hard partons lose energy when traversing the QGP. Therefore, the resulting jets are modified, which is observed as a angular broadening and modification of momentum distribution of jet particles. Hence, the study of jet modifications

helps to understand the properties of the QGP. In this research, jets are studied using π^0 -hadron azimuth correlations which use high momentum neutral pions as triggers to indicate the present of a jet. The azimuth correlations, known as jet functions, between the trigger π^0 and the charged hadrons are corrected for detector efficiency and underlying flow harmonics up to the fourth order. The jet functions are used to extract angular width and per trigger yields of the jets. This research found the angular broadening and enhancement of soft jet particles in $Au + Au$ collisions at 200 GeV compared to $p + p$ results, while hard jet particles are suppressed but no significant angular broadening is observed.

To be able to fully interpret the modification observed in heavy-ion collisions, a deeper understanding of the initial state of confined quarks in the nuclei is needed. Therefore, the next era of nuclear physics requires an Electron-Ion Collider (EIC) to construct the comprehensive nucleon tomography in different phase spaces. This dissertation details work performed to develop a compact aerogel ring-imaging Cherenkov detector called the mRICH with a focusing Fresnel lens to overcome the space limitation in the EIC detector

INDEX WORDS: Quark-gluon plasma, nuclear physics, PHENIX, jet, π^0 -hadron correlation, Electron-Ion collider, modular RICH

π^0 -HADRON CORRELATIONS IN 200 GeV Au+Au COLLISIONS

by

CHEUK-PING WONG

A Dissertation Submitted in Partial Fulfillment of the Requirements for the Degree of

Doctor of Philosophy

in the College of Arts and Sciences

Georgia State University

2020

Copyright by
Cheuk-Ping Wong
2020

π^0 -HADRON CORRELATIONS IN 200 GeV Au+Au COLLISIONS

by

CHEUK-PING WONG

Committee Chair:

Megan Connors

Committee:

Xiaochun He

Murad Sasour

Christine Nattrass

Electronic Version Approved:

Office of Graduate Studies

College of Arts and Sciences

Georgia State University

May 2020

DEDICATION

I dedicate this dissertation to my late grandmother. On my kindergarten graduation day, I asked her if I was done with school. She told me that I am going to graduate from primary school, secondary school, and university and then become a doctor. She shaped me as an independent woman at a young age. When everyone doubted my decision to attend graduate school in the United States, she was the only one who believed in me.

ACKNOWLEDGMENTS

As a high energy experimentalist, I would sincerely say that I could not have finished my graduate study by myself.

I would like to thank my advisors, Xiaochun He and Megan Connors. I will always thank Dr. He for giving me a chance to join the Nuclear and Particle Physics Group at Georgia State University at the very first place. Under his supervision, I was exposed and grew interest in detector development. I am grateful for having Megan as my advisor. She had the ability to smell the hidden problems and gave the great critiques on my work. She believed in me more than I could and gave me advise in both research and life.

Besides my advisors, members of the Nuclear Physics Group, especially Sawaiz, Tristan, Anthony and Saif, have been great supporters in the hardest times. Thank you for being friends with me and also working hard together for both the mRICH detector and the two-particle correlations analysis. I would also like to thank Fatemeh who took care of me at our lively apartment.

Thanks to my collaborators in PHENIX and the EIC PID R&D14 consortium for being brilliant. I have met some of the smartest people in the world in these collaborations. I will always be humbled knowing that I can succeed because of your help.

TABLE OF CONTENTS

ACKNOWLEDGMENTS	v
LIST OF TABLES	x
LIST OF FIGURES	xiv
1 Introduction	1
1.1 Standard Model	1
1.2 Quantum Chromodynamics	3
1.3 Quark-Gluon Plasma	7
1.4 Heavy-Ion Collider Experiments	8
<i>1.4.1 Quark-Gluon Plasma Evolution in Heavy-Ion Collisions</i>	9
<i>1.4.2 Variables and Terminology</i>	11
1.5 Probing the Quark-Gluon Plasma	16
<i>1.5.1 Collective Flow</i>	16
<i>1.5.2 Jet Modification</i>	20
1.6 Purpose of This Dissertation	37
2 Experiments	39
2.1 Relativistic Heavy Ion Collider	39
2.2 PHENIX Detector	41
<i>2.2.1 Global Detectors</i>	42
<i>2.2.2 Ring Imaging Cherenkov Detector</i>	47
<i>2.2.3 Tracking System</i>	49
<i>2.2.4 Electromagnetic Calorimeter</i>	55
<i>2.2.5 Data Sets</i>	58
3 π^0-Hadron Correlation Analysis	60

3.1	Data Selection	60
3.2	Event-Mixing	65
3.3	Run Selection	65
3.4	Correction for Detector Effects	66
3.4.1	<i>Charged Hadron Efficiency</i>	66
3.4.2	<i>Detector Acceptance</i>	68
3.5	Background Flow subtraction	74
3.5.1	<i>Coefficients of Flow Harmonics for Charged Hadron</i>	75
3.5.2	<i>Coefficients of Flow Harmonics for π^0 from Acoustic Scaling</i>	77
3.5.3	<i>Flow Level Estimation: Absolute Normalization</i>	79
3.6	Extracting Physics Quantities	82
4	Systematic Uncertainty	84
4.1	Flow Harmonics	84
4.2	Absolute Normalization	85
4.3	Hadron Efficiency	85
4.4	Combinatorial Background in π^0 Reconstruction	86
4.5	Uncertainty Propagation	92
4.6	Summary of Systematic Uncertainty	95
5	Results	114
5.1	Jet Functions	114
5.2	Yields	114
5.3	Away-side $I_{AA}(p_T)$	115
5.4	Jet Widths	115
5.5	$I_{AA}(\Delta\phi)$	116
6	Discussions	121

6.1	Comparisons to $A + A$ Collision Results	121
6.1.1	Comparison to <i>PHENIX Results</i>	121
6.1.2	<i>STAR Results in 200 GeV Au + Au</i>	125
6.1.3	<i>ALICE Results in 2.76 TeV Pb + Pb</i>	126
6.1.4	<i>ATLAS Results in 5.02 TeV Pb + Pb</i>	127
6.2	Comparison to Small System Results	129
7	Electron-Ion Collider Experiments	133
7.1	Electron-Ion Collisions	134
7.2	Modular RICH Detector	136
7.2.1	<i>Detector Design</i>	136
7.2.2	<i>Analytical Calculations of Cherenkov Ring Information</i> . .	139
7.2.3	<i>Simulation</i>	145
7.2.4	<i>First Beam Test</i>	148
7.2.5	<i>Second Prototype and Beam Test</i>	152
7.2.6	<i>Outlook</i>	154
7.2.7	<i>Summary</i>	154
8	Summary	156
REFERENCES		158
Appendices		166
A	Near-Side Normalization	166
B	Available PHENIX Dataset	173
B.1	2015 200 GeV $p + p$ <i>Data</i>	173
B.2	2014 200 GeV $Au + Au$ <i>Data</i>	174
C	Data Tables: Coefficients of Flow Harmonics	179
D	Data Table: ξ	180
E	Data Tables: Jet Functions	182
F	Data Tables: Jet Width	231

G Data Tables: Per Trigger Yield	235
H Data Tables: $I_{AA}(p_T)$	239
I Data Tables: $I_{AA}(\Delta\phi)$	241
J Good Run List: Run14	249

LIST OF TABLES

Table 1.1 List of hadrons discussed in this thesis	5
Table 2.1 Specifications of PHENIX Electromagnetic Calorimeter Specifications	57
Table 2.2 Summary of PHENIX minimum bias data sets	59
Table 3.1 Summary of cuts applied in particle selection	61
Table 3.2 Fit parameters of single charged hadron efficiency	67
Table 3.3 Fit parameters of the occupancy	68
Table 4.1 Sources of Systematic Uncertainty	93
Table 4.2 Uncorrelated errors in hadron efficiency study	94
Table 7.1 The radius of the Cherenkov ring image and the number of Cherenkov photons at the sensor plane from the 120 GeV proton beam incident at the center of the mRICH. The total number of photons is the number of photons which reach the sensor plane. The number of photons on the ring is the number of photons counted along the reconstructed ring image.	151
Table 1 Different single photon and photon pair cuts in this analysis and PPG106.166	166
Table 2 Run Groups	174
Table 3 Control Log Comments in run 409691 – 410500	175
Table 4 Interpolated charged hadron v_n	179
Table 5 Interpolated $\pi^0 v_2$	179
Table 6 Scaling factor g_n^h	179
Table 7 ξ in Run 10	180
Table 8 ξ in Run 11	181
Table 9 0–20%, 4.0–5.0 \otimes 0.5–1.0 GeV/c Jet Function	182

Table 10	0–20%, 4.0–5.0 \otimes 1.0–2.0 GeV/c Jet Function	183
Table 11	0–20%, 4.0–5.0 \otimes 2.0–3.0 GeV/c Jet Function	184
Table 12	0–20%, 4.0–5.0 \otimes 3.0–5.0 GeV/c Jet Function	185
Table 13	0–20%, 4.0–5.0 \otimes 5.0–7.0 GeV/c Jet Function	186
Table 14	0–20%, 5.0–7.0 \otimes 0.5–1.0 GeV/c Jet Function	187
Table 15	0–20%, 5.0–7.0 \otimes 1.0–2.0 GeV/c Jet Function	188
Table 16	0–20%, 5.0–7.0 \otimes 2.0–3.0 GeV/c Jet Function	189
Table 17	0–20%, 5.0–7.0 \otimes 3.0–5.0 GeV/c Jet Function	190
Table 18	0–20%, 5.0–7.0 \otimes 5.0–7.0 GeV/c Jet Function	191
Table 19	0–20%, 7.0–9.0 \otimes 0.5–1.0 GeV/c Jet Function	192
Table 20	0–20%, 7.0–9.0 \otimes 1.0–2.0 GeV/c Jet Function	193
Table 21	0–20%, 7.0–9.0 \otimes 2.0–3.0 GeV/c Jet Function	194
Table 22	0–20%, 7.0–9.0 \otimes 3.0–5.0 GeV/c Jet Function	195
Table 23	0–20%, 7.0–9.0 \otimes 5.0–7.0 GeV/c Jet Function	196
Table 24	0–20%, 9.0–12.0 \otimes 0.5–1.0 GeV/c Jet Function	197
Table 25	0–20%, 9.0–12.0 \otimes 1.0–2.0 GeV/c Jet Function	198
Table 26	0–20%, 9.0–12.0 \otimes 2.0–3.0 GeV/c Jet Function	199
Table 27	0–20%, 9.0–12.0 \otimes 3.0–5.0 GeV/c Jet Function	200
Table 28	0–20%, 9.0–12.0 \otimes 5.0–7.0 GeV/c Jet Function	201
Table 29	0–20%, 12.0–15.0 \otimes 0.5–1.0 GeV/c Jet Function	202
Table 30	0–20%, 12.0–15.0 \otimes 1.0–2.0 GeV/c Jet Function	203
Table 31	0–20%, 12.0–15.0 \otimes 2.0–3.0 GeV/c Jet Function	204
Table 32	0–20%, 12.0–15.0 \otimes 3.0–5.0 GeV/c Jet Function	205
Table 33	0–20%, 12.0–15.0 \otimes 5.0–7.0 GeV/c Jet Function	206
Table 34	20–40%, 4.0–5.0 \otimes 0.5–1.0 GeV/c Jet Function	207

Table 35	$20\text{--}40\%$, $4.0\text{--}5.0 \otimes 1.0\text{--}2.0 \text{ GeV}/c$ Jet Function	208
Table 36	$20\text{--}40\%$, $4.0\text{--}5.0 \otimes 2.0\text{--}3.0 \text{ GeV}/c$ Jet Function	209
Table 37	$20\text{--}40\%$, $4.0\text{--}5.0 \otimes 3.0\text{--}5.0 \text{ GeV}/c$ Jet Function	210
Table 38	$20\text{--}40\%$, $4.0\text{--}5.0 \otimes 5.0\text{--}7.0 \text{ GeV}/c$ Jet Function	211
Table 39	$20\text{--}40\%$, $5.0\text{--}7.0 \otimes 0.5\text{--}1.0 \text{ GeV}/c$ Jet Function	212
Table 40	$20\text{--}40\%$, $5.0\text{--}7.0 \otimes 1.0\text{--}2.0 \text{ GeV}/c$ Jet Function	213
Table 41	$20\text{--}40\%$, $5.0\text{--}7.0 \otimes 2.0\text{--}3.0 \text{ GeV}/c$ Jet Function	214
Table 42	$20\text{--}40\%$, $5.0\text{--}7.0 \otimes 3.0\text{--}5.0 \text{ GeV}/c$ Jet Function	215
Table 43	$20\text{--}40\%$, $5.0\text{--}7.0 \otimes 5.0\text{--}7.0 \text{ GeV}/c$ Jet Function	216
Table 44	$20\text{--}40\%$, $7.0\text{--}9.0 \otimes 0.5\text{--}1.0 \text{ GeV}/c$ Jet Function	217
Table 45	$20\text{--}40\%$, $7.0\text{--}9.0 \otimes 1.0\text{--}2.0 \text{ GeV}/c$ Jet Function	218
Table 46	$20\text{--}40\%$, $7.0\text{--}9.0 \otimes 2.0\text{--}3.0 \text{ GeV}/c$ Jet Function	219
Table 47	$20\text{--}40\%$, $7.0\text{--}9.0 \otimes 3.0\text{--}5.0 \text{ GeV}/c$ Jet Function	220
Table 48	$20\text{--}40\%$, $7.0\text{--}9.0 \otimes 5.0\text{--}7.0 \text{ GeV}/c$ Jet Function	221
Table 49	$20\text{--}40\%$, $9.0\text{--}12.0 \otimes 0.5\text{--}1.0 \text{ GeV}/c$ Jet Function	222
Table 50	$20\text{--}40\%$, $9.0\text{--}12.0 \otimes 1.0\text{--}2.0 \text{ GeV}/c$ Jet Function	222
Table 51	$20\text{--}40\%$, $9.0\text{--}12.0 \otimes 2.0\text{--}3.0 \text{ GeV}/c$ Jet Function	223
Table 52	$20\text{--}40\%$, $9.0\text{--}12.0 \otimes 3.0\text{--}5.0 \text{ GeV}/c$ Jet Function	224
Table 53	$20\text{--}40\%$, $9.0\text{--}12.0 \otimes 5.0\text{--}7.0 \text{ GeV}/c$ Jet Function	225
Table 54	$20\text{--}40\%$, $12.0\text{--}15.0 \otimes 0.5\text{--}1.0 \text{ GeV}/c$ Jet Function	226
Table 55	$20\text{--}40\%$, $12.0\text{--}15.0 \otimes 1.0\text{--}2.0 \text{ GeV}/c$ Jet Function	227
Table 56	$20\text{--}40\%$, $12.0\text{--}15.0 \otimes 2.0\text{--}3.0 \text{ GeV}/c$ Jet Function	228
Table 57	$20\text{--}40\%$, $12.0\text{--}15.0 \otimes 3.0\text{--}5.0 \text{ GeV}/c$ Jet Function	229
Table 58	$20\text{--}40\%$, $12.0\text{--}15.0 \otimes 5.0\text{--}7.0 \text{ GeV}/c$ Jet Function	230
Table 59	0–20%, Near side Width	231

Table 60	0–20%, Away side Width	232
Table 61	20–40%, Near side Width	233
Table 62	20–40%, Away side Width	234
Table 63	Near side yield, 0–20%	235
Table 64	Away side yield, 0–20%	236
Table 65	Near side yield, 20–40%	237
Table 66	Away side yield, 20–40%	238
Table 67	0–20%, Away-side $I_{AA}(p_T)$	239
Table 68	20–40%, Away-side $I_{AA}(p_T)$	240
Table 69	0–20%, trigger p_T 4.0–5.0 Away-side $I_{AA}(\Delta\phi)$	241
Table 70	0–20%, trigger p_T 5.0–7.0 Away-side $I_{AA}(\Delta\phi)$	242
Table 71	0–20%, trigger p_T 7.0–9.0 Away-side $I_{AA}(\Delta\phi)$	243
Table 72	0–20%, trigger p_T 9.0–12.0 Away-side $I_{AA}(\Delta\phi)$	244
Table 73	20–40%, trigger p_T 4.0–5.0 Away-side $I_{AA}(\Delta\phi)$	245
Table 74	20–40%, trigger p_T 5.0–7.0 Away-side $I_{AA}(\Delta\phi)$	246
Table 75	20–40%, trigger p_T 7.0–9.0 Away-side $I_{AA}(\Delta\phi)$	247
Table 76	20–40%, trigger p_T 9.0–12.0 Away-side $I_{AA}(\Delta\phi)$	248

LIST OF FIGURES

Figure 1.1 Stand model of elementary particles which are categorized into quarks (purple), leptons (green) and force carriers (blue). The particle properties such as mass, charge, spin, and name are labeled in each grid [2].	2
Figure 1.2 Feynman diagrams of strong interactions. Left: quark-gluon interaction. Center and Right: gluon-gluon interactions.	3
Figure 1.3 Potential (V) of quark-antiquark system as a function of particle distance (r) in arbitrary scale.	4
Figure 1.4 The coupling constant, α_s , of the strong interaction as a function of squared momentum transfer Q^2 obtained from different experiments [7]. . . .	7
Figure 1.5 QCD phase diagram. The curves are the phase transitions. The 900 MeV indicator separates nuclear matter from hadron gas in low temperature.	8
Figure 1.6 QGP evolution in heavy-ion collisions. (a) The relativistic heavy ions are under Lorentz contraction. (b) The heavy ions collide. The QGP starts to form. (c) Thermal expansion of QGP. (d) hadronization occurs as environment cools down. (e) The kinematics of the newly formed hadrons is determined in the thermal freeze-out stage.	10
Figure 1.7 Different perspectives of heavy-ion collisions. (a) Side view of the collisions. (b) Transverse plane of the collisions. b is the impact parameter, which is the distance between the centers of two ions. Participants and spectators are drawn as solid dots and open circles, respectively.	11
Figure 1.8 ((a)) Pseudorapidity η plotted as a function of θ . The blue dot is at $(90^\circ, 0)$. ((b)) A graphic relationship between the angle (θ) and pseudorapidity (η). The origin is at the collision point [10].	13
Figure 1.9 Demonstration of counting number of participant N_{part} and number of binary collision N_{coll} . The solid dots and open circles are the participants and spectators, respectively [11].	14
Figure 1.10 Cross-section illustrated as a function of charged particle multiplicity N_{ch} . The centrality classes which are the percentile of integrated cross-section are shown under the curve. The top two axes are the impact parameter b and number of participant N_{part} in the corresponding centrality class [12]. . . .	15

Figure 1.11 Directed flow harmonic coefficient v_1 of proton and π^- as a function of rapidity y from $Au + Au$ collisions at different energies [16].	17
Figure 1.12 Spatial anisotropy (left) of the overlap region transfers (in orange) to the momentum space (right) [20].	18
Figure 1.13 Coefficient of flow harmonics of charged hadrons as a function of transverse momentum in $Au + Au$ collisions at 200 GeV [21]. The magenta points are from previous PHENIX results of the same measurements, the blue points are the updated results. Different centrality classes are plotted in different column. The last row is the v_4 values obtained from the second event plane.	19
Figure 1.14 Coefficient of second order flow harmonics of neutral pions as a function of transverse momentum in $Au + Au$ collisions at 200 GeV [22].	19
Figure 1.15 Left: Charged hadron v_2 as a function of transverse momentum, p_T , and kinematic energy, KE_T , in transverse direction. Right: Charged hadron v_2 scaled by number of constituent quarks as a function of p_T and KE_T [23].	20
Figure 1.16 Three-jet event in an electron-positron collision measured in TASSO detector at DESY [24]. The dots are the hits in the detector made by the traversing particles. These hits are then reconstructed to tracks (lines) of the particle.	21
Figure 1.17 Nuclear modification factors of different mesons as a function of transverse momentum in central events of $Au + Au$ collisions at 200 GeV [42].	26
Figure 1.18 ((a)) $\pi^0 R_{AA}$ comparison between ZOWW models with different ϵ_0 values and PHENIX results. The red bold curve is using $\epsilon_0 = 1.88$ GeV/fm [43]. ((b)) $\pi^0 R_{AA}$ comparison between ACHNS model with K values and PHENIX results. The black solid curve is using $K = 4.1$ [38].	27
Figure 1.19 Left: drawing of a pair of jets. The trigger particle is in bold blue arrow. Associate particles in the near (away) side are drawn in blue (orange). $\Delta\phi$ is the correlation angle between trigger and associate particles. Right: sketch of two-particle azimuthal correlation function from $p+p$ collisions. The near (away) side correlation peaks at 0 (π) is in blue (orange). σ_{near} and σ_{away} are the Gaussian width of the peaks [45].	30
Figure 1.20 Left: jet functions from direct photon-hadron correlations in different ξ ranges. Black and blue data points are results from $Au + Au$ and $p + p$ at 200 GeV data, respectively. Right: Away-side per trigger yields (top) and I_{AA} (bottom) as a function of ξ obtained from the jet functions on the left [46].	32

Figure 1.21 Jet functions with second flow harmonic subtracted $Au + Au$ (black) and $p + p$ (blue) collisions at 200 GeV [49].	34
Figure 1.22 ((a)) Angular width of the away-side jets as a function of associate particle p_T . ((b)) Away-side I_{AA} as a function of associate particle p_T . Theoretical calculations are drawn as green and purple lines. The black box is the $\pi^0 R_{AA}$ results [49].	35
Figure 1.23 K values obtained from ACHNS fits on PHENIX R_{AA} and STAR I_{AA} results [38].	36
Figure 2.1 AGS facility and RHIC at Brookhaven National Laboratory.	40
Figure 2.2 Left: beam view of PHENIX central arms in 2010. The gray area is the central magnet. The beam line is pointing perpendicularly to the page. Right: slide view of PHENIX Muon arms.	41
Figure 2.3 Beam view of PHENIX central arms in 2011. The gray area is the central magnet. The beam line is pointing perpendicularly to the page.	41
Figure 2.4 Left: The beam-beam counter. In the front of the BBC are 64 photomultiplier tubes. In the back are the readout electronics. Right: one of the PMT inside the BBC. Connected in the front of the 54 mm long PMT tube which is the 30 mm long quartz Cherenkov radiator. The whole tube is covered with a hexagon tube [58].	43
Figure 2.5 Drawing of ZDC and dipole pair along the beam pipe. The black lines are the ion beams, Neutron and charged particle such as protons are drawn in green and red respectively. Unlike neutron, charged particle trajectory bends within the dipole magnet and misses the ZDC [59].	45
Figure 2.6 Segmentation of the PHENIX reaction plane detector in the central arms. The center circle is the space for the beam pipe. The red and the blue trapezoids are segments in the inner and the outer rings respectively. The numbers are the dimensions of the segments in centimeter [60].	47
Figure 2.7 Cut view of a sector of PHENIX RICH detector [61]	48
Figure 2.8 Left: mechanical drawing of the PHENIX Drift Chamber with dimension labelled. Center: drawing of a sector of the drift chamber with 6 layers of wire labelled as X1, X2, U1, U2, V1, and V2. Right: top view of the wire orientations from three adjacent sectors [62]	51
Figure 2.9 Anatomy of PHENIX pad chambers.	53

Figure 2.10 Schematic of track (solid) passes through the drift chamber and pad chamber 3 in arbitrary scale. The black dash line is the projected track from calculation, $d\phi$ is the angle between the actual and projected hit positions at the PC3.	54
Figure 2.11 Left: Design of lead-scintillator tower. Right: Design of lead-glass tower.	55
Figure 2.12 Illustration of electromagnetic shower [64].	56
Figure 3.1 Invariant mass spectra of photon pair in different centrality classes from Run 10 and Run11 data. The π^0 mass is peak at about 0.135 GeV. The peak near 0.548 GeV is the η meson which is not used in this analysis.	64
Figure 3.2 Transverse momentum distributions of trigger particles in different centrality classes from Run 10 and Run11 data.	64
Figure 3.3 Transverse momentum distributions of associate tracks in different centrality classes from Run 10 and Run 11 data.	64
Figure 3.4 Hadron efficiencies as a function of associate track transverse momentum in Run 10 and Run 11 [71].	67
Figure 3.5 Illustrations of detector acceptance effect on angular correlation measurements. The grey areas represent the PHENIX central arm detectors. Left: example of accepted correlation. Right: example of missed correlation where the trigger or associate particle is missed by the detector.	69
Figure 3.6 Azimuth correlations from the same-event (black dots) and mixed-event (red circles) in 0–20% centrality in Run 10 data.	70
Figure 3.7 Azimuth correlations from the same-event (black dots) and mixed-event (red circles) in 2–40% centrality in Run 10 data.	71
Figure 3.8 Correlation functions in Run 10 0–20% after hadron efficiency and detector acceptance corrections	72
Figure 3.9 Correlation functions in Run 10 20–40% after hadron efficiency and detector acceptance corrections	73
Figure 3.10 Different order of harmonic functions in arbitrary scale.	75
Figure 3.11 v_2^h values in different centrality classes. The open circles are from experimental results [21]. The black dots are the merged values from the open circles.	76

Figure 3.12 Merged (solid dots) and interpolated (open circles) v_n^h values. The blue dash lines are the fits of the nominal, upper and lower bounds values of the solid points.	76
Figure 3.13 Merged $v_2^{\pi^0}$ values (black dots) in 0–20% (left) and 20–40% (right) centrality. The red and blue data points are results from reference [22] in 10% centrality bin width. The black points are the merged values of the red and blue points.	77
Figure 3.14 Merged (dots) and interpolated (circle) $v_2^{\pi^0}$ values in 0–20% and 20–40% centrality. The red dash lines are the fits of the nominal, upper and lower bounds values of the merged $v_2^{\pi^0}$	77
Figure 3.15 g_3 (top row) and g_4 (bottom row) calculated using charged hadron v_n in reference [21] in different centrality classes. The dash lines are the constant fits and their upper and lower bound values.	79
Figure 3.16 Number of trigger (top) and associate particles (bottom) as function of N_{part} from Run 10 data.	80
Figure 3.17 Number of trigger (top) and associate particles (bottom) as function of N_{coll} from Run 10 data.	81
Figure 3.18 ξ as a function of centrality in different trigger and associate p_T ranges from Run 10 (top) and Run 11 (bottom) data.	81
Figure 4.1 Example of invariant mass spectrum. The blue dash line at the bottom is the fit for combinatorial background. The red solid line is the fit of the combinatorial background and the signal. The vertical dash lines indicate the signal π^0 mass window (red), and side-band mass windows (blue).	86
Figure 4.2 Photon pair invariant mass spectra with fits in different trigger $\pi^0 p_T$ bins. Mass spectra in 0–20% (top) and 20–40% (bottom) events are separated to the top and bottom rows, respectively.	90
Figure 4.3 Signal-to-background ratio of reconstructed π^0	90
Figure 4.4 Near (top) and away-side (bottom) per trigger yields as a function of associate p_T in different trigger p_T bins in 0–20% centrality. Per trigger yields obtained from side-band and π^0 mass peak regions are drawn in red and black, respectively. The ratios of per trigger yields from different mass windows are drawn at the bottom of each panel.	91

Figure 4.5 Near (top) and away-side (bottom) per trigger yields as a function of associate p_T in different trigger p_T bins in 20–40% centrality. See Figure 4.4 for description.	91
Figure 4.6 Relative background π^0 systematic uncertainty as a function of associate p_T in near (top) and away-side (bottom) peaks. The trigger p_T is labeled on the top of each panel.	92
Figure 4.7 Jet functions in 0–20% centrality with systematic uncertainty from the second order flow harmonic drawn as boxes which are small. The trigger and associate p_T ranges are labeled on the side and the top, respectively. The dash lines indicate zero per trigger yield.	98
Figure 4.8 Jet functions in 20–40% centrality with systematic uncertainty from the second order flow harmonic drawn as boxes which are small.	98
Figure 4.9 Jet functions in 0–20% centrality with systematic uncertainty from the third order flow harmonic drawn as boxes which are small.	99
Figure 4.10 Jet functions in 20–40% centrality with systematic uncertainty from the third order flow harmonic drawn as boxes which are small.	99
Figure 4.11 Jet functions in 0–20% centrality with systematic uncertainty from the fourth order flow harmonic drawn as boxes which are small.	100
Figure 4.12 Jet functions in 20–40% centrality with systematic uncertainty from the fourth order flow harmonic drawn as boxes which are small.	100
Figure 4.13 Jet functions in 0–20% centrality with systematic uncertainty from Absolute Normalization method drawn as box.	101
Figure 4.14 Jet functions in 20–40% centrality with systematic uncertainty from Absolute Normalization method drawn as box.	101
Figure 4.15 Jet functions in 0–20% centrality with systematic uncertainty from combinatorial background π^0 drawn as box.	102
Figure 4.16 Jet functions in 20–40% centrality with systematic uncertainty from combinatorial background π^0 drawn as box.	102
Figure 4.17 Relative uncertainties in near-side width in 0–20% centrality.	103
Figure 4.18 Relative uncertainties in near-side width in 20–40% centrality.	103
Figure 4.19 Relative uncertainties in away-side width in 0–20% centrality.	104
Figure 4.20 Relative uncertainties in away-side width in 20–40% centrality.	104

Figure 4.21 Relative uncertainties in near-side yield in 0–20% centrality.	105
Figure 4.22 Relative uncertainties in near-side yield in 20–40% centrality.	105
Figure 4.23 Relative uncertainties in away-side yield in 0–20% centrality.	106
Figure 4.24 Relative uncertainties in away-side yield in 20–40% centrality.	106
Figure 4.25 Relative uncertainties in away-side I_{AA} in 0–20% centrality.	107
Figure 4.26 Relative uncertainties in away-side I_{AA} in 20–40% centrality.	107
Figure 4.27 Away-side $I_{AA}(\Delta\phi)$ in 0–20% with systematic uncertainty, σ^{f^2} , raised by the second order flow harmonics drawn as box.	108
Figure 4.28 Away-side $I_{AA}(\Delta\phi)$ in 20–40% with systematic uncertainty, σ^{f^2} , raised by the second order flow harmonics drawn as box.	108
Figure 4.29 Away-side $I_{AA}(\Delta\phi)$ in 0–20% with systematic uncertainty, σ^{f^3} , raised by the third order flow harmonics drawn as box.	109
Figure 4.30 Away-side $I_{AA}(\Delta\phi)$ in 20–40% with systematic uncertainty, σ^{f^3} , raised by the third order flow harmonics drawn as box.	109
Figure 4.31 Away-side $I_{AA}(\Delta\phi)$ in 0–20% with systematic uncertainty, σ^{f^4} , raised by the fourth order flow harmonics drawn as box.	110
Figure 4.32 Away-side $I_{AA}(\Delta\phi)$ in 20–40% with systematic uncertainty, σ^{f^4} , raised by the fourth order flow harmonics drawn as box.	110
Figure 4.33 Away-side $I_{AA}(\Delta\phi)$ in 0–20% with systematic uncertainty, σ^ξ , raised by Absolute Normalization method drawn as box.	111
Figure 4.34 Away-side $I_{AA}(\Delta\phi)$ in 20–40% with systematic uncertainty, σ^ξ , raised by Absolute Normalization method drawn as box.	111
Figure 4.35 Away-side $I_{AA}(\Delta\phi)$ in 0–20% with systematic uncertainty, σ^{π^0} , raised by combinatorial background π^0 drawn as box.	112
Figure 4.36 Away-side $I_{AA}(\Delta\phi)$ in 20–40% with systematic uncertainty, σ^{π^0} , raised by combinatorial background π^0 drawn as box.	112
Figure 4.37 Away-side $I_{AA}(\Delta\phi)$ in 0–20% with systematic uncertainty, σ^{pp} , raised by $p + p$ measurement drawn as box.	113
Figure 4.38 Away-side $I_{AA}(\Delta\phi)$ in 20–40% with systematic uncertainty, σ^{pp} , in $p + p$ measurement drawn as box.	113

Figure 5.1 Jet functions in 0–20% of 200 GeV $Au + Au$ collisions. The trigger and associate p_T of each panel are labeled on the side and the top of the figure, respectively. The statistic and systematic errors are shown as vertical lines and boxes on the data, respectively. The red curves are the Gaussian fits to the jet functions. The horizontal red lines indicate zero per trigger yields.	117
Figure 5.2 Jet functions in 20–40% of 200 GeV $Au + Au$ collisions.	118
Figure 5.3 Near (top) and away-side (bottom) per trigger yields as a function of associate p_T	119
Figure 5.4 I_{AA} as a function of associate p_T in the away-side peaks. The filled blue box is the global scale uncertainty.	119
Figure 5.5 Near (top) and away-side (bottom) jet widths as a function of associate p_T	120
Figure 5.6 Away-side I_{AA} as a function of associate $\Delta\phi$ in 0–20% (top) and 20–40% (bottom) centrality events. The filled blue box is the global scale uncertainty.	120
Figure 6.1 Comparison of jet functions in 0–20 of 200 GeV $Au + Au$ collisions. Trigger p_T and associate p_T are labeled on the side and the top of the figure, respectively. The jet functions from this analysis are drawn as black dots, results from [49] are shown as red circles.	123
Figure 6.2 Comparison of jet functions in peripheral events 200 GeV $Au + Au$ collisions. The jet functions from this analysis are in 20–40% centrality, results from [49] are in 20–60% centrality.	124
Figure 6.3 Away-side I_{AA} as a function of z_T from 200 GeV $Au + Au$ data from STAR experiment [77]. The results from π^0 -hadron and direct photon–hadron correlations are drawn in blue and red respectively.	126
Figure 6.4 Near (left) and away-side (right) I_{AA} as a function of p_T from 2.76 TeV $Pb + Pb$ data from ALICE experiment [78]. The results from π^0 -hadron and hadron–hadron correlations are drawn in red and black, respectively.	127
Figure 6.5 Away-side yield ratio of 5.02 TeV $Pb + Pb$ to $p + p$ collisions. from ATLAS [79]. The x axis is the distance of the associate particle measured from the jet axis found in the jet reconstruction.	128
Figure 6.6 Near (left) and away-side (right) I_{AA} as a function of z_T in 200 GeV $d + Au$ collisions [81].	130

Figure 6.7 Left: R_I as a function of z_T in 200 GeV $d + Au$ collisions [81]. The vertical bars and boxes are the statistical and systematic uncertainty, respectively. Right: Comparison of R_I in 200 GeV $d + Au$ and $^3He + Au$ collisions [81]. The statistical error is drawn as vertical bar. Systematic uncertainty is not shown in this plot.	131
Figure 7.1 ((a)) The commonly known nucleon model with three valence quarks. ((b)) The updated nucleon model pictures the nucleon as a collection of valence quarks, sea quarks and gluons. The sea quarks and gluons interact constantly. ((c)) Parton distribution function of proton measured by HERA and ZEUS [82].	134
Figure 7.2 Electron-proton collision.	134
Figure 7.3 Kinematics of meson products in electron-ion collisions as a function of rapidity from simulation. The electron-going direction is in negative rapidity and the ion-going direction is in positive rapidity. The color code indicated amplitude in arbitrary unit [85].	136
Figure 7.4 Left: mRICH design. Right: simulation with 10 charged pions (red) which emits Cherenkov photons (green).	137
Figure 7.5 Left: optics diagram shows the parallel cherenkov photons are focused by the Fresnel lens on the sensor plane. The orange line, which passes through the center of the lens, is used as guide to find the focal point. Right: Cherenkov ring image from simulation with 10 incident charged pions launched at the center of the detector $x - y$ plane.	137
Figure 7.6 Left: optics diagram shows the shifting function of the Fresnel lens when the charged particles incident off the optical principle. Right: Cherenkov ring image simulation with 10 incident charged pions incident at the third quadrant as marked as star.	138
Figure 7.7 First mRICH prototype.	139
Figure 7.8 Components of the first mRICH prototype. ((a)) Aerogel, ((b)) Fresnel lens, ((c)) four-sided mirror set and ((d)) H8500 multianode PMT [92]. . . .	139
Figure 7.9 ((a)) Ring radius differences as a function of refractive index of radiator. ((b)) Number of photon survived as a function of aerogel radiator thickness.	142
Figure 7.10 Cut view of the groove geometry of the Fresnel lens.	146
Figure 7.11 mRICH subsystem (left) in JLEIC detector design (left).	148
Figure 7.12 mRICH subsystem in sPHENIX detector design.	148

Figure 7.13 First beam test setup.	149
Figure 7.14 Ring images of single events from the beam test data.	150
Figure 7.15 Accumulated hit map from 120 GeV proton beam incident at the center of the detector $x - y$ plane. Beam test results are shown on the left and simulation results are shown on the right.	151
Figure 7.16 Accumulated hit map from 120 GeV proton beam incident at the third quadrant of the detector $x - y$ plane. Beam test results are shown on the left and simulation results are shown on the right. The photon hits in the third quadrant are the Cherenkov photons emitted inside the glass window of the photon sensor.	152
Figure 7.17 ((a)) Drawing of the second mRICH prototype, ((b)) The second mRICH prototype.	152
Figure 7.18 Beam test results of the second mRICH prototype. Accumulated hit map from 120 GeV proton beam incident at the center of the detector $x - y$ plane.153	
Figure 1 Jet functions in 0–20% centrality events. Black: results in [49]. Blue: results from this analysis with cuts listed in section 3.1. Red: same as blue data but paring two inclusive photons in π^0 reconstruction.	168
Figure 2 Jet functions in 0–20% centrality events. Black: results in [49]. Blue: results from this analysis with cuts listed in section 3.1, but paring two inclusive photons in π^0 reconstruction. Red: same as blue data but switching photon probability cut to $\chi^2 > 3$ shower shape cut.	169
Figure 3 Jet functions in 0–20% centrality events. Black: results in [49]. Blue: results from this analysis with cuts listed in section 3.1, but paring two inclusive photons in π^0 reconstruction. Red: same as blue data but switching to the energy asymmetry cut that was applied in [49].	170
Figure 4 Jet functions in 0–20% centrality events. Black: results in [49]. Blue: results from this analysis with cuts listed in section 3.1, but paring two inclusive photons in π^0 reconstruction. Red: same as blue data but the invariant mass window is changed to 0.12–0.15 GeV for all photon pair.	171
Figure 5 Jet functions in 0–20% centrality events. Black: results in [49]. Blue: results from this analysis with cuts listed in section 3.1, but paring two inclusive photons in π^0 reconstruction. Red: same as blue data but using the oval veto track cut.	172

Figure 6 ϕ - z distributions of charged hadron tracks from 2015 200 GeV $p + p$ data (a) and simulations (b and c).	173
Figure 7 Summed event-mixing background correlations in different run groups. These correlations are normalized to 1.	175
Figure 8 Standard deviation distribution of the entire Run 14. The red curve is the Gaussian fit at the peak region. The red dash line indicates $\mu + 3\sigma$	176
Figure 9 Examples of bad runs in Run 14. The event-mixing background correlations from each run (black) and from the corresponding run group (red) are drawn on the left in each panel. The ratio of the correlation is shown on the right of each panel.	176
Figure 10 Number of charged hadron tracks per event vs run number (top) and number of event vs run number (bottom). The blue dash line indicate separation of run groups. From left to right are group 0 to group 5. Bad runs determined are drawn in red.	177
Figure 11 photon hit maps of each tower of the electromagnetic calorimeters. The lead-glass scintillator towers are denoted as tower 6 and 7.	178

CHAPTER 1

Introduction

Democritus, the ancient Greek philosopher, introduced his most famous philosophy concept: the cheese atom, an inseparable unit of cheese [1]. This philosophical idea has driven the discovery of three categories of elementary particles and developments of the theories of fundamental interactions. One of the theories, quantum chromodynamics (QCD), explains how these elementary particles form the world that we observed. Interestingly, the interactions between these elementary particles evolves with their environment. Just like when cheese is heated, it becomes cheese fondue, when these elementary particles are heated, they transform to a nearly perfect liquid.

This introductory chapter will briefly describe the concept of elementary particles and QCD, and then detail the making of this perfect particle soup in the laboratory along with methods of studying its properties.

1.1 Standard Model

We, humans, have spent thousand of years trying to understand the fundamental elements of the universe. We have found that there are three categories of elementary particles that make up this world with different properties and roles which can be summarised in the standard model of particle physics.

The standard model is the theory that describes the elementary particles and their interactions. All the visible matter in this universe is comprised of quarks, leptons and their anti-particles. Quarks and leptons are fermions, that is, spin-half particles. Quarks and

Mass→ Charge→ Spin→ Name→	3 MeV 2/3 1/2 u up	1.24 GeV 2/3 1/2 c charm	173.3 GeV 2/3 1/2 t top	0 0 1 γ photon
Quarks	6 MeV -1/3 1/2 d down	95 MeV -1/3 1/2 s strange	4.2 GeV -1/3 1/2 b bottom	0 0 1 g gluon
Leptons	< 2 eV 0 1/2 v_e electron neutrino	< 0.19 MeV 0 1/2 v_μ muon neutrino	< 18.2 MeV 0 1/2 v_τ tau neutrino	91.2 GeV 0 1 Z⁰ weak force
	0.511 MeV -1 1/2 e electron	106 MeV -1 1/2 μ muon	1.78 GeV -1 1/2 τ tau	80.4 GeV ±1 1 W[±] weak force
Bosons (forces)				

Figure 1.1: Standard model of elementary particles which are categorized into quarks (purple), leptons (green) and force carriers (blue). The particle properties such as mass, charge, spin, and name are labeled in each grid [2].

leptons have unique mass and flavor which is denoted by a unique name or a letter, as shown in Figure 1.1. Quarks are particles that carry fractional electric charge and color charge, while leptons are particles with integer electric charge and are colorless. The third type of particles, which are shown at the right most column of Figure 1.1, are bosons with integer spin. These particles are called force carriers, as they associate with different forces and mediate the interaction between particles.

Both quarks and leptons experience the weak interaction whose force carriers are the W and Z bosons. The weak interaction is described by quantum flavor dynamics (QFD). All electrically charged particles also experience the electromagnetic interaction whose force carrier is the photon. The electromagnetic interaction, which is described by quantum electrodynamics (QED), was unified with the weak interaction in the electroweak interactions

introduced in [3–5].

Only quarks, which have color charge, experience the strong force whose force carrier is the gluon. The nucleus is composed of particle containing quarks and gluons. The strong interaction is described by Quantum Chromodynamics (QCD) which is the focus of this study. This chapter will briefly explain QCD, the questions raised by QCD, and how can we find the answers to these questions.

1.2 Quantum Chromodynamics

Quantum Chromodynamics (QCD) is the theory that describes the strong interaction between quarks and gluons, collectively referred to as partons. Quarks have six color charges, red, blue, green, anti-red, anti-blue, and anti-green, which act in the strong interaction like the electrical charge in the electromagnetic interaction. A gluon is massless and electrically neutral but has eight color charge combinations, including charges that exchange colors between particles. That means gluons not only interact with quarks, but also interact with other gluons, as shown in Figure 1.2. Therefore, the strong interaction is more complicated than electromagnetic and weak interactions whose bosons do not interact.

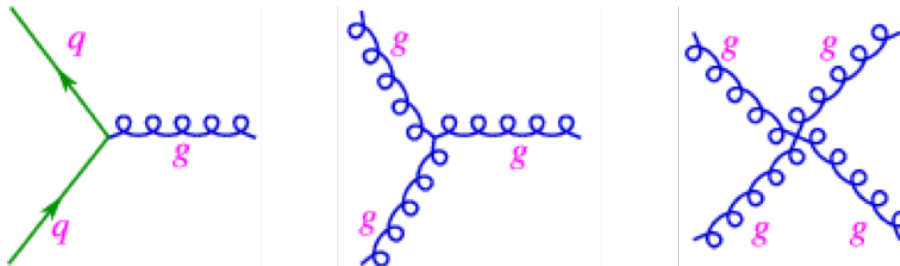


Figure 1.2: Feynman diagrams of strong interactions. Left: quark-gluon interaction. Center and Right: gluon-gluon interactions.

The effective potential of a quark-antiquark pair bounded by the strong force [6] plotted in Figure 1.3 is

$$V(r) = -\frac{a}{r} + br . \quad (1.1)$$

The first term in Equation (1.1) gives a repulsive force between partons. This repulsive force increases as partons become closer to each other, while the second term provides an attractive force that is proportional to the distance between two partons. There are two important phenomena of the strong potential: asymptotic freedom and confinement which distinguish the strong interaction from other fundamental forces.

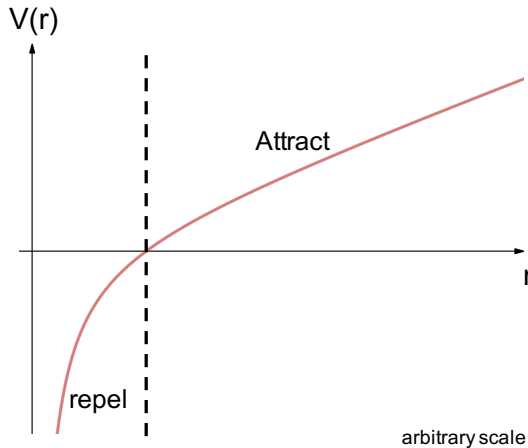


Figure 1.3: Potential (V) of quark-antiquark system as a function of particle distance (r) in arbitrary scale.

Confinement

The repulsive force dominates as the distance between two partons tends to zero, but the attractive force becomes stronger as the distance between two partons increases. Therefore, the partons must be bound together within a certain distance. Hence, partons cannot appear

alone. Thus, this physical world neither collapse nor fall apart. This phenomenon is known as confinement.

Consider a simple two-particle system with Coulomb or mechanical interactions, for example a positron-electron pair or two particles in spring system, if the particles are being pulled apart, these systems can be parted or broken apart if there is enough input energy. However, because of confinement, when a parton system, such as a quark-antiquark pair sepaes, the energy required produces another quark-antiquark pair following Einstein's Mass-Energy Equivalence ($E = mc^2$). Thus, regardless of how hard we pull, we can never observe a free quark under normal conditions.

The confined or bound quarks are called hadrons. A hadron must have integer charge and neutral color charge. Using the concept of optical color, color neutral can be seen in a meson which is a quark pair with opposite colors, or a baryon which is formed by three quarks with a (anti)red-(anti)blue-(anti)green color combination. The hadrons which will be discussed in this thesis, are listed in table 1.1.

Table 1.1: List of hadrons discussed in this thesis

Hadron	Constitutes	electrical charge	mass (kg)	mass (GeV)
Proton p	uud	1e	1.67×10^{-27}	0.938
Neutron n	udd	0	1.67×10^{-27}	0.939
Charged kaon κ^\pm	$u\bar{s}, \bar{u}s$	$\pm 1e$	8.80×10^{-28}	0.494
Charged pion π^\pm	$u\bar{d}, \bar{u}d$	$\pm 1e$	2.49×10^{-28}	0.139
Neutral pion π^0	$u\bar{u}, d\bar{d}$	0	2.41×10^{-28}	0.135

Asymptotic Freedom

Consider the first term in Equation (1.1), which gives an increasing repulsive force between partons as the partons move closer to each other. The coefficient a in the strong potential in Equation (1.1) can be expressed as

$$a = \frac{4}{3}\alpha_s, \quad (1.2)$$

where the factor $4/3$ is the number of gluon colors to number of quark flavors ratio ($8/6 = 4/3$), and α_s is the coupling constant of the strong interaction. Although the coupling constants α for other interactions, such as electromagnetic, do not change, α_s depends on the squared momentum transfer Q^2 between partons as shown in Equation (1.3)

$$\alpha_s(Q^2) = \frac{\alpha_s(\mu^2)}{1 + \frac{33-2N_f}{12\pi} \cdot \alpha_s(\mu^2) \ln \frac{Q^2}{\mu^2}}, \quad (1.3)$$

where N_f is the number of flavours of quarks that are involved in the interaction and $\alpha_s(\mu^2)$ is the reference coupling constant at squared momentum transfer μ^2 . Thus, α_s is known as a running constant. It is clear from Equation (1.3) that the coupling constant decreases logarithmically with increasing Q^2 . The relation between α_s and Q^2 is also demonstrated by experimental measurements as shown in Figure 1.4. Hence, the strength of forces in the strong interaction decreases as the momentum transfer increases.

Furthermore, the second term in the strong potential shown in Equation (1.1) tends to zero as the partons move so close to each other ($r \rightarrow 0$). Combining these two extreme

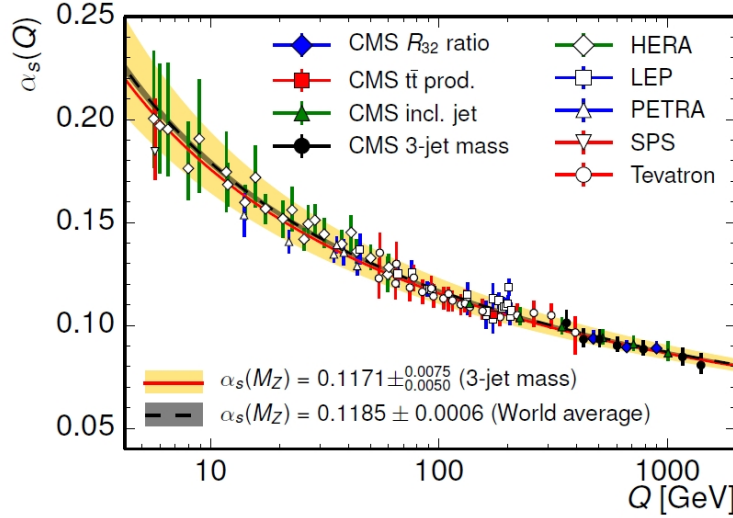


Figure 1.4: The coupling constant, α_s , of the strong interaction as a function of squared momentum transfer Q^2 obtained from different experiments [7].

conditions: large momentum transfer, and extremely close distance between partons, the strong potential drastically decreases. This phenomenon is known as asymptotic freedom, as quarks can behave as a free particle.

1.3 Quark-Gluon Plasma

Asymptotic freedom in QCD indicates that as the energy of a dense environment increases, the bonding between partons inside a hadron decreases. Hence, the phase of the nuclear matter changes with temperature and chemical potential as shown in the phase diagram in Figure 1.5. In the low temperature region, partons are confined in hadrons. As the chemical potential rises, the nucleons (neutrons and protons) are bound by the residual strong force and form nuclear matter. When the temperature increases, the bonding between partons inside the hadrons become weaker, and the hadrons start to melt. Above some critical

temperature, the hadrons become deconfined, and the partons can move freely. This free state of partons is called the Quark-Gluon Plasma (QGP). Lattice QCD calculations estimate that the critical temperature of the QGP phase transition is at 170 MeV when the energy density is at 1 GeV/fm³ [8]. The search for the QGP can be achieved with high energy heavy-ion collisions, which serve two purposes: testing Quantum Chromodynamics, and providing a glimpse into the beginning of the universe.

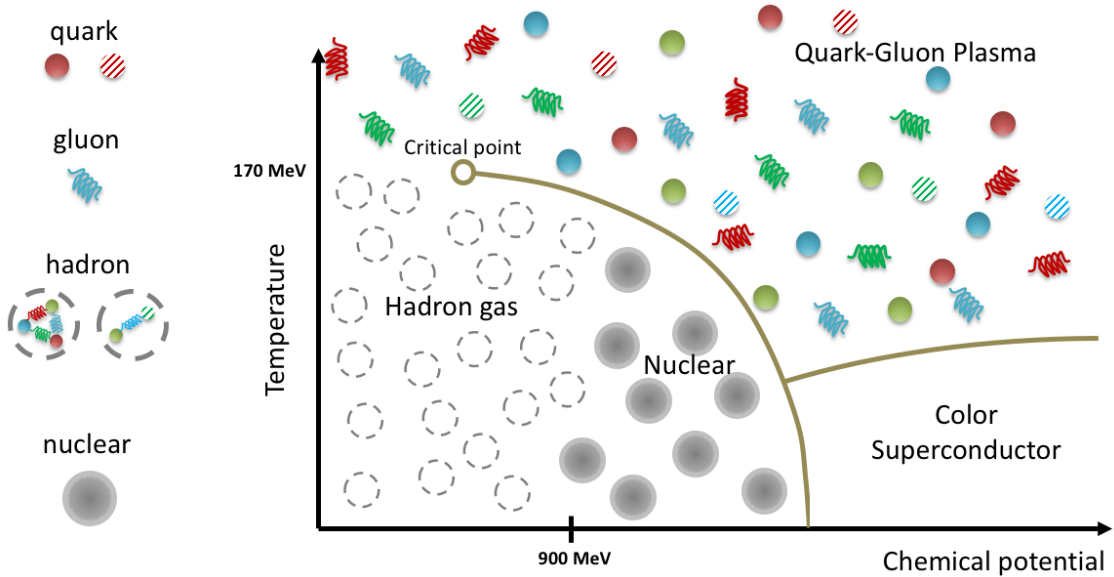


Figure 1.5: QCD phase diagram. The curves are the phase transitions. The 900 MeV indicator separates nuclear matter from hadron gas in low temperature.

1.4 Heavy-Ion Collider Experiments

To create the required conditions for QGP formation, physicists collide heavy ions, such as gold, lead and copper, at nearly the speed of light. The goal of the heavy-ion collision experiments is to map the transition of QCD matter from the hadronic phase to the QGP

phase, and understand the properties of the QGP, including the temperature, density, and energy transfer. This section details the evolution of the QGP produced by the heavy-ion collisions, introduces terminology and observables used in the experiments, and details the probes of QGP used in this study.

1.4.1 Quark-Gluon Plasma Evolution in Heavy-Ion Collisions

The following is a brief description of the evolution of the heavy-ion collisions which is also pictured in Figure 1.6.

Before the collisions

Heavy-ion beams travel near the speed of light. The longitudinal (direction of motion) dimension of these relativistic ions reduces, as illustrated in Figure 1.6a, because of Lorentz contraction. Hence, the particle density of the collision system rises.

Hard scattering

In the beginning of the collisions, some of the partons inside the nucleons undergo hard scattering, that is large momentum transfer ($Q^2 \gg 1$). These hard scattered partons later interact with the QGP; therefore, they can be used to probe the QGP. Discussion of related topics are included in the section 1.5.2.

QGP phase

During the collision, the temperature rises as the kinetic energy of the ions is transformed to thermal energy. The nucleons start melting, the bonding between the partons weakens and the QGP then forms (Figure 1.6b). The QGP phase can last for 1–10 fm/c (about

3×10^{-24} – 3×10^{-23} seconds) depending on the initial energy [9]. The QGP then undergoes a thermal expansion while cooling down (Figure 1.6c).

Chemical freeze-out

The temperature and density start falling as the QGP expands. Once the environment reaches temperatures below the QGP transition phase temperature, the bonding between the partons grows and formation of hadrons occurs (Figure 1.6d). The species of the hadrons are determined by the flavors of the partons inside the QGP.

Thermal freeze-out

In Figure 1.6e, the temperature is still high during chemical freeze-out, and the newly formed hadrons are in the gas phase which has higher degrees of freedom. Hadrons scatter off each other until the temperature further decreases. Motion of this hadron gas slows down, and the kinetic properties of the hadrons are then established.

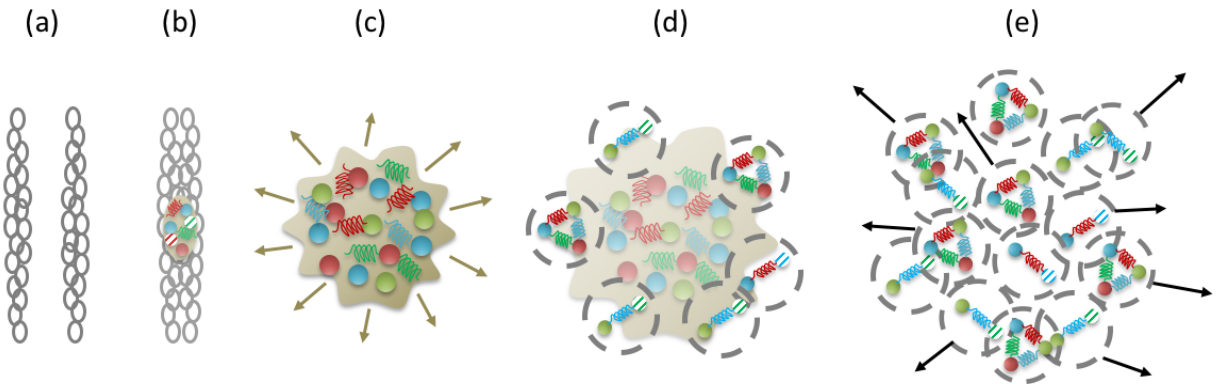


Figure 1.6: QGP evolution in heavy-ion collisions. (a) The relativistic heavy ions are under Lorentz contraction. (b) The heavy ions collide. The QGP starts to form. (c) Thermal expansion of QGP. (d) hadronization occurs as environment cools down. (e) The kinematics of the newly formed hadrons is determined in the thermal freeze-out stage.

1.4.2 Variables and Terminology

Before introducing the terminology, variables and observables that are used in this study, it is helpful to define the coordinates. In a collision, two heavy-ion projectiles move along the beam pipe which is used to define the z -axis as shown in Figure 1.7a. The coordinates of the transverse plane (xy -plane) are arbitrary and depend on the experiment or the detector setup. The polar angle, θ , is the angle between a vector and the z -axis. The azimuthal angle, ϕ , is the angle between the x and y components of the vector.

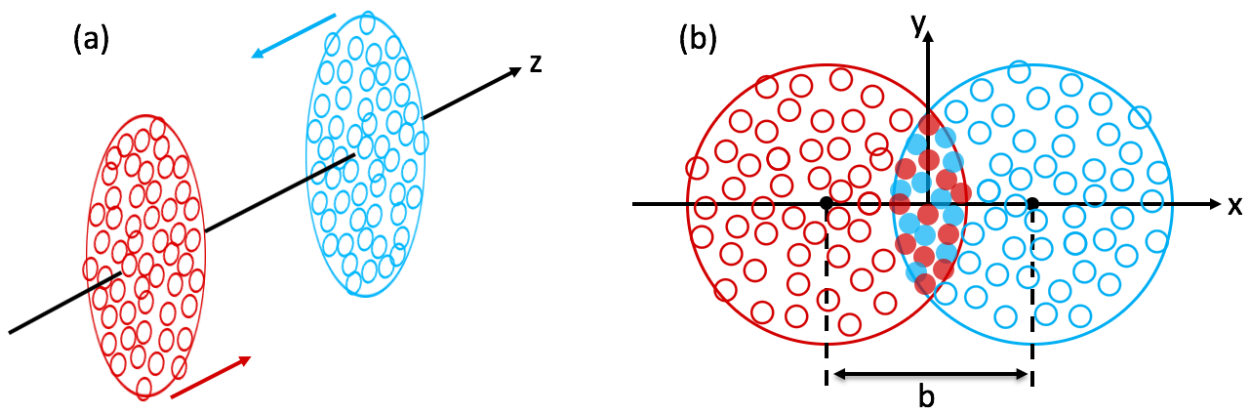


Figure 1.7: Different perspectives of heavy-ion collisions. (a) Side view of the collisions. (b) Transverse plane of the collisions. b is the impact parameter, which is the distance between the centers of two ions. Participants and spectators are drawn as solid dots and open circles, respectively.

Then, for a particle with four momentum

$$p = (E, p_x, p_y, p_z), \quad (1.4)$$

p_z is the longitudinal momentum, and the transverse momentum lies on the xy -plane and is

$$p_T = \sqrt{p_x^2 + p_y^2}. \quad (1.5)$$

Pseudorapidity

Since the particles are in relativistic motion in these high energy experiments, Lorentz invariant variables, such as rapidity, are preferred. Rapidity y is defined as

$$y = \frac{1}{2} \ln \frac{E + p_z}{E - p_z}. \quad (1.6)$$

Since $E^2 = m^2 + p^2$ ($c = 1$ in natural units), and $p_z = p \cos \theta$, Equation (1.6) becomes

$$y = \frac{1}{2} \ln \frac{\sqrt{m^2 + p^2} + p \cos \theta}{\sqrt{m^2 + p^2} - p \cos \theta}. \quad (1.7)$$

For energetic particles where $p \gg m$, the rapidity can be reduced to

$$\begin{aligned} \eta &= \frac{1}{2} \ln \frac{p + p \cos \theta}{p - p \cos \theta} \\ \eta &= \frac{1}{2} \ln \frac{1 + \cos \theta}{1 - \cos \theta} \\ \eta &\equiv -\frac{1}{2} \ln \tan\left(\frac{\theta}{2}\right). \end{aligned} \quad (1.8)$$

The reduced rapidity in Equation (1.8) is known as pseudorapidity η . η as a function of θ is plotted in Figure 1.8. To be familiar with η , consider $\theta = 0^\circ$, 90° and 180° which give

$\eta = +\infty$, 0 and $-\infty$, respectively.

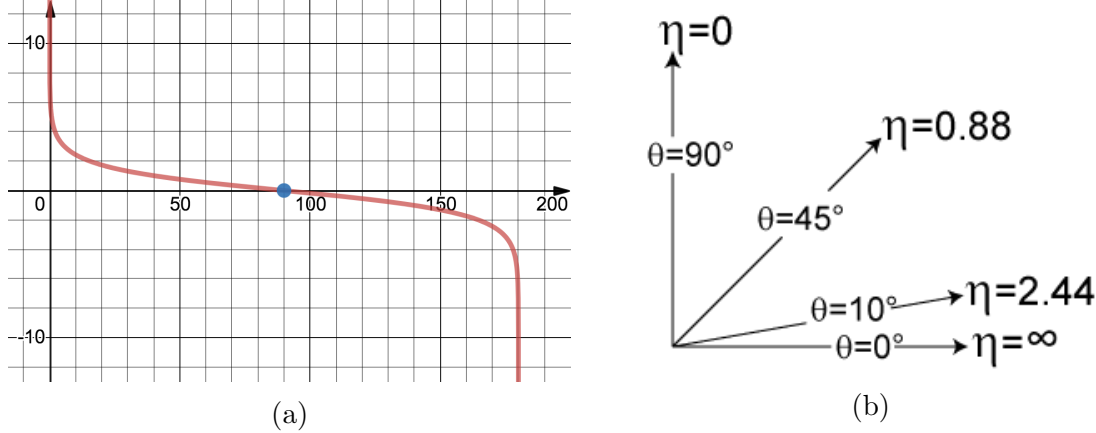


Figure 1.8: (a) Pseudorapidity η plotted as a function of θ . The blue dot is at $(90^\circ, 0)$. (b) A graphic relationship between the angle (θ) and pseudorapidity (η). The origin is at the collision point [10].

Participants and spectators

As drawn in Figure 1.7(b), the colliding ions may not hit head-on. Therefore, only part of the nucleons inside the ions are involved in the collisions, and participate in the formation of the QGP. These nucleons are described as wounded, or labeled as “participants.” On the other hand, the nucleons that are not involved in the collisions are labeled as “spectators.” The events with a higher number of participants, N_{part} , will produce a higher multiplicity of final state charged particles, as the probability of binary (nucleon-nucleon) collisions increases.

Binary collision

A binary collision is simply defined as the nucleon-nucleon collision, that is, a one-on-one collision. The number of binary collisions, N_{coll} , also affects the multiplicity of final charged particles. Figure 1.9 demonstrate the steps of counting N_{part} and N_{coll} . Collision 1 involves $N_{part} = 1 + 4 = 5$ participants from both ions and $N_{coll} = 1 \times 4 = 4$ binary collisions. In

the second collision, only one participant is counted as the other four participants have been counted in collision 1.

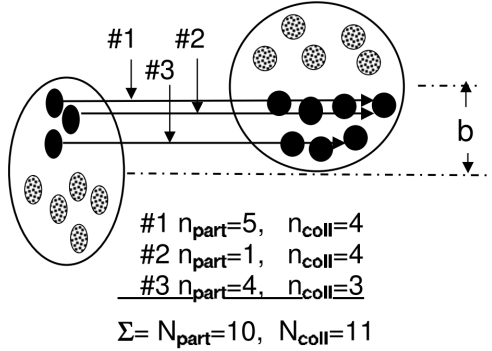


Figure 1.9: Demonstration of counting number of participant N_{part} and number of binary collision N_{coll} . The solid dots and open circles are the participants and spectators, respectively [11].

Impact parameter

Impact parameter, b , which describes the geometry of the collision, is defined as the distance between the centers of the collided ions as drawn in Figure 1.7b. Note that Figure 1.7b is a simplified illustration where the impact parameter is parallel to the x -axis. However, in reality, this may not be true. For a symmetric collision system, $b = 0$ for completely overlapping collisions. When $b \geq 2r$ where r is the radius of the ions, the ions miss each other. The completely overlapping collisions are categorized as central collisions, while those near misses are called peripheral.

It is clear that the impact parameter affects the number of participants, hence the multiplicity of final particles. The central collisions with $b = 0$ have the maximum number of participant N_{part} , thus highest multiplicity. The total multiplicity reduces in peripheral events with $b > 0$ as N_{part} decreases. The relation between N_{part} and b can be described

by the famous Glauber model which treats the nucleon collisions as a many-body system of uncorrelated nucleons with nuclear density, ρ , calculated using Woods-Saxon distribution [12, 13]

$$\rho(r) = \frac{\rho_0}{1 + e^{(r-R)/a}} , \quad (1.9)$$

where r is the distance from the center of the nucleus and a is the thickness of the nucleus shell. $R = r_0 A^{1/3}$ is the nucleus radius, where A is the nucleon number and $r_0 = 1.25$ fm.

Centrality

While the impact parameter b is useful to describe the geometry of the collisions, it is impossible to measure b directly with a detector. Therefore, an experimentally quantifiable

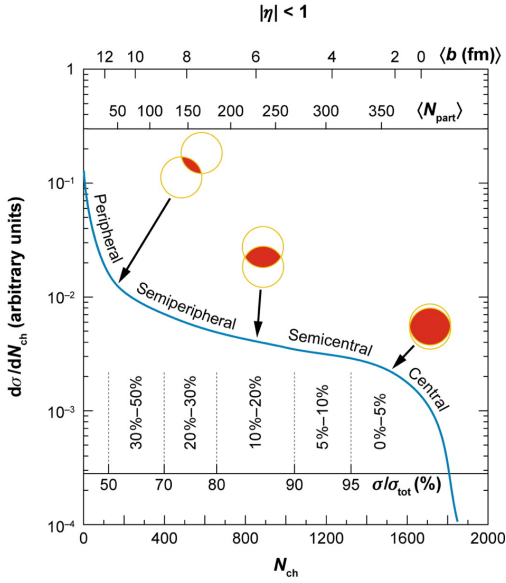


Figure 1.10: Cross-section illustrated as a function of charged particle multiplicity N_{ch} . The centrality classes which are the percentile of integrated cross-section are shown under the curve. The top two axes are the impact parameter b and number of participant N_{part} in the corresponding centrality class [12].

quantity - centrality is introduced. Centrality is the percentile class of the integrated cross-section, σ , of the charged hadron multiplicity, N_{ch} , as illustrated in Figure 1.10. Centrality equals to 0% refers for most central events with the highest multiplicity and 100% centrality refer to the ultra-peripheral events with the least multiplicity.

1.5 Probing the Quark-Gluon Plasma

This section introduces two different measurements to study the QGP. They are collective flow, and jet modification. Previous experimental results of these measurements and the physics implications are also shown in this section.

1.5.1 Collective Flow

The energetic QGP can expand freely causing hydrodynamic flow. The shape of the flow depends on the energy distribution of the QGP. Flow is measured via multiparticle angular correlations which can be expressed as a Fourier series

$$\frac{N_{\text{flow}}}{d\phi} \propto 1 + 2 \sum_{n=1} \langle v_n \rangle \cos(n[\phi - \psi_n]), \quad (1.10)$$

where N_{flow} is the number of particles at an azimuth angle ϕ and v_n in Equation (1.10) are the coefficient of flow harmonics [14]. The angle ψ_n , which is known as the event plane angle of the n^{th} order flow harmonic, is the estimation of the reaction plane angle measured from the experiment xz plane by measuring the direction of the spectator neutrons.

The first order harmonic $v_1 \cos(\Delta\phi)$ is known as directed flow. As the nuclei collide,

matter in nucleus A pushes matter in the other nucleus B away from the longitudinal direction (z -axis) [15]. Due to momentum conservation, matter deflected at opposite rapidities must have opposite directions but same magnitude of transverse momenta. This can be shown by the v_1 versus rapidity plots in Figure 1.11 [16]. Moreover, the v_1 near zero rapidity is negligible.

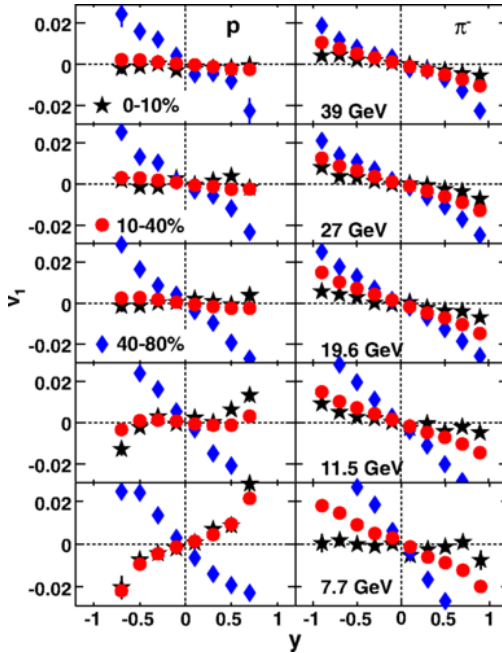


Figure 1.11: Directed flow harmonic coefficient v_1 of proton and π^- as a function of rapidity y from $Au + Au$ collisions at different energies [16].

In the higher order ($n \geq 2$) flow harmonics, the even order terms are created by the spatial anisotropy of the overlap region of the colliding ions. Since the density and pressure increases in the impact parameter, b , direction as illustrated in Figure 1.12 (where x -axis is the b direction), the momentum of the flow is higher in the reaction plane (xy -plane in Figure 1.12). However, the odd order flow harmonics, which are observed to be non-zero in

recent experiments [17–19], are caused by fluctuations in the colliding region.

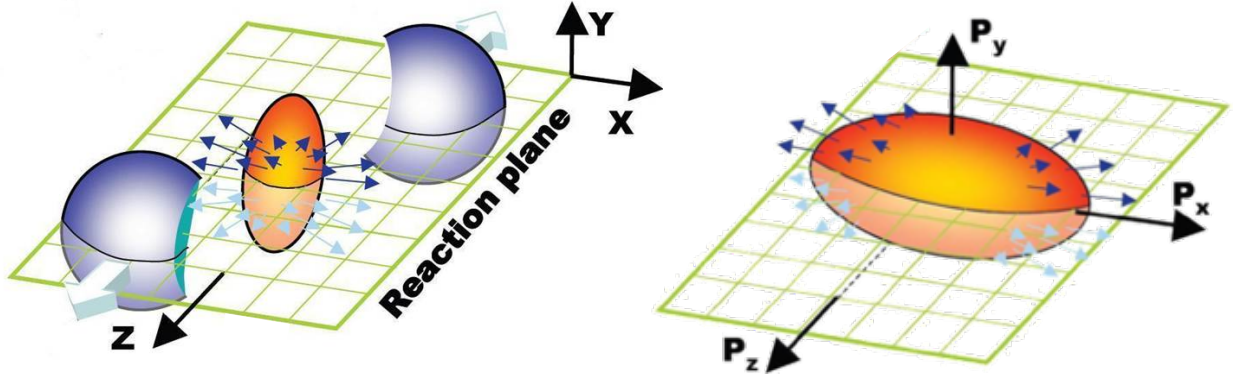


Figure 1.12: Spatial anisotropy (left) of the overlap region transfers (in orange) to the momentum space (right) [20].

Higher order v_n in $Au + Au$ Collisions at 200 GeV

The coefficients of second, third and fourth order flow harmonics of charged particles measured in $Au + Au$ collisions at 200 GeV with PHENIX 2007 data are plotted as a function of transverse momentum in Figure 1.13. Figure 1.13 shows that the v_n values increase in the low p_T region, then start falling after ≈ 3 GeV/c. The v_n values increase with centrality as well. The hierarchy of v_n values are also shown in these plots. The magnitudes of v_n values reduce in higher order.

Figure 1.14 shows the second flow harmonic of neutral pions as a function of transverse momentum v_2 in $Au + Au$ collisions at 200 GeV with PHENIX 2007 data. Like the charged hadrons, similar centrality and momentum dependencies are shown in the $\pi^0 v_2$ values. The higher order flow coefficients, v_3 and v_4 , of neutral pions are not shown as they have not been measured at RHIC in the high momentum region.

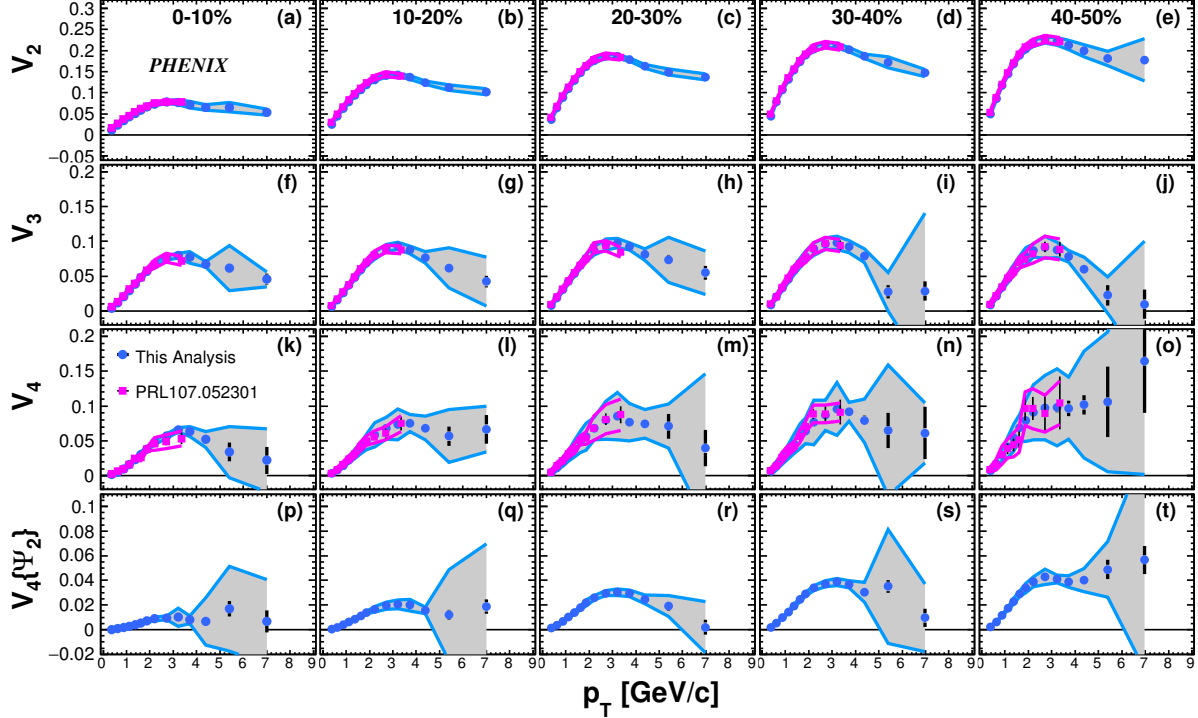


Figure 1.13: Coefficient of flow harmonics of charged hadrons as a function of transverse momentum in $Au + Au$ collisions at 200 GeV [21]. The magenta points are from previous PHENIX results of the same measurements, the blue points are the updated results. Different centrality classes are plotted in different column. The last row is the v_4 values obtained from the second event plane.

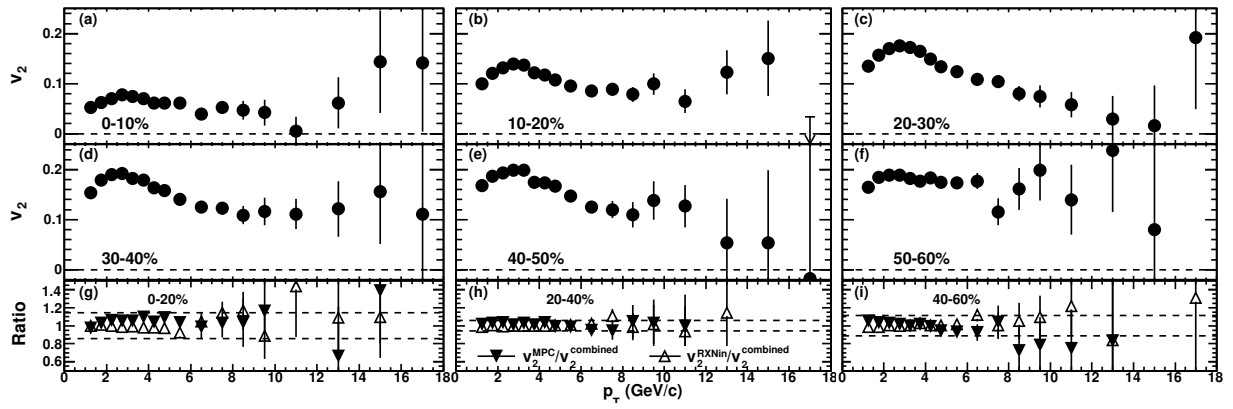


Figure 1.14: Coefficient of second order flow harmonics of neutral pions as a function of transverse momentum in $Au + Au$ collisions at 200 GeV [22].

Evidence of Quark-Gluon Plasma

Charged hadron v_2 as a function of p_T and transverse kinetic energy KE_T is shown on the left of Figure 1.15. It shows mass hierarchy in v_2 between the heavier baryons (p , \bar{p} , Λ , $\bar{\Lambda}$ and Ξ^\pm) and the lighter mesons (π^\pm and $\kappa^{0,\pm}$) in high p_T ($> 2 \text{ GeV}/c$) or KE_T ($> 1 \text{ GeV}$) regions. However, if v_2 , p_T and KE_T are scaled by number of constituent quarks, n_q , of the hadrons, this mass hierarchy feature reduces as demonstrated on the right of Figure 1.15 and even vanishes in v_2/n_q versus KE_T/n_q . The exceptional agreement in quark scaling in v_2 between different species of hadron indicates the degrees of freedom are at the quark level indicating that deconfined quarks are flowing, and therefore the quark-gluon plasma phase is formed [23].

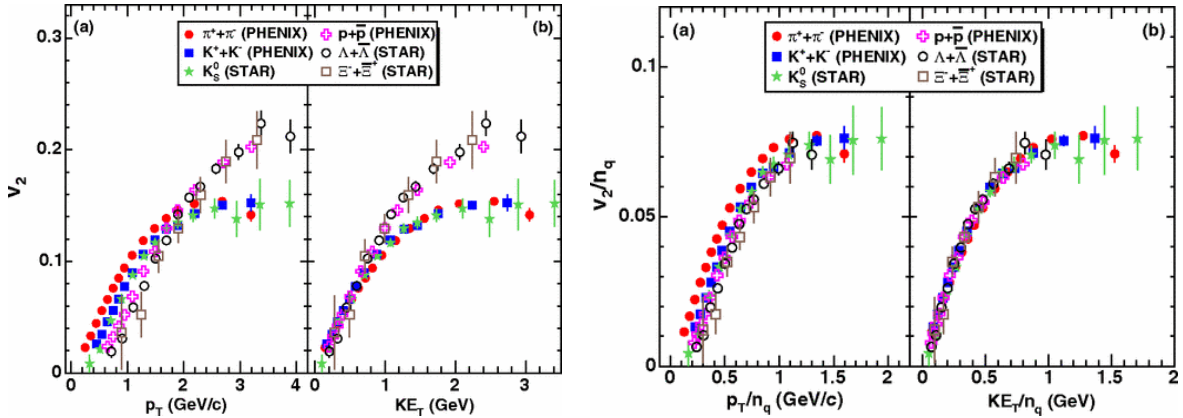


Figure 1.15: Left: Charged hadron v_2 as a function of transverse momentum, p_T , and kinematic energy, KE_T , in transverse direction. Right: Charged hadron v_2 scaled by number of constituent quarks as a function of p_T and KE_T [23].

1.5.2 Jet Modification

In the early stage of heavy-ion collisions, the partons of the colliding nuclei can experience collisions with a large momentum transfer known as a hard scattering. Because of confine-

ment, these hard partons then fragment into softer partons which then hadronize and form collimated sprays of particles known as jets.

Jet production is a phenomenon that has been researched and used to study QCD in high energy collisions. One of the most famous applications of jet measurements was the measurement of a tri-jet event in electron-positron collisions at 22 GeV in the TASSO experiment at DESY in 1979, as shown in Figure 1.16, which served as evidence of gluon production [24]. In the experiment, an electron and a positron annihilate to a photon which then decayed to a quark-antiquark pair. Because of baryon number conservation, a third quark could not have been the source of the additional third jet. The remaining possibilities were the production of two quarks and a gluon, or three-gluon interaction as shown in Figure 1.2.

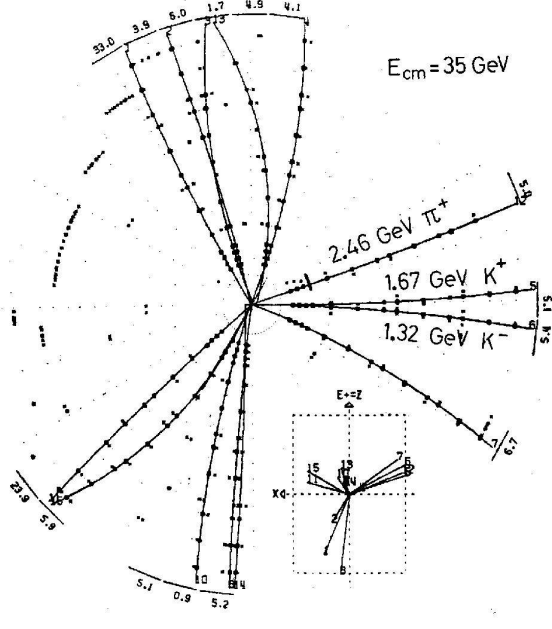


Figure 1.16: Three-jet event in an electron-positron collision measured in TASSO detector at DESY [24]. The dots are the hits in the detector made by the traversing particles. These hits are then reconstructed to tracks (lines) of the particle.

Jets in heavy-ion collisions

Hard scatterings also occur in heavy-ion collisions before the QGP formation. When the QGP is present, the hard scattered partons lose energy via gluon radiation when traversing the QGP [25]. Thus, the resulting jets are less energetic and appear broader compared to the case in $p + p$ collisions in which no QGP is formed. This partonic energy loss leads to softer jets and is known as jet quenching [26, 27].

The transport coefficient, which is the average squared transverse momentum broadening per unit length, is defined as

$$\hat{q} = \rho \int q_T^2 \frac{d\sigma}{dq_T^2} dq_T^2 , \quad (1.11)$$

where ρ is the parton density of the QGP, σ is the cross-section of interaction between the hard scattered parton and the QGP, and q_T is the transverse momentum. The transport coefficient carries information about the QGP that determines the partonic energy loss and thus, the jet modification. Therefore, the study of jet modification, including energy loss and broadening, is used to examine the properties of the QGP.

Examples of Energy Loss Models

Many partonic energy loss models have been proposed [28–36]. Two of them, ZOWW [37] and ACHNS [38], are introduced in this section. ZOWW [37], which considers gluon radiation as the key mechanism behind parton energy loss, models the QGP as a collection of gluons using a spherical nuclear geometry with less than 10% deviation from the Woods-Saxon density. ZOWW also simplifies the expansion of the QGP to one dimension. Gluon absorption by

the hard parton, which leads to parton energy gain, is also considered in the calculation. The total energy loss of a parton is recorded from a time $\tau = \tau_0$ until the QGP phase ends ($\tau = \infty$) is given by

$$\Delta E = \left\langle \frac{dE}{dL} \right\rangle \int_{\tau_0}^{\infty} \frac{\tau - \tau_0}{\tau_0 \rho_0} \rho_g(\tau, b, r, +n\tau) d\tau , \quad (1.12)$$

where ρ_g and ρ_0 are the gluon density of the QGP at times τ and τ_0 , respectively. ρ_g is a function of the impact parameter, b , the production location, r , of the parton which is moving in direction, n . $\left\langle \frac{dE}{dL} \right\rangle$, which is the averaged energy loss per unit length, can be expressed as

$$\left\langle \frac{dE}{dL} \right\rangle = \epsilon_0 (7.5 + E/\mu_0) (E/\mu_0 - 1.6)^{1.2} , \quad (1.13)$$

where ϵ_0 (GeV/fm), known as initial energy-loss parameter, is proportional to the reference gluon density, ρ_0 .

ACHNS [38], which was introduced in 2010, adapts a hydrodynamical model to construct the QGP at RHIC energies. The QGP is assumed to reach thermal equilibrium after $\tau_0 = 0.6$ fm/c when collective flow properties of the QGP occur. The interaction between a parton and the QGP is simplified to a parton travelling through the QGP in a straight path. The energy loss of the parton, which depends on the location, ξ of the parton, is via medium-induced gluon radiation estimated using the BDMPS [39]. In BDMPS calculations, the total energy loss, which is the sum of the energy distribution of the radiated gluons, is proportional

to the transport coefficients and the squared path length, L , as given by

$$\langle \Delta E \rangle \propto \alpha_s C_R \hat{q} L^2, \quad (1.14)$$

where α_s is the coupling constant of strong interaction. C_R is the color-factor, also known as Casimir coupling constant, is associate to the gluon emissions. $C_R = 3$ if the gluon is emitted from a gluon, and $C_R = \frac{4}{3}$ if the gluon is emitted from a quark.

This model assumes an ideal-gas-like QGP, and thus the transport coefficient, \hat{q}_{QGP} calculated in [40] is used according to

$$\hat{q} = K \cdot \hat{q}_{QGP}(\xi) , \quad (1.15)$$

where K is the fitting parameter which quantifies the deviation of the experimental results from the ideal-gas-like QGP, and $\hat{q}_{QGP} \approx 2[\epsilon(\xi)]^{3/4}$ [40]

$$\hat{q} = 2K [\epsilon(\xi)]^{3/4} . \quad (1.16)$$

Since the QGP properties are uncertain before the $\tau_0 = 0.6$ fm/c, the ACHNS model suggests three cases for the time before τ_0 , that is $\xi < \tau_0$:

1. $\hat{q}(\xi) = 0$: no energy loss before thermalization.
2. $\hat{q}(\xi) = \hat{q}(\tau_0)$: constant energy loss.
3. $\hat{q}(\xi) = \hat{q}(\tau_0)/\xi^{3/4}$: decreases of energy density of the QGP as the parton moves forward.

Comparisons between model calculations and experimental results are shown in this section. The end of this section will also show the extracted energy loss properties, ϵ_0 and K , and evaluate these two models.

Nuclear Modification Factor

Jet quenching leads to the suppression of high momentum particles. This can be measured using the nuclear modification factor, R_{AA} , which is the ratio of the per event yield of single particle production in $Au + Au$ and in $p + p$ collisions

$$R_{AA} = \frac{N_{AA}}{\langle N_{coll}^{AA} \rangle} / \frac{N_{pp}}{\langle N_{coll}^{pp} \rangle}, \quad (1.17)$$

where N_{AA} and N_{pp} are the single particle yields per event in $Au + Au$ and in $p + p$ collisions, respectively[41]. N_{coll}^{AA} and N_{coll}^{pp} are the number of binary collisions calculated using the Glauber model [13], for $Au + Au$ and in $p + p$ collisions. Since there can only be a single binary collision in a $p + p$ collision, Equation (1.17) can be simplified to

$$R_{AA} = \frac{1}{\langle N_{coll}^{AA} \rangle} \frac{N_{AA}}{N_{pp}}. \quad (1.18)$$

If there are no QGP effects, the $Au + Au$ collision will be a superposition of $p + p$ collisions. This superposition effect will then be canceled out by the normalization of the number of binary collisions, N_{coll}^{AA} . Then, $R_{AA} = 1$, implies that there is no modification. On the other hand, $R_{AA} > 1$ and $R_{AA} < 1$ indicate enhancement and suppression of particles in $Au + Au$ collisions, respectively.

The nuclear modification factor R_{AA} as a function of transverse momentum of different particles in $Au + Au$ collisions at 200 GeV using PHENIX data is shown in Figure 1.17. Figure 1.17 shows that the direct photon R_{AA} is consistent with 1, indicating no modification, while most of the hadrons experience suppression. The difference in R_{AA} between photons and hadrons is due to the fact that the photon is blind to the strong force and does not interact with the QGP when traversing the QGP. Thus, direct photons are unmodified by the QGP and have an $R_{AA} = 1$. However, hadrons, which consist of color charged partons that interacted with the QGP have an $R_{AA} < 1$ indicating suppression.

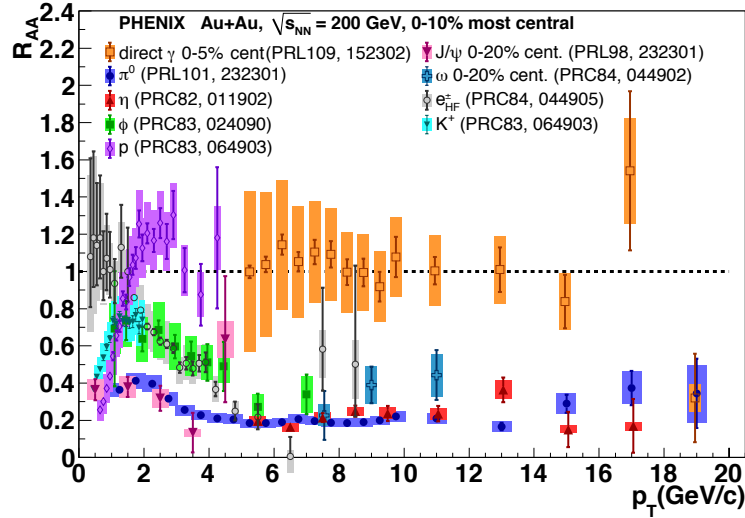


Figure 1.17: Nuclear modification factors of different mesons as a function of transverse momentum in central events of $Au + Au$ collisions at 200 GeV [42].

R_{AA} comparisons between PHENIX results [43] and models for π^0 mesons above 5 GeV/c are shown in Figure 1.18. Theoretical curves with different values of ϵ_0 and K are drawn. The red bold curve in Figure 1.18a is the best fit with $\epsilon_0 = 1.88$ GeV/fm which is in good agreement with the PHENIX R_{AA} at high p_T (> 5 GeV/c). The black solid curve

in Figure 1.18b, however, is not the best fit of R_{AA} from the ACHNS model, but instead results from combining best fit with $K = 4.1$ on different observables, the effect of which will be shown later in this section. Therefore, the best fit from the ZOWW model has better agreement to the experimental results compared the combined best fit from the ACHNS model which gives slightly higher values of R_{AA} than the ZOWW model.

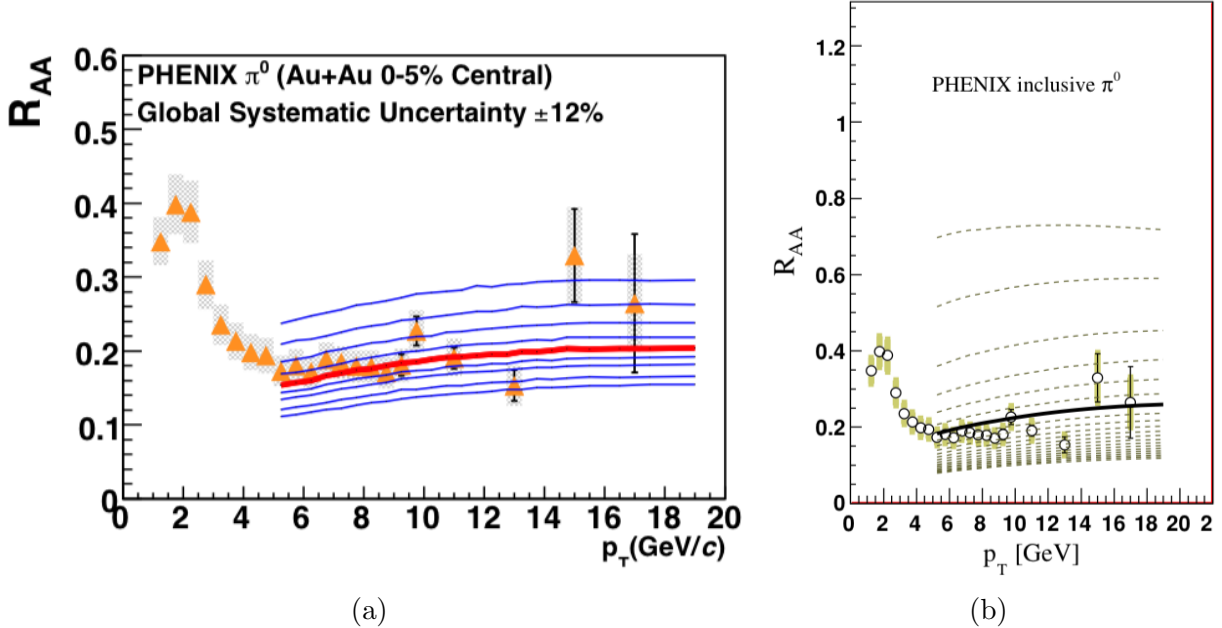


Figure 1.18: (a) π^0 R_{AA} comparison between ZOWW models with different ϵ_0 values and PHENIX results. The red bold curve is using $\epsilon_0 = 1.88 \text{ GeV/fm}$ [43]. (b) π^0 R_{AA} comparison between ACHNS model with K values and PHENIX results. The black solid curve is using $K = 4.1$ [38].

Fragmentation function

To express jet modification mathematically, consider nuclei A and B with partons a and b , respectively. When A and B collide, their partons, a and b scatter and produce another partons c and X . This daughter parton c , then, goes through fragmentation and hadronization, producing final state hadron h at the final state. The cross section of a hadron produced

from a hard scattering in a nucleon-nucleon collision is

$$d\sigma = \sum_{a,b,c} \int \int \int \overbrace{f_a^A(x_a) f_b^B(x_b)}^{\text{initial state}} \cdot \overbrace{d\sigma_{ab \rightarrow cX}}^{\text{hard scattering}} \cdot \overbrace{D_c^h(z)}^{\text{fragmentation}} dx_a dx_b dz. \quad (1.19)$$

Equation(1.19) shows that parton scattering can be factorized to an initial state, a hard scattering, and fragmentation [44]. Descriptions of each term in Equation (1.19) are shown in the following:

- x_a (x_b) is the momentum fraction of nucleus A (B) carried by parton a (b).
- $f_a^A(x_a)$ ($f_b^B(x_b)$), known as the parton distribution function (PDF) of nucleon or nucleus, is the probability of parton a (b) with momentum fraction x_a (x_b) to be found in nucleus A (B).
- $\sigma_{ab \rightarrow cX}$ is the differential cross section of the scattering processes, $a + b \rightarrow c + X$. It is a function of the momenta of parton a , b and c .
- z is the momentum fraction of parton c carried by the final hadron h .
- $D_c^h(z)$, known as the fragmentation function, is the probability that parton c fragments to hadron h with momentum fraction z .

While the cross section of the hard scattering process can be calculated, the PDF and fragmentation function can only be obtained from experimental results. Since the PDF only depends on the initial state of the nucleon or nucleus, any differences in the PDF found between nucleus and proton collisions are categorized as cold nuclear matter effects.

However, as the hard scattered partons lose energy to the QGP, the momentum fraction, z , shift depends of the fractional energy loss $-\frac{\Delta E}{E}$. If z is the momentum fraction in the case of $p + p$ collisions, the shifted momentum fraction, z' , in $Au + Au$ collisions can be expressed as

$$z' = \frac{z}{1 - \frac{\Delta E}{E}} . \quad (1.20)$$

Then, the fragmentation in $Au + Au$ collision can be written as

$$D_c^h(z') = D_c^h\left(\frac{z}{1 - \frac{\Delta E}{E}}\right) . \quad (1.21)$$

Thus, for the same value of the momentum fraction, the fragmentation function in $Au + Au$ is expected to differ from the $p + p$ collisions [44].

In experimental studies, different species of partons and final hadrons are considered. Thus, the fragmentation function $D_c^h(z)$ can be simplified to $D(z)$. Furthermore, the fragmentation function is proportional to the per trigger yield, Y , of the hadrons in two-particle correlations. Hence, the ratio of the per trigger yields in $Au + Au$ to $p + p$ measurements, denoted as I_{AA} , is used to quantify the jet modification in the QGP

$$I_{AA} = \frac{Y_{AA}}{Y_{pp}} \approx \frac{D_{AA}(z)}{D_{pp}(z)} . \quad (1.22)$$

Two-particle correlations

In two-particle correlations, a high momentum particle is assigned as a trigger particle to indicate the presence of a jet, while other hadrons found in the same event are labeled as associate particles. The angle, $\Delta\phi = \phi_{trig} - \phi_{assoc}$, between each trigger and associate particle pair is used to construct the angular correlation distribution known as the correlation function. The correlation functions after the removal of combinatorial pairs are known as jet functions. Since jets are usually produced in pairs moving in opposite directions as shown in Figure 1.19, the angular correlation functions are expected to peak around 0 and π radians for the jet associated with the trigger particle and the opposing jet, respectively. Comparing the widths and the integrated yields of the jet functions in $Au + Au$ collisions to those in $p + p$ collisions provides information on jet angular broadening and energy loss. Details of the two-particle correlation analysis is described in chapter 3.

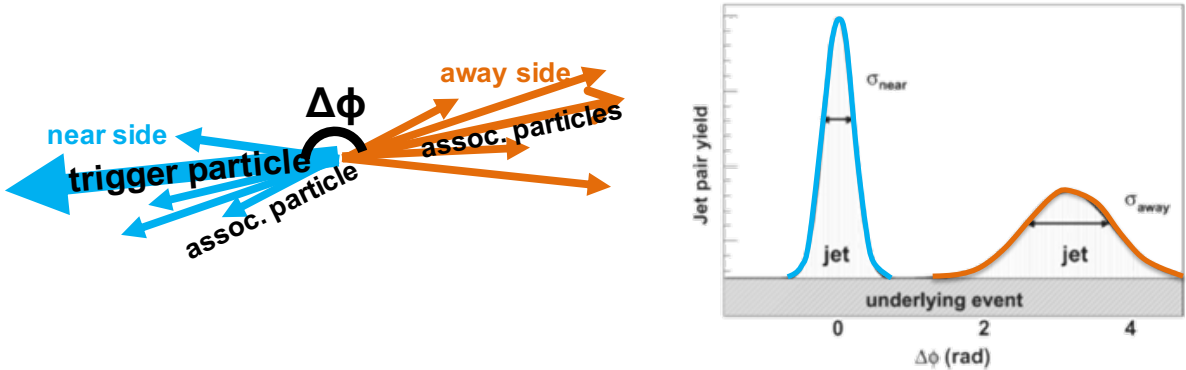


Figure 1.19: Left: drawing of a pair of jets. The trigger particle is in bold blue arrow. Associate particles in the near (away) side are drawn in blue (orange). $\Delta\phi$ is the correlation angle between trigger and associate particles. Right: sketch of two-particle azimuthal correlation function from $p+p$ collisions. The near (away) side correlation peaks at 0 (π) is in blue (orange). σ_{near} and σ_{away} are the Gaussian width of the peaks [45].

Direct photon-hadron correlations in $Au + Au$ Collisions at 200 GeV

Hard scatterings can produce photon-quark or photon-gluon pairs via QCD Compton scattering process, $q + g \rightarrow q + \gamma$, or quark-antiquark annihilation, $q + \bar{q} \rightarrow g + \gamma$. The daughter parton then fragments to a jet, while the photon does not fragment and appears isolated. Hence, a direct photon is a good option for trigger particle. Furthermore, since the photon is unmodified in the QGP, its kinematics are equivalent to its partner parton in the initial hard scattering. Hence, the energy difference between the trigger photon and the opposing jet is equal to the energy lost by the partner parton inside the QGP.

To estimate the photons from hard scattering processes, direct photons are selected in experimental measurements by eliminating photons from decay processes such as neutral pion decay, $\pi^0 \rightarrow \gamma\gamma$.

Figure 1.20 shows the jet functions from direct photon-hadron correlations in $Au + Au$ collisions at 200 GeV from PHENIX $p+p$ data collected in 2005 and 2006, and $Au + Au$ data collected in 2007 and 2010. The jet functions are shown in different ξ ranges. ξ is defined as

$$\xi = \ln \left(\frac{1}{z_T} \right) , \quad (1.23)$$

where $z_T = p_T^h/p_T^\gamma \approx p_T^h/p_T^{jet}$ is the ratio of associate particle transverse momentum to direct photon transverse momentum. It is an approximation to z in the fragmentation function in Equation (1.19). By converting z_T to ξ , one can focus on the low momentum region.

Since photons do not fragment, the near-side is only the trigger direct photon itself. Thus, the near-side of the jet functions in Figure 1.20 is flat compared to the away-side.

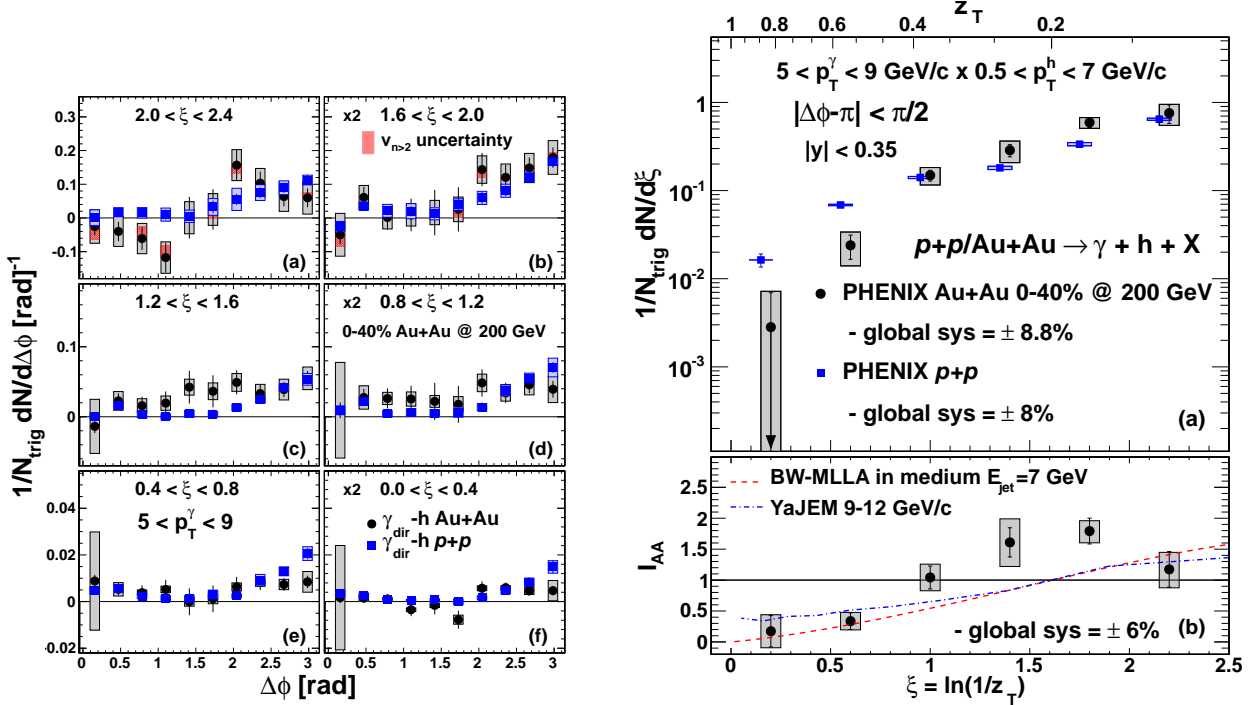


Figure 1.20: Left: jet functions from direct photon-hadron correlations in different ξ ranges. Black and blue data points are results from $Au + Au$ and $p + p$ at 200 GeV data, respectively. Right: Away-side per trigger yields (top) and I_{AA} (bottom) as a function of ξ obtained from the jet functions on the left [46].

The per trigger yields from both $Au + Au$ and $p + p$ data increase with increasing ξ , which corresponds to low associate p_T or high trigger p_T . The per trigger yield ratio, I_{AA} , indicates suppression at low ξ , but rises with ξ . The I_{AA} then passes 1 at $\xi \approx 1$. This transition can be interpreted as the hard partons losing energy to the QGP causing reduction of hard particles and enhancement of soft particles. The theoretical calculations of partonic energy loss using BW-MLLA [47] and YaJEM [48], which are shown on the bottom right of Figure 1.20, agree with the experimental results at low and high ξ ($\xi < 0.7$ and $\xi > 2$), but disagreements are shown in the mid ξ range.

π^0 -hadron correlations in $Au + Au$ Collisions at 200 GeV

While the direct photon triggers is great for parton energy loss studies, direct photon measurements suffer from low statistics because of the large photon background from neutral pion decays. To enhance statistics, which is crucial in the $Au + Au$ measurements where the number of combinatorial pairs is large, hadrons such as neutral pions are used as trigger particles instead of direct photons.

The jet functions from π^0 -hadron correlations $Au + Au$ and $p + p$ collisions at 200 GeV using PHENIX 2007 and 2006 data are shown in Figure 1.21. These results only subtracted the second order flow harmonics. The away-side peaks show noticeable angular broadening in $Au + Au$ collisions compared to $p + p$ collisions at low associate p_T . Furthermore, these away-side peaks in $Au + Au$ collisions appear less like Gaussian than their $p + p$ counterparts. When comparing the amplitude of the jet functions, the $Au + Au$ results show higher per trigger yield on the away-side at low associate p_T compared to the $p + p$ results.

The away-side angular widths and I_{AA} are plotted as a function of associate (partner) p_T in Figure 1.22a and 1.22b, respectively. Figure 1.22a shows that the not-so-Gaussian away-side peaks as shown in Figure 1.21 transfer to extremely high angular widths. The away-side widths in low trigger and associate p_T in the $Au + Au$ collisions show broadening compared to $p + p$ collisions, especially in the most central events. However, the away-side widths from $Au + Au$ and $p + p$ are consistent at high trigger and associate p_T . These angular width results indicate angular broadening of soft jet particles in $Au + Au$ collisions compared to $p + p$ collisions.

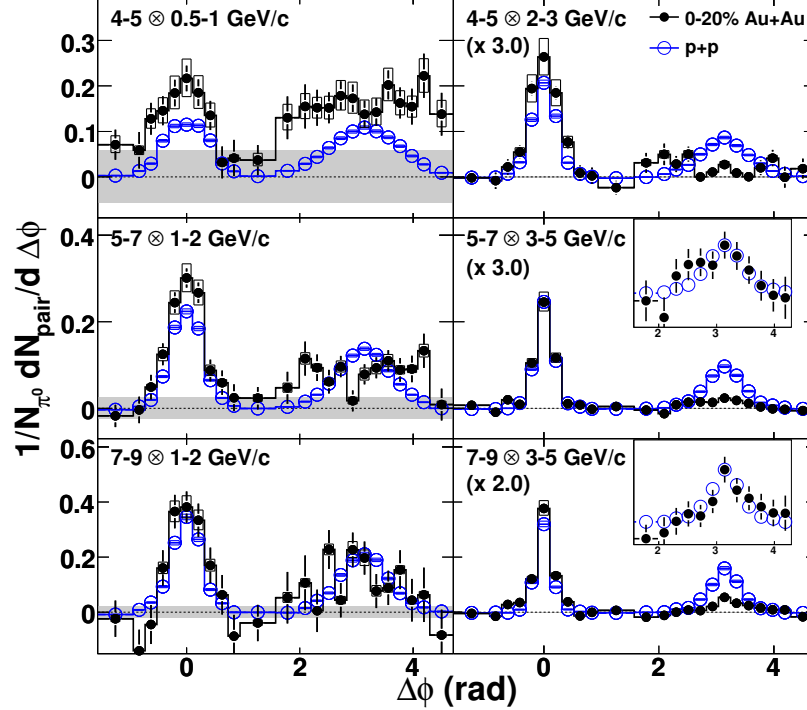


Figure 1.21: Jet functions with second flow harmonic subtracted $Au + Au$ (black) and $p + p$ (blue) collisions at 200 GeV [49].

Figure 1.22b shows the away-side I_{AA} is above 1 for low associate p_T hadrons. It decreases as the associate p_T increases, and reaches below 1 for high associate p_T particles. The I_{AA} results indicate partonic energy loss due in the QGP causing suppression of hard jet particles which are re-distributed to soft jet particles. Hence, enhancement is shown in soft jet particles.

The I_{AA} from ZOWW and ACHNS calculations are also shown in Figure 1.22b. The ZOWW calculations with $\epsilon_0 = 1.68$ GeV/fm are consistent with the experimental results that only the yields near the core of the away-side peak ($|Delta\phi - \pi| < \frac{\pi}{6}$) are included. However, the ACHNS calculations with $K = 4.1 \pm 0.6$ underestimate the I_{AA} values as shown in these comparisons.

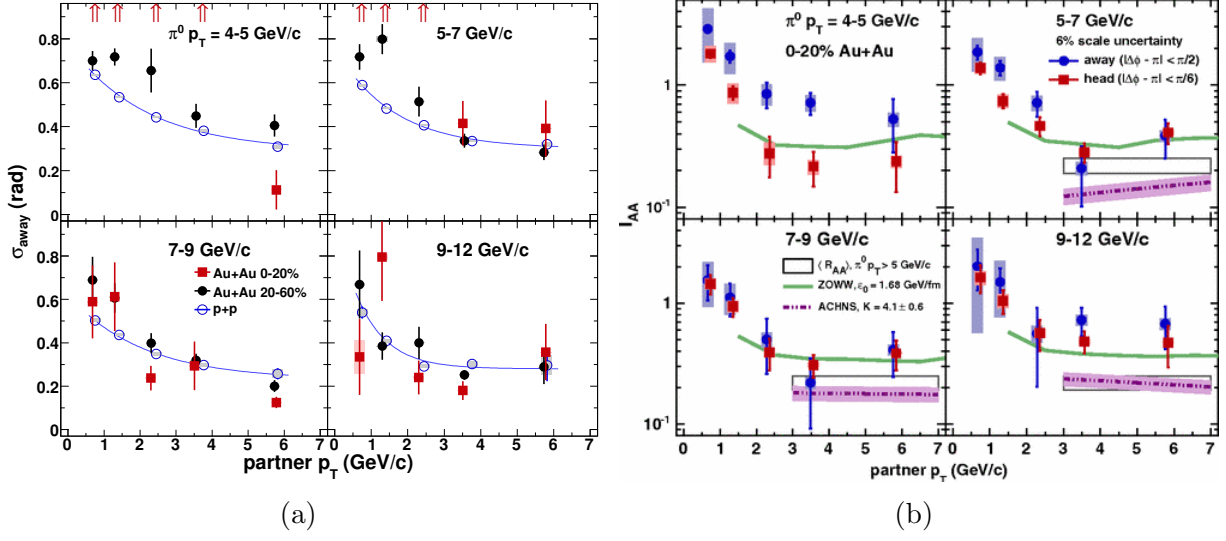


Figure 1.22: (a) Angular width of the away-side jets as a function of associate particle p_T . (b) Away-side I_{AA} as a function of associate particle p_T . Theoretical calculations are drawn as green and purple lines. The black box is the $\pi^0 R_{AA}$ results [49].

Results from Energy Loss Models

Based on the above $\pi^0 R_{AA}$ and I_{AA} comparisions, the ZOWW model shows agreement with each experimental result. However, the model gives $\epsilon_0 = 1.9 \pm 0.2$ and $1.68 \text{ GeV}/\text{fm}$ extracted from the R_{AA} and I_{AA} fits, respectively. Although the uncertainty on ϵ_0 from the I_{AA} fit is not given, the difference in ϵ_0 implies that the model indicates the R_{AA} measurements show stronger energy loss than the I_{AA} results, while both R_{AA} and I_{AA} results came from the same collision system. A best fit analysis for the I_{AA} calculation is needed for a conclusion.

This discrepancy also occurs in ACHNS model as shown in Figure 1.23. The ACHNS is struggling to provide consistent partonic energy loss predictions. The ACHNS calculations using the combined best fit $K = 4.1$ values shows agreement with $\pi^0 R_{AA}$ results in Figure 1.18b from $Au + Au$ collisions at 200 GeV. However, the $K = 4.1$ value gives an underestimated I_{AA} as shown in Figure 1.22b. Figure 1.23 shows the K values from the best

fit analysis done for each observable separately. The K value extracted from the R_{AA} fit is systematically greater than the I_{AA} fit in all three cases. The K values extracted from the fits of R_{AA} and I_{AA} show disagreement in case 1 which assumes no energy loss in the early stages of QGP formation. However, the K values in cases 2 and 3 show converging results.

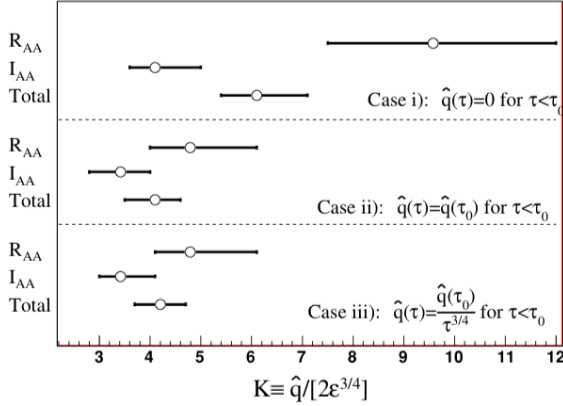


Figure 1.23: K values obtained from ACHNS fits on PHENIX R_{AA} and STAR I_{AA} results [38].

The R_{AA} and I_{AA} comparisons between experimental results and these theoretical calculations demonstrate the extraction of QGP properties from theoretical models and the struggles theories have to match multiple energy loss observables. Although different advanced theoretical models were introduced in the last decade, the discrepancy of the extracted QGP property quantities is still persisted. It is noteworthy that the experimental results play a significant role in constraints of these theoretical models. Therefore, efforts have been made in the heavy ion community, such as the JET collaboration, to evaluate the existing theory works by making systematic comparisons between models and experimental data [50]. Furthermore, JETSCAPE, a simulation of jets in heavy-ion collisions with implementation of various theoretical partonic energy loss models, has been developed to provide realistic

experiment prediction [51].

1.6 Purpose of This Dissertation

While the discovery of the QGP validates the QCD theory, the study of the QGP properties is key to understanding QCD in extreme energy regimes. Theorists have made attempts to build parton energy loss models to extract QGP properties, such as the energy-loss coefficient and the transport coefficients. The existing models show good agreement to different jet observables by varying the fitting parameters. However, these theoretical calculations fail because they cannot give consistent results of QGP property quantities. Therefore, a variety of experimental results are significant to fully evaluate and constrain theoretical models.

This study uses combined PHENIX 200 GeV $Au + Au$ data sets collected in 2010 and 2011 to study jet modification using π^0 -hadron correlations. This study is an improvement on the π^0 -hadron correlation study above. As discussed, results from 2007 PHENIX $Au + Au$ data [49] only removed second order flow harmonics with the assumption that the higher even order flow harmonics are negligible, and the odd order flow harmonics do not exist in heavy-ion collisions. In fact, the third order flow harmonics, which is due to the fluctuations in the initial collision geometry, is non-zero as demonstrated with PHENIX results in section 1.5.1, as well as in STAR and PHOBOS data [21, 18, 19].

When only the second flow harmonic is included in the background subtraction as in [49], the away-side peaks are not Gaussian in the low p_T ranges. The non-Gaussian shape leads to extremely wide away-side Gaussian widths as shown in the right of Figure 1.22a, and the

huge deviations in away-side width between the two centrality classes. The shoulder shape of the away-side jet function is believed to arise from the third order triangular flow harmonics. In order to further eliminate flow effects and extract jet functions, higher flow harmonics up to the fourth order are subtracted in the this analysis.

In addition to the increased statistics and the elimination of higher order flow harmonic effects, this study will obtain new I_{AA} measurements in 20–40% centrality events and introduce a new observable of yield modifications as a function of the correlation angle. These improvements in analysis and new measurements will give a better understanding of parton energy loss in different phase spaces and help constrain theoretical models.

This thesis is arranged in the following order. RHIC and the PHENIX detector systems are detailed in chapter 2. The analysis process of π^0 -hadron correlations in 200 GeV $Au + Au$ collisions, including data selections, corrections and subtraction of combinatorial pairs are laid out in chapter 3, which is followed by the systematic uncertainty evaluation shown in chapter 4. Then, the analysis results are presented in chapter 5. Chapter 6 discusses the comparisons with other recent results within and outside the PHENIX experiments. The comparison with $d + Au$ and ${}^3He + Au$ collisions results are also shown, which leads us to question our knowledge of basic nuclear matter, that is nucleons. Thus, chapter 7 introduces the future Electron-Ion Collider experiments and the modular RICH detector which will deliver the knowledge of the nucleon structure. At the end of this thesis, the findings of π^0 -hadron correlations analysis using 200 GeV $Au + Au$ data and the detector developments of the modular RICH detector are summarized in chapter 8.

CHAPTER 2

Experiments

To produce the QGP, physicists collide heavy ions (high parton density), such as gold, uranium, aluminum, lead and copper, at the speed of light (high energy) using the Relativistic Heavy Ion Collider (RHIC) at Brookhaven National Laboratory (BNL) or the Large Hadron Collider (LHC) at CERN to create the extremely dense and hot environment. RHIC can achieve 510 GeV $p+p$ and 200 GeV $Au+Au$ collisions, while LHC can accelerate lead ions to 5.02 TeV center-of-mass energy. Because of different energy ranges from both experiments, the QGP study can be studied in a broad kinematic range.

2.1 Relativistic Heavy Ion Collider

RHIC began operation in 2000 with four experiments, BRAHMS, PHOBOS, PHENIX and STAR at different locations as shown in Figure 2.1. While BRAHMS [52] and PHOBOS [53] finished their missions in 2006 and 2009 respectively, PHENIX [54] ended its last run in 2016 in preparation for a major upgrade. STAR [55] is continuing to collect data focusing on beam energy scan until 2021, and then will undergo an upgrade for its forward (high pseudorapidity) region.

RHIC provides a flexible range of center-of-mass energy ($\sqrt{s_{NN}} = 7.7\text{--}500$ GeV) for mapping the phase transition of nuclear matter. Besides heavy-ion collisions, small collision systems, such as $p + A$, $d/He^3 + A$ are included in the RHIC program to study cold nuclear matter effects which helps distinguish the QGP medium effects in heavy-ion collisions studies.

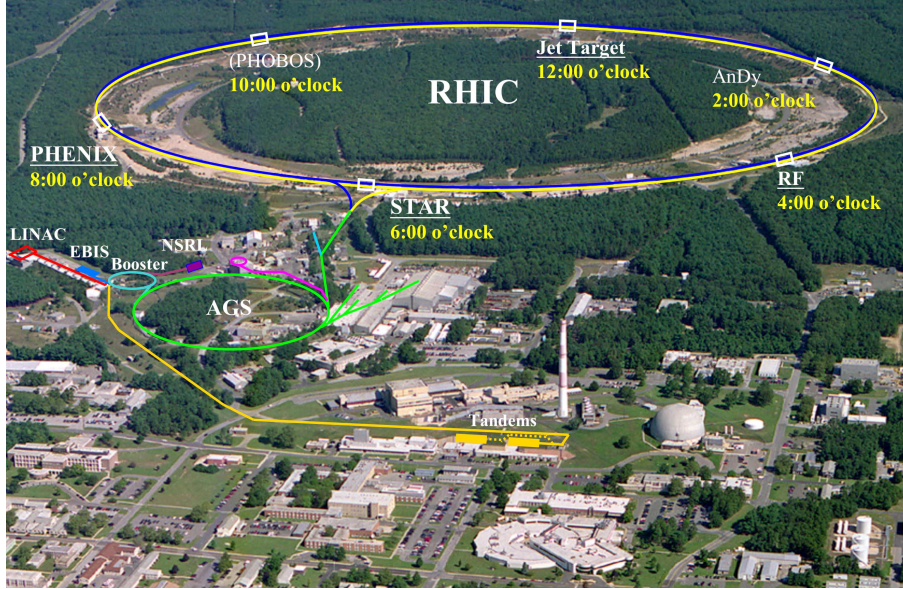


Figure 2.1: AGS facility and RHIC at Brookhaven National Laboratory.

Before injection to RHIC, the ion beams are accelerated using the Alternating Gradient Synchrotron (AGS) which was the most powerful accelerator in the world in the 1960s. Besides the synchrotron, the AGS facility consists of a linear accelerator (LINAC), Electron Beam Ion Source (EBIS), Tandem Van de Graaff accelerator (that is an atom stripper) and the Booster. The first three machines are used to produce different ion species. The Booster is an additional accelerator built in the 1990s to enhance the AGS energy.

The produced ion beam is first accelerated to 37% speed of light in the Booster [56], and then enters to the AGS for second acceleration to reach 99.7% speed of light [56]. When the beam exits the AGS and enters RHIC, it is separated into bunches. For the case of $Au + Au$ collisions, a beam is separated to 112 bunches, and each bunch contains 1.1 billion ions [57] which gives $2 \times 10^{26} \text{cm}^{-2}\text{s}^{-1}$ luminosity (number of events per unit time to cross-section $\frac{1}{\sigma} \frac{dN}{dt}$).

2.2 PHENIX Detector

PHENIX consists of four global detectors for event categorization, and four detector systems, known as arms, in each direction of PHENIX. Layouts of PHENIX in 2010 and 2011 are shown in Figure 2.2 and 2.3, respectively.

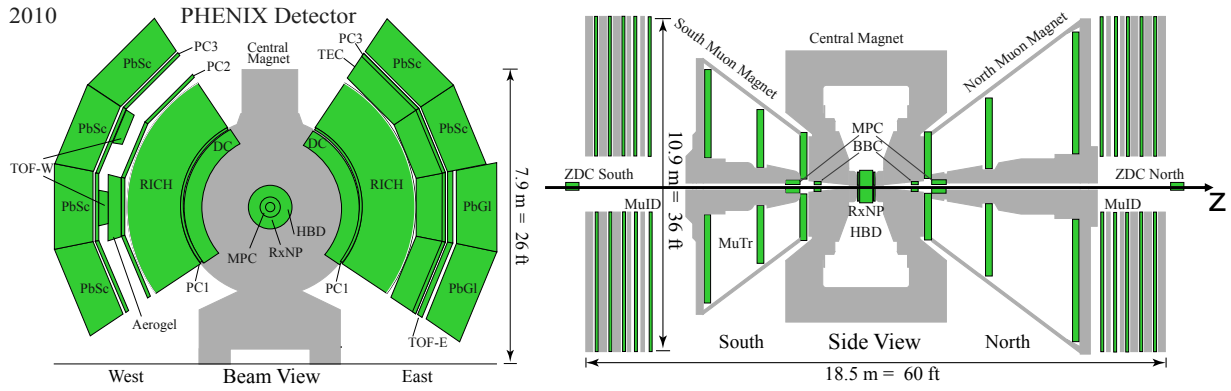


Figure 2.2: Left: beam view of PHENIX central arms in 2010. The gray area is the central magnet. The beam line is pointing perpendicularly to the page. Right: slide view of PHENIX Muon arms.

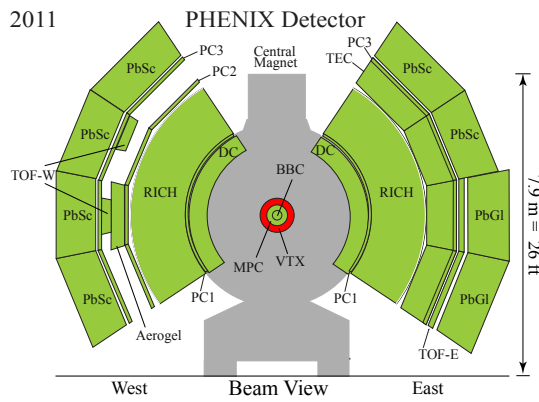


Figure 2.3: Beam view of PHENIX central arms in 2011. The gray area is the central magnet. The beam line is pointing perpendicularly to the page.

The beam pipe passes through the North and South arms of PHENIX which include

a pair of muon detectors which are specialized for muon tracking and identification with pseudorapidity $1.4 < |\eta| < 2.2$. Wrapped around the beam pipe are the East and West arms, collectively known as the central arms, centered at $\eta = 0$. The central arm detectors, which consist of particle identification systems, tracking systems and electromagnetic calorimeters, focus on photon, electron, and charged hadron measurements. Between the central arms are the central magnets which enhance particle identification ability and the resolution of momentum measurement as the bending trajectory of charged particle depends on particle mass and momentum. The 2011 setup had an addition of the vertex detector (VTX). However, it is not used in this study. The following sections will focus on the global detectors, the central tracking system, the RICH detector, and the Electromagnetic Calorimeters.

2.2.1 Global Detectors

The global detectors include a pair of beam-beam counters, a pair of zero degree calorimeters, and the reaction plane detector. The purpose of the global detectors is to categorize events by measuring centrality, vertex (origin of an event) and reaction plane.

2.2.1.1 Beam-Beam Counter

The beam-beam counters (BBC) [58] are two cylindrical detectors located on the beam pipe 144 cm from the collision area as shown in the right of Figure 2.2. It covers 3–3.9 in pseudorapidity and 2π in azimuth. The BBC consists of 64 photomultipliers tubes (PMT) with time resolution 52 ± 4 ps. Each tube, which has a 30 mm long quartz Cherenkov radiator at the front, is covered by a metal shell to prevent light leaks [58]. The BBCs are used to

measure the collision time, centrality, z-vertex (z coordinate of the vertex), and event plane.

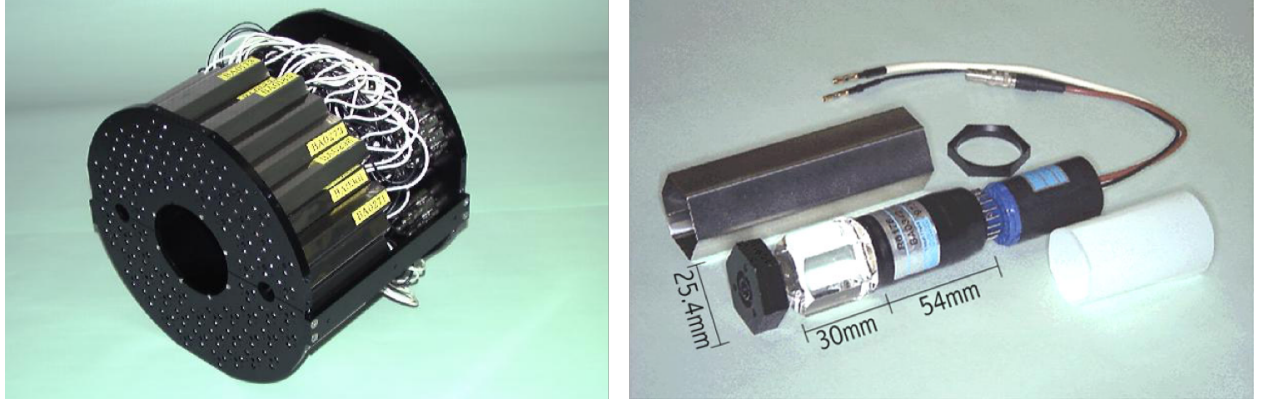


Figure 2.4: Left: The beam-beam counter. In the front of the BBC are 64 photomultiplier tubes. In the back are the readout electronics. Right: one of the PMT inside the BBC. Connected in the front of the 54 mm long PMT tube which is the 30 mm long quartz Cherenkov radiator. The whole tube is covered with a hexagon tube [58].

The charged particle multiplicity measured in the BBC is used to obtain centrality as explained in section 1.4.2. For a central 200 GeV $Au + Au$ collision, 15 charged particles per tube are expected. When these charged particles pass through the quartz Cherenkov radiator with a speed faster than the speed of light in the radiator, they radiates photons known as Cherenkov photons. This phenomenon is known as Cherenkov radiation. These Cherenkov photons are captured by the PMT and transferred to electrical signals which give the hit time in each tube. More details on Cherenkov radiation is covered in section 2.2.2

There are two arrival times, T_S and T_N , measured from the South and North BBCs,

respectively. T_s and T_N are the averaged hit time of the fired PMT tubes, that is,

$$T_{S/N} = \frac{1}{m} \sum_{i=1}^m T_i , \quad (2.1)$$

where m is the number of fired PMT tubes, and T_i is the hit time of the i^{th} fired PMT tubes.

Using the arrival times, the collision time t_0 can be estimated as

$$t_0 = \frac{T_s + T_N + 2L/c}{2}, \quad (2.2)$$

where $L = 144$ cm is the distance of the BBC to the interaction region. The z-vertex (vtx_z), which is the longitudinal position of the collision, can be calculated as

$$\text{vtx}_z = \frac{T_s - T_N}{2} \times c \quad (2.3)$$

The BBCs also act as a trigger for minimum bias events. When at least 2 or more PMT tubes are fired and the z-vertex is within ± 30 cm, the BBC will signal the data acquisition system to record the event when a collision occurred. According to PHENIX detector simulation studies with embedded simulation events, the trigger efficiency of the BBC is about 92%.

2.2.1.2 Zero-Degree Calorimeters

The zero-degree calorimeters (ZDC) [59] are a pair of hadron calorimeters located in the North and the South arms, 18 m from the collision area. The ZDCs are dedicated to neutron

measurements which can be used to measure event centrality and z -vertex position.

A dipole magnet sits in front of each ZDC. Unlike neutrons, charged particles bend their trajectory as they pass through the dipole magnet. Thus, only the neutrons can reach the ZDC. The z -vertex of the event can be estimated by the ZDC using Equation (2.3).

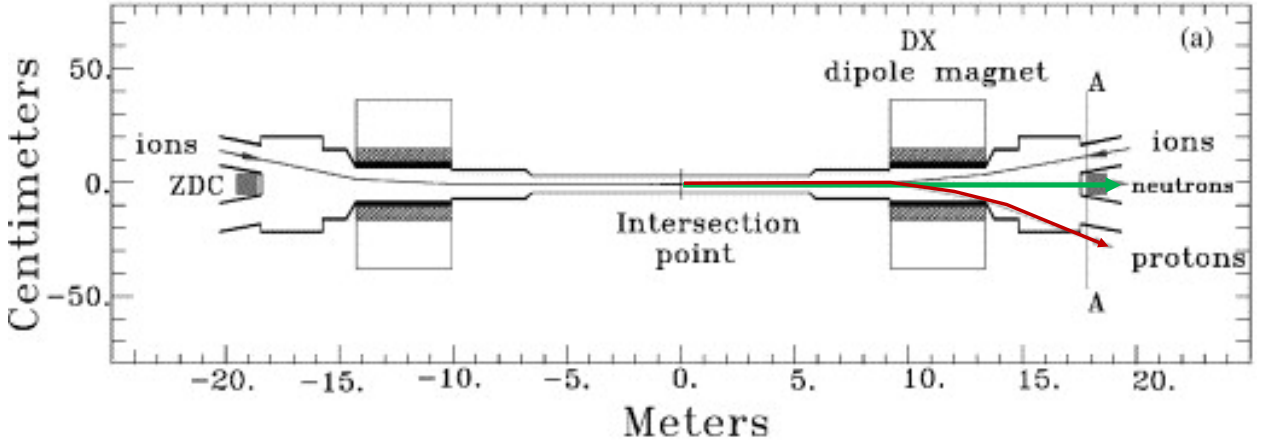


Figure 2.5: Drawing of ZDC and dipole pair along the beam pipe. The black lines are the ion beams, Neutron and charged particle such as protons are drawn in green and red respectively. Unlike neutron, charged particle trajectory bends within the dipole magnet and misses the ZDC [59].

2.2.1.3 Reaction Plane Detector

There is a reaction plane detector (RXNP) [60] at north and south arms of PHENIX close to the beam pipe. Although RXNPs are not used in this analysis, they are used to estimate the reaction plane angle for collective flow studies by measuring the event plane angle Ψ_n , which is the n^{th} harmonic distribution of the particles. The event flow vector of the n^{th}

harmonic Q_n can be decomposed to

$$\begin{aligned}
 Q_n &= Q_{n,x} + Q_{n,y} \\
 &= Q_n \cos(n\Psi_n) + Q_n \sin(n\Psi_n) \\
 &= \sum W_i \cos(n\phi_i) + \sum W_i \sin(n\phi_i) ,
 \end{aligned} \tag{2.4}$$

where ϕ_i is the measured azimuth angle of the i^{th} particle, and W_i is the weight which can be the particle transverse momentum or event multiplicity depending on the measurements [15].

Then the event plane angle can be calculated

$$\begin{aligned}
 n\Psi_n &= \tan^{-1} \left[\frac{Q_{n,x}}{Q_{n,y}} \right] \\
 \Psi_n &= \frac{1}{n} \tan^{-1} \left[\frac{Q_{n,x}}{Q_{n,y}} \right] \\
 &= \frac{1}{n} \tan^{-1} \left[\frac{\sum W_i \sin(n\phi_i)}{\sum W_i \cos(n\phi_i)} \right] .
 \end{aligned} \tag{2.5}$$

The RXNPs are attached at the center area of the central magnet as shown on the right of Figure 2.2. They are cylindrical in shape with 4 cm thickness, and placed around the beam pipe [60]. Each RXNP has an inner and an outer ring as shown in Figure 2.6. Each ring, which has full azimuthal and 1–2.8 in pseudorapidity coverage, is evenly segmented in azimuth into 12 trapezoids.

Each segment of the RXNP has a 2 cm thick scintillator at the back to convert deposited particle energy to photon signals. In the front of the scintillator is a 2 cm thick lead con-

verter to increase the neutral particle flux and reduce soft background. Thus the signal to background ratio is enhanced.

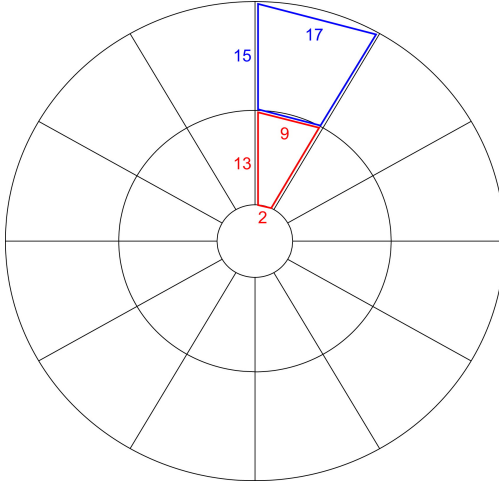


Figure 2.6: Segmentation of the PHENIX reaction plane detector in the central arms. The center circle is the space for the beam pipe. The red and the blue trapezoids are segments in the inner and the outer rings respectively. The numbers are the dimensions of the segments in centimeter [60].

2.2.2 Ring Imaging Cherenkov Detector

The PHENIX Ring Imaging Cherenkov (RICH) detector [61] is a gas RICH detector filled with ethane gas as the radiator. The PHENIX RICH is designed for electron/pion separation up to about 4 GeV/c. The mechanical design of the RICH is shown in Figure 2.7.

As explained in the previous section, when a charged particle travels faster than the speed of light for the ethane gas (radiator), it emits Cherenkov photons. These Cherenkov photons are emitted in a cone shape. The angle of the cone, known as the Cherenkov angle θ , is a function of the refractive index of the radiator (n), particle momentum (p), and

mass (m), as given by

$$\cos \theta = \frac{1}{n} \frac{\sqrt{m^2 + p^2}}{p} . \quad (2.6)$$

In PHENIX, the momentum is measured by the tracking system. The mass of the particle can be calculated using the measured Cherenkov angle from the RICH detector. The PHENIX RICH uses spherical mirrors with a bare aluminum surface to focus Cherenkov photons at the detection plane composed of 1280 photomultiplier tubes. To reduced fluctuations of the ring image, the mirror is required to have root-mean-squared surface roughness within 3 nm [61].

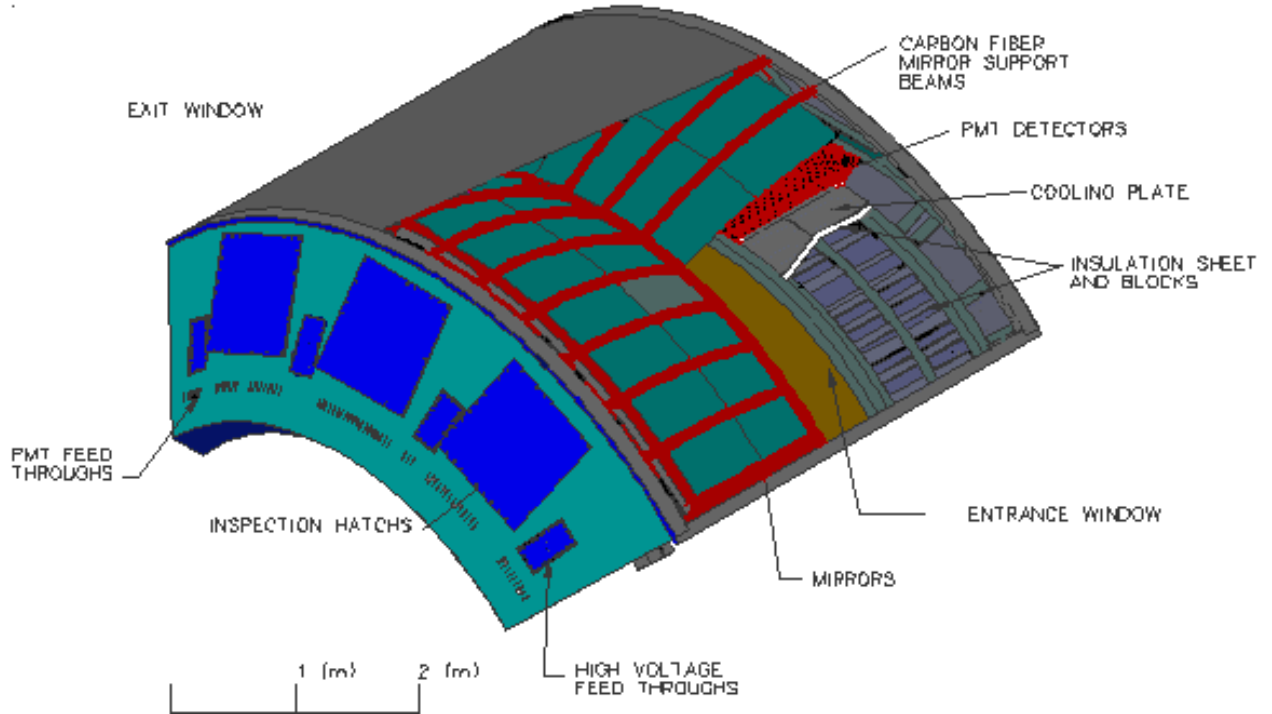


Figure 2.7: Cut view of a sector of PHENIX RICH detector [61]

2.2.2.1 Electron/Charged Hadron Separation

For $0 < \theta < \frac{\pi}{2}$,

$$\cos \theta < 1$$

$$\frac{p}{\sqrt{m^2 + p^2}} > \frac{1}{n} . \quad (2.7)$$

Equation 2.7 showing that there is a threshold momentum p of a particle with mass m for Cherenkov radiation to happen in a radiator with a refractive index n . The momentum thresholds of electrons and charged pions in the PHENIX RICH are 0.2 GeV/c and about 4 GeV/c respectively. Therefore, if the RICH detector is triggered by a particle with a momentum lower than 4 GeV/c, that particle must be an electron. Hence, the RICH detector is used to remove electron tracks from the charged hadron samples below 4 GeV/c.

2.2.3 Tracking System

Two tracking detectors in PHENIX are used in this study. They are the drift chambers and the pad chambers [62]. Both detector systems are variations of gas chamber detectors which utilize ionization to create electrical signals.

When an energetic charged particle passes through the gas-filled detector, the gas atoms along the charged particle track are ionized and electron-ion pairs are created. By placing anode and cathode as well as field wires inside the gas chamber, an electric field is provided to guide the produced ions and electron drift to the cathode and anode wires, respectively.

The ionized electron gains kinematic energy as it moves along the electric field, and then

releases its kinematic energy via a second ionization. Eventually, the kinematic energy gain balances the loss and the electron moves with a steady velocity. Moreover, the number of charges multiplies as the electron drifts to the anode. The number of ionized electrons, n , can be calculated

$$n = n_0 \exp \left[\int_0^r \alpha(r) dr \right] , \quad (2.8)$$

where n_0 is the initial number of charges, dr is the travel distance, and α is called the first Townsend coefficient which is the probability that an ionization occurs within a unit distance. If α is independent of r , then

$$n = n_0 \exp (\alpha r) . \quad (2.9)$$

That is, the number of the ionized charges multiplied exponentially through out the drifting path. This process, of producing a strong signal induced by a small number of charges, is called avalanching.

2.2.3.1 Drift Chamber

The drift chambers (DC) [62] are filled with a mixture of 50% Argon and 50% Ethane gas. They sit outside the beam pipe and centered at $\eta = 0$ as shown in the Figure 2.2. Each DC covers $\frac{\pi}{2}$ in azimuth angle, that is, π in total for both arms. Because of the central magnet, a charged particle's trajectory depends on the sign of its charge, e , and momentum, p . Hence,

using the bending radius, R , measured by the DC tracking, the momentum of the charged particle can be obtained using the Equation (2.10) derived from Lorentz force, where B is the magnetic field.

$$p = eBR . \quad (2.10)$$

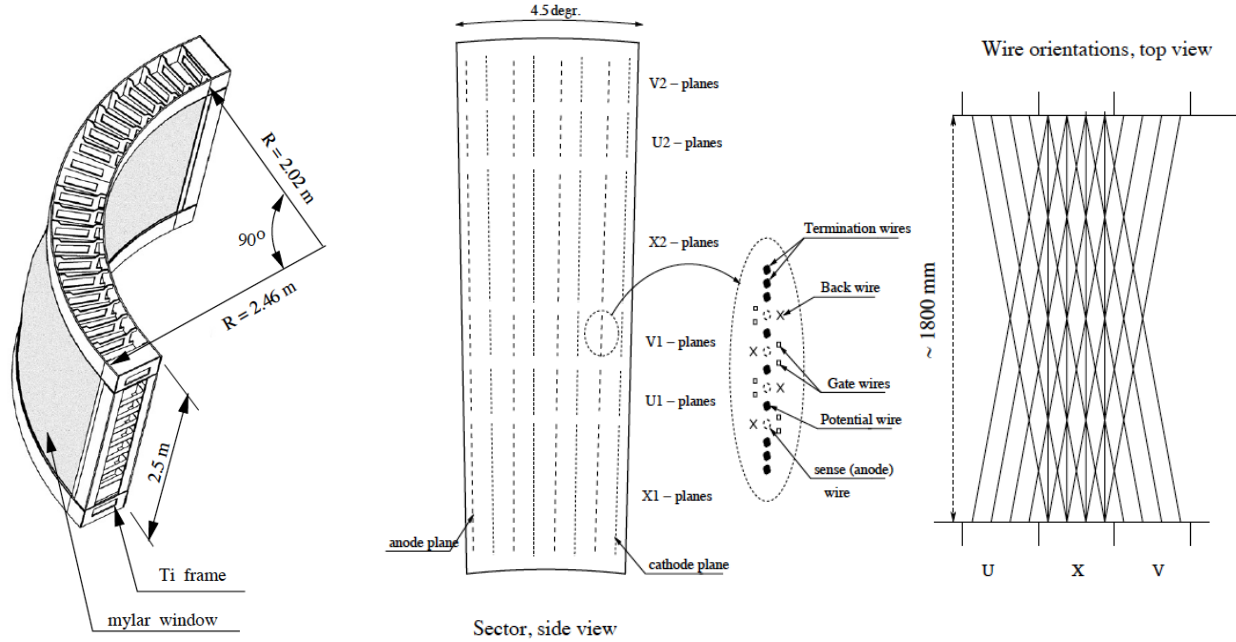


Figure 2.8: Left: mechanical drawing of the PHENIX Drift Chamber with dimension labelled. Center: drawing of a sector of the drift chamber with 6 layers of wire labelled as X1, X2, U1, U2, V1, and V2. Right: top view of the wire orientations from three adjacent sectors [62]

Mechanical drawings of the DC are shown in Figure 2.8. The inner and outer radii of the DC are 2.02 m and 2.46 m, respectively. Each DC is composed of 20 sectors. Each sector provides 4.5° coverage in ϕ as shown in the center of Figure 2.8. As shown in the center and

the right drawings in Figure 2.8, each sector has multiple planes (layers) of wires in three different orientations labeled as, X, U, and V. Each X plane has 12×4 anode wires, while each U and V plane has 4×4 anode wires. The wires in the X planes connect to the same sector on the other side of the DC, while the wires in the U and V planes connect to the adjacent sectors on the other side of the detector, such that the U and V wires form an 6° angle with respect to the X wires. This crossing design reduces ambiguity of hit positions in a high multiplicity event.

In addition to the potential (P) wire that generates the electric field, there are two gate (G) wires and a back (B) wire around each anode wire. The G wires guide the signal to the closest anode, while the B wire terminates the signal from a particular side such that the anode always receives signal from the same side (left or right). Hence, the left-right ambiguity is eliminated.

2.2.3.2 Pad Chamber System

The pad chamber system [62] of PHENIX has three layers which are called PC1, PC2, and PC3. They are used to reconstruct straight line tracks of charged particles outside the central magnet. Figure 2.9 shows the design of the PHENIX pad chamber. The anode and field wires line up in the wire plane which is sandwiched by two cathode panels. The top cathode plane is pixelated, and connected to readout cards (ROC) by kapton cables. Three pixels in the top cathode groups in one $8.4 \times 8.4 \text{ mm}^2$ cell which give $\pm 1.7 \text{ mm}$ z -position resolution. The ionized charges must fire 3 pixels, that is, one cell to create a signal to reduce electronic noise.

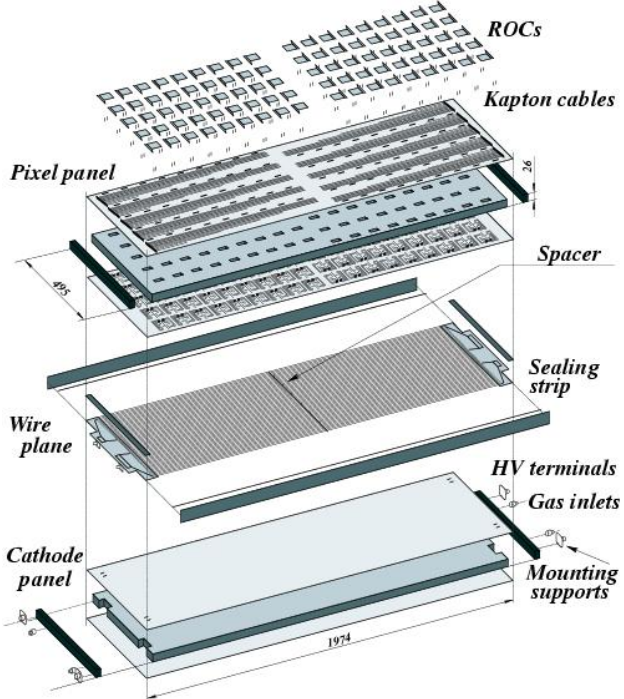


Figure 2.9: Anatomy of PHENIX pad chambers.

The PC1 sits right behind the Drift chamber. The PC2, which is not being used in this study, is behind the RICH detector in the West arm. The PC3 is right in front of the electromagnetic calorimeter. Since the PC1 is at the inner region of the central arms, the PC1 components are held together by honeycomb structure to limit material budget and reduce unwanted particle interactions. However, PC2 and PC3 are supported by fiberglass frames.

2.2.3.3 Track Selection

A charged track is reconstructed by the hits in the DC and PC1. In this analysis, the reconstructed track must pass the quality cut, PC3 matching cut, as well as veto RICH cut to be declared as a charged hadron.

Track Quality

A valid track defined in this analysis is required to have a hit in both X1 and X2 planes, a hit in either U or V plane of the DC, and a hit in the PC1.

PC3 Matching

To reject false tracks, a projection track between the DC and the PC3 is calculated using the track information from the DC as drawn in Figure 2.10. The difference in the azimuth angle ($d\phi$) as well as the z -position (dz) between the PC3 hit and the projection are used to determine bad tracks. $\sigma_{d\phi}$ and σ_{dz} , which are the standard deviations of $d\phi$ and dz , are found from the $d\phi$ and dz distribution in each run. A track is rejected if its $d\phi$ and dz are out of the deviation ranges.

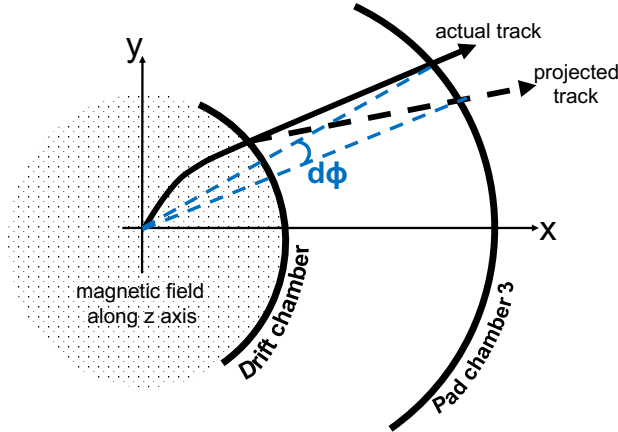


Figure 2.10: Schematic of track (solid) passes through the drift chamber and pad chamber 3 in arbitrary scale. The black dash line is the projected track from calculation, $d\phi$ is the angle between the actual and projected hit positions at the PC3.

RICH Veto

The RICH detector is used to exclude electrons from the charged hadron sample. Since the momentum threshold for charged hadrons at the RICH detector is about 4 GeV/c, any low

momentum ($< 5 \text{ GeV}/c$) track that produces hits within $5.9 \pm 2.5 \text{ cm}$, that is the expected Cherenkov ring radius from an electron, from the track at the RICH detector is considered an electron track and vetoed from the charged hadron pool.

2.2.4 Electromagnetic Calorimeter

The Electromagnetic Calorimeter (Emcal) [63] consists of four sectors of lead-scintillator (PbSc) calorimeters in the West arm. In the East arm, the Emcal has two sectors of lead-scintillator calorimeters and two sectors of lead-glass (PbGl) calorimeters. The Emcal is designed to identify and measure the energy of electrons, positrons and photons.

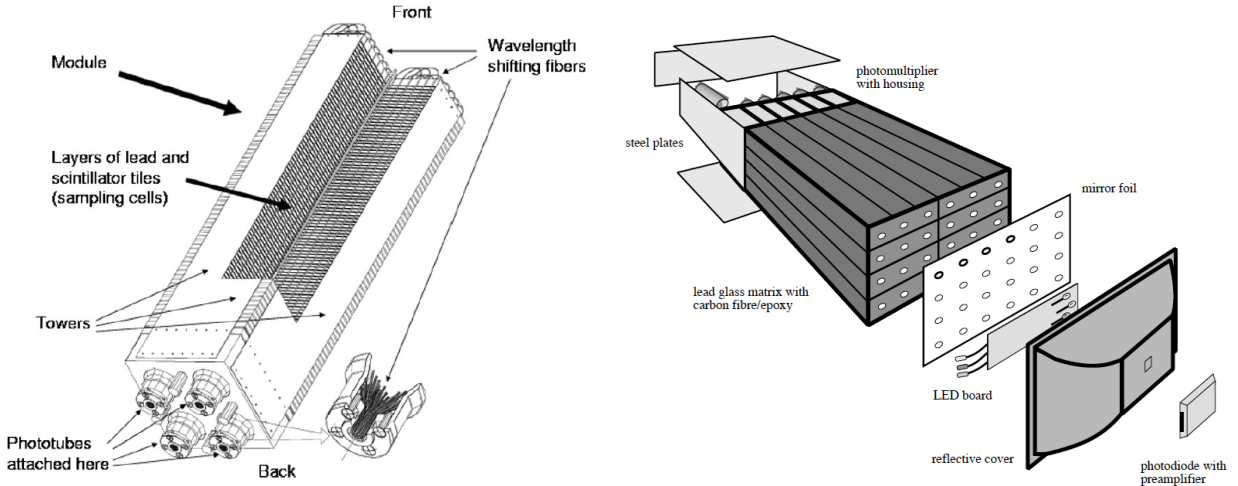


Figure 2.11: Left: Design of lead-scintillator tower. Right: Design of lead-glass tower.

2.2.4.1 Lead-Scintillator Calorimeters

The PbSc is a Shashlik style calorimeter with alternating lead and scintillator cells stacked together. There are 66 sample cells and 36 wavelength shifting fibers in between cells to compose one tower. Each tower is coated with aluminum to prevent light leaks. Four towers

are grouped to a module as drawn on the left of Figure 2.11. Bounding 36 of these modules by a stainless-steel skin forms a supermodule. Then 18 supermodules form a 48 m^2 sector. Therefore, 15,552 towers in total form a single sector.

When an electron travels near a lead atom in the Emcal, it decelerates via photon emission known as Bremsstrahlung radiation. This emitted photon than decays to an electron-positron pair. This cascade process of photon and electron-positron productions leads to an electromagnetic shower as illustrated in Figure 2.12. The scintillators in the Emcal absorb the energy of the showered $e^{+/-}$ and photons, and release the energy by emitting photons which are then carried by the wavelength shifting fiber and captured by phototubes.

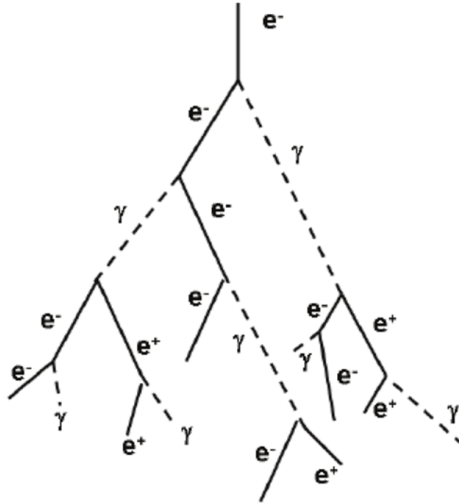


Figure 2.12: Illustration of electromagnetic shower [64].

2.2.4.2 Lead-Glass Calorimeter

Two sectors of lead-glass calorimeters sit at the lower East arm. Unlike the PbSc calorimeters, each PbGl module, which has dimension $40 \times 40 \times 400\text{ mm}^3$, is a mixture of lead and glass with carbon fibre inside. 24 PbGl modules are wrapped in aluminum individually to

avoid light leaks. They are then glued in a 4×6 array to form a supermodule, and then 192 supermodules assemble one sector.

Because of the mass scales, hadrons which are heavier than electrons, have a higher momentum threshold for Cherenkov radiation in the PbGl calorimeters. Thus, low momentum hadrons signals are reduced, while the multiplicity of high momentum hadron signals are low.

Table 2.1: Specifications of PHENIX Electromagnetic Calorimeter Specifications

	Lead–Scintillator Calorimeters	Lead–Glass Calorimeters
energy resolution	$8.1\% \sqrt{E}$ (GeV)	$5.9\% \sqrt{E}$ (GeV)
timing resolution	200 ps	300 ps
granularity	$5.54 \times 5.54 \text{ cm}^2$	$4 \times 4 \text{ cm}^2$

Resolutions of both PbSc and PbGl calorimeters are tabulated in Table 2.1. Although the PbSc calorimeters have better timing resolution than the PbGl calorimeters, the PbGl calorimeters have finer granularity and energy resolution. Different technologies of calorimeters and detector performances provide the ability to cross-check results from the same measurement, and study systematic uncertainties.

2.2.4.3 Particle Identification using Shower Shape

Since the shower patterns and energy depositions differ between electrons (photons) and hadrons, particle identification can be done by χ^2 analysis on the deposited energy in the Emcal as given by [65]

$$\chi^2 = \sum_i \left[\frac{E_i^{predict} - E_i^{measured}}{\sigma_i} \right]^2 , \quad (2.11)$$

where $E_i^{measured}$ is the deposited energy at the i^{th} tower from measurement, $E_i^{predict}$ is the same quantity but from a prediction given by test beam results, and σ_i is the fluctuation of the measurement [65].

2.2.5 Data Sets

A summary of PHENIX data sets is tabulated in Table 2.2 which lists each collision systems, center-of-mass energy, number of events collected and integrated luminosity of the accelerator. The collision system and energy vary for energy scan purposes. However, some of the collision configurations are repeated, such as 200 GeV $Au + Au$, to accumulate statistics for later analyses.

This study analyzes the 200 GeV $Au + Au$ data from Run 10 (2010) and 11 (2011) as highlighted in Table 2.2. Later Run 14 (2014) and 16 (2016) accumulated large data sets, but additional calibrations are needed to be performed prior to analysis. Therefore, Run 14 and 16 data sets are not included in this dissertation, but expected in future studies. The results of Run 6 (2006) and Run 15 (2015) 200 GeV $p + p$ [49, 66] are used as baseline measurement for in I_{AA} and angular width studies, respectively.

Table 2.2: Summary of PHENIX minimum bias data sets

Run Number	Year	Species	C.M. energy (GeV)	Number of events	integrated Luminosity (b^{-1})
1	2000	$Au + Au$	130	10 M	1μ
2	2001–2	$Au + Au$	200	170 M	24μ
		$p + p$	200	3.7 B	$0.15 p$
3	2002–3	$d + Au$	200	5.5 B	$2.74 n$
		$p + p$	200	6.6 B	$0.35 p$
4	2003–4	$Au + Au$	200	1.5 B	241μ
		$Au + Au$	62.4	58 M	9μ
5	2005	$Cu + Cu$	200	8.6 B	$3 n$
		$Cu + Cu$	62.4	400 M	$0.19 n$
		$Cu + Cu$	22.4	9 M	2.7μ
		$p + p$	200	85 B	$3.8 p$
6	2006	$p + p$	200	233 B	$10.7 p$
		$p + p$	62.4	28 B	$0.1 p$
7	2007	$Au + Au$	200	5.1 B	813μ
8	2008	$d + Au$	200	160 B	$80 n$
		$p + p$	200	115 B	$5.2 p$
9	2009	$p + p$	500	3.08 B	$14 p$
		$p + p$	200	9.36 B	$16 p$
10	2010	$Au + Au$	200	8.2 B	$1.3 m^*$
		$Au + Au$	62.4	700 M	$0.11 n$
		$Au + Au$	39	250 M	40μ
		$Au + Au$	7.7	1.6 M	0.26μ
11	2011	$p + p$	500	594 B*	$27 p$
		$Au + Au$	19	13 M	$2.17 \mu^*$
		$Au + Au$	27	2.2 B*	5.2μ
		$Au + Au$	200	5.7 B*	915μ
12	2012	$p + p$	200	4.5 B	$9.24 p$
		$p + p$	510	4.2 B	$30.03 p$
		$Cu + Au$	200	6.8 B	$2.8 n$
		$U + U$	192	3 B	171.19μ
13	2013	$p + p$	510	15 B	$156.49 p$
14	2014	$He + Au$	200	2.8 B	$134 n$
		$Au + Au$	15	15 M	44.2μ
		$Au + Au$	200	18 B*	$2.56 n$
15	2015	$p + p$	200	4 B*	$59.91 p$
		$p + Al$	200	2 B*	$691 n$
		$p + Au$	200	3.7 B*	$206.2 n$
16	2016	$Au + Au$	200	14.3 B	$2.3 m^*$
		$d + Au$	20	1.0 B*	
		$d + Au$	39	2.0 B*	
		$d + Au$	62	0.93 B*	
		$d + Au$	200	1.5 B*	$286 p^*$

* Estimated values

CHAPTER 3

π^0 -Hadron Correlation Analysis

The two-particle correlation analysis starts with data selection. The neutral pion is reconstructed by paring photons detected in the electromagnetic calorimeters. The reconstructed π^0 are correlated to every associate charged hadron track found in the same event. The azimuth angles $\Delta\phi$ between the trigger pions and associate tracks are measured in different transverse momentum p_T ranges and centrality classes.

The correlation functions are corrected for detector efficiency and detector geometry effects, and then the background flow is subtracted in order to obtain the jet functions. The jet functions, which are the crucial elements in this study, are used to extract physics quantities, including jet widths, I_{AA} and R_I .

3.1 Data Selection

Cuts are applied on events, trigger particles, and associate charged hadron tracks depending on detector properties discussed in Section 2.2. After passing all the cuts described below, the data are binned in centrality, trigger p_T and associate p_T , as shown in Table 3.1 which also summarizes the cuts applied. Furthermore, a run-by-run quality assurance, detailed in section 3.3, is also performed to remove exceptional deviations between data sets.

Event Selection

To make sure that the final particles fall within the PHENIX pseudorapidity acceptance ($\eta \leq 0.35$), a z-vertex of an event is required to be within 30 cm. Furthermore, this analysis focuses on two centrality classes, 0–20% and 20–40% to study influence of the QGP size.

Table 3.1: Summary of cuts applied in particle selection

	cuts	criteria
Event	z -vertex centrality	$ z_{\text{vtx}} \leq 30$ cm 0–20%, 20–40%
	tower cuts	remove clusters hit next to the dead towers remove clusters hit at the edge towers remove clusters hit at the hot towers
Single photon	energy	$E \geq 1$ GeV
	shower shape cut	remove clusters that are 2% least likely to be a photon using χ^2 method
	veto track cut	no cluster closer than 8 cm to projected tracks
	location	same arm of EMCals
	total energy	$E_{\text{total}} = E_{\gamma 1} + E_{\gamma 2} \geq 4$ GeV
Photon pair	energy asymmetry	$a \leq 0.15 + 0.85 \left[\frac{E_{\text{total}} - 4}{1.25} \right]^2$
	mass window cut	$0.12 \leq m_{\gamma\gamma} \leq 0.16$ GeV
	momentum binning	4–5 GeV/c, 5–7 GeV/c, 7–9 GeV/c, 9–12 GeV/c, 12–15 GeV/c
	track quality	keep track that gives a hit in both X1 and X2 planes of the DC, a hit in either U or V plane of the DC, and a hit in the PC1
Charged track	veto RICH cut	remove tracks that trigger RICH at $p_T \leq 5$ GeV/c
	PC3 matching cut	$\sqrt{\sigma_{d\phi}^2 + \sigma_{dz}^2} < 2$
	momentum binning	0.5–1 GeV/c, 1–2 GeV/c, 2–3 GeV/c, 3–5 GeV/c, 5–7 GeV/c

Single Photon Selection

Two sets of cuts are applied on the clusters measured by the electromagnetic calorimeters. The first set of cuts is used to reduce noise and avoid effects from ineffective areas in the detector. The other set separates photon signals from electrons and charged hadrons. In addition, the cluster must deposit at least 1 GeV energy to the EMCals. This 1 GeV energy cut reduces the combinatorial background in π^0 reconstruction. If a cluster passes all the single photon cuts, it is labeled as an inclusive photon.

If a cluster hits a dead tower or the edge of the electromagnetic calorimeters, the measured

cluster energy will deviate from the true value. To avoid such situation, clusters hit at the towers adjacent to the dead towers as well as the edge towers are removed. To reduce the noise in the detector, cluster hit at the hot towers that have higher accumulated hits than the average over the entire run is also be rejected.

To reject electron clusters, a confidence level cut based on shower shape technique, as discussed in section 2.2.4.3, is applied to remove the 2% of clusters that are the least likely to be photons. In addition, a veto cut is applied on the cluster to eliminate the charged hadron signal from the single photon pool. If the projected charged track from the drift chamber is within 8 cm of the cluster, the cluster is rejected. If the clusters passed all the single photon cuts except for the veto track cut, these clusters are labeled as loose photons. The clusters, which passed all the single photon cuts listed above, are categorized as inclusive photons.

Photon Pair Selection

After the single photon cuts, an inclusive photon is paired with a loose photon for π^0 reconstruction. The decay photon pair must be detected in the same Emcal arm. The total energy of the photon pair, $E_{total} = E_{\gamma 1} + E_{\gamma 2}$, must be at least 4 GeV. To further reduce combinatorial pairs, an energy asymmetry cut is applied on the photon pairs that have total energy less than 5.25 GeV. The energy asymmetry is defined as the ratio of the difference to the sum of the photon pair energies

$$a = \frac{|E_{\gamma 1} - E_{\gamma 2}|}{E_{\gamma 1} + E_{\gamma 2}} . \quad (3.1)$$

The asymmetry cut requires that

$$a \leq 0.15 + 0.85 \left[\frac{E_{total} - 4}{1.25} \right]^2 . \quad (3.2)$$

Then, the mass of the reconstructed π^0 is calculated according to the following

$$m_{\pi^0} = \sqrt{2E_{\gamma 1}E_{\gamma 2} \cos(1 - \psi)} , \quad (3.3)$$

where ψ is the open angle between the photon pair. The reconstructed π^0 mass distribution found in Run 10 and Run 11 data sets are shown in Figure 3.1. Although Figure 3.1 shows the mass spectra from 0–1 GeV/c², only the reconstructed π^0 with mass between 0.12 GeV/c² and 0.16 GeV/c² are selected which encompasses the true π^0 mass of 0.135 GeV/c² [67]. In addition, the momentum of the selected π^0 must be within 4–15 GeV/c to be used in the jet analysis. The momentum distributions of the trigger π^0 are shown in Figure 3.2. The plateau in Figure 3.2 at about 5 GeV is due to the energy asymmetry cut on photon pairs with total energy less than 5.25 GeV.

Charged Hadron Track selection

Charged particles are measured and tracked by the drift chamber and the pad chamber detectors. To ensure the track is valid, a track quality cut is applied. A signalized PC3 matching cut is set to

$$\sqrt{\sigma_{d\phi}^2 + \sigma_{dz}^2} < 2 . \quad (3.4)$$

The RICH veto cut is applied on tracks with $p_T < 5$ GeV/c rather than $p_T < 4$ GeV/c because the associated track p_T binning is across 3 to 5 GeV/c. Only tracks with momentum within 0.5–7 GeV/c are selected as associated tracks for correlations. The momentum distributions of the associated tracks are shown in Figure 3.3. The steps at 5 GeV/c in Figure 3.3 are caused by the RICH veto cut. Explanations of these track selections are detailed in section 2.2.3.3.

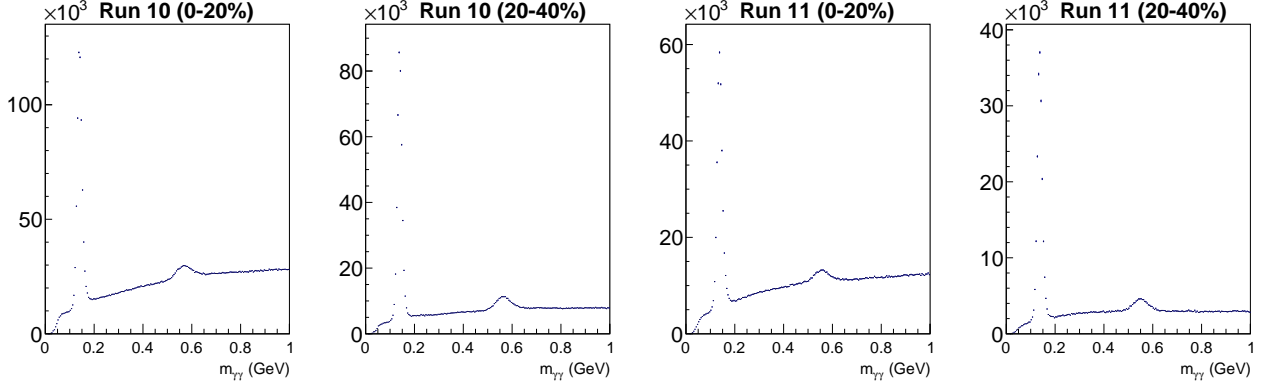


Figure 3.1: Invariant mass spectra of photon pair in different centrality classes from Run 10 and Run11 data. The π^0 mass is peak at about 0.135 GeV. The peak near 0.548 GeV is the η meson which is not used in this analysis.

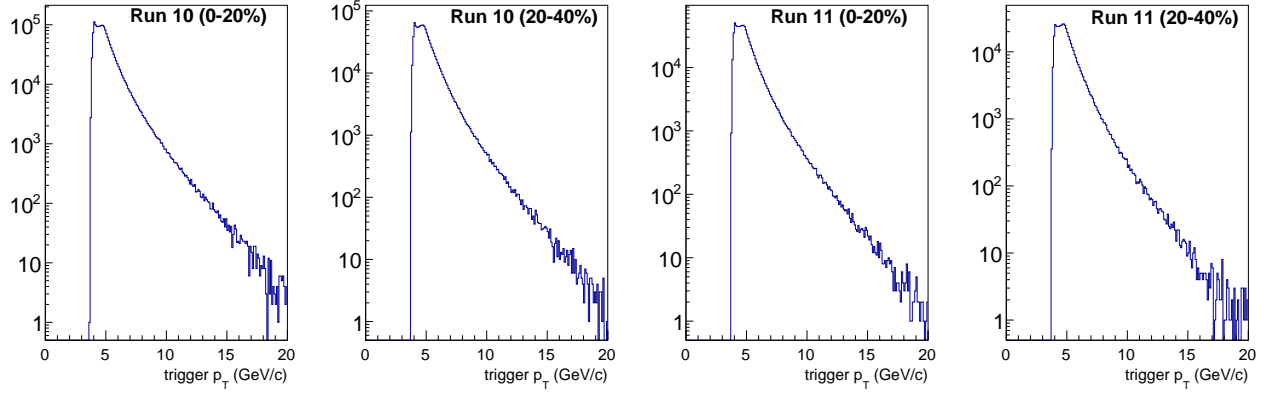


Figure 3.2: Transverse momentum distributions of trigger particles in different centrality classes from Run 10 and Run11 data.

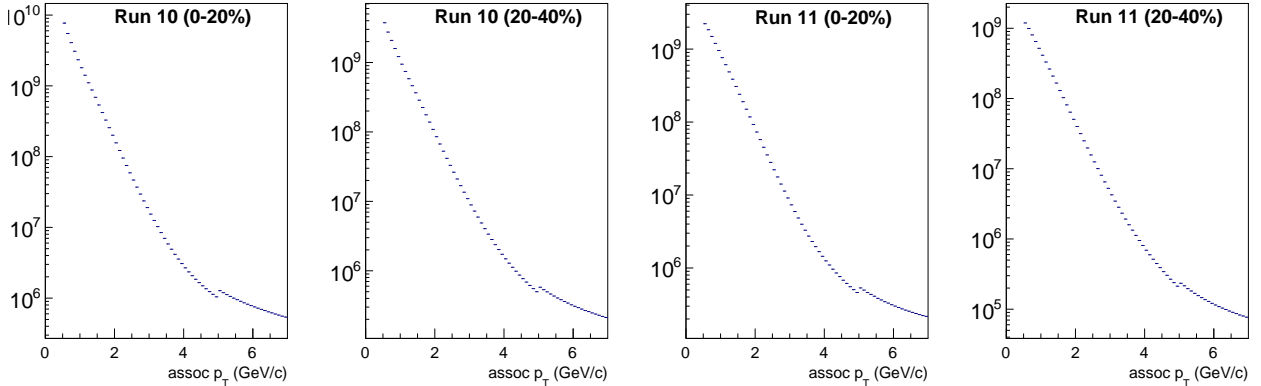


Figure 3.3: Transverse momentum distributions of associate tracks in different centrality classes from Run 10 and Run 11 data.

3.2 Event-Mixing

The event-mixing technique is developed to estimate combinatorial pairs, that are uncorrelated, in the same-event analysis but may yield a correlation due to detector acceptance effects. The event-mixing technique pairs trigger and associate particles from different events to mimic the combinatorial pair in the same-event analysis. To reduce bias, the centrality and z -vertex of the mixed-event pair are restricted to be less than 5% and 5 cm between two events, respectively. The correlation functions from the mixed-events are used to correct detector acceptance effects and estimate the level of underlying events as discussed in section 3.4.2 and 3.5.3.

3.3 Run Selection

Data collected in 2010 and 2011 in different data collecting sessions called runs with maximum 60 minutes duration. The detector setup and performance changes between runs cause a variation in detector efficiency and the measured correlations. Therefore, a run-by-run quality assurance is performed to remove runs that deviates from the majority of runs.

The run-by-run quality assurances (QA) was done in previous PHENIX analyses [68, 69] by applying a χ^2 method to the shapes of the correlations from event-mixing analysis. The mixed-event correlation in each run is compared to the summed correlations from mixed events by dividing the former by the latter in a data point by data point fashion. In an ideal case that there are no deviation between runs at all, the ratio plots of the mixed-event correlations should appear flat. Thus, flat lines are fitted on the ratio plots, then the ratios of χ^2 to the degree of freedom (dof) of the fits are used to qualify each run. While runs with $\chi^2/\text{dof} < 2$ are classified as good, runs with $\chi^2/\text{dof} > 2$ are inspected and classified manually. If a run is declared as bad, it will not be included

in the analysis.

3.4 Correction for Detector Effects

Corrections are applied to the correlation functions to account for detector efficiency and acceptance effects. The detector efficiency affects the per trigger yields of the correlation functions while the detector acceptance affects the shape of the correlation functions.

3.4.1 Charged Hadron Efficiency

The charged hadron efficiency, ϵ , can be factorized into two components

$$\epsilon = \epsilon^h \cdot \epsilon^{\text{occ}} , \quad (3.5)$$

where ϵ^h and ϵ^{occ} are the single hadron efficiency and occupancy, respectively.

Single Charged Hadron Efficiency

Due to detector design, aging, electrical or mechanical issues, the detector does not achieve 100% efficiency in the measurement of single hadrons. To estimate the detector efficiency, PHENIX detector properties including acceptance, materials, and dead areas of the drift chamber detectors found in the experimental data are included in the GEANT3 simulation [70]. Different species of charged particles, $\pi^{+/-}$, $K^{+/-}$ and p/\bar{p} , each with a flat momentum distribution, are simulated. The charged tracks are reconstructed with the same cuts applied in experimental data. Then the single charged hadron efficiency is defined as the ratio of the reconstructed tracks to the simulated tracks.

The single hadron efficiencies for Run 10 and Run 11 are obtained from previous PHENIX analyses [71]. The efficiency obtained from the simulation is fitted in three different p_T regions,

$p_T < 3 \text{ GeV}/c$, $3 < p_T < 5 \text{ GeV}/c$ and $p_T > 5 \text{ GeV}/c$ using the following function

$$\epsilon^h(p_T) = A + B \exp(C \cdot p_T) , \quad (3.6)$$

where A , B , and C are the fit parameters which are shown in Table 3.2 and plotted in Figure 3.4.

The efficiency is fitted in three p_T regions because of the veto RICH cut for hadron samples below $5 \text{ GeV}/c$. The additional $3\text{--}5 \text{ GeV}/c$ region is added to match the associate track p_T binning.

Note that azimuthal acceptance of the central arms is included in the single hadron efficiency as the central arm geometry is included in the simulation. As mentioned in section 2.2, the azimuthal acceptance of the central arms equal π ; therefore, the acceptance correction is a factor of 2.

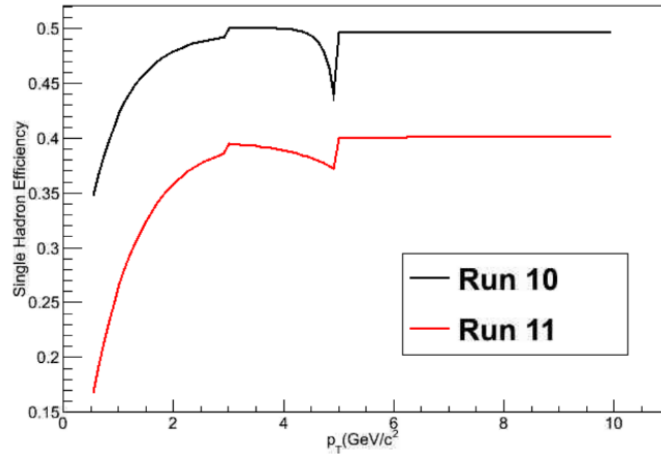


Figure 3.4: Hadron efficiencies as a function of associate track transverse momentum in Run 10 and Run 11 [71].

Table 3.2: Fit parameters of single charged hadron efficiency

Hadron momentum	Run 10			Run 11		
	A	B	C	A	B	C
< 3 GeV/C	0.496	-0.337	-1.50	0.4007	-0.4413	-1.167
3–5 GeV/C	0.500	-2.13×10^{-13}	5.36	0.3973	-7.951×10^{-5}	1.172
> 5 GeV/C	0.496	-0.337	-1.50	0.4007	-0.4413	-1.167

Occupancy

The occupancy correction accounts for the detector efficiency of track reconstruction in high multiplicity events. To simulate the detector's response in high multiplicity events, simulated tracks are embedded into the real events from experimental data.

The occupancy obtained from the simulation is fitted by flat lines for different centrality classes. Moreover, the occupancy is fitted separately in $p_T < 5 \text{ GeV}/c$ and $p_T > 5 \text{ GeV}/c$ due to the rejection of tracks consistent with an electron in the RICH below 5 GeV/c. The results of fit to the occupancy obtained from previous PHENIX analysis [71] are shown in Table 3.3.

Table 3.3: Fit parameters of the occupancy

Centrality (%)	$pT < 5 \text{ GeV}/c$	$pT > 5 \text{ GeV}/c$
0 – 20	0.680	$0.761 + 1.640e^{-4.734p_T}$
20 – 40	0.835	0.913

3.4.2 Detector Acceptance

Due to the gaps between the West and East arms at the 12 and 6 o'clock positions, the detector may bias the correlations at certain angles as illustrated in Figure 3.5. To correct for this problem, the same-event correlations are divided by the mixed-event correlations. As discussed in Section 3.2, the mixed-event correlations are constructed by combinatorial π^0 -hadron pairs. Therefore, the mixed-event correlations reflect the angular bias raised by the detector acceptance.

The mixed-event correlation functions, which are also corrected with charged hadron efficiency, are normalized to 2π . The idea is that for an ideal full azimuth acceptance detector, the mixed-event correlation functions should have a unitary $\Delta\phi$ distribution, as the probability of getting a combinatorial trigger-associate pair at any $\Delta\phi$ should be the same. Then, the integral of the $\Delta\phi$

distribution should satisfy

$$\int_{-\pi/2}^{3\pi/2} d(\Delta\phi) = 2\pi. \quad (3.7)$$

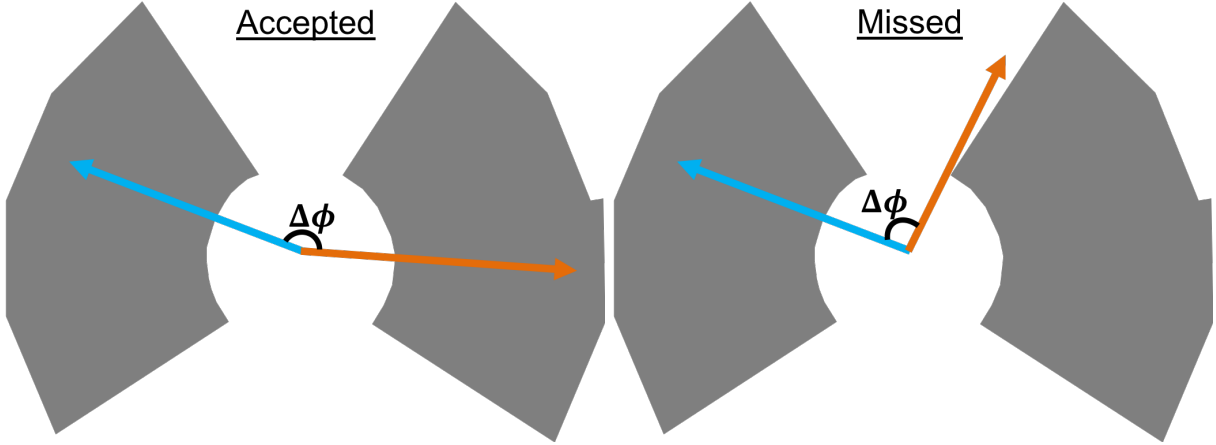


Figure 3.5: Illustrations of detector acceptance effect on angular correlation measurements. The grey areas represent the PHENIX central arm detectors. Left: example of accepted correlation. Right: example of missed correlation where the trigger or associate particle is missed by the detector.

The same-event correlation functions are divided by the normalized mixed-event correlation functions. Figure 3.6 and 3.7 show the comparisons of the same-event to the mixed-event correlation functions. These correlation functions are scaled to match the amplitudes of the near-side peaks in the mixed-event correlation functions. These figures show the importance of the detector geometry correction as the mixed-event correlations demonstrated that the detector favors correlation with $\Delta\phi$ closes to 0 or π . Moreover, the artificial wiggles in the away-side peaks are reduced after acceptance correction as observed in the comparisons between Figure 3.6 and 3.8, and the comparisons between Figure 3.7 and 3.9.

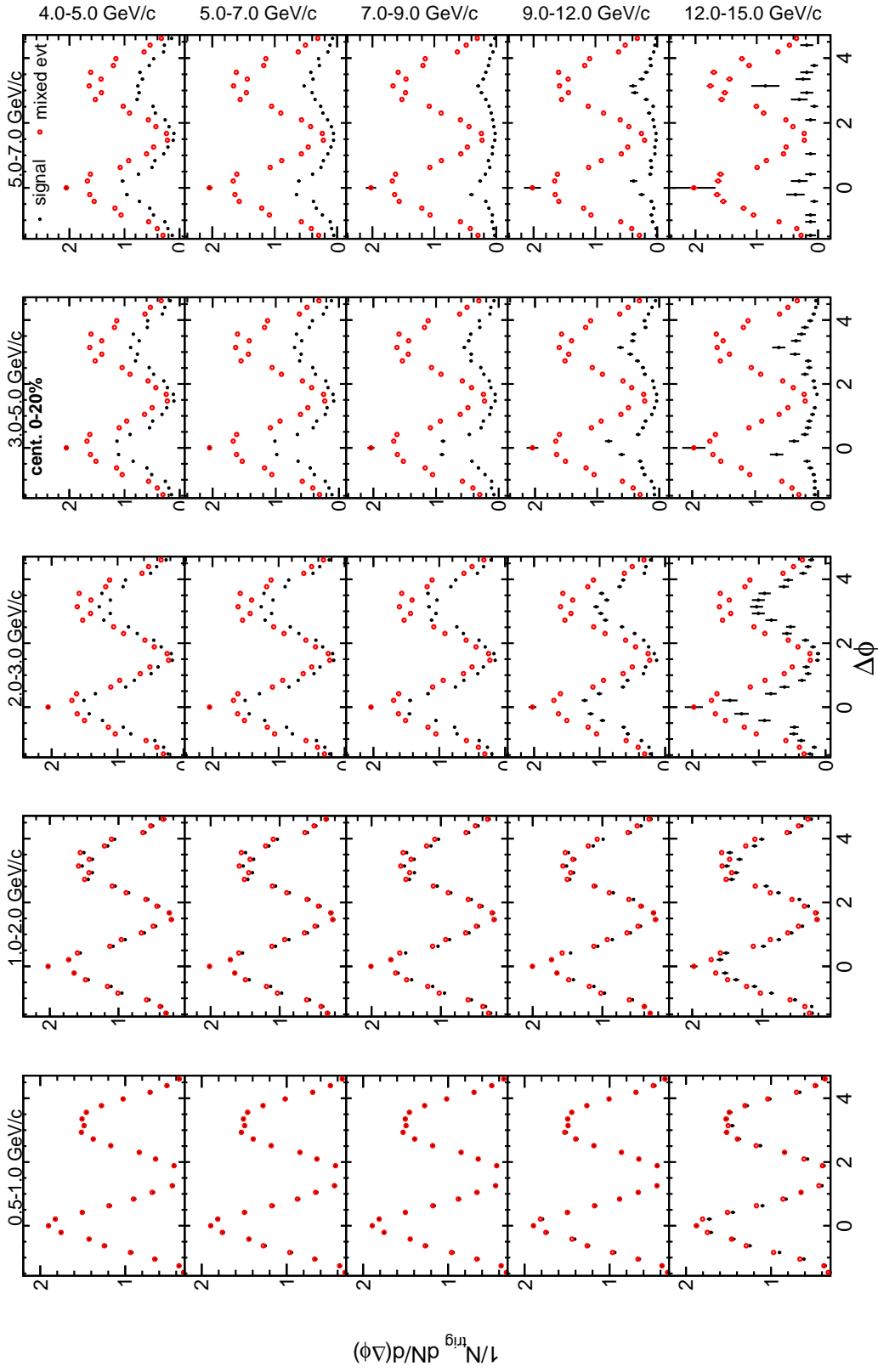


Figure 3.6: Azimuth correlations from the same-event (black dots) and mixed-event (red circles) in 0–20% centrality in Run 10 data.

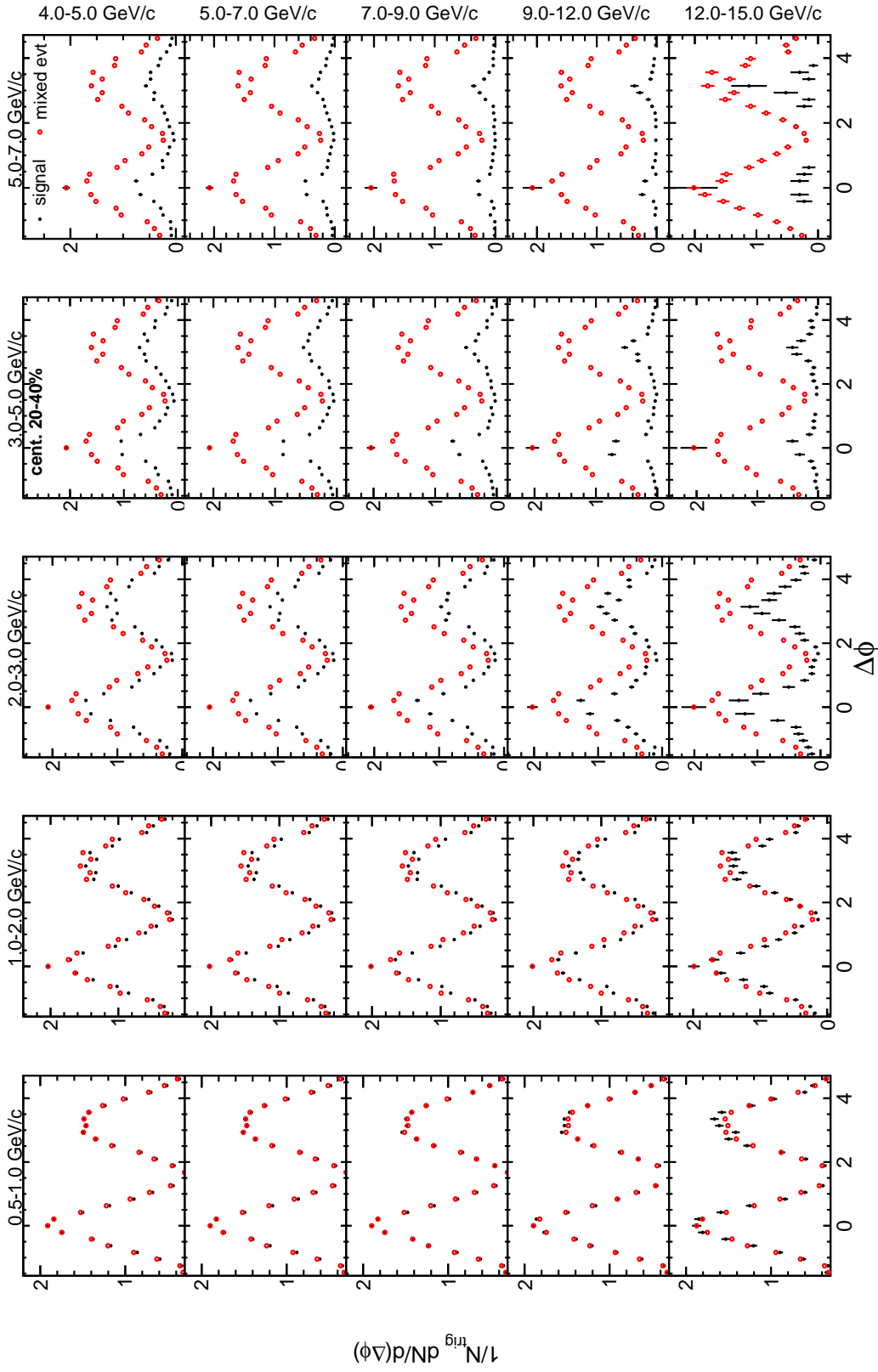


Figure 3.7: Azimuth correlations from the same-event (black dots) and mixed-event (red circles) in 2–40% centrality in Run 10 data.

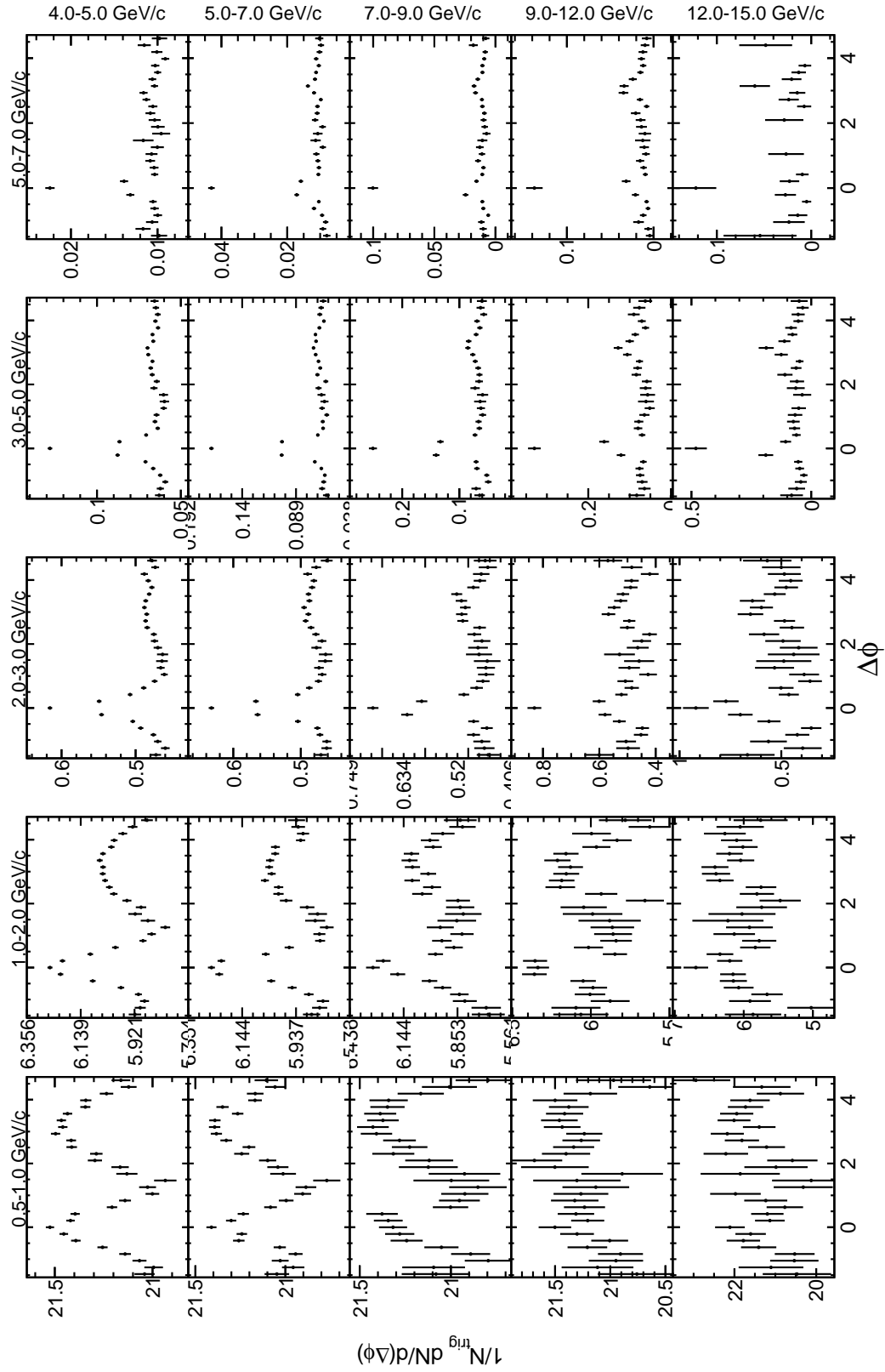


Figure 3.8: Correlation functions in Run 10 0–20% after hadron efficiency and detector acceptance corrections .

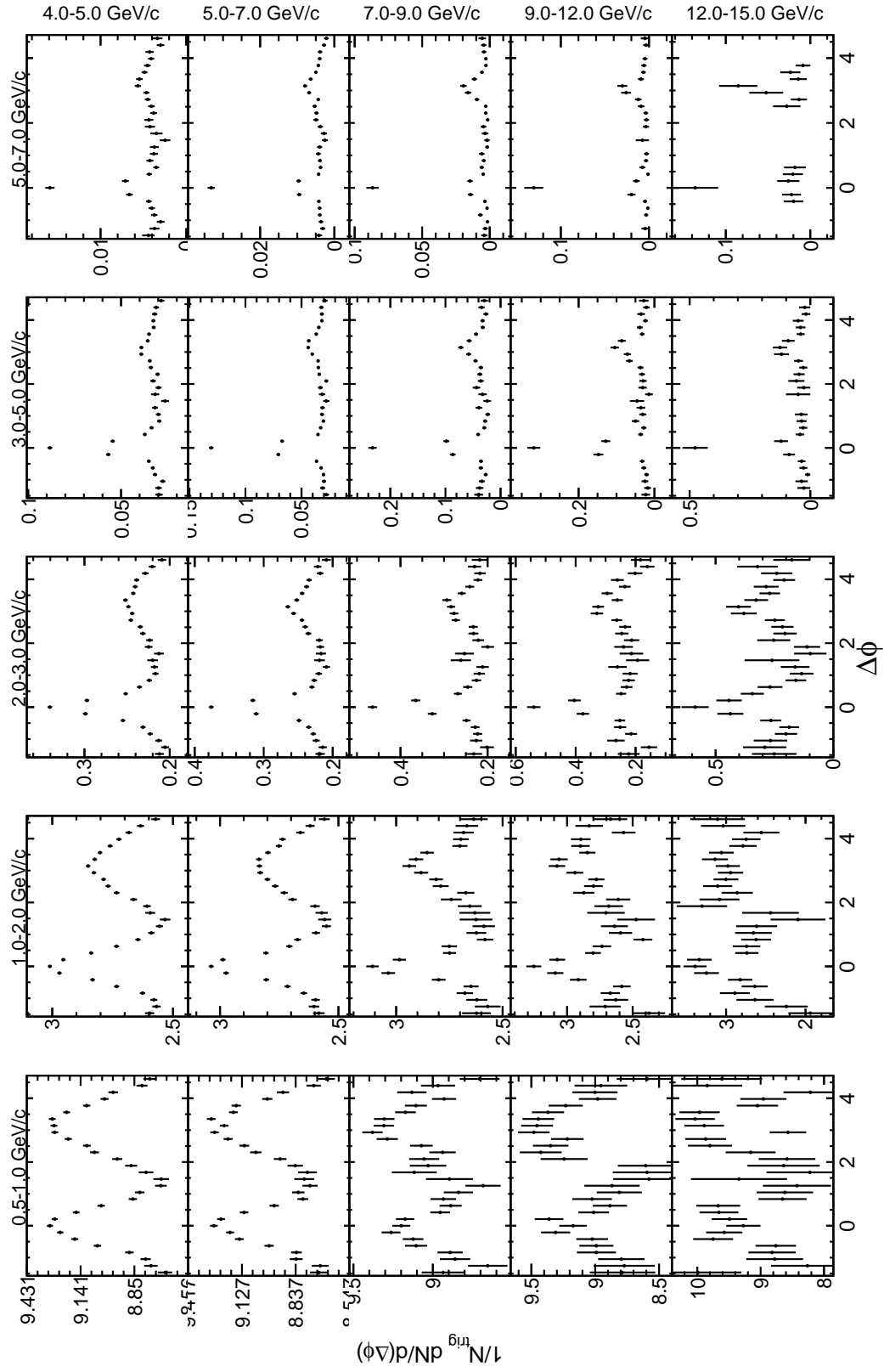


Figure 3.9: Correlation functions in Run 10 20–40% after hadron efficiency and detector acceptance corrections .

3.5 Background Flow subtraction

In $p + p$ collisions where no QGP is formed, the combinatorial pairs are expected to be distributed in $\Delta\phi$ space evenly. In $Au + Au$ collisions, however, the combinatorial distributions are convoluted with collective flow of the QGP. A common two-source model is used to describe the correlation function as a superposition of jet and flow

$$\overbrace{\frac{dN_{Corr}}{d\Delta\phi}}^{\text{correlation function}} = \overbrace{\frac{dN_{Jet}}{d\Delta\phi}}^{\text{jet function}} + \overbrace{\frac{dN_{Flow}}{d\Delta\phi}}^{\text{underlying flow}}, \quad (3.8)$$

where N_{Corr} , N_{jet} and N_{Flow} are the numbers of correlation pairs in the correlation function, jet function, and underlying flow as functions of the correlation angle $\Delta\phi$. The derivative with respect to $\Delta\phi$ accounts for $\Delta\phi$ bin width. Then, the jet function is simply the difference between the correlation function and the underlying flow

$$\overbrace{\frac{dN_{Jet}}{d\Delta\phi}}^{\text{jet function}} = \overbrace{\frac{dN_{Corr}}{d\Delta\phi}}^{\text{correlation function}} - \overbrace{\frac{dN_{Flow}}{d\Delta\phi}}^{\text{underlying flow}}. \quad (3.9)$$

As discussed in section 1.5.1, the flow can be expanded to a Fourier series

$$\frac{dN_{flow}}{d\Delta\phi} = b \left[1 + 2 \sum \langle v_n \rangle \cos(n \cdot \Delta\phi) \right], \quad (3.10)$$

where b is the level of the background flow which is estimated using Absolute Normalization method as described in later section 3.5.3. As demonstrated in several experimental observables [49, 72, 73], v_n in the p_T regions of interest is a product of $v_n^{\pi^0}$ and v_n^h which are the n^{th} order flow harmonic coefficients for π^0 and charged hadrons, respectively.

Since we assume the coefficient for the first order harmonic, v_1 , can be ignored and the coefficients for the higher order ($n \geq 5$) harmonics are negligible, this analysis subtracts flow harmonics from the second to the fourth order. Then, equation 3.10 can be rewritten as

$$\frac{dN_{flow}}{d\Delta\phi} = b \left[1 + 2 \sum_{n=2}^4 \langle v_n^{\pi^0} \rangle \langle v_n^h \rangle \cos n \cdot \Delta\phi \right]. \quad (3.11)$$

The second to fourth order harmonics are plotted in Figure 3.10 for visualization. This section details the process to obtain different order flow coefficients as well as the background level b .

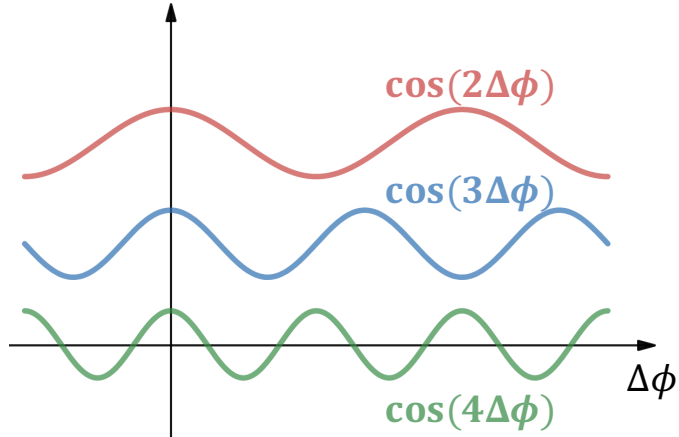


Figure 3.10: Different order of harmonic functions in arbitrary scale.

3.5.1 Coefficients of Flow Harmonics for Charged Hadron

The hadron v_2^h , v_3^h , and v_4^h values in 0.5–10 GeV/c are PHENIX results [21]. v_n^h values in reference [21] are obtained in 10% centrality bins. To match the centrality bins in this analysis, v_n^h values in ref [21] are merged from different centrality bins (0–10% and 10–20%, 20–30% and 30–40%). The v_n^h values are weighted by the number of hadrons in the corresponding centrality and hadron p_T bin. The merged v_2^h in 0–20% and 20–40% centrality classes are shown in Figure 3.11, as examples. Then, the v_n^h values, which correspond to the mean p_T values of the associate p_T bins that are used

in this analysis, are interpolated from a fit by the following function

$$v_n(p_T) = A \cdot e^{-(\frac{B-p_T}{C})^2} + (D - E \cdot e^{-F \cdot p_T}) . \quad (3.12)$$

Equation 3.12 is an arbitrary choice but captures the features of the v_n functions. The errors of the interpolated v_n^h values are the interpolated values of the upper and lower errors of the merged v_n^h values with the same fit functions. The interpolated v_n^h values are shown in Figure 3.12.

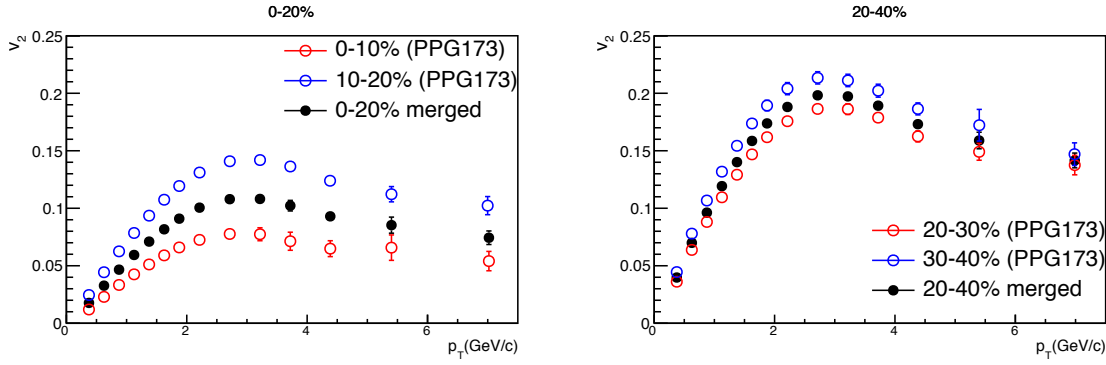


Figure 3.11: v_2^h values in different centrality classes. The open circles are from experimental results [21]. The black dots are the merged values from the open circles.

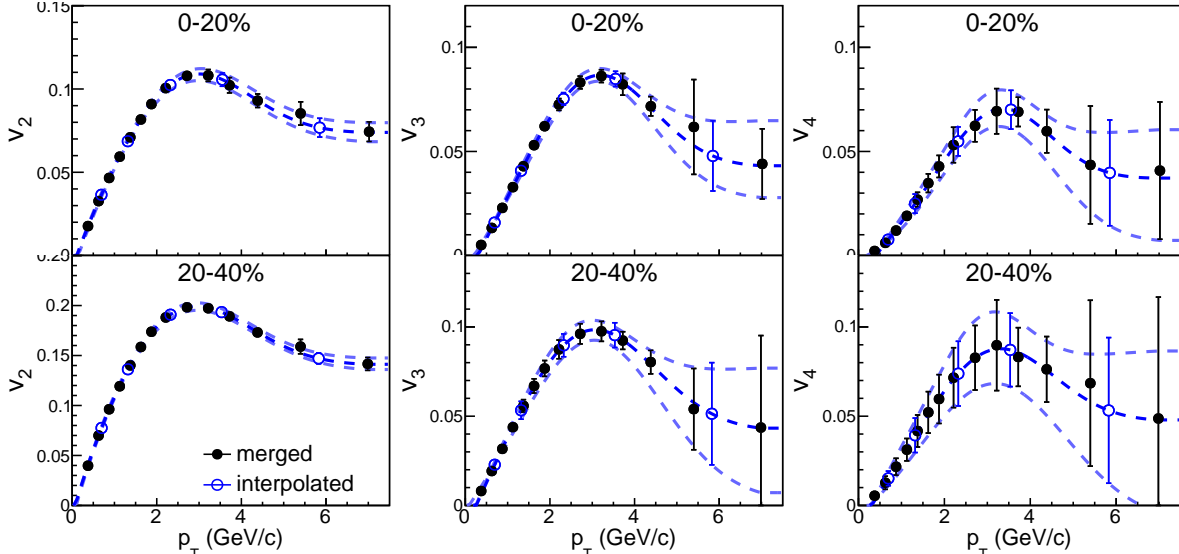


Figure 3.12: Merged (solid dots) and interpolated (open circles) v_n^h values. The blue dash lines are the fits of the nominal, upper and lower bounds values of the solid points.

3.5.2 Coefficients of Flow Harmonics for π^0 from Acoustic Scaling

Neutral pion $v_2^{\pi^0}$ values in 1–18 GeV/c are measured from previous PHENIX analysis [22], as shown in Figure 1.14. Similar to the charged hadron v_n^h values in reference [21], the $v_n^{\pi^0}$ values are obtained in 10% centrality bins. Therefore, the $v_n^{\pi^0}$ are also merged using the same procedure for merging v_n^h , and the results are shown in Figure 3.13.

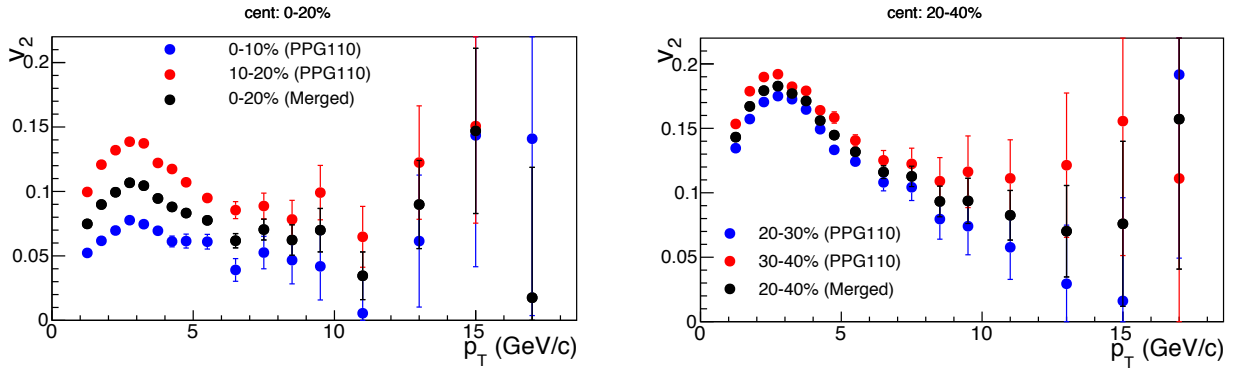


Figure 3.13: Merged $v_2^{\pi^0}$ values (black dots) in 0–20% (left) and 20–40% (right) centrality. The red and blue data points are results from reference [22] in 10% centrality bin width. The black points are the merged values of the red and blue points.

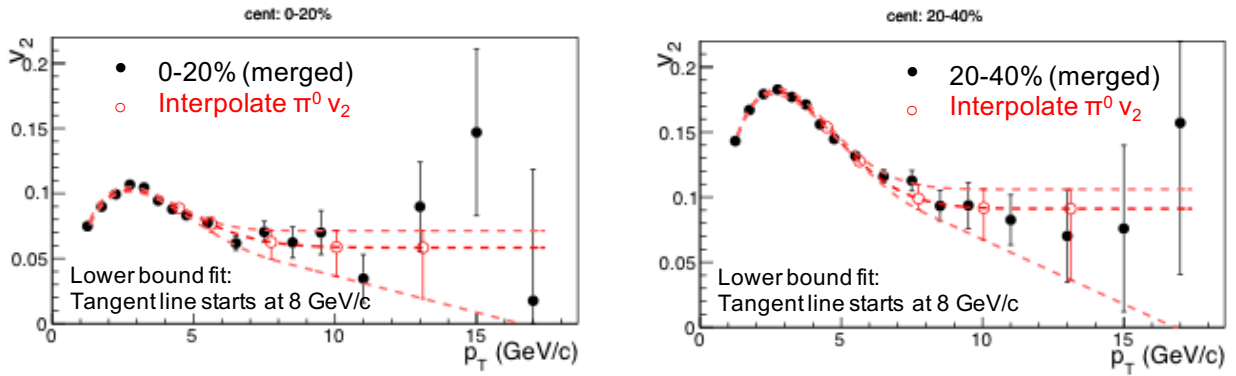


Figure 3.14: Merged (dots) and interpolated (circle) $v_2^{\pi^0}$ values in 0–20% and 20–40% centrality. The red dash lines are the fits of the nominal, upper and lower bounds values of the merged $v_2^{\pi^0}$.

To interpolate the $v_2^{\pi^0}$ values at a particular p_T , equation 3.12 is used to fit the merged $v_2^{\pi^0}$ values in 1–8 GeV/c. Since the coefficients are not expected to rise in high p_T (> 8 GeV/c) but potentially fall as p_T increases, the fits of the nominal and the upper bound in the high p_T region are set to be flat, while the lower bound is set as the tangent of the fits in the low p_T region. The interpolated $v_2^{\pi^0}$ values are shown in Figure 3.14.

Acoustic Scaling

While there are $v_2^{\pi^0}$ measurements available from PHENIX [22], higher order $v_n^{\pi^0}$ has not been measured at RHIC in the high momentum region. To estimate $v_3^{\pi^0}$ and $v_4^{\pi^0}$, Acoustic Scaling [74] is applied. Acoustic Scaling refers to the ratio of v_n ($n = 3, 4$) to $(v_2)^{n/2}$, that is,

$$g_n = \frac{v_n}{(v_2)^{n/2}}. \quad (3.13)$$

This ratio, denoted as g_n , is p_T independent up to 10 GeV/c as demonstrated with PHENIX data [74]. Thus, we can obtain charged hadron g_n^h with the existing PHENIX charged hadron v_n^h results

$$g_n^h = \frac{v_n^h}{(v_2^h)^{n/2}}, \quad (3.14)$$

and assume $g_n^h = g_n^{\pi^0}$. Applying equation (3.13) again to estimate neutral pion $v_3^{\pi^0}$ and $v_4^{\pi^0}$ gives

$$v_n^{\pi^0} = g_n^h (v_2^{\pi^0})^{n/2}. \quad (3.15)$$

Figure 3.15 shows g_n^h values that are calculated using equation (3.14) with v_n^h values from reference [21]. Since g_n^h is observed to be constant in 0–10 GeV/c, a flat line is fitted to extract the g_n^h values in different centrality bins. The uncertainties of g_n^h are from the fit errors. Then, $v_3^{\pi^0}$ and $v_4^{\pi^0}$ are estimated using equation 3.15 with the fitted g_n^h values from Figure 3.15 as input parameters.

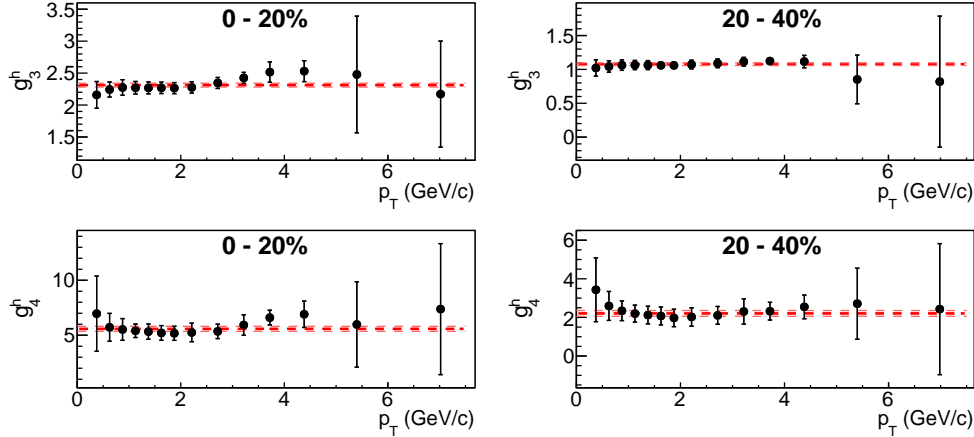


Figure 3.15: g_3 (top row) and g_4 (bottom row) calculated using charged hadron v_n in reference [21] in different centrality classes. The dash lines are the constant fits and their upper and lower bound values.

3.5.3 Flow Level Estimation: Absolute Normalization

Absolute Normalization, also known as Mean-Seeds Mean-Partners, uses the mixed-event correlations to estimate underlying flow amplitude which is denoted as b in equation 3.10. Absolute Normalization also includes a centrality correction, ξ , for the finite centrality binning effect in the event-mixing analysis. Then, b in equation 3.10 can be expressed as

$$b = \xi b_0 , \quad (3.16)$$

where b_0 is the per trigger yield found in mixed-event correlations

$$b_0 = \frac{\langle n^A n^B \rangle_{\text{mixed}}}{\langle n^A \rangle_{\text{mixed}}} , \quad (3.17)$$

and n^A and n^B are the number of trigger and associate particles, respectively.

ξ is defined as the ratio of the mean correlation pairs $\langle n^A n^B \rangle$ to the mean combinatorial pairs $\langle n^A \rangle \langle n^B \rangle$ as written in equation (3.18). Since $\langle n^A n^B \rangle$ and $\langle n^A \rangle \langle n^B \rangle$ depends on number

of collisions, N_{coll} , and number of participants, N_{part} , they can be estimated using the probability, w^{glaub} , of N_{coll} (N_{part}) contribution in a certainty centrality range calculated from Glauber Monte Carlo [12] as expressed in equation (3.19). The subscript i represents different N_{coll} (N_{part}) values in a centrality range, and w_i^{glaub} , n_i^A and n_i^B are the corresponding values.

$$\xi = \frac{\langle n^A n^B \rangle}{\langle n^A \rangle \langle n^B \rangle} \quad (3.18)$$

$$= \frac{\sum w_i^{glaub} n_i^A n_i^B}{\sum w_i^{glaub} n_i^A \times \sum w_i^{glaub} n_i^B}. \quad (3.19)$$

To find n_i^A and n_i^B , n^A and n^B as functions of N_{coll} (N_{part}) are fitted with Equations 3.20 and 3.21 in the N_{coll} (N_{part}) region which corresponds to the centrality classes (0–20% and 20–40%) as shown in Figure 3.16 and 3.17. Equation 3.20 and 3.21 are selected for their smoothness

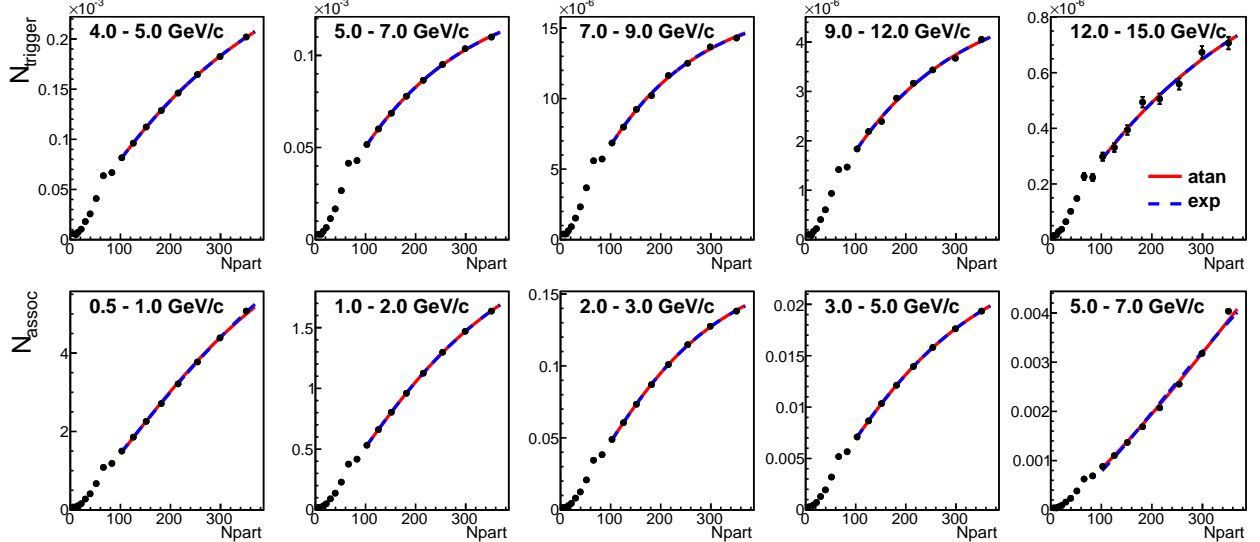


Figure 3.16: Number of trigger (top) and associate particles (bottom) as function of N_{part} from Run 10 data.

and well-controlled behavioral at large N_{coll} (N_{part}) [75]. Then, there is a total of four fits for determining the ξ values using equation 3.19. The final ξ values are the average of the calculations using these different fits and the deviation between these fits is used as uncertainty on ξ . The ξ

values for different runs are shown in Figure 3.18.

$$n^{A/B} = \gamma \tan^{-1}(\beta N_{part/coll}^\alpha) \quad (3.20)$$

$$n^{A/B} = \gamma(1 - e^{\beta N_{part/coll}^\alpha}) \quad (3.21)$$

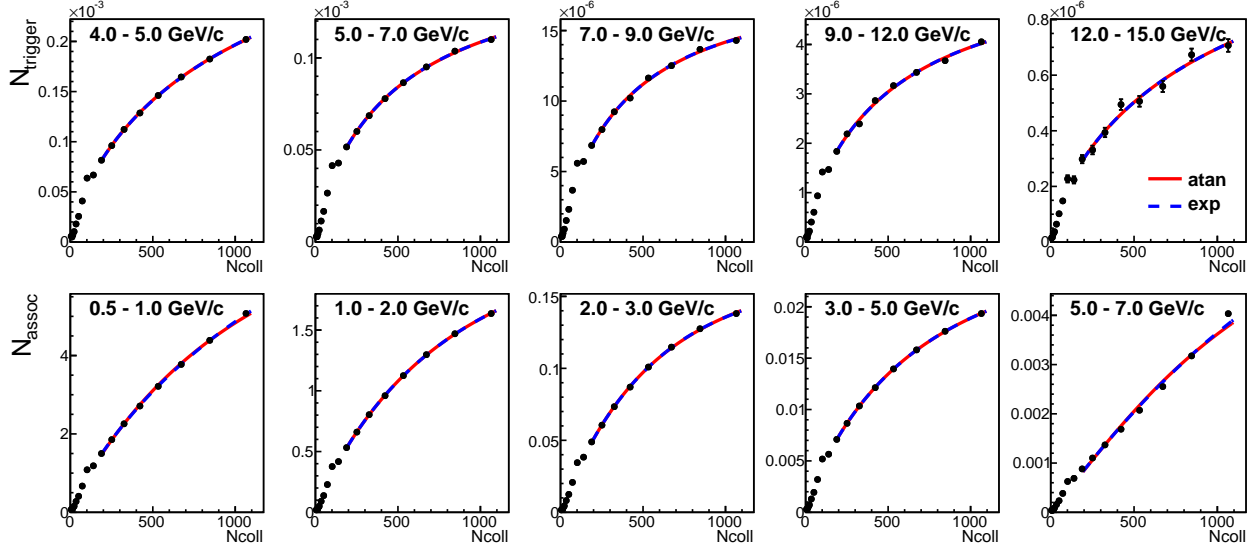


Figure 3.17: Number of trigger (top) and associate particles (bottom) as function of N_{coll} from Run 10 data.

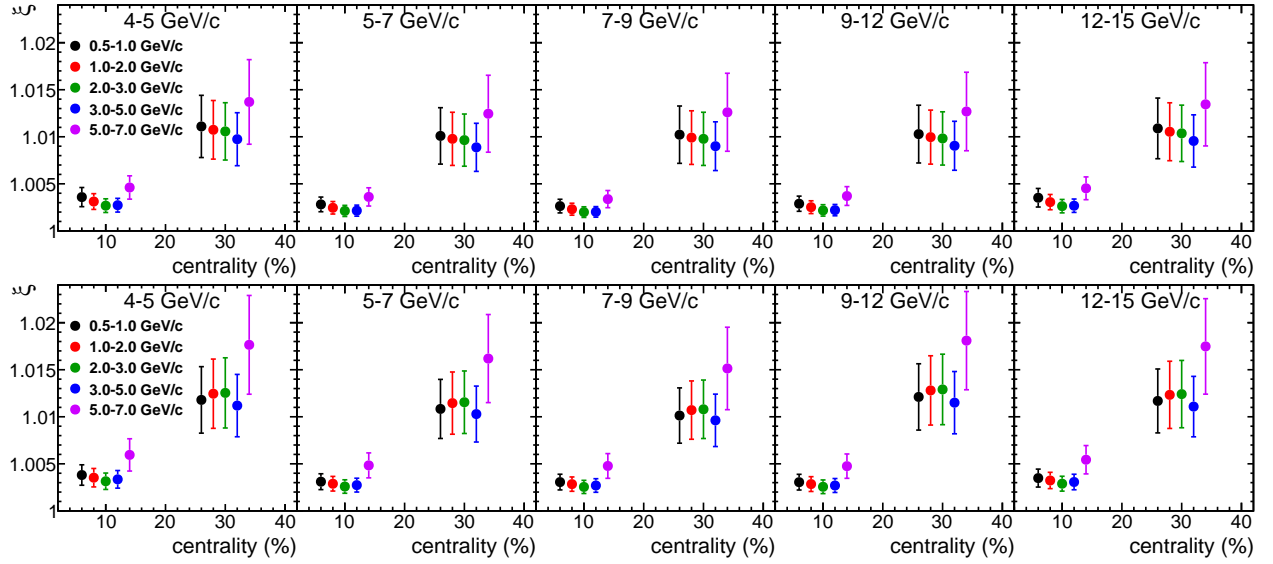


Figure 3.18: ξ as a function of centrality in different trigger and associate p_T ranges from Run 10 (top) and Run 11 (bottom) data.

3.6 Extracting Physics Quantities

The jet functions are obtained from the correlation function after removing underlying flow harmonics. The jet functions are used to extract different jet observables such as angular widths and yields. This section describes the extraction and calculation of these observables.

Jet Width

Jet widths in this analysis refer to the Gaussian widths of the near and away-side peaks in the jet functions. The widths are obtained from Gaussian fits

$$\frac{1}{N_{trig}} \frac{dN_{jet}}{d\Delta\phi} = \underbrace{A_{Near} e^{-(\frac{\Delta\phi-0}{2\sigma_{Near}})^2} + A_{Away} e^{-(\frac{\Delta\phi-\pi}{2\sigma_{Away}})^2}}_{\text{near-side peak}} + \underbrace{A_{Near} e^{-(\frac{\Delta\phi-2\pi}{2\sigma_{Near}})^2} + A_{Away} e^{-(\frac{\Delta\phi+\pi}{2\sigma_{Away}})^2}}_{\text{away-side peak}} + \underbrace{A_{Near} e^{-(\frac{\Delta\phi-2\pi}{2\sigma_{Near}})^2} + A_{Away} e^{-(\frac{\Delta\phi+\pi}{2\sigma_{Away}})^2}}_{\text{mirror functions}}, \quad (3.22)$$

where A_{Near} and A_{Away} and the amplitudes of the near and away-side peaks, and σ_{Near} and σ_{Away} are the widths of the near and away-side jets.

Since the jets are emitted in a cone shape, the far ends on both sides ($\Delta\phi = -\pi/2$ and $\Delta\phi = 3\pi/2$) of the jet functions should have the same yield. Therefore, two Gaussian functions are added in Equation (3.22) as mirror functions. The mirror functions share the same amplitudes and widths as the near and away-side peaks, but peak at $-\pi$ and 2π . This means that the influence of the away (near)-side is the same on both left and right of the near (away)-side peak.

Integrated Per Trigger Yields Modification $I_{AA}(p_T)$

The common definition of I_{AA} is the ratio of the integrated per trigger yields in $Au + Au$ to $p + p$

$$I_{AA} = \frac{Y_{AA}}{Y_{pp}} . \quad (3.23)$$

where Y_{AA} and Y_{pp} are the integrated per trigger yields from the jet functions measured in $Au + Au$ and $p + p$ collisions, respectively. They are defined as

$$Y = \frac{1}{N_{trig}} \int_{\Delta\phi^-}^{\Delta\phi^+} \frac{dN_{jet}}{d\Delta\phi} d\Delta\phi , \quad (3.24)$$

where $\Delta\phi^\pm$ are the integration ranges which are $[0 - \frac{\pi}{3}, 0 + \frac{\pi}{3}]$ and $[\pi - \frac{\pi}{2}, \pi + \frac{\pi}{2}]$ for the near and away-side peaks, respectively.

Per Trigger Yields Modification $I_{AA}(\Delta\phi)$

In this study, a point-by-point per trigger yield ratio is also calculated to obtain I_{AA} as a function of the correlation angle $\Delta\phi$. $I_{AA}(\Delta\phi)$, which is simply the quotient of the $Au + Au$ jet function divided by the $p + p$ jet function, describes the jet modification at jet substructure level.

Double Ratio R_I

R_I is the modification ratio of the away-side to the near-side jet functions. The definition of R_I is

$$R_I = \frac{I_{AA}^{Away}}{I_{AA}^{Near}} . \quad (3.25)$$

Although R_I in 200 GeV $Au + Au$ is not covered in this thesis, it is a useful observable in small system studies because the modification I_{AA} is small in $Au + Au$ collisions. More discussions of R_I measurements in small systems are shown in section 6.2.

CHAPTER 4

Systematic Uncertainty

There are five sources of systematic uncertainty accounted for in this analysis. They are the uncertainty associated with the coefficients of flow harmonics, the ξ uncertainty in the background level estimation using Absolute Normalization method, combinatorial background in π^0 reconstruction, hadron efficiency uncertainty, and the uncertainties associated with the $p + p$ baseline measurements. Since the systematic uncertainties (σ^{pp}), from $p + p$ results is obtained in [49], this chapter will discuss the other four sources of systematic uncertainty.

4.1 Flow Harmonics

Considering the differences in the shape of each order of flow harmonics, the systematic uncertainties from flow are separated by order. Since we used Acoustic Scaling to estimate the $\pi^0 v_3$ and v_4 values, the subtracted flow harmonics can be written as

$$\begin{aligned} \text{Flow}(\Delta\phi) &= 1 + 2[v_2^{\pi^0} v_2^h \cos(2\Delta\phi) + v_3^{\pi^0} v_3^h \cos(3\Delta\phi) + v_4^{\pi^0} v_4^h \cos(4\Delta\phi)] \\ &= 1 + 2[v_2^{\pi^0} v_2^h \cos(2\Delta\phi) + g_3(v_2^{\pi^0})^{3/2} v_3^h \cos(3\Delta\phi) + g_4(v_2^{\pi^0})^{4/2} v_4^h \cos(4\Delta\phi)] . \end{aligned} \quad (4.1)$$

To find the systematic uncertainty, σ^{f2} , arising from the second order flow harmonic, $v_2^{\pi^0}$ and v_2^h are set to their upper (lower) bound values in the $\cos(2\Delta\phi)$ term in Equation (4.1) only. For the systematic uncertainty, σ^{f3} , arising from the third order flow harmonic, g_3 , $v_2^{\pi^0}$ and v_3^h are set to their upper (lower) bound values in the $\cos(3\Delta\phi)$ term in Equation (4.1) only. Then set g_4 , $v_2^{\pi^0}$ and v_4^h to their upper (lower) bound values in the $\cos(4\Delta\phi)$ term in Equation (4.1) alone to find the systematic uncertainty, σ^{f4} , arising from the fourth order flow harmonic.

4.2 Absolute Normalization

The systematic uncertainty, σ^ξ , associated with the Absolute Normalization method, comes from the uncertainty on ξ . The uncertainty on ξ is defined as the deviation of the fits on the number of trigger (or associate) as written in Equations (3.20) and (3.21) in Section 3.5.3. Although ξ is close to 1, the jet function is very sensitive to ξ values especially in the low p_T regions where the background is large.

4.3 Hadron Efficiency

There are six sources of uncertainty in the hadron efficiency. They are: (1) the momentum resolution of the central arm detectors, (2) the PC3 matching recalibration uncertainty in simulation, (3) the differences between Monte Carlo simulation and real data, (4) the embedding efficiency in the occupancy study, (5) the particle ratios from the charged hadron p_T spectra measured at PHENIX [76] and (6) the statistical uncertainty in the simulation. The total uncertainty of the hadron efficiency is a quadrature sum of these uncertainties. The systematic uncertainty, σ^H , from hadron efficiency is presented as a global scale uncertainty shown at the far end of a figure separated from systematic uncertainties raised by other sources.

The uncertainties of hadron efficiency for $Au + Au$ collisions in Run 10 and Run 11 are 10% and 15%, respectively. The average for both Runs weighted by statistics is about 12%. However, some of these uncertainties, such as momentum resolution and PC3 matching cut in the simulation, are canceled out in I_{AA} analysis, as the associated uncertainties are correlated between the hadron efficiency studies for $Au + Au$ and $p + p$ collisions. Further discussion will be covered as Section 4.5.

4.4 Combinatorial Background in π^0 Reconstruction

After applying all kinematic cuts in the photon pair selection, all reconstructed π^0 candidates that fall under the π^0 mass peak, that is, within 0.12–0.16 GeV/ c^2 mass window, are used to construct the correlation functions. However, the π^0 mass peak is contaminated by combinatorial photon pairs which are labeled as background in Figure 4.1. These combinatorial photon pairs affect the features in both amplitudes and shapes of the jet functions. Although it is impossible to distinguish combinatorial background from the mass peak, the effect from the combinatorial background can be estimated using combinatorial photon pairs in the side-band regions with the assumption that the combinatorial pairs within the mass peak and side-band regions give the same features in jet functions.

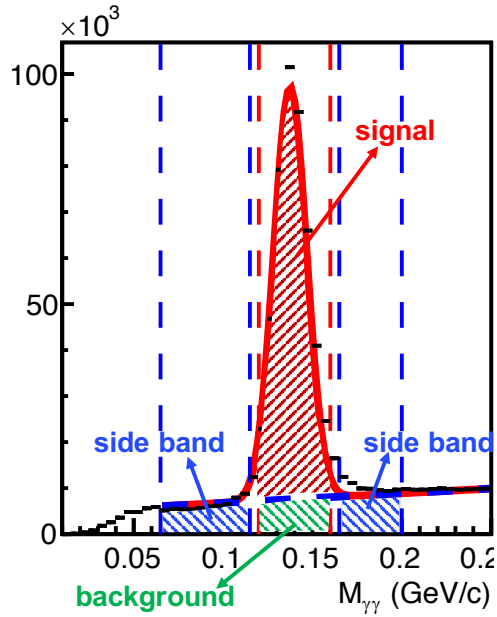


Figure 4.1: Example of invariant mass spectrum. The blue dash line at the bottom is the fit for combinatorial background. The red solid line is the fit of the combinatorial background and the signal. The vertical dash lines indicate the signal π^0 mass window (red), and side-band mass windows (blue).

The relative systematic uncertainty from the combinatorial photon pair is defined as

$$\frac{\sigma_Y^{\pi^0}}{Y_{peak}} = \frac{Y_{true} - Y_{peak}}{Y_{peak}} \quad (4.2)$$

where σ_{π^0} is the absolute uncertainty of the per trigger yield. Y_{peak} is the per trigger yields of the measured jets that use reconstructed π^0 within 0.12–0.16 GeV/c², and Y_{true} is the per trigger yields of the jets that are constructed by true π^0 found in the same mass window as indicated in the red area in Figure 4.1. Then, the total yields of jets from reconstructed π^0 found in π^0 mass peak can be written as

$$\begin{aligned} N_{FG}Y_{peak} &= N_{signal}Y_{signal} + N_{BG}Y_{BG} \\ N_{signal}Y_{signal} &= N_{FG}Y_{peak} - N_{BG}Y_{BG} \\ Y_{signal} &= \frac{N_{FG}}{N_{signal}}Y_{FG} - \frac{N_{BG}}{N_{signal}}Y_{BG} \end{aligned} \quad (4.3)$$

where N_{peak} , N_{true} , and N_{BG} are the number of reconstructed π^0 found in the peak region, number of true π^0 and number of combinatorial photon pairs, respectively. Y_{BG} is the per trigger yield of jets that use trigger constructed by combinatorial photon pairs found in the π^0 mass peak. Since the combinatorial photon pairs in the side-band regions are used to estimate the effect from combinatorial photon pairs within the peak region, Y_{BG} is replaced with Y_{side} . Then eq. (4.3) becomes

$$Y_{true} = \frac{N_{peak}}{N_{true}}Y_{peak} - \frac{N_{BG}}{N_{true}}Y_{side} . \quad (4.4)$$

Substitute eq. (4.4) in eq. (4.2), we have

$$\begin{aligned}\frac{\sigma_Y^{\pi^0}}{Y_{peak}} &= \frac{\frac{N_{peak}}{N_{true}} Y_{peak} - \frac{N_{BG}}{N_{true}} Y_{side} - Y_{peak}}{Y_{peak}} \\ &= \frac{\left(\frac{N_{peak}}{N_{true}} - 1\right) Y_{peak} - \frac{N_{BG}}{N_{true}} Y_{side}}{Y_{peak}} \\ &= \frac{\frac{N_{peak} - N_{true}}{N_{true}} Y_{peak} - \frac{N_{BG}}{N_{true}} Y_{side}}{Y_{peak}}.\end{aligned}$$

Since $N_{peak} = N_{true} + N_{BG}$,

$$\begin{aligned}\frac{\sigma_Y^{\pi^0}}{Y_{peak}} &= \frac{\frac{N_{BG}}{N_{true}} Y_{peak} - \frac{N_{BG}}{N_{true}} Y_{side}}{Y_{peak}} \\ &= \frac{N_{BG}}{N_{true}} \cdot \frac{Y_{peak} - Y_{side}}{Y_{peak}} \\ &= \frac{1}{N_{true}/N_{BG}} \cdot \left(1 - \frac{Y_{side}}{Y_{peak}}\right) \\ &= \frac{1}{S/B} \cdot \left(1 - \frac{Y_{side}}{Y_{peak}}\right)\end{aligned}\tag{4.5}$$

where S/B is a simplified notation for N_{true}/N_{BG} which is the signal-to-background ratio of the π^0 mass peak. Equation (4.5) defines relative uncertainty, $\sigma_Y^{\pi^0}/Y_{peak}$, as the difference of per trigger yields of jet functions obtained from side-band and the π^0 mass peak regions, scaled down by the signal-to-background ratio found in the π^0 mass peak. If per trigger yields of jet functions obtained from different mass windows are similar ($Y_{side} \approx Y_{peak}$) or the true π^0 dominates in the π^0 mass peak ($S/B \gg 1$), the relative uncertainty become small $\sigma_Y^{\pi^0}/Y_{peak} \approx 0$.

To find the signal to background ratio, the invariant mass spectrum is fitted by a sum of

Gaussian and linear equations as shown in Figure 4.2

$$\frac{dN_{peak}(m_{\gamma\gamma})}{dm_{\gamma\gamma}} = \overbrace{Ae^{-(\frac{m_{\gamma\gamma}-0.135}{2\sigma_m})^2}}^{\text{true } \pi^0 \text{ count}} + \overbrace{(Bm_{\gamma\gamma} + C)}^{\text{background count}}, \quad (4.6)$$

where A , B , C , and σ_m are the fitting parameters. Then, N_{BG} is estimated by integrating the linear fit from 0.12 to 0.16 GeV

$$N_{BG} = \int_{0.12}^{0.16} (Bm_{\gamma\gamma} + C) d(m_{\gamma\gamma}), \quad (4.7)$$

and N_{true} is the difference between the integral of the mass spectrum (data) in 0.12–0.16 GeV mass window and N_{BG}

$$N_{true} = \overbrace{\int_{0.12}^{0.16} \frac{dN_{peak}(m_{\gamma\gamma})}{dm_{\gamma\gamma}} d(m_{\gamma\gamma})}^{\text{data}} - \overbrace{N_{BG}}^{\text{background fit}}. \quad (4.8)$$

The π^0 signal-to-background ratio is plotted as a function of trigger $\pi^0 p_T$ in Figure 4.3. Figure 4.3 shows that the signal-to-background ratio of π^0 increases with trigger $\pi^0 p_T$, which indicates that the purity of reconstructed π^0 enhances in the high momentum region.

To obtain the side-band per trigger yield (Y_{side}), the reconstructed π^0 are picked from 0.165–0.2 GeV (upper side band) and 0.08–0.11 GeV (lower side band) in data selection. Then, the same procedures are followed as for the same procedures of jet functions and per trigger yields as explained in chapter 3. The per trigger yields obtained from side-band and π^0 mass peak regions, and their ratios are shown in Figure 4.4 and 4.5. These two figures show that the per trigger yields

from the side-band deviate more from the π^0 mass peak in the central events. This observation echoes to the centrality dependency in the signal-to-background ratio shown in Figure 4.3.

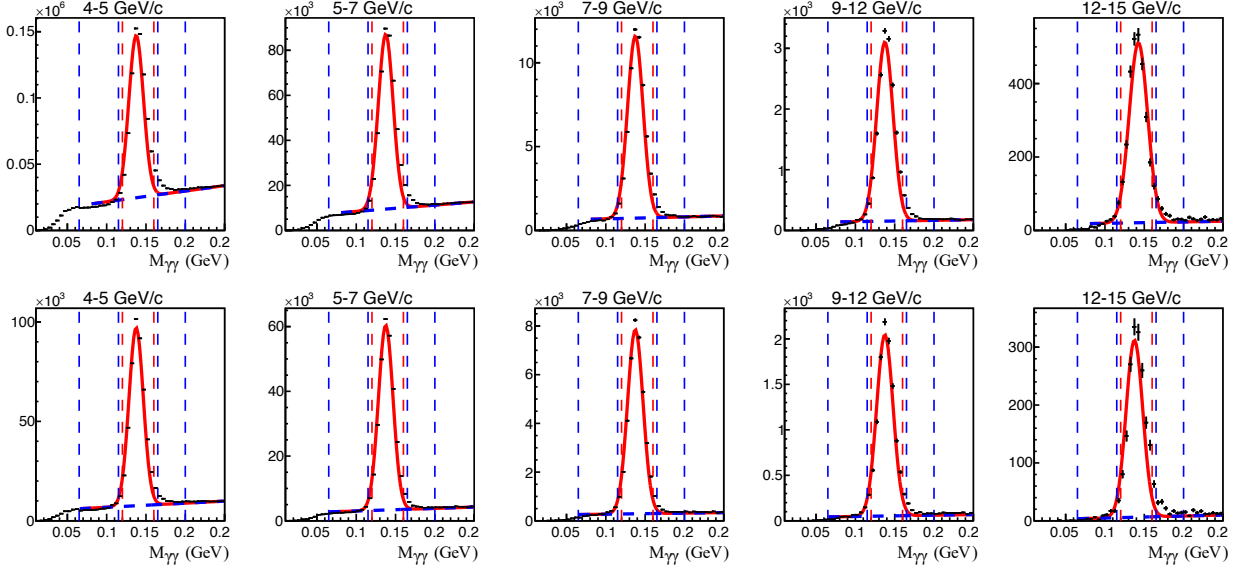


Figure 4.2: Photon pair invariant mass spectra with fits in different trigger π^0 p_T bins. Mass spectra in 0–20% (top) and 20–40% (bottom) events are separated to the top and bottom rows, respectively.

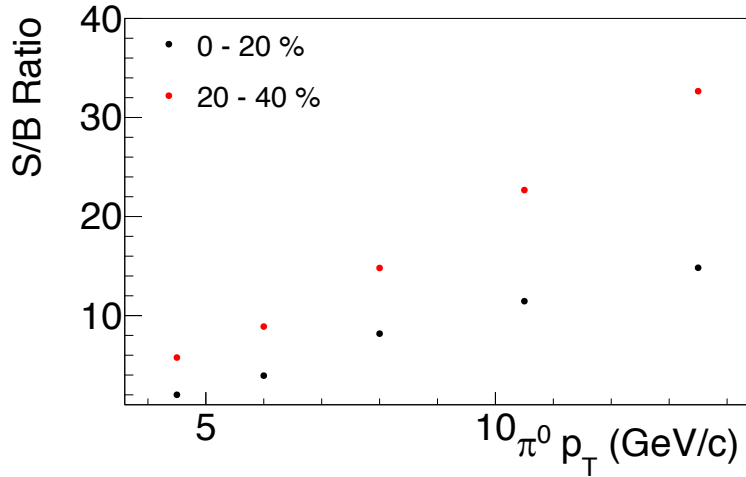


Figure 4.3: Signal-to-background ratio of reconstructed π^0 .

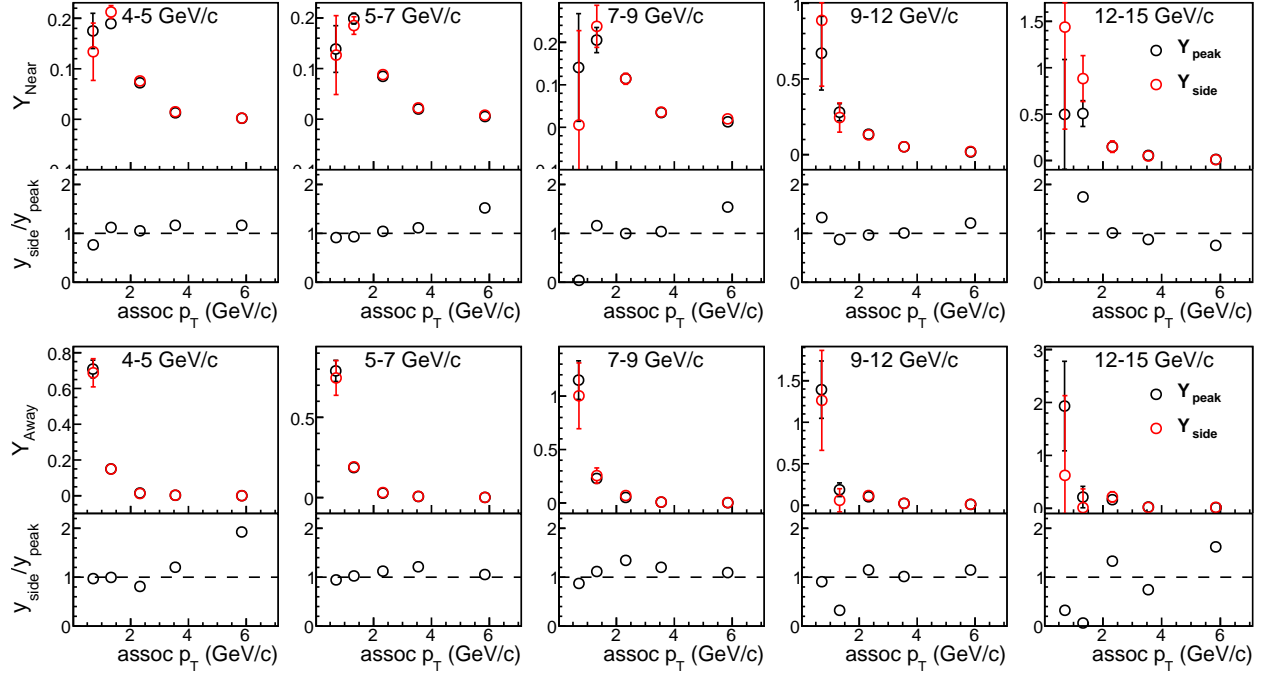


Figure 4.4: Near (top) and away-side (bottom) per trigger yields as a function of associate p_T in different trigger p_T bins in 0–20% centrality. Per trigger yields obtained from side-band and π^0 mass peak regions are drawn in red and black, respectively. The ratios of per trigger yields from different mass windows are drawn at the bottom of each panel.

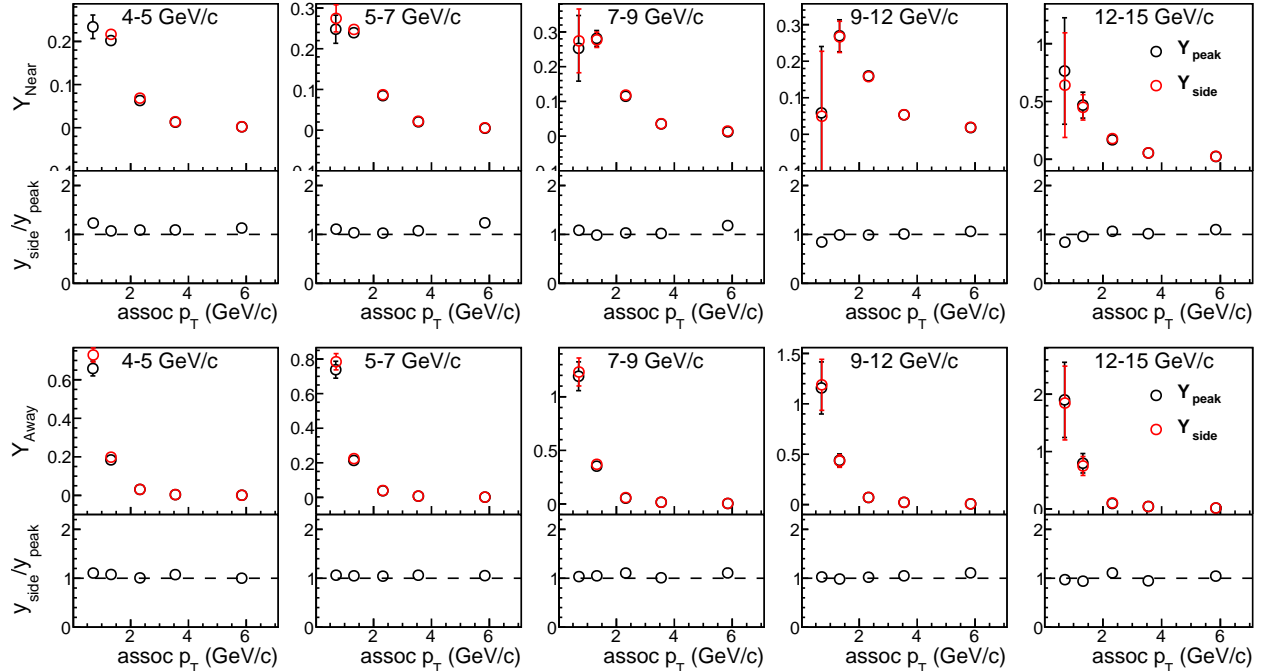


Figure 4.5: Near (top) and away-side (bottom) per trigger yields as a function of associate p_T in different trigger p_T bins in 20–40% centrality. See Figure 4.4 for description.

The relative systematic uncertainty, $\sigma_Y^{\pi^0}/Y_{peak}$, arising from the combinatorial background π^0 is plotted as a function of associate p_T in Figure 4.6. Since the signal-to-background ratio is higher in the 20–40% centrality events and the per trigger yield ratios of side-band to π^0 mass peak are close to 1, the relative systematic uncertainty in the 20–40% centrality events is also smaller.

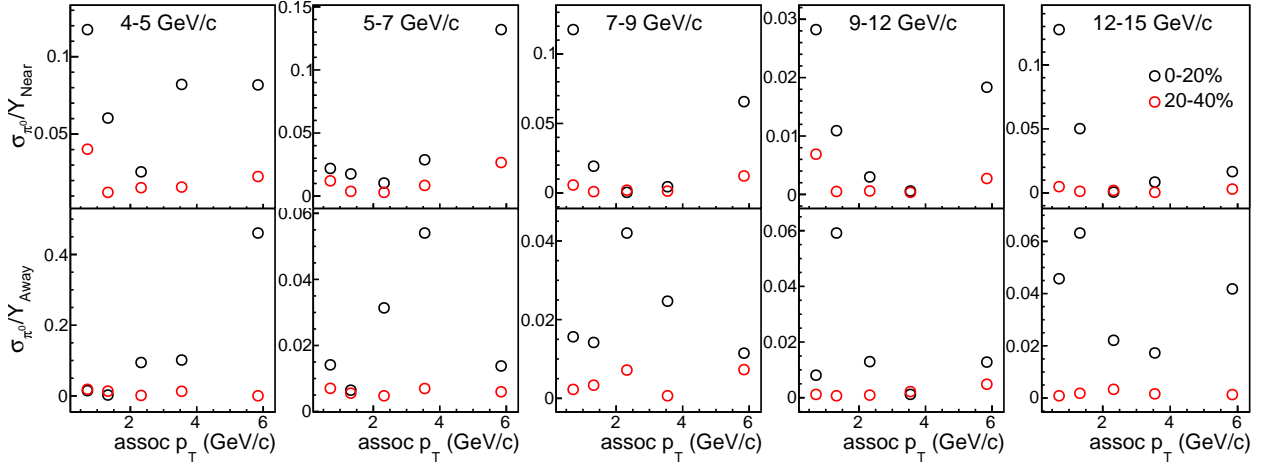


Figure 4.6: Relative background π^0 systematic uncertainty as a function of associate p_T in near (top) and away-side (bottom) peaks. The trigger p_T is labeled on the top of each panel.

4.5 Uncertainty Propagation

While absolute uncertainties arising from the flow harmonics and Absolute Normalization in different physics quantities are obtained by repeating the same analysis procedures by varying flow harmonics coefficients and ξ between their upper and lower bounds, the absolute uncertainties arising from the combinatorial background in the π^0 reconstruction and $p + p$ measurements are implemented analytically.

The total absolute systematic uncertainty is a quadrature sum of the absolute errors from

each source

$$\sigma^{total} = \sqrt{\sum(\sigma^i)^2}, \quad (4.9)$$

where σ^i is the systematic uncertainty from the i^{th} source. The sources of uncertainty for each physics quantity are listed in Table 4.1. In Table 4.1, the uncertainties ingredients are categorized into three types. Type A refers to an uncorrelated uncertainty for which each data point can move independently within its uncertainty range. Statistical error bars are considered Type A. Type B refers to uncertainty which is correlated (or anti-correlated) such that if one data point moves all data points would shift accordingly. Type C, which is known as global scaled uncertainty, is a percent error applied on all data points.

Table 4.1: Sources of Systematic Uncertainty

Quantity	Uncertainty						
	σ^{f2}	σ^{f3}	σ^{f4}	σ^ξ	σ^{π^0}	σ^{pp}	σ^H
Jet Function	B	B	B	B	B		C
Jet width	B	B	B	B			
Per trigger yields	B	B	B	B	B		C
Away-side $I_{AA}(p_T)$		B		B	B	B	C
Away-side $I_{AA}(\Delta\phi)$	B	B	B	B	C	B	C

B: Correlated systematic uncertainty

C: global scale uncertainty

Hadron Efficiency Uncertainty

The uncertainty from hadron efficiency, σ^H , is presented separately as a global scale uncertainty on the far end of the figures. As mentioned earlier, the systematic error from the hadron efficiency correction is smaller in the I_{AA} study than in the jet function analysis as some of the errors are correlated in $Au + Au$ and $p + p$ collisions. Therefore, only the uncorrelated errors remain in the global scale uncertainty in the I_{AA} measurement. The uncorrelated errors and their values are obtained

from a previous PHENIX analysis [49] and shown in Table 4.2. Note that these uncorrelated errors are not expected to change significantly between different data sets as the particle ratios shown in the PHENIX results [76] do not change for the same collision system, the statistical errors can be well controlled in the simulation, and the embedding efficiency is a conservative estimation based on statistics and the uncertainty arising from the PC3 matching criterion.

Table 4.2: Uncorrelated errors in hadron efficiency study

source	error
embedding efficiency	5%
particle ratios	3%
statistical errors	1%

Combinatorial Background Uncertainty from π^0 Reconstruction

The combinatorial background uncertainty from the π^0 reconstruction is applied on all per trigger yield related quantities including the jet functions and I_{AA} . Since the jet function amplitude and I_{AA} are proportional to the per trigger yield, the relative errors from the combinatorial background in the jet functions and I_{AA} equals the relative uncertainty in per trigger yield

$$\begin{aligned} \frac{\sigma_{jet}^{\pi^0}}{\text{jet}} &= \frac{\sigma_Y^{\pi^0}}{Y} \\ \sigma_{jet}^{\pi^0} &= \frac{\sigma_Y^{\pi^0}}{Y} \cdot \text{jet} \end{aligned} \quad (4.10)$$

and similarly,

$$\sigma_I^{\pi^0} = \frac{\sigma_Y^{\pi^0}}{Y} \cdot I_{AA} . \quad (4.11)$$

$p + p$ Uncertainty

Consider the per trigger yields, Y_{pp} , in $p + p$ measurement, with error $\sigma_Y^{pp\pm}$. The upper bound values of Y_{pp} , $Y_{pp} + \sigma_Y^{pp+}$, contributes to the lower bound values of I_{AA} , that is $I_{AA} - \sigma_I^{pp-}$

$$\begin{aligned}
 I_{AA} - \sigma_I^{pp-} &= \frac{Y_{AA}}{Y_{pp} + \sigma_Y^{pp+}} \\
 \sigma_I^{pp-} &= I_{AA} - \frac{Y_{AA}}{Y_{pp} + \sigma_Y^{pp+}} \\
 &= I_{AA} - \frac{Y_{AA}}{Y_{pp}} \cdot \frac{Y_{pp}}{Y_{pp} + \sigma_Y^{pp+}} \\
 &= I_{AA} \left[1 - \frac{Y_{pp}}{Y_{pp} + \sigma_Y^{pp+}} \right] \\
 &= I_{AA} \cdot \frac{Y_{pp} + \sigma_Y^{pp+} - Y_{pp}}{Y_{pp} + \sigma_Y^{pp+}} \\
 &= I_{AA} \cdot \frac{\sigma_Y^{pp+}}{Y_{pp} + \sigma_Y^{pp+}} .
 \end{aligned}$$

Using the same analytical procedure, the absolute uncertainty of I_{AA} from $p + p$ can be concluded in one formula

$$\sigma_I^{pp\pm} = I_{AA} \cdot \frac{\sigma_Y^{pp\mp}}{Y_{pp} \mp \sigma_Y^{pp\mp}} \quad (4.12)$$

4.6 Summary of Systematic Uncertainty

The following plots are break down of the systematic uncertainties associated with each quantity.

Jet Functions

The systematic uncertainties associated with the jet functions from different sources are shown separately in Figure 4.7 to 4.16. The Absolute Normalization method is the major contributor to the systematic uncertainty in the low p_T regions where underlying event is dominant. The combinatorial background π^0 has a larger influence in central events especially in the near-side where the trigger π^0 locate at.

Jet Widths

Figure 4.17 to Figure 4.20 are the systematic uncertainty contributions in the jet widths. Second order flow and ξ are the dominant factors in the systematic uncertainty in most p_T bins. However, the size of systematic uncertainty from different sources are comparable in the away-side jet width at the mid associate p_T (1–5 GeV/c) in 0–20% events.

Yields

Figure 4.21 to Figure 4.24 are the systematic uncertainty contributions in the per trigger yields. ξ uncertainty dominates in the low assoc p_T region. It is noteworthy that the even order flow has zero contribution in the away-side systematic uncertainty as the integrated yields of even order flow within $\pi/2$ to $3\pi/2$ are zero

$$\int_{\pi/2}^{3\pi/2} \cos(2n \cdot \phi) d\phi = \frac{1}{2n} \left[\sin(2n \cdot \frac{3\pi}{2}) - \sin(2n \cdot \frac{\pi}{2}) \right] = 0 \quad (4.13)$$

Hence, the changes of the second and fourth order flow harmonic coefficients do not affect the away side yield.

I_{AA}

Figure 4.25 to Figure 4.26 are the systematic uncertainty contributions in the $I_{AA}(p_T)$. In the low associate p_T region where underlying events are large, the systematic uncertainty of $I_{AA}(p_T)$ is dominated by ξ error of Absolute Normalization method. For the same reason discussed in the systematic errors in the per trigger yields, the even order flow harmonics uncertainties do not contribute to away-side $I_{AA}(p_T)$. In the high associate p_T region, the $p + p$ measurements become the major contributor to the $I_{AA}(p_T)$. In addition, the combinatorial background in the π^0 yield is also a major contributor in low trigger π^0 p_T in central events (0–20%).

The systematic uncertainties of $I_{AA}(\Delta\phi)$ from different sources are shown separately in Figure 4.27 to 4.38 which reflect the influences of different sources of systematic errors in the $I_{AA}(p_T)$. In addition, these figures show that the uncertainty grows on the skirt of the jet where both per trigger yields and statistics are low.

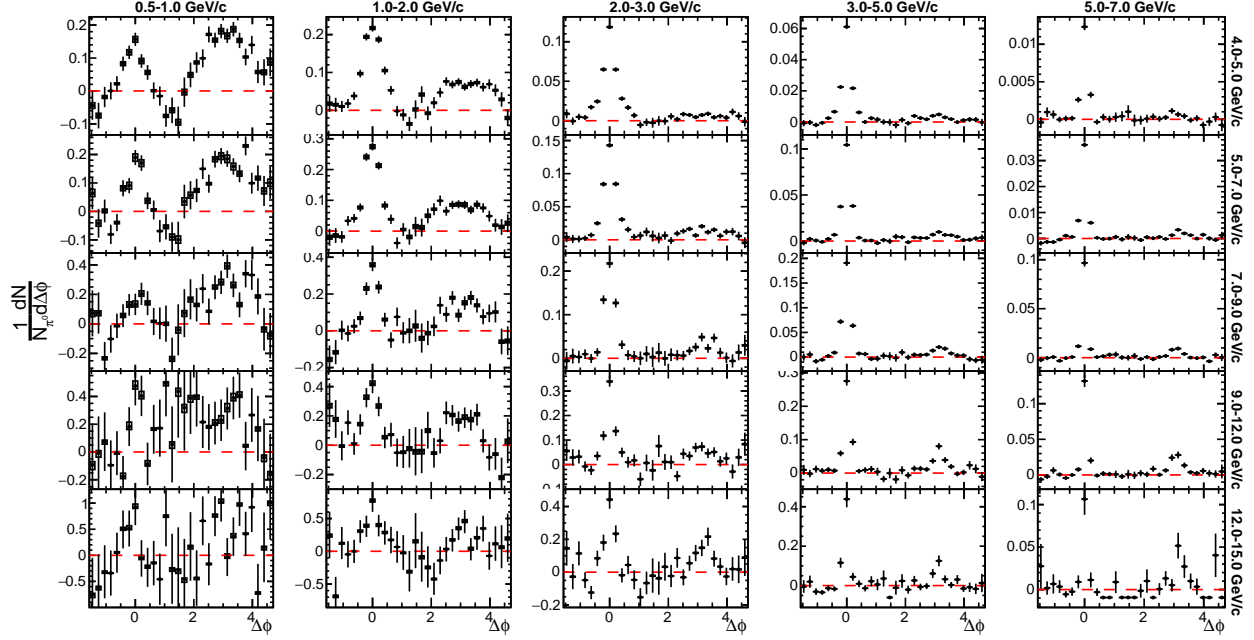


Figure 4.7: Jet functions in 0–20% centrality with systematic uncertainty from the second order flow harmonic drawn as boxes which are small. The trigger and associate p_T ranges are labeled on the side and the top, respectively. The dash lines indicate zero per trigger yield.

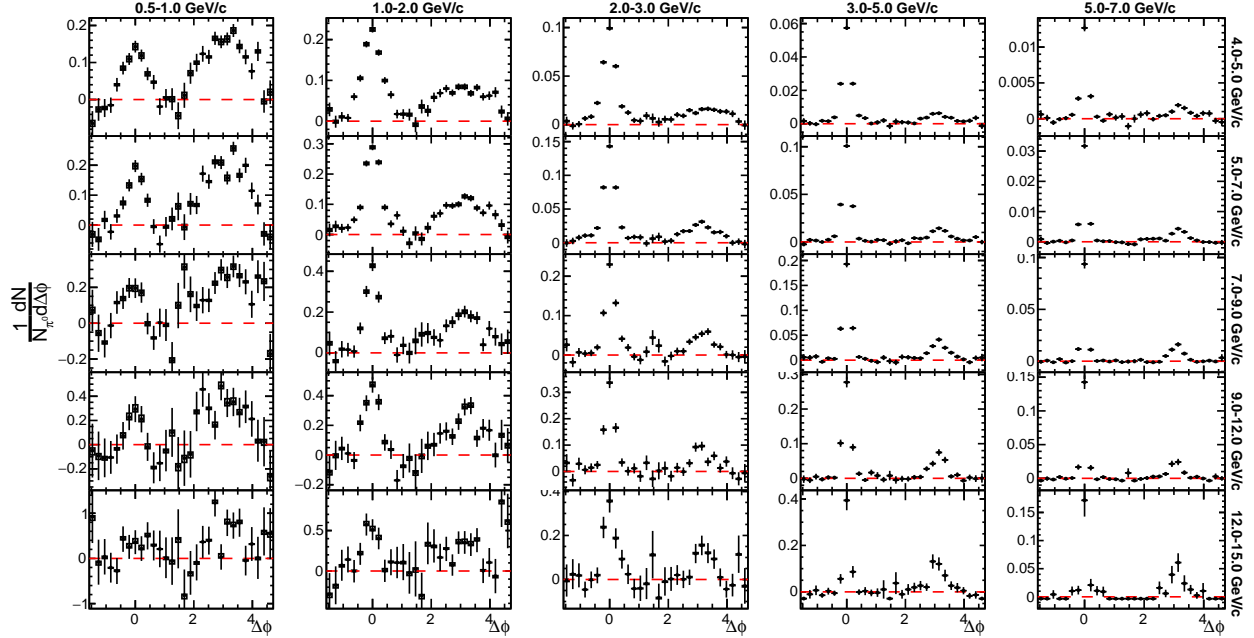


Figure 4.8: Jet functions in 20–40% centrality with systematic uncertainty from the second order flow harmonic drawn as boxes which are small.

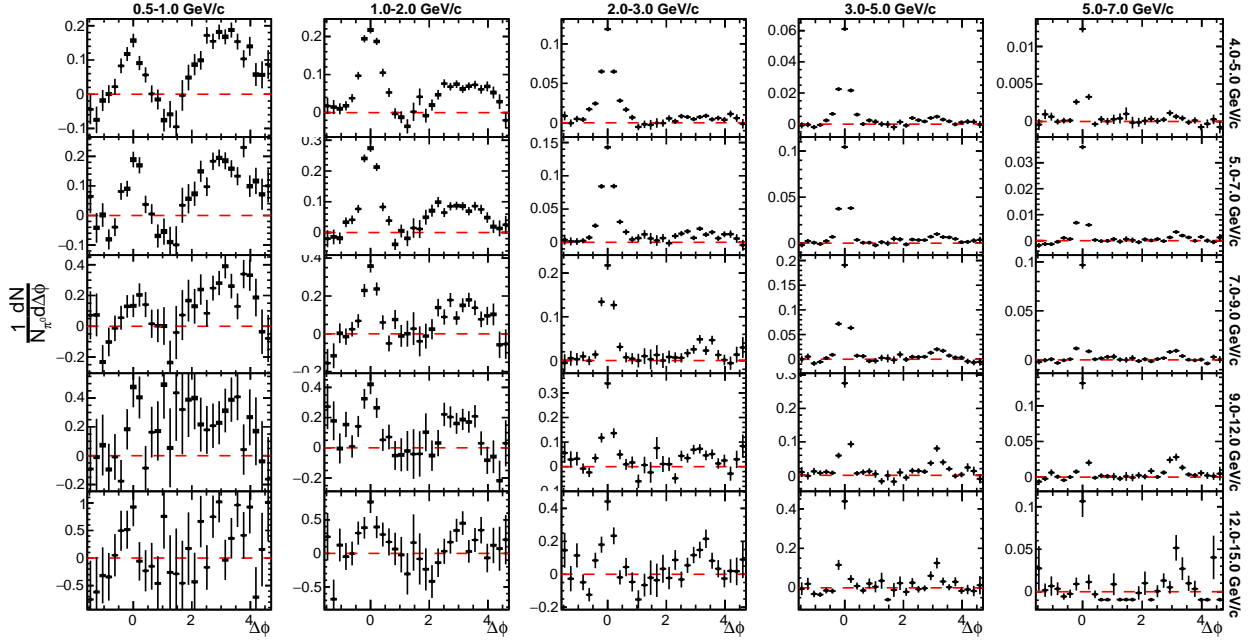


Figure 4.9: Jet functions in 0–20% centrality with systematic uncertainty from the third order flow harmonic drawn as boxes which are small.

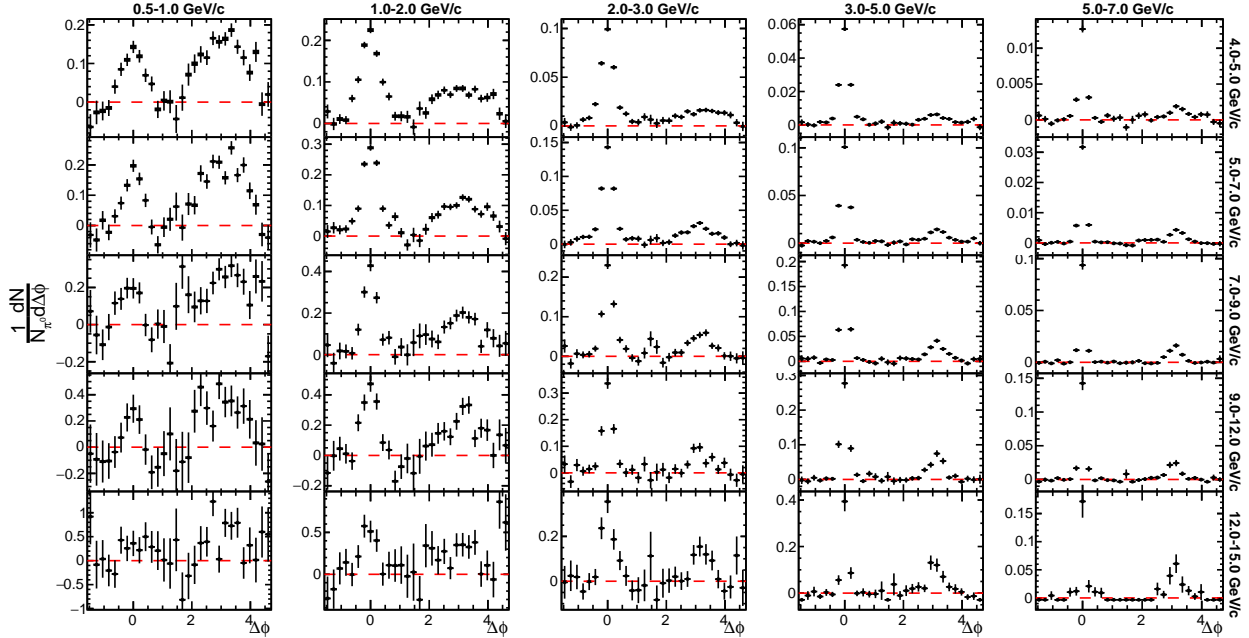


Figure 4.10: Jet functions in 20–40% centrality with systematic uncertainty from the third order flow harmonic drawn as boxes which are small.

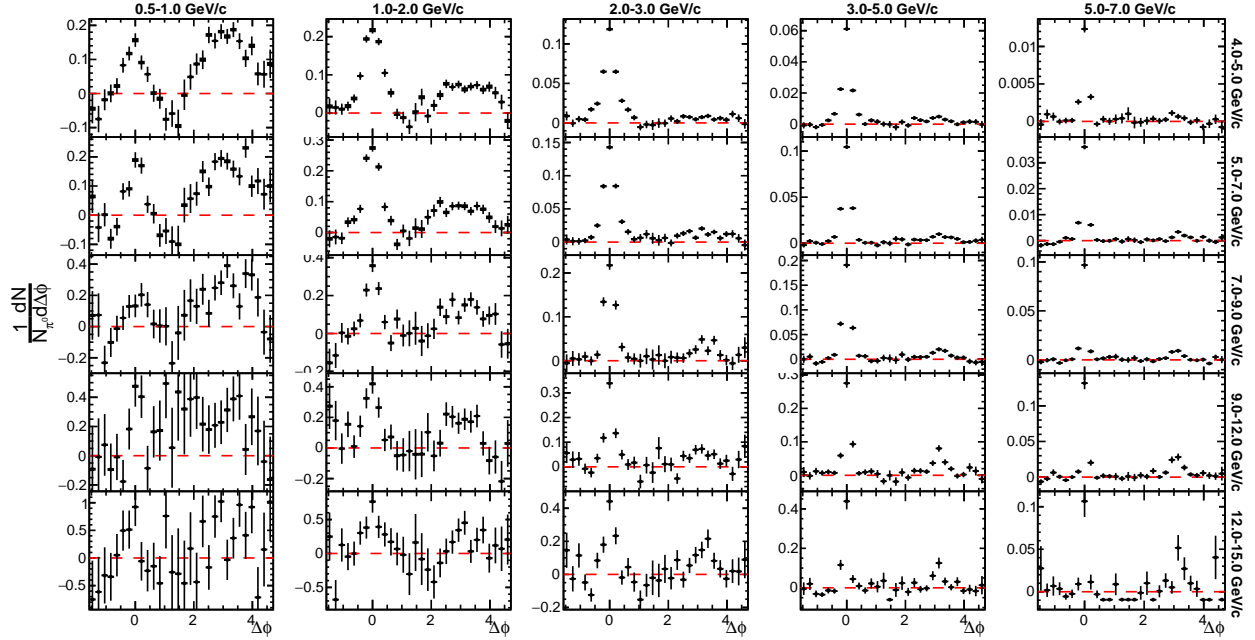


Figure 4.11: Jet functions in 0–20% centrality with systematic uncertainty from the fourth order flow harmonic drawn as boxes which are small.

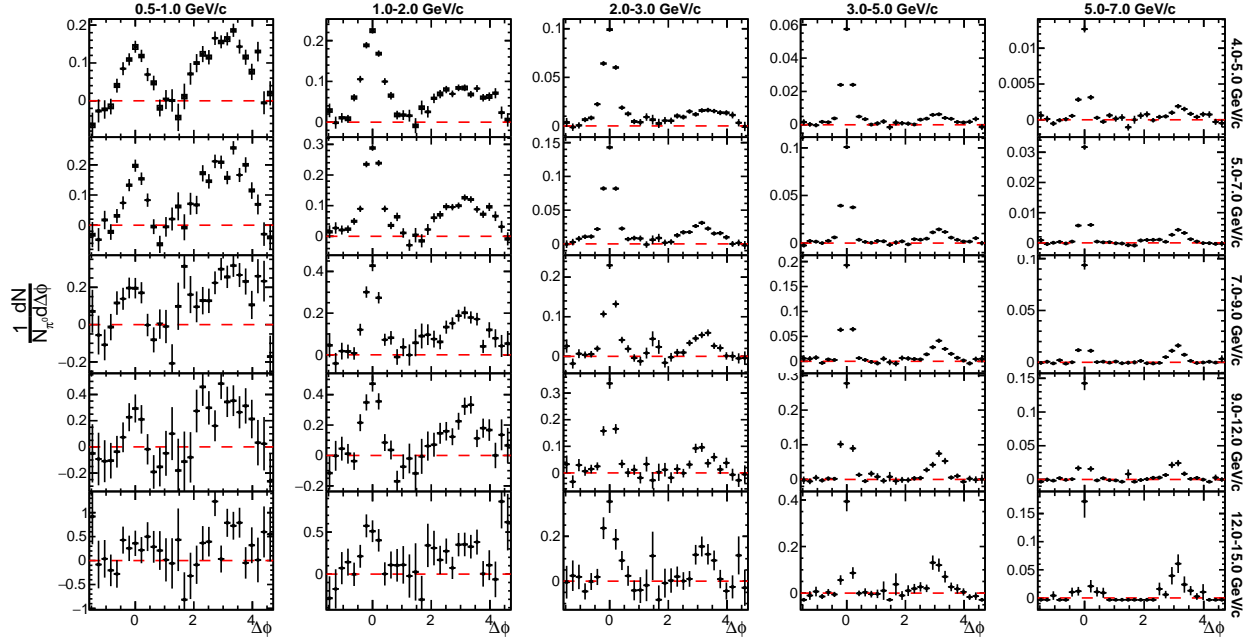


Figure 4.12: Jet functions in 20–40% centrality with systematic uncertainty from the fourth order flow harmonic drawn as boxes which are small.

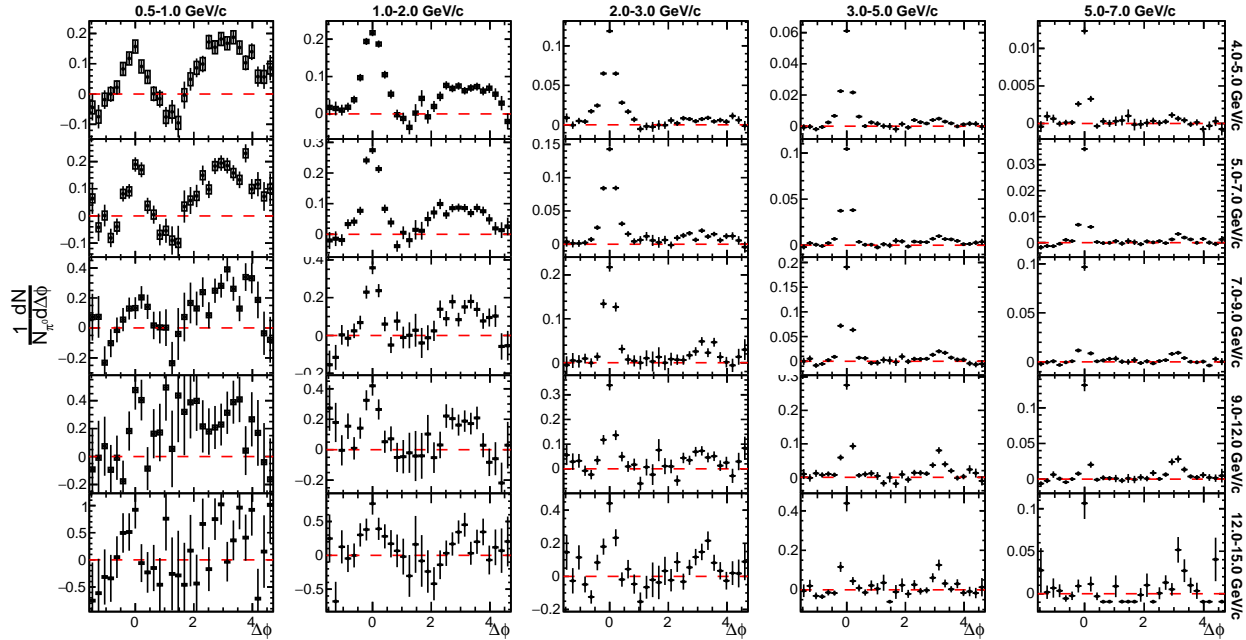


Figure 4.13: Jet functions in 0–20% centrality with systematic uncertainty from Absolute Normalization method drawn as box.

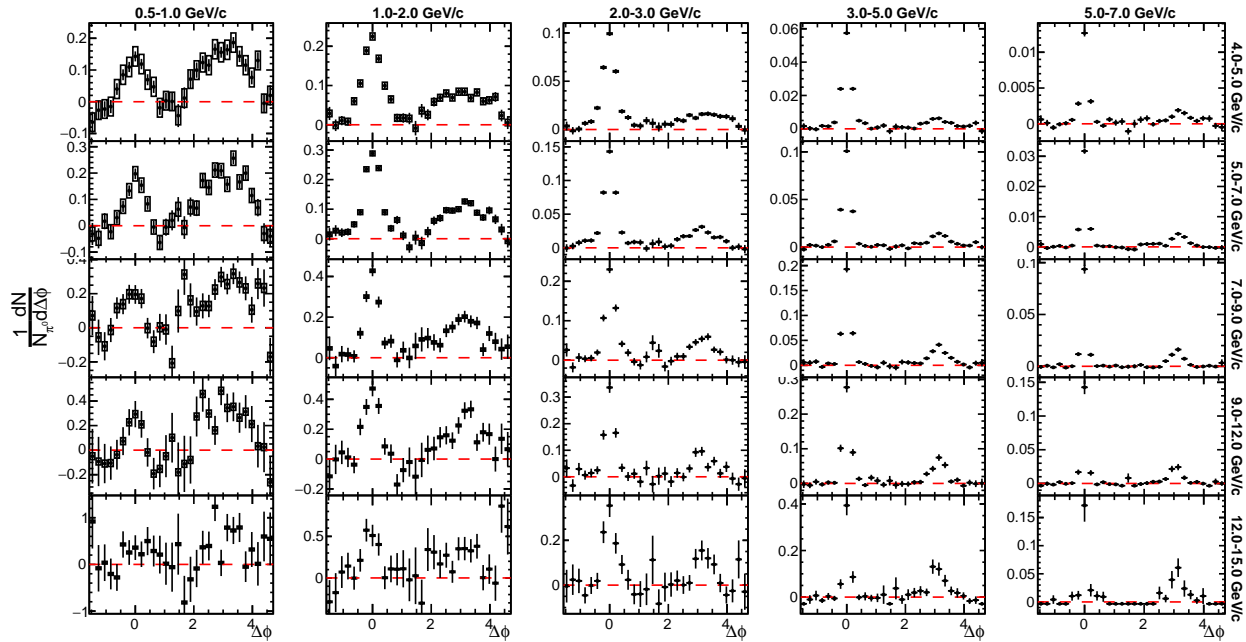


Figure 4.14: Jet functions in 20–40% centrality with systematic uncertainty from Absolute Normalization method drawn as box.

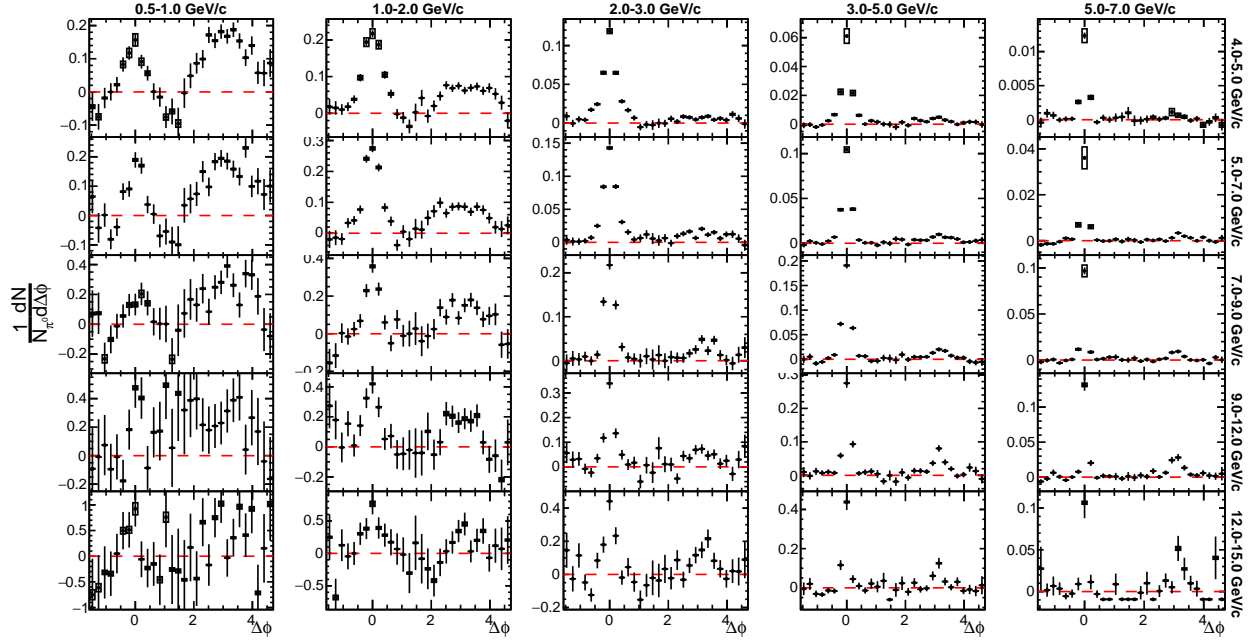


Figure 4.15: Jet functions in 0–20% centrality with systematic uncertainty from combinatorial background π^0 drawn as box.

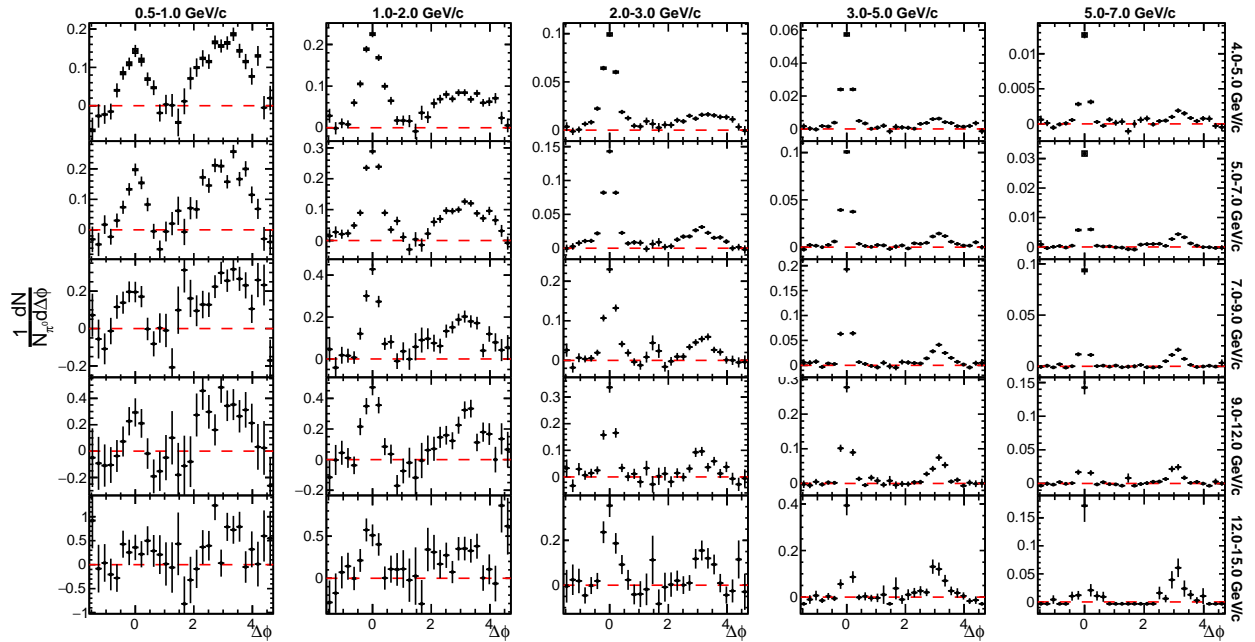


Figure 4.16: Jet functions in 20–40% centrality with systematic uncertainty from combinatorial background π^0 drawn as box.

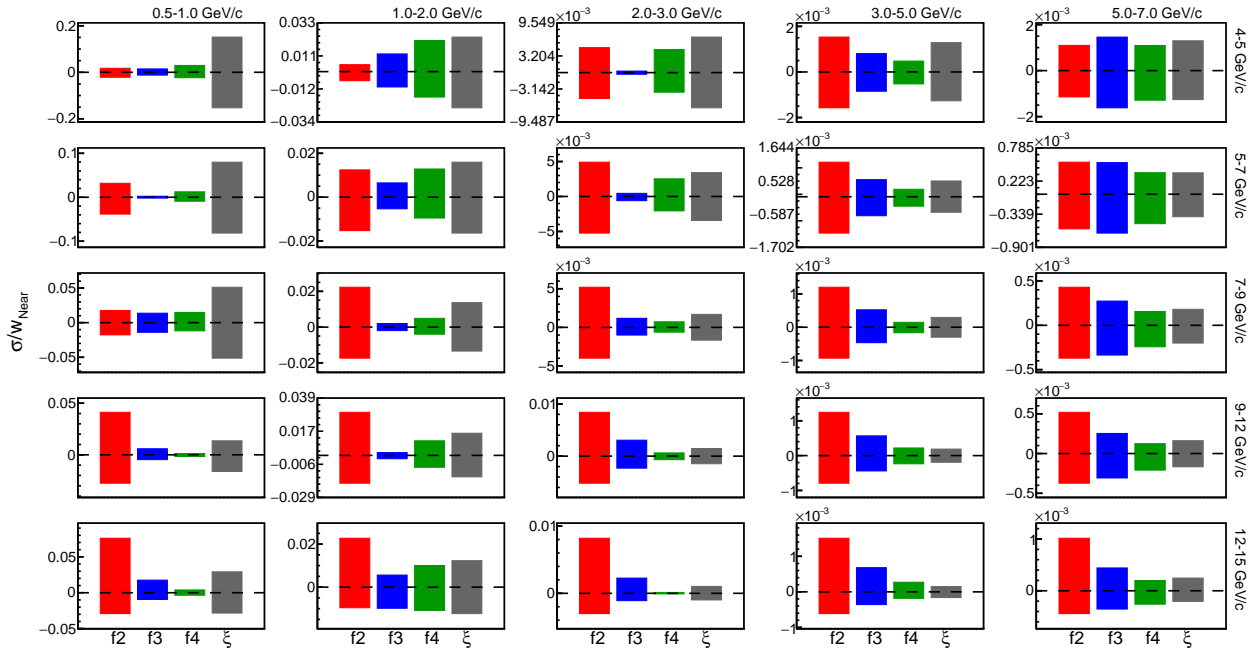


Figure 4.17: Relative uncertainties in near-side width in 0–20% centrality.

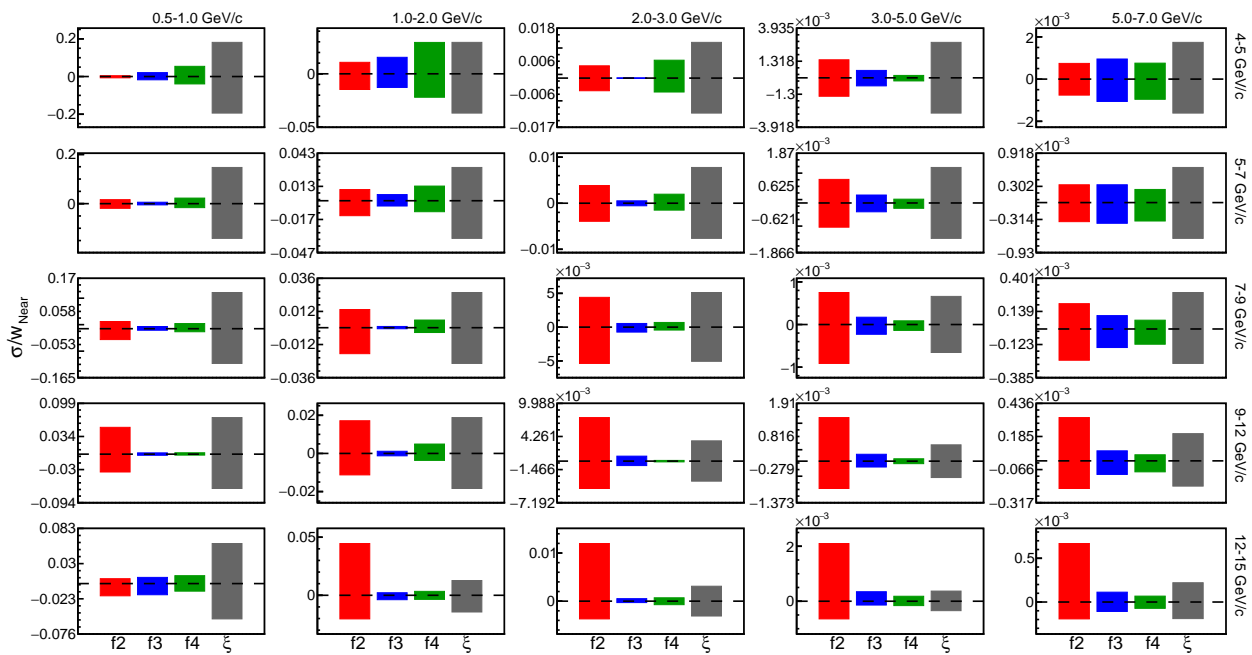


Figure 4.18: Relative uncertainties in near-side width in 20–40% centrality.

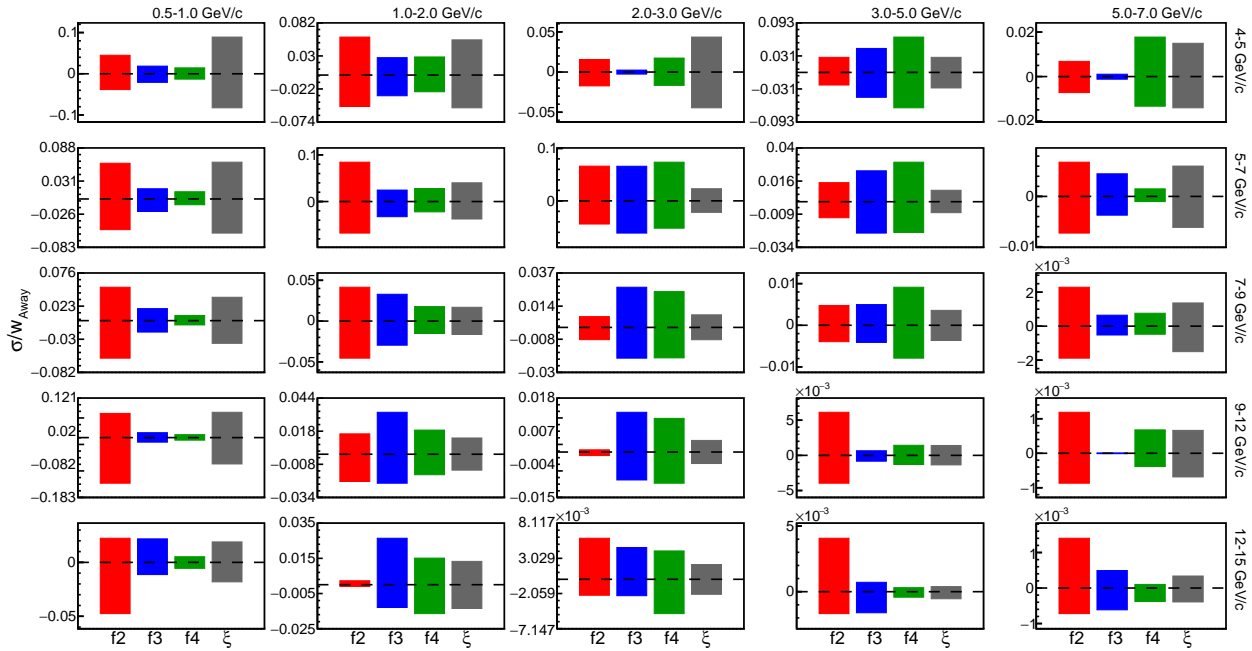


Figure 4.19: Relative uncertainties in away-side width in 0–20% centrality.

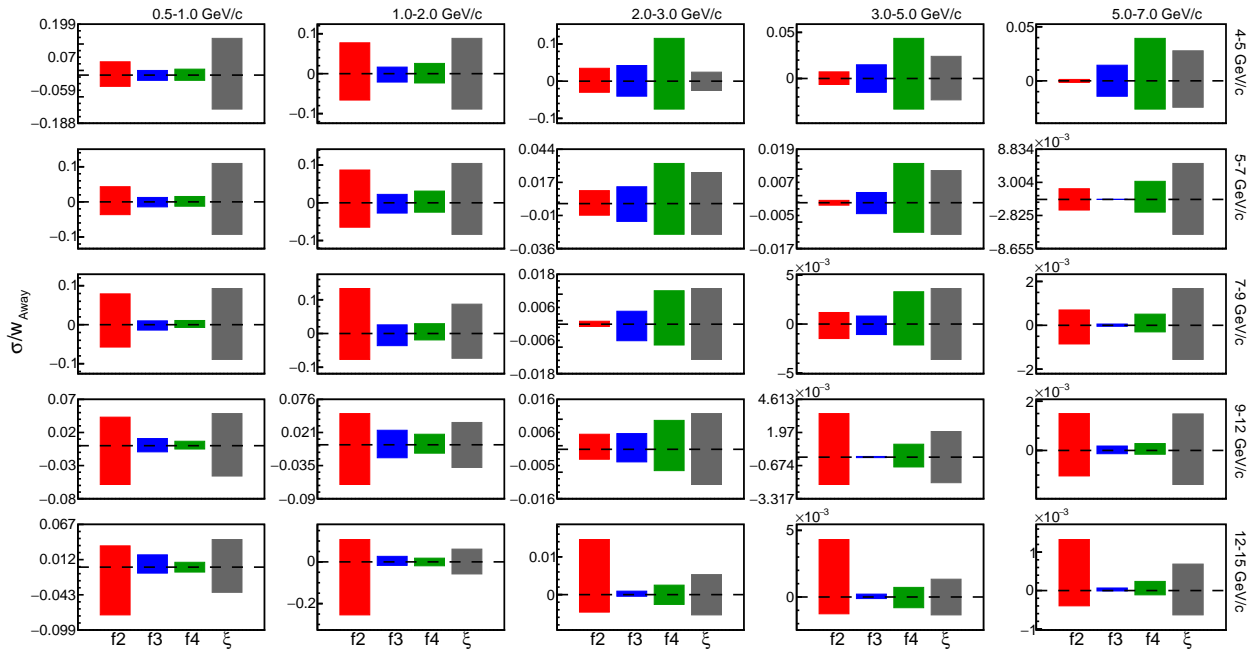


Figure 4.20: Relative uncertainties in away-side width in 20–40% centrality.

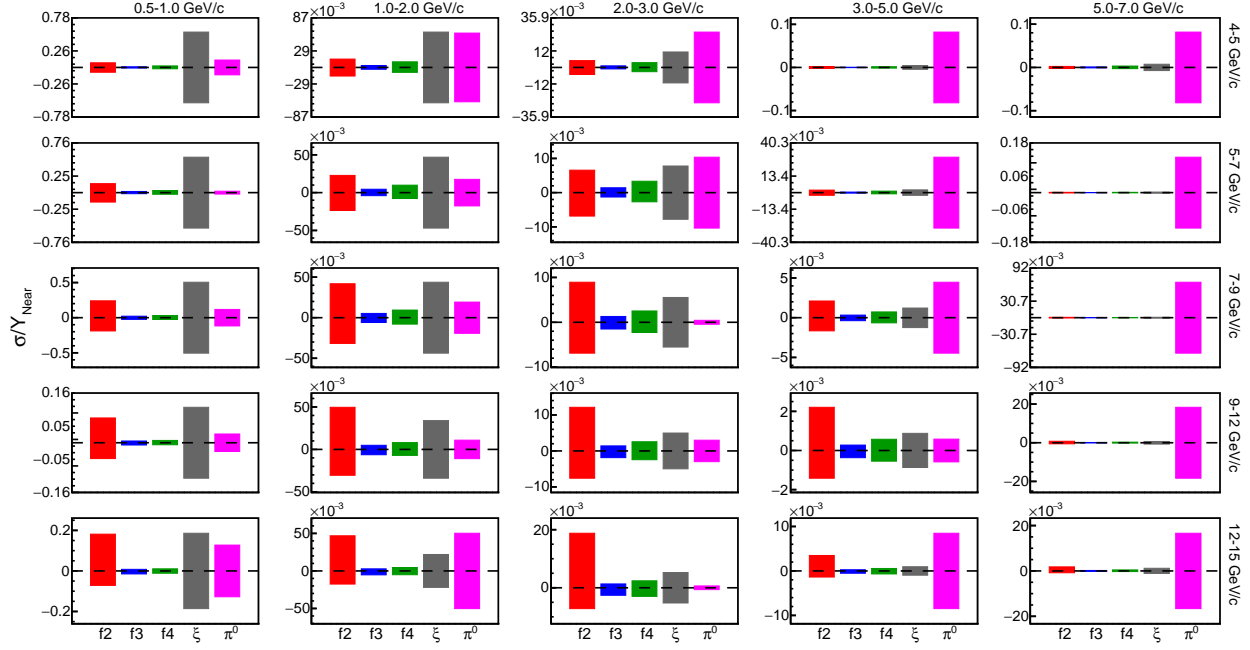


Figure 4.21: Relative uncertainties in near-side yield in 0–20% centrality.

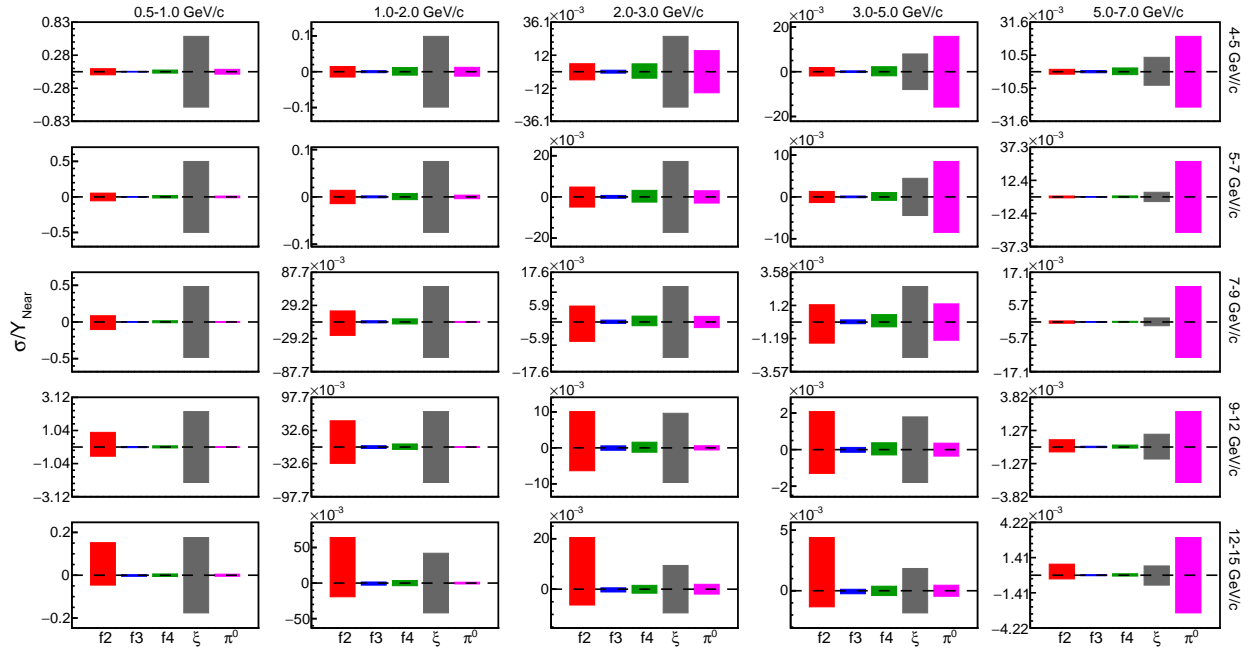


Figure 4.22: Relative uncertainties in near-side yield in 20–40% centrality.

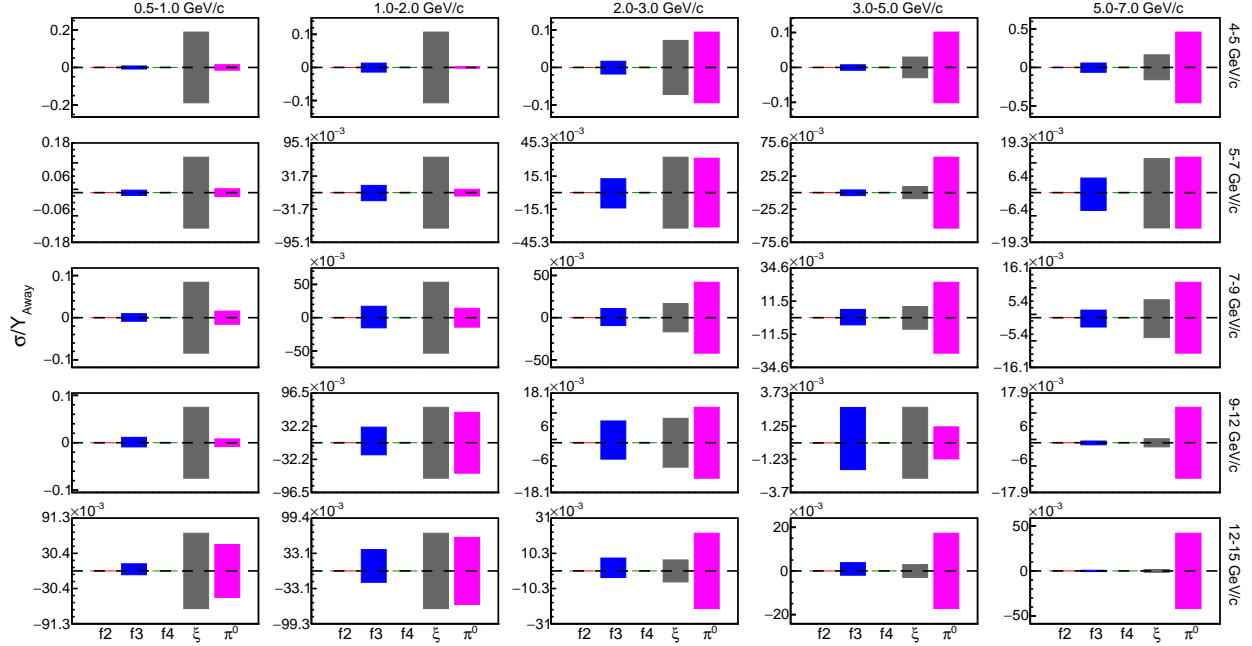


Figure 4.23: Relative uncertainties in away-side yield in 0–20% centrality.

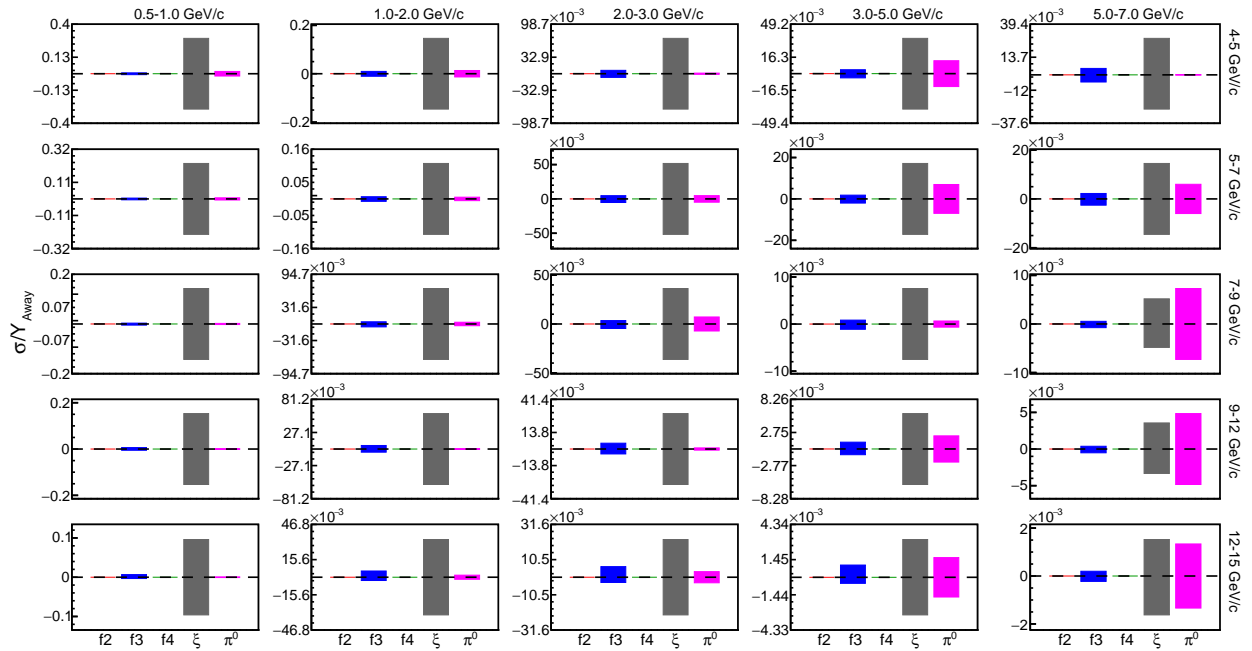


Figure 4.24: Relative uncertainties in away-side yield in 20–40% centrality.

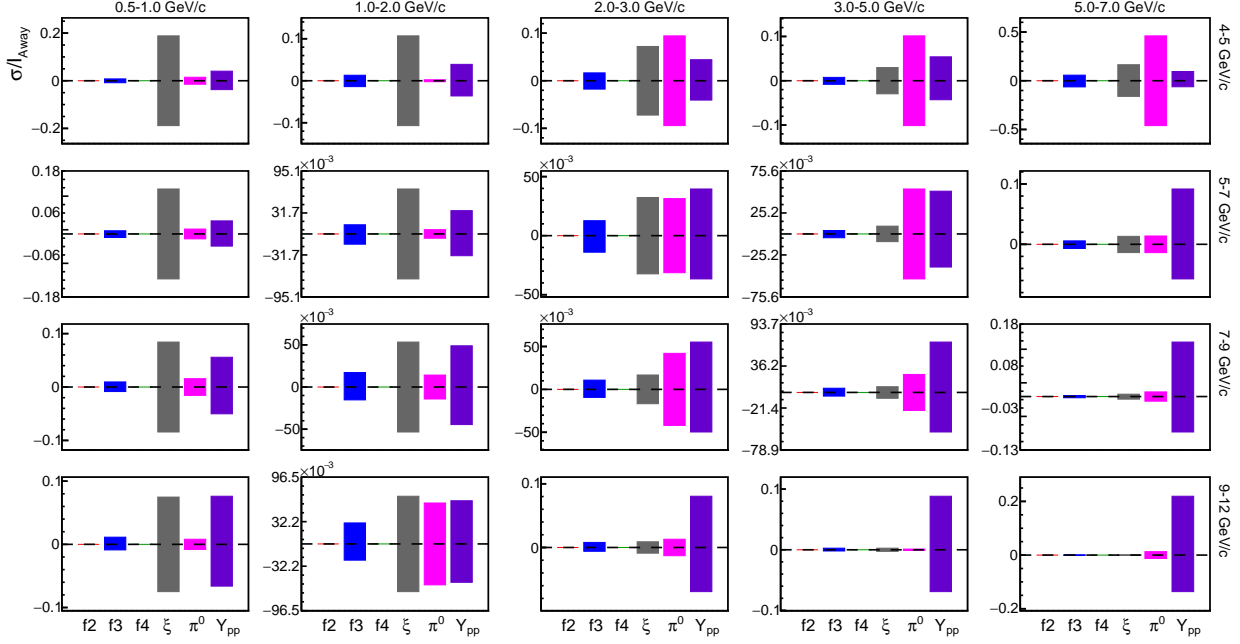


Figure 4.25: Relative uncertainties in away-side I_{AA} in 0–20% centrality.

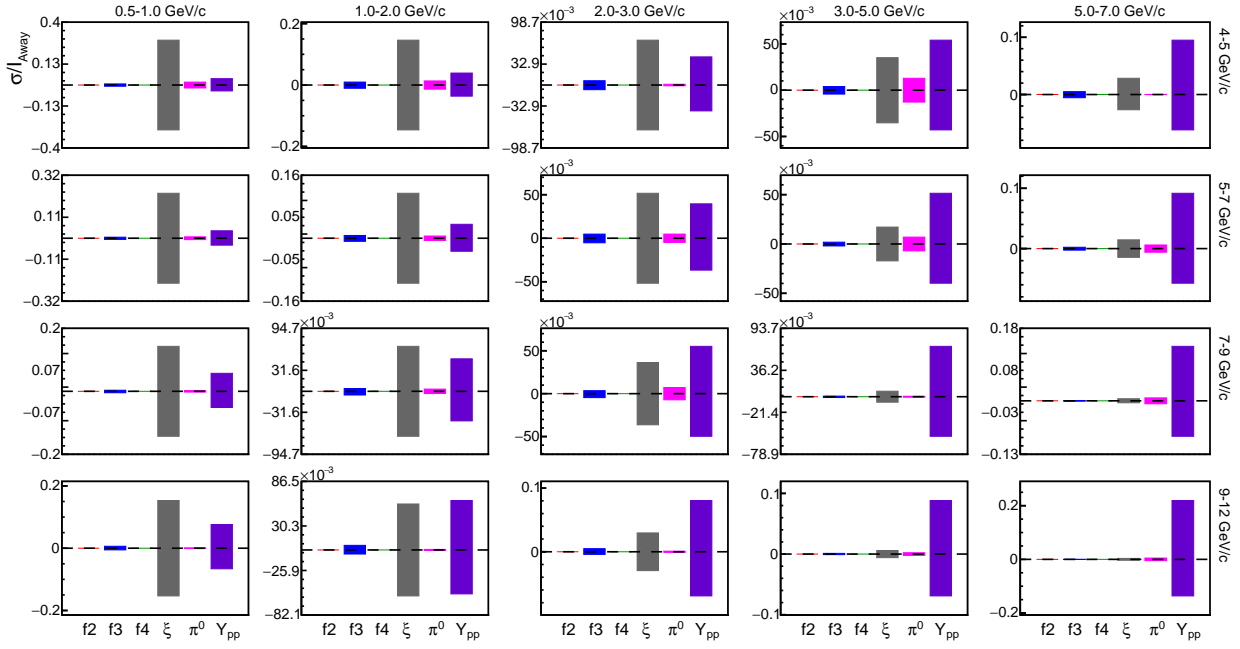


Figure 4.26: Relative uncertainties in away-side I_{AA} in 20–40% centrality.

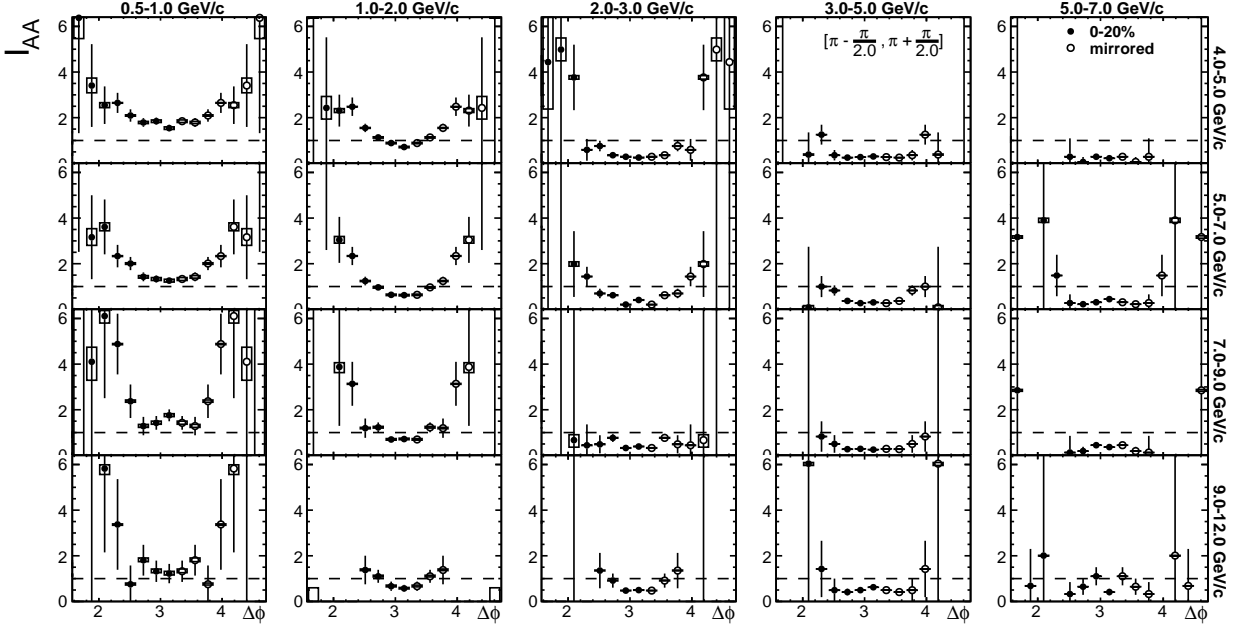


Figure 4.27: Away-side $I_{AA}(\Delta\phi)$ in 0–20% with systematic uncertainty, σ^{f2} , raised by the second order flow harmonics drawn as box.

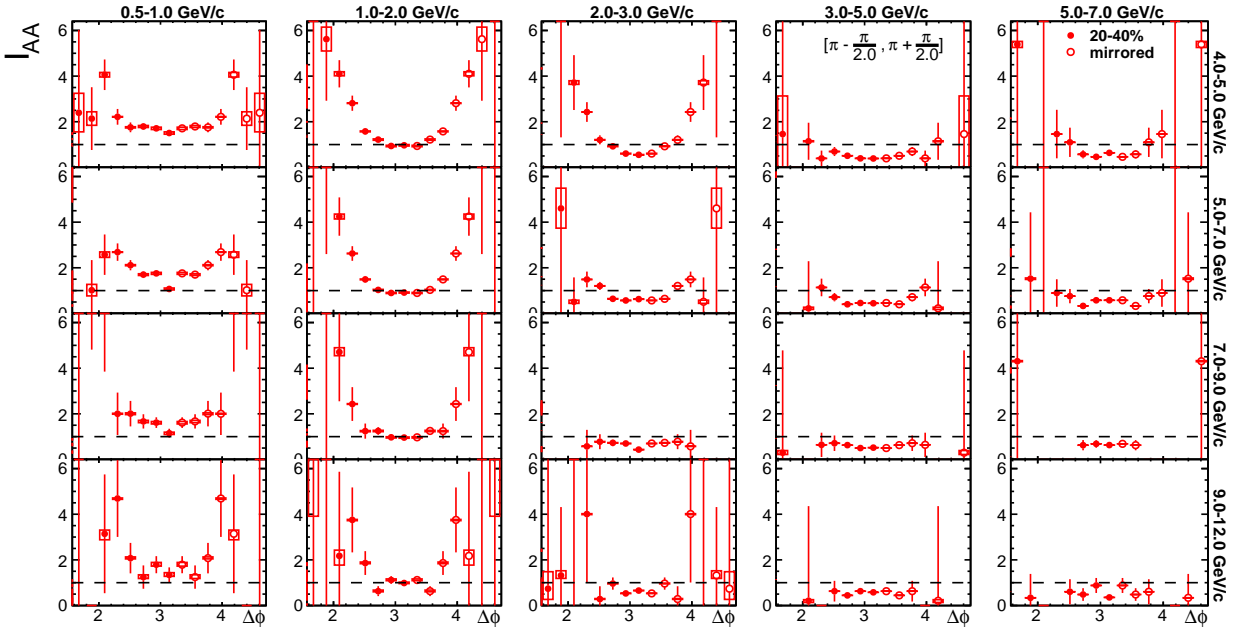


Figure 4.28: Away-side $I_{AA}(\Delta\phi)$ in 20–40% with systematic uncertainty, σ^{f2} , raised by the second order flow harmonics drawn as box.

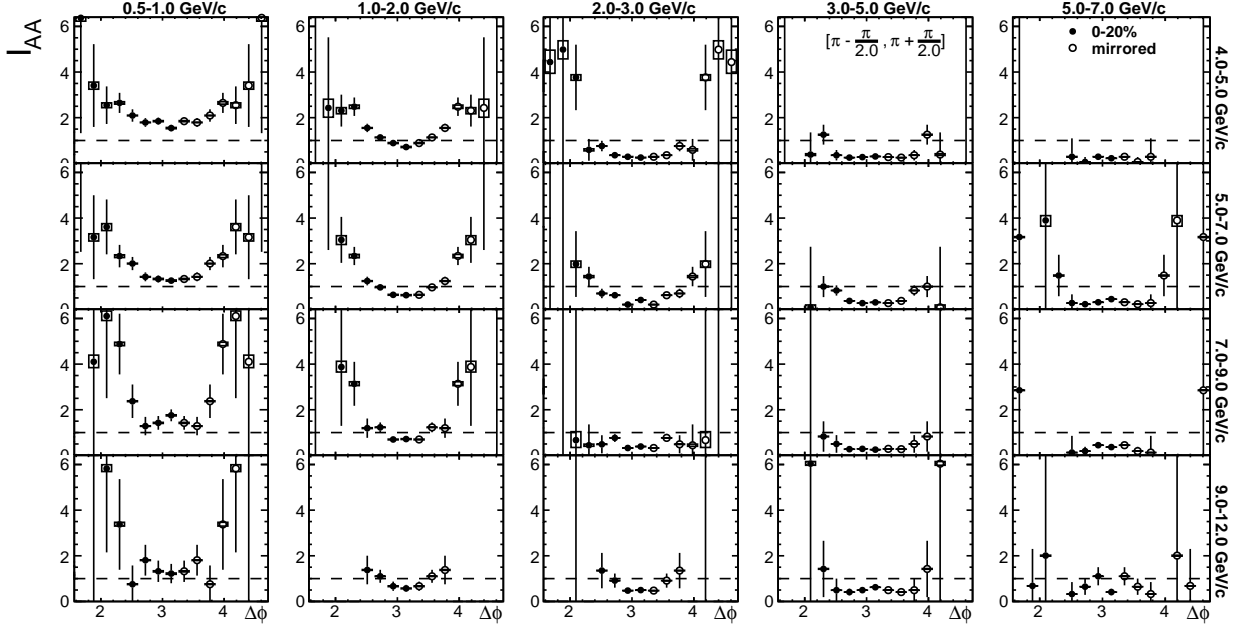


Figure 4.29: Away-side $I_{AA}(\Delta\phi)$ in 0–20% with systematic uncertainty, σ^{f3} , raised by the third order flow harmonics drawn as box.

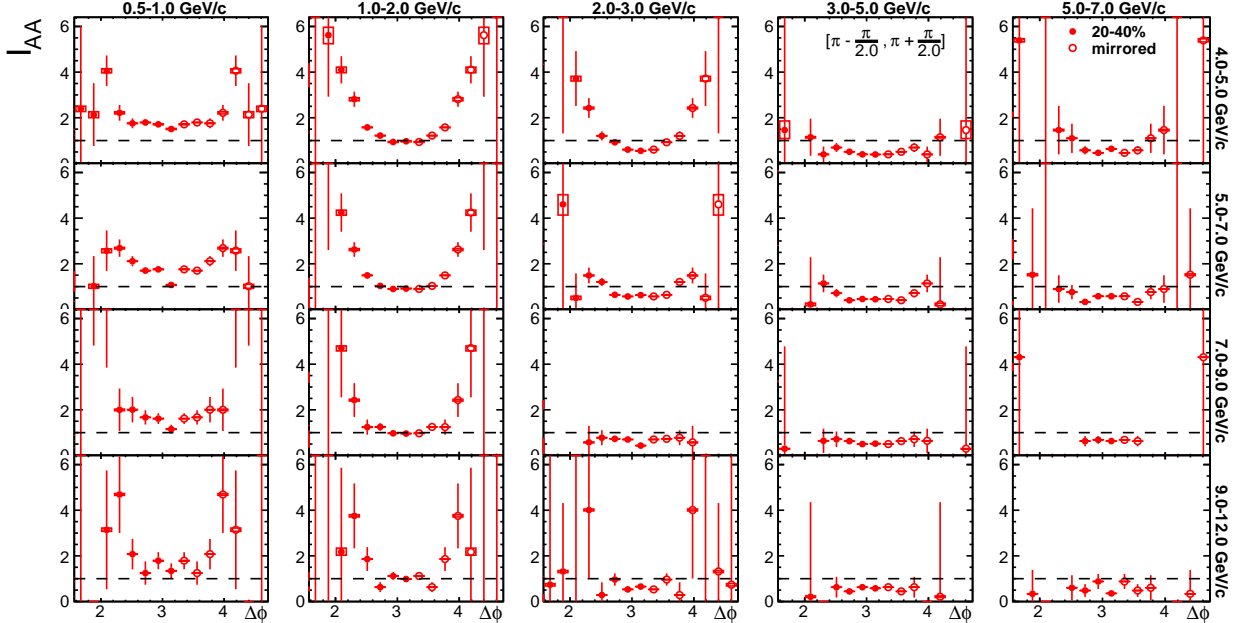


Figure 4.30: Away-side $I_{AA}(\Delta\phi)$ in 20–40% with systematic uncertainty, σ^{f3} , raised by the third order flow harmonics drawn as box.

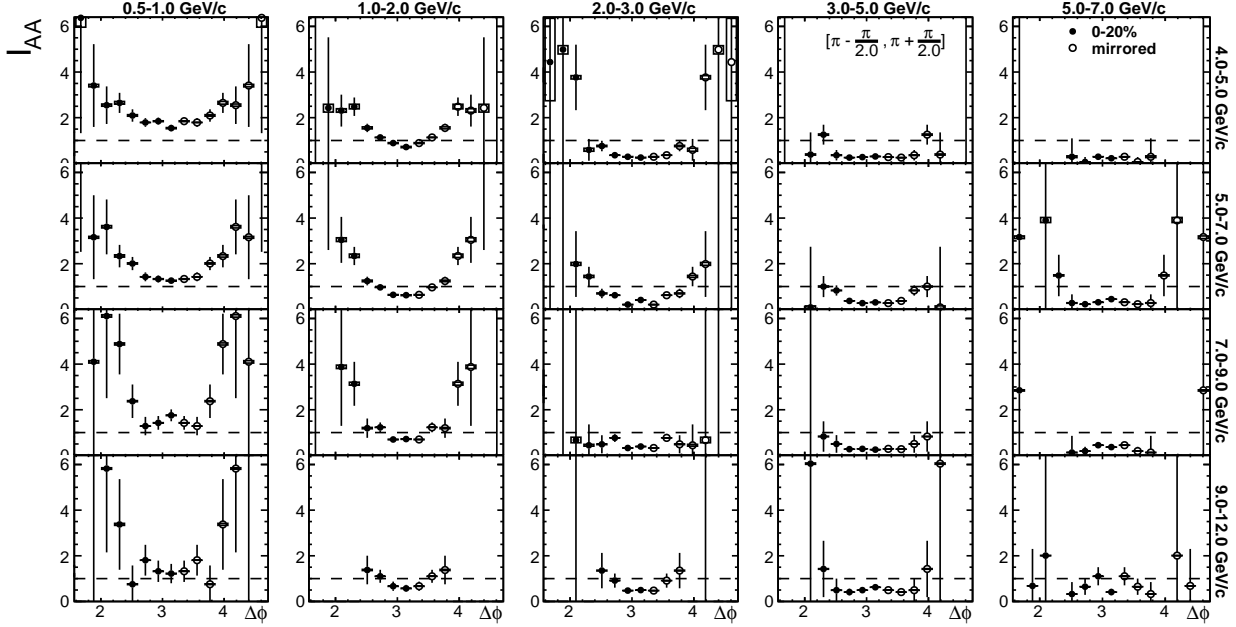


Figure 4.31: Away-side $I_{AA}(\Delta\phi)$ in 0–20% with systematic uncertainty, σ^{f4} , raised by the fourth order flow harmonics drawn as box.

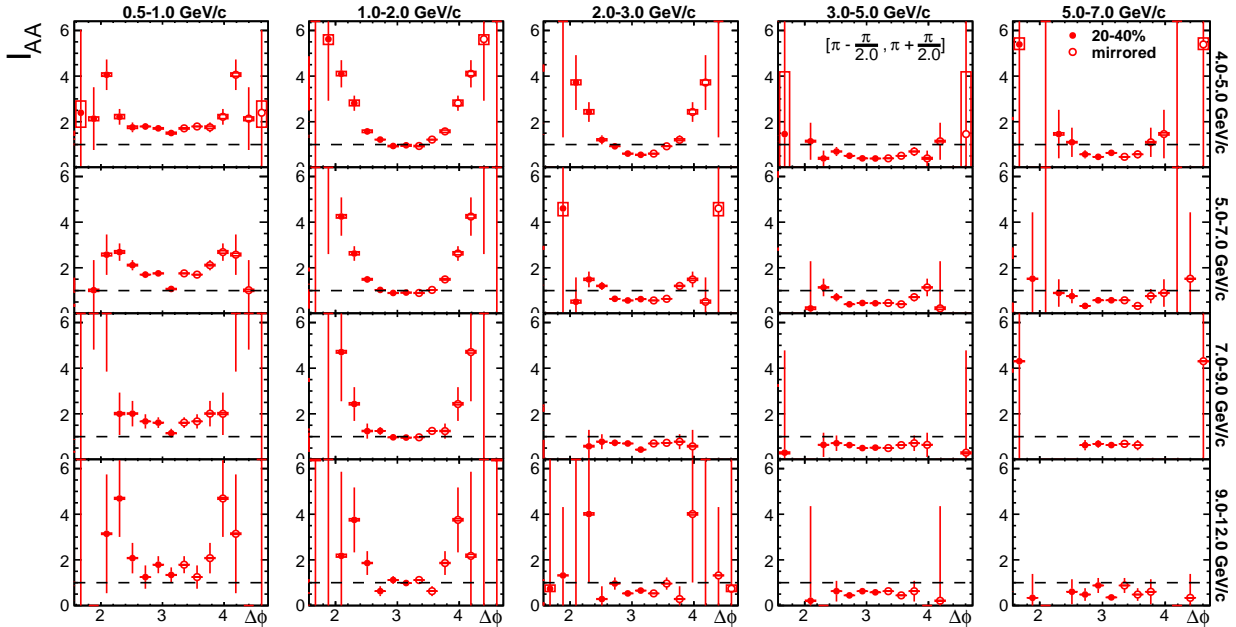


Figure 4.32: Away-side $I_{AA}(\Delta\phi)$ in 20–40% with systematic uncertainty, σ^{f4} , raised by the fourth order flow harmonics drawn as box.

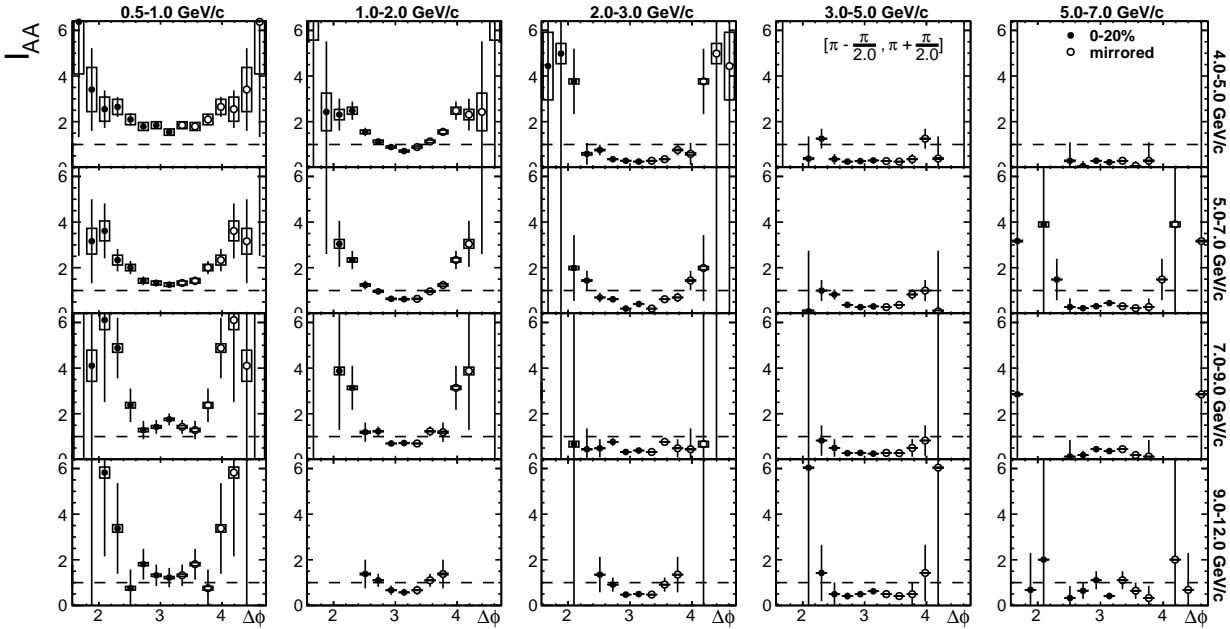


Figure 4.33: Away-side $I_{AA}(\Delta\phi)$ in 0–20% with systematic uncertainty, σ^ξ , raised by Absolute Normalization method drawn as box.

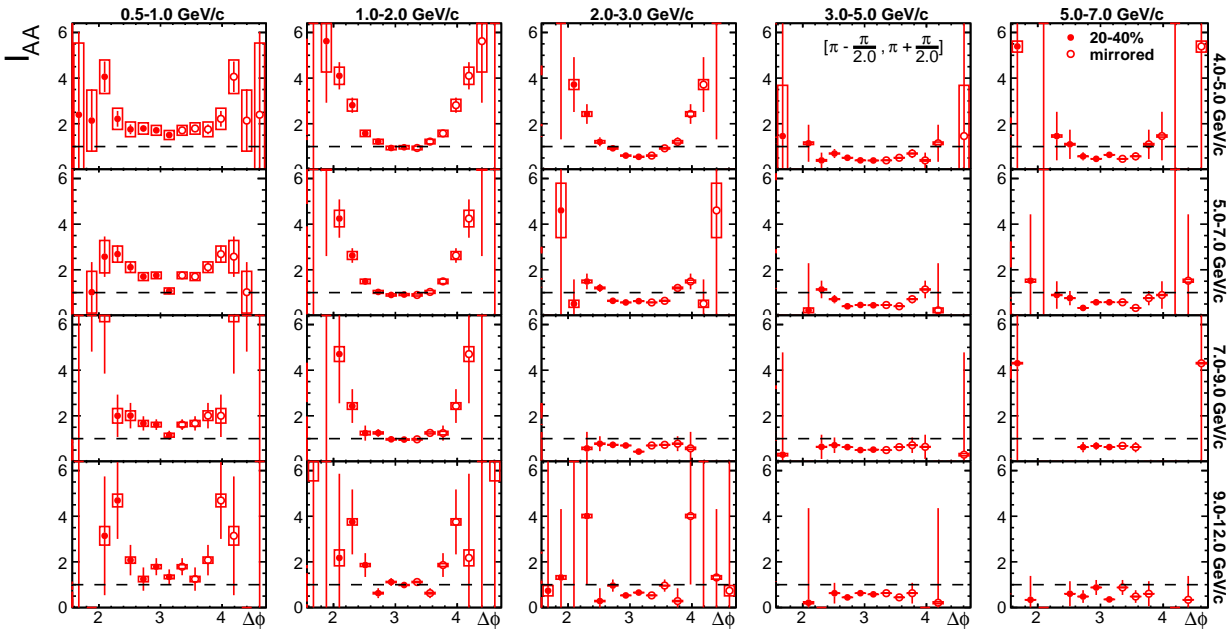


Figure 4.34: Away-side $I_{AA}(\Delta\phi)$ in 20–40% with systematic uncertainty, σ^ξ , raised by Absolute Normalization method drawn as box.

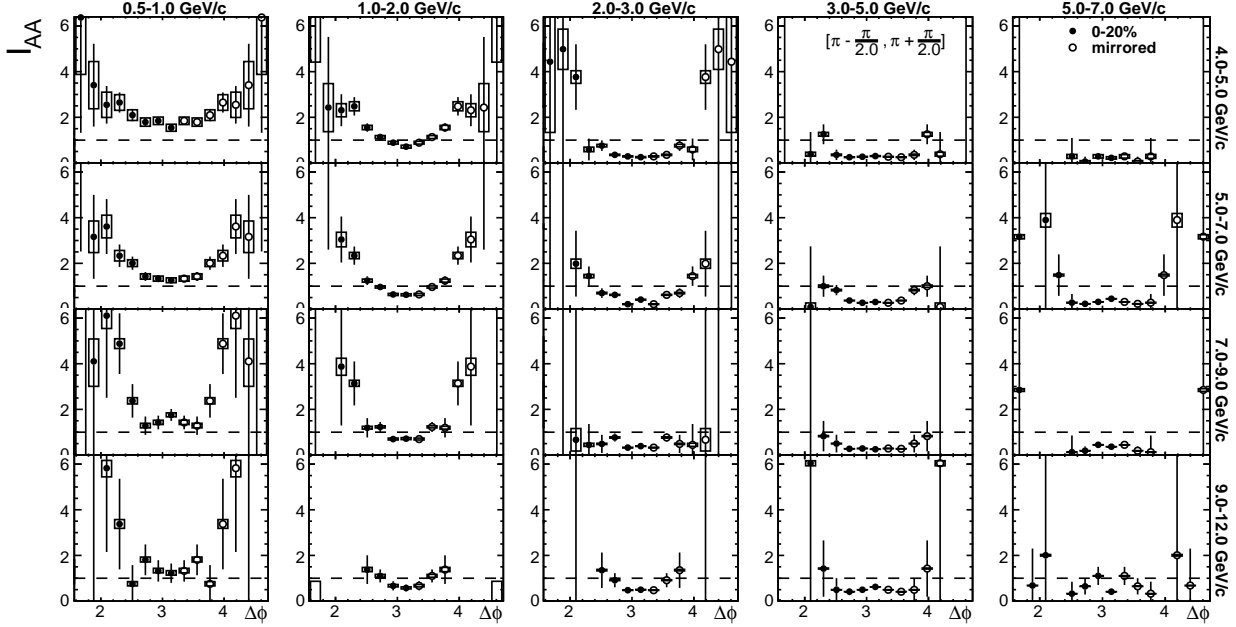


Figure 4.35: Away-side $I_{AA}(\Delta\phi)$ in 0–20% with systematic uncertainty, σ^{π^0} , raised by combinatorial background π^0 drawn as box.

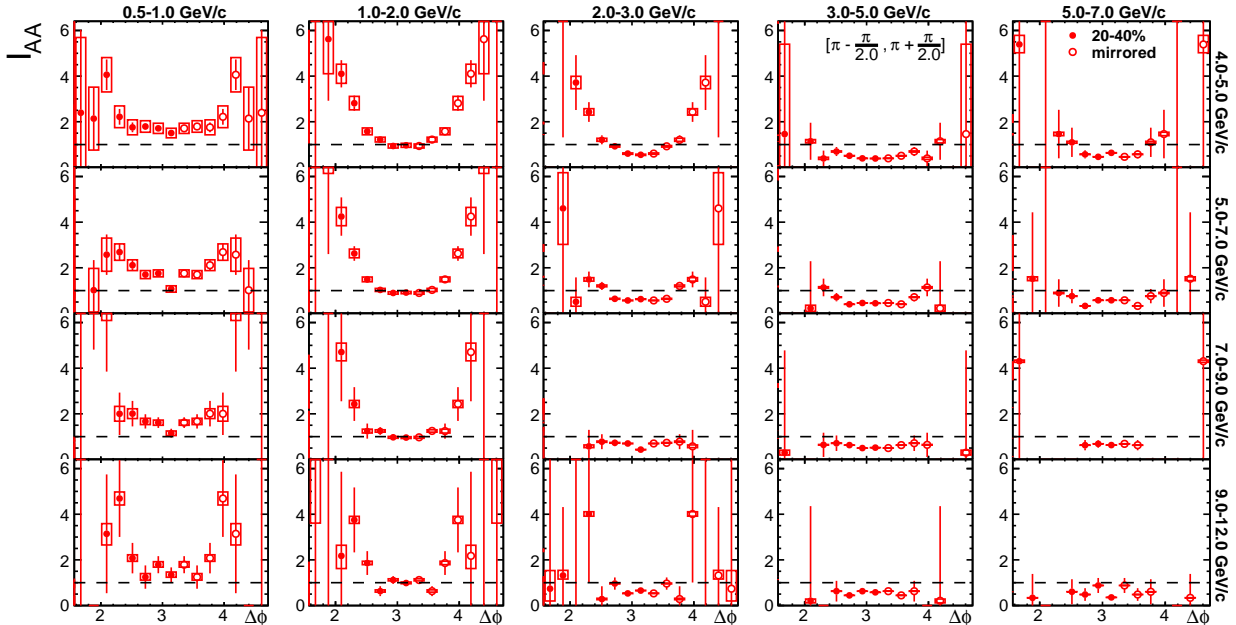


Figure 4.36: Away-side $I_{AA}(\Delta\phi)$ in 20–40% with systematic uncertainty, σ^{π^0} , raised by combinatorial background π^0 drawn as box.

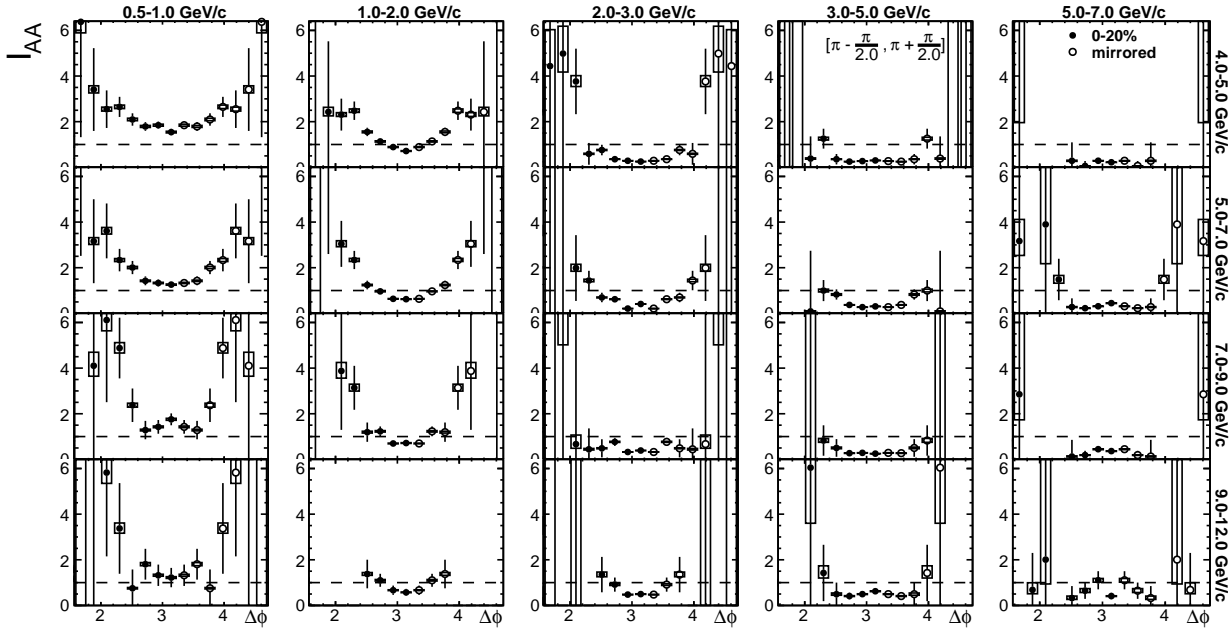


Figure 4.37: Away-side $I_{AA}(\Delta\phi)$ in 0–20% with systematic uncertainty, σ^{pp} , raised by $p + p$ measurement drawn as box.

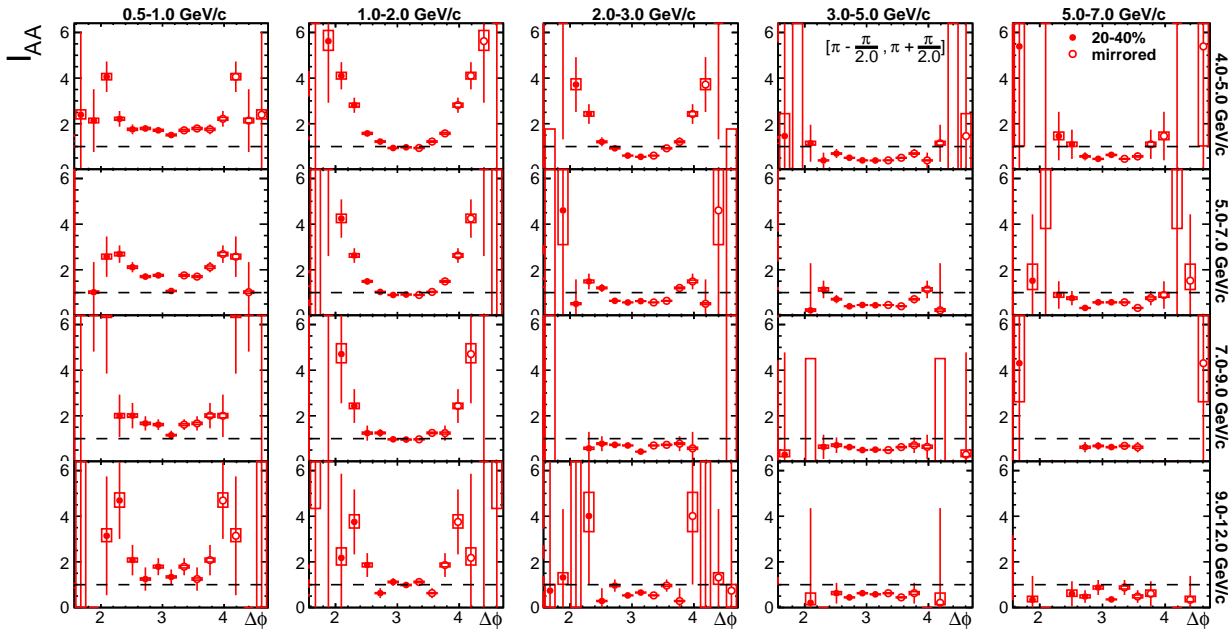


Figure 4.38: Away-side $I_{AA}(\Delta\phi)$ in 20–40% with systematic uncertainty, σ^{pp} , in $p + p$ measurement drawn as box.

CHAPTER 5

Results

5.1 Jet Functions

Jet functions, that is the per trigger yield as a function of $\Delta\phi$, in 0–20% and 20–40% centrality are shown in figure. 5.1 and figure. 5.2, respectively. The fits of the jet functions are drawn as red lines in these figures. The jet functions appear sharp and narrow at the high associate p_T , but broad and at the low associate p_T . While Absolute Normalization works well in the high p_T bins, it is clear that there are over subtractions in the low associate p_T bins.

5.2 Yields

Per trigger yields as a function of associate p_T are shown in Figure 5.3. It is the integrated per trigger yield of the jet functions between $\Delta\phi = \pi - \frac{\pi}{2}$ and $\Delta\phi = \pi + \frac{\pi}{2}$. There is a decreasing trend along the associate p_T axis in both near and away-side yields and in both $Au + Au$ and $p + p$ collisions. The near-side yields in $Au + Au$ and $p + p$ are consistent implying the near-side jets modification is small in $Au + Au$ collisions. The away-side jets in $Au + Au$ collisions have higher yields than the $p + p$ collision for low associate p_T (< 2 GeV/c), but the yields of away-side jets in $Au + Au$ collisions become consistent with those in $p + p$ collisions with increasing p_T .

Since more central events are expected to create a larger volume of QGP, centrality dependence studies can show path length effect of the QGP. The near-side yields are consistent between 0–20% and 20–40% centrality classes. While the away-side yields are consistent between these centrality classes at low associate p_T , the yields in 20–40% is systematically higher than in 0–20% at high associate p_T (> 2 GeV/c) within the 4–9 GeV/c trigger p_T range.

The differences in yields between $Au + Au$ and $p + p$ collisions are more noticeable in the away-side than the near-side jets. This is due to the fact that a relatively high momentum particles are used as trigger particles. Therefore, near-side jets, which travel shorter path length in the QGP and suffer less energy loss, are favored in the analysis. Since jets emerge back-to-back, the away-side jets travel a longer path length and lose more energy to the QGP than the near-side jets. Due to this path length bias, the away-side jets are more sensitive to the QGP effects.

5.3 Away-side $I_{AA}(p_T)$

To quantify the observed modification to the per trigger yield, away-side I_{AA} as a function of associate p_T , which is displayed in Figure 5.4, is calculated using the integrated per trigger yield within $\pi - \frac{\pi}{2} < \Delta\phi \leq \pi + \frac{\pi}{2}$. Figure 5.4 shows away-side I_{AA} greater than 1 at low associate p_T , but decreases as associate p_T increases, and is below 1 at high associate p_T . These results show enhancement of soft jet particles but suppression of hard jet particles, indicating the energy loss of partons in the QGP causes a reduction in the number of high momentum particles produced which leads to an enhancement of particles with low momenta. It is noteworthy to point out that the transition from enhancement to suppression happens at about 2 GeV/c in different trigger p_T ranges, suggesting the transition is independent of trigger particle momentum.

5.4 Jet Widths

There is a decreasing trend along the associate p_T axis in both near and away-side jet width and in both $Au + Au$ and $p + p$ collisions as shown in Figure 5.5. The azimuthal widths of the near-side jets measured in $Au + Au$ and $p + p$ are consistent. However, the enhanced soft particles of the away-side jets in $Au + Au$ collisions spread in a wider azimuthal range than in $p + p$ collisions, while

the angular widths of the suppressed hard particles of the away-side jets in $Au + Au$ collisions are consistent with the $p + p$ measurements.

5.5 $I_{AA}(\Delta\phi)$

The away-side angular widths and I_{AA} shown in Figure 5.4 and 5.5 suggest that the modifications has azimuthal dependent as well. To clearly show the relation between the yields modification and the correlation angle, the ratios of the differentiated yields of the away-side jet functions obtained from $Au + Au$ and $p + p$ measurements as a function of $\Delta\phi$ are shown in Figure 5.6. These $I_{AA}(\Delta\phi)$ plots reveal the details of modification at jet substructure level.

At the lowest associate p_T range, I_{AA} is greater than 1 overall in azimuth and increases at $\Delta\phi$ away from π , indicating soft jet particles are enhanced within the away-side jets, and stronger enhancement appears in the soft jet particles at the skirt of the away-side jets. This angular dependence changes with jet particle momentum. At $1 \leq p_T^{assoc} < 2$ GeV/c, I_{AA} is about 0.75 and 1 in 0–20% and 20–40% classes, respectively, at $\Delta\phi \approx \pi$. However, I_{AA} is above 1 as $\Delta\phi$ is away from π . This shows that the jet particles near the core of the away-side jets experience little to no modification. On the other hand, jet particles at the skirt of the away-side jets experience enhancement. At the even higher associate p_T , I_{AA} is mostly below 1 showing that the hard jet particles at different layers of the away-side jets are suppressed at all angles.

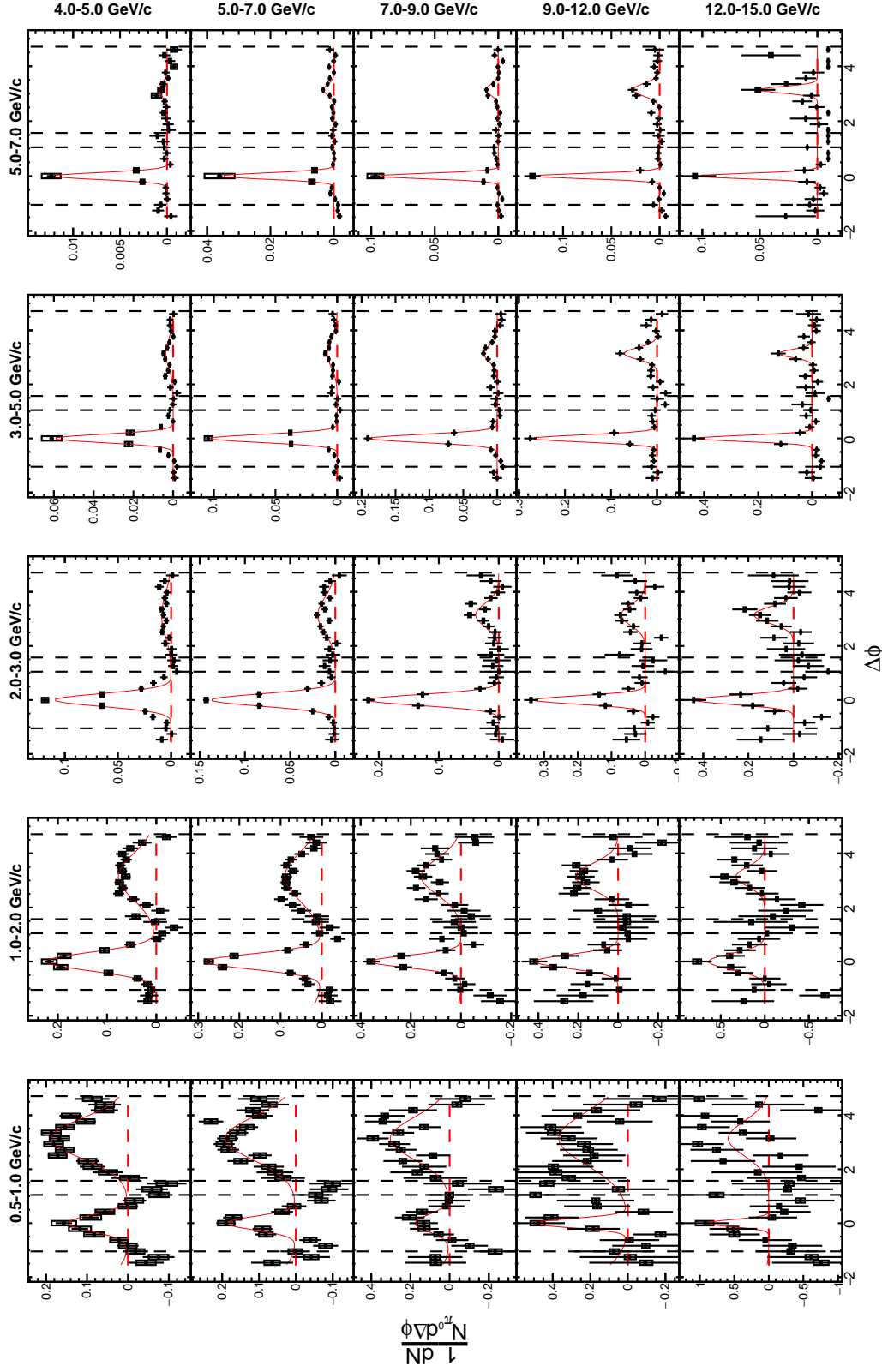


Figure 5.1: Jet functions in 0–20% of 200 GeV $Au + Au$ collisions. The trigger and associate p_T of each panel are labeled on the side and the top of the figure, respectively. The statistic and systematic errors are shown as vertical lines and boxes on the data, respectively. The red curves are the Gaussian fits to the jet functions. The horizontal red lines indicate zero per trigger yields.

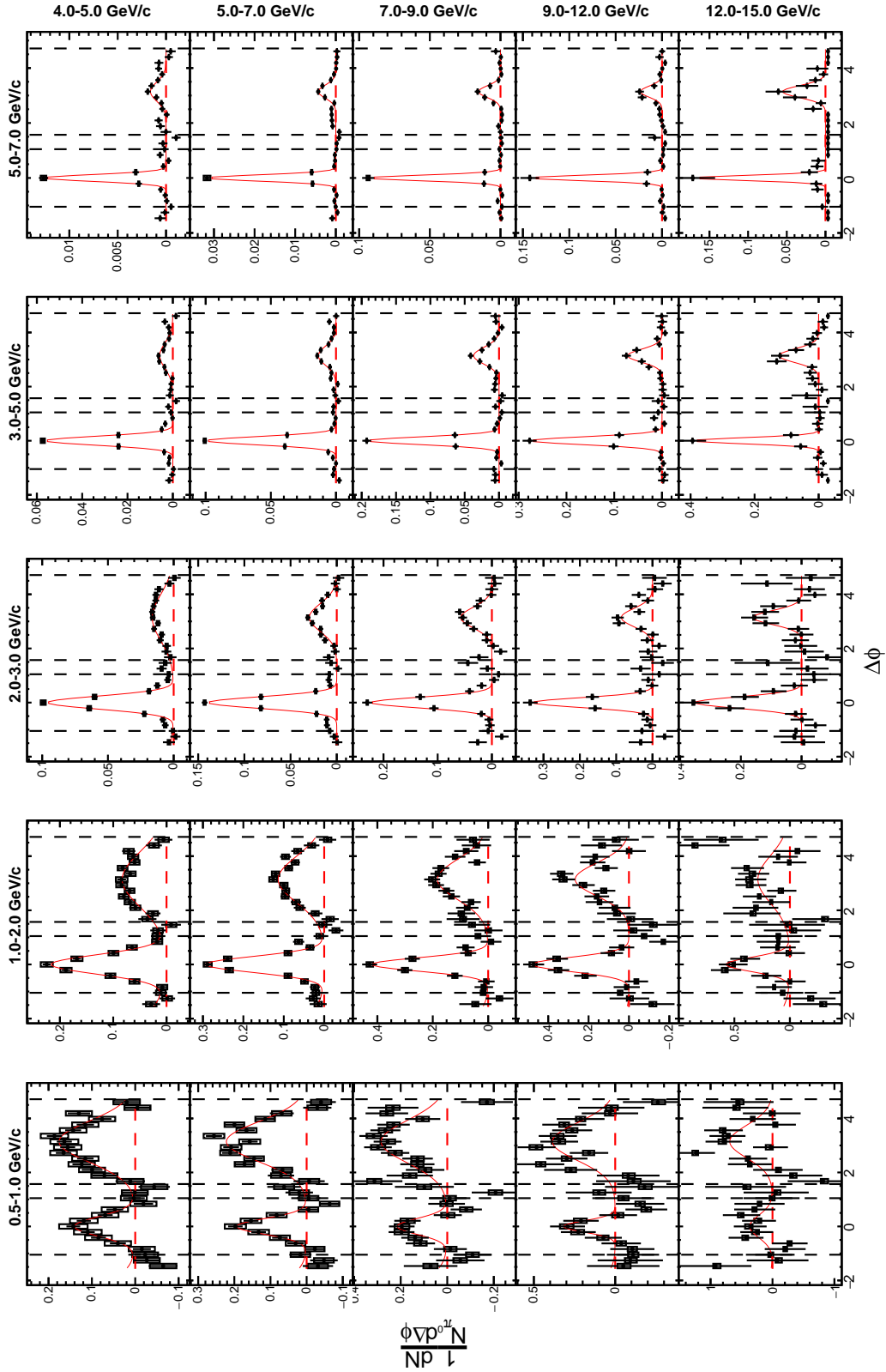


Figure 5.2: Jet functions in 20–40% of 200 GeV $Au + Au$ collisions.

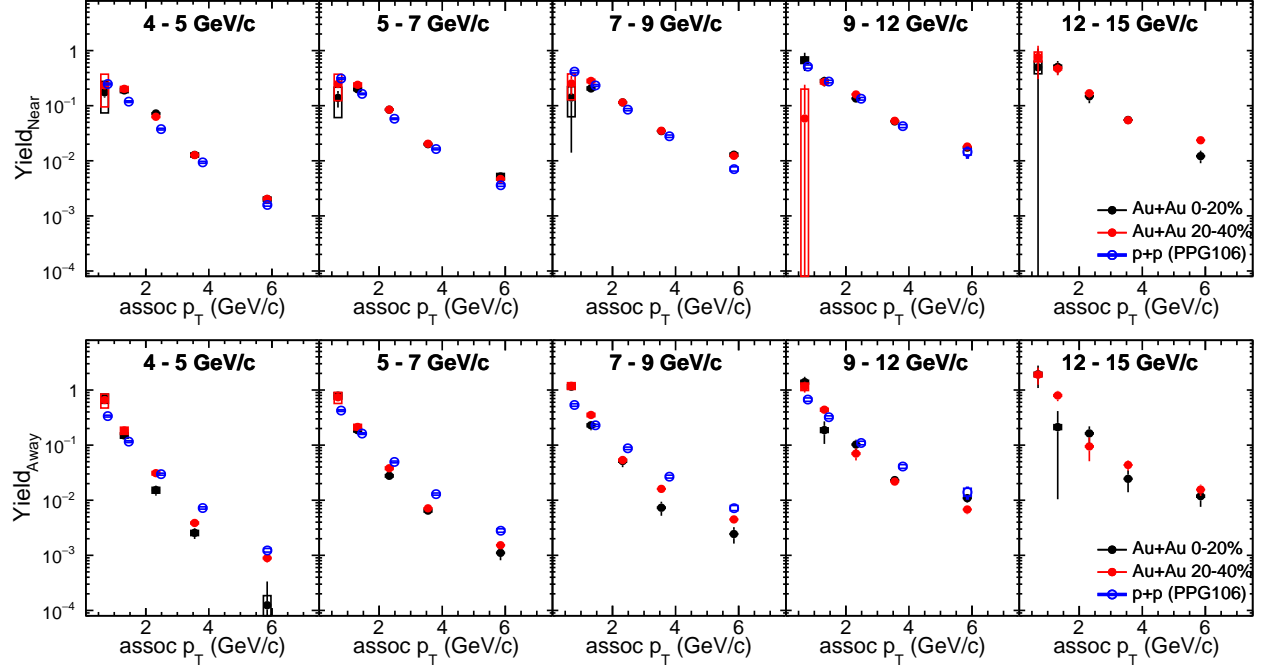


Figure 5.3: Near (top) and away-side (bottom) per trigger yields as a function of associate p_T .

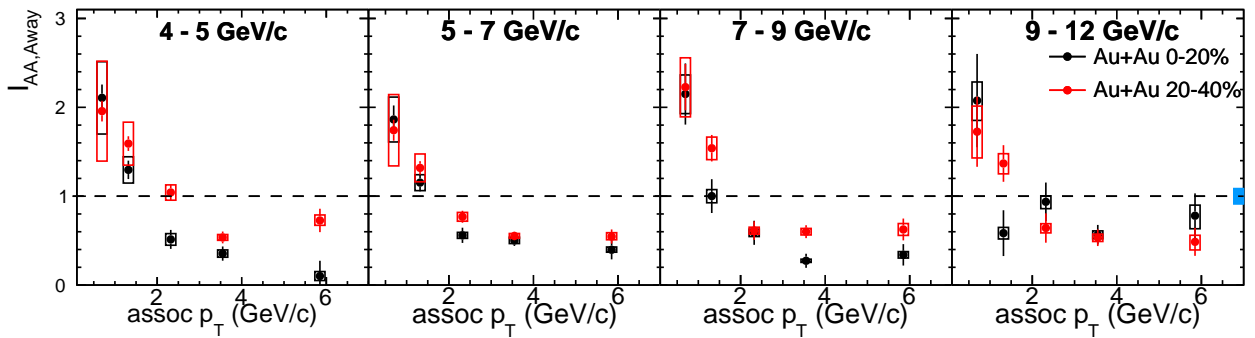


Figure 5.4: I_{AA} as a function of associate p_T in the away-side peaks. The filled blue box is the global scale uncertainty.

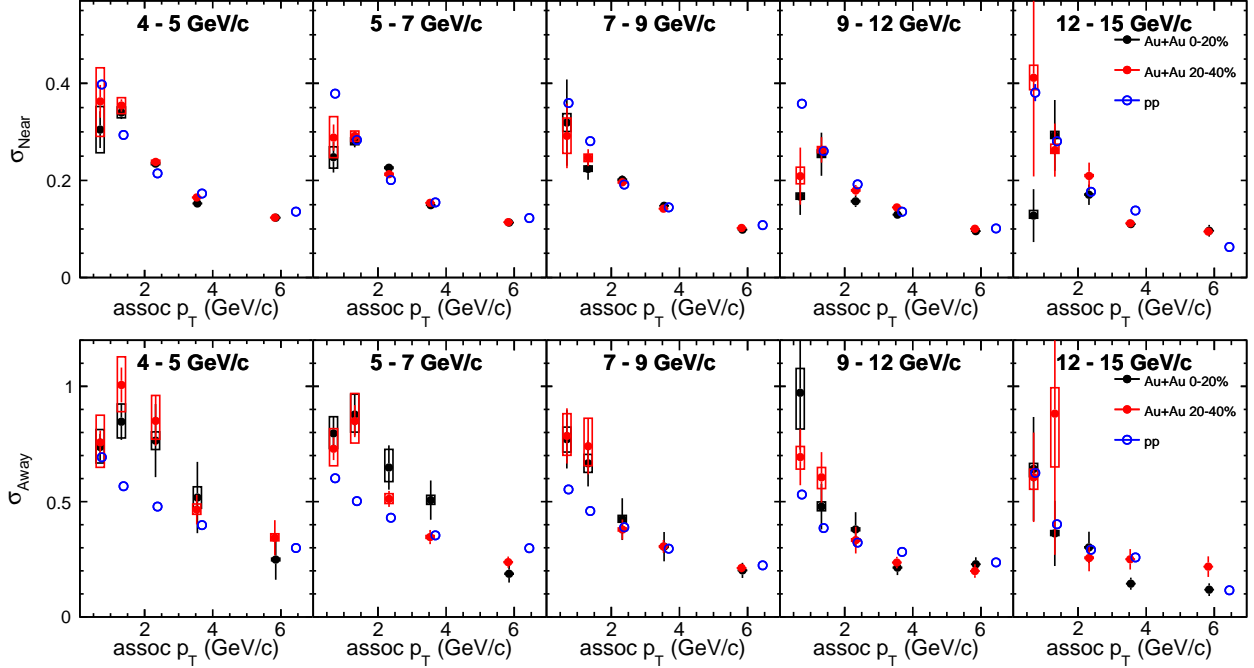


Figure 5.5: Near (top) and away-side (bottom) jet widths as a function of associate p_T .

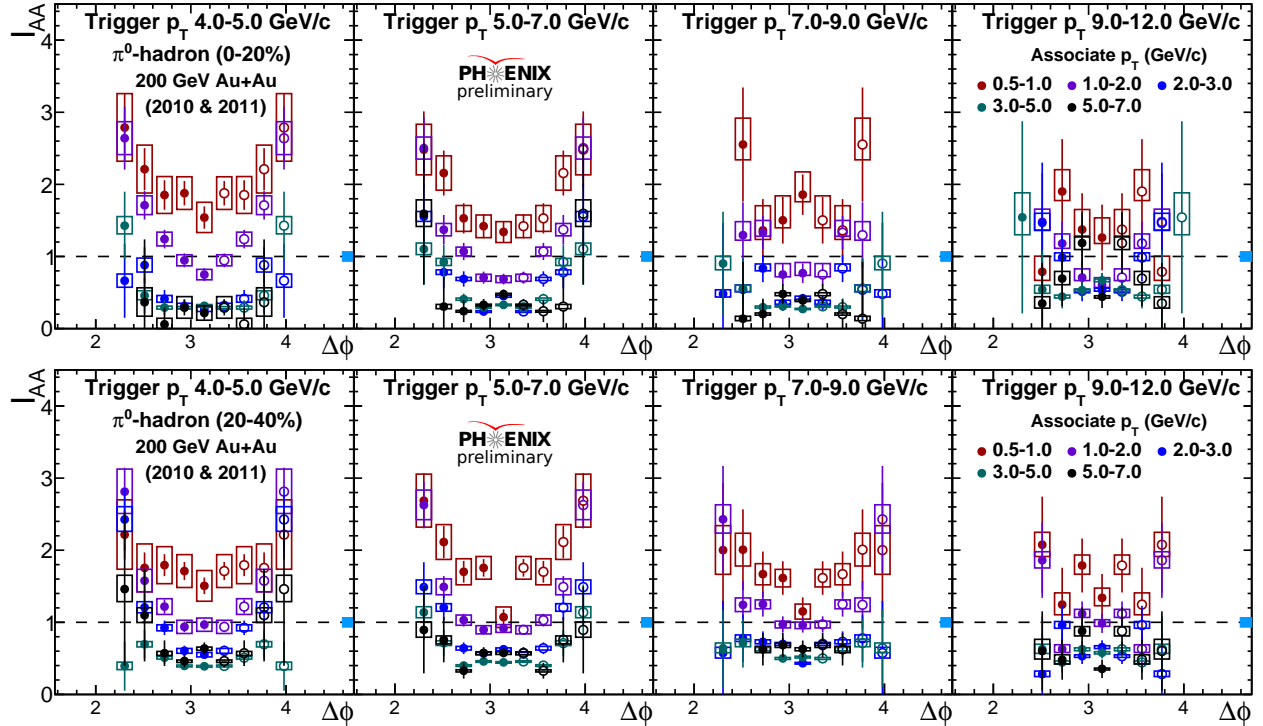


Figure 5.6: Away-side I_{AA} as a function of associate $\Delta\phi$ in 0-20% (top) and 20-40% (bottom) centrality events. The filled blue box is the global scale uncertainty.

CHAPTER 6

Discussions

π^0 -hadron correlation analysis is used to study jet modification in Quark-Gluon Plasma. This study analysed PHENIX data from 2010 and 2011 $Au + Au$ collisions at 200 GeV. Instead of considering only the second order flow harmonics in the background subtraction as in the previous PHENIX analysis [49], this analysis subtracted the second to fourth order flow harmonics to obtain jet functions. The second to fourth order flow harmonic coefficients of charged hadrons and the second order flow harmonic coefficients of neutral pions were measured by PHENIX. The third and fourth order flow harmonic coefficients of neutral pions are estimated using acoustic scaling. The Absolute Normalization method is applied to estimate the level of underlying event in the flow subtraction.

This chapter will compare results from this analysis to other experiment results, and discuss the implications of any agreements and discrepancies.

6.1 Comparisons to $A + A$ Collision Results

This section will show comparisons between the $Au + Au$ results from this analysis and other results from RHIC with the same collision systems. Any agreements between these comparisons are important to validate the experimental results at RHIC. Comparisons to $Pb + Pb$ results will also be shown to study the jet modification's dependencies on system size and energy.

6.1.1 Comparison to PHENIX Results

As mentioned earlier in Section 1.6, this work is an updated analysis of previous PHENIX π^0 -hadron correlations results published in [49]. Besides the increase of statistics from Run 10 and 11

combined data sets, the higher order flow harmonics are also accounted for background subtraction in this analysis. Therefore, this analysis gives results with higher accuracy than the previous PHENIX results [49], which included Run 7 data set alone and subtracted the second order flow harmonics only.

Jet Function Comparisons

The comparisons of jet functions are shown in Figures 6.1 and 6.2. While the systematic uncertainty is not shown in these two figures, the statistical uncertainties and fluctuations are reduced in this analysis because of the accumulated statistics from both data sets. Moreover, the away-side peaks are closer to a Gaussian in the updated analysis as the subtraction of the higher order flow harmonics reduces the shoulder shape in the away-side peak. The shape improvements of the away-side are more obvious at low associate p_T in the central events (0–20%) where the underlying events have stronger influence.

Since higher order flow harmonics are subtracted in this analysis, the near-side jet functions measured in this analysis are expected to be lower than in [49] at low associate p_T . At high associate p_T , the differences in near-side jet functions should be small as underlying flow influence is minimal at high momentum. However, Figures 6.1 and 6.2 shows that there are discrepancies between this analysis and [49] on the near-side peaks at high associate p_T . Because the away-side jet functions agree well between these two analyses, there is suspicion that the near-side discrepancies are due to single photon or photon pairs in data selection. To find the cause of the discrepancies, a detailed diagnostic investigation is documented in appendix A, which shows the effects on the near-side peaks with different single photon or photon pair cuts. However, these cuts do not influence the away-side peak.

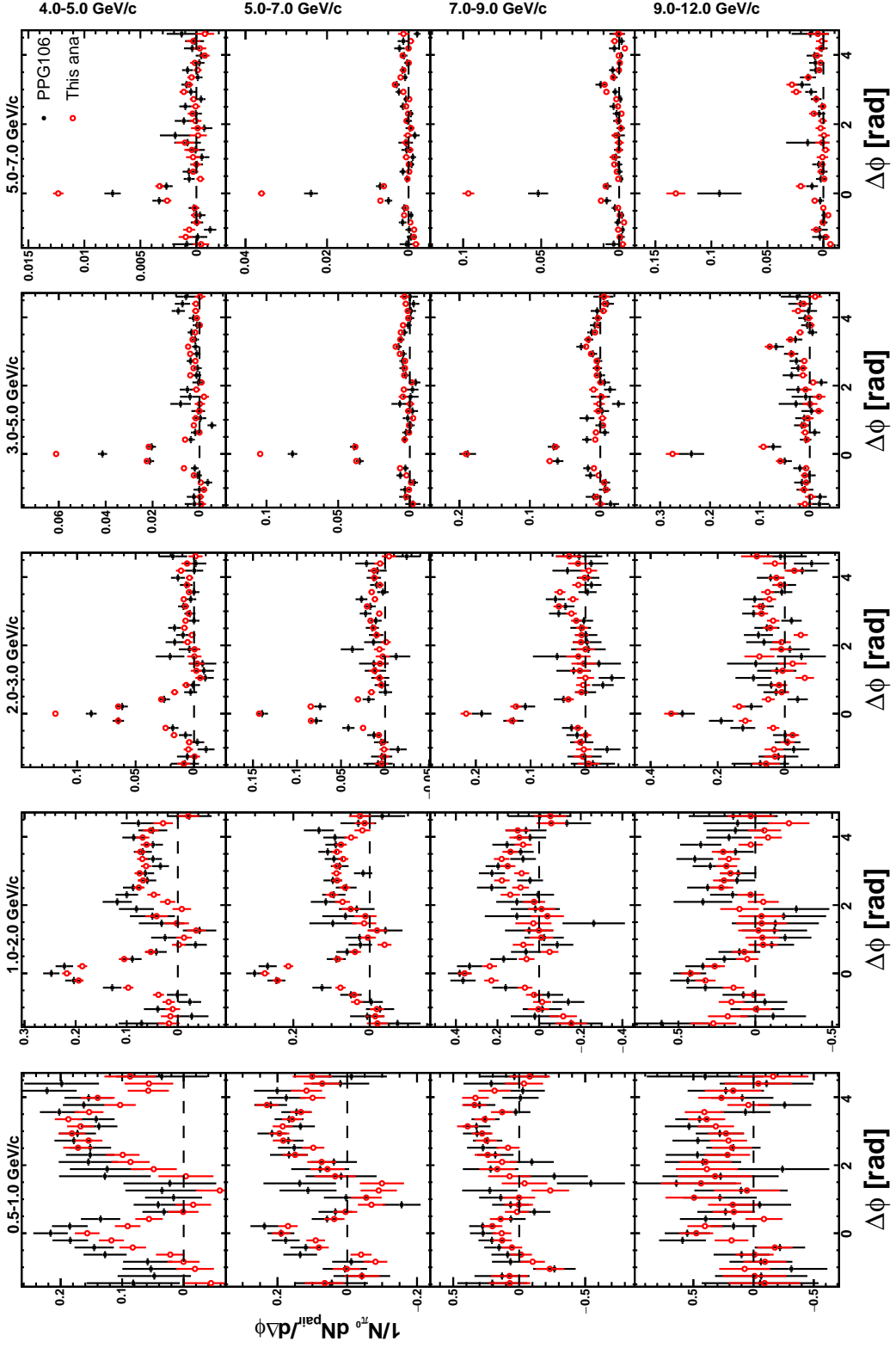


Figure 6.1: Comparison of jet functions in 0–20 of 200 GeV $Au + Au$ collisions. Trigger p_T and associate p_T are labeled on the side and the top of the figure, respectively. The jet functions from this analysis are drawn as black dots, results from [49] are shown as red circles.

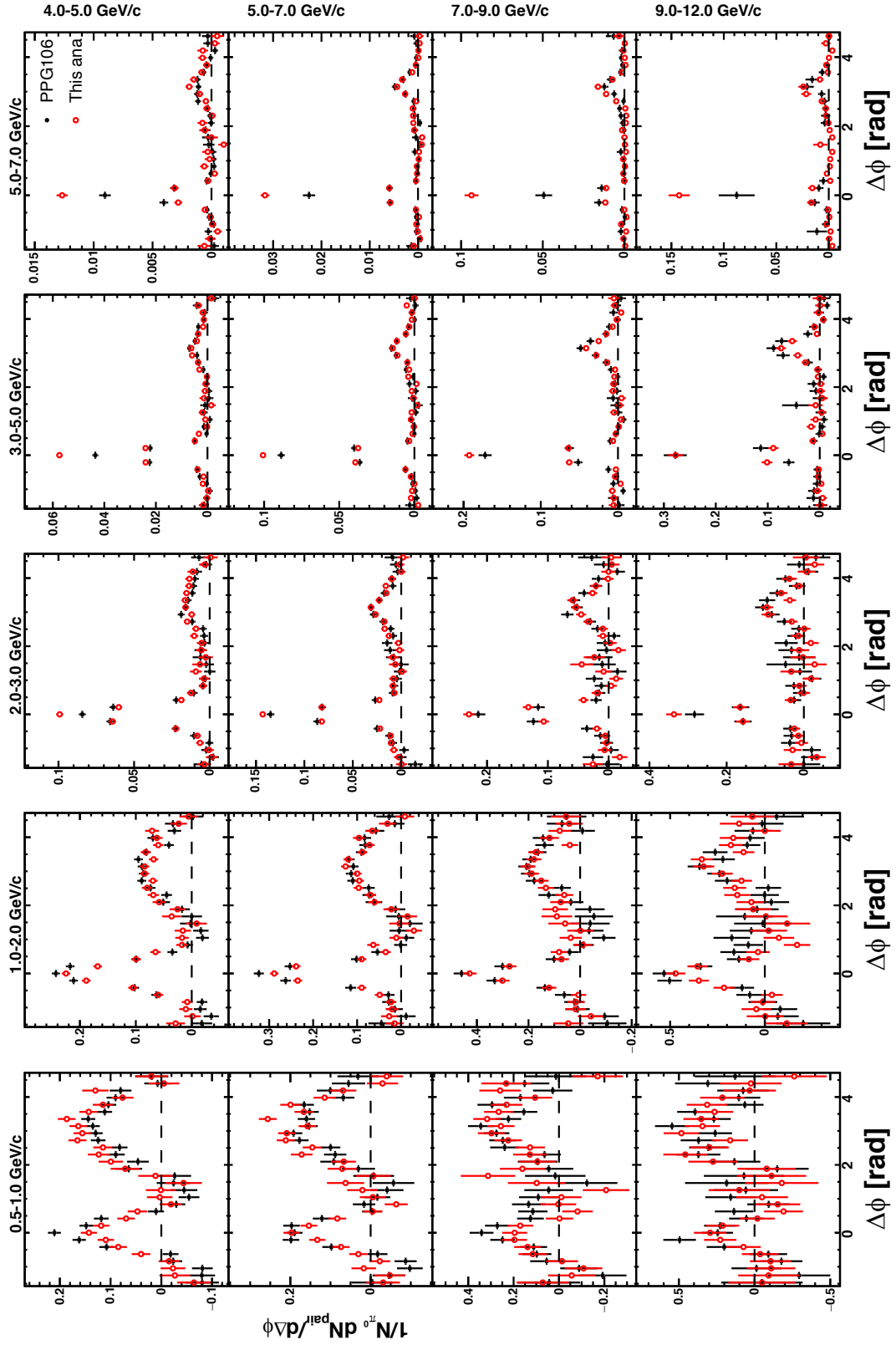


Figure 6.2: Comparison of jet functions in peripheral events 200 GeV $Au + Au$ collisions. The jet functions from this analysis are in 20–40% centrality, results from [49] are in 20–60% centrality.

I_{AA} Comparisons

The less prominent away-side shoulders lead to a reduction in the yields of the away-side in the updated analysis. Thus, the away-side I_{AA} is smaller than that in the previous analysis [49] at low associate p_T . This difference is more noticeable in the 0–20% centrality events where the combinatorial pairs are strong. At high associate p_T where the combinatorial pairs are weak, the difference between this and the previous analysis is small and both results show agreements.

Jet Width Comparisons

Because of the shoulder effect on the away-side is reduced, the away-side jet widths are lower in this analysis than in [49]. The effect is more noticeable in the 0–20% events causing the difference in the jet widths observed in different centrality classes in [49] to be reduced. Moreover, no significant centrality dependence is observed in the present analysis.

6.1.2 STAR Results in 200 GeV Au + Au

Since STAR and PHENIX are part of the RHIC program, crosschecking results between PHENIX and STAR serves as a verification of the physics messages in different studies.

Shown in Figure 6.3 is the away-side I_{AA} in 0–12% central events as a function of z_T from π^0 -hadron correlation analysis at STAR experiment [77] using 200 GeV Au + Au data. This result only includes higher trigger p_T , 12–20 GeV/c with associate p_T particles ranging 1.2–18 GeV/c. For comparison, consider the first two z_T points at about $(0.126, 1.205 \pm 0.038^{+0.45}_{-0.207})$ and $(0.23, 0.148 \pm 0.033^{+0.118}_{-0.068})$, which give p_T equal to 1.44 GeV/c and 2.64 GeV/c. Those are the second and the third associate p_T points in the analysis. The STAR results at $z_T = 0.126$ and 0.23 agree with this analysis at associate $p_T = 1.44$ GeV/c and 2.64 GeV/c in the 4–5 GeV/c, 5–7 GeV/c and 7–9 GeV/c trigger p_T bins (see Table 67 for the numerical results). The deviations in the 9–12 GeV/c

bins are due to statistical fluctuations.

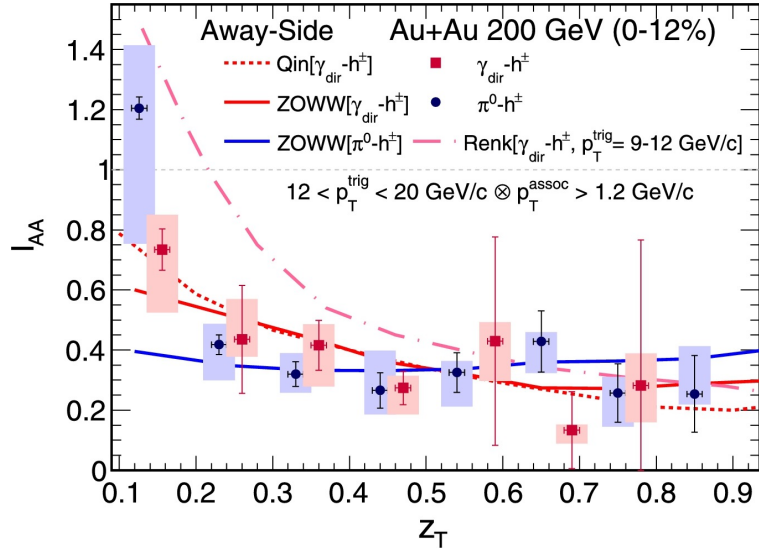


Figure 6.3: Away-side I_{AA} as a function of z_T from 200 GeV $Au + Au$ data from STAR experiment [77]. The results from π^0 -hadron and direct photon–hadron correlations are drawn in blue and red respectively.

6.1.3 ALICE Results in 2.76 TeV $Pb + Pb$

The ALICE experiment focuses on a larger system, $Pb + Pb$ collisions, with a higher kinematic range. Near and away-side I_{AA} results from 2.76 GeV $Pb + Pb$ collisions are shown in Figure 6.4. Similar to this analysis, the away-side I_{AA} is above unity at low associate p_T , but below 1 at high associate p_T . The away-side I_{AA} values in ALICE are close to the PHENIX analysis at high associate p_T . At low associate p_T , however, the ALICE results are noticeably higher than this analysis. Both ALICE results and this analysis show partonic energy loss causing suppression of hard particles in the away-side jets, and the enhancement of soft jet particles. The comparison between ALICE results and this analysis shows that the soft particles in the away-side are more enhanced in larger systems at higher energy.

The near-side I_{AA} results shown on the left of Figure 6.4 are above 1 in a wide associate p_T

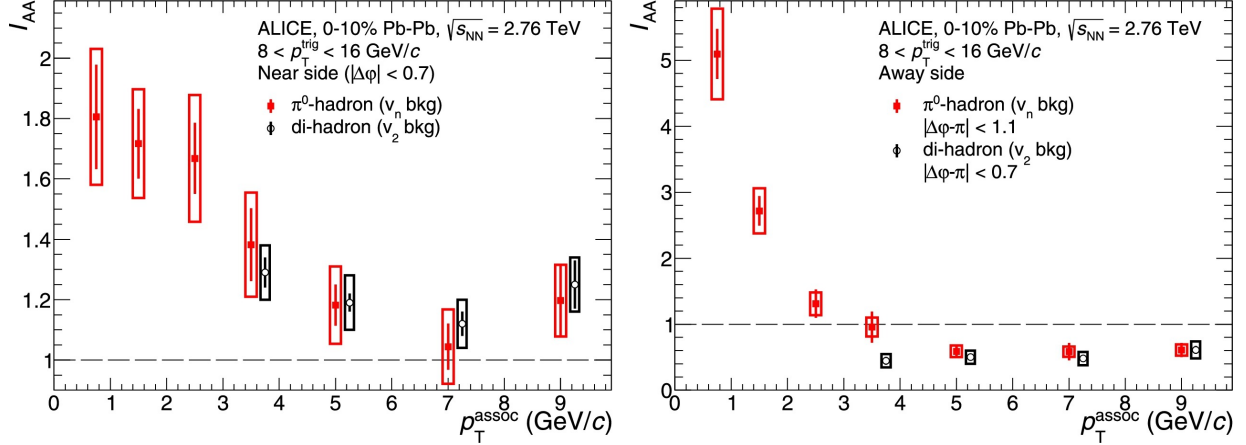


Figure 6.4: Near (left) and away-side (right) I_{AA} as a function of p_T from 2.76 TeV $Pb + Pb$ data from ALICE experiment [78]. The results from π^0 -hadron and hadron-hadron correlations are drawn in red and black, respectively.

range indicating that the near-side jet particles are enhanced. This observation could be due to the high energy of the collision system that jet particles in 2.76 TeV $Pb + Pb$ collisions are expected to have much higher energy compared to RHIC. Therefore, the path length bias raised by the 8–16 GeV/c p_T criteria on the trigger particles is expected to be smaller in ALICE than STAR or PHENIX. That is, the probability of finding trigger particles or near-side jets at the heart of the QGP could be higher at ALICE than at PHENIX or STAR and could lead to near-side jet modifications at ALICE.

6.1.4 ATLAS Results in 5.02 TeV $Pb + Pb$

The ATLAS experiment has similar measurements to I_{AA} as a function of $\Delta\phi$. After reconstructing the jets from data, the yield of the particles within an angular distance r from the jet axis is measured. r is defined as

$$r = \sqrt{\Delta\phi^2 + \Delta\eta^2} , \quad (6.1)$$

where $\Delta\phi$ and $\Delta\eta$ are the differences in azimuth and pseudorapidity between the particles and the jet axis. The yield ratio, that is the ratio of the fragmentation functions, $R_{D(p_T, r)}$, of $Pb + Pb$ to $p + p$ collisions at 5.02 TeV as a function of r measured by ATLAS is shown in Figure 6.5. $R_{D(p_T, r)}$,

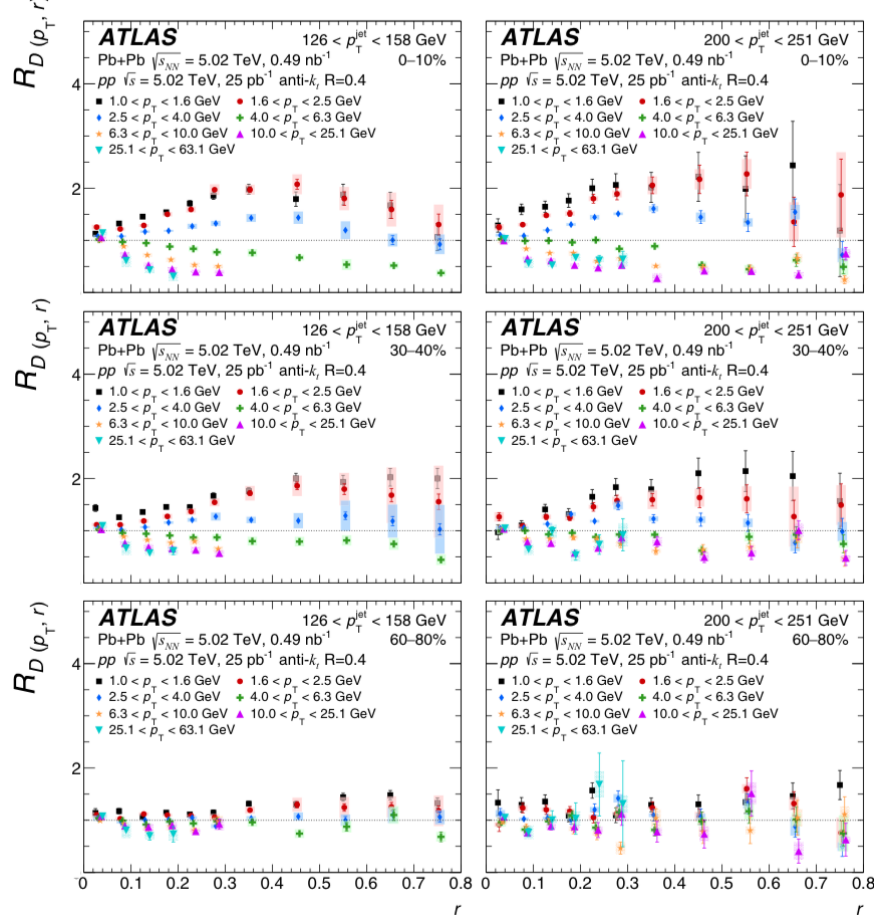


Figure 6.5: Away-side yield ratio of 5.02 TeV $Pb + Pb$ to $p + p$ collisions. from ATLAS [79]. The x axis is the distance of the associate particle measured from the jet axis found in the jet reconstruction.

which is equivalent to I_{AA} , also demonstrates the momentum and angular dependencies of the particle yield modification. At the most central events (0–10%), the soft particles are enhanced in the r range. Similar to the $I_{AA}(\Delta\phi)$ in this analysis where enhancement of soft jet particles rises at large $\Delta\phi$, the enhancement of soft jet particles in ATLAS results is more pronounced at large r .

At 4–6.3 GeV/c, the particles near the core of the jets ($r \approx 0$) experience little to no modification, while particles at the skirt of the jets ($r > 0$) are clearly suppressed. At even higher momentum, the particles are suppressed in the jets. However, in the peripheral events (60–80%), $R_{D(p_T,r)}$ is close to 1 in different traversed momentum indicating that the modifications are small due to the limited amount of the QGP produced in peripheral collisions.

6.2 Comparison to Small System Results

The purpose of small systems studies is to quantify the cold nuclear matter effects, that is the effects caused by initial nuclear stages rather than the QGP. However, recent PHENIX results showed non-zero flow harmonic coefficient v_n ($n = 2, 3$) at 200 GeV $p + Au$, $d + Au$ and $^3He + Au$ collisions, indicating the presence of the QGP in these small systems [80]. These results revolutionized our understanding of the QGP production. On the other hand, these results raised questions in jet modification studies in small systems: how much of the jet modifications are due to cold nuclear matter effects or QGP? Theoretical models are needed to distinguish the cold and hot nuclear matter effects in order to answer this questions. However, different experimental studies can help constrain theoretical models.

I_{AA} as a function of z_T measured in $d + Au$ and $^3He + Au$ collisions at 200 GeV is shown in Figures 6.6, where z_T is the p_T ratio of the associate particle to the trigger particle. z_T is used as an approximate of the fragmentation parameter, z , that was introduced in section 1.5.2. The near-side I_{AA} shown on the left of Figure 6.6 agrees with unity indicating no modification on the near-side jets. The away-side I_{AA} is smaller than unity at high z_T which corresponds to high associate p_T . At low z_T which corresponds to low associate p_T , away-side I_{AA} agrees with unity considering the size of the systematic uncertainty. The away-side I_{AA} suggests that the hard particles of the

away-side jets are suppressed. The away-side I_{AA} also hints to an enhancement of the soft particles of the away-side jets. However, the systematic uncertainties are too large at low z_T to make any conclusion of jet modification.

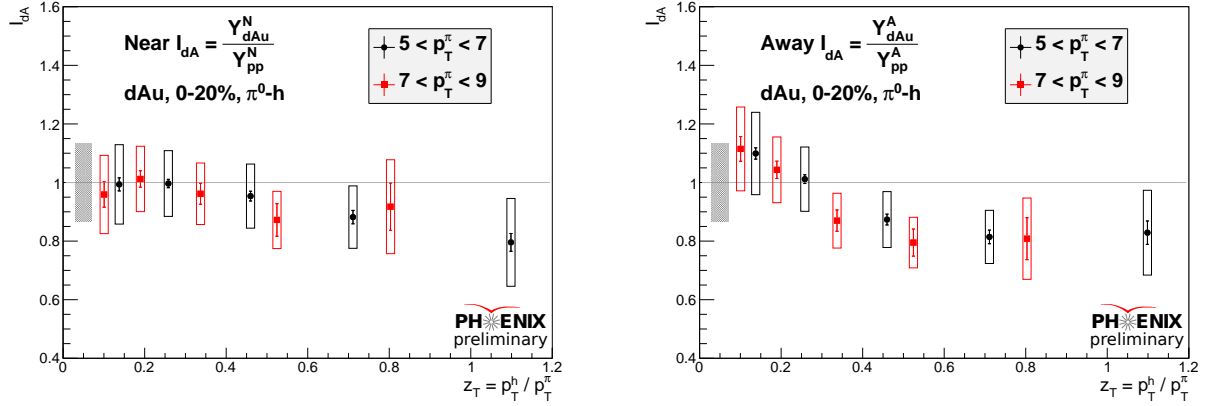


Figure 6.6: Near (left) and away-side (right) I_{AA} as a function of z_T in 200 GeV $d + Au$ collisions [81].

To reduce the systematic uncertainty of the away-side measurements in the small systems, a double ratio,

$$R_I = \frac{I_{AA}^{away}}{I_{AA}^{near}} , \quad (6.2)$$

is introduced. R_I , which is the I_{AA} ratio of the away-side to the near-side jets, is used to study away-side jet modification in small systems. Since $I_{AA}^{near} \approx 1$ indicating no or very little near-side jet modification, the double ratio measurements will give similar values as the away-side I_{AA} . The benefit of the double ratio is that the away and near-side I_{AA} is from the same jet function measurements, and some sources of the systematic uncertainties, such as hadron efficiency, cancel out in the ratio. Figure 6.7 shows R_I as a function of z_T from $d + Au$ collisions. R_I is mostly

below unity at high z_T (> 0.25) indicating suppression of hard particles in the away-side jets. With smaller systematic uncertainty compared to away-side I_{AA} , R_I is above 1 at low z_T (< 0.2) showing enhancement of the soft particles in the away-side jets.

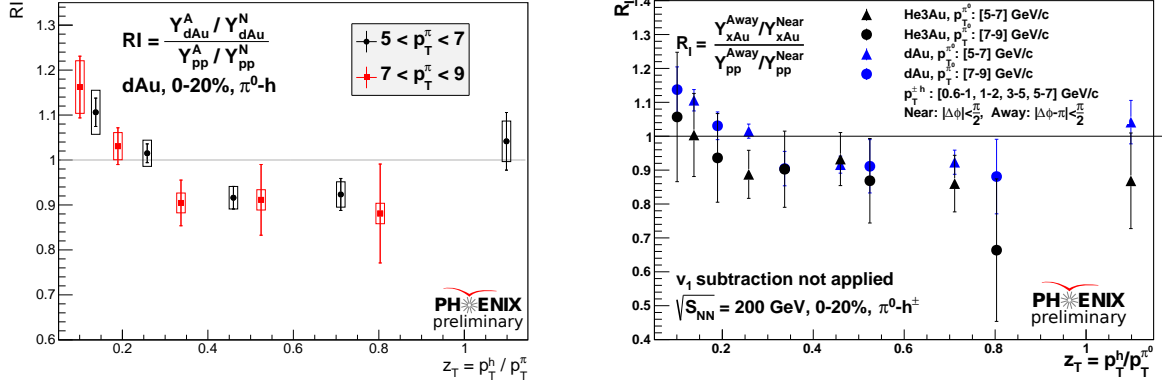


Figure 6.7: Left: R_I as a function of z_T in 200 GeV $d + Au$ collisions [81]. The vertical bars and boxes are the statistical and systematic uncertainty, respectively. Right: Comparison of R_I in 200 GeV $d + Au$ and $^3He + Au$ collisions [81]. The statistical error is drawn as vertical bar. Systematic uncertainty is not shown in this plot.

A comparison of R_I between $d + Au$ and $^3He + Au$ is also shown on the right of Figure 6.7.

R_I from $^3He + Au$ measurements is consistent with $d + Au$ results considering the size of the uncertainty. However, the $^3He + Au$ R_I is systematically lower than the $d + Au$ results, hinting to stronger suppression on hard particles of the away-side jets.

Comparing to the away-side I_{AA} results from $Au + Au$ collisions as show in Figure 5.4, the I_{AA} is about 72% higher than the R_I at low associate p_T (low z_T). However, I_{AA} is about 55% lower than the R_I at high associate p_T (high z_T). The differences between the $Au + Au$ and small systems shows that the away-side jets experience significantly more modification by the QGP produced in $Au + Au$ collisions than in small systems.

To summarize, away-side jet modifications in $d + Au$ and $^3He + Au$ collisions at 200 GeV are

shown. The modifications are small compared to the results in $Au + Au$ collisions from this analysis indicating the parton energy loss in small systems is less than in the $Au + Au$ collisions. However, the causes of the parton energy loss in small systems are unclear, as the recent PHENIX results [80], which show evidence of the QGP in $p + Au$, $d + Au$ and $^3He + Au$ collisions, shake the common belief that the jet modifications observed in small systems are purely arising from cold nuclear effects. Both theoretical and experimental efforts are needed to understand the partonic energy loss mechanisms in small systems in order to further study the QGP effects in large systems.

One way to further our understanding of these small systems is to probe the nucleus itself directly with an electromagnetic probe such as an electron. Therefore, Chapter 7 will review the evolution of the nucleon model and introduce proposed Electron-Ion Collider experiments which are required to advance our knowledge of nuclear matter.

CHAPTER 7

Electron-Ion Collider Experiments

To fully interpret the results from the π^0 -hadron correlations in small systems discussed in Chapter 6, a deeper understanding of cold nuclear matter is required. In fact, the smallest nuclear system, that is nucleon, is not even fully understood. The configuration of the confined partons gives rise to the different hadron species and their properties, such as mass and spin. However, even for familiar particles such as the proton, the exact nature of the partonic interactions that give rise to these properties remains unclear.

The commonly known model depicts nucleon constituents with three valence quarks as illustrated in Figure 7.1a. However, the parton distribution functions of a proton from DESY experiments in Figure 7.1c show that the common two-up-one-down-quark proton model is only true in a thin slice of x . At the small x region, the proton in fact is dominated by gluons and sea quarks which are quark-antiquark pairs mainly induced by the fluctuation of color field inside the proton via gluon splitting [83]. The parton distribution function in Figure 7.1c demonstrates that nucleon structure changes with kinematics. It suggests that the nucleon is a collection of valence quarks, sea quarks and gluons as illustrated in Figure 7.1b, where sea quarks and gluons interact constantly. In this updated nucleon model, the motion of the sea quarks and gluons also contribute to the nucleon properties including mass and spin. To construct the comprehensive nucleon tomography in spatial, momentum, flavor and spin space, and study gluon interaction inside the nucleon, the next era of nuclear physics requires an Electron-Ion Collider (EIC). That is, the finest resolution electron microscope in the world.

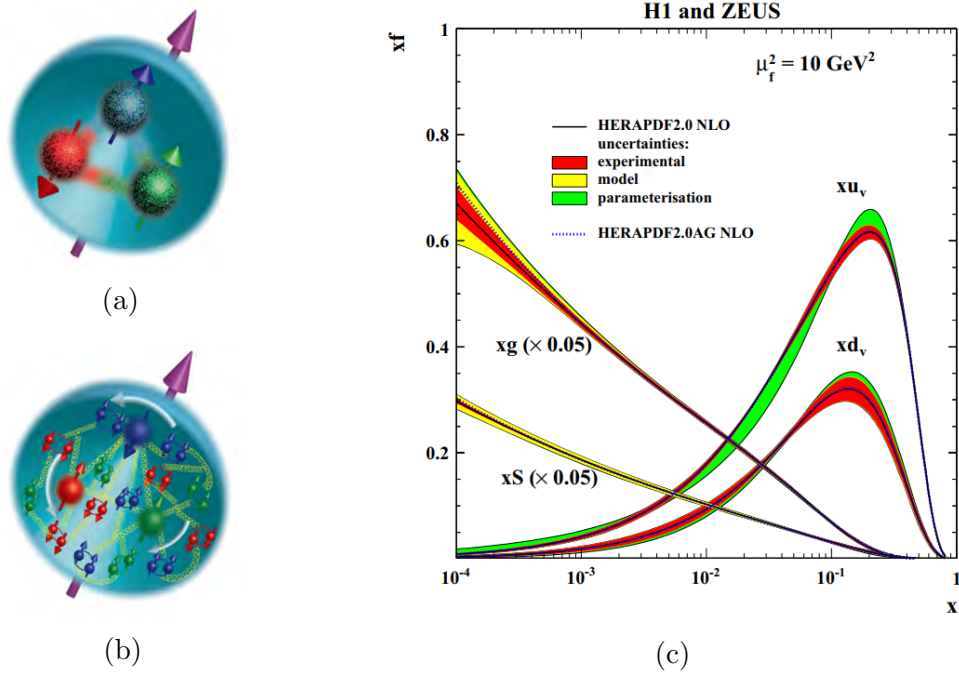


Figure 7.1: (a) The commonly known nucleon model with three valence quarks. (b) The updated nucleon model pictures the nucleon as a collection of valence quarks, sea quarks and gluons. The sea quarks and gluons interact constantly. (c) Parton distribution function of proton measured by HERA and ZEUS [82].

7.1 Electron-Ion Collisions

Figure 7.2 simplifies the electron-ion collision to electron-proton collision. It illustrates that when an electron travels near a proton, a virtual photon is created. This virtual photon will interact with the quarks inside the proton. Then, the electron and the proton lose energy and are deflected, and the struck quark fragments to other final products.

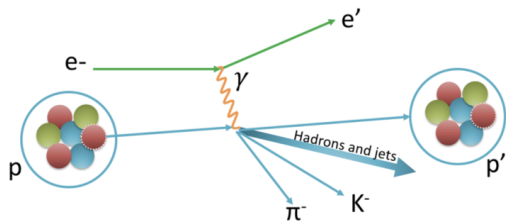


Figure 7.2: Electron-proton collision.

There are several advantages to using an electron as a projectile. The electron is structureless and blind to the strong interactions. Therefore, the interaction between the electron and quarks within the nucleon to purely QED interactions, which are well understood and calculable. Secondly, unlike the QCD, the QED interaction between the electron, the proton, and the induced virtual photon are well understood and calculable. Thirdly, by controlling the momentum of the electron, the wavelength of the virtual photon becomes controllable. The coherent scatterings, where the wavelength of the virtual photon is larger than the size of the target nucleus which thus stays intact, can be used to study multi-parton correlations and the space time distribution of the partons. On the other hand, the incoherent scatterings, where the virtual photon's wavelength is small enough to probe the partons inside the nucleus which breaks up after the scattering, will be used to obtain parton density and study gluon saturation [84]. Furthermore, the comparison between coherent and incoherent scatterings results can be used to study the hadronization of the final products inside or outside the nucleon.

One of the final products, the charged kaon, which has strange quark constituents is the key to access the strange sea quarks distribution of the nucleon. Therefore, charged kaon measurements are a major task in EIC experiments. Charged kaon measurement requires separation between charged kaons and charged pions as they share the same electric charge and have close masses as listed in Table 1.1. Figure 7.3, which shows the kinematic range of the final meson products obtained from simulated EIC events, shows that the kinematics of meson products varies at different rapidity. Therefore, particle identification detectors with different momentum requirements at different location of the EIC detector are suggested by the EIC R&D14 consortium. In the electron-going direction, a modular RICH detector, which is the focus of this chapter, is proposed for K^\pm/π^\pm separation up to 10 GeV/c.

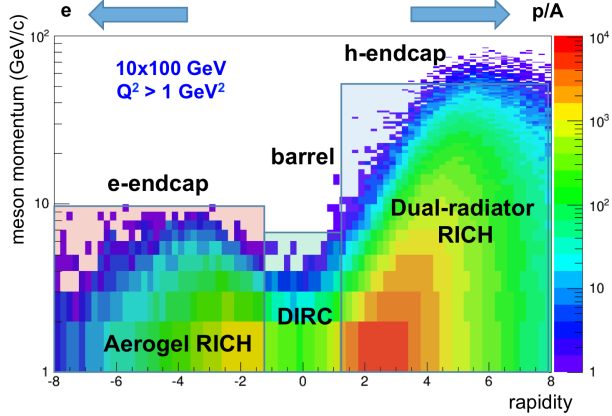


Figure 7.3: Kinematics of meson products in electron-ion collisions as a function of rapidity from simulation. The electron-going direction is in negative rapidity and the ion-going direction is in positive rapidity. The color code indicated amplitude in arbitrary unit [85].

7.2 Modular RICH Detector

The working principle of a RICH detector is detailed in section 2.2.1.1 and 2.2.2. However, this simple RICH design can only provide K^\pm/π^\pm separation at low momentum. Even though there are variations of RICH detectors in different experiments [86–89], these existing RICH designs require large space which is lacking in the EIC detector design. To reduce the size of the RICH detector while still providing sufficient PID performance, a lens-based modular RICH (mRICH) is proposed.

7.2.1 Detector Design

The mRICH detector [90] is a box composed of a block of aerogel, a piece of Fresnel lens, a four-sided mirror set, and a photon sensor plane as illustrated of in Figure 7.4. Aided by the focusing property of the Fresnel lens, the Cherenkov photons that move in parallel are focused to the same point on the sensor plane as illustrated in Figure 7.5. Therefore, the ring image becomes sharper. Furthermore, Figure 7.6 shows a case where the incident charged particles are moving parallel to but off the optical principle axis which is at center of the detector, the Cherenkov photons emitted at the corner of the aerogel will be shifted by the Fresnel lens to the center of the sensor plane,

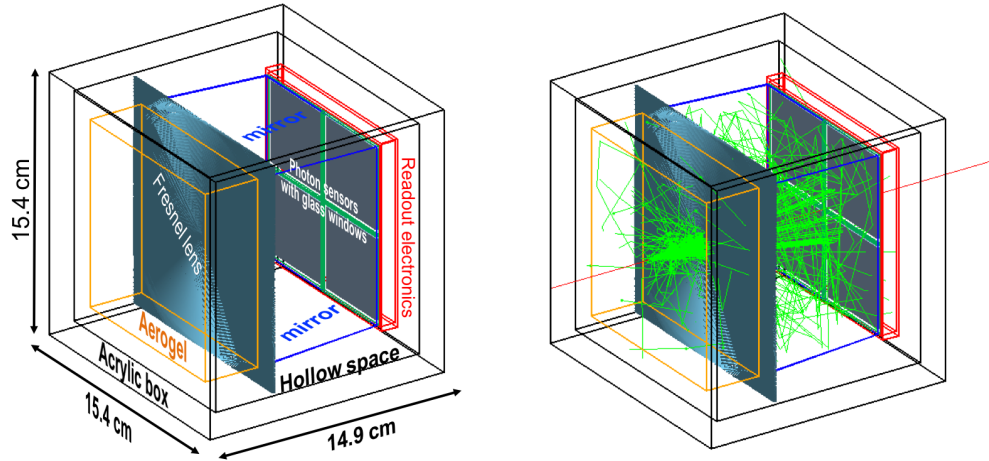


Figure 7.4: Left: mRICH design. Right: simulation with 10 charged pions (red) which emits Cherenkov photons (green).

meaning the ring image will be projected to the central area of the sensor plane.

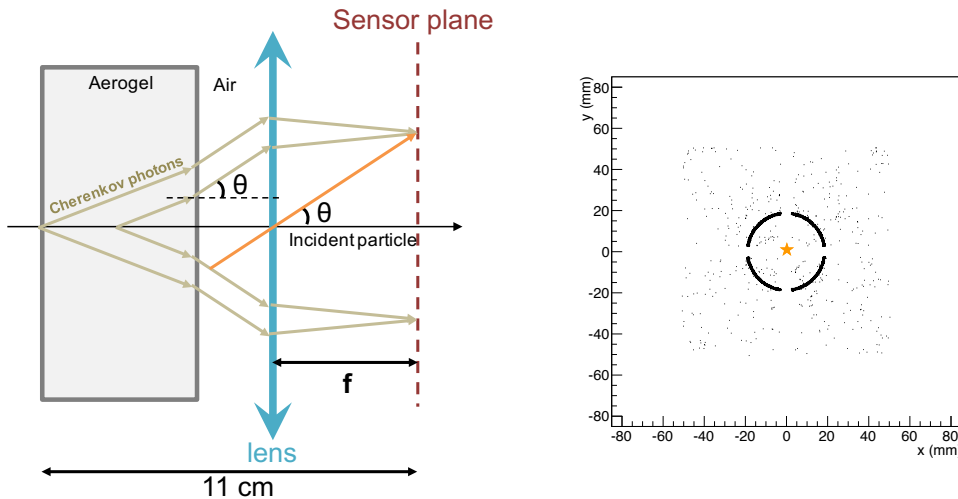


Figure 7.5: Left: optics diagram shows the parallel cherenkov photons are focused by the Fresnel lens on the sensor plane. The orange line, which passes through the center of the lens, is used as guide to find the focal point. Right: Cherenkov ring image from simulation with 10 incident charged pions launched at the center of the detector $x - y$ plane.

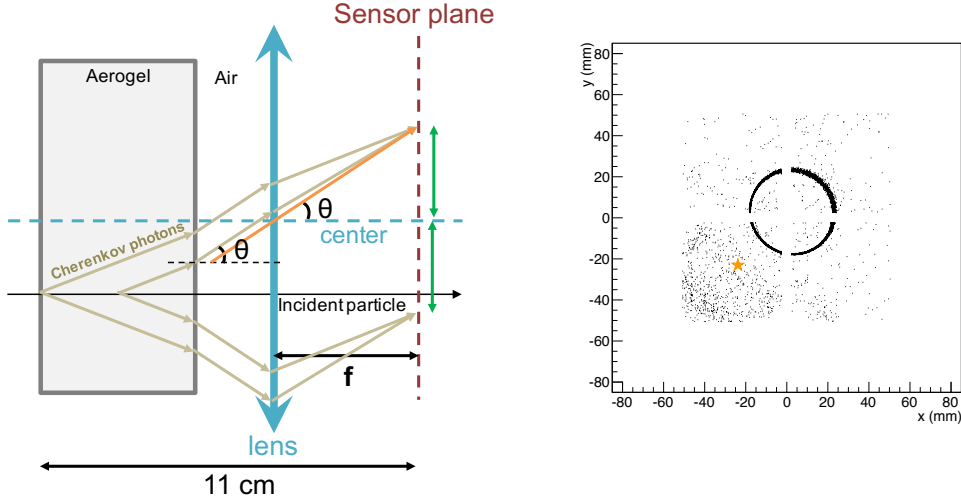


Figure 7.6: Left: optics diagram shows the shifting function of the Fresnel lens when the charged particles incident off the optical principle. Right: Cherenkov ring image simulation with 10 incident charged pions incident at the third quadrant as marked as star.

The first prototype and the key components are shown in Figure 7.7 and 7.8, respectively. The first prototype uses a 3.3 cm thick aerogel block with refractive index $n = 1.03$, an acrylic Fresnel lens with 100 grooves per inch with refraction index $n = 1.49$ and 3" (7.62 cm) long focal length [91]. The sensor plane is covered by four H8500 multianode photon multiplier tubes (PMT) from Hamamatsu [92]. Each H8500 multianode PMT is pixelated to 8×8 channels within a $49 \times 49 \text{ mm}^2$ effective area. Therefore, each anode is about $5.8 \times 5.8 \text{ mm}^2$. In front of the PMTs is a $52 \times 52 \times 1.5 \text{ mm}^3$ glass window. The H8500 multianode PMT is sensitive to visible to ultraviolet light (300–650 nm). The quantum efficiency, the rate of an incident photon convert to electrical signal, of H8500 multianode PMT peak at about 350 nm is around 30% efficiency. Details of the simulation setup and beam test of this prototype will be shown in later sections.

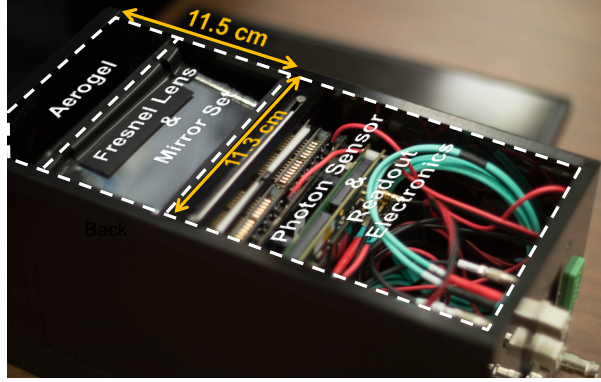


Figure 7.7: First mRICH prototype.

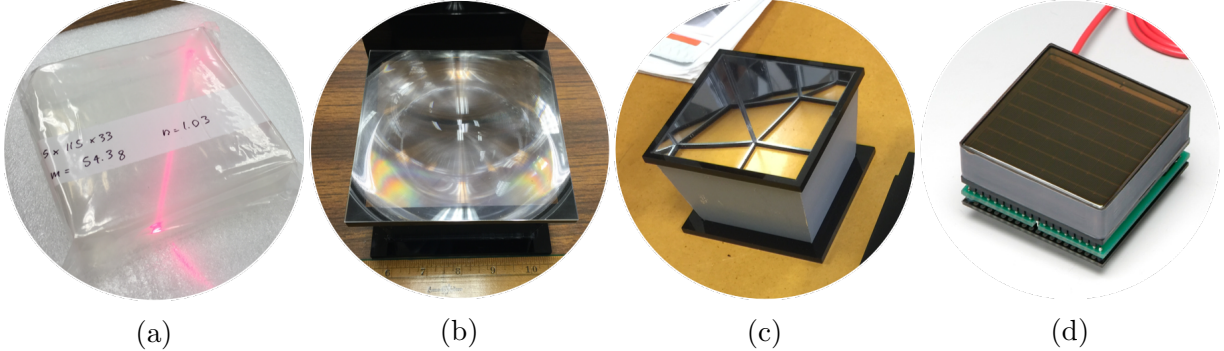


Figure 7.8: Components of the first mRICH prototype. (a) Aerogel, (b) Fresnel lens, (c) four-sided mirror set and (d) H8500 multianode PMT [92].

7.2.2 Analytical Calculations of Cherenkov Ring Information

The separation power, N_σ , which is also known as a number of sigmas, is used to evaluate the particle identification performance. It is defined as

$$N_\sigma = \frac{\Delta\theta}{\sigma_\theta} \sqrt{N_\gamma}, \quad (7.1)$$

where N_γ is the number of photons detected, $\Delta\theta$ is the angular difference between charged pions and charged kaons Cherenkov ring images and σ_θ is the uncertainty of the measurements. The calculations of these quantities will be elaborated in this section. They will help optimize the detector design for better particle identification performance.

7.2.2.1 Calculating Cherenkov Ring Radius

The emission angle of Cherenkov radiation θ_c is given by

$$\theta_c = \cos^{-1} \frac{1}{\beta n}, \quad (7.2)$$

where $\beta = \frac{v}{c}$ is the ratio of incident particle velocity to the speed of light inside the radiator, and n is the index of refraction of the radiator. Considering the refraction at the interface between the radiator and the air, the refracted angle θ of a Cherenkov photon can be calculated using Snell's law

$$\begin{aligned} \frac{\sin \theta}{\sin \theta_c} &= \frac{n}{n_{air}} \\ \sin \theta &= n \cdot \sin \theta_c. \end{aligned} \quad (7.3)$$

Using the Pythagorean theorem and Equation (7.2), Equation (7.3) becomes

$$\sin \theta = \frac{\sqrt{n^2 \beta^2 - 1}}{\beta}. \quad (7.4)$$

Applying the Pythagorean theorem again, then we can express θ as a inverse tangent function, such that

$$\theta = \tan^{-1} \sqrt{\frac{n^2 \beta^2 - 1}{1 - (n^2 - 1)\beta^2}}. \quad (7.5)$$

and the Cherenkov ring radius is

$$\begin{aligned} r &= f \cdot \tan \theta \\ &= f \sqrt{\frac{n^2 \beta^2 - 1}{1 - (n^2 - 1)\beta^2}} \end{aligned} \quad (7.6)$$

The Lorentz factor β can be expressed in terms of particle momentum and mass

$$\begin{aligned} \beta &= \frac{p}{\sqrt{p^2 + m^2}} \\ \beta^2 &= \frac{p^2}{p^2 + m^2}. \end{aligned} \quad (7.7)$$

Then, Equation (7.6) becomes

$$r = f \sqrt{\frac{(n^2 - 1)p^2 - m^2}{(2 - n^2)p^2 - m^2}}. \quad (7.8)$$

To determine the required pixel size of the photon sensor, it is important to study the radius difference of ring images between charged pions and kaons

$$\begin{aligned} \Delta r &= r_{\pi^\pm} - r_{K^\pm} \\ &= f \sqrt{\frac{(n^2 - 1)p^2 - m_{\pi^\pm}^2}{(2 - n^2)p^2 - m_{\pi^\pm}^2}} - f \sqrt{\frac{(n^2 - 1)p^2 - m_{K^\pm}^2}{(2 - n^2)p^2 - m_{K^\pm}^2}} \\ &= f \left(\sqrt{\frac{(n^2 - 1)p^2 - m_{\pi^\pm}^2}{(2 - n^2)p^2 - m_{\pi^\pm}^2}} - \sqrt{\frac{(n^2 - 1)p^2 - m_{K^\pm}^2}{(2 - n^2)p^2 - m_{K^\pm}^2}} \right). \end{aligned} \quad (7.9)$$

Equation (7.9) shows that the radius difference between charged pions and kaons' rings is a function of the Fresnel lens focal length, refractive index n of the radiator, incident particle mo-

mentum and mass. The first take away of Equation (7.9) is that the radius difference is proportional to the Fresnel lens focal length. Thus, a Fresnel lens with longer focal length will provide higher separation. Equation (7.9) is plotted as a function of refractive index of the radiator in Figure 7.9a which shows that the difference in ring radius, Δr , is a non-monotonic function. Δr exponentially increases as the refractive index reaches 1 or about 1.41. Therefore, extremely light weight and fragile materials such as aerogel or dense material such as water and glass may serve well as the Cherenkov radiator. However, dielectric materials with a refractive index of about 1.3 are rare, while materials with a refractive index above 1.41 reduces the momentum limits of a RICH detector due to internal refraction.

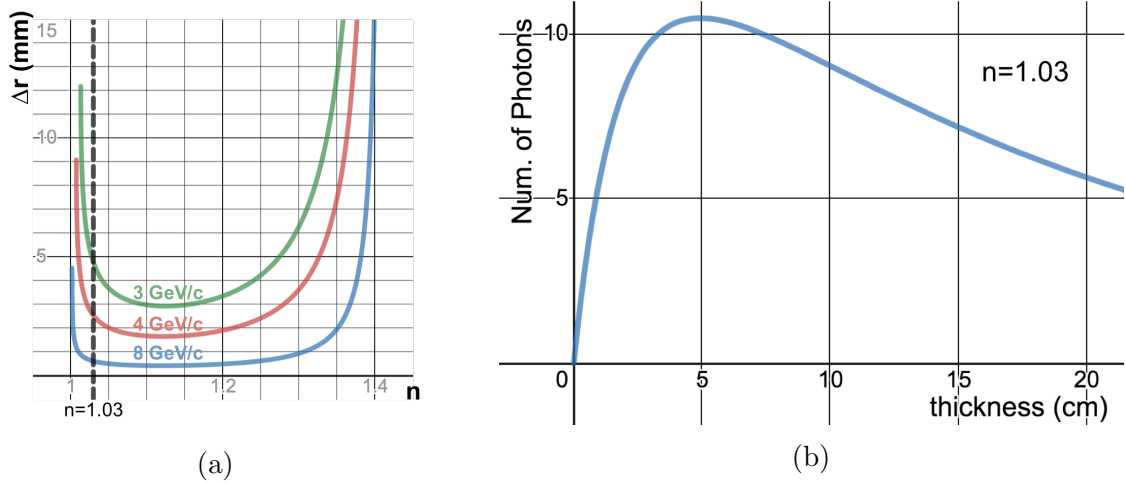


Figure 7.9: (a) Ring radius differences as a function of refractive index of radiator. (b) Number of photon survived as a function of aerogel radiator thickness.

7.2.2.2 Calculating Number of Photons detected

The number of photons emitted in the radiator is

$$N_\gamma = 2\pi\alpha L \left(1 - \frac{1}{\beta^2 n^2}\right) \int_{\lambda_1}^{\lambda_2} \frac{d\lambda}{\lambda^2}, \quad (7.10)$$

where L is the thickness of the radiator and α is the fine structure constant. However, not all photons survive to reach the photon sensors. Therefore, one should include the transmissions of each component. The number of surviving photons is

$$N_\gamma = 2\pi\alpha L \left(1 - \frac{1}{\beta^2 n^2}\right) \times \int_{\lambda_1}^{\lambda_2} QE(\lambda) \cdot T_{radiator}(\lambda, L) \cdot T_{lens}(\lambda) \cdot T_{glass\ window}(\lambda) \frac{d\lambda}{\lambda^2}, \quad (7.11)$$

where $QE(\lambda)$ is the quantum efficiency of the H8500 photon sensor. $T_{radiator}(\lambda)$, $T_{lens}(\lambda)$, and $T_{glass\ window}(\lambda)$ are the transmissions of the radiator block, Fresnel lens, and glass entrance window of the photon sensor, respectively. The measured transmission of an aerogel radiator that is used in the mRICH design and produced for CLAS12 experiment [93] is fitted with an exponential function

$$T_{radiator}(\lambda, L) = 0.83e^{\frac{-56.29 \times 10^{-20} L}{\lambda^4}}. \quad (7.12)$$

Hence, the number of photons survived is not proportional to the thickness of the aerogel radiator as shown in Figure 7.9b. Figure 7.9b shows that an aerogel with 1.03 refractive index will give a maximum of about 10 photons with an thickness of about 3 cm. If this aerogel is thicker than 5 cm, the number of survived photons decreases due to light absorption.

7.2.2.3 Uncertainty

There are three sources of uncertainty contributing to the measurements. They are the Cherenkov photon emission position, σ_{EP} , chromatic dispersion, σ_{chro} , and sensor pixel size, σ_{pix} . Therefore,

σ_θ in Equation (7.1) is expressed as

$$\sigma_\theta = \sqrt{\sigma_{EP}^2 + \sigma_{chro}^2 + \sigma_{pix}^2}. \quad (7.13)$$

Emission point error

Since Cherenkov photons are emitted along the radiator, the projected ring image has physical thickness in a simple RICH detector. However, in the lens-based design, the Cherenkov photons are focused on the sensor plane. Therefore, the emission point error is eliminated, $\sigma_{EP} \approx 0$.

Chromatic dispersion error

Chromatic dispersion error is due to the fact that the refractive index of the radiator changes with the wavelength of the Cherenkov photon. Thus, there is a fluctuation of the Cherenkov angle leading to image distortion. Chromatic dispersion can be measured by using known light source with different wavelength.

Pixel size error

The uncertainty raised by the pixel size error is given by

$$\sigma_{pix} = \frac{a}{f\sqrt{12}} \cos^2 \theta, \quad (7.14)$$

where a is the pixel dimension, and f is the focal length of the Fresnel lens. Therefore, σ_{pix} can be reduced by using a photon sensor with a smaller pixel size or a Fresnel lens with a longer focal length.

7.2.3 Simulation

Extensive simulation study of mRICH using GEANT4 software [94] is conducted to study detector performance as a standalone module and as a detector system. Although the working principle is well understood, a standalone simulation is crucial to study the causes of the ring image distortion and the development of the particle identification algorithm, while the detector system simulation studies the detector performance with simulated collision events and the effect raised by other detector systems.

7.2.3.1 Standalone Simulation

The standalone simulation discussed here follows the first mRICH prototype design described in section 7.2.1. The aerogel radiator is a $10 \times 10 \times 3.3$ cm 3 block of silica (SiO₂). The Fresnel lens, which is made of acrylic (C₅H₈O₂) with refractive index 1.49, is composed of circular grooves that sit on a 0.06" thick flat surface as shown in Figure 7.10. The tip of each groove is set to 0.0001 mm wide in the radial direction. While the groove width in the radial direction is fixed to 0.254 mm, the width, dz , in the z direction varies in order to achieve focusing performance. dz is determined by the curvature and radial positions, r_{inner} and r_{outer} , of the grooves

$$dz = \frac{\text{curvature}}{2} (r_{outer}^2 - r_{inner}^2) , \quad (7.15)$$

where curvature is a function of focal length and refractive index of the Fresnel lens

$$\text{curvature} = \frac{1}{(n - 1) \times f} . \quad (7.16)$$

The sensor plane is covered by four multianode PMT module. Each module is a layer of $52 \times 52 \times 1.5 \text{ mm}^3$ glass window made of borosilicate glass (also known as Pyrex glass) followed by a $48 \times 48 \text{ mm}^2$ sensor. Between each module, there is a 1 mm air gap which is for the supporting structure for each sensor module in the prototype. Note that the sensor material is simplified to a layer of air in the simulation. Furthermore, it is not pixelated to reduce the simulation processing time, but the pixelation is implemented in the simulation analysis.

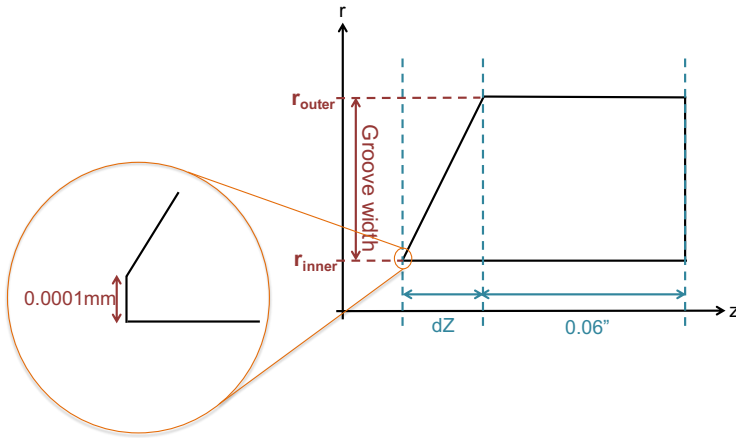


Figure 7.10: Cut view of the groove geometry of the Fresnel lens.

Besides components' geometry, the optical properties of the aerogel radiator, the Fresnel lens and the photon sensors, are key in a RICH detector simulation. These optical properties, including refractive index, transmission and Rayleigh scattering, are defined in the simulation setup as functions of photon energy, while the quantum efficiency of the photon sensors is implemented as a function of photon wavelength in the simulation analysis. Since transmission depends on both the material of the component and the path length travelled by the photon, an absorption length variable is implemented in the simulation in order to set up the transmission property. The absorption length is the average path length the photon travels before it is absorbed by the material.

Rayleigh scattering, a cause of Cherenkov ring image distortion, is also implemented as an

optical property of the aerogel radiator. Rayleigh scattering is the process in which photons are absorbed by a material's molecules, and then re-emitted. Although Rayleigh scattering is an elastic process where the re-emitted photon has the same energy as the absorbed photon, the emission angle is different to the incident angle of the photon [95]. Furthermore, the emission angle depends of the wavelength or energy of the photon. Similar to transmission, Rayleigh scattering is described by the Rayleigh scattering length, the average path length of the photon being scattered.

7.2.3.2 mRICH Subsystem Simulation

The mRICH is a highly adaptable detector that can be implemented in different EIC detector designs including JLEIC and BeAST from Thomas Jefferson National Laboratory and Brookhaven National Laboratory, respectively. The mRICH detector subsystem is integrated in the JLEIC detector simulation as shown in Figure 7.11. The mRICH subsystem, which is sitting at the electron going direction of the JLEIC detector, is arranged in a dish shape with a curvature depending on available space. The center of the mRICH subsystem is not covered to let the beam pipes pass through.

The mRICH subsystem is also implemented in the sPHENIX detector simulation. sPHENIX is the upgrade of the PHENIX detector. The first phase of the upgrade focuses on the brand new electromagnetic and hadron calorimeters with full azimuth and $|\eta| < 1.1$ coverage [96]. A proposed second phase of the upgrade will equip the forward region ($1 < \eta < 4$) of sPHENIX [97]. To enhance the physics capability, the mRICH subsystem is recommended for the the upgrade to the forward capabilities of sPHENIX. The mRICH subsystem is constructed in eight tilted sectors in the simulation as shown in Figure 7.12.

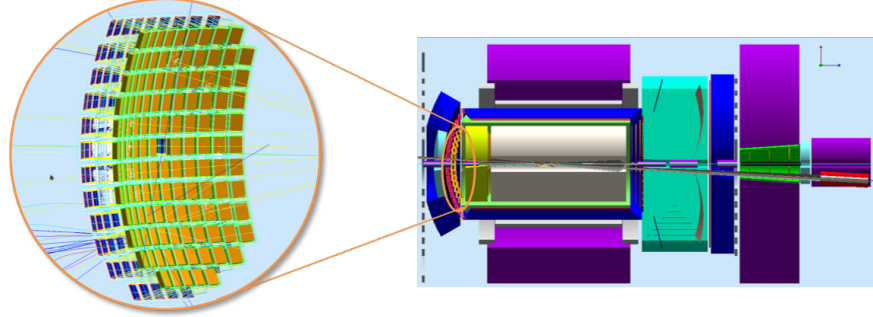


Figure 7.11: mRICH subsystem (left) in JLEIC detector design (left).

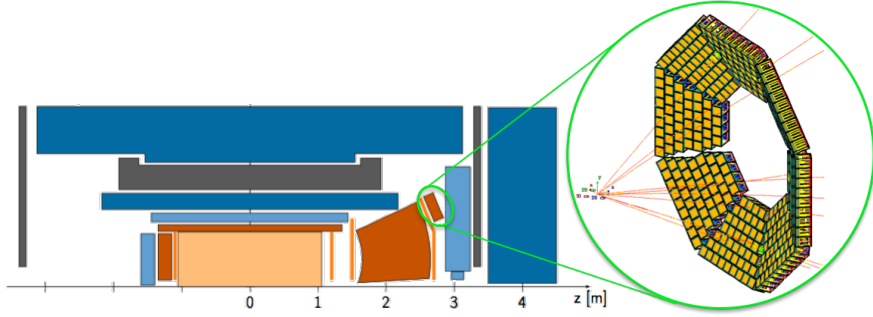


Figure 7.12: mRICH subsystem in sPHENIX detector design.

The fact that the mRICH subsystem can be fully implemented into both the JLEIC and sPHENIX detector designs demonstrates that the versatility of the modulated design of mRICH. The mRICH subsystem can occupy the available space of the detector and adopt different shapes. The modulated design also allows different orientations in order to adjust the incident angle of the particles produced in the experiments. Furthermore, different modules can be plugged in and out for easy maintenance.

7.2.4 First Beam Test

The first beam test was conducted at Fermi National Laboratory (Fermilab) in 2016. The Fermilab beam test facility provides primary proton beams at 120 GeV and secondary charged kaon and pion beam at 4 GeV and 8 GeV. The prototype was housed in an aluminum frame as shown in

Figure 7.13. Two sets of hodoscopes were setup on the front and the back of the prototype. Each hodoscope consisted of four scintillator rods aligned horizontally and four align vertically. In front of the hodoscope in the upstream direction were two plastic scintillator paddles as the event trigger.

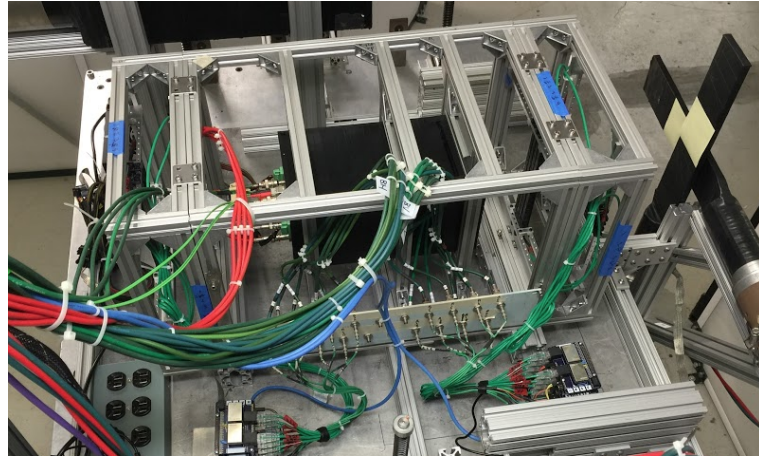


Figure 7.13: First beam test setup.

The 120 GeV primary proton beam was mainly used during the beam test. Benefited by the high momentum and smaller beam size, the primary proton beam provides a saturated ring image which is preferred for testing the detector's working principle in the first beam test. Using equation (7.8) and (7.10), an average ring radius 19.4 mm ring radius and a rate of about 10 detected photons per event were expected.

An event-by-event ring finder algorithm using a voting technique was developed for the both beam test and simulation study. In an event that has at least three photons detected, the algorithm calculates all the possible rings using the coordinates of the center of the fired photon sensor pixel. The ring radius and the center coordinates calculated are then filled in a probability density histogram which is used to extract the most probable ring in an event. Examples of rings from a single event are shown in Figure 7.14.

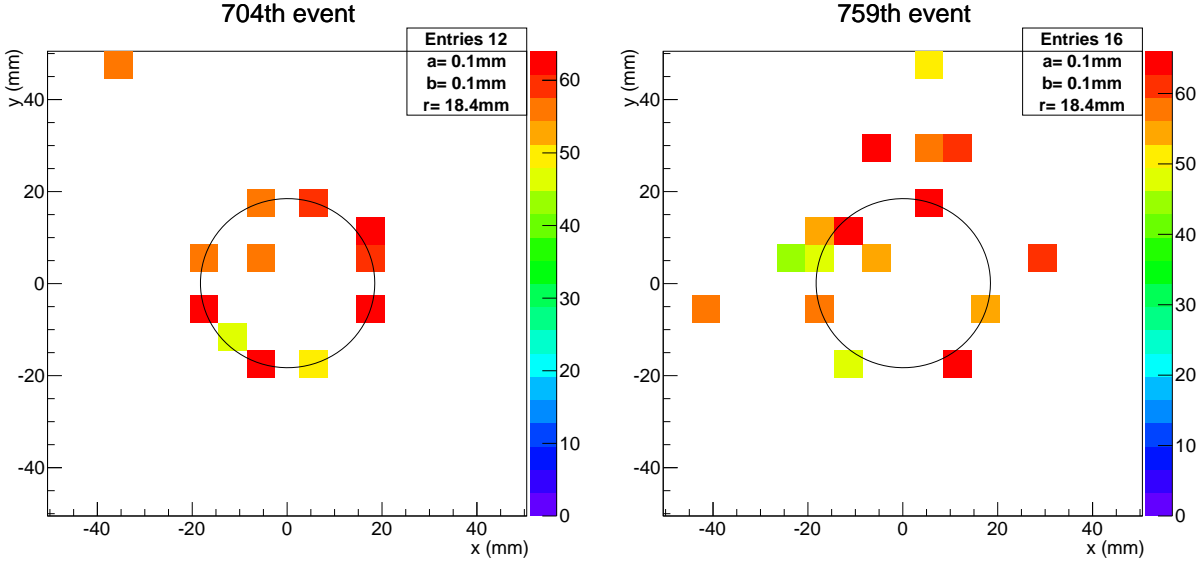


Figure 7.14: Ring images of single events from the beam test data.

The hit maps from accumulated event obtained from the beam test are shown on the left of Figure 7.15 and 7.16. Figure 7.15 shows a ring image formed at the center of the sensor plane when the primary proton beam passes the center of the detector. The hit maps comparison between the beam test and simulation results, shown on the right of Figure 7.15, shows that the beam test data has more noise than in the simulation. However, the numerical comparison in Table 7.1 shows good agreements between the beam test, simulation and the analytical calculation described in section 7.2.2. Note that the number of photons per event listed in the second row of Table 7.1 includes photons that were scattered. The number of photons on the ring found using the ring finding algorithm is about 6.0 per event.

Figure 7.16 shows the accumulated event from the beam test and simulation with 120 GeV/c proton beam hits at the third quadrant of the sensor plane. Both the beam test and simulation results demonstrate the advantage of a lens-based design where ring image is formed at the central area of the sensor plane when charged particles are incident off the center of the detector.

To summarize, the beam test results verified the working principle and the detector simulation with agreement on ring radius and number of photon per event measurements. The beam test results also demonstrate the benefit of using the lens-based design where ring image is formed at the central area of the sensor plane even when charged particles are incident off center of the detector.

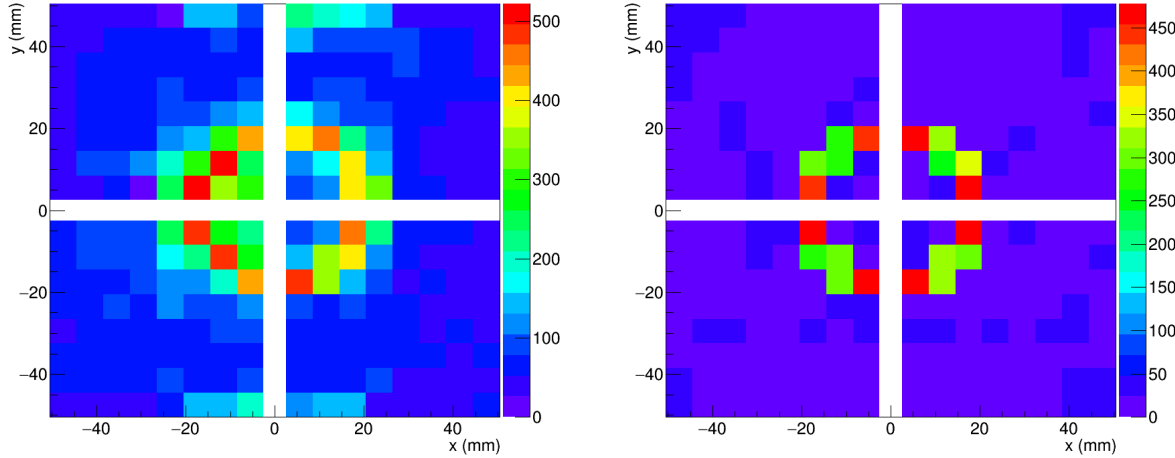


Figure 7.15: Accumulated hit map from 120 GeV proton beam incident at the center of the detector $x - y$ plane. Beam test results are shown on the left and simulation results are shown on the right.

Table 7.1: The radius of the Cherenkov ring image and the number of Cherenkov photons at the sensor plane from the 120 GeV proton beam incident at the center of the mRICH. The total number of photons is the number of photons which reach the sensor plane. The number of photons on the ring is the number of photons counted along the reconstructed ring image.

	Analytical Calculation	Test Beam Data	Simulation
Radius (mm)	19.4	19.0 ± 1.3	18.9 ± 1.0
Total number of photons	10.4	11.0 ± 2.9	11.1 ± 2.9
Number of photons on the ring		5.9 ± 1.8	5.8 ± 1.5

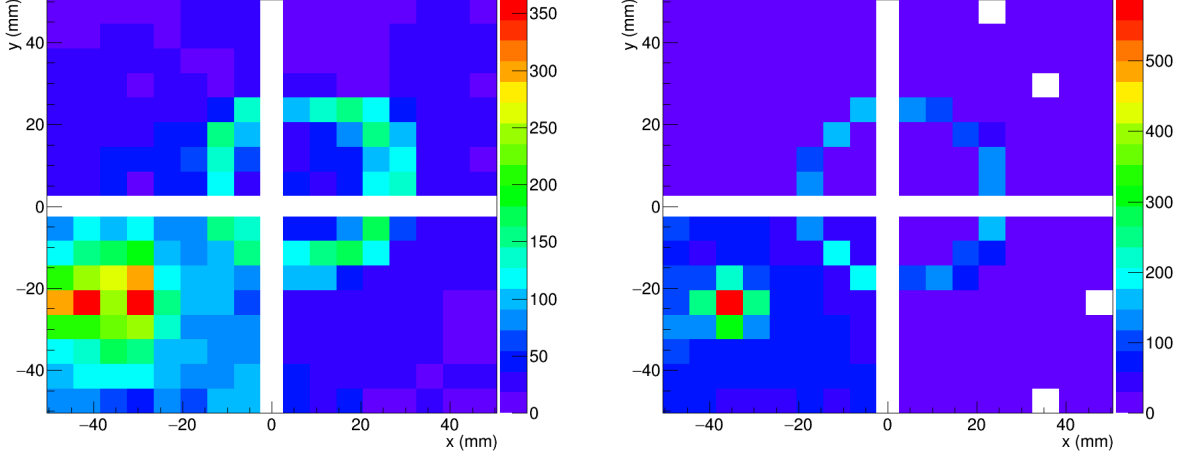


Figure 7.16: Accumulated hit map from 120 GeV proton beam incident at the third quadrant of the detector $x - y$ plane. Beam test results are shown on the left and simulation results are shown on the right. The photon hits in the third quadrant are the Cherenkov photons emitted inside the glass window of the photon sensor.

7.2.5 Second Prototype and Beam Test

To enhance the mRICH particle identification performance, the second prototype, which is shown in Figure 7.17, uses Fresnel lens with a longer focal length and photon sensors with a finer granularity.

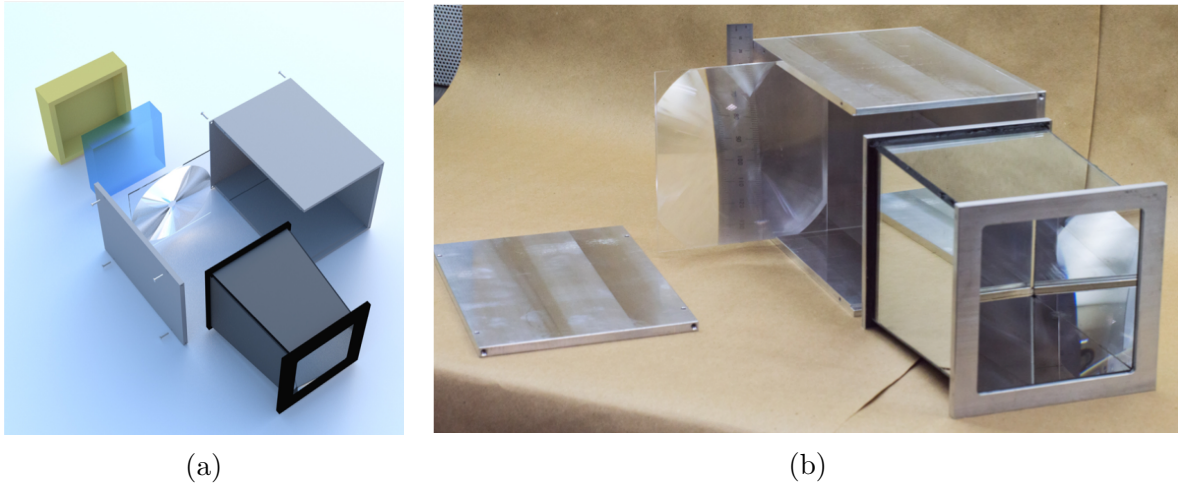


Figure 7.17: (a) Drawing of the second mRICH prototype, (b) The second mRICH prototype.

The Fresnel lens in the second prototype has a 6" (15.14 cm) focal length instead of 3" (7.62 cm).

According to Equations (7.8) and (7.9), both the ring radius, r , and difference of the ring radius, Δr , will be doubled by doubling the focal length of the Fresnel lens. The 6" focal length is expected to give ring radii of 38.7 mm and 38.0 mm for incident charged pions and kaons with 10 GeV/c momentum, respectively.

H13700 multianode PMTs from Hamamatsu with $48.5 \times 48.5 \text{ mm}^2$ effective area and $3 \times 3 \text{ mm}^2$ pixel size [98] are chosen for the second prototype for better resolution. According to Equation (7.13), the uncertainty raised by pixel size is expected to reduce by a factor of 2 as the pixel dimension is reduced from $6 \times 6 \text{ mm}^2$ to $3 \times 3 \text{ mm}^2$.

Figure 7.18 shows the accumulated event from the second beam test result using the second mRICH prototype. A 120 GeV/c primary proton beam was incident to the center of the detector. The accumulated ring image is noticeably larger and sharper which demonstrates the potential of the lens-based detector design.

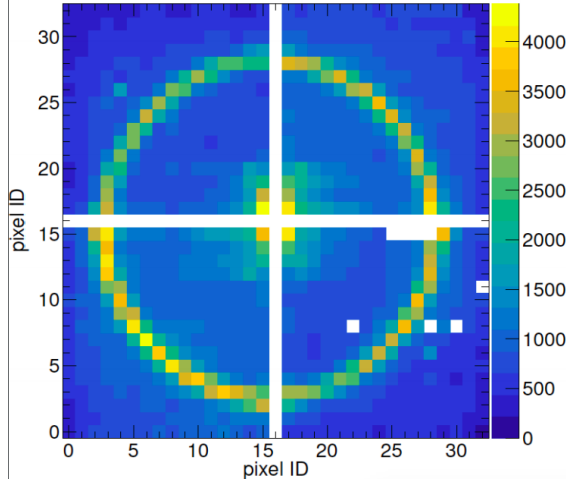


Figure 7.18: Beam test results of the second mRICH prototype. Accumulated hit map from 120 GeV proton beam incident at the center of the detector $x - y$ plane.

7.2.6 Outlook

There are a few more steps toward the realization of the mRICH detector. Firstly, the multianode PMTs do not work well in a strong magnetic field which will be applied near the mRICH subsystem in the EIC detector design. The EIC R&D14 consortium has been exploring the use of other photon sensors such as silicon photomultipliers (SiPMs). Besides the magnetic field, other concerns about the choice of photon sensor include timing resolution, dark rate and radiation tolerance. Secondly, an advanced particle identification algorithm using Bayesian likelihood technique is needed for fast performance in the high luminosity EIC experiments. Unlike the ring finding algorithm used in the beam test analysis, the likelihood technique, which processes different kinds of pattern, can handle different scenarios including different incident position and angle that give a non-circular image. Thirdly, detector simulations with simulated charged kaon and pion information from electron-ion collision events are needed to evaluate the detector subsystem design.

7.2.7 Summary

The future Electron-Ion Collider aims to obtain nuclear tomography in multi-phase space and study gluon and sea quark interactions inside the nucleon. One of the key focuses of the EIC is measuring the strange sea quark distribution via charged kaon measurement. Therefore, a modular RICH detector, a lens-based ring imaging Cherenkov detector, is introduced for charged kaon and pion separation for the EIC experiments. In this lens-based design, the ring image is focused by a piece of Fresnel lens on the photon sensor plane to achieve sharper ring images, allowing for better particle identification performance in a limited volume.

The first mRICH prototype uses an aerogel radiator with 1.03 refractive index, Fresnel lens with 3" focal length, and four H8500 multianode PMTs from Hamamatsu. The prototype was

tested with a 120 GeV/c proton beam at the Fermilab test beam facility, and the beam test results verified the detector working principle and validated the detector simulation. The second prototype with a Fresnel lens of a longer focal length and photon sensors with a finer granularity gives an improved ring image showing the potential particle identification ability of the lens-based detector design, and these improvements have been validated by a second beam test at Fermilab.

Toward detector realization, the EIC R&D consortium is looking for an alternative photon sensor that can perform in high magnetic field and are developing readout electronics that can handle high density of channels of the photon sensor. Likelihood method is under development for fast particle identification performance and for various incident position and angle. Furthermore, physics simulations need to be implemented in detector simulation to evaluate mRICH subsystem design.

CHAPTER 8

Summary

This thesis details two experimental studies which focus on two distinct features of the QCD, asymptotic freedom and confinement. The asymptotic freedom predicts an extreme phase of nuclear matter that is the QGP. Thus, the study of the QGP properties, such as transport coefficients, advances our knowledge of QCD in the extreme energy regime. To do so, this research uses π^0 -hadron correlations as a probe of jets to study parton energy loss in the QGP.

Using 200 GeV $Au + Au$ data with 0–20% and 20–40% centrality collected by PHENIX, this π^0 -hadron correlations analysis subtracts second to fourth order flow harmonics to extract the jet functions. The away-side jet functions are used to study jet angular broadening and yield modification relative to $p+p$ measurements. The results of I_{AA} as a function of transverse momentum indicate hard partons lose energy in the QGP causing a reduction of hard jet particles and an increase of soft particles. Furthermore, the angular width results show that the enhanced soft jet particles spread over a wider azimuthal angle compared to the results from $p + p$ collisions where no QGP is formed, while the suppressed hard jet particles in $Au + Au$ collisions show no significant angular broadening. A new observable, $I_{AA}(\Delta\phi)$, which studies the yield modification at jet substructure level, shows that the soft jet particles are enhanced over a wide range of azimuth but stronger enhancement is shown at the skirt of the jets. Enhancement also observed on the intermediate momentum jet particles found at the skirt of the jet, but little to no suppression occurs to jet particles at the core of the jets. The higher momentum jet particles are suppressed over the full away-side azimuthal range. This is consistent with expectations for gluon radiation as the leading parton traverses the QGP. These new results of yield modifications and angular widths along with the new observable, $I_{AA}(\Delta\phi)$, will provide stronger constraints on parton energy

loss models.

The next era of nuclear physics experiments aim to explore the confinement of QCD via nucleon structure measurements using an Electron-Ion Collider which will be the finest resolution microscope in the world. One of the goals of EIC is to obtain the strange sea quark distribution inside the nucleon through charged kaon measurements. Hence, a lens-based mRICH detector is proposed for K^\pm/π^\pm separation up to 10 GeV/c at the electron-going direction of the EIC detector.

Utilizing the focusing function of a Fresnel lens, the lens-based mRICH detector produces sharper ring images, and thus enhances the particle identification performance at high momentum within a finite volume. The first mRICH prototype was tested at Fermilab. The first beam test results with 120 GeV/c primary proton beams verified the detector's working principle and validated the detector simulation. The updated design with a Fresnel lens of a longer focal length and photon sensors with a finer granularity is implemented in the second mRICH prototype. The beam test results of the second prototype shows improvement in ring images which reaffirms the potential of the mRICH detector.

To conclude, this work cover the studies in both heavy-ion collisions and the future electron-ion collisions to help elucidate the phase diagram of nuclear matter with a deeper understanding of QCD.

REFERENCES

- [1] J. Osman, 100 Ideas that Changed the World, Ebury Publishing, 2011.
 URL <https://books.google.com/books?id=SescGntKYTkC>
- [2] D. I. Kazakov, The higgs boson is found: what is next?, *Physics-Uspekhi* 57 (9) (2014) 930–942.
 doi:[10.3367/ufne.0184.201409j.1004](https://doi.org/10.3367/ufne.0184.201409j.1004).
- [3] S.L. Glashow, The renormalizability of vector meson interactions, *Nucl. Phys.* 10 (1959) 107–117. doi:[10.1016/0029-5582\(59\)90196-8](https://doi.org/10.1016/0029-5582(59)90196-8).
- [4] A. Salam, Weak and Electromagnetic Interactions, *Conf. Proc. C* 680519 (1968) 367–377.
 doi:[10.1142/9789812795915_0034](https://doi.org/10.1142/9789812795915_0034).
- [5] S. Weinberg, A model of leptons, *Phys. Rev. Lett.* 19 (1967) 1264–1266. doi:[10.1103/PhysRevLett.19.1264](https://doi.org/10.1103/PhysRevLett.19.1264).
- [6] S. Narison, QCD as a Theory of Hadrons: From Partons to Confinement, Cambridge University Press, 2004. doi:[10.1017/CBO9780511535000](https://doi.org/10.1017/CBO9780511535000).
- [7] V. Khachatryan, et al., Measurement of the inclusive 3-jet production differential cross section in proton–proton collisions at 7 tev and determination of the strong coupling constant in the tevrage, *The European Physical Journal C* 75 (5) (2015) 186. doi:[10.1140/epjc/s10052-015-3376-y](https://doi.org/10.1140/epjc/s10052-015-3376-y).
- [8] S. Sarkar, et al., The Physics of the Quark-Gluon Plasma, Springer, Berlin, Heidelberg, 2010. doi:[10.1007/978-3-642-02286-9](https://doi.org/10.1007/978-3-642-02286-9).
- [9] M. Connors, et al., Jet measurements in heavy ion physics, *Rev. Mod. Phys.* 90 (2018) 025005. doi:[10.1103/RevModPhys.90.025005](https://doi.org/10.1103/RevModPhys.90.025005).
- [10] J. Wok, Pseudorapidity (2007).
 URL <https://commons.wikimedia.org/w/index.php?curid=5970403>
- [11] A. S. Carroll, et al., PHOBOS at RHIC: Some global observations, *Pramana* 61 (5) (2003) 865–876. doi:[10.1007/BF02704455](https://doi.org/10.1007/BF02704455).
- [12] M.L. Miller, et al., Glauber modeling in high-energy nuclear collisions, *Annual Review of Nuclear and Particle Science* 57 (1) (2007) 205–243. doi:[10.1146/annurev.nucl.57.090506.123020](https://doi.org/10.1146/annurev.nucl.57.090506.123020).
- [13] V. Franco, R. J. Glauber, High-energy deuteron cross sections, *Phys. Rev.* 142 (1966) 1195–1214. doi:[10.1103/PhysRev.142.1195](https://doi.org/10.1103/PhysRev.142.1195).
- [14] J. Ollitrault, Anisotropy as a signature of transverse collective flow, *Phys. Rev. D* 46 (1992) 229–245. doi:[10.1103/PhysRevD.46.229](https://doi.org/10.1103/PhysRevD.46.229).
- [15] S.A. Voloshin, et al., Collective phenomena in non-central nuclear collisions: Datasheet from

- landolt-börnstein - group i elementary particles, nuclei and atoms · volume 23: “relativistic heavy ion physics” in springermaterials. doi:[10.1007/978-3-642-01539-7_10](https://doi.org/10.1007/978-3-642-01539-7_10).
- [16] L. Adamczyk, et al., Beam-energy dependence of the directed flow of protons, antiprotons, and pions in au+au collisions, Phys. Rev. Lett. 112 (2014) 162301. doi:[10.1103/PhysRevLett.112.162301](https://doi.org/10.1103/PhysRevLett.112.162301).
 - [17] A. Adare, et al., Measurements of higher-order flow harmonics in au+au collisions at $\sqrt{s_{NN}} = 200$ GeV, Phys. Rev. Lett. 107 (2011) 252301. doi:[10.1103/PhysRevLett.107.252301](https://doi.org/10.1103/PhysRevLett.107.252301).
 - [18] L. Adamczyk, et al., Third harmonic flow of charged particles in au + au collisions at $\sqrt{s_{NN}} = 200$ gev, Phys. Rev. C 88 (2013) 014904. doi:[10.1103/PhysRevC.88.014904](https://doi.org/10.1103/PhysRevC.88.014904).
 - [19] B. Alver, G. Roland, Collision-geometry fluctuations and triangular flow in heavy-ion collisions, Phys. Rev. C 81 (2010) 054905. doi:[10.1103/PhysRevC.81.054905](https://doi.org/10.1103/PhysRevC.81.054905).
 - [20] X. Wei, PHENIX Reaction Plane Detector (2007).
URL <https://www.bnl.gov/rhic/news/061907/story2.asp>
 - [21] A. Adare, et al., Measurement of two-particle correlations with respect to second- and third-order event planes in Au + Au collisions at $\sqrt{s_{NN}} = 200$ GeV, Phys. Rev. C 99 (2019) 054903. doi:[10.1103/PhysRevC.99.054903](https://doi.org/10.1103/PhysRevC.99.054903).
 - [22] A. Adare, et al., Azimuthal anisotropy of π^0 production in Au + Au collisions at $\sqrt{s_{NN}} = 200$ GeV: Path-length dependence of jet quenching and the role of initial geometry, Phys. Rev. Lett. 105 (2010) 142301. doi:[10.1103/PhysRevLett.105.142301](https://doi.org/10.1103/PhysRevLett.105.142301).
 - [23] A. Adare, et al., Scaling properties of azimuthal anisotropy in Au + Au and Cu + Cu collisions at $\sqrt{s_{NN}} = 200$ GeV, Phys. Rev. Lett. 98 (2007) 162301. doi:[10.1103/PhysRevLett.98.162301](https://doi.org/10.1103/PhysRevLett.98.162301).
 - [24] R. Brandelik, et al., Evidence for planar events in e^+e^- annihilation at high energies, Physics Letters B 86 (2) (1979) 243 – 249. doi:[10.1016/0370-2693\(79\)90830-X](https://doi.org/10.1016/0370-2693(79)90830-X).
 - [25] R. Baier, et al., Induced gluon radiation in a qcd medium, Physics Letters B 345 (3) (1995) 277 – 286. doi:[10.1016/0370-2693\(94\)01617-L](https://doi.org/10.1016/0370-2693(94)01617-L).
 - [26] J. Bjorken, Energy Loss of Energetic Partons in Quark - Gluon Plasma: Possible Extinction of High p(t) Jets in Hadron - Hadron Collisions.
URL <https://s3.cern.ch/inspire-prod-files-b/b16cecc7217b868e2ac527ece99f418>
 - [27] M. Gyulassy, M. Plümer, Jet quenching in dense matter, Physics Letters B 243 (4) (1990) 432 – 438. doi:[10.1016/0370-2693\(90\)91409-5](https://doi.org/10.1016/0370-2693(90)91409-5).
 - [28] R. Kunnawalkam Elayavalli, K.C. Zapp, Medium response in JEWEL and its impact on jet shape observables in heavy ion collisions, JHEP 07 (2017) 141. doi:[10.1007/JHEP07\(2017\)141](https://doi.org/10.1007/JHEP07(2017)141)

141.

- [29] J. Qiu, et al., Factorization of jet cross sections in heavy-ion collisions, Phys. Rev. Lett. 122 (2019) 252301. doi:10.1103/PhysRevLett.122.252301.
- [30] J. Casalderrey-Solana, et al., Angular Structure of Jet Quenching Within a Hybrid Strong/Weak Coupling Model, JHEP 03 (2017) 135. arXiv:1609.05842, doi:10.1007/JHEP03(2017)135.
- [31] Y. He, et al., Interplaying mechanisms behind single inclusive jet suppression in heavy-ion collisions, Phys. Rev. C 99 (5) (2019) 054911. arXiv:1809.02525, doi:10.1103/PhysRevC.99.054911.
- [32] N. Chang, G. Qin, Full jet evolution in quark-gluon plasma and nuclear modification of jet production and jet shape in Pb+Pb collisions at 2.76ATeV at the CERN Large Hadron Collider, Phys. Rev. C 94 (2) (2016) 024902. arXiv:1603.01920, doi:10.1103/PhysRevC.94.024902.
- [33] B. Schenke, et al., MARTINI: An Event generator for relativistic heavy-ion collisions, Phys. Rev. C 80 (2009) 054913. arXiv:0909.2037, doi:10.1103/PhysRevC.80.054913.
- [34] M. Sievert, et al., A complete set of in-medium splitting functions to any order in opacity, Phys. Lett. B 795 (2019) 502–510. arXiv:1903.06170, doi:10.1016/j.physletb.2019.06.019.
- [35] Y. Chien, I. Vitev, Towards the understanding of jet shapes and cross sections in heavy ion collisions using soft-collinear effective theory, JHEP 05 (2016) 023. arXiv:1509.07257, doi:10.1007/JHEP05(2016)023.
- [36] I.P. Lokhtin, A.M. Snigirev, Nuclear geometry of jet quenching, Eur. Phys. J. C 16 (2000) 527–536. arXiv:hep-ph/0004176, doi:10.1007/s100520000437.
- [37] H. Zhang, et al., Dihadron tomography of high-energy nuclear collisions in next-to-leading order perturbative qcd, Phys. Rev. Lett. 98 (2007) 212301. doi:10.1103/PhysRevLett.98.212301.
- [38] N. Armesto, et al., Constraint fitting of experimental data with a jet quenching model embedded in a hydrodynamical bulk medium, Journal of Physics G: Nuclear and Particle Physics 37 (2) (2010) 025104. doi:10.1088/0954-3899/37/2/025104.
- [39] R. Baier, et al., Radiative energy loss of high energy quarks and gluons in a finite-volume quark-gluon plasma, Nuclear Physics B 483 (1) (1997) 291 – 320. doi:[https://doi.org/10.1016/S0550-3213\(96\)00553-6](https://doi.org/10.1016/S0550-3213(96)00553-6).
- [40] R. Baier, Jet quenching, Nuclear Physics A 715 (2003) 209c – 218c, quark Matter 2002. doi:[https://doi.org/10.1016/S0375-9474\(02\)01429-X](https://doi.org/10.1016/S0375-9474(02)01429-X).
- [41] V. Khachatryan, et al., Charged-particle nuclear modification factors in pbpb and ppb col-

- lisions at $\sqrt{s_{NN}} = 5.02$ tev, Journal of High Energy Physics 4 (2017) 39. doi:10.1007/JHEP04(2017)039.
- [42] D. Sharma, Measurement of light mesons by the PHENIX experiment at the RHIC, J. Phys. G38 (2011) 124082. doi:10.1088/0954-3899/38/12/124082.
 - [43] A. Adare, et al., Quantitative constraints on the transport properties of hot partonic matter from semi-inclusive single high transverse momentum pion suppression in au+au collisions at $\sqrt{s_{NN}} = 200$ gev, Phys. Rev. C 77 (2008) 064907. doi:10.1103/PhysRevC.77.064907.
 - [44] A. Majumder, A comparative study of jet-quenching schemes, Journal of Physics G: Nuclear and Particle Physics 34 (8) (2007) S377–S387. doi:10.1088/0954-3899/34/8/s25.
 - [45] A. Adare, et al., Dihadron azimuthal correlations in au+au collisions at $\sqrt{s_{NN}} = 200$ gev, Phys. Rev. C 78 (2008) 014901. doi:10.1103/PhysRevC.78.014901.
 - [46] S. S. Adler, et al., Dense-medium modifications to jet-induced hadron pair distributions in Au + Au collisions at $\sqrt{s_{NN}} = 200$ GeV, Phys. Rev. Lett. 97 (2006) 052301. doi:10.1103/PhysRevLett.97.052301.
 - [47] N. Borghini, U. Wiedemann, Distorting the hump-backed plateau of jets with dense QCD matter, arXiv:hep-ph/0506218.
 - [48] T. Renk, Using hard dihadron correlations to constrain elastic energy loss, Phys. Rev. C 84 (2011) 067902. doi:10.1103/PhysRevC.84.067902.
 - [49] A. Adare, et al., Transition in yield and azimuthal shape modification in dihadron correlations in relativistic heavy ion collisions, Phys. Rev. Lett. 104 (2010) 252301. doi:10.1103/PhysRevLett.104.252301.
 - [50] K. Burke, et al., Extracting the jet transport coefficient from jet quenching in high-energy heavy-ion collisions, Phys. Rev. C 90 (2014) 014909. doi:10.1103/PhysRevC.90.014909.
 - [51] J. Putschke, et al., The JETSCAPE framework, arXiv:1903.07706.
 - [52] I. Arsene, et al., Quarkgluon plasma and color glass condensate at rhic? the perspective from the brahms experiment, Nuclear Physics A 757 (1) (2005) 1 – 27, first Three Years of Operation of RHIC. doi:<https://doi.org/10.1016/j.nuclphysa.2005.02.130>.
 - [53] B. Back, et al., The phobos perspective on discoveries at rhic, Nuclear Physics A 757 (1) (2005) 28 – 101, first Three Years of Operation of RHIC. doi:<https://doi.org/10.1016/j.nuclphysa.2005.03.084>.
 - [54] K. Adcox, et al., Formation of dense partonic matter in relativistic nucleusnucleus collisions at rhic: Experimental evaluation by the phenix collaboration, Nuclear Physics A 757 (1) (2005) 184 – 283, first Three Years of Operation of RHIC. doi:<https://doi.org/10.1016/j.nuclphysa.2005.03.084>.

j.nuclphysa.2005.03.086.

- [55] J. Adams, et al., Experimental and theoretical challenges in the search for the quarkgluon plasma: The star collaboration's critical assessment of the evidence from rhic collisions, Nuclear Physics A 757 (1) (2005) 102 – 183, first Three Years of Operation of RHIC. doi:<https://doi.org/10.1016/j.nuclphysa.2005.03.085>.
- [56] R. Vogt, Chapter 1 - kinematics and invariants, in: R. Vogt (Ed.), Ultrarelativistic Heavy-Ion Collisions, Elsevier Science B.V., Amsterdam, 2007, pp. 3 – 24. doi:<https://doi.org/10.1016/B978-044452196-5/50001-3>.
- [57] Collider–Accelerator Department of RHIC, Relativistic heavy ion collider (rhic) configuration manual.
URL <https://www.bnl.gov/cad/accelerator/docs/pdf/RHICConfManual.pdf>
- [58] M. Allen, et al., Phenix inner detectors, Nuclear Instruments and Methods in Physics Research Section A: Accelerators, Spectrometers, Detectors and Associated Equipment 499 (2003) 549. doi:[10.1016/S0168-9002\(02\)01956-3](https://doi.org/10.1016/S0168-9002(02)01956-3).
- [59] C. Adler, et al., The rhic zero-degree calorimeters, Nuclear Instruments and Methods in Physics Research Section A: Accelerators, Spectrometers, Detectors and Associated Equipment 499 (2) (2003) 433 – 436, the Relativistic Heavy Ion Collider Project: RHIC and its Detectors. doi:[10.1016/j.nima.2003.08.112](https://doi.org/10.1016/j.nima.2003.08.112).
- [60] E. Richardson, et al., A reaction plane detector for phenix at rhic, Nuclear Instruments and Methods in Physics Research Section A: Accelerators, Spectrometers, Detectors and Associated Equipment 636 (1) (2011) 99 – 107. doi:[10.1016/j.nima.2011.01.034](https://doi.org/10.1016/j.nima.2011.01.034).
- [61] M. Aizawa, et al., Phenix central arm particle id detectors, Nuclear Instruments and Methods in Physics Research Section A: Accelerators, Spectrometers, Detectors and Associated Equipment 499 (2) (2003) 508 – 520, the Relativistic Heavy Ion Collider Project: RHIC and its Detectors. doi:[10.1016/S0168-9002\(02\)01953-8](https://doi.org/10.1016/S0168-9002(02)01953-8).
- [62] K. Adcox, et al., Phenix central arm tracking detectors, Nuclear Instruments and Methods in Physics Research Section A: Accelerators, Spectrometers, Detectors and Associated Equipment 499 (2) (2003) 489 – 507, the Relativistic Heavy Ion Collider Project: RHIC and its Detectors. doi:[10.1016/S0168-9002\(02\)01952-6](https://doi.org/10.1016/S0168-9002(02)01952-6).
- [63] L. Aphecetche, et al., Phenix calorimeter, Nuclear Instruments and Methods in Physics Research Section A: Accelerators, Spectrometers, Detectors and Associated Equipment 499 (2) (2003) 521 – 536, the Relativistic Heavy Ion Collider Project: RHIC and its Detectors. doi:[10.1016/S0168-9002\(02\)01954-X](https://doi.org/10.1016/S0168-9002(02)01954-X).
- [64] P. Rocca, F. Riggi, The Use of Avalanche Photodiodes in High Energy Electromagnetic Calorimetry, 2011. doi:[10.5772/14574](https://doi.org/10.5772/14574).

- [65] G. David, et al., Pattern recognition in the phenix pbsc electromagnetic calorimeter, *IEEE Transactions on Nuclear Science* 47 (6) (2000) 1982–1986. doi:10.1109/23.903833.
- [66] C. Aidala, et al., Nonperturbative transverse-momentum-dependent effects in dihadron and direct photon-hadron angular correlations in $p + p$ collisions at $\sqrt{s} = 200$ GeV, *Phys. Rev. D* 98 (2018) 072004. doi:10.1103/PhysRevD.98.072004.
- [67] J. Beringer, et al., Review of particle physics, *Phys. Rev. D* 86 (2012) 010001. doi:10.1103/PhysRevD.86.010001.
- [68] A. Hanks, et al., Analysis of Run 10 $Au + Au$ Direct Photon–Hadron correlations and combined Run 7 and Run 10 results for ppg113.
URL <https://www.phenix.bnl.gov/phenix/WWW/p/info/an/1045/Run10Ana-04.pdf>
- [69] H. Ge, et al., Direct photon–hadron correlations in Run 11 $Au + Au$ 200 GeV and combined results with Run 7, Run 10 and Run 11 for preliminary.
URL <https://www.phenix.bnl.gov/phenix/WWW/p/info/an/1272/ANrun11AuAu-01.pdf>
- [70] R. Brun, et al., GEANT3 users guide, CERN DD/EE/84-1 (1985).
- [71] T. Danley, Photon–Related Elliptic Azimuthal Asymmetry and Photon–Hadron Correlations with an Isolation Cut in $Au + Au$ Collisions at $\sqrt{s_{NN}} = 200$ GeV at RHIC–PHENIX, PhD dissertation, Ohio University (2018).
URL http://rave.ohiolink.edu/etdc/view?acc_num=ohiou1542201804266935
- [72] J. Adam, et al., Jet–like correlations with neutral pion triggers in pp and central $pb-pb$ collisions at 2.76 TeV, *Physics Letters B* 763 (2016) 238 – 250. doi:10.1016/j.physletb.2016.10.048.
- [73] L. Adamczyk, et al., Jet–like correlations with direct–photon and neutral–pion triggers at $\sqrt{s_{NN}} = 200$ GeV, *Physics Letters B* 760 (2016) 689 – 696. doi:10.1016/j.physletb.2016.07.046.
- [74] R. A. Lacey, et al., Scaling of the higher-order flow harmonics: implications for initial-eccentricity models and the viscous horizon, , arXiv:1105.3782 (2011).
- [75] A. Sickles, et al., Extraction of correlated jet pair signals in relativistic heavy ion collisions, *Phys. Rev. C* 81 (2010) 014908. doi:10.1103/PhysRevC.81.014908.
- [76] S. S. Adler, et al., Identified charged particle spectra and yields in $au + au$ collisions at $\sqrt{s_{NN}} = 200$ gev, *Phys. Rev. C* 69 (2004) 034909. doi:10.1103/PhysRevC.69.034909.
- [77] L. Adamczyk, et al., Jet-like correlations with direct-photon and neutral-pion triggers at snn=200 gev, *Physics Letters B* 760 (2016) 689 – 696. doi:10.1016/j.physletb.2016.07.046.

- [78] J. Adam, et al., Jet-like correlations with neutral pion triggers in pp and central pbpb collisions at 2.76 tev, Physics Letters B 763 (2016) 238 – 250. doi:[10.1016/j.physletb.2016.10.048](https://doi.org/10.1016/j.physletb.2016.10.048).
- [79] G. Aad, et al., Measurement of angular and momentum distributions of charged particles within and around jets in Pb + Pb and pp collisions at $\sqrt{s_{NN}} = 5.02$ tev with the atlas detector, Phys. Rev. C 100 (2019) 064901. doi:[10.1103/PhysRevC.100.064901](https://doi.org/10.1103/PhysRevC.100.064901).
- [80] Aidala, C. and others, Creation of quarkgluon plasma droplets with three distinct geometries, Nature Physics 15 (2019) 214. doi:[0.1038/s41567-018-0360-0](https://doi.org/10.1038/s41567-018-0360-0).
- [81] A. Pun, Gamma–hadron and related two–particle azimuthal correlations results in phenix, in: Proceedings of the 13th International Workshop in High pT Physics in the RHIC and LHC Era, Proceedings of Science, 2019, p. 1.
URL <https://pos.sissa.it/355/001/pdf>
- [82] H. Abramowicz, et al., Combination of measurements of inclusive deep inelastic $e^\pm p$ scattering cross sections and qcd analysis of hera data, Eur. Phys. J. C 75 (2015) 580. doi:[10.1140/epjc/s10052-015-3710-4](https://doi.org/10.1140/epjc/s10052-015-3710-4).
- [83] D. Geesaman, P. Reimer, The sea of quarks and antiquarks in the nucleon, Reports on Progress in Physics 82 (4) (2019) 046301. doi:[10.1088/1361-6633/ab05a7](https://doi.org/10.1088/1361-6633/ab05a7).
- [84] A. Accardi, et al., Electron-ion collider: The next qcd frontier, Eur. Phys. J. A 52 (2016) 268. doi:[10.1140/epja/i2016-16268-9](https://doi.org/10.1140/epja/i2016-16268-9).
- [85] eRD14 PID Consortium, An integrated program for particle identification (PID) for a future electron-ion collider (EIC) detector, 2016 (accessed 07.06.16).
URL https://wiki.bnl.gov/conferences/images/d/d2/ERD14_FY17.v2.pdf
- [86] T. Iijima, et al., A novel type of proximity focusing rich counter with multiple refractive index aerogel radiator, Nuclear Instruments and Methods in Physics Research Section A: Accelerators, Spectrometers, Detectors and Associated Equipment 548 (3) (2005) 383 – 390. doi:<https://doi.org/10.1016/j.nima.2005.05.030>.
- [87] R. Pestotnik, et al., Aerogel rich for forward pid at belle ii, Nuclear Instruments and Methods in Physics Research Section A: Accelerators, Spectrometers, Detectors and Associated Equipment 732 (2013) 371 – 374, vienna Conference on Instrumentation 2013. doi:<https://doi.org/10.1016/j.nima.2013.06.080>.
- [88] M. Contalbrigo, et al., The clas12 large area rich detector, Nuclear Instruments and Methods in Physics Research Section A: Accelerators, Spectrometers, Detectors and Associated Equipment 639 (1) (2011) 302 – 306, proceedings of the Seventh International Workshop on Ring Imaging Cherenkov Detectors. doi:<https://doi.org/10.1016/j.nima.2010.10.047>.
- [89] M. Adinolfi, et al., Performance of the lhcb rich detector at the lhc, The European Physical Journal C 73 (2013) 2431. doi:[10.1140/epjc/s10052-013-2431-9](https://doi.org/10.1140/epjc/s10052-013-2431-9).

- [90] C. Wong, et al., Modular focusing ring imaging cherenkov detector for electronion collider experiments, Nuclear Instruments and Methods in Physics Research Section A: Accelerators, Spectrometers, Detectors and Associated Equipment 871 (2017) 13 – 19. doi:<https://doi.org/10.1016/j.nima.2017.07.001>.
- [91] Edmund Optics, Specification of Fresnel Lens (stock no. 32–593) (2016 (accessed 01.09.17)). URL <http://www.edmundoptics.com/optics/optical-lenses/fresnel-lenses/fresnel-lenses/32593/>
- [92] Hamamatsu Photonics K.K., Flat panel type multianode PMT assembly H8500 series/ H10966 series (2011). URL https://www.hamamatsu.com/resources/pdf/etd/H8500_H10966 TPMH1327E.pdf
- [93] M. Contalbrigo, et al., Aerogel mass production for the clas12 rich: Novel characterization methods and optical performance, Nuclear Instruments and Methods in Physics Research Section A: Accelerators, Spectrometers, Detectors and Associated Equipment doi:[10.1016/j.nima.2017.02.068](https://doi.org/10.1016/j.nima.2017.02.068).
- [94] J. Allison, et al., Recent developments in Geant4, Nuclear Instruments and Methods in Physics Research Section A: Accelerators, Spectrometers, Detectors and Associated Equipment 835 (2016) 186 – 225. doi:[10.1016/j.nima.2016.06.125](https://doi.org/10.1016/j.nima.2016.06.125).
- [95] L. Rayleigh, XXXIV. on the transmission of light through an atmosphere containing small particles in suspension, and on the origin of the blue of the sky, The London, Edinburgh, and Dublin Philosophical Magazine and Journal of Science 47 (287) (1899) 375–384. doi:[10.1080/14786449908621276](https://doi.org/10.1080/14786449908621276).
- [96] A. Adare, et al., An Upgrade Proposal from the PHENIX Collaboration, [arXiv:1501.06197](https://arxiv.org/abs/1501.06197).
- [97] sPHENIX Forward Instrumentation. URL https://www.sphenix.bnl.gov/web/system/files/sPH-cQCD-2017-001_draft_2017_06_02.pdf
- [98] Hamamatsu Photonics K.K., Flat panel type multianode PMT assembly H13700 series (2011). URL <https://www.hamamatsu.com/resources/pdf/etd/H13700 TPMH1370E.pdf>
- [99] A. Adare, et al., Identified charged hadron production in $p + p$ collisions at $\sqrt{s} = 200$ and 62.4 gev, Phys. Rev. C 83 (2011) 064903. doi:[10.1103/PhysRevC.83.064903](https://doi.org/10.1103/PhysRevC.83.064903).

Appendix

A Near-Side Normalization

Discussed in section 6.1.1, there are near-side discrepancies between this analysis and [49]. To find the root of the discrepancies, this section details the difference of single photon as well as pair photon selections between this work and [49] as listed in Table 1.

Table 1: Different single photon and photon pair cuts in this analysis and PPG106.

	This analysis	[49]
Shower shape	photon probability > 2	$\chi^2 < 3$
Energy asymmetry	$\alpha \leq 0.15 + 0.85(\frac{E_{\gamma_1\gamma_2}-4}{1.25})^2$	$\alpha \leq \frac{E_{\gamma_1\gamma_2}-2E_{\gamma_{min}}}{E_{\gamma_1\gamma_2}}$ $E_{\gamma_{min}} = 0.7 + 0.8(1 - cent)e^{0.4(4-p_T)}$
invariant mass window	0.12–0.16 GeV	0.125–0.15 GeV for $p_T < 5$ GeV/c 0.12–0.16 GeV otherwise
veto track cut	$\sqrt{\Delta x^2 + \Delta y^2 + \Delta z^2} < 8$ cm	$\frac{\Delta z}{\Delta z_{max}^2} + \frac{\Delta \phi^2}{\Delta \phi_{max}^2} < 1$ $\Delta z_{max} = 10$ cm and $\Delta \phi_{max} = 0.02$ rad

Photon paring

In addition, this analysis pairs a photon that passes a looser single photon requirements and a photon that passes all the single photon requirements, while [49] pairs photons that both passes all the single photon requirements. The jet functions that using photon pairs that both photons meet the single photon selections as detailed in section 3.1 are compared to [49] results in Figure 1. However, the discrepancies still persist at high associate p_T . Moreover, the near-side peaks at 1–2 GeV/c associate p_T rises above the results from [49].

Shower shape cut

Shower shape cut on electromagnetic calorimeter cluster using χ^2 parameter is implemented in [49]. Figure 2 shows that if switching the photon probability requirement to χ^2 requirement in single photon selection, the near-side jet functions reduce slightly at most of the high associate p_T (> 2 GeV/c) region. Even though [49] near-side results still have lower yield. Although the near-side peaks are still higher at 1–2 GeV/c associate p_T compared to [49], clear reduction is shown on the near-side peaks, and the away-side peaks become less fluctuate.

Energy asymmetry cut

The energy asymmetry cut on photon pair used by [49] depends on both centrality and photon momentum. As shown in Figure 3, this energy asymmetry cut applied by [49] has similar effects on jet functions as the shower shape χ^2 cut.

Invariant mass cut

A narrower invariant mass window is used in [49] on low energy (< 5 GeV) photon pair to reduce the combinatorial photon pairs in π^0 reconstruction. For simplicity, a narrower invariant mass window is applied in all trigger p_T in order to study the effect on the near-side peak. The resulting

jet plotted in Figure 4 show that the narrower mass window has the similar influence on the jet functions as the shower shape χ^2 cut but gives slightly further reduction on the near-side peaks.

Even though the narrower mass window cut reduces near-side peak, the invariant mass distributions shown in Figure 4.2 shows that this cut could be too harsh at high trigger p_T where the combinatorial photon pairs are very limited compared to low trigger p_T .

Veto track cut

Instead of measured the transitional distance between the cluster and the projected track position at the EMCAL, [49] used an oval cut to remove charged hadron clusters. Figure 5 shows that the effect of the oval cut on the near-side peaks are inconsistent at high associate p_T . At low associate p_T , this cut reduces the near-side peak. Especially between 1–2 GeV/c, where the near-side peaks matches to [49] results very well after switching to the oval cut.

Accumulated effects of photon selection

The veto track cut is the dominate influence amount the photon selection requirements listed in this section.

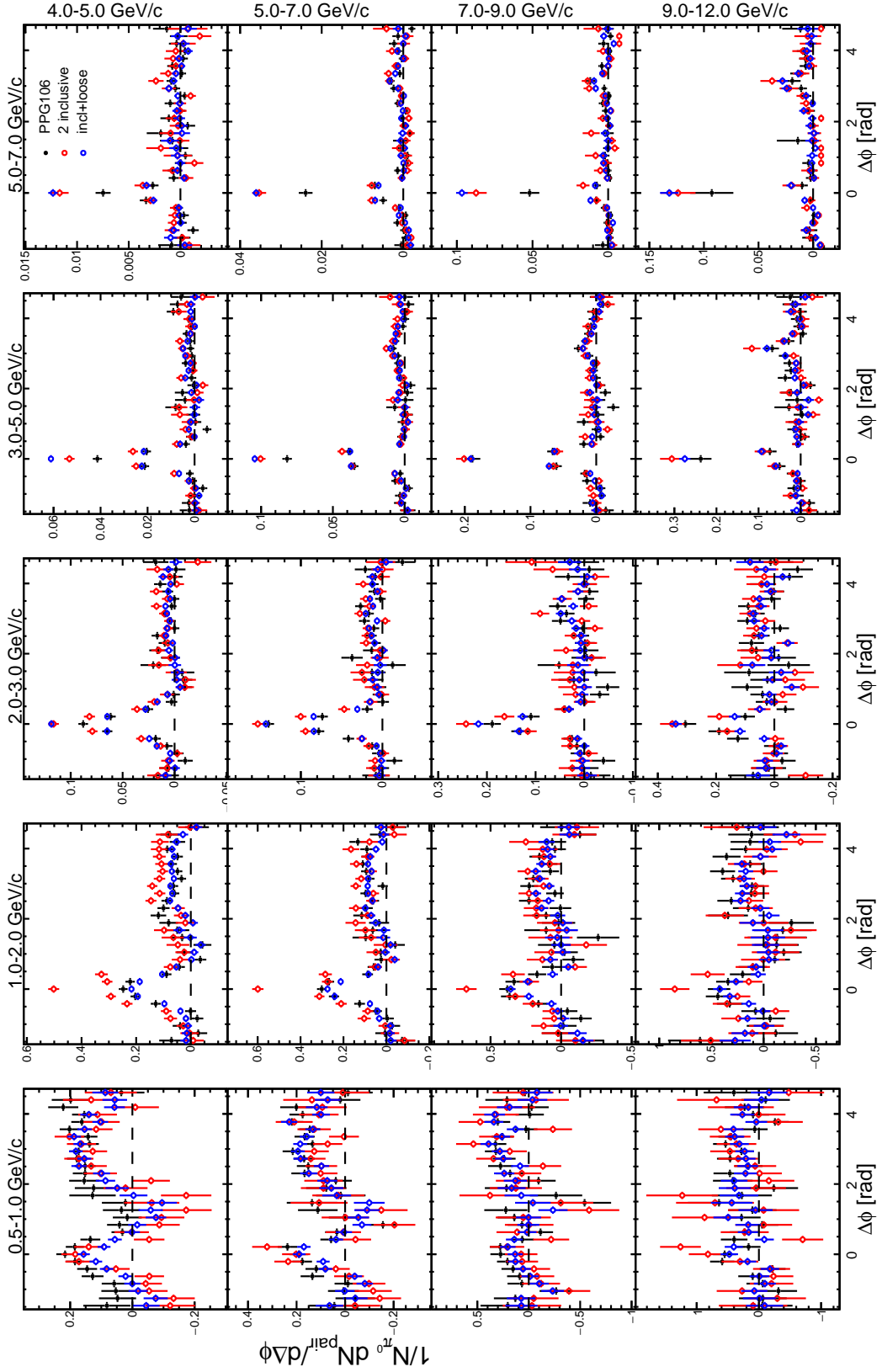


Figure 1: Jet functions in 0–20% centrality events. Black: results in [49]. Blue: results from this analysis with cuts listed in section 3.1. Red: same as blue data but pairing two inclusive photons in π^0 reconstruction.

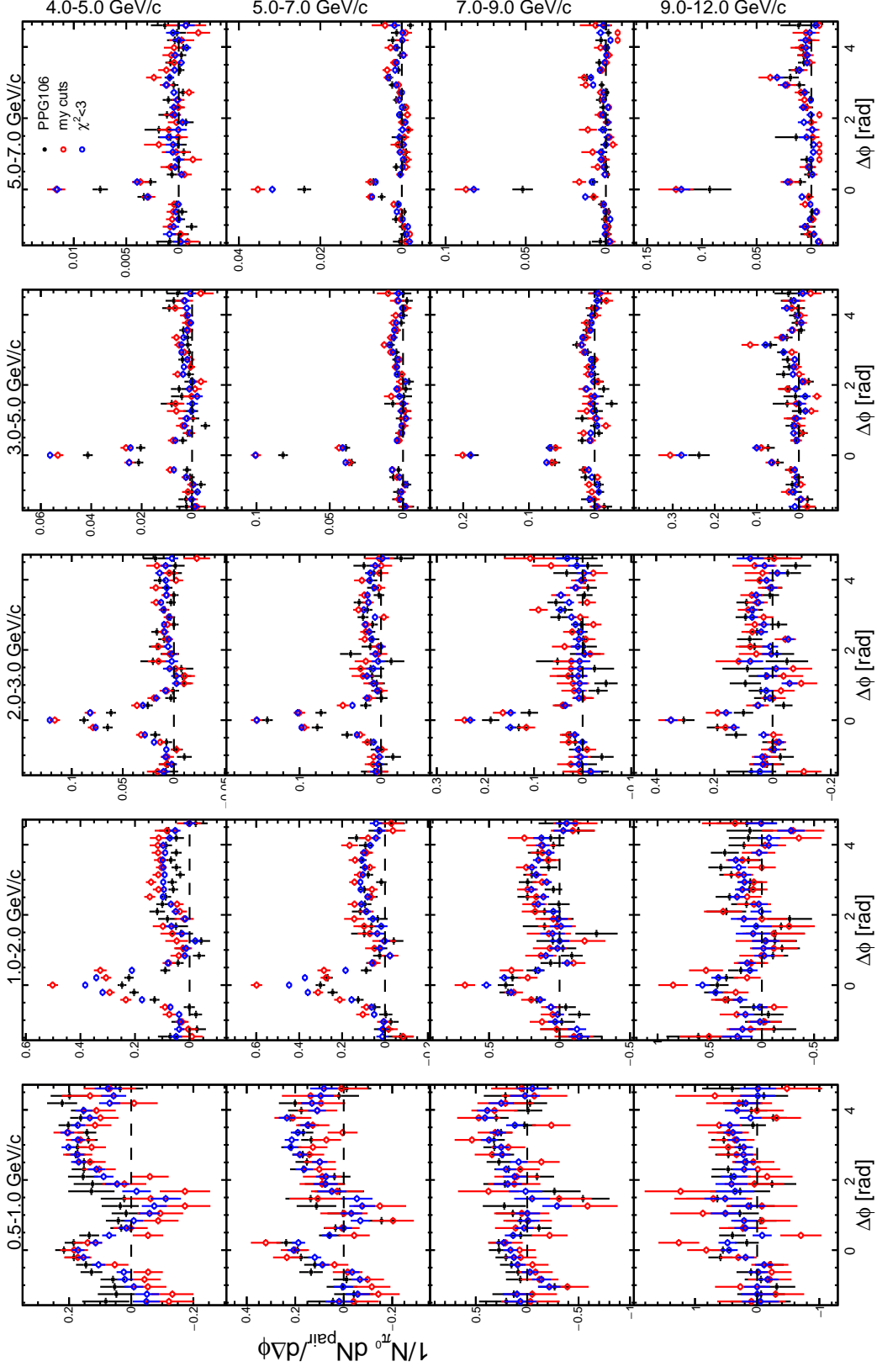


Figure 2: Jet functions in 0–20% centrality events. Black: results in [49]. Blue: results from this analysis with cuts listed in section 3.1, but pairing two inclusive photons in π^0 reconstruction. Red: same as blue data but switching photon probability cut to $\chi^2 > 3$ shower shape cut.

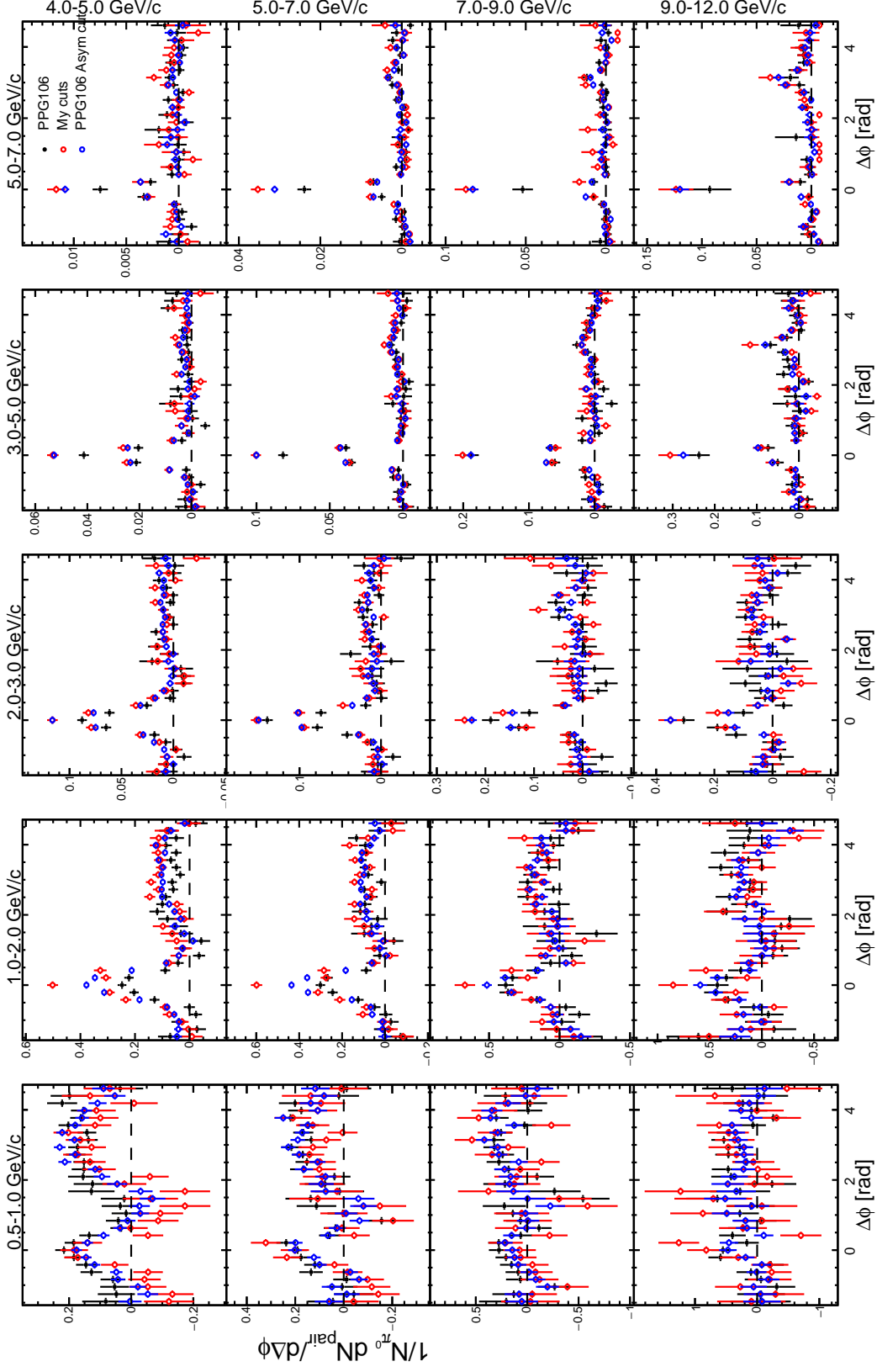


Figure 3: Jet functions in 0–20% centrality events. Black: results in [49]. Blue: results from this analysis with cuts listed in section 3.1, but pairing two inclusive photons in π^0 reconstruction. Red: same as blue data but switching to the energy asymmetry cut that was applied in [49].

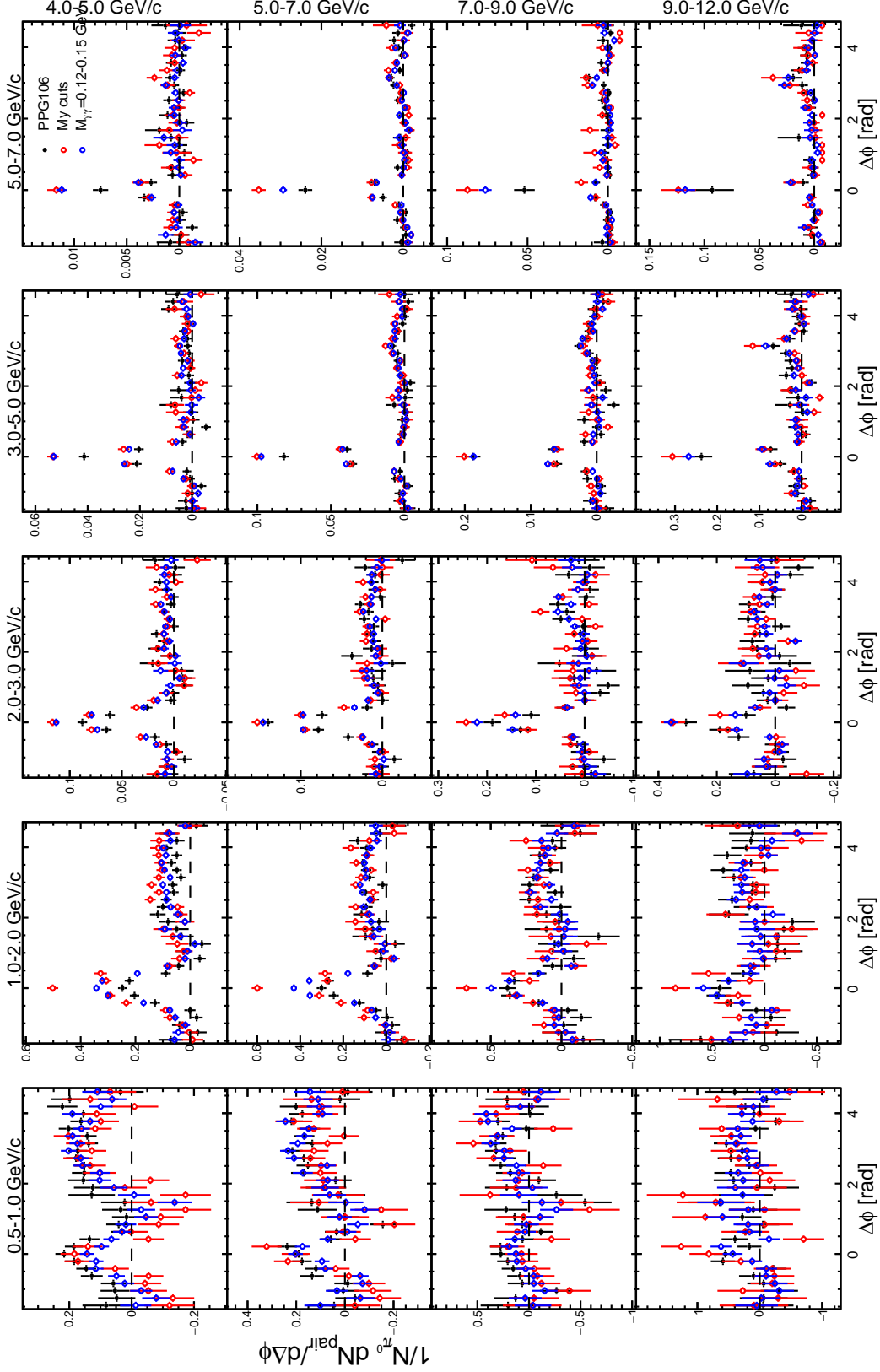


Figure 4: Jet functions in 0–20% centrality events. Black: results in [49]. Blue: results from this analysis with cuts listed in section 3.1, but pairing two inclusive photons in π^0 reconstruction. Red: same as blue data but the invariant mass window is changed to 0.12–0.15 GeV for all photon pair.

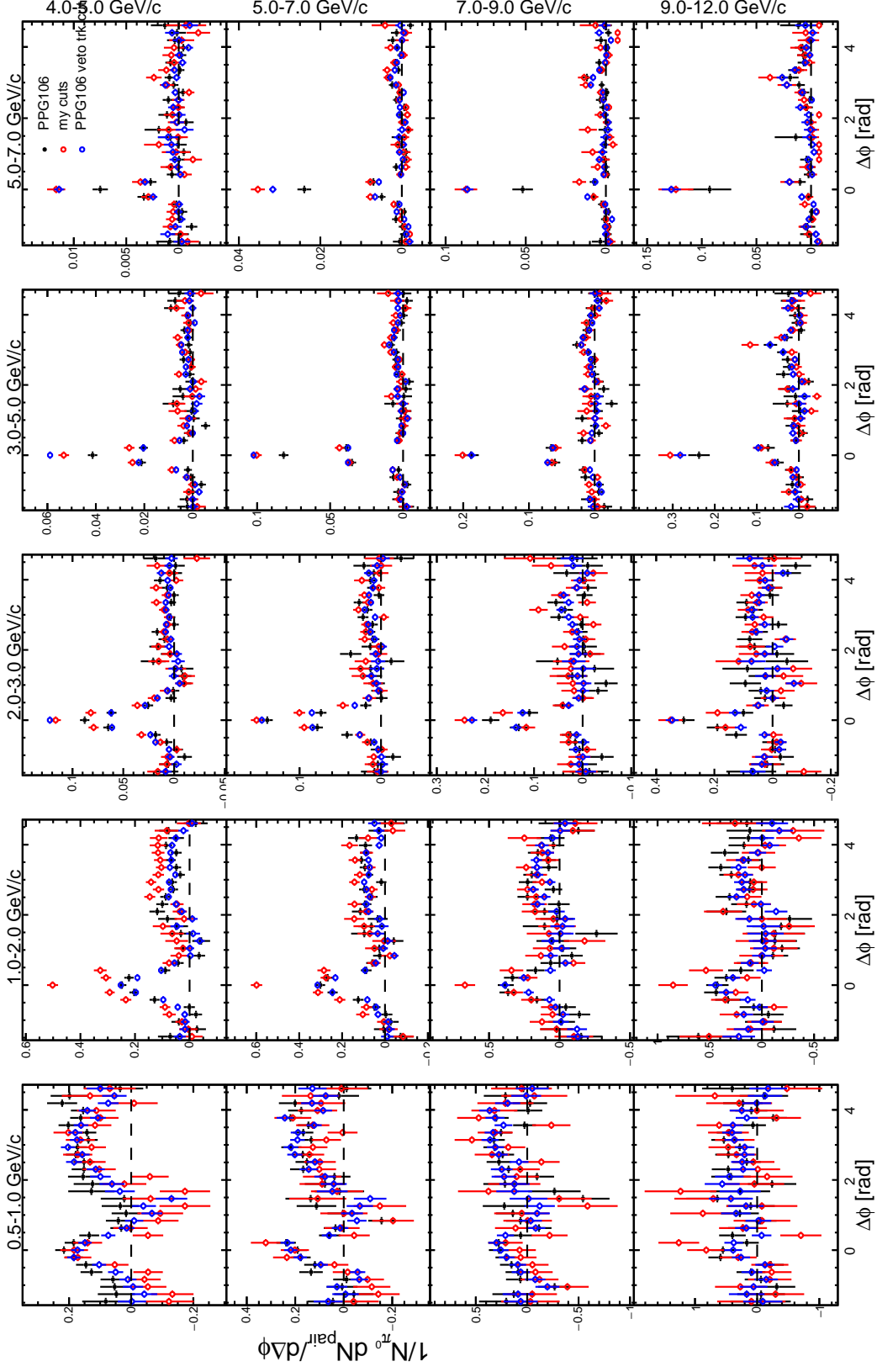


Figure 5: Jet functions in 0–20% centrality events. Black: results in [49]. Blue: results from this analysis with cuts listed in section 3.1, but pairing two inclusive photons in π^0 reconstruction. Red: same as blue data but using the oval veto track cut.

B Available PHENIX Dataset

There are additional 200 GeV $Au + Au$ and $p + p$ available later run years of PHENIX. However, hadron efficiency and data acquisition, which are run year dependent, are needed for these runs. This section will details works done for the available data and the steps needed to complete the analysis using these data sets.

B.1 2015 200 GeV $p + p$ Data

π^0 -hadron correlation analysis has been conduct by PHENIX collaboration using 2015 200 GeV $p + p$ data set. The statistics of 2015 data set is about 6 times of the 2006 data set as stated in Table 2.2. With higher statistics in 2015 data set, the statistical error in the results could be reduced by factor of $\sqrt{6} \approx 2.4$.

However, the hadron efficiency, which corrects the per trigger yields of the jet functions and I_{AA} , is still in progress. There are issues with the PHENIX detector simulation that is using 2012 drift and pad chamber setup. As shown the in Figure 6 (a) and (b), the $\phi-z$ distribution from simulation in Figure 6 (b) that is using 2012 Drift chamber efficiency information has fewer dead wires compared to the data in Figure 6 (a). Moreover, dead sections of pad chamber around $\phi = 2$ and $\phi = -0.5$ do not show up in the simulation indicating the pad chamber setup in simulation does not well describe the experiment setup. Since the ratio of live pixels and wires determines the efficiency of track reconstruction, these misalignment in simulation causes the over estimation of the hadron efficiency. Thus, lower per trigger yields in the results.

To obtain the an accurate hadron efficiency, the pad chamber mismatch issue has been resolved and the 2015 drift chamber efficiency file is produced. An additional fiducial cut is applied in the simulation analysis to remove charged hadron tracks that hit at the dead ϕ regions. The $\phi-z$ distribution from simulation using the updated drift and pad chambers information is shown in Figure 6 (c). Comparison between Figure 6 (a) and (c) shows that the simulation matches most

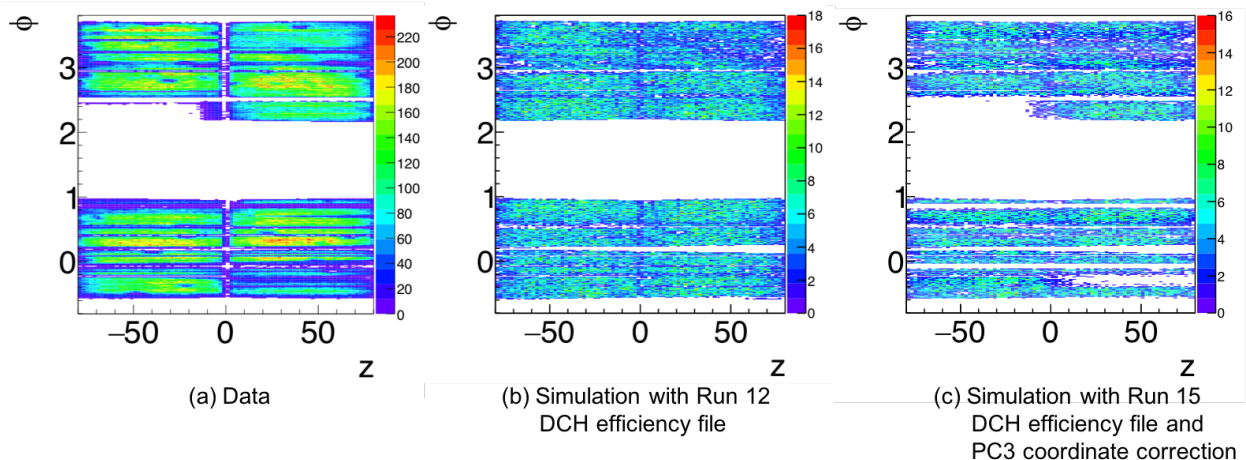


Figure 6: $\phi-z$ distributions of charged hadron tracks from 2015 200 GeV $p + p$ data (a) and simulations (b and c).

of the dead areas to experimental data after updating detector information. The next step to obtaining hadron efficiency is weighting the efficiency of each charged hadron species using the measured identified charged hadron spectrum from PHENIX [99].

B.2 2014 200 GeV Au + Au Data

Run Selection

Following description in section 3.3. The entire Run 14 is separated in six groups as shown in Table 2 as the drift chamber setup may changes between these runs. These changes of drift chamber setup could affect the shape of correlations from both same and mixed events. The decision of having group 3 is based on the shape of the mixed event correlation functions of the runs in group 3 share similar feature in the away-side peak as shown in Figure 7 which also displays mixed event correlation functions from other runs. Comments in the control logbook shows there were west arm Drift Chamber back packet and frames issues in run 409697, 409698, 409699, and 409714. The specific feature on the away-side peak of the correlations of group 3 (see Figure 7) started to show since these runs. Other related Drift Chamber issues documented in the control log in group 3 are listed in Table 3. The Drift chamber bad frames problems are found in run 409459 and 409714,

Table 2: Run Groups

Group	Run Numbers
0	405863 – 406500
1	406501 – 407000
2	407001 – 409690
3	409691 – 410500
4	410501 – 413300
5	413301 – 414988

near and within run group 3. The frames refer to the header frames which provides information for decoding the packets. Thus, the data from these two runs maybe disrupted. These two runs are listed as known bad runs, and are excluded from the run selection process.

Instead of using χ^2 analysis, standard deviation with respect to 1, which represent identical, of the ratio plot is calculated point-by-point. Then, there is a standard deviation distribution of the ratio plots from all runs as shown in Figure 8 which is fitted with a Gaussian function at the peak region. Runs with standard deviation greater than $\mu + 3\sigma$ are categorized as bad and excluded in the analysis, where μ and σ standard deviation extracted from the Gaussian fit in the peak region. These steps have been done twice in the same run groups as the standard deviation distribution could change after the first round of run selection. The standard deviation cut of all runs in the first and second rounds of run selection are 0.0618 and 0.0604. Examples of bad runs are displayed in Figure 9.

Top panel of Figure 10 is the number of tracks per event distribution in each run, and the bottom panel shows the number of events distribution in each run. The bad runs found in run selection are drawn in red in this figure. There are 145 bad runs out of 1140 runs found. Total of tracks in these bad runs is 2.91×10^9 out of 4.10×10^{10} tracks from all runs are removed, that is 7.1% of tracks in Run 14. The list of good runs can be found in the appendix J.

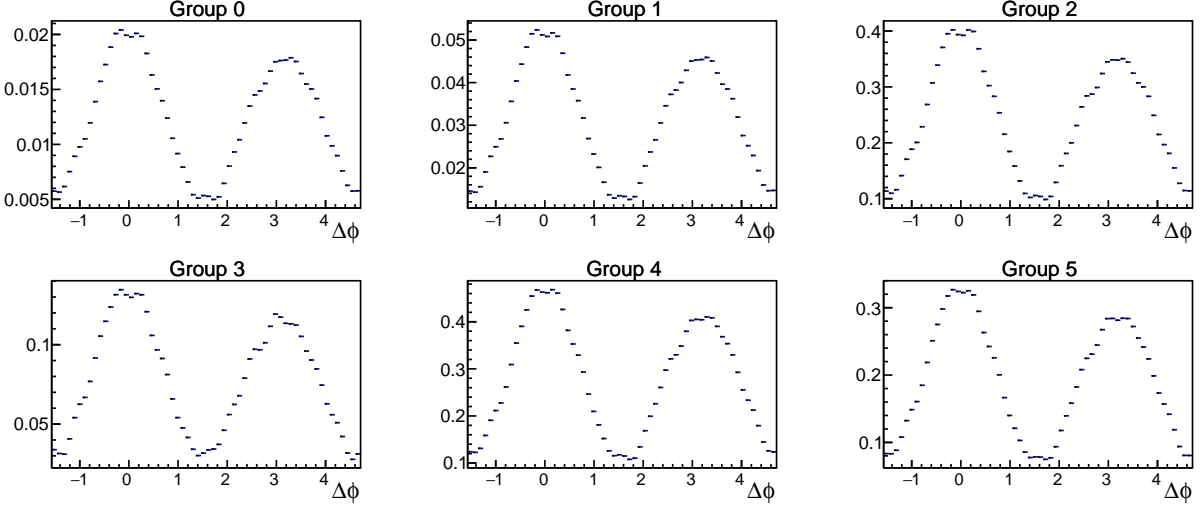


Figure 7: Summed event-mixing background correlations in different run groups. These correlations are normalized to 1.

Table 3: Control Log Comments in run 409691 – 410500

Run Num	Comments
409697	back packet errors in DCH west
409698	back packet errors in DCH west
409699	back packet errors in TOF west
409714	Many poor DCW frames
409839	DCH West high packet error rate
409840	DAQ erorrss in DCHW, MUTR S
409841	daq errors for MuTR S, and DCH W
409887	DC-W hang DAQ at the end
409891	DC.W hung at the end
409893	Ended with DC.W busy
409967	Ended when DC HV MF dropped dead
409973	Small FEMClk error rate in PCW
409974	Had to stop run due to many PCW daq errors
410065	Terminated with a DC.W glink dropout
410106	DC.E hung DAQ
410222	Stopped run a little early due to 4 DC x-sector HV trips
410267	some bbc laser hit errors and with 1 x-sector DC W HV tripped
410346	Stopped becausae of MuTrS DCM hung up
410406	MUTR.N DCM hung daq

Hadron Efficiency

Same as simulation study for 2015 data, the drift chamber wire efficiency file for 2014 detector setup has been generated recently. simulation study is still on going for obtaining 2014 hadron efficiency.

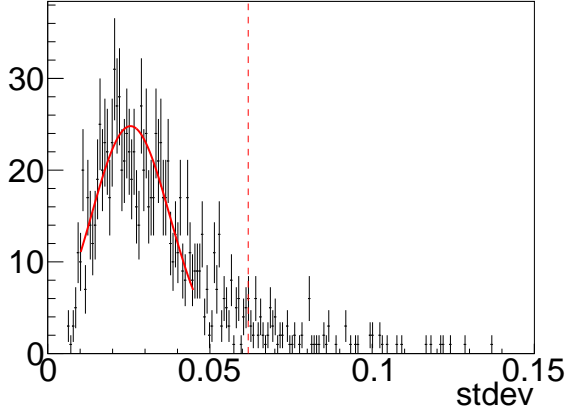


Figure 8: Standard deviation distribution of the entire Run 14. The red curve is the Gaussian fit at the peak region. The red dash line indicates $\mu + 3\sigma$.

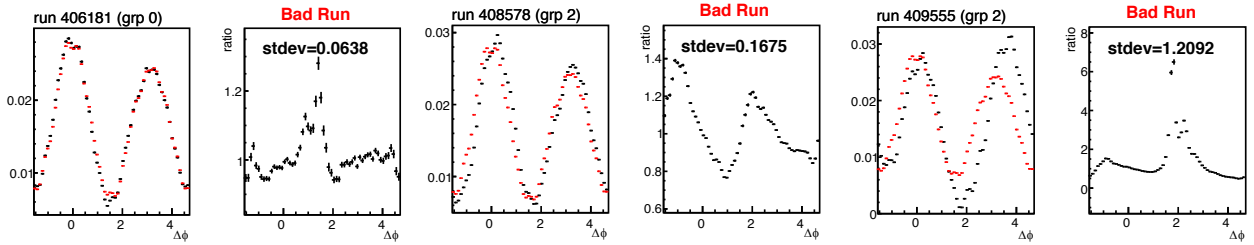


Figure 9: Examples of bad runs in Run 14. The event-mixing background correlations from each run (black) and from the corresponding run group (red) are drawn on the left in each panel. The ratio of the correlation is shown on the right of each panel.

Hot Towers in Electromagnetic Calorimeters

The hot tower maps are inherited from other PHENIX analysis using Run 14 data set. However, there are a few hot towers showing up in the photon hit maps in the tower 6 and 7, which are the lead-glass calorimeters, as demonstrated in Figure 11. Photon clusters hit at these hot towers needs to be removed before neutral pion reconstruction.

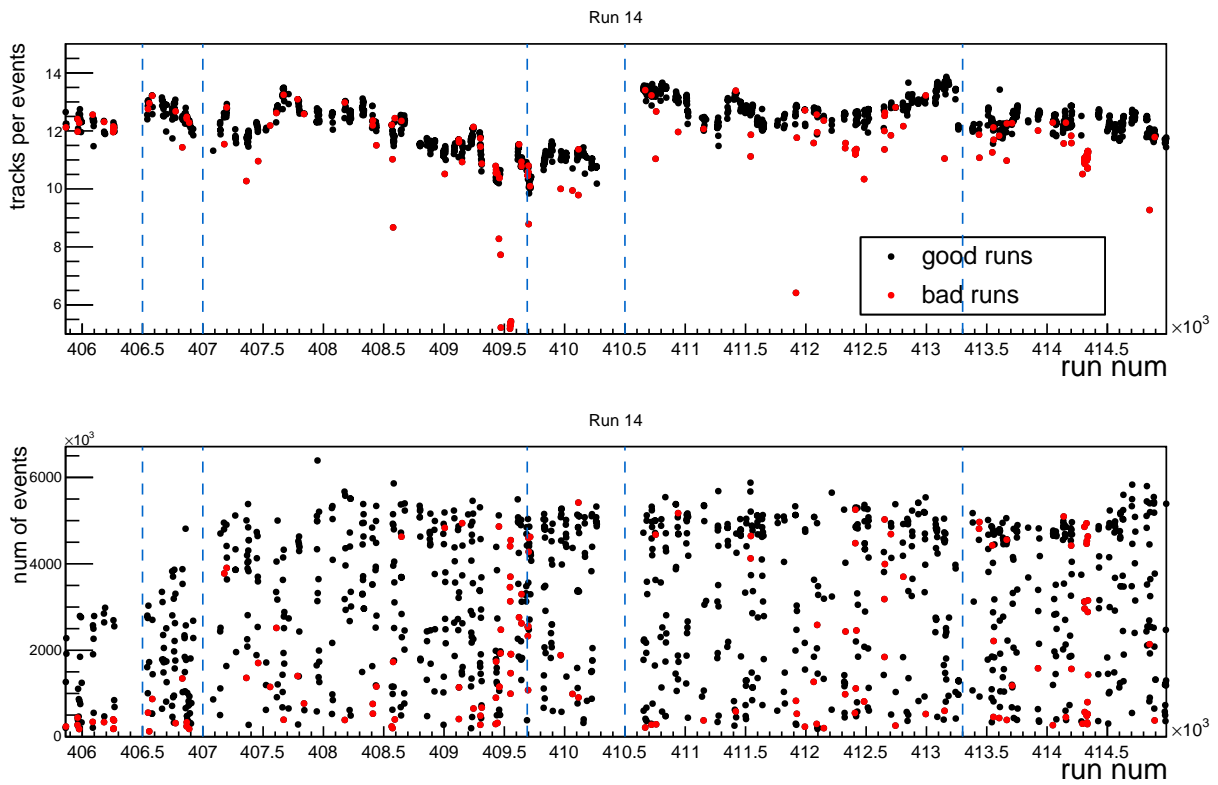


Figure 10: Number of charged hadron tracks per event vs run number (top) and number of event vs run number (bottom). The blue dash line indicate separation of run groups. From left to right are group 0 to group 5. Bad runs determined are drawn in red.

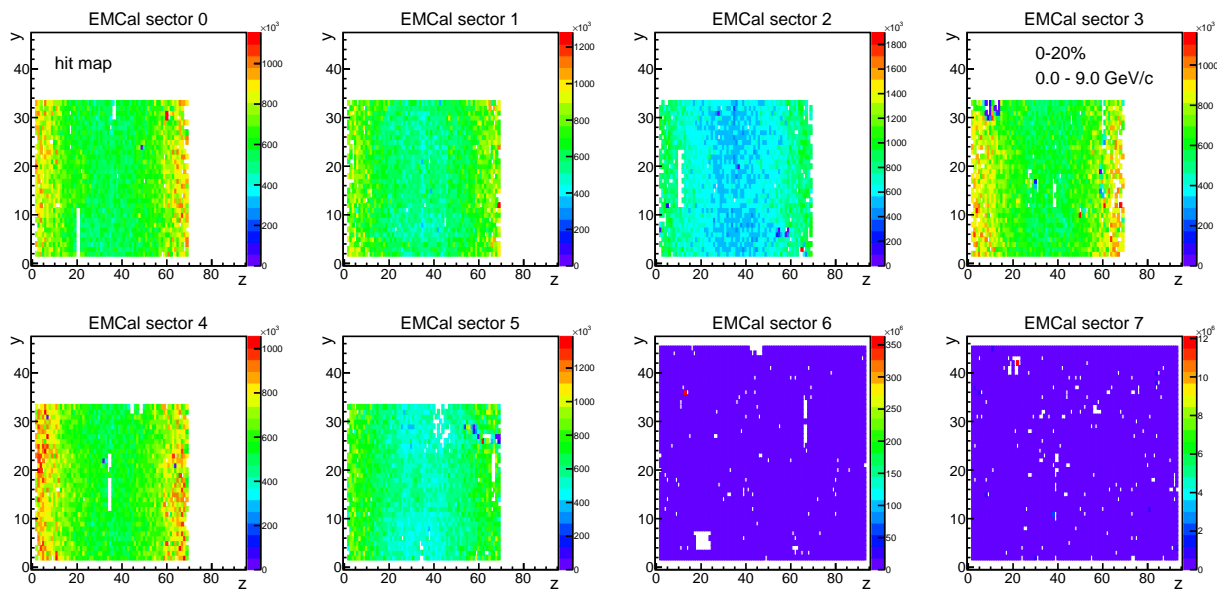


Figure 11: photon hit maps of each tower of the electromagnetic calorimeters. The lead-glass scintillator towers are denoted as tower 6 and 7.

C Data Tables: Coefficients of Flow Harmonics

Table 4: Interpolated charged hadron v_n

0–20%									
assoc p_T (GeV/c)	v_2	$\sigma_{v_2}^+$	$\sigma_{v_2}^-$	v_3	$\sigma_{v_3}^+$	$\sigma_{v_3}^-$	v_4	$\sigma_{v_4}^+$	$\sigma_{v_4}^-$
0.5–1.0	0.03648	0.00128	0.00128	0.01584	0.00085	0.00085	0.00767	0.00148	0.00148
1.0–2.0	0.06866	0.00167	0.00167	0.04074	0.00215	0.00215	0.02495	0.00458	0.00458
2.0–3.0	0.10240	0.00310	0.00310	0.07524	0.00301	0.00301	0.05482	0.00697	0.00697
3.0–5.0	0.10565	0.00401	0.00401	0.08484	0.00365	0.00365	0.07006	0.00931	0.00931
5.0–7.0	0.07678	0.00564	0.00564	0.04785	0.01684	0.01684	0.03972	0.02540	0.02540

20–40%									
assoc p_T (GeV/c)	v_2	$\sigma_{v_2}^+$	$\sigma_{v_2}^-$	v_3	$\sigma_{v_3}^+$	$\sigma_{v_3}^-$	v_4	$\sigma_{v_4}^+$	$\sigma_{v_4}^-$
0.5–1.0	0.07753	0.00148	0.00148	0.02280	0.00178	0.00178	0.01516	0.00407	0.00407
1.0–2.0	0.13623	0.00241	0.00241	0.05332	0.00499	0.00499	0.03929	0.00965	0.00965
2.0–3.0	0.19085	0.00399	0.00399	0.08970	0.00639	0.00639	0.07385	0.01813	0.01813
3.0–5.0	0.19341	0.00354	0.00354	0.09542	0.00693	0.00693	0.08715	0.02059	0.02059
5.0–7.0	0.14710	0.00541	0.00541	0.05137	0.02863	0.02863	0.05324	0.04081	0.04081

Table 5: Interpolated $\pi^0 v_2$

0–20%			
trigger p_T (GeV/c)	v_2	$\sigma_{v_2}^+$	$\sigma_{v_2}^-$
4–5	0.08875	0.00251	0.00251
5–7	0.07625	0.00585	0.00585
7–9	0.06262	0.00916	0.01324
9–12	0.05878	0.01256	0.02244
12–15	0.05832	0.01301	0.03909

20–40%			
trigger p_T (GeV/c)	v_2	$\sigma_{v_2}^+$	$\sigma_{v_2}^-$
4–5	0.15378	0.00283	0.00283
5–7	0.12754	0.00404	0.00404
7–9	0.09896	0.01060	0.00869
9–12	0.09177	0.01436	0.02469
12–15	0.09116	0.01491	0.05459

Table 6: Scaling factor g_n^h

centrality	g_3	σ_{g_3}	g_4	σ_{g_4}
0–20%	2.30	0.03	5.56	0.23
20–40%	1.07	0.02	2.20	0.15

D Data Table: ξ
Table 7: ξ in Run 10

Trigger p_T 4–5 GeV/c					
assoc p_T GeV/c	0–20%		20–40%		
	ξ	σ	ξ	σ	
0.5–1	1.00359	0.00102	1.01110	0.00331	
1.0–2	1.00312	0.00084	1.01074	0.00312	
2.0–3	1.00268	0.00073	1.01057	0.00305	
3.0–5	1.00273	0.00073	1.00974	0.00282	
5.0–7	1.00461	0.00124	1.01370	0.00450	
Trigger p_T 5–7 GeV/c					
assoc p_T GeV/c	0–20%		20–40%		
	ξ	σ	ξ	σ	
0.5–1	1.00281	0.00078	1.01009	0.00300	
1.0–2	1.00245	0.00066	1.00978	0.00283	
2.0–3	1.00212	0.00059	1.00964	0.00277	
3.0–5	1.00215	0.00059	1.00888	0.00256	
5.0–7	1.00361	0.00097	1.01245	0.00409	
Trigger p_T 7–9 GeV/c					
assoc p_T GeV/c	0–20%		20–40%		
	ξ	σ	ξ	σ	
0.5–1	1.00263	0.00073	1.01022	0.00305	
1.0–2	1.00230	0.00064	1.00991	0.00285	
2.0–3	1.00199	0.00057	1.00978	0.00283	
3.0–5	1.00202	0.00056	1.00900	0.00259	
5.0–7	1.00338	0.00091	1.01261	0.00415	
Trigger p_T 9–12 GeV/c					
assoc p_T GeV/c	0–20%		20–40%		
	ξ	σ	ξ	σ	
0.5–1	1.00289	0.00081	1.01028	0.00307	
1.0–2	1.00252	0.00068	1.00996	0.00287	
2.0–3	1.00217	0.00061	1.00982	0.00283	
3.0–5	1.00220	0.00060	1.00904	0.00260	
5.0–7	1.00370	0.00100	1.01269	0.00417	
Trigger p_T 12–15 GeV/c					
assoc p_T GeV/c	0–20%		20–40%		
	ξ	σ	ξ	σ	
0.5–1	1.00352	0.00099	1.01089	0.00322	
1.0–2	1.00306	0.00081	1.01054	0.00308	
2.0–3	1.00262	0.00071	1.01037	0.00300	
3.0–5	1.00267	0.00071	1.00955	0.00278	
5.0–7	1.00452	0.00121	1.01345	0.00442	

Table 8: ξ in Run 11

Trigger p_T 4–5 GeV/c					
assoc p_T	GeV/c	0–20%		20–40%	
		ξ	σ	ξ	σ
0.5–1		1.00381	0.00109	1.01179	0.00353
1.0–2		1.00353	0.00098	1.01245	0.00368
2.0–3		1.00315	0.00087	1.01254	0.00373
3.0–5		1.00335	0.00094	1.01119	0.00331
5.0–7		1.00595	0.00172	1.01765	0.00525
Trigger p_T 5–7 GeV/c					
assoc p_T	GeV/c	0–20%		20–40%	
		ξ	σ	ξ	σ
0.5–1		1.00310	0.00084	1.01083	0.00314
1.0–2		1.00288	0.00078	1.01145	0.00331
2.0–3		1.00259	0.00072	1.01155	0.00332
3.0–5		1.00274	0.00073	1.01029	0.00297
5.0–7		1.00483	0.00133	1.01619	0.00468
Trigger p_T 7–9 GeV/c					
assoc p_T	GeV/c	0–20%		20–40%	
		ξ	σ	ξ	σ
0.5–1		1.00306	0.00083	1.01013	0.00294
1.0–2		1.00284	0.00076	1.01071	0.00310
2.0–3		1.00254	0.00070	1.01080	0.00311
3.0–5		1.00270	0.00072	1.00962	0.00279
5.0–7		1.00477	0.00131	1.01514	0.00438
Trigger p_T 9–12 GeV/c					
assoc p_T	GeV/c	0–20%		20–40%	
		ξ	σ	ξ	σ
0.5–1		1.00305	0.00083	1.01211	0.00352
1.0–2		1.00285	0.00079	1.01280	0.00368
2.0–3		1.00256	0.00073	1.01291	0.00375
3.0–5		1.00270	0.00074	1.01150	0.00331
5.0–7		1.00475	0.00129	1.01809	0.00522
Trigger p_T 12–15 GeV/c					
assoc p_T	GeV/c	0–20%		20–40%	
		ξ	σ	ξ	σ
0.5–1		1.00348	0.00095	1.01168	0.00340
1.0–2		1.00323	0.00087	1.01233	0.00357
2.0–3		1.00289	0.00079	1.01241	0.00358
3.0–5		1.00307	0.00083	1.01108	0.00321
5.0–7		1.00544	0.00151	1.01748	0.00507

E Data Tables: Jet Functions

Table 9: 0–20%, 4.0–5.0 \otimes 0.5–1.0 GeV/c Jet Function

ϕ	per trig yield	σ_{stat}/y	systematic errors											
			$+\sigma_{f_2}/y$	$-\sigma_{f_2}/y$	$+\sigma_{f_3}/y$	$-\sigma_{f_3}/y$	$+\sigma_{f_4}/y$	$-\sigma_{f_4}/y$	$+\sigma_\xi/y$	$-\sigma_\xi/y$	$+\sigma_{\pi^0}/y$	$-\sigma_{\pi^0}/y$	$+\sigma_{total}/y$	$-\sigma_{total}/y$
-1.47	-0.04442	-0.97259	0.19534	-0.18923	0.03035	-0.02841	0.07451	-0.08525	0.47507	-0.47505	0.11751	-0.11751	0.53304	-0.53232
-1.26	-0.07493	-0.51836	0.09577	-0.09278	0.04710	-0.04410	0.01494	-0.01709	0.28154	-0.28152	0.11751	-0.11751	0.32355	-0.32235
-1.05	-0.01840	-1.67012	0.24099	-0.23345	0.23701	-0.22192	0.11261	-0.09843	1.14752	-1.14746	0.11751	-0.11751	1.20728	-1.20163
-0.84	0.00030	87.62950	3.10968	-3.01238	11.83548	-11.08168	13.59817	-11.88535	71.01677	-71.01329	0.11751	-0.11751	73.33522	-72.91119
-0.63	0.02180	1.06169	0.12180	-0.12573	0.06183	-0.05789	0.15382	-0.13445	0.97498	-0.97494	0.11751	-0.11751	1.00335	-1.00077
-0.42	0.08283	0.26114	0.06941	-0.07166	0.01524	-0.01627	0.00523	-0.00457	0.25764	-0.25763	0.11751	-0.11751	0.29200	-0.29258
-0.21	0.11745	0.17280	0.06683	-0.06899	0.02813	-0.03005	0.02064	-0.02361	0.18226	-0.18225	0.11751	-0.11751	0.22959	-0.23075
-0.00	0.15685	0.12793	0.05478	-0.05655	0.02604	-0.02781	0.02310	-0.02643	0.13663	-0.13662	0.11751	-0.11751	0.19154	-0.19273
0.21	0.09105	0.22796	0.08621	-0.08899	0.03629	-0.03876	0.02662	-0.03046	0.23509	-0.23508	0.11751	-0.11751	0.28024	-0.28182
0.42	0.05637	0.39551	0.10200	-0.10529	0.02239	-0.02391	0.00769	-0.00672	0.37858	-0.37857	0.11751	-0.11751	0.41000	-0.41088
0.63	0.00088	28.58653	3.02568	-3.12340	1.53594	-1.43812	3.82119	-3.33987	24.21989	-24.21870	0.11751	-0.11751	24.75343	-24.68882
0.84	-0.01553	-1.87851	0.05972	-0.05785	0.22729	-0.21281	0.26114	-0.22825	1.36381	-1.36374	0.11751	-0.11751	1.41323	-1.40511
1.05	-0.07586	-0.43659	0.05847	-0.05664	0.05750	-0.05384	0.02732	-0.02388	0.27840	-0.27838	0.11751	-0.11751	0.31430	-0.31302
1.26	-0.05879	-0.66427	0.12205	-0.11823	0.06002	-0.05620	0.01904	-0.02178	0.35878	-0.35877	0.11751	-0.11751	0.40174	-0.40017
1.47	-0.09524	-0.50231	0.09109	-0.08824	0.01415	-0.01325	0.03475	-0.03976	0.22155	-0.22154	0.11751	-0.11751	0.26944	-0.26913
1.68	-0.00360	-12.41688	2.40748	-2.33215	0.35019	-0.37401	0.91836	-1.05071	5.86224	-5.86196	0.01466	-0.01466	6.41312	-6.40668
1.88	0.04870	0.77072	0.14735	-0.14274	0.06785	-0.07246	0.02299	-0.02630	0.43455	-0.43453	0.01466	-0.01466	0.46464	-0.46405
2.09	0.08647	0.36072	0.05129	-0.04969	0.04723	-0.05044	0.02397	-0.02095	0.24519	-0.24517	0.01466	-0.01466	0.25645	-0.25647
2.30	0.09906	0.27576	0.00936	-0.00907	0.03335	-0.03562	0.04093	-0.03577	0.21441	-0.21440	0.01466	-0.01466	0.22150	-0.22094
2.51	0.17177	0.14102	0.01546	-0.01596	0.00735	-0.00785	0.01952	-0.01706	0.12388	-0.12388	0.01466	-0.01466	0.12742	-0.12715
2.72	0.15454	0.14502	0.03720	-0.03840	0.00872	-0.00817	0.00280	-0.00245	0.13792	-0.13791	0.01466	-0.01466	0.14389	-0.14416
2.93	0.18174	0.11951	0.04319	-0.04459	0.01942	-0.01818	0.01334	-0.01526	0.11741	-0.11741	0.01466	-0.01466	0.12814	-0.12865
3.14	0.16761	0.13069	0.05126	-0.05292	0.02602	-0.02437	0.02161	-0.02473	0.12736	-0.12736	0.01466	-0.01466	0.14216	-0.14297
3.35	0.18747	0.11755	0.04187	-0.04322	0.01882	-0.01762	0.01293	-0.01479	0.11383	-0.11382	0.01466	-0.01466	0.12428	-0.12477
3.56	0.15365	0.15137	0.03742	-0.03863	0.00877	-0.00821	0.00282	-0.00246	0.13871	-0.13871	0.01466	-0.01466	0.14471	-0.14498
3.77	0.10325	0.24511	0.02572	-0.02655	0.01222	-0.01305	0.03248	-0.02839	0.20610	-0.20609	0.01466	-0.01466	0.21108	-0.21063
3.98	0.13982	0.19768	0.00663	-0.00642	0.02363	-0.02524	0.02900	-0.02534	0.15192	-0.15191	0.01466	-0.01466	0.15728	-0.15688
4.19	0.05754	0.58156	0.07707	-0.07466	0.07097	-0.07580	0.03602	-0.03148	0.36843	-0.36841	0.01466	-0.01466	0.38501	-0.38504
4.40	0.05661	0.69958	0.12676	-0.12279	0.05836	-0.06233	0.01978	-0.02263	0.37381	-0.37380	0.01466	-0.01466	0.39977	-0.39927
4.61	0.08704	0.48143	0.09968	-0.09656	0.01450	-0.01549	0.03802	-0.04350	0.24271	-0.24270	0.01466	-0.01466	0.26592	-0.26566

Table 10: 0–20%, 4.0–5.0 \otimes 1.0–2.0 GeV/c Jet Function

ϕ	per trig yield	σ_{stat}/y	systematic errors											
			$+\sigma_{f2}/y$	$-\sigma_{f2}/y$	$+\sigma_{f3}/y$	$-\sigma_{f3}/y$	$+\sigma_{f4}/y$	$-\sigma_{f4}/y$	$+\sigma_\xi/y$	$-\sigma_\xi/y$	$+\sigma_{\pi^0}/y$	$-\sigma_{\pi^0}/y$	$+\sigma_{total}/y$	$-\sigma_{total}/y$
-1.47	0.01744	1.21192	0.21430	-0.20872	0.05495	-0.05148	0.16705	-0.19099	0.28883	-0.28883	0.06037	-0.06037	0.40486	-0.41201
-1.26	0.01455	1.27204	0.21241	-0.20688	0.17240	-0.16151	0.06772	-0.07743	0.34553	-0.34553	0.06037	-0.06037	0.44996	-0.44488
-1.05	0.01011	1.44020	0.18903	-0.18411	0.30685	-0.28746	0.18039	-0.15777	0.49807	-0.49807	0.06037	-0.06037	0.64354	-0.62700
-0.84	0.01792	0.67540	0.02229	-0.02171	0.14001	-0.13117	0.19904	-0.17408	0.28226	-0.28226	0.06037	-0.06037	0.37819	-0.36235
-0.63	0.03794	0.28502	0.03032	-0.03113	0.02526	-0.02367	0.07776	-0.06801	0.13439	-0.13439	0.06037	-0.06037	0.17120	-0.16691
-0.42	0.09700	0.10429	0.02567	-0.02636	0.00926	-0.00988	0.00393	-0.00344	0.05303	-0.05303	0.06037	-0.06037	0.08495	-0.08521
-0.21	0.19401	0.04898	0.01752	-0.01799	0.01212	-0.01293	0.01100	-0.01258	0.02670	-0.02670	0.06037	-0.06037	0.07023	-0.07075
-0.00	0.21728	0.04234	0.01713	-0.01759	0.01337	-0.01427	0.01468	-0.01678	0.02391	-0.02391	0.06037	-0.06037	0.07002	-0.07078
0.21	0.18705	0.05112	0.01818	-0.01866	0.01257	-0.01341	0.01141	-0.01304	0.02770	-0.02770	0.06037	-0.06037	0.07092	-0.07148
0.42	0.10502	0.09954	0.02371	-0.02435	0.00855	-0.00913	0.00363	-0.00317	0.04898	-0.04898	0.06037	-0.06037	0.08180	-0.08203
0.63	0.05289	0.22113	0.02174	-0.02233	0.01812	-0.01698	0.05578	-0.04879	0.09640	-0.09640	0.06037	-0.06037	0.12980	-0.12690
0.84	-0.00219	-6.22663	0.18244	-0.17769	1.14605	-1.07363	1.62917	-1.42493	2.31038	-2.31038	0.06037	-0.06037	3.05654	-2.92509
1.05	-0.01208	-1.28266	0.15810	-0.15398	0.25663	-0.24042	0.15087	-0.13196	0.41656	-0.41656	0.06037	-0.06037	0.53925	-0.52544
1.26	-0.03603	-0.52083	0.08579	-0.08356	0.06963	-0.06523	0.02735	-0.03127	0.13955	-0.13955	0.06037	-0.06037	0.18994	-0.18797
1.47	0.00224	10.71107	1.66853	-1.62507	0.42783	-0.40079	1.30064	-1.48708	2.24880	-2.24880	0.06037	-0.06037	3.11760	-3.17389
1.68	0.04158	0.53013	0.08988	-0.08754	0.02159	-0.02305	0.07007	-0.08011	0.12152	-0.12152	0.00231	-0.00231	0.16801	-0.17142
1.88	-0.00776	-2.34473	0.39832	-0.38794	0.30286	-0.32329	0.12699	-0.14519	0.65320	-0.65320	0.00231	-0.00231	0.83258	-0.83831
2.09	0.01989	0.74521	0.09604	-0.09354	0.14605	-0.15590	0.09165	-0.08016	0.25559	-0.25559	0.00231	-0.00231	0.32293	-0.32375
2.30	0.04697	0.27105	0.00850	-0.00828	0.05004	-0.05341	0.07593	-0.06641	0.10855	-0.10855	0.00231	-0.00231	0.14188	-0.13828
2.51	0.07632	0.14656	0.01507	-0.01547	0.01176	-0.01256	0.03865	-0.03381	0.06700	-0.06700	0.00231	-0.00231	0.07971	-0.07768
2.72	0.06817	0.14986	0.03653	-0.03751	0.01406	-0.01317	0.00559	-0.00489	0.07524	-0.07524	0.00231	-0.00231	0.08503	-0.08527
2.93	0.07479	0.13405	0.04546	-0.04668	0.03355	-0.03143	0.02853	-0.03262	0.06872	-0.06872	0.00231	-0.00231	0.09346	-0.09465
3.14	0.06209	0.16264	0.05994	-0.06154	0.04995	-0.04679	0.05136	-0.05873	0.08284	-0.08284	0.00231	-0.00231	0.12487	-0.12764
3.35	0.06945	0.14725	0.04895	-0.05026	0.03613	-0.03384	0.03073	-0.03513	0.07400	-0.07400	0.00231	-0.00231	0.10064	-0.10192
3.56	0.07311	0.14462	0.03406	-0.03497	0.01311	-0.01228	0.00521	-0.00456	0.07015	-0.07015	0.00231	-0.00231	0.07928	-0.07951
3.77	0.06116	0.18711	0.01880	-0.01931	0.01468	-0.01567	0.04824	-0.04219	0.08362	-0.08362	0.00231	-0.00231	0.09946	-0.09693
3.98	0.06886	0.19046	0.00580	-0.00565	0.03414	-0.03644	0.05180	-0.04531	0.07405	-0.07405	0.00231	-0.00231	0.09681	-0.09435
4.19	0.05290	0.29685	0.03611	-0.03517	0.05492	-0.05862	0.03446	-0.03014	0.09611	-0.09611	0.00231	-0.00231	0.12145	-0.12176
4.40	0.02888	0.66552	0.10704	-0.10425	0.08138	-0.08687	0.03412	-0.03901	0.17553	-0.17553	0.00231	-0.00231	0.22374	-0.22528
4.61	-0.02030	-1.04962	0.18409	-0.17929	0.04422	-0.04720	0.14350	-0.16407	0.24888	-0.24888	0.00231	-0.00231	0.34407	-0.35105

Table 11: 0–20%, 4.0–5.0 \otimes 2.0–3.0 GeV/c Jet Function

ϕ	per trig yield	σ_{stat}/y	systematic errors											
			$+\sigma_{f2}/y$	$-\sigma_{f2}/y$	$+\sigma_{f3}/y$	$-\sigma_{f3}/y$	$+\sigma_{f4}/y$	$-\sigma_{f4}/y$	$+\sigma_\xi/y$	$-\sigma_\xi/y$	$+\sigma_{\pi^0}/y$	$-\sigma_{\pi^0}/y$	$+\sigma_{total}/y$	$-\sigma_{total}/y$
-1.47	0.00875	0.65086	0.05501	-0.05343	0.01398	-0.01316	0.04528	-0.05126	0.03934	-0.03938	0.02562	-0.02562	0.08646	-0.08867
-1.26	-0.00042	-11.19667	0.94979	-0.92240	0.76409	-0.71927	0.31970	-0.36195	0.81761	-0.81835	0.02562	-0.02562	1.50243	-1.47293
-1.05	0.00486	0.81902	0.05069	-0.04923	0.08156	-0.07677	0.05057	-0.04467	0.07060	-0.07067	0.02562	-0.02562	0.13198	-0.12635
-0.84	0.00411	0.74491	0.01252	-0.01216	0.07796	-0.07339	0.11690	-0.10326	0.08399	-0.08406	0.02562	-0.02562	0.16617	-0.15466
-0.63	0.01711	0.17214	0.00863	-0.00889	0.00715	-0.00673	0.02322	-0.02051	0.02043	-0.02045	0.02562	-0.02562	0.04169	-0.04024
-0.42	0.02438	0.10874	0.01312	-0.01351	0.00473	-0.00502	0.02211	-0.00186	0.01456	-0.01458	0.02562	-0.02562	0.03267	-0.03286
-0.21	0.06492	0.04132	0.00673	-0.00693	0.00465	-0.00494	0.00447	-0.00506	0.00554	-0.00554	0.02562	-0.02562	0.02782	-0.02802
-0.00	0.11860	0.02177	0.00403	-0.00415	0.00314	-0.00334	0.00366	-0.00414	0.00303	-0.00303	0.02562	-0.02562	0.02655	-0.02667
0.21	0.06481	0.04156	0.00674	-0.00694	0.00465	-0.00494	0.00448	-0.00507	0.00555	-0.00555	0.02562	-0.02562	0.02782	-0.02803
0.42	0.02804	0.09703	0.01141	-0.01175	0.00411	-0.00437	0.00183	-0.00162	0.01267	-0.01268	0.02562	-0.02562	0.03110	-0.03125
0.63	0.01666	0.19181	0.00887	-0.00913	0.00734	-0.00691	0.02384	-0.02106	0.02098	-0.02100	0.02562	-0.02562	0.04240	-0.04089
0.84	0.00671	0.51320	0.00767	-0.00745	0.04777	-0.04497	0.07163	-0.06327	0.05146	-0.05151	0.02562	-0.02562	0.10381	-0.09690
1.05	-0.00528	-0.79476	0.04665	-0.04530	0.07505	-0.07065	0.04654	-0.04111	0.06497	-0.06503	0.02562	-0.02562	0.12187	-0.11670
1.26	-0.00197	-2.42798	0.20266	-0.19681	0.16303	-0.15347	0.06821	-0.07723	0.17445	-0.17461	0.02562	-0.02562	0.32155	-0.31527
1.47	-0.00260	-2.40776	0.18514	-0.17980	0.04705	-0.04429	0.15238	-0.17251	0.13241	-0.13253	0.02562	-0.02562	0.27910	-0.28683
1.68	-0.00023	-26.38887	2.09758	-2.03708	0.50183	-0.53311	1.72640	-1.95453	1.50873	-1.51010	0.09434	-0.09434	3.14917	-3.24706
1.88	-0.00045	-10.35824	0.88329	-0.85781	0.66890	-0.71059	0.29732	-0.33661	0.77182	-0.77252	0.09434	-0.09434	1.38587	-1.39992
2.09	0.00551	0.73239	0.04465	-0.04336	0.06762	-0.07183	0.04454	-0.03934	0.06334	-0.06340	0.09434	-0.09434	0.14650	-0.14666
2.30	0.00186	1.74878	0.02761	-0.02682	0.16186	-0.17194	0.25782	-0.22772	0.18800	-0.18818	0.09434	-0.09434	0.37105	-0.35560
2.51	0.00830	0.36239	0.01780	-0.01833	0.01388	-0.01474	0.04787	-0.04228	0.04236	-0.04240	0.09434	-0.09434	0.11617	-0.11419
2.72	0.00730	0.35678	0.04382	-0.04512	0.01676	-0.01578	0.00703	-0.00621	0.04837	-0.04842	0.09434	-0.09434	0.11615	-0.11648
2.93	0.00458	0.58541	0.09532	-0.09815	0.06993	-0.06583	0.06336	-0.07173	0.07734	-0.07741	0.09434	-0.09434	0.18131	-0.18440
3.14	0.00727	0.35472	0.06579	-0.06774	0.05450	-0.05130	0.05970	-0.06759	0.04883	-0.04888	0.09434	-0.09434	0.14882	-0.15191
3.35	0.00879	0.31456	0.04969	-0.05117	0.03646	-0.03432	0.03303	-0.03739	0.04032	-0.04036	0.09434	-0.09434	0.12416	-0.12539
3.56	0.00427	0.62209	0.07490	-0.07712	0.02865	-0.02697	0.01202	-0.01062	0.08268	-0.08275	0.09434	-0.09434	0.14937	-0.15012
3.77	0.00594	0.51467	0.02486	-0.02560	0.01939	-0.02059	0.06687	-0.05906	0.05917	-0.05923	0.09434	-0.09434	0.13367	-0.13029
3.98	0.00389	0.84782	0.01322	-0.01284	0.07751	-0.08234	0.12346	-0.10905	0.09003	-0.09011	0.09434	-0.09434	0.19604	-0.18936
4.19	0.01119	0.38107	0.02199	-0.02135	0.03330	-0.03538	0.02194	-0.01938	0.03120	-0.03122	0.09434	-0.09434	0.10930	-0.10935
4.40	0.00597	0.80596	0.06667	-0.06475	0.05049	-0.05364	0.02244	-0.02541	0.05826	-0.05831	0.09434	-0.09434	0.14069	-0.14148
4.61	-0.00124	-4.88647	0.38888	-0.37766	0.09304	-0.09884	0.32006	-0.36236	0.27971	-0.27997	0.09434	-0.09434	0.59115	-0.60908

Table 12: 0–20%, 4.0–5.0 \otimes 3.0–5.0 GeV/c Jet Function

ϕ	per trig yield	σ_{stat}/y	systematic errors												
			$+\sigma_{f2}/y$	$-\sigma_{f2}/y$	$+\sigma_{f3}/y$	$-\sigma_{f3}/y$	$+\sigma_{f4}/y$	$-\sigma_{f4}/y$	$+\sigma_\xi/y$	$-\sigma_\xi/y$	$+\sigma_{\pi^0}/y$	$-\sigma_{\pi^0}/y$	$+\sigma_{total}/y$	$-\sigma_{total}/y$	
-1.47	-0.00076	-2.65713	0.09986	-0.09666	0.02485	-0.02337	0.09145	-0.10364	0.06271	-0.06225	0.08208	-0.08208	0.17212	-0.17675	
-1.26	-0.00030	-5.45354	0.20812	-0.20144	0.16390	-0.15416	0.07794	-0.08833	0.15711	-0.15594	0.08208	-0.08208	0.32814	-0.32125	
-1.05	-0.00192	-0.72986	0.02019	-0.01954	0.03180	-0.02991	0.02244	-0.01980	0.02464	-0.02445	0.08208	-0.08208	0.09627	-0.09489	
-0.84	-0.00051	-2.09521	0.01588	-0.01537	0.09678	-0.09103	0.16510	-0.14568	0.09328	-0.09258	0.08208	-0.08208	0.22872	-0.21226	
-0.63	0.00242	0.43930	0.00957	-0.00989	0.00779	-0.00733	0.02878	-0.02539	0.01993	-0.01979	0.08208	-0.08208	0.09009	-0.08903	
-0.42	0.00663	0.14581	0.00755	-0.00780	0.00267	-0.00284	0.00135	-0.00120	0.00739	-0.00733	0.08208	-0.08208	0.08282	-0.08284	
-0.21	0.02246	0.04713	0.00305	-0.00315	0.00206	-0.00219	0.00226	-0.00256	0.00221	-0.00220	0.08208	-0.08208	0.08223	-0.08224	
-0.00	0.06112	0.01904	0.00122	-0.00127	0.00094	-0.00100	0.00124	-0.00141	0.00082	-0.00081	0.08208	-0.08208	0.08211	-0.08212	
0.21	0.02163	0.04944	0.00316	-0.00327	0.00214	-0.00228	0.00235	-0.00266	0.00230	-0.00228	0.08208	-0.08208	0.08224	-0.08226	
0.42	0.00615	0.16241	0.00814	-0.00841	0.00288	-0.00306	0.00146	-0.00129	0.00796	-0.00790	0.08208	-0.08208	0.08293	-0.08296	
0.63	0.00004	31.19426	0.62436	-0.64507	0.50801	-0.47783	1.87657	-1.65586	1.29997	-1.29025	0.08208	-0.08208	2.42199	-2.24895	
0.84	0.00243	0.51762	0.00333	-0.00323	0.02031	-0.01911	0.03465	-0.03058	0.01958	-0.01943	0.08208	-0.08208	0.09352	-0.09179	
1.05	0.00158	1.00986	0.02443	-0.02365	0.03848	-0.03620	0.02715	-0.02396	0.02981	-0.02959	0.08208	-0.08208	0.10218	-0.10028	
1.26	0.00006	28.88087	0.40414	-0.00771	0.81992	-0.77122	0.38992	-0.44189	0.78597	-0.78010	0.08208	-0.08208	1.59147	-1.55590	
1.47	-0.00015	-14.69950	0.50418	-0.48799	0.12544	-0.11799	0.46169	-0.52323	0.31662	-0.31426	0.08208	-0.08208	0.76816	-0.79455	
1.68	-0.00191	-1.12342	0.03962	-0.03834	0.00927	-0.00986	0.03628	-0.04111	0.02504	-0.02485	0.10132	-0.10132	0.11774	-0.11891	
1.88	0.00135	1.24519	0.04649	-0.04500	0.03444	-0.03661	0.01741	-0.01973	0.03569	-0.03543	0.10132	-0.10132	0.12325	-0.12359	
2.09	-0.00078	-1.85399	0.04946	-0.04787	0.07328	-0.07790	0.05496	-0.04850	0.06162	-0.06116	0.10132	-0.10132	0.15779	-0.15722	
2.30	0.00394	0.30415	0.00205	-0.00199	0.01177	-0.01251	0.02135	-0.01884	0.01227	-0.01217	0.10132	-0.10132	0.10495	-0.10454	
2.51	0.00254	0.43400	0.00911	-0.00941	0.00697	-0.00741	0.02737	-0.02415	0.01908	-0.01894	0.10132	-0.10132	0.10728	-0.10654	
2.72	0.00175	0.53148	0.02859	-0.02954	0.01074	-0.01011	0.00513	-0.00452	0.02780	-0.02759	0.10132	-0.10132	0.10953	-0.10964	
2.93	0.00398	0.25089	0.01719	-0.01776	0.01239	-0.01165	0.01276	-0.01446	0.01229	-0.01220	0.10132	-0.10132	0.10501	-0.10523	
3.14	0.00484	0.19653	0.01546	-0.01597	0.01258	-0.01183	0.01566	-0.01775	0.01011	-0.01004	0.10132	-0.10132	0.10493	-0.10524	
3.35	0.00296	0.34593	0.02310	-0.02387	0.01664	-0.01566	0.01714	-0.01942	0.01652	-0.01639	0.10132	-0.10132	0.10790	-0.10828	
3.56	0.00182	0.52481	0.02746	-0.02837	0.01032	-0.00971	0.00493	-0.00435	0.02670	-0.02650	0.10132	-0.10132	0.10892	-0.10902	
3.77	-0.00011	-9.94205	0.20872	-0.21565	0.15974	-0.16983	0.62734	-0.55356	0.43735	-0.43408	0.10132	-0.10132	0.81497	-0.76188	
3.98	0.00111	1.06722	0.00726	-0.00703	0.04163	-0.04426	0.07550	-0.06662	0.04338	-0.04305	0.10132	-0.10132	0.14012	-0.13625	
4.19	0.00163	0.97143	0.02374	-0.02297	0.03517	-0.03739	0.02638	-0.02327	0.02957	-0.02935	0.10132	-0.10132	0.11677	-0.11659	
4.40	0.00152	1.13156	0.04116	-0.03984	0.03049	-0.03242	0.01542	-0.01747	0.03160	-0.03137	0.10132	-0.10132	0.11885	-0.11913	
4.61	-0.00023	-9.96173	0.33183	-0.32118	0.07765	-0.08256	0.30387	-0.34437	0.20974	-0.20817	0.10132	-0.10132	0.51257	-0.53119	

Table 13: 0–20%, 4.0–5.0 \otimes 5.0–7.0 GeV/c Jet Function

ϕ	per trig yield	σ_{stat}/y	systematic errors												
			$+\sigma_{f2}/y$	$-\sigma_{f2}/y$	$+\sigma_{f3}/y$	$-\sigma_{f3}/y$	$+\sigma_{f4}/y$	$-\sigma_{f4}/y$	$+\sigma_{\xi}/y$	$-\sigma_{\xi}/y$	$+\sigma_{\pi^0}/y$	$-\sigma_{\pi^0}/y$	$+\sigma_{total}/y$	$-\sigma_{total}/y$	
-1.47	-0.00042	-1.74135	0.03134	-0.03007	0.01707	-0.01554	0.04793	-0.05602	0.03064	-0.02988	0.08179	-0.08179	0.10583	-0.10893	
-1.26	0.00095	0.66656	0.01142	-0.01096	0.01970	-0.01793	0.00715	-0.00835	0.01347	-0.01313	0.08179	-0.08179	0.08625	-0.08586	
-1.05	0.00064	0.83836	0.01050	-0.01007	0.03619	-0.03294	0.02009	-0.01719	0.02002	-0.01953	0.08179	-0.08179	0.09441	-0.09248	
-0.84	-0.00003	-14.13041	0.05138	-0.04929	0.68554	-0.62401	0.92004	-0.78725	0.47109	-0.45951	0.08179	-0.08179	1.24407	-1.10879	
-0.63	0.00011	3.46655	0.03613	-0.03766	0.06493	-0.05910	0.18868	-0.16145	0.11788	-0.11498	0.08179	-0.08179	0.24841	-0.22558	
-0.42	0.00014	2.50130	0.06355	-0.06625	0.04801	-0.05275	0.01981	-0.01695	0.09681	-0.09443	0.08179	-0.08179	0.15099	-0.15187	
-0.21	0.00261	0.14423	0.00451	-0.00470	0.00653	-0.00718	0.00564	-0.00659	0.00508	-0.00495	0.08179	-0.08179	0.08252	-0.08265	
-0.00	0.01233	0.03751	0.00105	-0.00109	0.00171	-0.00188	0.00178	-0.00208	0.00108	-0.00105	0.08179	-0.08179	0.08184	-0.08185	
0.21	0.00328	0.12235	0.00359	-0.00375	0.00521	-0.00572	0.00449	-0.00525	0.00404	-0.00395	0.08179	-0.08179	0.08225	-0.08233	
0.42	-0.00035	-0.99945	0.02433	-0.02536	0.01838	-0.02019	0.00758	-0.00649	0.03706	-0.03615	0.08179	-0.08179	0.09513	-0.09533	
0.63	0.00029	1.60498	0.01392	-0.01451	0.02502	-0.02278	0.07272	-0.06222	0.04543	-0.04432	0.08179	-0.08179	0.12191	-0.11513	
0.84	0.00001	33.06768	0.09878	-0.09476	1.31802	-1.19971	1.76886	-1.51357	0.90572	-0.88345	0.08179	-0.08179	2.38806	-2.12752	
1.05	0.00029	2.14097	0.02287	-0.02194	0.07885	-0.07177	0.04376	-0.03745	0.04362	-0.04255	0.08179	-0.08179	0.13133	-0.12463	
1.26	0.00041	1.66139	0.02682	-0.02573	0.04624	-0.04209	0.01677	-0.01960	0.03161	-0.03083	0.08179	-0.08179	0.10405	-0.10226	
1.47	0.00102	0.84616	0.01291	-0.01239	0.00703	-0.00640	0.01975	-0.02308	0.01262	-0.01231	0.08179	-0.08179	0.08634	-0.08699	
1.68	-0.00015	-5.29570	0.08899	-0.08536	0.04412	-0.04847	0.13609	-0.15905	0.08730	-0.08515	0.46073	-0.46073	0.49828	-0.50444	
1.88	-0.00012	-5.03371	0.09218	-0.08843	0.14466	-0.15892	0.05766	-0.06738	0.10968	-0.10698	0.46073	-0.46073	0.50700	-0.51121	
2.09	0.00009	6.23727	0.07803	-0.07485	0.24490	-0.26905	0.14932	-0.12777	0.15060	-0.14690	0.46073	-0.46073	0.56861	-0.57286	
2.30	0.00035	1.24618	0.00405	-0.00389	0.04923	-0.05408	0.07258	-0.06211	0.03752	-0.03659	0.46073	-0.46073	0.47052	-0.46948	
2.51	0.00007	6.01727	0.05955	-0.06208	0.09742	-0.10703	0.31103	-0.26614	0.19501	-0.19022	0.46073	-0.46073	0.60007	-0.57844	
2.72	0.00025	1.38165	0.03488	-0.03636	0.02895	-0.02635	0.01087	-0.00930	0.05294	-0.05164	0.46073	-0.46073	0.46610	-0.46588	
2.93	0.00112	0.34074	0.01049	-0.01093	0.01669	-0.01519	0.01311	-0.01532	0.01170	-0.01141	0.46073	-0.46073	0.46149	-0.46151	
3.14	0.00065	0.55388	0.01968	-0.02052	0.03537	-0.03220	0.03360	-0.03927	0.02008	-0.01958	0.46073	-0.46073	0.46416	-0.46439	
3.35	0.00043	0.90166	0.02746	-0.02863	0.04371	-0.03978	0.03434	-0.04013	0.03063	-0.02987	0.46073	-0.46073	0.46589	-0.46603	
3.56	-0.00011	-3.19686	0.07722	-0.08050	0.06409	-0.05834	0.02407	-0.02059	0.11722	-0.11434	0.46073	-0.46073	0.48648	-0.48544	
3.77	0.00014	3.01873	0.02872	-0.02993	0.04697	-0.05161	0.14997	-0.12833	0.09403	-0.09172	0.46073	-0.46073	0.49663	-0.49063	
3.98	-0.00075	-0.57805	0.00187	-0.00180	0.02274	-0.02498	0.03352	-0.02868	0.01733	-0.01690	0.46073	-0.46073	0.46284	-0.46261	
4.19	-0.00031	-1.89540	0.02200	-0.02110	0.06903	-0.07584	0.04209	-0.03602	0.04245	-0.04141	0.46073	-0.46073	0.47021	-0.47062	
4.40	0.00028	2.21117	0.03823	-0.03668	0.06000	-0.06592	0.02391	-0.02795	0.04549	-0.04437	0.46073	-0.46073	0.46902	-0.46980	
4.61	-0.00076	-1.09768	0.01739	-0.01668	0.00862	-0.00947	0.02660	-0.03109	0.01706	-0.01664	0.46073	-0.46073	0.46222	-0.46248	

Table 14: 0–20%, 5.0–7.0 \otimes 0.5–1.0 GeV/c Jet Function

ϕ	per trig yield	σ_{stat}/y	systematic errors											
			$+\sigma_{f2}/y$	$-\sigma_{f2}/y$	$+\sigma_{f3}/y$	$-\sigma_{f3}/y$	$+\sigma_{f4}/y$	$-\sigma_{f4}/y$	$+\sigma_\xi/y$	$-\sigma_\xi/y$	$+\sigma_{\pi^0}/y$	$-\sigma_{\pi^0}/y$	$+\sigma_{total}/y$	$-\sigma_{total}/y$
-1.47	0.06444	0.88341	0.20235	-0.19265	0.02860	-0.02559	0.04817	-0.06130	0.25088	-0.25084	0.02194	-0.02194	0.32788	-0.32393
-1.26	-0.04191	-1.20636	0.25735	-0.24502	0.11515	-0.10301	0.02505	-0.03188	0.38572	-0.38566	0.02194	-0.02194	0.47893	-0.46998
-1.05	0.00152	26.38479	4.39450	-4.18398	3.93275	-3.51809	1.42543	-1.12003	10.66836	-10.66682	0.02194	-0.02194	12.27291	-12.03821
-0.84	-0.08091	-0.41981	0.01722	-0.01640	0.05964	-0.05335	0.05227	-0.04107	0.20044	-0.20041	0.02194	-0.02194	0.21736	-0.21319
-0.63	-0.03948	-0.76360	0.09935	-0.10435	0.04669	-0.04177	0.08861	-0.06963	0.41212	-0.41206	0.02194	-0.02194	0.43615	-0.43330
-0.42	0.08137	0.34814	0.10437	-0.10962	0.02026	-0.02265	0.00555	-0.00436	0.20061	-0.20058	0.02194	-0.02194	0.22817	-0.23079
-0.21	0.09060	0.29471	0.12798	-0.13442	0.04765	-0.05326	0.02509	-0.03194	0.18063	-0.18061	0.02194	-0.02194	0.22888	-0.23457
-0.00	0.18935	0.13997	0.06703	-0.07040	0.02818	-0.03150	0.01794	-0.02284	0.08651	-0.08649	0.02194	-0.02194	0.11651	-0.12014
0.21	0.16987	0.16215	0.06826	-0.07169	0.02541	-0.02841	0.01338	-0.01703	0.09634	-0.09632	0.02194	-0.02194	0.12347	-0.12648
0.42	0.03740	0.78961	0.22708	-0.23851	0.04409	-0.04929	0.01209	-0.00950	0.43647	-0.43641	0.02194	-0.02194	0.49462	-0.50034
0.63	0.00489	6.82085	0.80155	-0.84188	0.37671	-0.33699	0.71493	-0.56175	3.32506	-3.32457	0.02194	-0.02194	3.51454	-3.49159
0.84	-0.06931	-0.56231	0.02011	-0.01914	0.06963	-0.06229	0.06103	-0.04795	0.23400	-0.23397	0.02194	-0.02194	0.25341	-0.24853
1.05	-0.05438	-0.81712	0.12257	-0.11670	0.10969	-0.09813	0.03976	-0.03124	0.29756	-0.29752	0.02194	-0.02194	0.34302	-0.33648
1.26	-0.09026	-0.57676	0.11948	-0.11375	0.05346	-0.04782	0.01163	-0.01480	0.17908	-0.17905	0.02194	-0.02194	0.22320	-0.21906
1.47	-0.09945	-0.63653	0.13111	-0.12483	0.01853	-0.01658	0.03121	-0.03972	0.16255	-0.16253	0.02194	-0.02194	0.21310	-0.21055
1.68	0.03469	1.70928	0.37591	-0.35790	0.04754	-0.05314	0.08948	-0.11388	0.46652	-0.46645	0.01414	-0.01414	0.60779	-0.60138
1.88	0.05683	0.87264	0.18976	-0.18067	0.07596	-0.08491	0.01847	-0.02351	0.28513	-0.28509	0.01414	-0.01414	0.35159	-0.34911
2.09	0.07355	0.55843	0.09062	-0.08628	0.07255	-0.08110	0.02940	-0.02310	0.22069	-0.22066	0.01414	-0.01414	0.25148	-0.25188
2.30	0.14958	0.24004	0.00932	-0.00887	0.02886	-0.03226	0.02828	-0.02222	0.10869	-0.10868	0.01414	-0.01414	0.11719	-0.11672
2.51	0.09743	0.32586	0.04025	-0.04228	0.01692	-0.01892	0.03590	-0.02821	0.16714	-0.16712	0.01414	-0.01414	0.17701	-0.17627
2.72	0.18349	0.16034	0.04628	-0.04861	0.01005	-0.00899	0.00246	-0.00194	0.08888	-0.08886	0.01414	-0.01414	0.10173	-0.10269
2.93	0.19452	0.14655	0.05960	-0.06260	0.02483	-0.02219	0.01169	-0.01487	0.08392	-0.08391	0.01414	-0.01414	0.10746	-0.10896
3.14	0.18506	0.15547	0.06858	-0.07203	0.03223	-0.02883	0.01836	-0.02336	0.08824	-0.08823	0.01414	-0.01414	0.11860	-0.12062
3.35	0.15801	0.18318	0.07338	-0.07707	0.03054	-0.02732	0.01439	-0.01831	0.10331	-0.10329	0.01414	-0.01414	0.13190	-0.13376
3.56	0.13295	0.23071	0.06387	-0.06709	0.01386	-0.01240	0.00340	-0.00267	0.12266	-0.12264	0.01414	-0.01414	0.13974	-0.14108
3.77	0.23029	0.14537	0.01703	-0.01789	0.00716	-0.00800	0.01519	-0.01194	0.07071	-0.07070	0.01414	-0.01414	0.07598	-0.07567
3.98	0.09926	0.36813	0.01404	-0.01337	0.04349	-0.04862	0.04261	-0.03348	0.16380	-0.16378	0.01414	-0.01414	0.17588	-0.17517
4.19	0.11688	0.38180	0.05703	-0.05429	0.04565	-0.05103	0.01850	-0.01453	0.13887	-0.13885	0.01414	-0.01414	0.15863	-0.15888
4.40	0.07175	0.73664	0.15031	-0.14311	0.06016	-0.06726	0.01463	-0.01862	0.22585	-0.22582	0.01414	-0.01414	0.27863	-0.27666
4.61	0.10029	0.55975	0.13002	-0.12379	0.01644	-0.01838	0.03095	-0.03939	0.16136	-0.16133	0.01414	-0.01414	0.21064	-0.20842

Table 15: 0–20%, 5.0–7.0 \otimes 1.0–2.0 GeV/c Jet Function

ϕ	per trig yield	σ_{stat}/y	systematic errors											
			$+\sigma_{f2}/y$	$-\sigma_{f2}/y$	$+\sigma_{f3}/y$	$-\sigma_{f3}/y$	$+\sigma_{f4}/y$	$-\sigma_{f4}/y$	$+\sigma_\xi/y$	$-\sigma_\xi/y$	$+\sigma_{\pi^0}/y$	$-\sigma_{\pi^0}/y$	$+\sigma_{total}/y$	$-\sigma_{total}/y$
-1.47	-0.02012	-1.37618	0.30503	-0.29398	0.06549	-0.05865	0.13711	-0.17408	0.19855	-0.19859	0.01759	-0.01759	0.39480	-0.39989
-1.26	-0.01441	-1.66960	0.35215	-0.33938	0.23933	-0.21431	0.06473	-0.08219	0.27681	-0.27686	0.01759	-0.01759	0.51226	-0.49480
-1.05	-0.01866	-1.01071	0.16806	-0.16197	0.22844	-0.20455	0.10269	-0.08088	0.21401	-0.21404	0.01759	-0.01759	0.37024	-0.34748
-0.84	0.03334	0.47334	0.01967	-0.01896	0.10348	-0.09266	0.11248	-0.08859	0.12032	-0.12034	0.01759	-0.01759	0.19630	-0.17772
-0.63	0.04136	0.34044	0.04518	-0.04688	0.03186	-0.02853	0.07499	-0.05906	0.09763	-0.09764	0.01759	-0.01759	0.13609	-0.12784
-0.42	0.07666	0.17243	0.05277	-0.05476	0.01539	-0.01719	0.00523	-0.00412	0.05305	-0.05306	0.01759	-0.01759	0.07857	-0.08022
-0.21	0.24099	0.05201	0.02292	-0.02378	0.01282	-0.01431	0.00838	-0.01064	0.01697	-0.01698	0.01759	-0.01759	0.03684	-0.03849
-0.00	0.27444	0.04441	0.02203	-0.02286	0.01391	-0.01554	0.01100	-0.01397	0.01494	-0.01494	0.01759	-0.01759	0.03650	-0.03862
0.21	0.21293	0.05945	0.02594	-0.02692	0.01451	-0.01620	0.00949	-0.01205	0.01921	-0.01921	0.01759	-0.01759	0.04064	-0.04255
0.42	0.08309	0.16621	0.04869	-0.05052	0.01420	-0.01586	0.00482	-0.00380	0.04894	-0.04895	0.01759	-0.01759	0.07280	-0.07432
0.63	0.03850	0.40352	0.04852	-0.05035	0.03422	-0.03064	0.08054	-0.06344	0.10486	-0.10487	0.01759	-0.01759	0.14600	-0.13713
0.84	-0.03865	-0.47096	0.01697	-0.01635	0.08925	-0.07992	0.09702	-0.07641	0.10378	-0.10380	0.01759	-0.01759	0.16954	-0.15354
1.05	0.00494	4.23309	0.63511	-0.61208	0.86328	-0.77303	0.38807	-0.30566	0.80875	-0.80888	0.01759	-0.01759	1.39771	-1.31158
1.26	-0.01910	-1.31175	0.26575	-0.25611	0.18061	-0.16173	0.04885	-0.06202	0.20889	-0.20893	0.01759	-0.01759	0.38675	-0.37357
1.47	0.01461	2.17437	0.42011	-0.40488	0.09020	-0.08077	0.18883	-0.23975	0.27346	-0.27350	0.01759	-0.01759	0.54348	-0.55049
1.68	0.01151	2.52842	0.53312	-0.51379	0.10250	-0.11447	0.23963	-0.30424	0.34787	-0.34793	0.00648	-0.00648	0.68790	-0.70053
1.88	0.04976	0.48717	0.10199	-0.09829	0.06207	-0.06931	0.01875	-0.02380	0.08069	-0.08070	0.00648	-0.00648	0.14546	-0.14692
2.09	0.07113	0.27593	0.04410	-0.04250	0.05367	-0.05994	0.02694	-0.02122	0.05660	-0.05661	0.00648	-0.00648	0.09379	-0.09537
2.30	0.09884	0.16997	0.06663	-0.06639	0.03125	-0.03490	0.03794	-0.02988	0.04084	-0.04085	0.00648	-0.00648	0.06457	-0.06215
2.51	0.06488	0.22565	0.02880	-0.02988	0.01819	-0.02031	0.04780	-0.03765	0.06238	-0.06239	0.00648	-0.00648	0.08590	-0.08160
2.72	0.08530	0.15702	0.04743	-0.04921	0.01545	-0.01383	0.00470	-0.00370	0.04756	-0.04757	0.00648	-0.00648	0.06938	-0.07023
2.93	0.08711	0.15087	0.06340	-0.06579	0.03960	-0.03546	0.02319	-0.02944	0.04666	-0.04667	0.00648	-0.00648	0.09135	-0.09313
3.14	0.08565	0.15532	0.07059	-0.07324	0.04978	-0.04457	0.03525	-0.04475	0.04749	-0.04749	0.00648	-0.00648	0.10488	-0.10794
3.35	0.06925	0.19419	0.07976	-0.08276	0.04981	-0.04460	0.02917	-0.03704	0.05869	-0.05870	0.00648	-0.00648	0.11480	-0.11704
3.56	0.08588	0.16249	0.04711	-0.04888	0.01534	-0.01374	0.00467	-0.00367	0.04724	-0.04725	0.00648	-0.00648	0.06892	-0.06976
3.77	0.07527	0.20065	0.02482	-0.02576	0.01567	-0.01750	0.04120	-0.03245	0.05377	-0.05378	0.00648	-0.00648	0.07411	-0.07041
3.98	0.04873	0.35606	0.01346	-0.01297	0.06338	-0.07078	0.07694	-0.06060	0.08283	-0.08284	0.00648	-0.00648	0.13046	-0.12552
4.19	0.01927	1.08005	0.16279	-0.15689	0.19814	-0.22128	0.09947	-0.07835	0.20895	-0.20898	0.00648	-0.00648	0.34548	-0.35133
4.40	0.01346	1.91243	0.37706	-0.36339	0.22947	-0.25627	0.06931	-0.08800	0.29831	-0.29836	0.00648	-0.00648	0.53728	-0.54270
4.61	0.02548	1.13156	0.24080	-0.23207	0.04630	-0.05170	0.10823	-0.13742	0.15713	-0.15715	0.00648	-0.00648	0.31076	-0.31647

Table 16: 0–20%, 5.0–7.0 \otimes 2.0–3.0 GeV/c Jet Function

ϕ	per trig yield	σ_{stat}/y	systematic errors											
			$+\sigma_{f2}/y$	$-\sigma_{f2}/y$	$+\sigma_{f3}/y$	$-\sigma_{f3}/y$	$+\sigma_{f4}/y$	$-\sigma_{f4}/y$	$+\sigma_{\xi}/y$	$-\sigma_{\xi}/y$	$+\sigma_{\pi^0}/y$	$-\sigma_{\pi^0}/y$	$+\sigma_{total}/y$	$-\sigma_{total}/y$
-1.47	0.00386	1.92785	0.19621	-0.18799	0.04583	-0.04145	0.10496	-0.13016	0.07269	-0.07277	0.01037	-0.01037	0.23876	-0.24373
-1.26	0.00131	4.69991	0.48012	-0.46000	0.35496	-0.32107	0.10504	-0.13026	0.21438	-0.21462	0.01037	-0.01037	0.64312	-0.61467
-1.05	0.00116	4.41763	0.33271	-0.31877	0.49195	-0.44498	0.23633	-0.19056	0.24051	-0.24079	0.01037	-0.01037	0.68302	-0.62771
-0.84	0.00225	1.76971	0.03600	-0.03449	0.20598	-0.18631	0.23926	-0.19293	0.12521	-0.12536	0.01037	-0.01037	0.34169	-0.29824
-0.63	0.00715	0.53071	0.03207	-0.03348	0.02475	-0.02239	0.06225	-0.05020	0.03981	-0.03986	0.01037	-0.01037	0.08491	-0.07641
-0.42	0.02497	0.13902	0.01989	-0.02076	0.00641	-0.00709	0.00230	-0.00186	0.01154	-0.01156	0.01037	-0.01037	0.02613	-0.02694
-0.21	0.08410	0.04259	0.00806	-0.00842	0.00498	-0.00551	0.00353	-0.00438	0.00346	-0.00347	0.01037	-0.01037	0.01489	-0.01549
-0.00	0.14288	0.02435	0.00520	-0.00542	0.00363	-0.00401	0.00311	-0.00385	0.00205	-0.00205	0.01037	-0.01037	0.01271	-0.01312
0.21	0.08438	0.04291	0.00804	-0.00839	0.00497	-0.00549	0.00352	-0.00436	0.00345	-0.00346	0.01037	-0.01037	0.01487	-0.01546
0.42	0.03077	0.11745	0.01614	-0.01685	0.00520	-0.00575	0.00187	-0.00151	0.00937	-0.00938	0.01037	-0.01037	0.02205	-0.02269
0.63	0.01549	0.27363	0.01480	-0.01545	0.01142	-0.01033	0.02874	-0.02317	0.01838	-0.01840	0.01037	-0.01037	0.04026	-0.03645
0.84	0.00431	1.06745	0.01879	-0.01800	0.10749	-0.09723	0.12486	-0.10069	0.06534	-0.06542	0.01037	-0.01037	0.17854	-0.15589
1.05	0.00643	0.89300	0.06027	-0.05775	0.08912	-0.08061	0.04281	-0.03452	0.04357	-0.04362	0.01037	-0.01037	0.12416	-0.11417
1.26	0.01190	0.54622	0.05268	-0.05047	0.03894	-0.03523	0.01152	-0.01429	0.02352	-0.02355	0.01037	-0.01037	0.07131	-0.06822
1.47	0.00571	1.46072	0.13268	-0.12712	0.03099	-0.02803	0.07097	-0.08802	0.04915	-0.04921	0.01037	-0.01037	0.16163	-0.16499
1.68	0.00273	2.94748	0.27803	-0.26638	0.05874	-0.06494	0.14873	-0.18444	0.10347	-0.10359	0.03138	-0.03138	0.33847	-0.34772
1.88	0.00636	0.97993	0.09854	-0.09441	0.06590	-0.07286	0.02156	-0.02674	0.04453	-0.04458	0.03138	-0.03138	0.13223	-0.13382
2.09	-0.00126	-4.20557	0.30825	-0.29533	0.41227	-0.45579	0.21895	-0.17655	0.22612	-0.22638	0.03138	-0.03138	0.60418	-0.61512
2.30	0.00952	0.45383	0.00851	-0.00815	0.04405	-0.04870	0.05657	-0.04561	0.02995	-0.02999	0.03138	-0.03138	0.08422	-0.08001
2.51	0.01311	0.30214	0.01750	-0.01826	0.01221	-0.01350	0.03396	-0.02739	0.02182	-0.02184	0.03138	-0.03138	0.05540	-0.05223
2.72	0.01645	0.20951	0.03020	-0.03152	0.01076	-0.00973	0.00350	-0.00282	0.01745	-0.01747	0.03138	-0.03138	0.04826	-0.04885
2.93	0.00659	0.53342	0.10295	-0.10746	0.07035	-0.06364	0.04508	-0.05591	0.04370	-0.04375	0.03138	-0.03138	0.14309	-0.14704
3.14	0.02044	0.16837	0.03632	-0.03791	0.02803	-0.02535	0.02171	-0.02693	0.01410	-0.01412	0.03138	-0.03138	0.06132	-0.06316
3.35	0.01155	0.31562	0.05871	-0.06127	0.04012	-0.03629	0.02571	-0.03188	0.02492	-0.02495	0.03138	-0.03138	0.08557	-0.08772
3.56	0.01521	0.23313	0.03267	-0.03409	0.01164	-0.01053	0.00378	-0.00305	0.01888	-0.01890	0.03138	-0.03138	0.05057	-0.05123
3.77	0.00600	0.66970	0.03821	-0.03988	0.02667	-0.02949	0.07417	-0.05980	0.04765	-0.04770	0.03138	-0.03138	0.10453	-0.09642
3.98	0.01214	0.36489	0.00667	-0.00639	0.03451	-0.03816	0.04432	-0.03574	0.02347	-0.02350	0.03138	-0.03138	0.06882	-0.06566
4.19	0.01232	0.45984	0.03144	-0.03012	0.04205	-0.04649	0.02233	-0.01801	0.02306	-0.02309	0.03138	-0.03138	0.06908	-0.07007
4.40	0.00568	1.14211	0.11036	-0.10574	0.07380	-0.08159	0.02414	-0.02994	0.04987	-0.04992	0.03138	-0.03138	0.14724	-0.14903
4.61	-0.00442	-1.86008	0.17139	-0.16420	0.03621	-0.04003	0.09168	-0.11370	0.06378	-0.06386	0.03138	-0.03138	0.21010	-0.21577

Table 17: 0–20%, 5.0–7.0 \otimes 3.0–5.0 GeV/c Jet Function

ϕ	per trig yield	σ_{stat}/y	systematic errors												
			$+\sigma_{f2}/y$	$-\sigma_{f2}/y$	$+\sigma_{f3}/y$	$-\sigma_{f3}/y$	$+\sigma_{f4}/y$	$-\sigma_{f4}/y$	$+\sigma_{\xi}/y$	$-\sigma_{\xi}/y$	$+\sigma_{\pi^0}/y$	$-\sigma_{\pi^0}/y$	$+\sigma_{total}/y$	$-\sigma_{total}/y$	
-1.47	-0.00200	-1.30736	0.05648	-0.05369	0.01352	-0.01221	0.03520	-0.04375	0.01908	-0.01875	0.02879	-0.02879	0.07619	-0.07827	
-1.26	0.00229	0.95492	0.04079	-0.03878	0.03091	-0.02791	0.01040	-0.01292	0.01659	-0.01630	0.02879	-0.02879	0.06190	-0.05954	
-1.05	0.00059	3.15409	0.09794	-0.09311	0.14840	-0.13402	0.08123	-0.06535	0.06444	-0.06332	0.02879	-0.02879	0.20783	-0.18905	
-0.84	-0.00087	-1.60010	0.01390	-0.01322	0.08152	-0.07362	0.10789	-0.08680	0.04401	-0.04325	0.02879	-0.02879	0.14576	-0.12581	
-0.63	0.00234	0.59005	0.01448	-0.01523	0.01154	-0.01042	0.03308	-0.02661	0.01651	-0.01622	0.02879	-0.02879	0.05038	-0.04627	
-0.42	0.00681	0.18646	0.01076	-0.01132	0.00358	-0.00396	0.00147	-0.00118	0.00575	-0.00564	0.02879	-0.02879	0.03151	-0.03172	
-0.21	0.03737	0.04042	0.00268	-0.00282	0.00171	-0.00189	0.00138	-0.00171	0.00106	-0.00104	0.02879	-0.02879	0.02902	-0.02906	
-0.00	0.10443	0.01717	0.00105	-0.00110	0.00076	-0.00084	0.00074	-0.00092	0.00038	-0.00037	0.02879	-0.02879	0.02883	-0.02884	
0.21	0.03799	0.04062	0.00264	-0.00277	0.00168	-0.00186	0.00135	-0.00168	0.00104	-0.00102	0.02879	-0.02879	0.02901	-0.02905	
0.42	0.00361	0.35816	0.02029	-0.02134	0.00674	-0.00747	0.00277	-0.00222	0.01083	-0.01064	0.02879	-0.02879	0.03756	-0.03819	
0.63	0.00051	3.01379	0.06623	-0.06967	0.05278	-0.04767	0.15127	-0.12170	0.07548	-0.07416	0.02879	-0.02879	0.19127	-0.16813	
0.84	0.00056	2.95094	0.02149	-0.02043	0.12599	-0.11378	0.16676	-0.13416	0.06803	-0.06684	0.02879	-0.02879	0.22271	-0.19147	
1.05	-0.00231	-0.90456	0.02498	-0.02375	0.03786	-0.03419	0.02072	-0.01667	0.01644	-0.01615	0.02879	-0.02879	0.05988	-0.05568	
1.26	0.00104	2.21995	0.08973	-0.08531	0.06798	-0.06140	0.02287	-0.02843	0.03650	-0.03586	0.02879	-0.02879	0.12393	-0.11820	
1.47	-0.00022	-13.25199	0.51025	-0.48509	0.12213	-0.11029	0.31798	-0.39524	0.17239	-0.16938	0.02879	-0.02879	0.63791	-0.65819	
1.68	0.00483	0.62076	0.02333	-0.02218	0.00504	-0.00558	0.01454	-0.01807	0.00792	-0.00778	0.05403	-0.05403	0.06135	-0.06189	
1.88	0.00416	0.54521	0.02245	-0.02134	0.01536	-0.01701	0.00572	-0.00711	0.00925	-0.00909	0.05403	-0.05403	0.06146	-0.06162	
2.09	-0.00134	-1.42084	0.04317	-0.04104	0.05908	-0.06542	0.03581	-0.02881	0.02888	-0.02838	0.05403	-0.05403	0.10193	-0.10256	
2.30	0.00393	0.39962	0.00307	-0.00291	0.01623	-0.01798	0.02379	-0.01914	0.00984	-0.00966	0.05403	-0.05403	0.06209	-0.06092	
2.51	0.00341	0.42632	0.00994	-0.01046	0.00716	-0.00793	0.02271	-0.01827	0.01139	-0.01119	0.05403	-0.05403	0.06095	-0.05959	
2.72	0.00330	0.37361	0.02220	-0.02336	0.00817	-0.00738	0.00303	-0.00243	0.01179	-0.01158	0.05403	-0.05403	0.06023	-0.06050	
2.93	0.00696	0.19194	0.01438	-0.01512	0.01015	-0.00916	0.00739	-0.00919	0.00561	-0.00551	0.05403	-0.05403	0.05758	-0.05786	
3.14	0.00985	0.13184	0.01113	-0.01170	0.00887	-0.00801	0.00781	-0.00971	0.00397	-0.00390	0.05403	-0.05403	0.05656	-0.05683	
3.35	0.00666	0.20764	0.01504	-0.01582	0.01061	-0.00959	0.00773	-0.00961	0.00587	-0.00577	0.05403	-0.05403	0.05790	-0.05820	
3.56	0.00630	0.20734	0.01164	-0.01225	0.00428	-0.00387	0.00159	-0.00128	0.00618	-0.00607	0.05403	-0.05403	0.05581	-0.05589	
3.77	0.00470	0.32278	0.00720	-0.00758	0.00518	-0.00574	0.01645	-0.01324	0.00825	-0.00811	0.05403	-0.05403	0.05777	-0.05702	
3.98	0.00110	1.43940	0.01091	-0.01037	0.05778	-0.06398	0.08469	-0.06813	0.03501	-0.03440	0.05403	-0.05403	0.12155	-0.11378	
4.19	0.00143	1.44437	0.04040	-0.03841	0.05528	-0.06121	0.03351	-0.02696	0.02703	-0.02655	0.05403	-0.05403	0.09727	-0.09784	
4.40	0.00279	0.84478	0.03342	-0.03177	0.02286	-0.02532	0.00852	-0.01059	0.01378	-0.01354	0.05403	-0.05403	0.06944	-0.06975	
4.61	0.00374	0.87623	0.03017	-0.02868	0.00652	-0.00722	0.01880	-0.02337	0.01025	-0.01007	0.05403	-0.05403	0.06581	-0.06665	

Table 18: 0–20%, 5.0–7.0 \otimes 5.0–7.0 GeV/c Jet Function

ϕ	per trig yield	σ_{stat}/y	systematic errors												
			$+\sigma_{f2}/y$	$-\sigma_{f2}/y$	$+\sigma_{f3}/y$	$-\sigma_{f3}/y$	$+\sigma_{f4}/y$	$-\sigma_{f4}/y$	$+\sigma_\xi/y$	$-\sigma_\xi/y$	$+\sigma_{\pi^0}/y$	$-\sigma_{\pi^0}/y$	$+\sigma_{total}/y$	$-\sigma_{total}/y$	
-1.47	-0.00180	-0.48876	0.00929	-0.00861	0.00389	-0.00319	0.00853	-0.01161	0.00513	-0.00532	0.13197	-0.13197	0.13272	-0.13290	
-1.26	-0.00130	-0.56119	0.01066	-0.00989	0.01412	-0.01159	0.00401	-0.00545	0.00710	-0.00737	0.13197	-0.13197	0.13340	-0.13316	
-1.05	-0.00136	-0.45564	0.00628	-0.00582	0.01664	-0.01365	0.00841	-0.00618	0.00678	-0.00703	0.13197	-0.13197	0.13360	-0.13313	
-0.84	-0.00043	-1.13446	0.00413	-0.00383	0.04238	-0.03477	0.05178	-0.03806	0.02143	-0.02223	0.13197	-0.13197	0.14956	-0.14346	
-0.63	0.00108	0.47932	0.00451	-0.00487	0.00645	-0.00529	0.01705	-0.01253	0.00860	-0.00892	0.13197	-0.13197	0.13357	-0.13305	
-0.42	0.00063	0.72603	0.01687	-0.01820	0.00913	-0.01113	0.00380	-0.00280	0.01497	-0.01554	0.13197	-0.13197	0.13424	-0.13461	
-0.21	0.00691	0.08347	0.00209	-0.00226	0.00217	-0.00265	0.00163	-0.00221	0.00137	-0.00142	0.13197	-0.13197	0.13202	-0.13204	
-0.00	0.03607	0.02489	0.00044	-0.00047	0.00051	-0.00063	0.00047	-0.00063	0.00026	-0.00027	0.13197	-0.13197	0.13197	-0.13197	
0.21	0.00607	0.09740	0.00239	-0.00257	0.00248	-0.00302	0.00185	-0.00252	0.00156	-0.00162	0.13197	-0.13197	0.13203	-0.13206	
0.42	0.00027	1.83967	0.03990	-0.04303	0.02159	-0.02632	0.00900	-0.00661	0.03541	-0.03674	0.13197	-0.13197	0.14425	-0.14613	
0.63	-0.00017	-3.44731	0.02893	-0.03121	0.04133	-0.03391	0.10935	-0.08036	0.05512	-0.05719	0.13197	-0.13197	0.18696	-0.17108	
0.84	-0.00004	-15.17886	0.04313	-0.03999	0.44216	-0.36273	0.54022	-0.39702	0.22353	-0.23193	0.13197	-0.13197	0.74604	-0.60167	
1.05	0.00058	1.47009	0.01482	-0.01374	0.03925	-0.03220	0.01983	-0.01457	0.01598	-0.01658	0.13197	-0.13197	0.14080	-0.13830	
1.26	-0.00032	-2.68716	0.04323	-0.04008	0.05726	-0.04697	0.01624	-0.02210	0.02880	-0.02989	0.13197	-0.13197	0.15381	-0.15037	
1.47	0.00061	1.82223	0.02733	-0.02534	0.01144	-0.00938	0.02511	-0.03417	0.01509	-0.01566	0.13197	-0.13197	0.13839	-0.13985	
1.68	0.00017	6.15997	0.09705	-0.08998	0.03331	-0.04061	0.08916	-0.12131	0.05374	-0.05575	0.01380	-0.01380	0.14682	-0.16662	
1.88	-0.00059	-1.29605	0.02355	-0.02183	0.02559	-0.03119	0.00885	-0.01204	0.01581	-0.01640	0.01380	-0.01380	0.04157	-0.04532	
2.09	0.00047	1.54331	0.01824	-0.01691	0.03964	-0.04832	0.02441	-0.01794	0.01986	-0.02061	0.01380	-0.01380	0.05554	-0.05965	
2.30	0.00010	5.48034	0.01740	-0.01613	0.14633	-0.17837	0.21793	-0.16016	0.09085	-0.09427	0.01380	-0.01380	0.27866	-0.25846	
2.51	0.00060	0.90044	0.00821	-0.00885	0.00962	-0.01172	0.03101	-0.02279	0.01568	-0.01627	0.01380	-0.01380	0.03947	-0.03450	
2.72	-0.00016	-2.67269	0.06499	-0.07009	0.04287	-0.03517	0.01466	-0.01077	0.05752	-0.05968	0.01380	-0.01380	0.09887	-0.10009	
2.93	0.00126	0.39635	0.01150	-0.01241	0.01455	-0.01194	0.00894	-0.01216	0.00747	-0.00776	0.01380	-0.01380	0.02589	-0.02636	
3.14	0.00336	0.15719	0.00471	-0.00508	0.00673	-0.00552	0.00500	-0.00680	0.00280	-0.00291	0.01380	-0.01380	0.01705	-0.01736	
3.35	0.00196	0.28110	0.00739	-0.00797	0.00935	-0.00767	0.00374	-0.00782	0.00480	-0.00499	0.01380	-0.01380	0.01971	-0.01997	
3.56	0.00125	0.40072	0.00847	-0.00913	0.00558	-0.00458	0.00191	-0.00140	0.00749	-0.00777	0.01380	-0.01380	0.01879	-0.01890	
3.77	-0.00004	-13.99411	0.12626	-0.13617	0.14796	-0.18035	0.47714	-0.35066	0.24120	-0.25027	0.01380	-0.01380	0.56909	-0.48668	
3.98	0.00147	0.44177	0.00122	-0.00113	0.01025	-0.01249	0.01526	-0.01121	0.00636	-0.00660	0.01380	-0.01380	0.02388	-0.02274	
4.19	0.00002	37.04111	0.40100	-0.37180	0.87140	-1.06221	0.53670	-0.39443	0.43661	-0.45302	0.01380	-0.01380	1.18280	-1.27574	
4.40	-0.00053	-1.56912	0.02615	-0.02425	0.02841	-0.03463	0.00982	-0.01337	0.01755	-0.01821	0.01380	-0.01380	0.04567	-0.04988	
4.61	0.00124	1.07144	0.01346	-0.01248	0.00462	-0.00563	0.01236	-0.01682	0.00745	-0.00773	0.01380	-0.01380	0.02452	-0.02684	

Table 19: 0–20%, 7.0–9.0 \otimes 0.5–1.0 GeV/c Jet Function

ϕ	per trig yield	σ_{stat}/y	systematic errors											
			$+\sigma_{f2}/y$	$-\sigma_{f2}/y$	$+\sigma_{f3}/y$	$-\sigma_{f3}/y$	$+\sigma_{f4}/y$	$-\sigma_{f4}/y$	$+\sigma_\xi/y$	$-\sigma_\xi/y$	$+\sigma_{\pi^0}/y$	$-\sigma_{\pi^0}/y$	$+\sigma_{total}/y$	$-\sigma_{total}/y$
-1.47	0.07163	2.18123	0.24228	-0.30845	0.03107	-0.03489	0.04511	-0.05394	0.21418	-0.21421	0.11756	-0.11756	0.34841	-0.39872
-1.26	0.07385	1.88744	0.19435	-0.24743	0.07889	-0.08859	0.01480	-0.01770	0.20773	-0.20775	0.11756	-0.11756	0.31810	-0.35548
-1.05	-0.23205	-0.47209	0.03823	-0.04867	0.03103	-0.03485	0.00911	-0.00762	0.06617	-0.06618	0.11756	-0.11756	0.14390	-0.14779
-0.84	-0.10174	-0.91867	0.01823	-0.02321	0.05726	-0.06431	0.04066	-0.03401	0.15121	-0.15123	0.11756	-0.11756	0.20482	-0.20621
-0.63	-0.01335	-6.21555	0.52268	-0.41055	0.16664	-0.18714	0.25623	-0.21429	1.15497	-1.15512	0.11756	-0.11756	1.30935	-1.26397
-0.42	0.05548	1.40155	0.27243	-0.21398	0.04505	-0.04011	0.00797	-0.00666	0.27873	-0.27877	0.11756	-0.11756	0.40966	-0.37279
-0.21	0.12926	0.56784	0.15964	-0.12539	0.05062	-0.04507	0.01831	-0.02189	0.11987	-0.11989	0.11756	-0.11756	0.23785	-0.21547
-0.00	0.13241	0.54913	0.17059	-0.13399	0.06108	-0.05439	0.02671	-0.03194	0.11710	-0.11712	0.11756	-0.11756	0.24714	-0.22241
0.21	0.20348	0.37129	0.10141	-0.07965	0.03216	-0.02863	0.01163	-0.01391	0.07615	-0.07616	0.11756	-0.11756	0.17627	-0.16425
0.42	0.14063	0.57777	0.10747	-0.08442	0.01777	-0.01582	0.00314	-0.00263	0.10996	-0.10997	0.11756	-0.11756	0.19439	-0.18248
0.63	0.01647	5.57072	0.42379	-0.33287	0.13511	-0.15174	0.20775	-0.17374	0.93645	-0.93657	0.11756	-0.11756	1.06384	-1.02713
0.84	0.00373	28.75375	0.49749	-0.63337	1.56291	-1.75519	1.10979	-0.92813	4.12705	-4.12759	0.11756	-0.11756	4.57910	-4.62537
1.05	0.00184	66.58672	4.82081	-6.13753	3.91359	-4.39506	1.14923	-0.96111	8.34488	-8.34596	0.11756	-0.11756	10.46556	-11.29507
1.26	-0.23535	-0.60414	0.06099	-0.07765	0.02476	-0.02780	0.00464	-0.00555	0.06519	-0.06519	0.11756	-0.11756	0.14974	-0.15781
1.47	-0.04039	-4.28562	0.42967	-0.54702	0.05510	-0.06188	0.08000	-0.09566	0.37983	-0.37988	0.11756	-0.11756	0.59342	-0.68582
1.68	0.07277	2.23652	0.23847	-0.30360	0.03434	-0.03058	0.04440	-0.05309	0.21096	-0.21099	0.01564	-0.01564	0.32368	-0.37509
1.88	0.16654	0.81756	0.08618	-0.10972	0.03929	-0.03498	0.00656	-0.00785	0.09229	-0.09230	0.01564	-0.01564	0.13333	-0.14862
2.09	0.12979	0.87014	0.06835	-0.08702	0.06231	-0.05549	0.01629	-0.01363	0.11859	-0.11860	0.01564	-0.01564	0.15207	-0.15858
2.30	0.23874	0.41403	0.00777	-0.00989	0.02741	-0.02440	0.01733	-0.01449	0.06456	-0.06457	0.01564	-0.01564	0.07433	-0.07292
2.51	0.08440	1.03321	0.08270	-0.06495	0.02961	-0.02637	0.04054	-0.03390	0.18286	-0.18289	0.01564	-0.01564	0.20747	-0.19939
2.72	0.24820	0.32666	0.06089	-0.04783	0.00897	-0.01007	0.00178	-0.00149	0.06226	-0.06227	0.01564	-0.01564	0.08895	-0.08070
2.93	0.28104	0.28000	0.07342	-0.05767	0.02073	-0.02328	0.00842	-0.01007	0.05503	-0.05504	0.01564	-0.01564	0.09573	-0.08511
3.14	0.39078	0.20385	0.05780	-0.04540	0.01843	-0.02070	0.00905	-0.01082	0.03959	-0.03959	0.01564	-0.01564	0.07466	-0.06647
3.35	0.26136	0.30605	0.07895	-0.06201	0.02229	-0.02503	0.00906	-0.01083	0.05917	-0.05918	0.01564	-0.01564	0.10275	-0.09131
3.56	0.12919	0.65202	0.11699	-0.09189	0.01723	-0.01934	0.00342	-0.00286	0.11961	-0.11963	0.01564	-0.01564	0.16895	-0.15291
3.77	0.33946	0.27238	0.02056	-0.01615	0.00736	-0.00656	0.01008	-0.00843	0.04547	-0.04547	0.01564	-0.01564	0.05376	-0.05184
3.98	0.33160	0.30487	0.00559	-0.00712	0.01973	-0.01757	0.01248	-0.01043	0.04648	-0.04649	0.01564	-0.01564	0.05460	-0.05361
4.19	0.18683	0.65609	0.04748	-0.06045	0.04329	-0.03855	0.01132	-0.00947	0.08238	-0.08239	0.01564	-0.01564	0.10624	-0.11074
4.40	-0.03577	-4.04194	0.40129	-0.51089	0.18292	-0.16289	0.03056	-0.03654	0.42971	-0.42977	0.01564	-0.01564	0.61671	-0.68835
4.61	-0.07907	-1.93665	0.21947	-0.27942	0.03161	-0.02814	0.04087	-0.04886	0.19416	-0.19418	0.01564	-0.01564	0.29796	-0.34527

Table 20: 0–20%, 7.0–9.0 \otimes 1.0–2.0 GeV/c Jet Function

ϕ	per trig yield	σ_{stat}/y	systematic errors											
			$+\sigma_{f2}/y$	$-\sigma_{f2}/y$	$+\sigma_{f3}/y$	$-\sigma_{f3}/y$	$+\sigma_{f4}/y$	$-\sigma_{f4}/y$	$+\sigma_\xi/y$	$-\sigma_\xi/y$	$+\sigma_{\pi^0}/y$	$-\sigma_{\pi^0}/y$	$+\sigma_{total}/y$	$-\sigma_{total}/y$
-1.47	-0.15474	-0.48440	0.05503	-0.07257	0.01031	-0.01160	0.01876	-0.02225	0.02492	-0.02492	0.01925	-0.01925	0.06692	-0.08299
-1.26	-0.11569	-0.56907	0.06088	-0.08028	0.03609	-0.04063	0.00849	-0.01007	0.03331	-0.03330	0.01925	-0.01925	0.08100	-0.09837
-1.05	0.00325	16.01398	1.33948	-1.76636	1.58811	-1.78796	0.57991	-0.48891	1.18725	-1.18715	0.01925	-0.01925	2.46222	-2.82233
-0.84	-0.01454	-2.97363	0.06258	-0.08252	0.28713	-0.32326	0.25353	-0.21375	0.26625	-0.26622	0.01925	-0.01925	0.47106	-0.47775
-0.63	0.02455	1.57484	0.14450	-0.10958	0.06496	-0.07313	0.12420	-0.10471	0.15852	-0.15851	0.01925	-0.01925	0.25696	-0.23198
-0.42	0.06834	0.53075	0.11240	-0.08524	0.02627	-0.02334	0.00576	-0.00486	0.05727	-0.05726	0.01925	-0.01925	0.13042	-0.10716
-0.21	0.22908	0.15003	0.04578	-0.03472	0.02052	-0.01823	0.00928	-0.01101	0.01716	-0.01716	0.01925	-0.01925	0.05717	-0.04820
-0.00	0.35780	0.09429	0.03209	-0.02433	0.01624	-0.01442	0.00888	-0.01053	0.01100	-0.01100	0.01925	-0.01925	0.04317	-0.03745
0.21	0.23699	0.14666	0.04425	-0.03356	0.01983	-0.01762	0.00897	-0.01064	0.01659	-0.01659	0.01925	-0.01925	0.05548	-0.04686
0.42	0.06020	0.62916	0.12761	-0.09677	0.02983	-0.02649	0.00654	-0.00552	0.06502	-0.06501	0.01925	-0.01925	0.14770	-0.12122
0.63	-0.05050	-0.83797	0.07024	-0.05327	0.03158	-0.03555	0.06038	-0.05090	0.07706	-0.07705	0.01925	-0.01925	0.12604	-0.11402
0.84	0.07593	0.66592	0.01198	-0.01580	0.05499	-0.06191	0.04855	-0.04094	0.05099	-0.05099	0.01925	-0.01925	0.09217	-0.09343
1.05	-0.01060	-5.42471	0.41072	-0.54161	0.48695	-0.54823	0.17781	-0.14991	0.36404	-0.36401	0.01925	-0.01925	0.75520	-0.86559
1.26	0.00091	75.11139	7.70417	-10.15941	4.56710	-5.14182	1.07410	-1.27401	4.21511	-4.21475	0.01925	-0.01925	9.95659	-12.20818
1.47	0.02754	3.15812	0.30916	-0.40769	0.05790	-0.06519	0.10539	-0.12501	0.14000	-0.13998	0.01925	-0.01925	0.36057	-0.45393
1.68	-0.03949	-2.00930	0.21563	-0.28435	0.04547	-0.04038	0.07351	-0.08719	0.09782	-0.09781	0.01420	-0.01420	0.25247	-0.31600
1.88	-0.01186	-5.56351	0.59398	-0.78328	0.39643	-0.35212	0.08281	-0.09822	0.32654	-0.32651	0.01420	-0.01420	0.78972	-0.92410
2.09	0.02441	2.19388	0.17830	-0.23512	0.23799	-0.21139	0.07719	-0.06508	0.15897	-0.15895	0.01420	-0.01420	0.34621	-0.36010
2.30	0.13867	0.33396	0.00656	-0.00865	0.03390	-0.03011	0.02659	-0.02241	0.02805	-0.02805	0.01420	-0.01420	0.05373	-0.04972
2.51	0.08904	0.45262	0.03984	-0.03021	0.02016	-0.01791	0.03424	-0.02887	0.04379	-0.04378	0.01420	-0.01420	0.07270	-0.06470
2.72	0.17872	0.20808	0.04298	-0.03259	0.00892	-0.01005	0.00220	-0.00186	0.02186	-0.02186	0.01420	-0.01420	0.05110	-0.04297
2.93	0.08385	0.43075	0.12507	-0.09485	0.04979	-0.05606	0.02536	-0.03008	0.04666	-0.04666	0.01420	-0.01420	0.14541	-0.12418
3.14	0.15092	0.24379	0.07607	-0.05769	0.03420	-0.03850	0.02106	-0.02497	0.02594	-0.02594	0.01420	-0.01420	0.09096	-0.07942
3.35	0.17986	0.20754	0.05831	-0.04422	0.02321	-0.02613	0.01182	-0.01402	0.02175	-0.02175	0.01420	-0.01420	0.06894	-0.05924
3.56	0.13772	0.27970	0.05578	-0.04230	0.01158	-0.01304	0.00286	-0.00241	0.02837	-0.02836	0.01420	-0.01420	0.06526	-0.05451
3.77	0.07688	0.54024	0.04614	-0.03499	0.02335	-0.02074	0.03966	-0.03344	0.05071	-0.05071	0.01420	-0.01420	0.08379	-0.07447
3.98	0.09506	0.50262	0.00957	-0.01262	0.04945	-0.04392	0.03878	-0.03270	0.04092	-0.04092	0.01420	-0.01420	0.07692	-0.07095
4.19	0.10279	0.56026	0.04235	-0.05584	0.05653	-0.05021	0.01833	-0.01546	0.03776	-0.03775	0.01420	-0.01420	0.08338	-0.08663
4.40	-0.05798	-1.20690	0.12146	-0.16017	0.08107	-0.07200	0.01693	-0.02009	0.06677	-0.06677	0.01420	-0.01420	0.16209	-0.18948
4.61	-0.05405	-1.45231	0.15754	-0.20775	0.03322	-0.02950	0.05371	-0.06370	0.07147	-0.07146	0.01420	-0.01420	0.18471	-0.23108

Table 21: 0–20%, 7.0–9.0 \otimes 2.0–3.0 GeV/c Jet Function

ϕ	per trig yield	σ_{stat}/y	systematic errors											
			$+\sigma_{f_2}/y$	$-\sigma_{f_2}/y$	$+\sigma_{f_3}/y$	$-\sigma_{f_3}/y$	$+\sigma_{f_4}/y$	$-\sigma_{f_4}/y$	$+\sigma_\xi/y$	$-\sigma_\xi/y$	$+\sigma_{\pi^0}/y$	$-\sigma_{\pi^0}/y$	$+\sigma_{total}/y$	$-\sigma_{total}/y$
-1.47	-0.00559	-3.60923	0.18440	-0.23927	0.03929	-0.04539	0.08333	-0.09234	0.04851	-0.04839	0.00044	-0.00044	0.21176	-0.26491
-1.26	0.00507	3.36339	0.16831	-0.21840	0.11353	-0.13115	0.03111	-0.03447	0.05343	-0.05330	0.00044	-0.00044	0.21223	-0.26255
-1.05	0.00308	4.59921	0.17095	-0.22183	0.23061	-0.26642	0.09166	-0.08272	0.08789	-0.08768	0.00044	-0.00044	0.31390	-0.36704
-0.84	0.00949	1.16647	0.01161	-0.01507	0.06062	-0.07004	0.05827	-0.05258	0.02870	-0.02863	0.00044	-0.00044	0.08960	-0.09336
-0.63	-0.00035	-29.79290	1.21789	-0.93858	0.63307	-0.73136	1.31751	-1.18897	0.79134	-0.78940	0.00044	-0.00044	2.06060	-1.85812
-0.42	0.01379	0.68402	0.06638	-0.05116	0.01841	-0.01594	0.00428	-0.00387	0.02011	-0.02006	0.00044	-0.00044	0.07189	-0.05735
-0.21	0.13426	0.07631	0.00931	-0.00717	0.00495	-0.00428	0.00254	-0.00282	0.00208	-0.00208	0.00044	-0.00044	0.01105	-0.00907
-0.00	0.21749	0.04661	0.00629	-0.00485	0.00378	-0.00327	0.00234	-0.00260	0.00129	-0.00128	0.00044	-0.00044	0.00782	-0.00654
0.21	0.12683	0.08130	0.00985	-0.00759	0.00524	-0.00453	0.00269	-0.00298	0.00220	-0.00220	0.00044	-0.00044	0.01169	-0.00960
0.42	0.03115	0.31850	0.02938	-0.02264	0.00815	-0.00705	0.00190	-0.00171	0.00890	-0.00888	0.00044	-0.00044	0.03182	-0.02538
0.63	0.00731	1.57603	0.05783	-0.04457	0.03006	-0.03473	0.06256	-0.05646	0.03757	-0.03748	0.00044	-0.00044	0.09784	-0.08823
0.84	0.00419	3.03559	0.02627	-0.03409	0.13713	-0.15843	0.13180	-0.11894	0.06493	-0.06477	0.00044	-0.00044	0.20269	-0.21119
1.05	0.00001	2157.73438	72.42388	-93.97707	97.69952	-112.86895	38.83195	-35.04343	37.23523	-37.14401	0.00044	-0.00044	132.98419	-155.49538
1.26	0.01015	1.77594	0.08403	-0.10904	0.05668	-0.06548	0.01553	-0.01721	0.02667	-0.02661	0.00044	-0.00044	0.10596	-0.13108
1.47	0.00277	8.21749	0.37236	-0.48317	0.07935	-0.09167	0.16827	-0.18646	0.09796	-0.09772	0.00044	-0.00044	0.42762	-0.53496
1.68	0.01296	1.71553	0.07954	-0.10321	0.01958	-0.01695	0.03594	-0.03983	0.02099	-0.02094	0.04201	-0.04201	0.10103	-0.12136
1.88	-0.00007	-251.03328	12.62167	-16.37785	9.83512	-8.51329	2.33274	-2.58493	4.04200	-4.03210	0.04201	-0.04201	16.66785	-19.06965
2.09	0.00812	1.80285	0.06492	-0.08424	0.10118	-0.08758	0.03481	-0.03141	0.03374	-0.03366	0.04201	-0.04201	0.13626	-0.13657
2.30	0.00692	1.71086	0.01593	-0.02067	0.09606	-0.08315	0.07992	-0.07212	0.03972	-0.03962	0.04201	-0.04201	0.13860	-0.12601
2.51	0.00613	1.75687	0.06893	-0.05312	0.04139	-0.03583	0.07456	-0.06729	0.04494	-0.04483	0.04201	-0.04201	0.12573	-0.11139
2.72	0.01680	0.56464	0.05448	-0.04198	0.01308	-0.01511	0.00352	-0.00317	0.01645	-0.01641	0.04201	-0.04201	0.07201	-0.06352
2.93	0.02561	0.38357	0.04880	-0.03760	0.02246	-0.02595	0.01333	-0.01477	0.01082	-0.01079	0.04201	-0.04201	0.07032	-0.06470
3.14	0.04852	0.20160	0.02819	-0.02172	0.01465	-0.01693	0.01051	-0.01165	0.00571	-0.00570	0.04201	-0.04201	0.05401	-0.05188
3.35	0.02282	0.44193	0.05476	-0.04220	0.02521	-0.02912	0.01496	-0.01657	0.01214	-0.01211	0.04201	-0.04201	0.07595	-0.06939
3.56	0.04657	0.21620	0.01965	-0.01514	0.00472	-0.00545	0.00127	-0.00114	0.00593	-0.00592	0.04201	-0.04201	0.04701	-0.04539
3.77	0.01297	0.85856	0.03258	-0.02511	0.01957	-0.01694	0.03525	-0.03181	0.02124	-0.02119	0.04201	-0.04201	0.07002	-0.06436
3.98	0.00128	9.41944	0.08636	-0.11206	0.52082	-0.45082	0.43329	-0.39102	0.21533	-0.21480	0.04201	-0.04201	0.71735	-0.64544
4.19	-0.00602	-2.52017	0.08748	-0.11352	0.13634	-0.11801	0.04691	-0.04233	0.04547	-0.04536	0.04201	-0.04201	0.17965	-0.18007
4.40	0.01351	1.34496	0.06312	-0.08190	0.04918	-0.04257	0.01167	-0.01293	0.02021	-0.02016	0.04201	-0.04201	0.09334	-0.10420
4.61	0.02980	0.79919	0.03459	-0.04489	0.00852	-0.00737	0.01563	-0.01732	0.00913	-0.00911	0.04201	-0.04201	0.05798	-0.06494

Table 22: 0–20%, 7.0–9.0 \otimes 3.0–5.0 GeV/c Jet Function

ϕ	per trig yield	σ_{stat}/y	systematic errors											
			$+\sigma_{f2}/y$	$-\sigma_{f2}/y$	$+\sigma_{f3}/y$	$-\sigma_{f3}/y$	$+\sigma_{f4}/y$	$-\sigma_{f4}/y$	$+\sigma_\xi/y$	$-\sigma_\xi/y$	$+\sigma_{\pi^0}/y$	$-\sigma_{\pi^0}/y$	$+\sigma_{total}/y$	$-\sigma_{total}/y$
-1.47	0.00002	460.26941	9.43310	-11.96328	2.10686	-2.42493	5.05767	-5.63937	2.26069	-2.32295	0.00446	-0.00446	11.14060	-13.64548
-1.26	0.00532	1.16937	0.02326	-0.02950	0.01644	-0.01893	0.00510	-0.00569	0.00672	-0.00691	0.00446	-0.00446	0.03004	-0.03645
-1.05	-0.00849	-0.55198	0.00901	-0.01143	0.01274	-0.01466	0.00577	-0.00517	0.00421	-0.00433	0.00446	-0.00446	0.01773	-0.02027
-0.84	-0.00532	-0.68925	0.00300	-0.00381	0.01644	-0.01892	0.01800	-0.01614	0.00676	-0.00694	0.00446	-0.00446	0.02586	-0.02648
-0.63	0.00224	1.69199	0.02679	-0.02112	0.01493	-0.01719	0.03539	-0.03174	0.01621	-0.01666	0.00446	-0.00446	0.04976	-0.04524
-0.42	0.00907	0.39236	0.01432	-0.01129	0.00424	-0.00369	0.00113	-0.00101	0.00404	-0.00416	0.00446	-0.00446	0.01614	-0.01339
-0.21	0.07186	0.06702	0.00247	-0.00195	0.00140	-0.00122	0.00082	-0.00091	0.00051	-0.00053	0.00446	-0.00446	0.00538	-0.00513
-0.00	0.19070	0.03201	0.00102	-0.00080	0.00065	-0.00057	0.00046	-0.00051	0.00019	-0.00020	0.00446	-0.00446	0.00465	-0.00460
0.21	0.06356	0.07444	0.00279	-0.00220	0.00158	-0.00138	0.00092	-0.00103	0.00058	-0.00060	0.00446	-0.00446	0.00560	-0.00530
0.42	0.00717	0.50970	0.01811	-0.01428	0.00537	-0.00466	0.00143	-0.00128	0.00512	-0.00526	0.00446	-0.00446	0.02012	-0.01658
0.63	0.00613	0.73109	0.00978	-0.00771	0.00545	-0.00628	0.01293	-0.01159	0.00592	-0.00608	0.00446	-0.00446	0.01864	-0.01704
0.84	-0.00381	-1.13070	0.00420	-0.00533	0.02298	-0.02644	0.02515	-0.02256	0.00944	-0.00970	0.00446	-0.00446	0.03588	-0.03675
1.05	-0.00306	-1.86407	0.02504	-0.03176	0.03541	-0.04075	0.01603	-0.01438	0.01171	-0.01204	0.00446	-0.00446	0.04790	-0.05514
1.26	0.00281	2.34601	0.04412	-0.05596	0.03119	-0.03590	0.00967	-0.01079	0.01275	-0.01310	0.00446	-0.00446	0.05653	-0.06876
1.47	0.00163	4.98630	0.09187	-0.11651	0.02052	-0.02362	0.04926	-0.05492	0.02202	-0.02262	0.00446	-0.00446	0.10859	-0.13297
1.68	-0.00167	-4.65107	0.08990	-0.11402	0.02311	-0.02008	0.04820	-0.05375	0.02163	-0.02222	0.02469	-0.02469	0.10962	-0.13189
1.88	0.00955	0.67487	0.01296	-0.01644	0.01055	-0.00916	0.00284	-0.00317	0.00378	-0.00389	0.02469	-0.02469	0.03019	-0.03145
2.09	-0.00049	-10.71853	0.15683	-0.19890	0.25523	-0.22176	0.10039	-0.09004	0.07427	-0.07632	0.02469	-0.02469	0.32549	-0.32137
2.30	0.00482	0.89869	0.00332	-0.00421	0.02091	-0.01817	0.01989	-0.01783	0.00754	-0.00775	0.02469	-0.02469	0.03886	-0.03654
2.51	0.00434	0.92137	0.01381	-0.01089	0.00886	-0.00770	0.01825	-0.01636	0.00839	-0.00862	0.02469	-0.02469	0.03581	-0.03361
2.72	0.00513	0.67123	0.02532	-0.01996	0.00652	-0.00750	0.00200	-0.00179	0.00713	-0.00732	0.02469	-0.02469	0.03671	-0.03348
2.93	0.01320	0.29077	0.01343	-0.01059	0.00663	-0.00763	0.00445	-0.00497	0.00278	-0.00285	0.02469	-0.02469	0.02935	-0.02851
3.14	0.02010	0.19064	0.00966	-0.00761	0.00538	-0.00620	0.00437	-0.00487	0.00183	-0.00188	0.02469	-0.02469	0.02746	-0.02708
3.35	0.01714	0.23662	0.01034	-0.00815	0.00511	-0.00588	0.00343	-0.00382	0.00214	-0.00220	0.02469	-0.02469	0.02755	-0.02702
3.56	0.00741	0.49379	0.01753	-0.01382	0.00451	-0.00519	0.00138	-0.00124	0.00493	-0.00507	0.02469	-0.02469	0.03104	-0.02924
3.77	0.00330	1.25169	0.01820	-0.01435	0.01168	-0.01014	0.02405	-0.02157	0.01106	-0.01136	0.02469	-0.02469	0.04216	-0.03889
3.98	0.00321	1.37046	0.00498	-0.00632	0.03139	-0.02727	0.02985	-0.02677	0.01132	-0.01163	0.02469	-0.02469	0.05137	-0.04738
4.19	-0.00438	-1.25310	0.01746	-0.02215	0.02842	-0.02469	0.01118	-0.01002	0.00827	-0.00850	0.02469	-0.02469	0.04377	-0.04339
4.40	-0.00651	-0.88998	0.01901	-0.02410	0.01547	-0.01344	0.00417	-0.00465	0.00555	-0.00570	0.02469	-0.02469	0.03547	-0.03775
4.61	-0.00536	-1.47764	0.02791	-0.03540	0.00717	-0.00623	0.01496	-0.01669	0.00671	-0.00690	0.02469	-0.02469	0.04134	-0.04719

Table 23: 0–20%, 7.0–9.0 \otimes 5.0–7.0 GeV/c Jet Function

ϕ	per trig yield	σ_{stat}/y	systematic errors												
			$+\sigma_{f2}/y$	$-\sigma_{f2}/y$	$+\sigma_{f3}/y$	$-\sigma_{f3}/y$	$+\sigma_{f4}/y$	$-\sigma_{f4}/y$	$+\sigma_\xi/y$	$-\sigma_\xi/y$	$+\sigma_{\pi^0}/y$	$-\sigma_{\pi^0}/y$	$+\sigma_{total}/y$	$-\sigma_{total}/y$	
-1.47	-0.00220	-1.06976	0.00921	-0.01072	0.00304	-0.00248	0.00523	-0.00814	0.00405	-0.00450	0.06571	-0.06571	0.06675	-0.06727	
-1.26	-0.00041	-5.08082	0.04078	-0.04749	0.04262	-0.03475	0.00947	-0.01474	0.02164	-0.02404	0.06571	-0.06571	0.09140	-0.09260	
-1.05	0.00060	3.23795	0.01737	-0.02023	0.03632	-0.02961	0.01645	-0.01056	0.01493	-0.01659	0.06571	-0.06571	0.08020	-0.07740	
-0.84	-0.00315	-0.35484	0.00069	-0.00080	0.00558	-0.00455	0.00611	-0.00392	0.00285	-0.00316	0.06571	-0.06571	0.06629	-0.06606	
-0.63	-0.00043	-3.03248	0.01719	-0.01476	0.01543	-0.01258	0.03659	-0.02349	0.02073	-0.02303	0.06571	-0.06571	0.08136	-0.07600	
-0.42	0.00067	1.88302	0.02429	-0.02085	0.00821	-0.01007	0.00308	-0.00198	0.01361	-0.01512	0.06571	-0.06571	0.07190	-0.07132	
-0.21	0.01165	0.15303	0.00190	-0.00163	0.00123	-0.00151	0.00072	-0.00113	0.00078	-0.00087	0.06571	-0.06571	0.06575	-0.06576	
-0.00	0.09671	0.03947	0.00025	-0.00021	0.00018	-0.00022	0.00013	-0.00020	0.00009	-0.00010	0.06571	-0.06571	0.06571	-0.06571	
0.21	0.00865	0.20793	0.00255	-0.00219	0.00165	-0.00203	0.00098	-0.00152	0.00105	-0.00117	0.06571	-0.06571	0.06579	-0.06580	
0.42	0.00058	2.38645	0.02812	-0.02415	0.00950	-0.01166	0.00357	-0.00229	0.001576	-0.01751	0.06571	-0.06571	0.07389	-0.07313	
0.63	0.00149	1.24441	0.00500	-0.00429	0.00448	-0.00366	0.01063	-0.00683	0.00602	-0.00669	0.06571	-0.06571	0.06717	-0.06664	
0.84	0.00307	0.65948	0.00071	-0.00082	0.00572	-0.00466	0.00626	-0.00402	0.00292	-0.00324	0.06571	-0.06571	0.06632	-0.06608	
1.05	0.00330	0.87674	0.00315	-0.00366	0.00658	-0.00536	0.00298	-0.00191	0.00270	-0.00300	0.06571	-0.06571	0.06623	-0.06612	
1.26	0.00023	9.64672	0.07146	-0.08322	0.07469	-0.06089	0.01659	-0.02584	0.03792	-0.04213	0.06571	-0.06571	0.12929	-0.13188	
1.47	-0.00004	75.75134	0.52773	-0.61463	0.17427	-0.14208	0.29961	-0.46660	0.23188	-0.25765	0.06571	-0.06571	0.67581	-0.82847	
1.68	0.00193	1.50834	0.01050	-0.01223	0.00283	-0.00347	0.00396	-0.00929	0.00462	-0.00514	0.01148	-0.01148	0.01752	-0.02015	
1.88	-0.00118	-1.70328	0.01428	-0.01663	0.01217	-0.01492	0.00332	-0.00516	0.00762	-0.00847	0.01148	-0.01148	0.02351	-0.02701	
2.09	0.00057	3.42725	0.01821	-0.02121	0.03103	-0.03806	0.01724	-0.01107	0.01576	-0.01751	0.01148	-0.01148	0.04441	-0.04959	
2.30	-0.00150	-0.94161	0.00144	-0.00168	0.00951	-0.01167	0.01278	-0.00820	0.00598	-0.00665	0.01148	-0.01148	0.02058	-0.01956	
2.51	0.00078	1.88893	0.00960	-0.00824	0.00702	-0.00862	0.02043	-0.01312	0.01160	-0.01289	0.01148	-0.01148	0.02873	-0.02474	
2.72	0.00178	0.75108	0.00906	-0.00778	0.00376	-0.00306	0.00115	-0.00074	0.00507	-0.00563	0.01148	-0.01148	0.01597	-0.01530	
2.93	0.00820	0.21875	0.00269	-0.00231	0.00214	-0.00175	0.00103	-0.00160	0.00111	-0.00123	0.01148	-0.01148	0.01208	-0.01202	
3.14	0.00933	0.19366	0.00259	-0.00222	0.00233	-0.00190	0.00135	-0.00211	0.00097	-0.00108	0.01148	-0.01148	0.01212	-0.01208	
3.35	0.00388	0.41281	0.00569	-0.00489	0.00453	-0.00369	0.00218	-0.00339	0.00234	-0.00260	0.01148	-0.01148	0.01396	-0.01370	
3.56	0.00014	9.43715	0.11720	-0.10063	0.04858	-0.03960	0.01484	-0.00956	0.06555	-0.07283	0.01148	-0.01148	0.14403	-0.13123	
3.77	-0.00043	-3.36723	0.01754	-0.01506	0.01284	-0.01574	0.03733	-0.02397	0.02119	-0.02355	0.01148	-0.01148	0.04947	-0.04166	
3.98	0.00029	5.89956	0.00740	-0.00862	0.04881	-0.05987	0.06556	-0.04209	0.03070	-0.03411	0.01148	-0.01148	0.08837	-0.08201	
4.19	-0.00367	-0.39796	0.00283	-0.00329	0.00482	-0.00591	0.00267	-0.00172	0.00244	-0.00272	0.01148	-0.01148	0.01327	-0.01371	
4.40	0.00290	0.84504	0.00580	-0.00675	0.00494	-0.00606	0.00135	-0.00210	0.00309	-0.00344	0.01148	-0.01148	0.01419	-0.01518	
4.61	0.00025	14.21369	0.08065	-0.09393	0.02171	-0.02663	0.04579	-0.07131	0.03551	-0.03946	0.01148	-0.01148	0.10230	-0.12769	

Table 24: 0–20%, 9.0–12.0 \otimes 0.5–1.0 GeV/c Jet Function

ϕ	per trig yield	σ_{stat}/y	systematic errors												
			$+\sigma_{f2}/y$	$-\sigma_{f2}/y$	$+\sigma_{f3}/y$	$-\sigma_{f3}/y$	$+\sigma_{f4}/y$	$-\sigma_{f4}/y$	$+\sigma_\xi/y$	$-\sigma_\xi/y$	$+\sigma_{\pi^0}/y$	$-\sigma_{\pi^0}/y$	$+\sigma_{total}/y$	$-\sigma_{total}/y$	
-1.47	-0.09205	-3.23346	0.24243	-0.37973	0.03038	-0.03919	0.04235	-0.04878	0.17938	-0.17939	0.02823	-0.02823	0.30735	-0.42555	
-1.26	-0.00847	-31.22208	2.17792	-3.41142	0.86402	-1.11445	0.15561	-0.17924	1.94842	-1.94858	0.02823	-0.02823	3.05143	-4.08774	
-1.05	0.07409	2.85246	0.15396	-0.24116	0.12216	-0.15757	0.03317	-0.02880	0.22307	-0.22309	0.02823	-0.02823	0.30047	-0.36658	
-0.84	-0.09477	-1.87792	0.02516	-0.03941	0.07726	-0.09965	0.05073	-0.04405	0.17469	-0.17471	0.02823	-0.02823	0.20122	-0.21153	
-0.63	-0.00847	-18.70940	1.30403	-0.83252	0.33027	-0.42600	0.46961	-0.40770	1.95972	-1.95988	0.02823	-0.02823	2.42310	-2.20969	
-0.42	-0.17690	-0.83513	0.13516	-0.08629	0.02039	-0.01581	0.00290	-0.00252	0.09403	-0.09404	0.02823	-0.02823	0.16832	-0.13169	
-0.21	0.18271	0.76662	0.17866	-0.11406	0.05169	-0.04007	0.01563	-0.01800	0.09121	-0.09121	0.02823	-0.02823	0.20965	-0.15510	
-0.00	0.47559	0.29433	0.07513	-0.04797	0.02455	-0.01903	0.00897	-0.01034	0.03506	-0.03507	0.02823	-0.02823	0.09140	-0.06925	
0.21	0.40402	0.36053	0.08080	-0.05158	0.02338	-0.01812	0.00707	-0.00814	0.04125	-0.04125	0.02823	-0.02823	0.09810	-0.07452	
0.42	-0.08627	-1.78493	0.27715	-0.17694	0.04181	-0.03242	0.00596	-0.00517	0.19281	-0.19283	0.02823	-0.02823	0.34142	-0.26526	
0.63	0.16342	1.07700	0.06757	-0.04314	0.01711	-0.02207	0.02433	-0.02113	0.10154	-0.10155	0.02823	-0.02823	0.12868	-0.11792	
0.84	0.17203	1.19648	0.01386	-0.02171	0.04256	-0.05490	0.02795	-0.02426	0.09624	-0.09624	0.02823	-0.02823	0.11333	-0.11889	
1.05	0.49421	0.48063	0.02308	-0.03615	0.01831	-0.02362	0.00497	-0.00432	0.03344	-0.03344	0.02823	-0.02823	0.05299	-0.06163	
1.26	0.05467	5.01100	0.33759	-0.52878	0.13393	-0.17274	0.02412	-0.02778	0.30201	-0.30204	0.02823	-0.02823	0.47380	-0.63423	
1.47	0.43663	0.76457	0.05111	-0.08005	0.00641	-0.00826	0.00893	-0.01028	0.03781	-0.03782	0.02823	-0.02823	0.07042	-0.09386	
1.68	0.31981	0.97081	0.06977	-0.10929	0.01128	-0.00874	0.01219	-0.01404	0.05166	-0.05166	0.00809	-0.00809	0.08876	-0.12228	
1.88	0.38778	0.66562	0.04759	-0.07455	0.02435	-0.01888	0.00340	-0.00392	0.04265	-0.04266	0.00809	-0.00809	0.06895	-0.08840	
2.09	0.39842	0.54025	0.02863	-0.04484	0.02930	-0.02272	0.00617	-0.00536	0.04157	-0.04157	0.00809	-0.00809	0.05924	-0.06595	
2.30	0.21584	0.86689	0.01105	-0.01731	0.04376	-0.03392	0.02228	-0.01934	0.07683	-0.07684	0.00809	-0.00809	0.09220	-0.08828	
2.51	0.17902	0.92802	0.06168	-0.03938	0.02015	-0.01562	0.02221	-0.01928	0.09276	-0.09276	0.00809	-0.00809	0.11364	-0.10410	
2.72	0.20803	0.74059	0.11494	-0.07338	0.01344	-0.01734	0.00247	-0.00214	0.07991	-0.07992	0.00809	-0.00809	0.14089	-0.11019	
2.93	0.22892	0.65440	0.14260	-0.09104	0.03198	-0.04125	0.01247	-0.01437	0.07267	-0.07268	0.00809	-0.00809	0.16389	-0.12468	
3.14	0.31345	0.48325	0.11400	-0.07278	0.02887	-0.03724	0.01361	-0.01568	0.05309	-0.05309	0.00809	-0.00809	0.13000	-0.09907	
3.35	0.38907	0.39554	0.08390	-0.05356	0.01882	-0.02427	0.00734	-0.00845	0.04276	-0.04276	0.00809	-0.00809	0.09665	-0.07365	
3.56	0.40883	0.39802	0.05848	-0.03734	0.00684	-0.00882	0.00126	-0.00109	0.04066	-0.04067	0.00809	-0.00809	0.07203	-0.05650	
3.77	0.04250	4.11531	0.25982	-0.16587	0.08488	-0.06580	0.09357	-0.08123	0.39071	-0.39074	0.00809	-0.00809	0.48599	-0.43725	
3.98	0.26650	0.72825	0.00895	-0.01402	0.03544	-0.02747	0.01804	-0.01566	0.06223	-0.06223	0.00809	-0.00809	0.07483	-0.07166	
4.19	0.16926	1.39036	0.06739	-0.10556	0.06897	-0.05347	0.01452	-0.01261	0.09784	-0.09785	0.00809	-0.00809	0.13838	-0.15428	
4.40	-0.04014	-6.97001	0.45984	-0.72027	0.23530	-0.18243	0.03286	-0.03784	0.41208	-0.41212	0.00809	-0.00809	0.66164	-0.85053	
4.61	-0.16300	-1.80003	0.13690	-0.21443	0.02213	-0.01716	0.02392	-0.02755	0.10136	-0.10137	0.00809	-0.00809	0.17361	-0.23953	

Table 25: 0–20%, 9.0–12.0 \otimes 1.0–2.0 GeV/c Jet Function

ϕ	per trig yield	σ_{stat}/y	systematic errors												
			$+\sigma_{f2}/y$	$-\sigma_{f2}/y$	$+\sigma_{f3}/y$	$-\sigma_{f3}/y$	$+\sigma_{f4}/y$	$-\sigma_{f4}/y$	$+\sigma_\xi/y$	$-\sigma_\xi/y$	$+\sigma_{\pi^0}/y$	$-\sigma_{\pi^0}/y$	$+\sigma_{total}/y$	$-\sigma_{total}/y$	
-1.47	0.27318	0.54774	0.04078	-0.06643	0.00734	-0.00950	0.01288	-0.01468	0.01494	-0.01494	0.01091	-0.01091	0.04717	-0.07114	
-1.26	0.17893	0.71949	0.05150	-0.08388	0.02935	-0.03796	0.00665	-0.00758	0.02280	-0.02280	0.01091	-0.01091	0.06478	-0.09578	
-1.05	-0.00404	-24.60875	1.41031	-2.29726	1.60765	-2.07945	0.54373	-0.47710	1.01152	-1.01144	0.01091	-0.01091	2.42744	-3.29428	
-0.84	0.15453	0.54256	0.00770	-0.01255	0.03399	-0.04396	0.02779	-0.02439	0.02652	-0.02652	0.01091	-0.01091	0.05300	-0.05922	
-0.63	0.00903	8.14935	0.63463	-0.38961	0.22206	-0.28723	0.39325	-0.34506	0.45582	-0.45578	0.01091	-0.01091	0.90256	-0.74915	
-0.42	0.14173	0.49162	0.08758	-0.05377	0.01831	-0.01415	0.00324	-0.00284	0.02920	-0.02920	0.01091	-0.01091	0.09481	-0.06381	
-0.21	0.32437	0.20335	0.05225	-0.03208	0.02094	-0.01619	0.00795	-0.00906	0.01281	-0.01281	0.01091	-0.01091	0.05929	-0.04070	
-0.00	0.41957	0.15419	0.04422	-0.02714	0.02001	-0.01547	0.00918	-0.01047	0.00992	-0.00992	0.01091	-0.01091	0.05155	-0.03610	
0.21	0.26421	0.25073	0.06415	-0.03938	0.02571	-0.01988	0.00976	-0.01112	0.01573	-0.01573	0.01091	-0.01091	0.07237	-0.04936	
0.42	0.05238	1.39119	0.23700	-0.14550	0.04954	-0.03830	0.00876	-0.00769	0.07902	-0.07902	0.01091	-0.01091	0.25508	-0.17047	
0.63	0.07155	1.14128	0.08012	-0.04919	0.02803	-0.03626	0.04965	-0.04356	0.05755	-0.05754	0.01091	-0.01091	0.11446	-0.09520	
0.84	-0.05074	-1.88978	0.02346	-0.03822	0.10351	-0.13389	0.08465	-0.07428	0.08077	-0.08076	0.01091	-0.01091	0.15835	-0.17761	
1.05	-0.04592	-2.38749	0.12401	-0.20200	0.14136	-0.18285	0.04781	-0.04195	0.08894	-0.08894	0.01091	-0.01091	0.21372	-0.28987	
1.26	-0.02033	-6.47806	0.45315	-0.73813	0.25828	-0.33407	0.05855	-0.06673	0.20062	-0.20061	0.01091	-0.01091	0.56200	-0.83741	
1.47	-0.04135	-3.97970	0.26943	-0.43887	0.04851	-0.06275	0.08513	-0.09701	0.09871	-0.09871	0.01091	-0.01091	0.30341	-0.46456	
1.68	-0.04031	-3.73044	0.27639	-0.45022	0.06437	-0.04977	0.08733	-0.09952	0.10143	-0.10143	0.05916	-0.05916	0.31930	-0.47840	
1.88	0.10282	1.22052	0.08961	-0.14597	0.06607	-0.05108	0.01158	-0.01320	0.03985	-0.03984	0.05916	-0.05916	0.13273	-0.17082	
2.09	-0.05201	-1.93518	0.10948	-0.17834	0.16143	-0.12480	0.04221	-0.03704	0.07895	-0.07894	0.05916	-0.05916	0.22262	-0.24183	
2.30	0.03108	2.80559	0.03831	-0.06240	0.21857	-0.16898	0.13820	-0.12126	0.13242	-0.13241	0.05916	-0.05916	0.29895	-0.26112	
2.51	0.22108	0.35032	0.02593	-0.01592	0.01174	-0.00907	0.01607	-0.01410	0.01866	-0.01865	0.05916	-0.05916	0.07012	-0.06620	
2.72	0.20392	0.34716	0.06088	-0.03737	0.00984	-0.01272	0.00225	-0.00198	0.02026	-0.02026	0.05916	-0.05916	0.08785	-0.07398	
2.93	0.16174	0.42760	0.10478	-0.06433	0.03247	-0.04200	0.01594	-0.01817	0.02558	-0.02558	0.05916	-0.05916	0.12823	-0.10191	
3.14	0.18775	0.37440	0.09881	-0.06066	0.03457	-0.04472	0.02052	-0.02339	0.02205	-0.02205	0.05916	-0.05916	0.12396	-0.10106	
3.35	0.17152	0.41517	0.09881	-0.06066	0.03062	-0.03960	0.01503	-0.01713	0.02413	-0.02412	0.05916	-0.05916	0.12251	-0.09810	
3.56	0.20858	0.35599	0.05951	-0.03654	0.00962	-0.01244	0.00220	-0.00193	0.01981	-0.01981	0.05916	-0.05916	0.08679	-0.07339	
3.77	0.02966	2.67476	0.19330	-0.11867	0.08749	-0.06764	0.11978	-0.10510	0.13907	-0.13906	0.05916	-0.05916	0.28672	-0.22922	
3.98	-0.08272	-1.09064	0.01439	-0.02344	0.08212	-0.06349	0.05192	-0.04556	0.04975	-0.04975	0.05916	-0.05916	0.12499	-0.11239	
4.19	-0.05899	-1.83843	0.09654	-0.15725	0.14234	-0.11005	0.03722	-0.03266	0.06961	-0.06961	0.05916	-0.05916	0.19827	-0.21506	
4.40	-0.21842	-0.61151	0.04218	-0.06871	0.03110	-0.02404	0.00945	-0.00621	0.01876	-0.01876	0.05916	-0.05916	0.08141	-0.09587	
4.61	0.02985	5.12018	0.37317	-0.60785	0.08691	-0.06719	0.11790	-0.13437	0.13695	-0.13694	0.05916	-0.05916	0.42774	-0.64367	

Table 26: 0–20%, 9.0–12.0 \otimes 2.0–3.0 GeV/c Jet Function

ϕ	per trig yield	σ_{stat}/y	systematic errors											
			$+\sigma_{f_2}/y$	$-\sigma_{f_2}/y$	$+\sigma_{f_3}/y$	$-\sigma_{f_3}/y$	$+\sigma_{f_4}/y$	$-\sigma_{f_4}/y$	$+\sigma_\xi/y$	$-\sigma_\xi/y$	$+\sigma_{\pi^0}/y$	$-\sigma_{\pi^0}/y$	$+\sigma_{total}/y$	$-\sigma_{total}/y$
-1.47	0.05600	0.73040	0.02389	-0.03823	0.00499	-0.00664	0.01050	-0.01098	0.00513	-0.00513	0.00299	-0.00299	0.02723	-0.04076
-1.26	0.02913	1.14785	0.03799	-0.06079	0.02511	-0.03343	0.00683	-0.00714	0.00985	-0.00985	0.00299	-0.00299	0.04719	-0.07050
-1.05	0.03240	0.86013	0.02111	-0.03378	0.02790	-0.03715	0.01039	-0.00993	0.00887	-0.00887	0.00299	-0.00299	0.03768	-0.05203
-0.84	-0.00778	-2.67662	0.01837	-0.02940	0.09398	-0.12512	0.08463	-0.08090	0.03710	-0.03710	0.00299	-0.00299	0.13310	-0.15636
-0.63	-0.02336	-0.82097	0.02895	-0.01809	0.01196	-0.01592	0.02332	-0.02229	0.01246	-0.01246	0.00299	-0.00299	0.04110	-0.03524
-0.42	0.03468	0.52902	0.04223	-0.02639	0.01073	-0.00806	0.00203	-0.00194	0.00847	-0.00847	0.00299	-0.00299	0.04454	-0.02908
-0.21	0.11768	0.16378	0.01699	-0.01062	0.00828	-0.00622	0.00366	-0.00383	0.00251	-0.00251	0.00299	-0.00299	0.01964	-0.01347
-0.00	0.33858	0.06208	0.00646	-0.00404	0.00356	-0.00267	0.00190	-0.00199	0.00088	-0.00088	0.00299	-0.00299	0.00823	-0.00609
0.21	0.13622	0.14547	0.01468	-0.00917	0.00715	-0.00537	0.00316	-0.00331	0.00217	-0.00217	0.00299	-0.00299	0.01704	-0.01173
0.42	0.04949	0.39201	0.02960	-0.01850	0.00752	-0.00565	0.00142	-0.00136	0.00593	-0.00593	0.00299	-0.00299	0.03128	-0.02049
0.63	0.00951	2.31915	0.07116	-0.04447	0.02939	-0.03913	0.05731	-0.05479	0.03061	-0.03061	0.00299	-0.00299	0.10079	-0.08635
0.84	0.01702	1.43149	0.00840	-0.01344	0.04297	-0.05722	0.03870	-0.03699	0.01696	-0.01696	0.00299	-0.00299	0.06092	-0.07155
1.05	-0.05956	-0.46178	0.01148	-0.01838	0.01518	-0.02021	0.00565	-0.00540	0.00483	-0.00483	0.00299	-0.00299	0.02065	-0.02842
1.26	0.00677	4.98951	0.16353	-0.26166	0.10808	-0.14389	0.02939	-0.03075	0.04242	-0.04242	0.00299	-0.00299	0.20271	-0.30319
1.47	-0.02339	-1.79628	0.05720	-0.09153	0.01194	-0.01590	0.02514	-0.02630	0.01229	-0.01229	0.00299	-0.00299	0.06486	-0.09738
1.68	0.07572	0.59056	0.01767	-0.02828	0.00491	-0.00369	0.00777	-0.00812	0.00381	-0.00381	0.01296	-0.01296	0.02407	-0.03258
1.88	0.01081	3.00710	0.10239	-0.16384	0.09010	-0.06767	0.01840	-0.01925	0.02677	-0.02677	0.01296	-0.01296	0.14080	-0.18077
2.09	0.00964	2.86978	0.07096	-0.11354	0.12487	-0.09379	0.03493	-0.03339	0.03011	-0.03011	0.01296	-0.01296	0.15140	-0.15452
2.30	-0.04754	-0.44536	0.00301	-0.00481	0.02049	-0.01539	0.01386	-0.01325	0.00612	-0.00612	0.01296	-0.01296	0.02874	-0.02531
2.51	0.04401	0.48390	0.01537	-0.00961	0.00845	-0.00635	0.01238	-0.01183	0.00663	-0.00663	0.01296	-0.01296	0.02594	-0.02201
2.72	0.03474	0.53310	0.04217	-0.02635	0.00804	-0.01071	0.00203	-0.00194	0.00843	-0.00843	0.01296	-0.01296	0.04567	-0.03243
2.93	0.06932	0.28170	0.02885	-0.01803	0.01055	-0.01405	0.00621	-0.00650	0.00423	-0.00423	0.01296	-0.01296	0.03417	-0.02739
3.14	0.07276	0.26134	0.03008	-0.01880	0.01243	-0.01654	0.00885	-0.00925	0.00403	-0.00403	0.01296	-0.01296	0.03636	-0.02995
3.35	0.04598	0.42978	0.04349	-0.02718	0.01591	-0.02118	0.00937	-0.00980	0.00638	-0.00638	0.01296	-0.01296	0.04940	-0.03862
3.56	0.05104	0.38234	0.02869	-0.01793	0.00547	-0.00729	0.00138	-0.00132	0.00573	-0.00573	0.01296	-0.01296	0.03250	-0.02403
3.77	0.01297	1.64417	0.05214	-0.03259	0.02867	-0.02154	0.04199	-0.04014	0.02250	-0.02250	0.01296	-0.01296	0.07732	-0.06174
3.98	0.02510	0.95123	0.00570	-0.00912	0.03880	-0.02914	0.02624	-0.02509	0.01160	-0.01160	0.01296	-0.01296	0.05029	-0.04318
4.19	-0.02839	-1.01340	0.02409	-0.03855	0.04240	-0.03185	0.01186	-0.01134	0.01022	-0.01022	0.01296	-0.01296	0.05283	-0.05386
4.40	0.02964	1.19085	0.03734	-0.05975	0.03286	-0.02468	0.00671	-0.00702	0.00976	-0.00976	0.01296	-0.01296	0.05275	-0.06702
4.61	0.08354	0.56160	0.01602	-0.02563	0.00445	-0.00334	0.00704	-0.00736	0.00345	-0.00345	0.01296	-0.01296	0.02249	-0.03004

Table 27: 0–20%, 9.0–12.0 \otimes 3.0–5.0 GeV/c Jet Function

ϕ	per trig yield	σ_{stat}/y	systematic errors												
			$+\sigma_{f2}/y$	$-\sigma_{f2}/y$	$+\sigma_{f3}/y$	$-\sigma_{f3}/y$	$+\sigma_{f4}/y$	$-\sigma_{f4}/y$	$+\sigma_\xi/y$	$-\sigma_\xi/y$	$+\sigma_{\pi^0}/y$	$-\sigma_{\pi^0}/y$	$+\sigma_{total}/y$	$-\sigma_{total}/y$	
-1.47	0.00968	1.54015	0.01981	-0.03088	0.00438	-0.00580	0.01041	-0.01097	0.00402	-0.00398	0.00058	-0.00058	0.02316	-0.03353	
-1.26	-0.00169	-6.59937	0.09402	-0.14661	0.06577	-0.08720	0.02021	-0.02130	0.02299	-0.02279	0.00058	-0.00058	0.11875	-0.17341	
-1.05	0.01189	0.88641	0.00825	-0.01286	0.01154	-0.01529	0.00489	-0.00464	0.00326	-0.00324	0.00058	-0.00058	0.01536	-0.02077	
-0.84	0.00712	1.10238	0.00288	-0.00449	0.01559	-0.02067	0.01598	-0.01516	0.00548	-0.00543	0.00058	-0.00058	0.02317	-0.02659	
-0.63	0.01009	0.75860	0.00936	-0.00600	0.00420	-0.00557	0.00932	-0.00884	0.00390	-0.00386	0.00058	-0.00058	0.01441	-0.01267	
-0.42	0.00735	0.91461	0.02783	-0.01785	0.00764	-0.00577	0.00165	-0.00157	0.00540	-0.00535	0.00058	-0.00058	0.02941	-0.01958	
-0.21	0.05906	0.14725	0.00473	-0.00303	0.00249	-0.00188	0.00125	-0.00132	0.00068	-0.00067	0.00058	-0.00058	0.00556	-0.00391	
-0.00	0.27522	0.04909	0.00111	-0.00071	0.00066	-0.00050	0.00040	-0.00042	0.00013	-0.00014	0.00058	-0.00058	0.00148	-0.00114	
0.21	0.09303	0.10835	0.00300	-0.00192	0.00158	-0.00119	0.00079	-0.00084	0.00043	-0.00043	0.00058	-0.00058	0.00356	-0.00252	
0.42	0.00579	1.18725	0.03531	-0.02264	0.00970	-0.00731	0.00210	-0.00199	0.00685	-0.00679	0.00058	-0.00058	0.03732	-0.02483	
0.63	0.00918	0.92017	0.01029	-0.00660	0.00461	-0.00612	0.01024	-0.00972	0.00428	-0.00424	0.00058	-0.00058	0.01583	-0.01392	
0.84	0.01177	0.80134	0.00174	-0.00272	0.00943	-0.01250	0.00966	-0.00917	0.00331	-0.00328	0.00058	-0.00058	0.01402	-0.01609	
1.05	0.00410	2.87247	0.02391	-0.03728	0.03345	-0.04435	0.01418	-0.01345	0.00947	-0.00938	0.00058	-0.00058	0.04452	-0.06022	
1.26	-0.01777	-0.54769	0.00893	-0.01392	0.00624	-0.00828	0.00192	-0.00202	0.00218	-0.00216	0.00058	-0.00058	0.01129	-0.01647	
1.47	-0.00036	-41.29550	0.52573	-0.81978	0.11618	-0.15403	0.27626	-0.29122	0.10659	-0.10565	0.00058	-0.00058	0.61447	-0.88980	
1.68	-0.01873	-0.67030	0.01024	-0.01597	0.00300	-0.00226	0.00538	-0.00567	0.00208	-0.00206	0.00120	-0.00120	0.01219	-0.01726	
1.88	0.00853	1.41352	0.01860	-0.02900	0.01725	-0.01301	0.00400	-0.00421	0.00459	-0.00455	0.00120	-0.00120	0.02611	-0.03240	
2.09	-0.00667	-1.41091	0.01470	-0.02292	0.02726	-0.02056	0.00872	-0.00827	0.00589	-0.00583	0.00120	-0.00120	0.03273	-0.03243	
2.30	0.01367	0.64359	0.00150	-0.00234	0.01076	-0.00812	0.00832	-0.00789	0.00288	-0.00285	0.00120	-0.00120	0.01404	-0.01197	
2.51	0.01330	0.61042	0.00710	-0.00455	0.00422	-0.00318	0.00707	-0.00671	0.00297	-0.00294	0.00120	-0.00120	0.01133	-0.00927	
2.72	0.01102	0.62668	0.01857	-0.01191	0.00385	-0.00510	0.00110	-0.00105	0.00359	-0.00356	0.00120	-0.00120	0.01937	-0.01353	
2.93	0.03633	0.22875	0.00769	-0.00493	0.00305	-0.00405	0.00203	-0.00214	0.00109	-0.00108	0.00120	-0.00120	0.00867	-0.00692	
3.14	0.08030	0.12181	0.00381	-0.00244	0.00171	-0.00226	0.00137	-0.00145	0.00049	-0.00049	0.00120	-0.00120	0.00458	-0.00386	
3.35	0.03902	0.22654	0.00716	-0.00459	0.00284	-0.00377	0.00189	-0.00199	0.00102	-0.00101	0.00120	-0.00120	0.00808	-0.00646	
3.56	0.01945	0.38714	0.01051	-0.00674	0.00218	-0.00289	0.00062	-0.00059	0.00203	-0.00202	0.00120	-0.00120	0.01101	-0.00772	
3.77	-0.00216	-3.49384	0.04377	-0.02807	0.02603	-0.01963	0.04358	-0.04135	0.01828	-0.01812	0.00120	-0.00120	0.06949	-0.05668	
3.98	0.00215	3.81957	0.00953	-0.01487	0.06844	-0.05162	0.05292	-0.05020	0.01831	-0.01815	0.00120	-0.00120	0.08895	-0.07574	
4.19	0.02337	0.54236	0.00419	-0.00654	0.00778	-0.00587	0.00249	-0.00236	0.00168	-0.00166	0.00120	-0.00120	0.00941	-0.00933	
4.40	0.01272	1.04502	0.01247	-0.01945	0.01157	-0.00872	0.00268	-0.00283	0.00308	-0.00305	0.00120	-0.00120	0.01753	-0.02175	
4.61	-0.01074	-1.25978	0.01786	-0.02784	0.00523	-0.00395	0.00938	-0.00989	0.00363	-0.00360	0.00120	-0.00120	0.02119	-0.03005	

Table 28: 0–20%, 9.0–12.0 \otimes 5.0–7.0 GeV/c Jet Function

ϕ	per trig yield	σ_{stat}/y	systematic errors											
			$+\sigma_{f2}/y$	$-\sigma_{f2}/y$	$+\sigma_{f3}/y$	$-\sigma_{f3}/y$	$+\sigma_{f4}/y$	$-\sigma_{f4}/y$	$+\sigma_\xi/y$	$-\sigma_\xi/y$	$+\sigma_{\pi^0}/y$	$-\sigma_{\pi^0}/y$	$+\sigma_{total}/y$	$-\sigma_{total}/y$
-1.47	-0.00627	-0.47926	0.00399	-0.00561	0.00119	-0.00099	0.00179	-0.00308	0.00158	-0.00164	0.01835	-0.01835	0.01897	-0.01953
-1.26	-0.00223	-1.51838	0.00926	-0.01304	0.00874	-0.00730	0.00170	-0.00292	0.00444	-0.00460	0.01835	-0.01835	0.02284	-0.02429
-1.05	0.00637	0.72153	0.00201	-0.00282	0.00379	-0.00316	0.00166	-0.00097	0.00156	-0.00161	0.01835	-0.01835	0.01898	-0.01893
-0.84	0.00060	4.61894	0.00446	-0.00628	0.03257	-0.02720	0.03449	-0.02009	0.01662	-0.01720	0.01835	-0.01835	0.03370	-0.04261
-0.63	-0.00431	-0.44301	0.00258	-0.00183	0.00173	-0.00144	0.00396	-0.00231	0.00232	-0.00240	0.01835	-0.01835	0.01917	-0.01880
-0.42	0.00003	74.06316	0.77659	-0.55160	0.20072	-0.24035	0.07121	-0.04147	0.32493	-0.33626	0.01835	-0.01835	0.86854	-0.69076
-0.21	0.00772	0.39519	0.00426	-0.00302	0.00211	-0.00253	0.00107	-0.00183	0.00131	-0.00136	0.01835	-0.01835	0.01903	-0.01891
-0.00	0.13173	0.06433	0.00027	-0.00019	0.00015	-0.00018	0.00009	-0.00016	0.00008	-0.00008	0.01835	-0.01835	0.01836	-0.01836
0.21	0.02022	0.21122	0.00162	-0.00115	0.00081	-0.00096	0.00041	-0.00070	0.00050	-0.00052	0.01835	-0.01835	0.01845	-0.01844
0.42	-0.00079	-3.06568	0.03043	-0.02162	0.00787	-0.00942	0.00279	-0.00162	0.01273	-0.01318	0.01835	-0.01835	0.03866	-0.03270
0.63	0.00189	1.84152	0.00589	-0.00418	0.00394	-0.00329	0.00904	-0.00527	0.00530	-0.00548	0.01835	-0.01835	0.02229	-0.02057
0.84	0.00119	2.67020	0.00225	-0.00317	0.01643	-0.01372	0.01740	-0.01013	0.00838	-0.00868	0.01835	-0.01835	0.03138	-0.02670
1.05	0.00084	6.10063	0.01520	-0.02139	0.02868	-0.02395	0.01256	-0.00731	0.01180	-0.01221	0.01835	-0.01835	0.04107	-0.03963
1.26	-0.00201	-1.81167	0.01031	-0.01451	0.00972	-0.00812	0.00189	-0.00325	0.00494	-0.00511	0.01835	-0.01835	0.02378	-0.02550
1.47	0.00099	6.29467	0.02515	-0.03540	0.00750	-0.00626	0.01130	-0.01941	0.00998	-0.01033	0.01835	-0.01835	0.03539	-0.04596
1.68	-0.00056	-9.25857	0.04468	-0.06291	0.01112	-0.01332	0.02008	-0.03449	0.01777	-0.01839	0.01280	-0.01280	0.05480	-0.07633
1.88	0.00247	1.83484	0.00835	-0.01176	0.00658	-0.00788	0.00154	-0.00264	0.00402	-0.00416	0.01280	-0.01280	0.01719	-0.01971
2.09	0.00077	4.99154	0.01667	-0.02347	0.02628	-0.03146	0.01378	-0.00802	0.01303	-0.01348	0.01280	-0.01280	0.03862	-0.04417
2.30	0.00862	0.48129	0.00031	-0.00044	0.00189	-0.00226	0.00239	-0.00139	0.00116	-0.00120	0.01280	-0.01280	0.01321	-0.01313
2.51	0.00034	7.90969	0.03255	-0.02312	0.01822	-0.02181	0.05002	-0.02913	0.02936	-0.03039	0.01280	-0.01280	0.07014	-0.05428
2.72	0.00639	0.46809	0.00377	-0.00267	0.00117	-0.00097	0.00035	-0.00020	0.00157	-0.00163	0.01280	-0.01280	0.01349	-0.01321
2.93	0.02420	0.19515	0.00136	-0.00096	0.00081	-0.00067	0.00034	-0.00058	0.00042	-0.00043	0.01280	-0.01280	0.01291	-0.01287
3.14	0.02806	0.17688	0.00128	-0.00091	0.00086	-0.00072	0.00044	-0.00075	0.00036	-0.00037	0.01280	-0.01280	0.01290	-0.01288
3.35	0.01340	0.29949	0.00245	-0.00174	0.00145	-0.00121	0.00061	-0.00105	0.00075	-0.00078	0.01280	-0.01280	0.01315	-0.01304
3.56	0.00370	0.77565	0.00650	-0.00462	0.00201	-0.00168	0.00060	-0.00035	0.00272	-0.00281	0.01280	-0.01280	0.01476	-0.01400
3.77	0.00244	1.33565	0.00456	-0.00324	0.00255	-0.00306	0.00701	-0.00408	0.00411	-0.00426	0.01280	-0.01280	0.01604	-0.01478
3.98	0.00570	0.74281	0.00047	-0.00066	0.00285	-0.00342	0.00362	-0.00211	0.00175	-0.00181	0.01280	-0.01280	0.01372	-0.01355
4.19	0.00227	2.08629	0.00562	-0.00791	0.00885	-0.01060	0.00464	-0.00270	0.00439	-0.00454	0.01280	-0.01280	0.01774	-0.01915
4.40	0.00135	3.85852	0.01530	-0.02155	0.01206	-0.01444	0.00281	-0.00483	0.00737	-0.00763	0.01280	-0.01280	0.02461	-0.03030
4.61	0.00488	1.97451	0.00512	-0.00721	0.00127	-0.00153	0.00230	-0.00395	0.00204	-0.00211	0.01280	-0.01280	0.01418	-0.01543

Table 29: 0–20%, 12.0–15.0 \otimes 0.5–1.0 GeV/c Jet Function

ϕ	per trig yield	σ_{stat}/y	systematic errors												
			$+\sigma_{f2}/y$	$-\sigma_{f2}/y$	$+\sigma_{f3}/y$	$-\sigma_{f3}/y$	$+\sigma_{f4}/y$	$-\sigma_{f4}/y$	$+\sigma_{\xi}/y$	$-\sigma_{\xi}/y$	$+\sigma_{\pi^0}/y$	$-\sigma_{\pi^0}/y$	$+\sigma_{total}/y$	$-\sigma_{total}/y$	
-1.47	-0.75119	-0.93581	0.03083	-0.07846	0.00385	-0.00722	0.00672	-0.00614	0.02657	-0.02657	0.12758	-0.12758	0.13414	-0.15241	
-1.26	-0.61363	-1.03417	0.03122	-0.07944	0.01235	-0.02315	0.00278	-0.00254	0.03253	-0.03253	0.12758	-0.12758	0.13591	-0.15553	
-1.05	-0.31536	-1.61226	0.03754	-0.09554	0.02971	-0.05569	0.00800	-0.00877	0.06335	-0.06335	0.12758	-0.12758	0.15049	-0.18055	
-0.84	-0.34056	-1.27055	0.00727	-0.01849	0.02226	-0.04172	0.01450	-0.01588	0.05876	-0.05877	0.12758	-0.12758	0.14314	-0.14855	
-0.63	0.05044	7.61726	0.36914	-0.14505	0.05741	-0.10759	0.08096	-0.08868	0.39768	-0.39771	0.12758	-0.12758	0.56616	-0.46361	
-0.42	0.49583	0.73368	0.08132	-0.03195	0.01095	-0.00584	0.00106	-0.00117	0.04055	-0.04056	0.12758	-0.12758	0.15702	-0.13776	
-0.21	0.51340	0.67244	0.10722	-0.04213	0.02767	-0.01477	0.00721	-0.00658	0.03924	-0.03924	0.12758	-0.12758	0.17358	-0.14090	
-0.00	0.92287	0.37448	0.06529	-0.02566	0.01903	-0.01015	0.00899	-0.00547	0.02184	-0.02184	0.12758	-0.12758	0.14634	-0.13246	
0.21	-0.05973	-5.84781	0.92157	-0.36213	0.23786	-0.12692	0.06194	-0.05655	0.33723	-0.33726	0.12758	-0.12758	1.01966	-0.52959	
0.42	-0.23063	-1.62455	0.17483	-0.06870	0.02353	-0.01256	0.00229	-0.00251	0.08719	-0.08719	0.12758	-0.12758	0.23453	-0.16960	
0.63	-0.15008	-2.83854	0.12407	-0.04875	0.01930	-0.03616	0.02721	-0.02981	0.13366	-0.13368	0.12758	-0.12758	0.22506	-0.19677	
0.84	-0.45799	-1.07325	0.00540	-0.01375	0.01650	-0.03102	0.01078	-0.01181	0.04370	-0.04370	0.12758	-0.12758	0.13641	-0.13956	
1.05	0.75884	0.77310	0.01560	-0.03970	0.01235	-0.02314	0.00333	-0.00364	0.02633	-0.02633	0.12758	-0.12758	0.13182	-0.13819	
1.26	-0.25815	-2.60284	0.07421	-0.18885	0.02937	-0.05504	0.00662	-0.00604	0.07732	-0.07733	0.12758	-0.12758	0.16932	-0.24695	
1.47	-0.28654	-2.87290	0.08083	-0.20570	0.01011	-0.01894	0.01763	-0.01609	0.06966	-0.06966	0.12758	-0.12758	0.16756	-0.25310	
1.68	-0.45882	-1.68635	0.05048	-0.12846	0.01183	-0.00631	0.01101	-0.01005	0.04353	-0.04353	0.04569	-0.04569	0.08241	-0.14362	
1.88	0.17032	3.86474	0.11247	-0.28623	0.08342	-0.04451	0.01003	-0.00916	0.11739	-0.11740	0.04569	-0.04569	0.18862	-0.31601	
2.09	-0.43607	-1.22010	0.02715	-0.06909	0.04027	-0.02149	0.00579	-0.00634	0.04591	-0.04591	0.04569	-0.04569	0.08117	-0.09732	
2.30	0.66173	0.70672	0.00374	-0.00952	0.02147	-0.01146	0.00746	-0.00817	0.03029	-0.03030	0.04569	-0.04569	0.05946	-0.05739	
2.51	-0.17109	-2.36380	0.10884	-0.04277	0.03172	-0.01693	0.02387	-0.02615	0.11732	-0.11733	0.04569	-0.04569	0.17110	-0.13658	
2.72	0.75044	0.51121	0.05373	-0.02111	0.00386	-0.00723	0.00070	-0.00077	0.02678	-0.02678	0.04569	-0.04569	0.07554	-0.05748	
2.93	1.02236	0.36640	0.05384	-0.02116	0.00742	-0.01390	0.00362	-0.00330	0.01967	-0.01967	0.04569	-0.04569	0.07377	-0.05591	
3.14	-0.03361	-10.85827	1.79278	-0.70447	0.27881	-0.52251	0.16451	-0.15019	0.59848	-0.59853	0.04569	-0.04569	1.91811	-1.07340	
3.35	0.35933	1.02357	0.15320	-0.06020	0.02110	-0.03954	0.01030	-0.00940	0.05597	-0.05597	0.04569	-0.04569	0.17100	-0.10245	
3.56	0.96275	0.41454	0.04188	-0.01646	0.00301	-0.00564	0.00055	-0.00060	0.02087	-0.02087	0.04569	-0.04569	0.06547	-0.05316	
3.77	0.40984	1.03688	0.04543	-0.01785	0.01324	-0.00707	0.00996	-0.01091	0.04898	-0.04898	0.04569	-0.04569	0.08261	-0.07053	
3.98	0.92182	0.51555	0.00268	-0.00683	0.01541	-0.00822	0.00536	-0.00587	0.02175	-0.02175	0.04569	-0.04569	0.05324	-0.05205	
4.19	-0.71438	-0.76993	0.01657	-0.04217	0.02458	-0.01312	0.00353	-0.00387	0.02802	-0.02803	0.04569	-0.04569	0.06136	-0.06956	
4.40	0.15306	4.36527	0.12515	-0.31850	0.09283	-0.04953	0.01116	-0.01019	0.13063	-0.13064	0.04569	-0.04569	0.20870	-0.35093	
4.61	1.01522	0.70239	0.02281	-0.05806	0.00535	-0.00285	0.00498	-0.00454	0.01967	-0.01967	0.04569	-0.04569	0.05521	-0.07664	

Table 30: 0–20%, 12.0–15.0 \otimes 1.0–2.0 GeV/c Jet Function

ϕ	per trig yield	σ_{stat}/y	systematic errors											
			$+\sigma_{f_2}/y$	$-\sigma_{f_2}/y$	$+\sigma_{f_3}/y$	$-\sigma_{f_3}/y$	$+\sigma_{f_4}/y$	$-\sigma_{f_4}/y$	$+\sigma_\xi/y$	$-\sigma_\xi/y$	$+\sigma_{\pi^0}/y$	$-\sigma_{\pi^0}/y$	$+\sigma_{total}/y$	$-\sigma_{total}/y$
-1.47	0.24853	1.42734	0.04656	-0.12455	0.00835	-0.01570	0.01839	-0.01656	0.01917	-0.01917	0.05022	-0.05022	0.07393	-0.13756
-1.26	-0.68023	-0.42565	0.01407	-0.03764	0.00799	-0.01502	0.00227	-0.00205	0.00700	-0.00700	0.05022	-0.05022	0.05328	-0.06494
-1.05	0.12544	1.95078	0.04715	-0.12614	0.05353	-0.10068	0.01796	-0.01995	0.03801	-0.03801	0.05022	-0.05022	0.09685	-0.17439
-0.84	-0.04637	-4.32144	0.02667	-0.07134	0.11717	-0.22036	0.09506	-0.10556	0.10318	-0.10317	0.05022	-0.05022	0.19143	-0.27921
-0.63	-0.00137	-128.89073	7.11603	-2.66003	1.51006	-2.83985	2.65289	-2.94588	3.49801	-3.49775	0.05022	-0.05022	8.49675	-6.00463
-0.42	0.30197	0.56977	0.07012	-0.02621	0.01292	-0.00687	0.00156	-0.00173	0.01600	-0.01600	0.05022	-0.05022	0.08869	-0.05929
-0.21	0.38115	0.42461	0.07585	-0.02835	0.02681	-0.01425	0.00878	-0.00791	0.01273	-0.01273	0.05022	-0.05022	0.09609	-0.06127
-0.00	0.76403	0.21274	0.04142	-0.01548	0.01653	-0.00879	0.00655	-0.00590	0.00636	-0.00636	0.05022	-0.05022	0.06778	-0.05399
0.21	0.39166	0.41902	0.07381	-0.02759	0.02609	-0.01387	0.00855	-0.00770	0.01239	-0.01239	0.05022	-0.05022	0.09422	-0.06074
0.42	0.28053	0.63592	0.07548	-0.02822	0.01391	-0.00740	0.00168	-0.00186	0.01722	-0.01722	0.05022	-0.05022	0.09334	-0.06061
0.63	0.17134	1.17631	0.05707	-0.02133	0.01211	-0.02278	0.02128	-0.02363	0.02805	-0.02805	0.05022	-0.05022	0.08465	-0.06958
0.84	0.06637	3.63543	0.01863	-0.04984	0.08186	-0.15395	0.06642	-0.07375	0.07209	-0.07208	0.05022	-0.05022	0.13849	-0.19835
1.05	-0.01866	-14.21719	0.31701	-0.84806	0.35993	-0.67689	0.12076	-0.13410	0.25559	-0.25557	0.05022	-0.05022	0.55900	-1.12393
1.26	-0.30404	-1.01568	0.03148	-0.08421	0.01787	-0.03360	0.00509	-0.00458	0.01567	-0.01566	0.05022	-0.05022	0.06406	-0.10492
1.47	0.16189	2.59565	0.07147	-0.19121	0.01282	-0.02411	0.02824	-0.02543	0.02944	-0.02943	0.05022	-0.05022	0.09726	-0.20292
1.68	-0.08259	-4.62268	0.14011	-0.37481	0.04725	-0.02513	0.05535	-0.04983	0.05780	-0.05779	0.06319	-0.06319	0.17961	-0.38850
1.88	-0.23835	-1.31710	0.04015	-0.10741	0.04287	-0.02279	0.00649	-0.00584	0.02007	-0.02007	0.06319	-0.06319	0.08881	-0.12840
2.09	-0.41951	-0.58433	0.01410	-0.03772	0.03010	-0.01601	0.00537	-0.00596	0.01143	-0.01143	0.06319	-0.06319	0.07251	-0.07641
2.30	-0.13918	-1.52509	0.00888	-0.02377	0.07341	-0.03903	0.03167	-0.03517	0.03452	-0.03452	0.06319	-0.06319	0.10796	-0.09225
2.51	0.03122	6.01146	0.31326	-0.11710	0.12502	-0.06648	0.11679	-0.12968	0.15424	-0.15423	0.06319	-0.06319	0.39394	-0.25046
2.72	0.16784	1.02379	0.12616	-0.04716	0.01236	-0.02325	0.00281	-0.00312	0.02874	-0.02874	0.06319	-0.06319	0.14456	-0.08714
2.93	0.34386	0.50044	0.08407	-0.03143	0.01580	-0.02971	0.00974	-0.00877	0.01405	-0.01405	0.06319	-0.06319	0.10772	-0.07835
3.14	0.45184	0.38952	0.07004	-0.02618	0.01486	-0.02795	0.01107	-0.00997	0.01070	-0.01070	0.06319	-0.06319	0.09673	-0.07532
3.35	0.03078	5.51239	0.93928	-0.35111	0.17651	-0.33195	0.10879	-0.09797	0.15695	-0.15694	0.06319	-0.06319	0.97666	-0.52124
3.56	0.20064	0.89126	0.10554	-0.03945	0.01034	-0.01945	0.00235	-0.00261	0.02404	-0.02404	0.06319	-0.06319	0.12579	-0.08070
3.77	0.34552	0.57015	0.02830	-0.01058	0.01129	-0.00601	0.01055	-0.01172	0.01394	-0.01393	0.06319	-0.06319	0.07230	-0.06688
3.98	-0.06890	-3.09312	0.01795	-0.04801	0.14830	-0.07886	0.06398	-0.07104	0.06974	-0.06973	0.06319	-0.06319	0.18779	-0.14975
4.19	0.11810	2.23361	0.05008	-0.13398	0.10694	-0.05686	0.01908	-0.02119	0.04059	-0.04059	0.06319	-0.06319	0.14124	-0.16515
4.40	0.06955	4.72124	0.13761	-0.36813	0.14691	-0.07812	0.02223	-0.02002	0.06878	-0.06877	0.06319	-0.06319	0.22302	-0.38826
4.61	0.20489	1.79925	0.05647	-0.15108	0.01905	-0.01013	0.02231	-0.02009	0.02330	-0.02329	0.06319	-0.06319	0.09266	-0.16693

Table 31: 0–20%, 12.0–15.0 \otimes 2.0–3.0 GeV/c Jet Function

ϕ	per trig yield	σ_{stat}/y	systematic errors											
			$+\sigma_{f2}/y$	$-\sigma_{f2}/y$	$+\sigma_{f3}/y$	$-\sigma_{f3}/y$	$+\sigma_{f4}/y$	$-\sigma_{f4}/y$	$+\sigma_\xi/y$	$-\sigma_\xi/y$	$+\sigma_{\pi^0}/y$	$-\sigma_{\pi^0}/y$	$+\sigma_{total}/y$	$-\sigma_{total}/y$
-1.47	0.14564	0.72768	0.00952	-0.02491	0.00198	-0.00387	0.00537	-0.00434	0.00228	-0.00228	0.00064	-0.00064	0.01136	-0.02569
-1.26	-0.02667	-2.87595	0.04301	-0.11248	0.02836	-0.05529	0.00991	-0.00802	0.01241	-0.01241	0.00064	-0.00064	0.05392	-0.12620
-1.05	0.11462	0.63962	0.00619	-0.01618	0.00816	-0.01590	0.00302	-0.00373	0.00289	-0.00289	0.00064	-0.00064	0.01108	-0.02318
-0.84	-0.04879	-0.98632	0.00304	-0.00795	0.01551	-0.03023	0.01387	-0.01716	0.00683	-0.00683	0.00064	-0.00064	0.02212	-0.03631
-0.63	-0.12412	-0.32589	0.00923	-0.00353	0.00233	-0.00454	0.00451	-0.00558	0.00270	-0.00270	0.00064	-0.00064	0.01090	-0.00848
-0.42	0.08394	0.56090	0.02956	-0.01130	0.00671	-0.00344	0.00086	-0.00107	0.00403	-0.00403	0.00064	-0.00064	0.03060	-0.01255
-0.21	0.17982	0.27211	0.01884	-0.00720	0.00820	-0.00421	0.00318	-0.00257	0.00190	-0.00190	0.00064	-0.00064	0.02089	-0.00896
-0.00	0.44133	0.12402	0.00840	-0.00321	0.00413	-0.00212	0.00194	-0.00157	0.00077	-0.00077	0.00064	-0.00064	0.00961	-0.00428
0.21	0.23352	0.21975	0.01451	-0.00555	0.00632	-0.00324	0.00245	-0.00198	0.00146	-0.00146	0.00064	-0.00064	0.01609	-0.00691
0.42	-0.01898	-2.27829	0.13073	-0.04999	0.02968	-0.01522	0.00381	-0.00471	0.01783	-0.01783	0.00064	-0.00064	0.13529	-0.05542
0.63	0.04363	1.27984	0.02626	-0.01004	0.00662	-0.01291	0.01283	-0.01587	0.00769	-0.00769	0.00064	-0.00064	0.03095	-0.02406
0.84	-0.04653	-1.24449	0.00319	-0.00833	0.01626	-0.03170	0.01455	-0.01799	0.00716	-0.00716	0.00064	-0.00064	0.02319	-0.03807
1.05	-0.15272	-0.36516	0.00464	-0.01214	0.00612	-0.01194	0.00227	-0.00280	0.00217	-0.00217	0.00064	-0.00064	0.00832	-0.01740
1.26	-0.06563	-1.05408	0.01748	-0.04571	0.01153	-0.02247	0.00403	-0.00326	0.00504	-0.00504	0.00064	-0.00064	0.02192	-0.05129
1.47	-0.02064	-5.07190	0.06719	-0.17572	0.01400	-0.02729	0.03787	-0.03062	0.01606	-0.01606	0.00064	-0.00064	0.08002	-0.18116
1.68	-0.03651	-2.77141	0.03799	-0.09935	0.01543	-0.00791	0.02141	-0.01731	0.00911	-0.00911	0.02212	-0.02212	0.05208	-0.10394
1.88	0.03322	2.56449	0.03453	-0.09030	0.04439	-0.02277	0.00796	-0.00643	0.01004	-0.01004	0.02212	-0.02212	0.06177	-0.09646
2.09	-0.02298	-2.94701	0.03086	-0.08069	0.07933	-0.04070	0.01505	-0.01862	0.01456	-0.01456	0.02212	-0.02212	0.09041	-0.09600
2.30	0.08688	0.68905	0.00171	-0.00446	0.01697	-0.00871	0.00779	-0.00963	0.00386	-0.00386	0.02212	-0.02212	0.02926	-0.02632
2.51	-0.03179	-1.52176	0.03605	-0.01378	0.01772	-0.00909	0.01761	-0.02178	0.01059	-0.01059	0.02212	-0.02212	0.05025	-0.03672
2.72	0.05418	0.85163	0.04580	-0.01751	0.00533	-0.01040	0.00133	-0.00165	0.00623	-0.00623	0.02212	-0.02212	0.05154	-0.03075
2.93	0.11648	0.42667	0.02909	-0.01112	0.00650	-0.01266	0.00492	-0.00397	0.00290	-0.00290	0.02212	-0.02212	0.03755	-0.02824
3.14	0.14784	0.33815	0.02508	-0.00959	0.00633	-0.01233	0.00579	-0.00468	0.00229	-0.00229	0.02212	-0.02212	0.03460	-0.02758
3.35	0.21571	0.25889	0.01571	-0.00601	0.00351	-0.00684	0.00265	-0.00215	0.00157	-0.00157	0.02212	-0.02212	0.02753	-0.02407
3.56	0.08227	0.59055	0.03016	-0.01153	0.00351	-0.00685	0.00088	-0.00109	0.00410	-0.00410	0.02212	-0.02212	0.03780	-0.02621
3.77	0.03375	1.55657	0.03396	-0.01299	0.01669	-0.00856	0.01659	-0.02052	0.00997	-0.00997	0.02212	-0.02212	0.04791	-0.03538
3.98	-0.02614	-2.04216	0.00567	-0.01483	0.05641	-0.02894	0.02589	-0.03202	0.01284	-0.01284	0.02212	-0.02212	0.06737	-0.05231
4.19	0.01971	3.64680	0.03597	-0.09406	0.09247	-0.04744	0.01755	-0.02170	0.01698	-0.01698	0.02212	-0.02212	0.10454	-0.11111
4.40	0.01766	4.76375	0.06498	-0.16993	0.08353	-0.04285	0.01498	-0.01211	0.01890	-0.01890	0.02212	-0.02212	0.11078	-0.17806
4.61	0.08933	1.25812	0.01553	-0.04061	0.00631	-0.00323	0.00875	-0.00708	0.00372	-0.00372	0.02212	-0.02212	0.02934	-0.04704

Table 32: 0–20%, 12.0–15.0 \otimes 3.0–5.0 GeV/c Jet Function

ϕ	per trig yield	σ_{stat}/y	systematic errors											
			$+\sigma_{f2}/y$	$-\sigma_{f2}/y$	$+\sigma_{f3}/y$	$-\sigma_{f3}/y$	$+\sigma_{f4}/y$	$-\sigma_{f4}/y$	$+\sigma_{\xi}/y$	$-\sigma_{\xi}/y$	$+\sigma_{\pi^0}/y$	$-\sigma_{\pi^0}/y$	$+\sigma_{total}/y$	$-\sigma_{total}/y$
-1.47	-0.00456	-7.06469	0.04343	-0.10987	0.00959	-0.01859	0.02924	-0.02387	0.00977	-0.00991	0.00848	-0.00848	0.05477	-0.11471
-1.26	0.01994	1.54208	0.00821	-0.02076	0.00573	-0.01112	0.00226	-0.00184	0.00223	-0.00226	0.00848	-0.00848	0.01350	-0.02520
-1.05	-0.03064	-0.55578	0.00330	-0.00835	0.00461	-0.00894	0.00194	-0.00238	0.00145	-0.00147	0.00848	-0.00848	0.01048	-0.01515
-0.84	-0.03445	-0.33694	0.00061	-0.00155	0.00332	-0.00644	0.00338	-0.00414	0.00130	-0.00132	0.00848	-0.00848	0.00982	-0.01160
-0.63	-0.01367	-1.09350	0.01157	-0.00457	0.00319	-0.00619	0.00704	-0.00863	0.00329	-0.00334	0.00848	-0.00848	0.01662	-0.01472
-0.42	-0.01661	-0.78100	0.02061	-0.00815	0.00510	-0.00263	0.00075	-0.00092	0.00273	-0.00278	0.00848	-0.00848	0.02304	-0.01240
-0.21	0.11596	0.21868	0.00403	-0.00159	0.00191	-0.00099	0.00084	-0.00069	0.00039	-0.00040	0.00848	-0.00848	0.00963	-0.00872
-0.00	0.43797	0.09323	0.00117	-0.00046	0.00063	-0.00032	0.00033	-0.00027	0.00010	-0.00011	0.00848	-0.00848	0.00859	-0.00850
0.21	0.04442	0.45296	0.01052	-0.00416	0.00499	-0.00257	0.00220	-0.00179	0.00103	-0.00105	0.00848	-0.00848	0.01461	-0.01001
0.42	0.00914	1.93347	0.03748	-0.01481	0.00927	-0.00478	0.00136	-0.00167	0.00497	-0.00505	0.00848	-0.00848	0.03986	-0.01850
0.63	-0.01371	-1.15029	0.01153	-0.00456	0.00319	-0.00618	0.00702	-0.00860	0.00328	-0.00333	0.00848	-0.00848	0.01659	-0.01470
0.84	0.02193	1.17020	0.00096	-0.00244	0.00521	-0.01011	0.00531	-0.00650	0.00204	-0.00207	0.00848	-0.00848	0.01150	-0.01505
1.05	0.00544	5.24398	0.01859	-0.04702	0.02597	-0.05036	0.01094	-0.01340	0.00816	-0.00829	0.00848	-0.00848	0.03575	-0.07118
1.26	0.03593	1.13194	0.00455	-0.01152	0.00318	-0.00617	0.00125	-0.00102	0.00124	-0.00125	0.00848	-0.00848	0.01029	-0.01566
1.47	-0.06020	-0.00000	0.00329	-0.00831	0.00073	-0.00141	0.00221	-0.00181	0.00074	-0.00075	0.00848	-0.00848	0.00942	-0.01212
1.68	-0.01080	-3.25292	0.01831	-0.04634	0.00784	-0.00404	0.01233	-0.01007	0.00413	-0.00420	0.01727	-0.01727	0.02940	-0.05080
1.88	0.02340	1.47046	0.00699	-0.01770	0.00948	-0.00489	0.00193	-0.00157	0.00191	-0.00194	0.01727	-0.01727	0.02108	-0.02533
2.09	-0.02043	-0.98875	0.00495	-0.01253	0.01342	-0.00692	0.00291	-0.00357	0.00220	-0.00223	0.01727	-0.01727	0.02272	-0.02282
2.30	0.02594	0.89700	0.00082	-0.00206	0.00855	-0.00441	0.00449	-0.00550	0.00174	-0.00176	0.01727	-0.01727	0.01988	-0.01885
2.51	-0.00729	-2.33831	0.02170	-0.00858	0.01162	-0.00599	0.01321	-0.01619	0.00620	-0.00629	0.01727	-0.01727	0.03343	-0.02664
2.72	-0.00253	-6.02863	0.13540	-0.05352	0.01727	-0.03349	0.00492	-0.00603	0.01790	-0.01817	0.01727	-0.01727	0.13883	-0.06819
2.93	0.06101	0.37458	0.00766	-0.00303	0.00187	-0.00363	0.00160	-0.00131	0.00074	-0.00076	0.01727	-0.01727	0.01907	-0.01797
3.14	0.12547	0.21868	0.00408	-0.00161	0.00113	-0.00218	0.00116	-0.00095	0.00036	-0.00037	0.01727	-0.01727	0.01783	-0.01751
3.35	0.03206	0.61830	0.01458	-0.00576	0.00357	-0.00691	0.00304	-0.00248	0.00142	-0.00144	0.01727	-0.01727	0.02313	-0.01969
3.56	0.00279	5.65886	0.12283	-0.04855	0.01567	-0.03038	0.00446	-0.00547	0.01624	-0.01649	0.01727	-0.01727	0.12615	-0.06229
3.77	0.03069	0.73907	0.00515	-0.00204	0.00276	-0.00142	0.00314	-0.00384	0.00147	-0.00149	0.01727	-0.01727	0.01856	-0.01793
3.98	-0.01518	-1.09563	0.00139	-0.00352	0.01460	-0.00753	0.00767	-0.00939	0.00297	-0.00301	0.01727	-0.01727	0.02411	-0.02156
4.19	-0.00854	-2.81035	0.01184	-0.02996	0.03209	-0.01655	0.00697	-0.00854	0.00526	-0.00534	0.01727	-0.01727	0.03930	-0.03964
4.40	-0.01639	-1.60911	0.00999	-0.02527	0.01353	-0.00698	0.00275	-0.00224	0.00273	-0.00277	0.01727	-0.01727	0.02442	-0.03159
4.61	0.01316	3.52240	0.01503	-0.03804	0.00643	-0.00332	0.01012	-0.00826	0.00339	-0.00344	0.01727	-0.01727	0.02607	-0.04285

Table 33: 0–20%, 12.0–15.0 \otimes 5.0–7.0 GeV/c Jet Function

ϕ	per trig yield	σ_{stat}/y	systematic errors											
			$+\sigma_{f2}/y$	$-\sigma_{f2}/y$	$+\sigma_{f3}/y$	$-\sigma_{f3}/y$	$+\sigma_{f4}/y$	$-\sigma_{f4}/y$	$+\sigma_\xi/y$	$-\sigma_\xi/y$	$+\sigma_{\pi^0}/y$	$-\sigma_{\pi^0}/y$	$+\sigma_{total}/y$	$-\sigma_{total}/y$
-1.47	0.02749	0.95317	0.00093	-0.00207	0.00028	-0.00029	0.00045	-0.00071	0.00045	-0.00042	0.01662	-0.01662	0.01666	-0.01677
-1.26	0.00179	4.40856	0.01188	-0.02630	0.01109	-0.01153	0.00233	-0.00370	0.00684	-0.00647	0.01662	-0.01662	0.02434	-0.03400
-1.05	0.00670	1.69381	0.00196	-0.00434	0.00366	-0.00381	0.00160	-0.00100	0.00183	-0.00173	0.01662	-0.01662	0.01730	-0.01770
-0.84	0.00352	2.14889	0.00078	-0.00173	0.00564	-0.00587	0.00595	-0.00375	0.00350	-0.00331	0.01662	-0.01662	0.01887	-0.01840
-0.63	-0.00561	-0.67556	0.00321	-0.00145	0.00135	-0.00141	0.00309	-0.00194	0.00221	-0.00208	0.01662	-0.01662	0.01740	-0.01698
-0.42	-0.00244	-2.03767	0.01596	-0.00721	0.00323	-0.00311	0.00092	-0.00058	0.00510	-0.00482	0.01662	-0.01662	0.02383	-0.01901
-0.21	0.00907	0.83840	0.00586	-0.00265	0.00227	-0.00219	0.00099	-0.00158	0.00138	-0.00130	0.01662	-0.01662	0.01785	-0.01709
-0.00	0.10637	0.17351	0.00055	-0.00025	0.00024	-0.00023	0.00013	-0.00020	0.00012	-0.00011	0.01662	-0.01662	0.01663	-0.01662
0.21	0.01139	0.77007	0.00466	-0.00211	0.00181	-0.00174	0.00079	-0.00126	0.00110	-0.00104	0.01662	-0.01662	0.01741	-0.01692
0.42	-0.00304	-1.48745	0.01278	-0.00578	0.00259	-0.00249	0.00073	-0.00046	0.00409	-0.00386	0.01662	-0.01662	0.02153	-0.01819
0.63	-0.00938	-0.00000	0.00191	-0.00087	0.00081	-0.00084	0.00184	-0.00116	0.00132	-0.00125	0.01662	-0.01662	0.01690	-0.01675
0.84	-0.00933	-0.00000	0.00029	-0.00065	0.00213	-0.00221	0.00224	-0.00141	0.00132	-0.00125	0.01662	-0.01662	0.01696	-0.01688
1.05	0.00877	1.46228	0.00150	-0.00332	0.00280	-0.00291	0.00122	-0.00077	0.00140	-0.00132	0.01662	-0.01662	0.01702	-0.01726
1.26	-0.00929	-0.00000	0.00229	-0.00506	0.00214	-0.00222	0.00045	-0.00071	0.00132	-0.00125	0.01662	-0.01662	0.01697	-0.01757
1.47	-0.00930	-0.00000	0.00276	-0.00612	0.00081	-0.00085	0.00132	-0.00210	0.00132	-0.00125	0.01662	-0.01662	0.01697	-0.01789
1.68	-0.00932	-0.00000	0.00276	-0.00610	0.00085	-0.00081	0.00132	-0.00210	0.00132	-0.00125	0.04180	-0.04180	0.04194	-0.04232
1.88	-0.00135	-5.92895	0.01571	-0.03476	0.01525	-0.01466	0.00308	-0.00489	0.00909	-0.00859	0.04180	-0.04180	0.04815	-0.05717
2.09	0.01003	1.37214	0.00131	-0.00290	0.00254	-0.00245	0.00107	-0.00067	0.00123	-0.00116	0.04180	-0.04180	0.04193	-0.04200
2.30	-0.00938	-0.00000	0.00029	-0.00065	0.00220	-0.00212	0.00223	-0.00140	0.00132	-0.00125	0.04180	-0.04180	0.04194	-0.04190
2.51	0.00055	12.90957	0.03291	-0.01487	0.01443	-0.01388	0.03171	-0.01996	0.02269	-0.02144	0.04180	-0.04180	0.06752	-0.05495
2.72	0.01315	0.65112	0.00296	-0.00134	0.00058	-0.00060	0.00017	-0.00011	0.00094	-0.00089	0.04180	-0.04180	0.04192	-0.04184
2.93	0.00514	1.43572	0.01033	-0.00467	0.00386	-0.00401	0.00175	-0.00279	0.00242	-0.00229	0.04180	-0.04180	0.04334	-0.04241
3.14	0.05164	0.29198	0.00113	-0.00051	0.00047	-0.00049	0.00026	-0.00041	0.00024	-0.00023	0.04180	-0.04180	0.04182	-0.04181
3.35	0.02712	0.49402	0.00196	-0.00089	0.00073	-0.00076	0.00033	-0.00053	0.00046	-0.00043	0.04180	-0.04180	0.04186	-0.04182
3.56	0.00988	0.91057	0.00394	-0.00178	0.00077	-0.00080	0.00023	-0.00014	0.00126	-0.00119	0.04180	-0.04180	0.04201	-0.04186
3.77	0.00343	2.76803	0.00524	-0.00237	0.00230	-0.00221	0.00504	-0.00317	0.00361	-0.00341	0.04180	-0.04180	0.04264	-0.04219
3.98	-0.00938	-0.00000	0.00029	-0.00065	0.00220	-0.00212	0.00223	-0.00140	0.00132	-0.00125	0.04180	-0.04180	0.04194	-0.04190
4.19	-0.00936	-0.00000	0.00140	-0.00311	0.00272	-0.00262	0.00114	-0.00072	0.00132	-0.00125	0.04180	-0.04180	0.04195	-0.04202
4.40	0.04035	0.63435	0.00053	-0.00117	0.00051	-0.00049	0.00010	-0.00016	0.00030	-0.00029	0.04180	-0.04180	0.04181	-0.04182
4.61	-0.00932	-0.00000	0.00276	-0.00610	0.00085	-0.00081	0.00132	-0.00210	0.00132	-0.00125	0.04180	-0.04180	0.04194	-0.04232

Table 34: 20–40%, 4.0–5.0 \otimes 0.5–1.0 GeV/c Jet Function

ϕ	per trig yield	σ_{stat}/y	systematic errors											
			$+\sigma_{f2}/y$	$-\sigma_{f2}/y$	$+\sigma_{f3}/y$	$-\sigma_{f3}/y$	$+\sigma_{f4}/y$	$-\sigma_{f4}/y$	$+\sigma_\xi/y$	$-\sigma_\xi/y$	$+\sigma_{\pi^0}/y$	$-\sigma_{\pi^0}/y$	$+\sigma_{total}/y$	$-\sigma_{total}/y$
-1.47	-0.06439	-0.51497	0.12259	-0.12032	0.01763	-0.01631	0.07406	-0.09094	0.45094	-0.45093	0.04024	-0.04024	0.47517	-0.47747
-1.26	-0.02673	-1.14376	0.24427	-0.23975	0.11119	-0.10286	0.06036	-0.07411	1.08814	-1.08813	0.04024	-0.04024	1.12310	-1.12214
-1.05	-0.02291	-1.06315	0.17613	-0.17288	0.16035	-0.14833	0.13991	-0.11394	1.27674	-1.27673	0.04024	-0.04024	1.30691	-1.30251
-0.84	-0.01525	-1.35796	0.05532	-0.05430	0.19489	-0.18029	0.41119	-0.33487	1.93625	-1.93623	0.04024	-0.04024	1.99017	-1.97438
-0.63	0.04003	0.45925	0.06114	-0.06230	0.02836	-0.02623	0.12955	-0.10550	0.74620	-0.74620	0.04024	-0.04024	0.76142	-0.75771
-0.42	0.08488	0.20232	0.06244	-0.06362	0.01237	-0.01337	0.0789	-0.06463	0.35599	-0.35598	0.04024	-0.04024	0.36395	-0.36416
-0.21	0.10951	0.14660	0.06608	-0.06732	0.02510	-0.02714	0.03190	-0.03917	0.27826	-0.27826	0.04024	-0.04024	0.29165	-0.29300
-0.00	0.14285	0.11100	0.05545	-0.05650	0.02379	-0.02572	0.03655	-0.04488	0.21398	-0.21398	0.04024	-0.04024	0.22887	-0.23081
0.21	0.11870	0.13734	0.06096	-0.06211	0.02316	-0.02504	0.02943	-0.03614	0.25671	-0.25671	0.04024	-0.04024	0.26952	-0.27076
0.42	0.06941	0.25054	0.07636	-0.07779	0.01513	-0.01635	0.00965	-0.00786	0.43531	-0.43531	0.04024	-0.04024	0.44415	-0.44440
0.63	0.04701	0.41202	0.05206	-0.05304	0.02415	-0.02234	0.11031	-0.08983	0.63539	-0.63538	0.04024	-0.04024	0.64869	-0.64553
0.84	-0.01897	-1.17625	0.04446	-0.04364	0.15663	-0.14490	0.33047	-0.26913	1.55614	-1.55612	0.04024	-0.04024	1.59966	-1.58697
1.05	0.00320	7.87577	1.26042	-1.23711	1.14746	-1.06147	1.00117	-0.81535	9.13645	-9.13635	0.04024	-0.04024	9.34794	-9.31646
1.26	0.00094	31.61469	6.96015	-6.83143	3.16819	-2.93076	1.71977	-2.11173	31.00533	-31.00502	0.04024	-0.04024	31.98079	-31.95356
1.47	-0.04371	-0.82793	0.18061	-0.17727	0.02597	-0.02403	0.10912	-0.13399	0.66435	-0.66435	0.04024	-0.04024	0.69870	-0.70209
1.68	0.01151	2.94433	0.68600	-0.67331	0.09126	-0.09863	0.41445	-0.50891	2.52812	-2.52810	0.01849	-0.01849	2.65376	-2.66715
1.88	0.07120	0.40227	0.09170	-0.09000	0.03863	-0.04174	0.02266	-0.02782	0.41049	-0.41048	0.01849	-0.01849	0.42338	-0.42362
2.09	0.09952	0.24126	0.04054	-0.03979	0.03414	-0.03691	0.03220	-0.02623	0.29567	-0.29566	0.01849	-0.01849	0.30267	-0.30231
2.30	0.12349	0.17274	0.00683	-0.00670	0.02226	-0.02407	0.05078	-0.04135	0.24026	-0.24025	0.01849	-0.01849	0.24736	-0.24576
2.51	0.11513	0.16539	0.02126	-0.02166	0.00912	-0.00986	0.04504	-0.03668	0.25994	-0.25993	0.01849	-0.01849	0.26547	-0.26423
2.72	0.16538	0.10749	0.03205	-0.03265	0.00686	-0.00635	0.00405	-0.00330	0.18238	-0.18238	0.01849	-0.01849	0.18627	-0.18634
2.93	0.15586	0.11038	0.04643	-0.04730	0.01907	-0.01764	0.02241	-0.02752	0.19458	-0.19458	0.01849	-0.01849	0.20304	-0.20374
3.14	0.16368	0.10624	0.04839	-0.04930	0.02244	-0.02076	0.03189	-0.03916	0.18566	-0.18565	0.01849	-0.01849	0.19665	-0.19800
3.35	0.18640	0.09389	0.03882	-0.03955	0.01594	-0.01475	0.01874	-0.02301	0.16271	-0.16271	0.01849	-0.01849	0.17008	-0.17066
3.56	0.14326	0.12832	0.03700	-0.03769	0.00792	-0.00733	0.00468	-0.00381	0.21054	-0.21054	0.01849	-0.01849	0.21476	-0.21484
3.77	0.11516	0.17353	0.02126	-0.02166	0.00912	-0.00986	0.04503	-0.03668	0.25988	-0.25988	0.01849	-0.01849	0.26541	-0.26418
3.98	0.07641	0.28208	0.01104	-0.01084	0.03598	-0.03889	0.08206	-0.06683	0.38829	-0.38828	0.01849	-0.01849	0.39907	-0.39649
4.19	0.12998	0.19930	0.03104	-0.03047	0.02614	-0.02826	0.02466	-0.02008	0.22640	-0.22640	0.01849	-0.01849	0.23206	-0.23179
4.40	-0.00516	-5.88621	1.26592	-1.24251	0.53305	-0.57624	0.31279	-0.38408	5.66706	-5.66700	0.01849	-0.01849	5.83956	-5.84283
4.61	0.01983	1.61427	0.39812	-0.39076	0.05296	-0.05725	0.24053	-0.29535	1.46720	-1.46718	0.01849	-0.01849	1.54018	-1.54795

Table 35: 20–40%, 4.0–5.0 \otimes 1.0–2.0 GeV/c Jet Function

ϕ	per trig yield	σ_{stat}/y	systematic errors												
			$+\sigma_{f2}/y$	$-\sigma_{f2}/y$	$+\sigma_{f3}/y$	$-\sigma_{f3}/y$	$+\sigma_{f4}/y$	$-\sigma_{f4}/y$	$+\sigma_{\xi}/y$	$-\sigma_{\xi}/y$	$+\sigma_{\pi^0}/y$	$-\sigma_{\pi^0}/y$	$+\sigma_{total}/y$	$-\sigma_{total}/y$	
-1.47	0.02884	0.58162	0.13618	-0.13374	0.03057	-0.02817	0.11877	-0.14515	0.28498	-0.28496	0.01238	-0.01238	0.33905	-0.34799	
-1.26	-0.00125	-11.79404	2.59149	-2.54509	1.84162	-1.69663	0.92440	-1.12965	6.56486	-6.56432	0.01238	-0.01238	7.35251	-7.32957	
-1.05	0.01056	1.11542	0.19009	-0.18669	0.27017	-0.24890	0.21693	-0.17752	0.78589	-0.78583	0.01238	-0.01238	0.87975	-0.86371	
-0.84	0.00798	1.22481	0.05259	-0.05165	0.28925	-0.26648	0.56161	-0.45957	1.05710	-1.05701	0.01238	-0.01238	1.23266	-1.18419	
-0.63	0.06001	0.14796	0.02030	-0.02067	0.01469	-0.01353	0.06177	-0.05054	0.14363	-0.14362	0.01238	-0.01238	0.15883	-0.15474	
-0.42	0.10532	0.07869	0.02505	-0.02551	0.00771	-0.00837	0.00455	-0.00372	0.08364	-0.08363	0.01238	-0.01238	0.08864	-0.08878	
-0.21	0.18869	0.04150	0.01909	-0.01944	0.01127	-0.01223	0.01330	-0.01625	0.04745	-0.04745	0.01238	-0.01238	0.05543	-0.05653	
-0.00	0.22488	0.03366	0.01753	-0.01785	0.01169	-0.01269	0.01667	-0.02037	0.04003	-0.04003	0.01238	-0.01238	0.04979	-0.05150	
0.21	0.16822	0.04627	0.02141	-0.02180	0.01264	-0.01372	0.01491	-0.01822	0.05322	-0.05322	0.01238	-0.01238	0.06186	-0.06310	
0.42	0.09960	0.08422	0.02649	-0.02697	0.00816	-0.00885	0.00481	-0.00393	0.08845	-0.08844	0.01238	-0.01238	0.09364	-0.09379	
0.63	0.06481	0.14346	0.01880	-0.01914	0.01360	-0.01253	0.05720	-0.04680	0.13300	-0.13299	0.01238	-0.01238	0.14715	-0.14337	
0.84	0.01740	0.60938	0.02412	-0.02369	0.13265	-0.12221	0.25757	-0.21077	0.48480	-0.48476	0.01238	-0.01238	0.56543	-0.54320	
1.05	0.01723	0.69770	0.11647	-0.11439	0.16554	-0.15251	0.13292	-0.10877	0.48155	-0.48151	0.01238	-0.01238	0.53915	-0.52932	
1.26	0.01592	0.91603	0.20406	-0.20041	0.14501	-0.13360	0.07279	-0.08895	0.51694	-0.51689	0.01238	-0.01238	0.57909	-0.57728	
1.47	-0.00863	-2.13752	0.45490	-0.44676	0.10213	-0.09409	0.39676	-0.48486	0.95197	-0.95189	0.01238	-0.01238	1.13189	-1.16180	
1.68	0.03592	0.47344	0.10933	-0.10737	0.02261	-0.02454	0.09535	-0.11652	0.22980	-0.22978	0.01337	-0.01337	0.27302	-0.28051	
1.88	0.02540	0.55451	0.12786	-0.12557	0.08371	-0.09086	0.04561	-0.05573	0.32765	-0.32763	0.01337	-0.01337	0.36465	-0.36694	
2.09	0.05835	0.20046	0.03440	-0.03378	0.04504	-0.04889	0.03926	-0.03212	0.14424	-0.14423	0.01337	-0.01337	0.16043	-0.15983	
2.30	0.06878	0.14814	0.00610	-0.00599	0.03092	-0.03356	0.06516	-0.05332	0.12403	-0.12402	0.01337	-0.01337	0.14422	-0.13987	
2.51	0.07995	0.11325	0.01524	-0.01552	0.01016	-0.01103	0.04637	-0.03794	0.10827	-0.10826	0.01337	-0.01337	0.11994	-0.11705	
2.72	0.06936	0.11969	0.03804	-0.03873	0.01271	-0.01171	0.00690	-0.00565	0.12648	-0.12647	0.01337	-0.01337	0.13353	-0.13357	
2.93	0.08422	0.09737	0.04277	-0.04355	0.02741	-0.02525	0.02979	-0.03640	0.10517	-0.10517	0.01337	-0.01337	0.12128	-0.12287	
3.14	0.08427	0.09778	0.04679	-0.04764	0.03386	-0.03119	0.04449	-0.05437	0.10548	-0.10547	0.01337	-0.01337	0.12892	-0.13229	
3.35	0.06822	0.12223	0.05280	-0.05376	0.03383	-0.03117	0.03677	-0.04494	0.12984	-0.12983	0.01337	-0.01337	0.14941	-0.15138	
3.56	0.08242	0.10438	0.03201	-0.03259	0.01070	-0.00985	0.00581	-0.00475	0.10643	-0.10643	0.01337	-0.01337	0.11260	-0.11264	
3.77	0.05986	0.15424	0.02035	-0.02072	0.01357	-0.01473	0.06192	-0.05067	0.14459	-0.14458	0.01337	-0.01337	0.15974	-0.15587	
3.98	0.06255	0.16703	0.00671	-0.00659	0.03399	-0.03690	0.07164	-0.05863	0.13638	-0.13637	0.01337	-0.01337	0.15846	-0.15368	
4.19	0.07092	0.17574	0.02830	-0.02780	0.03706	-0.04023	0.03230	-0.02643	0.11869	-0.11868	0.01337	-0.01337	0.13222	-0.13173	
4.40	0.02349	0.63215	0.13825	-0.13577	0.09051	-0.09824	0.04931	-0.06026	0.35428	-0.35425	0.01337	-0.01337	0.39424	-0.39672	
4.61	0.00561	2.95354	0.70025	-0.68771	0.14483	-0.15721	0.61074	-0.74635	1.47190	-1.47178	0.01337	-0.01337	1.74671	-1.79472	

Table 36: 20–40%, 4.0–5.0 \otimes 2.0–3.0 GeV/c Jet Function

ϕ	per trig yield	σ_{stat}/y	systematic errors											
			$+\sigma_{f_2}/y$	$-\sigma_{f_2}/y$	$+\sigma_{f_3}/y$	$-\sigma_{f_3}/y$	$+\sigma_{f_4}/y$	$-\sigma_{f_4}/y$	$+\sigma_\xi/y$	$-\sigma_\xi/y$	$+\sigma_{\pi^0}/y$	$-\sigma_{\pi^0}/y$	$+\sigma_{total}/y$	$-\sigma_{total}/y$
-1.47	0.00359	1.27501	0.13632	-0.13370	0.02879	-0.02666	0.14750	-0.18028	0.18287	-0.18287	0.01539	-0.01539	0.27359	-0.29115
-1.26	-0.00129	-2.97580	0.31481	-0.30875	0.21047	-0.19488	0.13931	-0.17027	0.51031	-0.51031	0.01539	-0.01539	0.65074	-0.65035
-1.05	0.00052	6.26987	0.48268	-0.47339	0.64540	-0.59761	0.68347	-0.55919	1.27900	-1.27900	0.01539	-0.01539	1.65913	-1.59060
-0.84	0.00640	0.40036	0.00817	-0.00801	0.04226	-0.03913	0.10822	-0.08854	0.10588	-0.10588	0.01539	-0.01539	0.15815	-0.14450
-0.63	0.00822	0.29874	0.01845	-0.01882	0.01258	-0.01165	0.06975	-0.05707	0.08516	-0.08516	0.01539	-0.01539	0.11337	-0.10600
-0.42	0.02231	0.10113	0.01472	-0.01500	0.00429	-0.00463	0.00332	-0.00272	0.03241	-0.03241	0.01539	-0.01539	0.03915	-0.03926
-0.21	0.06425	0.03686	0.00698	-0.00711	0.00390	-0.00421	0.00604	-0.00738	0.01154	-0.01154	0.01539	-0.01539	0.02168	-0.02220
-0.00	0.09922	0.02303	0.00495	-0.00504	0.00312	-0.00337	0.00584	-0.00714	0.00754	-0.00754	0.01539	-0.01539	0.01903	-0.01953
0.21	0.06017	0.03888	0.00745	-0.00760	0.00416	-0.00450	0.00644	-0.00788	0.01232	-0.01232	0.01539	-0.01539	0.02243	-0.02299
0.42	0.01879	0.11938	0.01747	-0.01781	0.00509	-0.00550	0.00394	-0.00322	0.03848	-0.03848	0.01539	-0.01539	0.04543	-0.04555
0.63	0.01242	0.20970	0.01221	-0.01245	0.00832	-0.00771	0.04614	-0.03775	0.05633	-0.05633	0.01539	-0.01539	0.07588	-0.07106
0.84	0.00448	0.60900	0.01169	-0.01146	0.06047	-0.05599	0.15484	-0.12668	0.15148	-0.15148	0.01539	-0.01539	0.22573	-0.20615
1.05	0.00379	0.88238	0.06606	-0.06479	0.08834	-0.08179	0.09355	-0.07654	0.17506	-0.17506	0.01539	-0.01539	0.22760	-0.21824
1.26	0.00915	0.42193	0.04425	-0.04340	0.02958	-0.02739	0.01958	-0.02393	0.07173	-0.07173	0.01539	-0.01539	0.09272	-0.09267
1.47	0.00645	0.77697	0.07582	-0.07436	0.01601	-0.01483	0.08204	-0.10027	0.10171	-0.10171	0.01539	-0.01539	0.15270	-0.16244
1.68	0.00259	1.83907	0.18904	-0.18540	0.03697	-0.03993	0.20454	-0.25000	0.25551	-0.25551	0.0122	-0.00122	0.37977	-0.40466
1.88	0.00552	0.67037	0.07329	-0.07188	0.04537	-0.04900	0.03243	-0.03964	0.12117	-0.12117	0.00122	-0.00122	0.15221	-0.15435
2.09	0.00531	0.60869	0.04707	-0.04616	0.05827	-0.06293	0.06664	-0.05453	0.12774	-0.12774	0.00122	-0.00122	0.16240	-0.15932
2.30	0.01023	0.26446	0.00511	-0.00501	0.02448	-0.02644	0.06771	-0.05540	0.06752	-0.06752	0.00122	-0.00122	0.09884	-0.09140
2.51	0.00907	0.27557	0.01672	-0.01705	0.01056	-0.01140	0.06321	-0.05172	0.07772	-0.07772	0.00122	-0.00122	0.10213	-0.09559
2.72	0.01487	0.14917	0.02207	-0.02251	0.00695	-0.00643	0.00498	-0.00407	0.04828	-0.04828	0.00122	-0.00122	0.05378	-0.05382
2.93	0.01193	0.19105	0.03758	-0.03832	0.02269	-0.02101	0.03252	-0.03974	0.06105	-0.06105	0.00122	-0.00122	0.08193	-0.08495
3.14	0.01593	0.13869	0.03081	-0.03141	0.02100	-0.01945	0.03639	-0.04448	0.04595	-0.04595	0.00122	-0.00122	0.06948	-0.07387
3.35	0.01628	0.14459	0.02753	-0.02807	0.01662	-0.01539	0.02382	-0.02911	0.04472	-0.04472	0.00122	-0.00122	0.06002	-0.06223
3.56	0.01528	0.14877	0.02149	-0.02191	0.00677	-0.00627	0.00485	-0.00397	0.04701	-0.04701	0.00122	-0.00122	0.05237	-0.05241
3.77	0.01362	0.18832	0.01113	-0.01135	0.00703	-0.00759	0.04208	-0.03443	0.05174	-0.05174	0.00122	-0.00122	0.06799	-0.06364
3.98	0.01342	0.20524	0.00390	-0.00382	0.01867	-0.02017	0.05164	-0.04225	0.05149	-0.05149	0.00122	-0.00122	0.07539	-0.06971
4.19	0.01118	0.31048	0.02237	-0.02194	0.02769	-0.02991	0.03167	-0.02591	0.06071	-0.06071	0.00122	-0.00122	0.07718	-0.07572
4.40	0.00326	1.15684	0.12427	-0.12188	0.07693	-0.08308	0.05499	-0.06721	0.20544	-0.20544	0.00122	-0.00122	0.25806	-0.26169
4.61	-0.00054	-8.95160	0.90791	-0.89045	0.17756	-0.19176	0.98236	-1.20069	1.22717	-1.22717	0.00122	-0.00122	1.82395	-1.94352

Table 37: 20–40%, 4.0–5.0 \otimes 3.0–5.0 GeV/c Jet Function

ϕ	per trig yield	σ_{stat}/y	systematic errors											
			$+\sigma_{f2}/y$	$-\sigma_{f2}/y$	$+\sigma_{f3}/y$	$-\sigma_{f3}/y$	$+\sigma_{f4}/y$	$-\sigma_{f4}/y$	$+\sigma_\xi/y$	$-\sigma_\xi/y$	$+\sigma_{\pi^0}/y$	$-\sigma_{\pi^0}/y$	$+\sigma_{total}/y$	$-\sigma_{total}/y$
-1.47	0.00164	1.03630	0.03859	-0.03789	0.00907	-0.00840	0.05071	-0.06185	0.04981	-0.05004	0.01580	-0.01580	0.08290	-0.08992
-1.26	0.00026	5.36190	0.20372	-0.20003	0.15164	-0.14044	0.10948	-0.13354	0.31735	-0.31882	0.01580	-0.01580	0.42124	-0.42363
-1.05	-0.00028	-4.21115	0.11559	-0.11350	0.17207	-0.15937	0.19837	-0.16262	0.29403	-0.29539	0.01580	-0.01580	0.41112	-0.39016
-0.84	0.00178	0.52039	0.00379	-0.00372	0.02182	-0.02021	0.06082	-0.04986	0.04713	-0.04734	0.01580	-0.01580	0.08161	-0.07348
-0.63	0.00151	0.59341	0.01296	-0.01320	0.00983	-0.00910	0.05932	-0.04863	0.05741	-0.05767	0.01580	-0.01580	0.08560	-0.07872
-0.42	0.00383	0.21427	0.01109	-0.01130	0.00360	-0.00388	0.00303	-0.00248	0.02348	-0.02359	0.01580	-0.01580	0.03076	-0.03090
-0.21	0.02397	0.04232	0.00242	-0.00246	0.00150	-0.00162	0.00254	-0.00310	0.00385	-0.00387	0.01580	-0.01580	0.01670	-0.01682
-0.00	0.05739	0.02031	0.00111	-0.00113	0.00078	-0.00084	0.00158	-0.00193	0.00162	-0.00163	0.01580	-0.01580	0.01602	-0.01606
0.21	0.02401	0.04235	0.00241	-0.00246	0.00150	-0.00162	0.00253	-0.00309	0.00384	-0.00386	0.01580	-0.01580	0.01670	-0.01681
0.42	0.00490	0.17096	0.00866	-0.00882	0.00281	-0.00303	0.00236	-0.00194	0.01833	-0.01841	0.01580	-0.01580	0.02596	-0.02606
0.63	0.00334	0.29488	0.00587	-0.00598	0.00445	-0.00412	0.02687	-0.02203	0.02601	-0.02613	0.01580	-0.01580	0.04126	-0.03835
0.84	0.00014	6.95271	0.04814	-0.04727	0.27734	-0.25687	0.77311	-0.63380	0.59901	-0.60178	0.01580	-0.01580	1.01784	-0.91230
1.05	0.00081	1.55321	0.03996	-0.03924	0.05949	-0.05510	0.06858	-0.05622	0.10165	-0.10212	0.01580	-0.01580	0.14291	-0.13570
1.26	0.00197	0.70955	0.02655	-0.02607	0.01976	-0.01830	0.01427	-0.01740	0.04136	-0.04155	0.01580	-0.01580	0.05708	-0.05738
1.47	-0.00146	-1.18555	0.04336	-0.04257	0.01020	-0.00944	0.05697	-0.06949	0.05596	-0.05622	0.01580	-0.01580	0.09279	-0.10070
1.68	0.00133	1.33658	0.04755	-0.04669	0.01036	-0.01118	0.06248	-0.07622	0.06187	-0.06215	0.01286	-0.01286	0.10132	-0.11020
1.88	0.00093	1.44171	0.05651	-0.05549	0.03896	-0.04207	0.03037	-0.03704	0.08990	-0.09031	0.01286	-0.01286	0.11782	-0.12059
2.09	0.00072	1.65143	0.04499	-0.04418	0.06204	-0.06698	0.07721	-0.06330	0.11741	-0.11796	0.01286	-0.01286	0.16058	-0.15660
2.30	0.00019	5.13462	0.03631	-0.03565	0.19373	-0.20917	0.58308	-0.47801	0.46103	-0.46316	0.01286	-0.01286	0.76912	-0.69871
2.51	0.00309	0.30481	0.00635	-0.00647	0.00446	-0.00482	0.02908	-0.02384	0.02836	-0.02849	0.01286	-0.01286	0.04330	-0.04013
2.72	0.00368	0.22212	0.01153	-0.01175	0.00404	-0.00374	0.00315	-0.00258	0.02424	-0.02435	0.01286	-0.01286	0.03020	-0.03028
2.93	0.00597	0.14829	0.00970	-0.00988	0.00651	-0.00603	0.01018	-0.01242	0.01516	-0.01523	0.01286	-0.01286	0.02521	-0.02619
3.14	0.00629	0.13375	0.01009	-0.01028	0.00765	-0.00709	0.01446	-0.01764	0.01449	-0.01455	0.01286	-0.01286	0.02729	-0.02906
3.35	0.00413	0.21525	0.01403	-0.01429	0.00942	-0.00873	0.01473	-0.01797	0.02192	-0.02203	0.01286	-0.01286	0.03389	-0.03541
3.56	0.00360	0.23169	0.01180	-0.01201	0.00413	-0.00382	0.00322	-0.00264	0.02479	-0.02490	0.01286	-0.01286	0.03076	-0.03085
3.77	0.00168	0.55447	0.01165	-0.01186	0.00818	-0.00883	0.05329	-0.04368	0.05196	-0.05220	0.01286	-0.01286	0.07686	-0.07083
3.98	0.00140	0.69995	0.00483	-0.00475	0.02579	-0.02785	0.07762	-0.06363	0.06137	-0.06166	0.01286	-0.01286	0.10318	-0.09388
4.19	0.00182	0.70823	0.01780	-0.01748	0.02454	-0.02650	0.03055	-0.02504	0.04645	-0.04667	0.01286	-0.01286	0.06462	-0.06307
4.40	0.00352	0.40832	0.01484	-0.01457	0.01023	-0.01105	0.00798	-0.00973	0.02361	-0.02372	0.01286	-0.01286	0.03334	-0.03401
4.61	-0.00141	-1.25504	0.04496	-0.04415	0.00979	-0.01057	0.05908	-0.07206	0.05849	-0.05876	0.01286	-0.01286	0.09589	-0.10427

Table 38: 20–40%, 4.0–5.0 \otimes 5.0–7.0 GeV/c Jet Function

ϕ	per trig yield	σ_{stat}/y	systematic errors											
			$+\sigma_{f2}/y$	$-\sigma_{f2}/y$	$+\sigma_{f3}/y$	$-\sigma_{f3}/y$	$+\sigma_{f4}/y$	$-\sigma_{f4}/y$	$+\sigma_\xi/y$	$-\sigma_\xi/y$	$+\sigma_{\pi^0}/y$	$-\sigma_{\pi^0}/y$	$+\sigma_{total}/y$	$-\sigma_{total}/y$
-1.47	0.00061	0.95595	0.01384	-0.01351	0.00747	-0.00673	0.02264	-0.02899	0.02548	-0.02389	0.02260	-0.02260	0.04382	-0.04637
-1.26	0.00011	3.87278	0.06095	-0.05948	0.10411	-0.09385	0.04076	-0.05221	0.13575	-0.12732	0.02260	-0.02260	0.18750	-0.17831
-1.05	-0.00052	-0.66794	0.00818	-0.00798	0.02794	-0.02518	0.01834	-0.01432	0.02972	-0.02788	0.02260	-0.02260	0.05077	-0.04681
-0.84	-0.00007	-4.18997	0.01326	-0.01294	0.17524	-0.15797	0.27816	-0.21716	0.23439	-0.21983	0.02260	-0.02260	0.40461	-0.34802
-0.63	0.00008	3.73864	0.03417	-0.03501	0.05980	-0.05391	0.20555	-0.16047	0.21430	-0.20098	0.02260	-0.02260	0.30566	-0.26606
-0.42	0.00055	0.47853	0.01010	-0.01035	0.00736	-0.00816	0.00362	-0.00283	0.02995	-0.02809	0.02260	-0.02260	0.03971	-0.03849
-0.21	0.00282	0.11627	0.00271	-0.00278	0.00379	-0.00420	0.00356	-0.00456	0.00599	-0.00562	0.02260	-0.02260	0.02411	-0.02426
-0.00	0.01268	0.03752	0.00066	-0.00068	0.00104	-0.00116	0.00118	-0.00152	0.00134	-0.00126	0.02260	-0.02260	0.02271	-0.02273
0.21	0.00313	0.10860	0.00244	-0.00250	0.00341	-0.00378	0.00321	-0.00411	0.00540	-0.00506	0.02260	-0.02260	0.02383	-0.02396
0.42	0.00028	0.92517	0.01971	-0.02019	0.01436	-0.01593	0.00707	-0.00552	0.05845	-0.05482	0.02260	-0.02260	0.06762	-0.06487
0.63	-0.00026	-1.11815	0.00981	-0.01005	0.01716	-0.01547	0.05899	-0.04605	0.06150	-0.05768	0.02260	-0.02260	0.09036	-0.07937
0.84	0.00061	0.58207	0.00146	-0.00143	0.01935	-0.01744	0.03072	-0.02398	0.02588	-0.02428	0.02260	-0.02260	0.05001	-0.04452
1.05	0.00016	2.71663	0.02751	-0.02685	0.09399	-0.08472	0.06170	-0.04817	0.10000	-0.09379	0.02260	-0.02260	0.15462	-0.13974
1.26	0.00032	1.46198	0.02167	-0.02115	0.03702	-0.03337	0.01449	-0.01856	0.04827	-0.04527	0.02260	-0.02260	0.06994	-0.06683
1.47	-0.00104	-0.44608	0.00803	-0.00784	0.00433	-0.00391	0.01313	-0.01682	0.01478	-0.01386	0.02260	-0.02260	0.03139	-0.03260
1.68	0.00001	68.25418	1.03090	-1.00608	0.50147	-0.55630	1.68559	-2.15910	1.90525	-1.78689	0.00021	-0.00021	2.79023	-3.02925
1.88	0.00058	0.78347	0.01195	-0.01166	0.01839	-0.02040	0.00799	-0.01023	0.02690	-0.02523	0.00021	-0.00021	0.03562	-0.03597
2.09	0.00077	0.54486	0.00558	-0.00545	0.01719	-0.01907	0.01252	-0.00977	0.02056	-0.01929	0.00021	-0.00021	0.03010	-0.02934
2.30	-0.00007	-4.59638	0.01353	-0.01321	0.16129	-0.17893	0.28401	-0.22172	0.24193	-0.22690	0.00021	-0.00021	0.40668	-0.36447
2.51	0.00039	0.78974	0.00667	-0.00684	0.01053	-0.01168	0.04015	-0.03134	0.04203	-0.03942	0.00021	-0.00021	0.05945	-0.05215
2.72	0.00047	0.55895	0.01182	-0.01211	0.00955	-0.00861	0.00424	-0.00331	0.03492	-0.03275	0.00021	-0.00021	0.03832	-0.03611
2.93	0.00100	0.29981	0.00766	-0.00785	0.01187	-0.01070	0.01006	-0.01289	0.01677	-0.01573	0.00021	-0.00021	0.02412	-0.02428
3.14	0.00189	0.16449	0.00442	-0.00453	0.00774	-0.00698	0.00793	-0.01016	0.00888	-0.00833	0.00021	-0.00021	0.01488	-0.01556
3.35	0.00150	0.21688	0.00511	-0.00523	0.00791	-0.00713	0.00671	-0.00859	0.01118	-0.01049	0.00021	-0.00021	0.01609	-0.01619
3.56	0.00084	0.33933	0.00670	-0.00686	0.00541	-0.00488	0.00240	-0.00188	0.01979	-0.01856	0.00021	-0.00021	0.02172	-0.02047
3.77	0.00040	0.76207	0.00640	-0.00656	0.01010	-0.01121	0.03852	-0.03007	0.04032	-0.03782	0.00021	-0.00021	0.05703	-0.05003
3.98	0.00077	0.46857	0.00117	-0.00114	0.01393	-0.01545	0.02452	-0.01914	0.02089	-0.01959	0.00021	-0.00021	0.03512	-0.03147
4.19	0.00074	0.62117	0.00582	-0.00568	0.01793	-0.01989	0.01306	-0.01019	0.02146	-0.02012	0.00021	-0.00021	0.03141	-0.03061
4.40	-0.00029	-1.48529	0.02425	-0.02367	0.03734	-0.04143	0.01622	-0.02077	0.05462	-0.05123	0.00021	-0.00021	0.07232	-0.07303
4.61	-0.00048	-1.07687	0.01741	-0.01699	0.00847	-0.00939	0.02847	-0.03646	0.03218	-0.03018	0.00021	-0.00021	0.04712	-0.05116

Table 39: 20–40%, 5.0–7.0 \otimes 0.5–1.0 GeV/c Jet Function

ϕ	per trig yield	σ_{stat}/y	systematic errors											
			$+\sigma_{f2}/y$	$-\sigma_{f2}/y$	$+\sigma_{f3}/y$	$-\sigma_{f3}/y$	$+\sigma_{f4}/y$	$-\sigma_{f4}/y$	$+\sigma_\xi/y$	$-\sigma_\xi/y$	$+\sigma_{\pi^0}/y$	$-\sigma_{\pi^0}/y$	$+\sigma_{total}/y$	$-\sigma_{total}/y$
-1.47	-0.03120	-1.34208	0.28507	-0.27835	0.03184	-0.02885	0.10957	-0.13954	0.83915	-0.83919	0.01211	-0.01211	0.89364	-0.89564
-1.26	-0.04783	-0.79869	0.15381	-0.15018	0.05438	-0.04927	0.02418	-0.03079	0.54829	-0.54831	0.01211	-0.01211	0.57268	-0.57160
-1.05	0.01716	1.77944	0.26488	-0.25864	0.18731	-0.16970	0.13882	-0.10901	1.53531	-1.53539	0.01211	-0.01211	1.57539	-1.57008
-0.84	-0.02266	-1.14371	0.04195	-0.04096	0.11480	-0.10401	0.20574	-0.16155	1.17226	-1.17232	0.01211	-0.01211	1.19650	-1.18873
-0.63	0.03054	0.75317	0.08982	-0.09199	0.03253	-0.02947	0.12623	-0.09911	0.87788	-0.87793	0.01211	-0.01211	0.89212	-0.88885
-0.42	0.07396	0.29115	0.08032	-0.08226	0.01217	-0.01343	0.00674	-0.00529	0.36590	-0.36592	0.01211	-0.01211	0.37507	-0.37552
-0.21	0.13280	0.15277	0.06107	-0.06255	0.01774	-0.01959	0.01885	-0.02401	0.20515	-0.20516	0.01211	-0.01211	0.21595	-0.21705
-0.00	0.19716	0.10211	0.04503	-0.04612	0.01477	-0.01631	0.01898	-0.02417	0.13852	-0.13853	0.01211	-0.01211	0.14812	-0.14938
0.21	0.15394	0.13462	0.05269	-0.05396	0.01531	-0.01690	0.01626	-0.02071	0.17698	-0.17699	0.01211	-0.01211	0.18639	-0.18734
0.42	0.08301	0.26635	0.07157	-0.07329	0.01084	-0.01197	0.00600	-0.00471	0.32601	-0.32603	0.01211	-0.01211	0.33422	-0.33463
0.63	-0.00488	-5.04834	0.56237	-0.57595	0.20364	-0.18449	0.79027	-0.62052	5.49619	-5.49648	0.01211	-0.01211	5.58485	-5.56437
0.84	-0.06363	-0.44985	0.01494	-0.01459	0.04088	-0.03703	0.07326	-0.05752	0.41740	-0.41742	0.01211	-0.01211	0.42618	-0.42342
1.05	-0.00547	-5.93586	0.83078	-0.81119	0.58749	-0.53224	0.43541	-0.34189	4.81539	-4.81564	0.01211	-0.01211	4.94095	-4.92430
1.26	0.02051	1.85563	0.35866	-0.35020	0.12681	-0.11489	0.05638	-0.07180	1.27851	-1.27857	0.01211	-0.01211	1.33515	-1.33263
1.47	0.06244	0.74277	0.14243	-0.13908	0.01591	-0.01441	0.05474	-0.06972	0.41927	-0.41930	0.01211	-0.01211	0.44663	-0.44762
1.68	-0.00688	-6.26958	1.29259	-1.26210	0.13081	-0.14438	0.49680	-0.63270	3.81028	-3.81047	0.00703	-0.00703	4.05622	-4.06618
1.88	0.07094	0.51281	0.10369	-0.10125	0.03322	-0.03666	0.01630	-0.02076	0.37100	-0.37102	0.00703	-0.00703	0.38706	-0.38695
2.09	0.06698	0.45271	0.06787	-0.06627	0.04348	-0.04799	0.03557	-0.02793	0.39518	-0.39520	0.00703	-0.00703	0.40494	-0.40461
2.30	0.17185	0.15710	0.00553	-0.00540	0.01371	-0.01513	0.02712	-0.02130	0.15511	-0.15512	0.00703	-0.00703	0.15831	-0.15755
2.51	0.14531	0.16531	0.01888	-0.01934	0.00619	-0.00684	0.02653	-0.02083	0.18477	-0.18478	0.00703	-0.00703	0.18785	-0.18721
2.72	0.21141	0.10610	0.02810	-0.02878	0.00470	-0.00426	0.00236	-0.00185	0.12783	-0.12784	0.00703	-0.00703	0.13118	-0.13131
2.93	0.20889	0.10403	0.03883	-0.03977	0.01245	-0.01128	0.01199	-0.01527	0.12996	-0.12997	0.00703	-0.00703	0.13691	-0.13741
3.14	0.15749	0.13922	0.05637	-0.05773	0.02041	-0.01849	0.02376	-0.03026	0.17265	-0.17266	0.00703	-0.00703	0.18443	-0.18561
3.35	0.25632	0.08665	0.03164	-0.03241	0.01015	-0.00919	0.00977	-0.01244	0.10591	-0.10591	0.00703	-0.00703	0.11165	-0.11206
3.56	0.16634	0.14022	0.03571	-0.03658	0.00597	-0.00541	0.00299	-0.00235	0.16246	-0.16247	0.00703	-0.00703	0.16662	-0.16679
3.77	0.19967	0.12734	0.01374	-0.01407	0.00451	-0.00498	0.01931	-0.01516	0.13447	-0.13448	0.00703	-0.00703	0.13680	-0.13633
3.98	0.11467	0.23962	0.00829	-0.00809	0.02055	-0.02268	0.04065	-0.03192	0.23245	-0.23247	0.00703	-0.00703	0.23712	-0.23599
4.19	0.06870	0.48019	0.06618	-0.06462	0.04240	-0.04680	0.03468	-0.02723	0.38532	-0.38534	0.00703	-0.00703	0.39484	-0.39451
4.40	-0.02955	-1.32074	0.24894	-0.24307	0.07974	-0.08802	0.03913	-0.04983	0.89068	-0.89073	0.00703	-0.00703	0.92910	-0.92885
4.61	-0.03980	-1.03078	0.22346	-0.21819	0.02261	-0.02496	0.08589	-0.10938	0.65871	-0.65875	0.00703	-0.00703	0.70127	-0.70299

Table 40: 20–40%, 5.0–7.0 \otimes 1.0–2.0 GeV/c Jet Function

ϕ	per trig yield	σ_{stat}/y	systematic errors											
			$+\sigma_{f_2}/y$	$-\sigma_{f_2}/y$	$+\sigma_{f_3}/y$	$-\sigma_{f_3}/y$	$+\sigma_{f_4}/y$	$-\sigma_{f_4}/y$	$+\sigma_\xi/y$	$-\sigma_\xi/y$	$+\sigma_{\pi^0}/y$	$-\sigma_{\pi^0}/y$	$+\sigma_{total}/y$	$-\sigma_{total}/y$
-1.47	0.01490	1.41169	0.29981	-0.29305	0.05102	-0.04596	0.16535	-0.20943	0.50037	-0.50041	0.00376	-0.00376	0.60845	-0.61829
-1.26	0.02712	0.68830	0.13628	-0.13321	0.07341	-0.06613	0.03074	-0.03893	0.27545	-0.27547	0.00376	-0.00376	0.31748	-0.31549
-1.05	0.02047	0.72131	0.11159	-0.10907	0.12022	-0.10830	0.08346	-0.06590	0.36773	-0.36777	0.00376	-0.00376	0.41123	-0.40402
-0.84	0.02305	0.53158	0.02072	-0.02025	0.08637	-0.07781	0.14500	-0.11448	0.33104	-0.33107	0.00376	-0.00376	0.37218	-0.35943
-0.63	0.04870	0.22696	0.02833	-0.02899	0.01561	-0.01407	0.05676	-0.04481	0.15944	-0.15946	0.00376	-0.00376	0.17235	-0.16878
-0.42	0.08963	0.11557	0.03333	-0.03410	0.00764	-0.00848	0.00398	-0.00315	0.08815	-0.08816	0.00376	-0.00376	0.09471	-0.09503
-0.21	0.23510	0.04227	0.01735	-0.01775	0.00763	-0.00847	0.00768	-0.00972	0.03404	-0.03405	0.00376	-0.00376	0.03989	-0.04068
-0.00	0.28845	0.03350	0.01548	-0.01584	0.00769	-0.00853	0.00935	-0.01185	0.02788	-0.02788	0.00376	-0.00376	0.03432	-0.03543
0.21	0.23880	0.04179	0.01708	-0.01748	0.00751	-0.00834	0.00756	-0.00957	0.03352	-0.03352	0.00376	-0.00376	0.03928	-0.04005
0.42	0.08959	0.11844	0.03335	-0.03412	0.00765	-0.00849	0.00399	-0.00315	0.08819	-0.08820	0.00376	-0.00376	0.09475	-0.09508
0.63	0.03512	0.33514	0.03929	-0.04020	0.02165	-0.01951	0.07871	-0.06214	0.22111	-0.22113	0.00376	-0.00376	0.23898	-0.23403
0.84	0.06333	0.21807	0.00754	-0.00737	0.03143	-0.02832	0.05277	-0.04166	0.12048	-0.12049	0.00376	-0.00376	0.13550	-0.13086
1.05	0.01087	1.43045	0.21017	-0.20543	0.22642	-0.20398	0.15720	-0.12411	0.69261	-0.69267	0.00376	-0.00376	0.77451	-0.76093
1.26	-0.02898	-0.63830	0.12754	-0.12466	0.06870	-0.06189	0.02877	-0.03644	0.25777	-0.25779	0.00376	-0.00376	0.29711	-0.29524
1.47	0.00363	6.49918	1.23262	-1.20483	0.20976	-0.18897	0.67982	-0.86104	2.05718	-2.05736	0.00376	-0.00376	2.50150	-2.54194
1.68	-0.01464	-1.46733	0.30529	-0.29841	0.04680	-0.05195	0.16837	-0.21326	0.51121	-0.51126	0.00556	-0.00556	0.62057	-0.63138
1.88	0.02229	0.80476	0.16583	-0.16209	0.08047	-0.08933	0.03741	-0.04738	0.33809	-0.33812	0.00556	-0.00556	0.38692	-0.38840
2.09	0.06040	0.24516	0.03782	-0.03696	0.03670	-0.04074	0.02829	-0.02233	0.12595	-0.12597	0.00556	-0.00556	0.13955	-0.13937
2.30	0.06988	0.18374	0.00683	-0.00668	0.02566	-0.02849	0.04783	-0.03776	0.11013	-0.11014	0.00556	-0.00556	0.12309	-0.12018
2.51	0.09655	0.11822	0.01429	-0.01462	0.00709	-0.00788	0.02863	-0.02260	0.08068	-0.08069	0.00556	-0.00556	0.08726	-0.08560
2.72	0.09510	0.11013	0.03142	-0.03214	0.00800	-0.00720	0.00376	-0.00297	0.08283	-0.08284	0.00556	-0.00556	0.08920	-0.08937
2.93	0.10004	0.10313	0.04078	-0.04172	0.01990	-0.01793	0.01804	-0.02285	0.07936	-0.07937	0.00556	-0.00556	0.09334	-0.09441
3.14	0.12612	0.08313	0.03541	-0.03622	0.01951	-0.01758	0.02139	-0.02709	0.06313	-0.06313	0.00556	-0.00556	0.07815	-0.07982
3.35	0.12023	0.08834	0.03393	-0.03471	0.01656	-0.01492	0.01501	-0.01901	0.06603	-0.06603	0.00556	-0.00556	0.07772	-0.07861
3.56	0.08788	0.12376	0.03400	-0.03478	0.00865	-0.00780	0.00406	-0.00321	0.08963	-0.08964	0.00556	-0.00556	0.09650	-0.09668
3.77	0.07178	0.16329	0.01922	-0.01967	0.00954	-0.01059	0.03851	-0.03040	0.10852	-0.10853	0.00556	-0.00556	0.11726	-0.11503
3.98	0.09585	0.13965	0.00498	-0.00487	0.01871	-0.02077	0.03487	-0.02753	0.08029	-0.08029	0.00556	-0.00556	0.08982	-0.08770
4.19	0.06563	0.24245	0.03480	-0.03402	0.03378	-0.03749	0.02603	-0.02055	0.11592	-0.11593	0.00556	-0.00556	0.12844	-0.12828
4.40	0.03118	0.61753	0.11854	-0.11587	0.05752	-0.06385	0.02674	-0.03387	0.24167	-0.24169	0.00556	-0.00556	0.27660	-0.27766
4.61	-0.00839	-2.55079	0.53275	-0.52073	0.08167	-0.09066	0.29382	-0.37215	0.89209	-0.89217	0.00556	-0.00556	1.08290	-1.10176

Table 41: 20–40%, 5.0–7.0 \otimes 2.0–3.0 GeV/c Jet Function

ϕ	per trig yield	σ_{stat}/y	systematic errors												
			$+\sigma_{f2}/y$	$-\sigma_{f2}/y$	$+\sigma_{f3}/y$	$-\sigma_{f3}/y$	$+\sigma_{f4}/y$	$-\sigma_{f4}/y$	$+\sigma_\xi/y$	$-\sigma_\xi/y$	$+\sigma_{\pi^0}/y$	$-\sigma_{\pi^0}/y$	$+\sigma_{total}/y$	$-\sigma_{total}/y$	
-1.47	-0.00036	-15.92901	1.52608	-1.48832	0.25437	-0.23080	1.06595	-1.35035	1.66990	-1.66990	0.00299	-0.00299	2.51365	-2.62305	
-1.26	0.00263	1.85011	0.17132	-0.16708	0.09039	-0.08201	0.04894	-0.06200	0.22681	-0.22681	0.00299	-0.00299	0.30227	-0.29989	
-1.05	0.00763	0.54251	0.03650	-0.03559	0.03851	-0.03494	0.03458	-0.02730	0.07892	-0.07892	0.00299	-0.00299	0.10124	-0.09732	
-0.84	0.01060	0.30590	0.00550	-0.00536	0.02244	-0.02036	0.04872	-0.03846	0.05793	-0.05793	0.00299	-0.00299	0.07920	-0.07271	
-0.63	0.01089	0.28285	0.01543	-0.01582	0.00835	-0.00757	0.03924	-0.03097	0.05786	-0.05786	0.00299	-0.00299	0.07214	-0.06800	
-0.42	0.02188	0.12913	0.01662	-0.01704	0.00377	-0.00415	0.00252	-0.00199	0.02955	-0.02955	0.00299	-0.00299	0.03434	-0.03455	
-0.21	0.08208	0.03738	0.00605	-0.00620	0.00263	-0.00290	0.00340	-0.00430	0.00803	-0.00803	0.00299	-0.00299	0.01134	-0.01178	
-0.00	0.14302	0.02154	0.00380	-0.00390	0.00187	-0.00206	0.00291	-0.00369	0.00464	-0.00464	0.00299	-0.00299	0.00754	-0.00797	
0.21	0.08198	0.03739	0.00606	-0.00621	0.00263	-0.00290	0.00340	-0.00431	0.00804	-0.00804	0.00299	-0.00299	0.01135	-0.01180	
0.42	0.02272	0.12590	0.01601	-0.01641	0.00363	-0.00400	0.00243	-0.00192	0.02846	-0.02846	0.00299	-0.00299	0.03308	-0.03328	
0.63	0.00706	0.46422	0.02379	-0.02440	0.01287	-0.01168	0.06051	-0.04777	0.08923	-0.08923	0.00299	-0.00299	0.11120	-0.10481	
0.84	0.00859	0.41450	0.00678	-0.00662	0.02770	-0.02514	0.06015	-0.04748	0.07151	-0.07151	0.00299	-0.00299	0.09775	-0.08974	
1.05	0.00800	0.54953	0.03482	-0.03395	0.03674	-0.03333	0.03299	-0.02604	0.07529	-0.07529	0.00299	-0.00299	0.09658	-0.09284	
1.26	-0.00094	-5.17142	0.48185	-0.46993	0.25423	-0.23067	0.13765	-0.17437	0.63793	-0.63793	0.00299	-0.00299	0.85013	-0.84345	
1.47	0.00614	1.04122	0.08882	-0.08662	0.01480	-0.01343	0.06204	-0.07859	0.09719	-0.09719	0.00299	-0.00299	0.14633	-0.15269	
1.68	0.00877	0.70193	0.06215	-0.06061	0.00940	-0.01036	0.04341	-0.05499	0.06839	-0.06839	0.00478	-0.00478	0.10264	-0.10726	
1.88	0.00171	2.73862	0.26375	-0.25722	0.12626	-0.13916	0.07534	-0.09545	0.35436	-0.35436	0.00478	-0.00478	0.46559	-0.46928	
2.09	0.00290	1.40353	0.09597	-0.09359	0.09188	-0.10127	0.09092	-0.07177	0.21130	-0.21130	0.00478	-0.00478	0.26569	-0.26237	
2.30	0.01264	0.27110	0.00461	-0.00450	0.01708	-0.01882	0.04086	-0.03226	0.04929	-0.04929	0.00478	-0.00478	0.06660	-0.06219	
2.51	0.01715	0.18595	0.00979	-0.01004	0.00481	-0.00530	0.02491	-0.01966	0.03693	-0.03693	0.00478	-0.00478	0.4611	-0.04361	
2.72	0.01740	0.16095	0.02090	-0.02143	0.00522	-0.00474	0.00317	-0.00250	0.03696	-0.03696	0.00478	-0.00478	0.04316	-0.04332	
2.93	0.02647	0.11105	0.01876	-0.01923	0.00899	-0.00815	0.01054	-0.01335	0.02457	-0.02457	0.00478	-0.00478	0.03421	-0.03523	
3.14	0.03125	0.09155	0.01739	-0.01783	0.00941	-0.00854	0.01334	-0.01689	0.02090	-0.02090	0.00478	-0.00478	0.03207	-0.03370	
3.35	0.02274	0.13222	0.02183	-0.02239	0.01046	-0.00949	0.01226	-0.01554	0.02860	-0.02860	0.00478	-0.00478	0.03972	-0.04091	
3.56	0.01538	0.18616	0.02364	-0.02424	0.00591	-0.00536	0.00359	-0.00283	0.04181	-0.04181	0.00478	-0.00478	0.04876	-0.04894	
3.77	0.01594	0.20528	0.01054	-0.01081	0.00517	-0.00570	0.02680	-0.02116	0.03974	-0.03974	0.00478	-0.00478	0.04958	-0.04690	
3.98	0.00978	0.35472	0.00596	-0.00581	0.02207	-0.02432	0.05280	-0.04168	0.06368	-0.06368	0.00478	-0.00478	0.08595	-0.08025	
4.19	-0.00006	-68.96778	4.45696	-4.34666	4.26727	-4.70309	4.22262	-3.33328	9.81326	-9.81326	0.00478	-0.00478	12.33713	-12.18292	
4.40	0.00160	3.03494	0.28184	-0.27487	0.13492	-0.14870	0.08051	-0.10199	0.37867	-0.37867	0.00478	-0.00478	0.49753	-0.50148	
4.61	-0.00190	-3.27226	0.28742	-0.28031	0.04347	-0.04791	0.20076	-0.25432	0.31629	-0.31629	0.00478	-0.00478	0.47420	-0.49559	

Table 42: 20–40%, 5.0–7.0 \otimes 3.0–5.0 GeV/c Jet Function

ϕ	per trig yield	σ_{stat}/y	systematic errors											
			$+\sigma_{f2}/y$	$-\sigma_{f2}/y$	$+\sigma_{f3}/y$	$-\sigma_{f3}/y$	$+\sigma_{f4}/y$	$-\sigma_{f4}/y$	$+\sigma_\xi/y$	$-\sigma_\xi/y$	$+\sigma_{\pi^0}/y$	$-\sigma_{\pi^0}/y$	$+\sigma_{total}/y$	$-\sigma_{total}/y$
-1.47	-0.00246	-0.80206	0.02913	-0.02847	0.00532	-0.00483	0.02435	-0.03077	0.03012	-0.03012	0.00847	-0.00847	0.04948	-0.05253
-1.26	0.00225	0.79379	0.02629	-0.02569	0.01520	-0.01379	0.00898	-0.01136	0.03285	-0.03285	0.00847	-0.00847	0.04641	-0.04616
-1.05	0.00151	1.00489	0.02422	-0.02366	0.02799	-0.02541	0.02739	-0.02167	0.04940	-0.04940	0.00847	-0.00847	0.06806	-0.06471
-0.84	-0.00000	-718.21112	4.88688	-4.77498	21.86075	-19.84282	51.71229	-40.91504	48.58969	-48.58969	0.00847	-0.00847	74.41030	-66.71983
-0.63	0.00240	0.47319	0.00921	-0.00943	0.00545	-0.00495	0.02791	-0.02208	0.03255	-0.03255	0.00847	-0.00847	0.04500	-0.04162
-0.42	0.00597	0.17744	0.00803	-0.00821	0.00199	-0.00219	0.00145	-0.00115	0.01346	-0.01346	0.00847	-0.00847	0.01798	-0.01807
-0.21	0.03927	0.03688	0.00167	-0.00170	0.00079	-0.00087	0.00112	-0.00141	0.00209	-0.00209	0.00847	-0.00847	0.00899	-0.00905
-0.00	0.10073	0.01792	0.00071	-0.00073	0.00038	-0.00042	0.00065	-0.00082	0.00082	-0.00082	0.00847	-0.00847	0.00858	-0.00859
0.21	0.03749	0.03847	0.00174	-0.00179	0.00083	-0.00091	0.00117	-0.00148	0.00219	-0.00219	0.00847	-0.00847	0.00904	-0.00910
0.42	0.00349	0.29834	0.01372	-0.01405	0.00340	-0.00375	0.00248	-0.00196	0.02302	-0.02302	0.00847	-0.00847	0.02842	-0.02858
0.63	0.00125	0.96598	0.01773	-0.01815	0.01049	-0.00952	0.05373	-0.04251	0.06266	-0.06266	0.00847	-0.00847	0.08550	-0.07890
0.84	0.00032	3.92593	0.02382	-0.02327	0.10655	-0.09671	0.25205	-0.19942	0.23683	-0.23683	0.00847	-0.00847	0.36278	-0.32530
1.05	0.00229	0.72907	0.01599	-0.01562	0.01848	-0.01677	0.01808	-0.01430	0.03261	-0.03261	0.00847	-0.00847	0.04538	-0.04319
1.26	0.00185	0.96704	0.03200	-0.03127	0.01849	-0.01679	0.01094	-0.01382	0.03999	-0.03999	0.00847	-0.00847	0.05618	-0.05587
1.47	-0.00180	-1.22164	0.03974	-0.03883	0.00726	-0.00659	0.03320	-0.04197	0.04108	-0.04108	0.00847	-0.00847	0.06703	-0.07121
1.68	0.00057	3.91769	0.12479	-0.12193	0.02068	-0.02279	0.10427	-0.13179	0.12977	-0.12977	0.00697	-0.00697	0.20919	-0.22281
1.88	0.00179	0.96538	0.03314	-0.03238	0.01739	-0.01915	0.01133	-0.01431	0.04207	-0.04207	0.00697	-0.00697	0.05785	-0.05864
2.09	-0.00135	-1.07123	0.02713	-0.02651	0.02847	-0.03136	0.03068	-0.02428	0.05642	-0.05642	0.00697	-0.00697	0.07563	-0.07421
2.30	0.00407	0.31463	0.00188	-0.00184	0.00764	-0.00842	0.01992	-0.01576	0.01901	-0.01901	0.00697	-0.00697	0.02947	-0.02707
2.51	0.00353	0.33634	0.00627	-0.00642	0.00337	-0.00371	0.01900	-0.01503	0.02228	-0.02228	0.00697	-0.00697	0.03093	-0.02874
2.72	0.00465	0.22399	0.01030	-0.01054	0.00281	-0.00255	0.00186	-0.00147	0.01717	-0.01717	0.00697	-0.00697	0.02147	-0.02153
2.93	0.01127	0.10575	0.00580	-0.00594	0.00304	-0.00276	0.00389	-0.00492	0.00718	-0.00718	0.00697	-0.00697	0.01258	-0.01293
3.14	0.01438	0.08201	0.00498	-0.00510	0.00295	-0.00267	0.00456	-0.00576	0.00565	-0.00565	0.00697	-0.00697	0.01161	-0.01212
3.35	0.01168	0.10553	0.00560	-0.00573	0.00293	-0.00266	0.00376	-0.00475	0.00692	-0.00692	0.00697	-0.00697	0.01227	-0.01261
3.56	0.00575	0.18906	0.00833	-0.00852	0.00228	-0.00207	0.00151	-0.00119	0.01389	-0.01389	0.00697	-0.00697	0.01784	-0.01789
3.77	0.00345	0.35260	0.00642	-0.00657	0.00345	-0.00380	0.01944	-0.01538	0.02280	-0.02280	0.00697	-0.00697	0.03162	-0.02937
3.98	0.00167	0.75406	0.00458	-0.00447	0.01859	-0.02048	0.04844	-0.03833	0.04622	-0.04622	0.00697	-0.00697	0.06999	-0.06398
4.19	0.00159	1.02573	0.02311	-0.02258	0.02425	-0.02672	0.02614	-0.02068	0.04806	-0.04806	0.00697	-0.00697	0.06452	-0.06332
4.40	0.00512	0.37512	0.01159	-0.01132	0.00608	-0.00670	0.00396	-0.00500	0.01471	-0.01471	0.00697	-0.00697	0.02126	-0.02152
4.61	-0.00010	-23.83983	0.72011	-0.70362	0.11935	-0.13149	0.60173	-0.76053	0.74886	-0.74886	0.00697	-0.00697	1.20654	-1.28515

Table 43: 20–40%, 5.0–7.0 \otimes 5.0–7.0 GeV/c Jet Function

ϕ	per trig yield	σ_{stat}/y	systematic errors											
			$+\sigma_{f_2}/y$	$-\sigma_{f_2}/y$	$+\sigma_{f_3}/y$	$-\sigma_{f_3}/y$	$+\sigma_{f_4}/y$	$-\sigma_{f_4}/y$	$+\sigma_\xi/y$	$-\sigma_\xi/y$	$+\sigma_{\pi^0}/y$	$-\sigma_{\pi^0}/y$	$+\sigma_{total}/y$	$-\sigma_{total}/y$
-1.47	0.00088	0.86431	0.00984	-0.00951	0.00406	-0.00354	0.01074	-0.01439	0.01549	-0.01549	0.02662	-0.02662	0.03431	-0.03548
-1.26	-0.00040	-1.28910	0.01791	-0.01731	0.02340	-0.02037	0.00800	-0.01071	0.03415	-0.03415	0.02662	-0.02662	0.05298	-0.05200
-1.05	0.00005	9.43161	0.08710	-0.08419	0.22764	-0.19817	0.13633	-0.10180	0.27078	-0.27078	0.02662	-0.02662	0.38990	-0.36160
-0.84	0.00035	1.09222	0.00267	-0.00258	0.02704	-0.02354	0.03917	-0.02925	0.04034	-0.04034	0.02662	-0.02662	0.06788	-0.06125
-0.63	-0.00019	-1.78109	0.01378	-0.01426	0.01864	-0.01622	0.05844	-0.04364	0.07414	-0.07414	0.02662	-0.02662	0.10078	-0.09260
-0.42	0.00043	0.76085	0.01326	-0.01372	0.00721	-0.00828	0.00335	-0.00250	0.03357	-0.03357	0.02662	-0.02662	0.04554	-0.04581
-0.21	0.00574	0.08664	0.00136	-0.00141	0.00142	-0.00163	0.00120	-0.00161	0.00255	-0.00255	0.02662	-0.02662	0.02684	-0.02688
-0.00	0.03171	0.02844	0.00027	-0.00028	0.00032	-0.00036	0.00033	-0.00044	0.00046	-0.00046	0.02662	-0.02662	0.02663	-0.02663
0.21	0.00595	0.08667	0.00131	-0.00136	0.00137	-0.00157	0.00116	-0.00155	0.00246	-0.00246	0.02662	-0.02662	0.02682	-0.02686
0.42	0.00042	0.81489	0.01357	-0.01404	0.00737	-0.00847	0.00343	-0.00256	0.03435	-0.03435	0.02662	-0.02662	0.04624	-0.04651
0.63	0.00017	2.35101	0.01512	-0.01564	0.02044	-0.01780	0.06410	-0.04787	0.08133	-0.08133	0.02662	-0.02662	0.10990	-0.10087
0.84	0.00023	1.90315	0.00405	-0.00391	0.04095	-0.03565	0.05931	-0.04429	0.06108	-0.06108	0.02662	-0.02662	0.09824	-0.08768
1.05	-0.00014	-3.34524	0.03091	-0.02987	0.08078	-0.07032	0.04838	-0.03612	0.09609	-0.09609	0.02662	-0.02662	0.14058	-0.13070
1.26	-0.00021	-2.54330	0.03451	-0.03336	0.04510	-0.03926	0.01541	-0.02063	0.06580	-0.06580	0.02662	-0.02662	0.09220	-0.09010
1.47	-0.00078	-0.80125	0.01113	-0.01075	0.00459	-0.00400	0.01215	-0.01627	0.01752	-0.01752	0.02662	-0.02662	0.03616	-0.03757
1.68	-0.00086	-0.71164	0.01008	-0.00974	0.00362	-0.00416	0.01100	-0.01473	0.01592	-0.01592	0.00599	-0.00599	0.02292	-0.02487
1.88	0.00079	0.74603	0.00907	-0.00877	0.01032	-0.01186	0.00405	-0.00542	0.01744	-0.01744	0.00599	-0.00599	0.02336	-0.02423
2.09	0.00096	0.56507	0.00461	-0.00446	0.01050	-0.01206	0.00722	-0.00539	0.01449	-0.01449	0.00599	-0.00599	0.02073	-0.02099
2.30	0.00101	0.43417	0.00091	-0.00088	0.00802	-0.00921	0.01334	-0.00996	0.01385	-0.01385	0.00599	-0.00599	0.02170	-0.02031
2.51	0.00108	0.38665	0.00244	-0.00252	0.00287	-0.00329	0.01033	-0.00771	0.01314	-0.01314	0.00599	-0.00599	0.01815	-0.01689
2.72	0.00037	0.88347	0.01540	-0.01593	0.00962	-0.00837	0.00390	-0.00291	0.03887	-0.03887	0.00599	-0.00599	0.04349	-0.04335
2.93	0.00268	0.16371	0.00291	-0.00301	0.00348	-0.00303	0.00258	-0.00345	0.00543	-0.00543	0.00599	-0.00599	0.00963	-0.00978
3.14	0.00433	0.10967	0.00197	-0.00204	0.00266	-0.00232	0.00238	-0.00319	0.00337	-0.00337	0.00599	-0.00599	0.00800	-0.00819
3.35	0.00329	0.14901	0.00237	-0.00245	0.00284	-0.00247	0.00210	-0.00281	0.00442	-0.00442	0.00599	-0.00599	0.00857	-0.00869
3.56	0.00122	0.30802	0.00469	-0.00485	0.00293	-0.00255	0.00119	-0.00089	0.01184	-0.01184	0.00599	-0.00599	0.01443	-0.01439
3.77	0.00045	0.89025	0.00589	-0.00609	0.00693	-0.00796	0.02496	-0.01864	0.03177	-0.03177	0.00599	-0.00599	0.04185	-0.03864
3.98	-0.00007	-5.64422	0.01368	-0.01322	0.12046	-0.13838	0.20040	-0.14965	0.20808	-0.20808	0.00599	-0.00599	0.31335	-0.29163
4.19	-0.00010	-5.02717	0.04462	-0.04312	0.10151	-0.11661	0.06984	-0.05215	0.14014	-0.14014	0.00599	-0.00599	0.19196	-0.19455
4.40	-0.00031	-1.76895	0.02274	-0.02198	0.02587	-0.02972	0.01015	-0.01360	0.04373	-0.04373	0.00599	-0.00599	0.05690	-0.05915
4.61	-0.00027	-3.25372	0.03218	-0.03110	0.01157	-0.01329	0.03513	-0.04704	0.05083	-0.05083	0.00599	-0.00599	0.07087	-0.07731

Table 44: 20–40%, 7.0–9.0 \otimes 0.5–1.0 GeV/c Jet Function

ϕ	per trig yield	σ_{stat}/y	systematic errors											
			$+\sigma_{f2}/y$	$-\sigma_{f2}/y$	$+\sigma_{f3}/y$	$-\sigma_{f3}/y$	$+\sigma_{f4}/y$	$-\sigma_{f4}/y$	$+\sigma_\xi/y$	$-\sigma_\xi/y$	$+\sigma_{\pi^0}/y$	$-\sigma_{\pi^0}/y$	$+\sigma_{total}/y$	$-\sigma_{total}/y$
-1.47	0.07147	1.61175	0.23892	-0.19665	0.01703	-0.01287	0.03384	-0.05325	0.36419	-0.36419	0.00572	-0.00572	0.43725	-0.41754
-1.26	-0.05607	-1.85566	0.25187	-0.20731	0.05684	-0.04295	0.01459	-0.02296	0.46489	-0.46488	0.00572	-0.00572	0.53201	-0.51137
-1.05	-0.10854	-0.76156	0.08041	-0.06619	0.03629	-0.02742	0.01919	-0.01219	0.24111	-0.24111	0.00572	-0.00572	0.25753	-0.25189
-0.84	-0.01334	-5.29980	0.13675	-0.11255	0.23884	-0.18046	0.30538	-0.19406	1.97329	-1.97327	0.00572	-0.00572	2.01567	-1.99417
-0.63	0.11557	0.54546	0.03842	-0.04667	0.01053	-0.00796	0.02916	-0.01853	0.22948	-0.22948	0.00572	-0.00572	0.23480	-0.23511
-0.42	0.13852	0.42614	0.06940	-0.08432	0.00664	-0.00879	0.00314	-0.00200	0.19279	-0.19279	0.00572	-0.00572	0.20512	-0.21070
-0.21	0.19650	0.28259	0.06680	-0.08115	0.01225	-0.01622	0.00901	-0.01419	0.13658	-0.13658	0.00572	-0.00572	0.15291	-0.16043
-0.00	0.19536	0.28151	0.07354	-0.08935	0.01523	-0.02016	0.01355	-0.02132	0.13762	-0.13762	0.00572	-0.00572	0.15747	-0.16678
0.21	0.17085	0.33248	0.07682	-0.09334	0.01409	-0.01865	0.01037	-0.01631	0.15708	-0.15708	0.00572	-0.00572	0.17583	-0.18448
0.42	-0.00222	-27.16191	4.33691	-5.26920	0.41491	-0.54914	0.19643	-0.12483	12.04722	-12.04704	0.00572	-0.00572	12.81230	-13.16104
0.63	-0.08171	0.82272	0.05434	-0.06602	0.01490	-0.01126	0.04124	-0.02621	0.32458	-0.32457	0.00572	-0.00572	0.33205	-0.33249
0.84	0.00285	27.64845	0.64095	-0.52754	1.11947	-0.84583	1.43132	-0.90956	9.24895	-9.24882	0.00572	-0.00572	9.44753	-9.34675
1.05	-0.01021	-8.73011	0.85465	-0.70343	0.38573	-0.29145	0.20395	-0.12961	2.56253	-2.56250	0.00572	-0.00572	2.73632	-2.67637
1.26	-0.20773	-0.49402	0.06798	-0.05595	0.01534	-0.01159	0.00394	-0.00620	0.12547	-0.12547	0.00572	-0.00572	0.14370	-0.13813
1.47	0.09836	1.28663	0.17359	-0.14288	0.01238	-0.00935	0.02459	-0.03869	0.26461	-0.26461	0.00572	-0.00572	0.31771	-0.30339
1.68	0.31286	0.38374	0.05458	-0.04492	0.00294	-0.00389	0.00773	-0.01216	0.08327	-0.08327	0.00227	-0.00227	0.09993	-0.09550
1.88	0.16110	0.61801	0.08766	-0.07215	0.01495	-0.01978	0.00508	-0.00799	0.16220	-0.16220	0.00227	-0.00227	0.18506	-0.17881
2.09	0.09524	0.86790	0.09164	-0.07543	0.03125	-0.04136	0.02187	-0.01390	0.27563	-0.27563	0.00227	-0.00227	0.29297	-0.28908
2.30	0.12845	0.57182	0.01420	-0.01169	0.01875	-0.02481	0.03172	-0.02016	0.20548	-0.20548	0.00227	-0.00227	0.20926	-0.20829
2.51	0.12756	0.51385	0.03480	-0.04229	0.00721	-0.00954	0.02642	-0.01679	0.20810	-0.20810	0.00227	-0.00227	0.21277	-0.21324
2.72	0.22419	0.27247	0.04288	-0.05210	0.00543	-0.00410	0.00194	-0.00123	0.11901	-0.11901	0.00227	-0.00227	0.12665	-0.13000
2.93	0.29781	0.19979	0.04407	-0.05355	0.01070	-0.00809	0.00595	-0.00936	0.08990	-0.08990	0.00227	-0.00227	0.10089	-0.10539
3.14	0.25620	0.23445	0.05608	-0.06813	0.01538	-0.01162	0.01033	-0.01626	0.10463	-0.10463	0.00227	-0.00227	0.12017	-0.12647
3.35	0.31683	0.19214	0.04143	-0.05033	0.01006	-0.00760	0.00559	-0.00880	0.08450	-0.08450	0.00227	-0.00227	0.09484	-0.09906
3.56	0.26591	0.24203	0.03615	-0.04393	0.00458	-0.00346	0.00164	-0.00104	0.10034	-0.10033	0.00227	-0.00227	0.10679	-0.10961
3.77	0.23108	0.30314	0.01921	-0.02334	0.00398	-0.00527	0.01458	-0.00927	0.11488	-0.11488	0.00227	-0.00227	0.11748	-0.11773
3.98	0.10550	0.71636	0.01730	-0.01424	0.02282	-0.03021	0.03862	-0.02454	0.25019	-0.25019	0.00227	-0.00227	0.25478	-0.25361
4.19	0.25950	0.35285	0.03363	-0.02768	0.01147	-0.01518	0.00803	-0.00510	0.10116	-0.10116	0.00227	-0.00227	0.10754	-0.10611
4.40	0.23301	0.46862	0.06061	-0.04988	0.01033	-0.01368	0.00351	-0.00552	0.11214	-0.11214	0.00227	-0.00227	0.12796	-0.12364
4.61	-0.17054	-0.65227	0.10012	-0.08241	0.00539	-0.00714	0.01418	-0.02231	0.15276	-0.15276	0.00227	-0.00227	0.18329	-0.17516

Table 45: 20–40%, 7.0–9.0 \otimes 1.0–2.0 GeV/c Jet Function

ϕ	per trig yield	σ_{stat}/y	systematic errors											
			$+\sigma_{f2}/y$	$-\sigma_{f2}/y$	$+\sigma_{f3}/y$	$-\sigma_{f3}/y$	$+\sigma_{f4}/y$	$-\sigma_{f4}/y$	$+\sigma_\xi/y$	$-\sigma_\xi/y$	$+\sigma_{\pi^0}/y$	$-\sigma_{\pi^0}/y$	$+\sigma_{total}/y$	$-\sigma_{total}/y$
-1.47	0.04604	1.26279	0.18938	-0.15586	0.01943	-0.01462	0.03836	-0.05999	0.16060	-0.16061	0.00095	-0.00095	0.25201	-0.23216
-1.26	-0.04125	-1.21963	0.17482	-0.14387	0.05678	-0.04271	0.01448	-0.02265	0.17957	-0.17958	0.00095	-0.00095	0.25738	-0.23513
-1.05	0.01774	2.26540	0.25117	-0.20671	0.16316	-0.12273	0.08519	-0.05447	0.42013	-0.42015	0.00095	-0.00095	0.52295	-0.48711
-0.84	0.01574	2.12165	0.05920	-0.04872	0.14883	-0.11195	0.18792	-0.12015	0.47877	-0.47879	0.00095	-0.00095	0.53869	-0.50851
-0.63	0.00664	4.51206	0.34164	-0.41514	0.13484	-0.10142	0.36864	-0.23571	1.15067	-1.15072	0.00095	-0.00095	1.26287	-1.24994
-0.42	0.12054	0.23566	0.04072	-0.04948	0.00558	-0.00742	0.00262	-0.00168	0.06416	-0.06416	0.00095	-0.00095	0.07625	-0.08139
-0.21	0.30103	0.09069	0.02226	-0.02705	0.00585	-0.00778	0.00430	-0.00672	0.02594	-0.02594	0.00095	-0.00095	0.03495	-0.03887
-0.00	0.42802	0.06301	0.01714	-0.02083	0.00509	-0.00676	0.00452	-0.00706	0.01830	-0.01830	0.00095	-0.00095	0.02600	-0.02942
0.21	0.27385	0.09988	0.02447	-0.02974	0.00643	-0.00855	0.00472	-0.00739	0.02851	-0.02851	0.00095	-0.00095	0.03842	-0.04273
0.42	0.07225	0.40170	0.06794	-0.08255	0.00931	-0.01238	0.00437	-0.00280	0.10705	-0.10705	0.00095	-0.00095	0.12720	-0.13578
0.63	0.08151	0.39892	0.02781	-0.03379	0.01098	-0.00826	0.03001	-0.01919	0.09367	-0.09367	0.00095	-0.00095	0.10281	-0.10175
0.84	-0.01038	-3.61239	0.08974	-0.07385	0.22559	-0.16969	0.28483	-0.18212	0.72569	-0.72572	0.00095	-0.00095	0.81652	-0.77077
1.05	0.03652	1.17844	0.12204	-0.10043	0.07928	-0.05963	0.04139	-0.02647	0.20413	-0.20414	0.00095	-0.00095	0.25409	-0.23668
1.26	-0.00090	-56.66001	8.01343	-6.59480	2.60282	-1.95780	0.66382	-1.03821	8.23112	-8.23146	0.00095	-0.00095	11.79753	-10.77772
1.47	0.05819	1.11986	0.14984	-0.12332	0.01538	-0.01157	0.03035	-0.04747	0.12707	-0.12708	0.00095	-0.00095	0.19940	-0.18369
1.68	0.09027	0.66099	0.09658	-0.07949	0.00748	-0.00991	0.01956	-0.03060	0.08209	-0.08209	0.00334	-0.00334	0.12852	-0.11876
1.88	0.09666	0.51479	0.07460	-0.06140	0.01823	-0.02423	0.00618	-0.00967	0.07708	-0.07709	0.00334	-0.00334	0.10904	-0.10200
2.09	0.07544	0.53572	0.05907	-0.04862	0.02887	-0.03838	0.02004	-0.01281	0.09953	-0.09953	0.00334	-0.00334	0.12100	-0.11797
2.30	0.06170	0.56737	0.01510	-0.01243	0.02855	-0.03796	0.04793	-0.03065	0.12282	-0.12283	0.00334	-0.00334	0.13579	-0.13279
2.51	0.13282	0.23610	0.01707	-0.02074	0.00507	-0.00674	0.01842	-0.01177	0.05761	-0.05761	0.00334	-0.00334	0.06313	-0.06280
2.72	0.15090	0.19131	0.03253	-0.03953	0.00593	-0.00446	0.00209	-0.00134	0.05114	-0.05114	0.00334	-0.00334	0.06103	-0.06489
2.93	0.18795	0.15164	0.03566	-0.04333	0.01246	-0.00937	0.00688	-0.01076	0.04131	-0.04131	0.00334	-0.00334	0.05649	-0.06163
3.14	0.20226	0.14249	0.03627	-0.04407	0.01431	-0.01077	0.00956	-0.01495	0.03847	-0.03847	0.00334	-0.00334	0.05570	-0.06142
3.35	0.17925	0.16282	0.03739	-0.04543	0.01307	-0.00983	0.00722	-0.01129	0.04331	-0.04331	0.00334	-0.00334	0.05922	-0.06461
3.56	0.17106	0.17658	0.02869	-0.03487	0.00523	-0.00393	0.00185	-0.00118	0.04511	-0.04512	0.00334	-0.00334	0.05386	-0.05726
3.77	0.04007	0.79528	0.05658	-0.06875	0.01680	-0.02233	0.06105	-0.03903	0.19097	-0.19097	0.00334	-0.00334	0.20902	-0.20792
3.98	0.11927	0.31164	0.00781	-0.00643	0.01477	-0.01964	0.02480	-0.01585	0.06354	-0.06354	0.00334	-0.00334	0.07030	-0.06876
4.19	0.07904	0.55299	0.05639	-0.04641	0.02755	-0.03663	0.01913	-0.01223	0.09500	-0.09501	0.00334	-0.00334	0.11550	-0.11262
4.40	0.04248	1.24510	0.16977	-0.13972	0.04148	-0.05514	0.01406	-0.02200	0.17541	-0.17542	0.00334	-0.00334	0.24804	-0.23201
4.61	0.05449	1.09668	0.16000	-0.13167	0.01235	-0.01642	0.03241	-0.05068	0.13599	-0.13599	0.00334	-0.00334	0.21285	-0.19668

Table 46: 20–40%, 7.0–9.0 \otimes 2.0–3.0 GeV/c Jet Function

ϕ	per trig yield	σ_{stat}/y	systematic errors											
			$+\sigma_{f2}/y$	$-\sigma_{f2}/y$	$+\sigma_{f3}/y$	$-\sigma_{f3}/y$	$+\sigma_{f4}/y$	$-\sigma_{f4}/y$	$+\sigma_\xi/y$	$-\sigma_\xi/y$	$+\sigma_{\pi^0}/y$	$-\sigma_{\pi^0}/y$	$+\sigma_{total}/y$	$-\sigma_{total}/y$
-1.47	0.02598	0.64306	0.03960	-0.03259	0.00434	-0.00329	0.01050	-0.01643	0.02300	-0.02298	0.00200	-0.00200	0.04723	-0.04330
-1.26	-0.01824	-0.69468	0.04666	-0.03840	0.01620	-0.01225	0.00506	-0.00791	0.03281	-0.03279	0.00200	-0.00200	0.05955	-0.05260
-1.05	0.00667	1.68660	0.07890	-0.06493	0.05479	-0.04144	0.03504	-0.02240	0.09050	-0.09045	0.00200	-0.00200	0.13656	-0.12092
-0.84	0.00361	2.42407	0.03048	-0.02508	0.08191	-0.06195	0.12666	-0.08097	0.16973	-0.16964	0.00200	-0.00200	0.22912	-0.19951
-0.63	0.00540	1.53311	0.04957	-0.06024	0.02092	-0.01582	0.07004	-0.04477	0.11566	-0.11560	0.00200	-0.00200	0.14554	-0.13875
-0.42	0.01944	0.39330	0.02979	-0.03620	0.00439	-0.00581	0.00251	-0.00161	0.03272	-0.03271	0.00200	-0.00200	0.04459	-0.04920
-0.21	0.10690	0.08104	0.00740	-0.00899	0.00209	-0.00276	0.00187	-0.00292	0.00604	-0.00603	0.00200	-0.00200	0.01015	-0.01172
-0.00	0.22998	0.04053	0.00376	-0.00457	0.00120	-0.00159	0.00130	-0.00203	0.00282	-0.00282	0.00200	-0.00200	0.00541	-0.00629
0.21	0.13221	0.06803	0.00598	-0.00727	0.00169	-0.00224	0.00151	-0.00236	0.00488	-0.00488	0.00200	-0.00200	0.00829	-0.00955
0.42	0.04131	0.19738	0.01402	-0.01704	0.00207	-0.00273	0.00118	-0.00076	0.01540	-0.01539	0.00200	-0.00200	0.02106	-0.02322
0.63	0.01893	0.48494	0.01413	-0.01717	0.00596	-0.00451	0.01997	-0.01276	0.03297	-0.03296	0.00200	-0.00200	0.04154	-0.03960
0.84	-0.00410	-2.29087	0.02680	-0.02206	0.07203	-0.05448	0.11138	-0.07119	0.14925	-0.14917	0.00200	-0.00200	0.20147	-0.17544
1.05	-0.01236	-0.91032	0.04257	-0.03503	0.02956	-0.02236	0.01890	-0.01208	0.04883	-0.04880	0.00200	-0.00200	0.07370	-0.06526
1.26	0.00828	1.66963	0.10282	-0.08461	0.03570	-0.02700	0.01115	-0.01744	0.07229	-0.07226	0.00200	-0.00200	0.13116	-0.11584
1.47	0.04427	0.42719	0.02324	-0.01913	0.00255	-0.00193	0.00616	-0.00964	0.01350	-0.01349	0.00200	-0.00200	0.02776	-0.02546
1.68	0.02372	0.73244	0.04337	-0.03569	0.00360	-0.00476	0.01150	-0.01799	0.02528	-0.02527	0.00719	-0.00719	0.05213	-0.04807
1.88	-0.01612	-0.75934	0.05280	-0.04345	0.01387	-0.01833	0.00572	-0.00896	0.03749	-0.03747	0.00719	-0.00719	0.06686	-0.06132
2.09	-0.00234	-4.66870	0.22439	-0.18465	0.11786	-0.15582	0.09965	-0.06369	0.26053	-0.26040	0.00719	-0.00719	0.37696	-0.36096
2.30	0.00956	0.97224	0.01150	-0.00946	0.02338	-0.03091	0.04780	-0.03055	0.06467	-0.06464	0.00719	-0.00719	0.08484	-0.07879
2.51	0.00960	0.88947	0.02786	-0.03385	0.00889	-0.01175	0.03936	-0.02516	0.06523	-0.06520	0.00719	-0.00719	0.08192	-0.07887
2.72	0.03371	0.23306	0.01718	-0.02088	0.00335	-0.00253	0.00145	-0.00093	0.01881	-0.01880	0.00719	-0.00719	0.02672	-0.02913
2.93	0.04531	0.18263	0.01745	-0.02121	0.00652	-0.00493	0.00441	-0.00690	0.01411	-0.01410	0.00719	-0.00719	0.02485	-0.02779
3.14	0.05395	0.15082	0.01605	-0.01950	0.00677	-0.00512	0.00554	-0.00866	0.01189	-0.01188	0.00719	-0.00719	0.02296	-0.02597
3.35	0.05944	0.14722	0.01331	-0.01617	0.00497	-0.00376	0.00336	-0.00526	0.01076	-0.01075	0.00719	-0.00719	0.01951	-0.02169
3.56	0.02653	0.30074	0.02183	-0.02653	0.00425	-0.00322	0.00184	-0.00118	0.02390	-0.02388	0.00719	-0.00719	0.03348	-0.03658
3.77	0.02102	0.42961	0.01273	-0.01547	0.00406	-0.00537	0.01798	-0.01150	0.02981	-0.02979	0.00719	-0.00719	0.03798	-0.03660
3.98	0.00108	8.72728	0.10218	-0.08408	0.20769	-0.27459	0.42461	-0.27141	0.57454	-0.57425	0.00719	-0.00719	0.75101	-0.69710
4.19	0.00020	57.83266	2.56867	-2.11376	1.34917	-1.78381	1.14070	-0.72915	2.98245	-2.98094	0.00719	-0.00719	4.31446	-4.13131
4.40	-0.00514	-2.50135	0.16551	-0.13620	0.04347	-0.05747	0.01795	-0.02807	0.11754	-0.11748	0.00719	-0.00719	0.20850	-0.19104
4.61	-0.00420	-4.00467	0.24489	-0.20152	0.02032	-0.02686	0.06492	-0.10157	0.14274	-0.14267	0.00719	-0.00719	0.29159	-0.26843

Table 47: 20–40%, 7.0–9.0 \otimes 3.0–5.0 GeV/c Jet Function

ϕ	per trig yield	σ_{stat}/y	systematic errors											
			$+\sigma_{f_2}/y$	$-\sigma_{f_2}/y$	$+\sigma_{f_3}/y$	$-\sigma_{f_3}/y$	$+\sigma_{f_4}/y$	$-\sigma_{f_4}/y$	$+\sigma_\xi/y$	$-\sigma_\xi/y$	$+\sigma_{\pi^0}/y$	$-\sigma_{\pi^0}/y$	$+\sigma_{total}/y$	$-\sigma_{total}/y$
-1.47	0.00571	1.09114	0.02434	-0.02003	0.00285	-0.00216	0.00755	-0.01178	0.01301	-0.01295	0.00131	-0.00131	0.02878	-0.02672
-1.26	0.00522	0.99708	0.02204	-0.01813	0.00817	-0.00618	0.00280	-0.00436	0.01426	-0.01419	0.00131	-0.00131	0.02767	-0.02428
-1.05	0.00742	0.60766	0.00958	-0.00788	0.00711	-0.00538	0.00497	-0.00318	0.01011	-0.01006	0.00131	-0.00131	0.01646	-0.01429
-0.84	-0.00329	-0.88451	0.00452	-0.00372	0.01297	-0.00981	0.02192	-0.01405	0.02315	-0.02304	0.00131	-0.00131	0.03474	-0.02898
-0.63	0.00374	0.84637	0.00968	-0.01176	0.00436	-0.00330	0.01596	-0.01023	0.02079	-0.02069	0.00131	-0.00131	0.02831	-0.02614
-0.42	0.00270	1.02120	0.02896	-0.03520	0.00456	-0.00603	0.00285	-0.00183	0.02931	-0.02917	0.00131	-0.00131	0.04158	-0.04617
-0.21	0.06316	0.07280	0.00169	-0.00206	0.00051	-0.00068	0.00050	-0.00078	0.00127	-0.00127	0.00131	-0.00131	0.00259	-0.00294
-0.00	0.19270	0.03344	0.00061	-0.00074	0.00021	-0.00027	0.00025	-0.00038	0.00042	-0.00042	0.00131	-0.00131	0.00154	-0.00163
0.21	0.06427	0.07143	0.00166	-0.00202	0.00050	-0.00066	0.00049	-0.00077	0.00125	-0.00125	0.00131	-0.00131	0.00256	-0.00290
0.42	0.00645	0.45605	0.01213	-0.01474	0.0191	-0.00252	0.00119	-0.00076	0.01228	-0.01222	0.00131	-0.00131	0.01745	-0.01937
0.63	0.00285	1.21536	0.01266	-0.01539	0.00571	-0.00432	0.02089	-0.01338	0.02720	-0.02707	0.00131	-0.00131	0.03703	-0.03419
0.84	-0.00117	-2.90372	0.01266	-0.01042	0.03634	-0.02749	0.06140	-0.03935	0.06486	-0.06454	0.00131	-0.00131	0.09726	-0.08112
1.05	-0.00399	-1.04374	0.01783	-0.01467	0.01322	-0.01000	0.00924	-0.00592	0.01881	-0.01872	0.00131	-0.00131	0.03055	-0.02650
1.26	0.00515	0.98364	0.02235	-0.01839	0.00829	-0.00627	0.00284	-0.00442	0.01446	-0.01439	0.00131	-0.00131	0.02805	-0.02461
1.47	-0.00196	-3.00377	0.07078	-0.05824	0.00829	-0.00627	0.02196	-0.03426	0.03784	-0.03766	0.00131	-0.00131	0.08363	-0.07762
1.68	-0.00458	-1.19246	0.03034	-0.02496	0.02689	-0.00355	0.00941	-0.01469	0.01629	-0.01621	0.00065	-0.00065	0.03580	-0.03338
1.88	0.00658	0.77295	0.01748	-0.01438	0.00490	-0.00648	0.00222	-0.00346	0.01143	-0.01138	0.00065	-0.00065	0.02158	-0.01976
2.09	0.00570	0.77193	0.01246	-0.01026	0.00699	-0.00924	0.00646	-0.00414	0.01333	-0.01326	0.00065	-0.00065	0.02059	-0.01960
2.30	0.00463	0.76484	0.00321	-0.00264	0.00698	-0.00922	0.01558	-0.00999	0.01663	-0.01655	0.00065	-0.00065	0.02406	-0.02159
2.51	0.00376	0.86069	0.00962	-0.01169	0.00328	-0.00434	0.01587	-0.01017	0.02075	-0.02065	0.00065	-0.00065	0.02803	-0.02618
2.72	0.01392	0.22975	0.00562	-0.00683	0.00117	-0.00089	0.00055	-0.00035	0.00567	-0.00564	0.00065	-0.00065	0.00811	-0.00893
2.93	0.02805	0.13624	0.00381	-0.00463	0.00152	-0.00115	0.00113	-0.00176	0.00284	-0.00282	0.00065	-0.00065	0.00516	-0.00585
3.14	0.04130	0.09818	0.00283	-0.00344	0.00128	-0.00097	0.00114	-0.00178	0.00193	-0.00192	0.00065	-0.00065	0.00389	-0.00448
3.35	0.02493	0.15434	0.00429	-0.00521	0.00171	-0.00129	0.00127	-0.00198	0.00319	-0.00318	0.00065	-0.00065	0.00579	-0.00658
3.56	0.01508	0.22351	0.00519	-0.00631	0.00108	-0.00082	0.00051	-0.00033	0.00523	-0.00521	0.00065	-0.00065	0.00750	-0.00825
3.77	0.00709	0.50913	0.00510	-0.00620	0.00174	-0.00230	0.00841	-0.00539	0.01100	-0.01095	0.00065	-0.00065	0.01487	-0.01389
3.98	0.00160	2.15717	0.00931	-0.00766	0.02021	-0.02672	0.04515	-0.02893	0.04819	-0.04795	0.00065	-0.00065	0.06969	-0.06253
4.19	-0.00418	-0.95240	0.01702	-0.01400	0.00955	-0.01262	0.00882	-0.00565	0.01819	-0.01811	0.00065	-0.00065	0.02811	-0.02675
4.40	0.00432	1.17638	0.02664	-0.02192	0.00747	-0.00988	0.00338	-0.00527	0.01742	-0.01734	0.00065	-0.00065	0.03288	-0.03012
4.61	0.00520	1.44112	0.02674	-0.02201	0.00237	-0.00313	0.00830	-0.01295	0.01436	-0.01429	0.00065	-0.00065	0.03156	-0.02943

Table 48: 20–40%, 7.0–9.0 \otimes 5.0–7.0 GeV/c Jet Function

ϕ	per trig yield	σ_{stat}/y	systematic errors											
			$+\sigma_{f2}/y$	$-\sigma_{f2}/y$	$+\sigma_{f3}/y$	$-\sigma_{f3}/y$	$+\sigma_{f4}/y$	$-\sigma_{f4}/y$	$+\sigma_{\xi}/y$	$-\sigma_{\xi}/y$	$+\sigma_{\pi^0}/y$	$-\sigma_{\pi^0}/y$	$+\sigma_{total}/y$	$-\sigma_{total}/y$
-1.47	-0.00052	-3.03669	0.02696	-0.02218	0.00590	-0.00427	0.01108	-0.01864	0.02735	-0.02549	0.01223	-0.01223	0.04221	-0.04071
-1.26	0.00059	2.59102	0.01971	-0.01622	0.01366	-0.00988	0.00331	-0.00557	0.02422	-0.02258	0.01223	-0.01223	0.03636	-0.03242
-1.05	-0.00102	-1.02270	0.00711	-0.00585	0.00985	-0.00713	0.00526	-0.00313	0.01423	-0.01327	0.01223	-0.01223	0.02296	-0.02050
-0.84	0.00202	0.62815	0.00075	-0.00062	0.00402	-0.00291	0.00519	-0.00308	0.00725	-0.00676	0.01223	-0.01223	0.01567	-0.01461
-0.63	-0.00126	-0.60038	0.00292	-0.00355	0.00246	-0.00178	0.00688	-0.00409	0.01179	-0.01100	0.01223	-0.01223	0.01872	-0.01740
-0.42	0.00005	16.97435	0.15932	-0.19365	0.04483	-0.06196	0.02239	-0.01331	0.30125	-0.28083	0.01223	-0.01223	0.34466	-0.34717
-0.21	0.01167	0.14936	0.00093	-0.00113	0.00050	-0.00069	0.00036	-0.00061	0.00130	-0.00121	0.01223	-0.01223	0.01235	-0.01237
-0.00	0.09367	0.04559	0.00013	-0.00015	0.00008	-0.00011	0.00007	-0.00011	0.00016	-0.00015	0.01223	-0.01223	0.01223	-0.01223
0.21	0.01115	0.15743	0.00097	-0.00118	0.00053	-0.00073	0.00038	-0.00064	0.00136	-0.00127	0.01223	-0.01223	0.01236	-0.01239
0.42	0.00020	4.14661	0.03896	-0.04736	0.01096	-0.01515	0.00548	-0.00326	0.07367	-0.06868	0.01223	-0.01223	0.08512	-0.08572
0.63	0.00065	1.65759	0.00562	-0.00683	0.00473	-0.00342	0.01324	-0.00787	0.02269	-0.02115	0.01223	-0.01223	0.02989	-0.02678
0.84	-0.00034	-2.94403	0.00444	-0.00365	0.02379	-0.01721	0.03073	-0.01826	0.04294	-0.04003	0.01223	-0.01223	0.05936	-0.04894
1.05	0.00074	1.94777	0.00983	-0.00808	0.01362	-0.00985	0.00727	-0.00432	0.01967	-0.01833	0.01223	-0.01223	0.02952	-0.02582
1.26	-0.00091	-1.56894	0.01290	-0.01062	0.00894	-0.00647	0.00217	-0.00365	0.01586	-0.01478	0.01223	-0.01223	0.02553	-0.02315
1.47	-0.00035	-5.02509	0.04024	-0.03311	0.00881	-0.00637	0.01654	-0.02782	0.04082	-0.03805	0.01223	-0.01223	0.06153	-0.05923
1.68	-0.00005	-41.54073	0.31093	-0.25582	0.04924	-0.06806	0.12779	-0.21497	0.31612	-0.29469	0.00730	-0.00730	0.46413	-0.45076
1.88	0.00141	1.19160	0.00831	-0.00683	0.00416	-0.00575	0.00140	-0.00235	0.01026	-0.00957	0.00730	-0.00730	0.01571	-0.01517
2.09	-0.00087	-1.26822	0.00831	-0.00684	0.00833	-0.01152	0.00615	-0.00366	0.01675	-0.01562	0.00730	-0.00730	0.02259	-0.02213
2.30	-0.00109	-0.79147	0.00139	-0.00114	0.00539	-0.00745	0.00962	-0.00572	0.01352	-0.01260	0.00730	-0.00730	0.01896	-0.01736
2.51	-0.00055	-1.63344	0.00665	-0.00809	0.00405	-0.00560	0.01567	-0.00932	0.02692	-0.02509	0.00730	-0.00730	0.03292	-0.02943
2.72	0.00500	0.26448	0.00159	-0.00193	0.00062	-0.00045	0.00022	-0.00013	0.00300	-0.00280	0.00730	-0.00730	0.00808	-0.00806
2.93	0.01117	0.16689	0.00097	-0.00118	0.00073	-0.00053	0.00038	-0.00064	0.00135	-0.00126	0.00730	-0.00730	0.00753	-0.00755
3.14	0.01617	0.12841	0.00074	-0.00089	0.00062	-0.00045	0.00039	-0.00066	0.00094	-0.00087	0.00730	-0.00730	0.00743	-0.00745
3.35	0.00734	0.22442	0.00148	-0.00180	0.00110	-0.00080	0.00058	-0.00098	0.00206	-0.00192	0.00730	-0.00730	0.00783	-0.00786
3.56	0.00140	0.73243	0.00570	-0.00693	0.00222	-0.00160	0.00080	-0.00048	0.01076	-0.01003	0.00730	-0.00730	0.01439	-0.01431
3.77	-0.00063	-1.49938	0.00581	-0.00707	0.00354	-0.00490	0.01369	-0.00814	0.02352	-0.02192	0.00730	-0.00730	0.02899	-0.02596
3.98	-0.00017	-6.98288	0.00909	-0.00748	0.03527	-0.04876	0.06298	-0.03744	0.08852	-0.08252	0.00730	-0.00730	0.11482	-0.10343
4.19	0.00059	2.64979	0.01232	-0.01014	0.01235	-0.01707	0.00912	-0.00542	0.02483	-0.02315	0.00730	-0.00730	0.03252	-0.03182
4.40	-0.00026	-5.33259	0.04567	-0.03758	0.02289	-0.03165	0.00768	-0.01291	0.05645	-0.05262	0.00730	-0.00730	0.07687	-0.07350
4.61	0.00334	1.01821	0.00423	-0.00348	0.00067	-0.00093	0.00174	-0.00292	0.00430	-0.00401	0.00730	-0.00730	0.00965	-0.00953

Table 49: 20–40%, 9.0–12.0 \otimes 0.5–1.0 GeV/c Jet Function

ϕ	per trig yield	σ_{stat}/y	systematic errors											
			$+\sigma_{f_2}/y$	$-\sigma_{f_2}/y$	$+\sigma_{f_3}/y$	$-\sigma_{f_3}/y$	$+\sigma_{f_4}/y$	$-\sigma_{f_4}/y$	$+\sigma_\xi/y$	$-\sigma_\xi/y$	$+\sigma_{\pi^0}/y$	$-\sigma_{\pi^0}/y$	$+\sigma_{total}/y$	$-\sigma_{total}/y$
-1.47	-0.04946	-4.50117	0.44682	-0.71387	0.02864	-0.03354	0.06040	-0.08078	0.56262	-0.56260	0.00689	-0.00689	0.72160	-0.91314
-1.26	-0.09263	-2.16825	0.19731	-0.31524	0.04003	-0.04689	0.01091	-0.01459	0.30081	-0.30081	0.00689	-0.00689	0.36220	-0.43854
-1.05	-0.10934	-1.46598	0.10330	-0.16505	0.04192	-0.04910	0.02000	-0.01495	0.25578	-0.25577	0.00689	-0.00689	0.27982	-0.30878
-0.84	-0.10536	-1.28930	0.02241	-0.03581	0.03519	-0.04122	0.04060	-0.03035	0.26695	-0.26695	0.00689	-0.00689	0.27331	-0.27425
-0.63	-0.03694	-3.27677	0.30191	-0.18897	0.03834	-0.04491	0.09576	-0.07160	0.76648	-0.76646	0.00689	-0.00689	0.83026	-0.79395
-0.42	0.07311	1.55749	0.33033	-0.20676	0.02269	-0.01937	0.00625	-0.00467	0.38975	-0.38974	0.00689	-0.00689	0.51149	-0.44169
-0.21	0.22680	0.47288	0.14538	-0.09100	0.01915	-0.01635	0.00965	-0.01290	0.12622	-0.12621	0.00689	-0.00689	0.19384	-0.15714
-0.00	0.29326	0.36557	0.12307	-0.07703	0.01831	-0.01563	0.01115	-0.01491	0.09777	-0.09777	0.00689	-0.00689	0.15879	-0.12652
0.21	0.21027	0.51807	0.15681	-0.09815	0.02066	-0.01764	0.01040	-0.01392	0.13614	-0.13614	0.00689	-0.00689	0.20906	-0.16947
0.42	-0.01838	-6.31079	1.31409	-0.82250	0.09027	-0.07707	0.02487	-0.01860	1.55048	-1.55044	0.00689	-0.00689	2.03461	-1.75691
0.63	-0.19142	-0.67105	0.05827	-0.03647	0.00740	-0.00867	0.01848	-0.01382	0.14792	-0.14792	0.00689	-0.00689	0.16038	-0.15338
0.84	-0.15300	-0.97216	0.01543	-0.02466	0.02424	-0.02839	0.02796	-0.02090	0.18383	-0.18383	0.00689	-0.00689	0.18828	-0.18892
1.05	-0.04922	-3.48432	0.22951	-0.36669	0.09313	-0.10908	0.04443	-0.03322	0.56827	-0.56826	0.00689	-0.00689	0.62154	-0.63588
1.26	0.10127	1.99813	0.18048	-0.28835	0.03662	-0.04289	0.00998	-0.01334	0.27515	-0.27515	0.00689	-0.00689	0.33132	-0.40115
1.47	-0.17995	-1.34704	0.12280	-0.19619	0.00787	-0.00922	0.01660	-0.02220	0.15462	-0.15462	0.00689	-0.00689	0.19843	-0.25105
1.68	-0.11186	-2.04794	0.19754	-0.31561	0.01483	-0.01266	0.02670	-0.03571	0.24895	-0.24894	0.00118	-0.00118	0.31927	-0.40375
1.88	-0.07995	-2.40869	0.22859	-0.36521	0.05432	-0.04638	0.01264	-0.01690	0.34928	-0.34927	0.00118	-0.00118	0.42114	-0.50775
2.09	0.27403	0.59513	0.04122	-0.06586	0.01959	-0.01673	0.00798	-0.00597	0.10234	-0.10234	0.00118	-0.00118	0.11235	-0.12299
2.30	0.45770	0.31615	0.00516	-0.00824	0.00949	-0.00810	0.00935	-0.00699	0.06159	-0.06159	0.00118	-0.00118	0.06323	-0.06306
2.51	0.29805	0.42844	0.03742	-0.02342	0.00557	-0.00475	0.01187	-0.00887	0.09508	-0.09508	0.00118	-0.00118	0.10303	-0.09845
2.72	0.16104	0.73381	0.14997	-0.09387	0.00880	-0.01030	0.00284	-0.00212	0.17681	-0.17680	0.00118	-0.00118	0.23203	-0.20046
2.93	0.48333	0.24169	0.06822	-0.04270	0.00767	-0.00899	0.00453	-0.00605	0.05910	-0.05910	0.00118	-0.00118	0.09070	-0.07372
3.14	0.34402	0.33736	0.10492	-0.06567	0.01332	-0.01561	0.00950	-0.01271	0.08312	-0.08312	0.00118	-0.00118	0.13486	-0.10783
3.35	0.35274	0.33293	0.09348	-0.05851	0.01051	-0.01231	0.00620	-0.00830	0.08098	-0.08097	0.00118	-0.00118	0.12428	-0.10101
3.56	0.26435	0.46525	0.09136	-0.05718	0.00536	-0.00628	0.00173	-0.00129	0.10771	-0.10770	0.00118	-0.00118	0.14135	-0.12212
3.77	0.31310	0.43122	0.03562	-0.02230	0.00530	-0.00452	0.01130	-0.00845	0.09051	-0.09051	0.00118	-0.00118	0.09807	-0.09371
3.98	0.21267	0.69156	0.01110	-0.01774	0.02042	-0.01744	0.02011	-0.01504	0.13255	-0.13255	0.00118	-0.00118	0.13607	-0.13570
4.19	0.03232	5.36643	0.34949	-0.55837	0.16610	-0.14182	0.06765	-0.05058	0.86772	-0.86770	0.00118	-0.00118	0.95250	-1.04276
4.40	0.02421	8.42221	0.75506	-1.20633	0.17943	-0.15320	0.04174	-0.05583	1.15370	-1.15367	0.00118	-0.00118	1.39107	-1.67713
4.61	-0.26215	-0.81862	0.08429	-0.13467	0.00633	-0.00540	0.01139	-0.01524	0.10623	-0.10623	0.00118	-0.00118	0.13624	-0.17229

 Table 50: 20–40%, 9.0–12.0 \otimes 1.0–2.0 GeV/c Jet Function

ϕ	per trig yield	σ_{stat}/y	systematic errors											
			$+\sigma_{f_2}/y$	$-\sigma_{f_2}/y$	$+\sigma_{f_3}/y$	$-\sigma_{f_3}/y$	$+\sigma_{f_4}/y$	$-\sigma_{f_4}/y$	$+\sigma_\xi/y$	$-\sigma_\xi/y$	$+\sigma_{\pi^0}/y$	$-\sigma_{\pi^0}/y$	$+\sigma_{total}/y$	$-\sigma_{total}/y$
-1.47	-0.11557	-0.95296	0.09801	-0.15743	0.08891	-0.01008	0.01930	-0.02523	0.06845	-0.06845	0.0050	-0.0050	5.12142	-0.17380
-1.26	-0.00228	43.07028	4.10544	-6.59443	1.18089	-1.33708	0.33067	-0.43223	3.47295	-3.47295	0.00500	-0.00500	5.51542	-7.58436
-1.05	0.04475	1.75514	0.12940	-0.20785	0.07444	-0.08429	0.03567	-0.02729	0.17819	-0.17819	0.00500	-0.00500	0.23518	-0.28775
-0.84	0.01095	5.90616	0.11051	-0.17751	0.24603	-0.27857	0.28504	-0.21807	0.73518	-0.73518	0.00500	-0.00500	0.83335	-0.83495
-0.63	-0.03736	-1.54029	0.15384	-0.09578	0.02755	-0.03119	0.06912	-0.05287	0.21816	-0.21816	0.00500	-0.00500	0.27713	-0.24604
-0.42	0.21554	0.25892	0.05774	-0.03595	0.00541	-0.00478	0.00155	-0.00118	0.03827	-0.03827	0.00500	-0.00500	0.06950	-0.05274
-0.21	0.34891	0.15265	0.04070	-0.03032	0.00874	-0.00772	0.00468	-0.00612	0.02384	-0.02384	0.00500	-0.00500	0.05513	-0.03981
-0.00	0.47210	0.11012	0.03940	-0.02453	0.00799	-0.00706	0.00517	-0.00676	0.01768	-0.01768	0.00500	-0.00500	0.04422	-0.03178
0.21	0.35559	0.15041	0.04779	-0.02975	0.00858	-0.00758	0.00460	-0.00601	0.02340	-0.02340	0.00500	-0.00500	0.05409	-0.03907
0.42	0.08492	0.65609	0.14657	-0.09125	0.01372	-0.01212	0.00393	-0.00301	0.09713	-0.09713	0.00500	-0.00500	0.17641	-0.13385
0.63	0.03596	1.72779	0.15983	-0.09950	0.02862	-0.03242	0.01780	-0.015493	0.22663	-0.22665	0.00500	-0.00500	0.28790	-0.25561
0.84	-0.17043	-0.01038	0.07170	-0.01441	0.15811	-0.00490	0.02127	-0.01729	0.07179	-0.07179	0.00500	-0.00500	0.53356	-0.05366
1.05	-0.07307	-0.09733	0.07057	-0.12523	0.04043	-0.05099	0.02132	-0.01651	0.10779	-0.10779	0.00500	-0.00500	0.14068	-0.0106
1.26	-0.09389	-4.91324	0.47095	-0.75648	0.13547	-0.15338	0.03793	-0.04958	0.39840	-0.39840	0.00500	-0.00500	0.63270	-0.87004
1.47	-0.11772	-1.03806	0.09622	-0.15456	0.00874	-0.00990	0.01895	-0.02477	0.06720	-0.06720	0.00500	-0.00500	0.11921	-0.17064
1.68	-0.00583	-19.76442	1.94347	-0.312174	0.19996	-0.17661	0.38275	-0.50031	1.36006	-1.36006	0.00700	-0.00700	2.41109	-3.44623
1.88	0.06175	1.55313	0.15172	-0.24371	0.04941	-0.04364	0.01222	-0.01597	0.12902	-0.12902	0.00700	-0.00700	0.20557	-0.27965
2.09	0.07079	1.11203	0.08179	-0.13138	0.05328	-0.04705	0.02254	-0.01725	0.11336	-0.11336	0.00700	-0.00700	0.15128	-0.18061
2.30	0.14572	0.47124	0.00831	-0.01334	0.02094	-0.01849	0.02143	-0.01639	0.05554	-0.05554	0.00700	-0.00700	0.06366	-0.06224
2.51	0.15922	0.38314	0.03610	-0.02248	0.00732	-0.00646	0.01622	-0.01241	0.05129	-0.05129	0.00700	-0.00700	0.06520	-0.05773
2.72	0.12318	0.45200	0.10104	-0.06290	0.00836	-0.00946	0.00271	-0.00207	0.06683	-0.06683	0.00700	-0.00700	0.12146	-0.09229
2.93	0.22502	0.24711	0.07552	-0.04701	0.01198	-0.01356	0.00726	-0.00949	0.03679	-0.03679	0.00700	-0.00700	0.08516	-0.06195
3.14	0.32356	0.17552	0.05749	-0.0										

Table 51: 20–40%, 9.0–12.0 \otimes 2.0–3.0 GeV/c Jet Function

ϕ	per trig yield	σ_{stat}/y	systematic errors												
			$+\sigma_{f2}/y$	$-\sigma_{f2}/y$	$+\sigma_{f3}/y$	$-\sigma_{f3}/y$	$+\sigma_{f4}/y$	$-\sigma_{f4}/y$	$+\sigma_\xi/y$	$-\sigma_\xi/y$	$+\sigma_{\pi^0}/y$	$-\sigma_{\pi^0}/y$	$+\sigma_{total}/y$	$-\sigma_{total}/y$	
-1.47	0.03276	1.00228	0.04055	-0.06435	0.00403	-0.00476	0.01051	-0.01375	0.01949	-0.01951	0.00059	-0.00059	0.04638	-0.06881	
-1.26	-0.03302	-0.72106	0.03327	-0.05280	0.01046	-0.01237	0.00353	-0.00461	0.01937	-0.01939	0.00059	-0.00059	0.04006	-0.05778	
-1.05	0.02928	0.78401	0.02319	-0.03680	0.01458	-0.01725	0.00842	-0.00644	0.02202	-0.02204	0.00059	-0.00059	0.03614	-0.04668	
-0.84	0.00636	2.69960	0.02233	-0.03544	0.05434	-0.06428	0.07588	-0.05799	0.10282	-0.10293	0.00059	-0.00059	0.14065	-0.13909	
-0.63	0.01433	1.14114	0.04648	-0.02928	0.00921	-0.01089	0.02784	-0.02128	0.04642	-0.04647	0.00059	-0.00059	0.07194	-0.05991	
-0.42	0.02462	0.60745	0.05857	-0.03691	0.00634	-0.00536	0.00209	-0.00160	0.02750	-0.02752	0.00059	-0.00059	0.06505	-0.04638	
-0.21	0.15785	0.11399	0.01247	-0.00786	0.00259	-0.00219	0.00160	-0.00209	0.00434	-0.00435	0.00059	-0.00059	0.01357	-0.00950	
-0.00	0.33647	0.06009	0.00641	-0.00404	0.00150	-0.00127	0.00112	-0.00147	0.00203	-0.00205	0.00059	-0.00059	0.00701	-0.00496	
0.21	0.16550	0.10915	0.01190	-0.00750	0.00247	-0.00209	0.00152	-0.00199	0.00414	-0.00415	0.00059	-0.00059	0.01294	-0.00906	
0.42	0.03391	0.46065	0.04252	-0.02679	0.00460	-0.00389	0.00152	-0.00116	0.01996	-0.01998	0.00059	-0.00059	0.04723	-0.03367	
0.63	0.00105	16.09724	0.63211	-0.39828	0.12522	-0.14812	0.37861	-0.28937	0.63135	-0.63201	0.00059	-0.00059	0.97836	-0.81471	
0.84	0.01166	1.64079	0.01217	-0.01931	0.02961	-0.03503	0.04135	-0.03160	0.05603	-0.05609	0.00059	-0.00059	0.07665	-0.07580	
1.05	-0.01837	-1.15566	0.03696	-0.05865	0.02324	-0.02749	0.01342	-0.01026	0.03509	-0.03512	0.00059	-0.00059	0.05760	-0.07440	
1.26	0.03293	0.84206	0.03337	-0.05296	0.01049	-0.01241	0.00354	-0.00463	0.01943	-0.01945	0.00059	-0.00059	0.04017	-0.05795	
1.47	-0.02783	-1.11783	0.04773	-0.07575	0.00474	-0.00561	0.01237	-0.01619	0.02295	-0.02297	0.00059	-0.00059	0.05460	-0.08100	
1.68	0.00241	13.42146	0.55037	-0.87348	0.06466	-0.05466	0.14265	-0.18664	0.26550	-0.26578	0.00093	-0.00093	0.63082	-0.93350	
1.88	0.01205	2.11941	0.09114	-0.14465	0.03390	-0.02865	0.00966	-0.01264	0.05354	-0.05359	0.00093	-0.00093	0.11143	-0.15741	
2.09	-0.01801	-1.13809	0.03770	-0.05983	0.02804	-0.02370	0.01369	-0.01046	0.03618	-0.03622	0.00093	-0.00093	0.06087	-0.07459	
2.30	0.01439	1.26349	0.00986	-0.01565	0.02839	-0.02400	0.03351	-0.02561	0.04581	-0.04585	0.00093	-0.00093	0.06423	-0.05983	
2.51	-0.00094	-17.21125	0.71002	-0.44738	0.16638	-0.14065	0.42528	-0.32504	0.71149	-0.71224	0.00093	-0.00093	1.10404	-0.91262	
2.72	0.03139	0.48347	0.04595	-0.02895	0.00420	-0.00497	0.00164	-0.00126	0.02150	-0.02152	0.00093	-0.00093	0.05094	-0.03645	
2.93	0.09233	0.18780	0.02132	-0.01344	0.00374	-0.00443	0.00273	-0.00357	0.00737	-0.00737	0.00093	-0.00093	0.02305	-0.01637	
3.14	0.09594	0.17579	0.02246	-0.01415	0.00445	-0.00526	0.00393	-0.00514	0.00711	-0.00712	0.00093	-0.00093	0.02432	-0.01749	
3.35	0.03631	0.44739	0.05422	-0.03417	0.00954	-0.01125	0.00694	-0.00909	0.01873	-0.01875	0.00093	-0.00093	0.05857	-0.04158	
3.56	0.05899	0.27679	0.02445	-0.01540	0.00224	-0.00265	0.00087	-0.00067	0.01144	-0.01145	0.00093	-0.00093	0.02711	-0.01941	
3.77	0.01284	1.33256	0.05189	-0.03269	0.01216	-0.01028	0.03108	-0.02375	0.05199	-0.05205	0.00093	-0.00093	0.08069	-0.06670	
3.98	0.03760	0.51989	0.00377	-0.00599	0.01087	-0.00919	0.01283	-0.00980	0.01753	-0.01755	0.00093	-0.00093	0.02460	-0.02292	
4.19	-0.00670	-3.35393	0.10128	-0.16073	0.07533	-0.06368	0.03677	-0.02811	0.09720	-0.09731	0.00093	-0.00093	0.16350	-0.20037	
4.40	-0.02785	-0.89387	0.03945	-0.06260	0.01467	-0.01240	0.00418	-0.00547	0.02317	-0.02320	0.00093	-0.00093	0.04823	-0.06813	
4.61	-0.00536	-6.32290	0.24784	-0.39335	0.02912	-0.02462	0.06424	-0.08405	0.11956	-0.11969	0.00093	-0.00093	0.28407	-0.42038	

Table 52: 20–40%, 9.0–12.0 \otimes 3.0–5.0 GeV/c Jet Function

ϕ	per trig yield	σ_{stat}/y	systematic errors												
			$+\sigma_{f2}/y$	$-\sigma_{f2}/y$	$+\sigma_{f3}/y$	$-\sigma_{f3}/y$	$+\sigma_{f4}/y$	$-\sigma_{f4}/y$	$+\sigma_\xi/y$	$-\sigma_\xi/y$	$+\sigma_{\pi^0}/y$	$-\sigma_{\pi^0}/y$	$+\sigma_{total}/y$	$-\sigma_{total}/y$	
-1.47	-0.00235	-4.56212	0.07664	-0.12279	0.00809	-0.00959	0.02333	-0.03024	0.03358	-0.03370	0.00035	-0.00035	0.08724	-0.13122	
-1.26	-0.00549	-1.48615	0.02715	-0.04350	0.00908	-0.01076	0.00338	-0.00438	0.01440	-0.01445	0.00035	-0.00035	0.03223	-0.04729	
-1.05	0.00486	1.72917	0.01896	-0.03038	0.01268	-0.01502	0.00801	-0.00618	0.01639	-0.01645	0.00035	-0.00035	0.02921	-0.03818	
-0.84	-0.00287	-1.99616	0.00671	-0.01075	0.01736	-0.02057	0.02652	-0.02047	0.02813	-0.02824	0.00035	-0.00035	0.04291	-0.04189	
-0.63	0.00259	2.31502	0.03526	-0.02201	0.00736	-0.00872	0.02434	-0.01878	0.03178	-0.03190	0.00035	-0.00035	0.05386	-0.04394	
-0.42	0.00191	2.72749	0.10345	-0.06456	0.01181	-0.00997	0.00426	-0.00329	0.04386	-0.04402	0.00035	-0.00035	0.11306	-0.07884	
-0.21	0.10137	0.10307	0.00266	-0.00166	0.00058	-0.00049	0.00040	-0.00051	0.00084	-0.00084	0.00035	-0.00035	0.00290	-0.00202	
-0.00	0.27720	0.05310	0.00107	-0.00067	0.00026	-0.00022	0.00022	-0.00028	0.00031	-0.00031	0.00035	-0.00035	0.00121	-0.00089	
0.21	0.08946	0.11193	0.00302	-0.00188	0.00066	-0.00056	0.00045	-0.00058	0.00095	-0.00095	0.00035	-0.00035	0.00328	-0.00229	
0.42	0.01334	0.48802	0.01482	-0.00925	0.00169	-0.00143	0.00061	-0.00047	0.00628	-0.00631	0.00035	-0.00035	0.01620	-0.01130	
0.63	-0.00495	-1.13110	0.01844	-0.01151	0.00385	-0.00456	0.01273	-0.00982	0.01662	-0.01668	0.00035	-0.00035	0.02816	-0.02298	
0.84	0.01661	0.50660	0.00116	-0.00186	0.00300	-0.00356	0.00459	-0.00354	0.00486	-0.00488	0.00035	-0.00035	0.00743	-0.00725	
1.05	0.00792	1.26096	0.01164	-0.01865	0.00778	-0.00922	0.00492	-0.00379	0.01006	-0.01010	0.00035	-0.00035	0.01793	-0.02344	
1.26	-0.00374	-2.09355	0.03987	-0.06388	0.01333	-0.01580	0.00496	-0.00643	0.02115	-0.02123	0.00035	-0.00035	0.04732	-0.06944	
1.47	0.00788	1.74856	0.02290	-0.03669	0.00242	-0.00287	0.00697	-0.00903	0.01003	-0.01007	0.00035	-0.00035	0.02607	-0.03921	
1.68	-0.00468	-2.28340	0.03852	-0.06171	0.00482	-0.00407	0.01173	-0.01520	0.01694	-0.01700	0.00218	-0.00218	0.04400	-0.06595	
1.88	-0.00135	-6.44568	0.11082	-0.17756	0.04390	-0.03705	0.01380	-0.01788	0.05933	-0.05955	0.00218	-0.00218	0.13388	-0.19176	
2.09	-0.00170	-4.45410	0.05413	-0.08672	0.04289	-0.03619	0.02287	-0.01764	0.04734	-0.04752	0.00218	-0.00218	0.08682	-0.10680	
2.30	0.00315	2.10666	0.00611	-0.00979	0.01873	-0.01581	0.02415	-0.01863	0.02585	-0.02595	0.00218	-0.00218	0.04055	-0.03703	
2.51	0.00412	1.52634	0.02214	-0.01382	0.00547	-0.00462	0.01528	-0.01179	0.02002	-0.02010	0.00218	-0.00218	0.03405	-0.02757	
2.72	0.02751	0.25674	0.00718	-0.00448	0.00069	-0.00082	0.00030	-0.00023	0.00304	-0.00305	0.00218	-0.00218	0.00813	-0.00591	
2.93	0.04239	0.19550	0.00637	-0.00397	0.00118	-0.00139	0.00095	-0.00123	0.00199	-0.00199	0.00218	-0.00218	0.00718	-0.00529	
3.14	0.07461	0.12781	0.00396	-0.00247	0.00083	-0.00098	0.00081	-0.00104	0.00113	-0.00114	0.00218	-0.00218	0.00480	-0.00377	
3.35	0.05307	0.17106	0.00508	-0.00317	0.00094	-0.00111	0.00076	-0.00098	0.00159	-0.00159	0.00218	-0.00218	0.00588	-0.00442	
3.56	0.00547	1.05983	0.03615	-0.02256	0.00348	-0.00413	0.00149	-0.00115	0.01527	-0.01533	0.00218	-0.00218	0.03948	-0.02770	
3.77	0.01008	0.70193	0.00906	-0.00565	0.00224	-0.00189	0.00625	-0.00482	0.00819	-0.00822	0.00218	-0.00218	0.01407	-0.01145	
3.98	-0.00657	-0.87111	0.00293	-0.00470	0.00900	-0.00759	0.01160	-0.00895	0.01242	-0.01246	0.00218	-0.00218	0.01957	-0.01788	
4.19	0.00228	3.76261	0.04046	-0.06483	0.03206	-0.02706	0.01709	-0.01319	0.03539	-0.03552	0.00218	-0.00218	0.06492	-0.07985	
4.40	-0.00081	-11.95136	0.18315	-0.29345	0.07256	-0.06123	0.02280	-0.02955	0.09806	-0.09842	0.00218	-0.00218	0.22125	-0.31690	
4.61	0.00066	19.70056	0.27254	-0.43666	0.03411	-0.02879	0.08297	-0.10753	0.11984	-0.12028	0.00218	-0.00218	0.31095	-0.46641	

Table 53: 20–40%, 9.0–12.0 \otimes 5.0–7.0 GeV/c Jet Function

ϕ	per trig yield	σ_{stat}/y	systematic errors												
			$+\sigma_{f2}/y$	$-\sigma_{f2}/y$	$+\sigma_{f3}/y$	$-\sigma_{f3}/y$	$+\sigma_{f4}/y$	$-\sigma_{f4}/y$	$+\sigma_\xi/y$	$-\sigma_\xi/y$	$+\sigma_{\pi^0}/y$	$-\sigma_{\pi^0}/y$	$+\sigma_{total}/y$	$-\sigma_{total}/y$	
-1.47	-0.00331	-0.00000	0.00537	-0.000803	0.00096	-0.00071	0.00164	-0.00296	0.00453	-0.00424	0.00273	-0.00273	0.00777	-0.00996	
-1.26	-0.00033	-8.95037	0.04404	-0.06587	0.02500	-0.01846	0.00549	-0.00992	0.04501	-0.04209	0.00273	-0.00273	0.06803	-0.08098	
-1.05	-0.00170	-0.96158	0.00533	-0.00798	0.00605	-0.00447	0.00314	-0.00174	0.00887	-0.00830	0.00273	-0.00273	0.01269	-0.01276	
-0.84	0.00196	1.22252	0.00097	-0.00145	0.00426	-0.00314	0.00535	-0.00296	0.00780	-0.00729	0.00273	-0.00273	0.01077	-0.00902	
-0.63	-0.00053	-3.17412	0.01594	-0.01066	0.00605	-0.00447	0.01645	-0.00911	0.02937	-0.02747	0.00273	-0.00273	0.03784	-0.03128	
-0.42	0.00046	3.79262	0.03922	-0.02622	0.00508	-0.00687	0.00242	-0.00134	0.03381	-0.03161	0.00273	-0.00273	0.05216	-0.04175	
-0.21	0.01671	0.23491	0.00149	-0.00099	0.00037	-0.00050	0.00024	-0.00043	0.00095	-0.00089	0.00273	-0.00273	0.00328	-0.00310	
-0.00	0.14257	0.07110	0.00019	-0.00013	0.00005	-0.00007	0.00004	-0.00008	0.00011	-0.00010	0.00273	-0.00273	0.00274	-0.00273	
0.21	0.01571	0.25851	0.00158	-0.00106	0.00039	-0.00053	0.00025	-0.00046	0.00101	-0.00094	0.00273	-0.00273	0.00334	-0.00315	
0.42	-0.00137	-1.13045	0.01329	-0.00888	0.00172	-0.00233	0.00082	-0.00045	0.01145	-0.01071	0.00273	-0.00273	0.01785	-0.01437	
0.63	0.00178	1.31158	0.00473	-0.00316	0.00180	-0.00133	0.00488	-0.00270	0.00872	-0.00815	0.00273	-0.00273	0.01153	-0.00964	
0.84	-0.00105	-1.56828	0.00181	-0.00271	0.00795	-0.00587	0.00999	-0.00553	0.01456	-0.01362	0.00273	-0.00273	0.01965	-0.01629	
1.05	-0.00139	-1.39893	0.00653	-0.00976	0.00741	-0.00547	0.00385	-0.00213	0.01086	-0.01016	0.00273	-0.00273	0.01542	-0.01550	
1.26	-0.00332	-0.00000	0.00443	-0.00663	0.00252	-0.00186	0.00055	-0.00100	0.00453	-0.00424	0.00273	-0.00273	0.00736	-0.00859	
1.47	0.00806	0.84805	0.00220	-0.00330	0.00040	-0.00029	0.00067	-0.00121	0.00186	-0.00174	0.00273	-0.00273	0.00405	-0.00479	
1.68	-0.00332	-0.00000	0.00536	-0.00802	0.00071	-0.00096	0.00163	-0.00295	0.00453	-0.00424	0.00484	-0.00484	0.00871	-0.01074	
1.88	-0.00087	-2.84720	0.01695	-0.02535	0.00710	-0.00962	0.00211	-0.00382	0.01741	-0.01628	0.00484	-0.00484	0.02586	-0.03222	
2.09	0.00051	5.42354	0.01798	-0.02689	0.01507	-0.02041	0.01060	-0.00587	0.03011	-0.02815	0.00484	-0.00484	0.03991	-0.04461	
2.30	0.00252	1.05529	0.00076	-0.00113	0.00245	-0.00332	0.00417	-0.00231	0.00611	-0.00571	0.00484	-0.00484	0.00920	-0.00858	
2.51	0.00281	0.90909	0.00299	-0.00200	0.00084	-0.00114	0.00309	-0.00171	0.00552	-0.00517	0.00484	-0.00484	0.00855	-0.00764	
2.72	0.00662	0.42399	0.00275	-0.00184	0.00048	-0.00036	0.00017	-0.00009	0.00237	-0.00221	0.00484	-0.00484	0.00607	-0.00564	
2.93	0.02150	0.21869	0.00116	-0.00077	0.00039	-0.00029	0.00018	-0.00033	0.00073	-0.00069	0.00484	-0.00484	0.00505	-0.00497	
3.14	0.02425	0.19415	0.00112	-0.00075	0.00043	-0.00031	0.00024	-0.00044	0.00065	-0.00061	0.00484	-0.00484	0.00503	-0.00496	
3.35	0.00845	0.39950	0.00294	-0.00197	0.00099	-0.00073	0.00047	-0.00085	0.00186	-0.00174	0.00484	-0.00484	0.00606	-0.00562	
3.56	0.00091	1.96345	0.02000	-0.01337	0.00350	-0.00259	0.00123	-0.00068	0.01721	-0.01609	0.00484	-0.00484	0.02708	-0.02164	
3.77	0.00237	1.13104	0.00354	-0.00237	0.00099	-0.00134	0.00366	-0.00202	0.00654	-0.00612	0.00484	-0.00484	0.00965	-0.00851	
3.98	-0.00021	-8.54968	0.00884	-0.01323	0.02870	-0.03886	0.04881	-0.02701	0.07150	-0.06686	0.00484	-0.00484	0.09176	-0.08311	
4.19	-0.00336	-0.00000	0.00271	-0.00405	0.00227	-0.00307	0.00160	-0.00088	0.00453	-0.00424	0.00484	-0.00484	0.00768	-0.00824	
4.40	0.00276	1.61765	0.00533	-0.00797	0.00223	-0.00302	0.00066	-0.00120	0.00547	-0.00512	0.00484	-0.00484	0.00934	-0.01112	
4.61	-0.00008	-42.67049	0.23361	-0.34945	0.03094	-0.04189	0.07121	-0.12866	0.19750	-0.18467	0.00484	-0.00484	0.31564	-0.41779	

Table 54: 20–40%, 12.0–15.0 \otimes 0.5–1.0 GeV/c Jet Function

ϕ	per trig yield	σ_{stat}/y	systematic errors											
			$+\sigma_{f2}/y$	$-\sigma_{f2}/y$	$+\sigma_{f3}/y$	$-\sigma_{f3}/y$	$+\sigma_{f4}/y$	$-\sigma_{f4}/y$	$+\sigma_\xi/y$	$-\sigma_\xi/y$	$+\sigma_{\pi^0}/y$	$-\sigma_{\pi^0}/y$	$+\sigma_{total}/y$	$-\sigma_{total}/y$
-1.47	0.91967	0.63002	0.02503	-0.08245	0.00159	-0.00316	0.00445	-0.00443	0.03115	-0.03115	0.00490	-0.00490	0.04053	-0.08844
-1.26	-0.08282	-6.00896	0.22987	-0.75721	0.04618	-0.09191	0.01670	-0.01665	0.34638	-0.34637	0.00490	-0.00490	0.41863	-0.83791
-1.05	0.03640	10.78682	0.32326	-1.06485	0.12987	-0.25849	0.06131	-0.06150	0.79109	-0.79107	0.00490	-0.00490	0.86658	-1.35289
-0.84	-0.20481	-1.61188	0.01201	-0.03956	0.01867	-0.03717	0.02132	-0.02138	0.14139	-0.14138	0.00490	-0.00490	0.14478	-0.15302
-0.63	-0.27925	-1.02832	0.08578	-0.02604	0.00523	-0.01041	0.01293	-0.01297	0.10439	-0.10438	0.00490	-0.00490	0.13592	-0.10897
-0.42	0.42711	0.65974	0.12144	-0.03687	0.00681	-0.00342	0.00109	-0.00110	0.06868	-0.06868	0.00490	-0.00490	0.13977	-0.07818
-0.21	0.25521	1.03838	0.27748	-0.08424	0.02983	-0.01498	0.01174	-0.01170	0.11546	-0.11546	0.00490	-0.00490	0.30229	-0.14426
-0.00	0.35955	0.73643	0.21559	-0.06545	0.02617	-0.01315	0.01245	-0.01241	0.08209	-0.08209	0.00490	-0.00490	0.23256	-0.10664
0.21	0.21756	1.25747	0.32550	-0.09881	0.03499	-0.01758	0.01377	-0.01373	0.13544	-0.13544	0.00490	-0.00490	0.35458	-0.16920
0.42	0.49970	0.60332	0.10380	-0.03151	0.00582	-0.00292	0.00093	-0.00094	0.05870	-0.05870	0.00490	-0.00490	0.11949	-0.06687
0.63	0.28674	1.15700	0.08354	-0.02536	0.00509	-0.01014	0.01259	-0.01263	0.10166	-0.10165	0.00490	-0.00490	0.13237	-0.10613
0.84	0.20974	1.93004	0.01173	-0.03863	0.01823	-0.03629	0.02082	-0.02088	0.13806	-0.13806	0.00490	-0.00490	0.14138	-0.14943
1.05	0.01492	30.25184	0.78879	-2.59835	0.31690	-0.63075	0.14961	-0.15007	1.93034	-1.93029	0.00490	-0.00490	2.11453	-3.30119
1.26	-0.05908	-8.89812	0.32224	-1.06150	0.06473	-0.12884	0.02342	-0.02335	0.48558	-0.48556	0.00490	-0.00490	0.58684	-1.17462
1.47	0.43400	1.50545	0.05304	-0.17471	0.00337	-0.00670	0.00942	-0.00939	0.06601	-0.06600	0.00490	-0.00490	0.08540	-0.18718
1.68	-0.81628	-0.69995	0.02820	-0.09289	0.00356	-0.00179	0.00501	-0.00500	0.03512	-0.03512	0.00088	-0.00088	0.04547	-0.09945
1.88	-0.31958	-1.51467	0.05957	-0.19623	0.02382	-0.01197	0.00433	-0.00432	0.08997	-0.08996	0.00088	-0.00088	0.11059	-0.21625
2.09	-0.08761	-4.56028	0.13430	-0.44240	0.10739	-0.05396	0.02547	-0.02555	0.32956	-0.32955	0.00088	-0.00088	0.37260	-0.55487
2.30	0.36620	0.96659	0.00672	-0.02213	0.02079	-0.01044	0.01192	-0.01196	0.07925	-0.07924	0.00088	-0.00088	0.08307	-0.08380
2.51	0.39433	0.78357	0.06075	-0.01844	0.00737	-0.00370	0.00916	-0.00919	0.07398	-0.07398	0.00088	-0.00088	0.09645	-0.07689
2.72	1.23417	0.24782	0.04203	-0.01276	0.00118	-0.00236	0.00038	-0.00038	0.02375	-0.02375	0.00088	-0.00088	0.04830	-0.02708
2.93	0.03209	8.77772	2.20706	-0.67000	0.11919	-0.23723	0.09337	-0.09308	0.91638	-0.91636	0.00088	-0.00088	2.39453	-1.16343
3.14	0.78805	0.37166	0.09837	-0.02986	0.00600	-0.01194	0.00568	-0.00566	0.03735	-0.03735	0.00088	-0.00088	0.10555	-0.04962
3.35	0.72689	0.39955	0.09742	-0.02957	0.00526	-0.01047	0.00412	-0.00411	0.04045	-0.04045	0.00088	-0.00088	0.10570	-0.05136
3.56	0.79071	0.39422	0.06560	-0.01991	0.00185	-0.00368	0.00059	-0.00059	0.03707	-0.03707	0.00088	-0.00088	0.07538	-0.04225
3.77	-0.04856	-6.76926	0.49330	-0.14975	0.05987	-0.03008	0.07436	-0.07459	0.60079	-0.60078	0.00088	-0.00088	0.78321	-0.62436
3.98	0.31951	1.17158	0.00770	-0.02536	0.02382	-0.01197	0.01366	-0.01371	0.09083	-0.09083	0.00088	-0.00088	0.09521	-0.09604
4.19	0.01220	38.23568	0.96469	-3.17779	0.77141	-0.38737	0.18297	-0.18354	2.36726	-2.36721	0.00088	-0.00088	2.67640	-3.98571
4.40	0.59790	0.89107	0.03184	-0.10489	0.01273	-0.00640	0.00231	-0.00231	0.04809	-0.04809	0.00088	-0.00088	0.05911	-0.11559
4.61	0.54807	1.03057	0.04200	-0.13835	0.00530	-0.00267	0.00746	-0.00744	0.05231	-0.05231	0.00088	-0.00088	0.06771	-0.14812

Table 55: 20–40%, 12.0–15.0 \otimes 1.0–2.0 GeV/c Jet Function

ϕ	per trig yield	σ_{stat}/y	systematic errors											
			$+\sigma_{f2}/y$	$-\sigma_{f2}/y$	$+\sigma_{f3}/y$	$-\sigma_{f3}/y$	$+\sigma_{f4}/y$	$-\sigma_{f4}/y$	$+\sigma_\xi/y$	$-\sigma_\xi/y$	$+\sigma_{\pi^0}/y$	$-\sigma_{\pi^0}/y$	$+\sigma_{total}/y$	$-\sigma_{total}/y$
-1.47	-0.28723	-0.90917	0.04109	-0.13641	0.00369	-0.00698	0.01078	-0.01037	0.02877	-0.02877	0.00126	-0.00126	0.05145	-0.13997
-1.26	-0.17678	-1.32560	0.05522	-0.18331	0.01570	-0.02971	0.00592	-0.00570	0.04682	-0.04683	0.00126	-0.00126	0.07433	-0.19160
-1.05	0.07088	2.70187	0.08512	-0.28257	0.04840	-0.09158	0.02299	-0.02391	0.11749	-0.11750	0.00126	-0.00126	0.15467	-0.32033
-0.84	0.14279	1.12379	0.00883	-0.02932	0.01944	-0.03678	0.02233	-0.02322	0.05890	-0.05890	0.00126	-0.00126	0.06652	-0.07888
-0.63	-0.00251	-55.31182	4.92589	-1.48384	0.42190	-0.79828	1.04946	-1.09110	3.38745	-3.38760	0.00126	-0.00126	6.08429	-3.93769
-0.42	0.21199	0.64125	0.12643	-0.03809	0.00946	-0.00500	0.00161	-0.00167	0.04063	-0.04063	0.00126	-0.00126	0.13315	-0.05595
-0.21	0.57444	0.23759	0.06370	-0.01919	0.00914	-0.00483	0.00395	-0.00380	0.01512	-0.01512	0.00126	-0.00126	0.06624	-0.02522
-0.00	0.51040	0.25370	0.07848	-0.02364	0.01272	-0.00672	0.00664	-0.00639	0.01707	-0.01707	0.00126	-0.00126	0.08160	-0.03063
0.21	0.40231	0.33297	0.09096	-0.02740	0.01305	-0.00690	0.00564	-0.00542	0.02159	-0.02159	0.00126	-0.00126	0.09457	-0.03599
0.42	0.00244	56.54071	10.98116	-3.30789	0.82184	-0.43436	0.13960	-0.14514	3.52862	-3.52878	0.00126	-0.00126	11.56425	-4.85842
0.63	0.10835	1.48506	0.11424	-0.03441	0.00978	-0.01851	0.02434	-0.02530	0.07856	-0.07856	0.00126	-0.00126	0.14111	-0.09133
0.84	0.10494	1.85069	0.01202	-0.03990	0.02645	-0.05004	0.03038	-0.03159	0.08014	-0.08014	0.00126	-0.00126	0.09050	-0.10732
1.05	0.11025	2.02751	0.05472	-0.18166	0.03112	-0.05888	0.01478	-0.01537	0.07554	-0.07554	0.00126	-0.00126	0.09944	-0.20594
1.26	-0.02277	-11.30447	0.42865	-1.42297	0.12188	-0.23060	0.04599	-0.04423	0.36349	-0.36350	0.00126	-0.00126	0.57691	-1.48732
1.47	0.02596	13.14550	0.45470	-1.50946	0.04084	-0.07728	0.11928	-0.11472	0.31834	-0.31835	0.00126	-0.00126	0.56920	-1.54885
1.68	-0.30358	-0.93250	0.03888	-0.12906	0.00661	-0.00349	0.01020	-0.00981	0.02727	-0.02727	0.00183	-0.00183	0.04905	-0.13234
1.88	0.34156	0.75567	0.02858	-0.09488	0.01538	-0.00813	0.00307	-0.00295	0.02436	-0.02436	0.00183	-0.00183	0.04074	-0.09835
2.09	0.31013	0.66325	0.01945	-0.06458	0.02093	-0.01106	0.00526	-0.00546	0.02702	-0.02702	0.00183	-0.00183	0.03972	-0.07111
2.30	0.16844	1.00062	0.00749	-0.02486	0.03118	-0.01648	0.01893	-0.01968	0.05018	-0.05019	0.00183	-0.00183	0.06251	-0.06163
2.51	0.27329	0.55011	0.04529	-0.01364	0.00734	-0.00388	0.00963	-0.01003	0.03121	-0.03121	0.00183	-0.00183	0.05635	-0.03577
2.72	0.07371	1.79214	0.36360	-0.10953	0.01438	-0.02721	0.00462	-0.00481	0.11662	-0.11662	0.00183	-0.00183	0.38215	-0.16237
2.93	0.35058	0.39668	0.10438	-0.03144	0.00792	-0.01498	0.00647	-0.00622	0.02466	-0.02466	0.00183	-0.00183	0.10775	-0.04316
3.14	0.35297	0.39827	0.11348	-0.03418	0.00972	-0.01839	0.00960	-0.00923	0.02454	-0.02454	0.00183	-0.00183	0.11692	-0.04688
3.35	0.32651	0.43080	0.11207	-0.03376	0.00850	-0.01608	0.00693	-0.00668	0.02647	-0.02647	0.00183	-0.00183	0.11569	-0.04634
3.56	0.38121	0.38978	0.07031	-0.02118	0.00278	-0.00526	0.00089	-0.00093	0.02255	-0.02255	0.00183	-0.00183	0.07392	-0.03145
3.77	0.00320	47.56808	3.86789	-1.16514	0.62682	-0.33128	0.82405	-0.85675	2.66501	-2.66514	0.00183	-0.00183	4.80987	-3.05029
3.98	0.10619	1.67529	0.01188	-0.03943	0.04946	-0.02614	0.03003	-0.03122	0.07960	-0.07961	0.00183	-0.00183	0.09914	-0.09774
4.19	-0.06285	-3.37665	0.09599	-0.31865	0.10328	-0.05458	0.02593	-0.02696	0.13334	-0.13335	0.00183	-0.00183	0.19580	-0.35075
4.40	0.86415	0.37051	0.01130	-0.03750	0.00608	-0.00321	0.00121	-0.00117	0.00963	-0.00963	0.00183	-0.00183	0.01619	-0.03891
4.61	0.61821	0.54474	0.01909	-0.06338	0.00324	-0.00171	0.00501	-0.00482	0.01339	-0.01339	0.00183	-0.00183	0.02414	-0.06500

Table 56: 20–40%, 12.0–15.0 \otimes 2.0–3.0 GeV/c Jet Function

ϕ	per trig yield	σ_{stat}/y	systematic errors											
			$+\sigma_{f2}/y$	$-\sigma_{f2}/y$	$+\sigma_{f3}/y$	$-\sigma_{f3}/y$	$+\sigma_{f4}/y$	$-\sigma_{f4}/y$	$+\sigma_{\xi}/y$	$-\sigma_{\xi}/y$	$+\sigma_{\pi^0}/y$	$-\sigma_{\pi^0}/y$	$+\sigma_{total}/y$	$-\sigma_{total}/y$
-1.47	-0.00465	-15.69697	0.29651	-0.96767	0.02918	-0.05896	0.10239	-0.09861	0.14131	-0.14131	0.00195	-0.00195	0.34529	-0.98466
-1.26	0.02431	2.79844	0.04692	-0.15313	0.01462	-0.02953	0.00663	-0.00638	0.02708	-0.02708	0.00195	-0.00195	0.05654	-0.15843
-1.05	0.01888	2.89183	0.03734	-0.12187	0.02327	-0.04701	0.01330	-0.01381	0.03515	-0.03515	0.00195	-0.00195	0.05789	-0.13598
-0.84	-0.04572	-0.79012	0.00322	-0.01052	0.00777	-0.01570	0.01074	-0.01115	0.01471	-0.01471	0.00195	-0.00195	0.02016	-0.02649
-0.63	-0.00156	-24.20384	0.90873	-0.27844	0.08674	-0.17525	0.25959	-0.26953	0.43745	-0.43745	0.00195	-0.00195	1.04502	-0.61013
-0.42	0.01870	1.92781	0.16464	-0.05045	0.01466	-0.00726	0.00281	-0.00291	0.03724	-0.03724	0.00195	-0.00195	0.16947	-0.06322
-0.21	0.23623	0.20575	0.01779	-0.00545	0.00304	-0.00150	0.00148	-0.00142	0.00299	-0.00299	0.00195	-0.00195	0.01846	-0.00684
-0.00	0.35504	0.14344	0.01296	-0.00397	0.00250	-0.00124	0.00147	-0.00141	0.00200	-0.00200	0.00195	-0.00195	0.01357	-0.00520
0.21	0.18654	0.24604	0.02253	-0.00690	0.00385	-0.00190	0.00187	-0.00180	0.00378	-0.00378	0.00195	-0.00195	0.02333	-0.00852
0.42	0.09201	0.46279	0.03346	-0.01025	0.00298	-0.00148	0.00057	-0.00059	0.00757	-0.00757	0.00195	-0.00195	0.03450	-0.01299
0.63	0.02372	1.87365	0.05995	-0.01837	0.00572	-0.01156	0.01713	-0.01778	0.02886	-0.02886	0.00195	-0.00195	0.06897	-0.04030
0.84	-0.04135	-1.06760	0.00356	-0.01163	0.00853	-0.01736	0.01188	-0.01233	0.01627	-0.01627	0.00195	-0.00195	0.02227	-0.02928
1.05	-0.03987	-1.44947	0.01768	-0.05771	0.01102	-0.02226	0.00630	-0.00654	0.01664	-0.01664	0.00195	-0.00195	0.02747	-0.06442
1.26	-0.01854	-3.81283	0.06153	-0.20081	0.01917	-0.03873	0.00869	-0.00837	0.03552	-0.03552	0.00195	-0.00195	0.07412	-0.20775
1.47	0.11279	0.95619	0.01223	-0.03990	0.00120	-0.00243	0.00422	-0.00407	0.00583	-0.00583	0.00195	-0.00195	0.01437	-0.04065
1.68	-0.08293	-0.77273	0.01663	-0.05428	0.00331	-0.00164	0.00574	-0.00553	0.00795	-0.00795	0.00335	-0.00335	0.01987	-0.05526
1.88	-0.00882	-7.32143	0.12940	-0.42231	0.08145	-0.04031	0.01828	-0.01760	0.07535	-0.07535	0.00335	-0.00335	0.17147	-0.43125
2.09	0.00272	19.96630	0.25897	-0.84517	0.32599	-0.16135	0.09222	-0.09575	0.24637	-0.24637	0.00335	-0.00335	0.49250	-0.90013
2.30	0.02031	2.21093	0.00726	-0.02369	0.03536	-0.01750	0.02419	-0.02511	0.03341	-0.03341	0.00335	-0.00335	0.05491	-0.05124
2.51	0.00049	81.30302	2.92216	-0.89538	0.56356	-0.27893	0.83476	-0.86672	1.41125	-1.41125	0.00335	-0.00335	3.39780	-1.90325
2.72	0.00996	3.52538	0.30923	-0.09475	0.01363	-0.02754	0.00527	-0.00547	0.06973	-0.06973	0.00335	-0.00335	0.31735	-0.12100
2.93	0.11781	0.37210	0.03568	-0.01093	0.00302	-0.00609	0.00296	-0.00285	0.00594	-0.00594	0.00335	-0.00335	0.03657	-0.01454
3.14	0.15470	0.28728	0.02975	-0.00911	0.00284	-0.00574	0.00337	-0.00325	0.00454	-0.00454	0.00335	-0.00335	0.03059	-0.01258
3.35	0.11986	0.38091	0.03507	-0.01075	0.00296	-0.00599	0.00291	-0.00280	0.00584	-0.00584	0.00335	-0.00335	0.03595	-0.01430
3.56	0.09239	0.47702	0.03333	-0.01021	0.00147	-0.00297	0.00057	-0.00059	0.00752	-0.00752	0.00335	-0.00335	0.03436	-0.01346
3.77	0.00932	4.39662	0.15263	-0.04677	0.02944	-0.01457	0.04360	-0.04527	0.07371	-0.07371	0.00335	-0.00335	0.17751	-0.09947
3.98	-0.04394	-0.86772	0.00335	-0.01095	0.01634	-0.00809	0.01118	-0.01160	0.01544	-0.01544	0.00335	-0.00335	0.02555	-0.02386
4.19	-0.02555	-2.01041	0.02759	-0.09004	0.03473	-0.01719	0.00982	-0.01020	0.02625	-0.02625	0.00335	-0.00335	0.05257	-0.09595
4.40	0.11482	0.73876	0.00993	-0.03242	0.00625	-0.00309	0.00140	-0.00135	0.00578	-0.00578	0.00335	-0.00335	0.01358	-0.03328
4.61	-0.02921	-2.77030	0.04722	-0.15410	0.00939	-0.00465	0.01631	-0.01570	0.02258	-0.02258	0.00335	-0.00335	0.05572	-0.15664

Table 57: 20–40%, 12.0–15.0 \otimes 3.0–5.0 GeV/c Jet Function

ϕ	per trig yield	σ_{stat}/y	systematic errors												
			$+\sigma_{f2}/y$	$-\sigma_{f2}/y$	$+\sigma_{f3}/y$	$-\sigma_{f3}/y$	$+\sigma_{f4}/y$	$-\sigma_{f4}/y$	$+\sigma_\xi/y$	$-\sigma_\xi/y$	$+\sigma_{\pi^0}/y$	$-\sigma_{\pi^0}/y$	$+\sigma_{total}/y$	$-\sigma_{total}/y$	
-1.47	-0.02883	-0.00000	0.00655	-0.02168	0.00069	-0.00139	0.00267	-0.00254	0.00288	-0.00287	0.00046	-0.00046	0.00769	-0.02207	
-1.26	-0.01033	-1.79733	0.01513	-0.05007	0.00501	-0.01015	0.00252	-0.00239	0.00806	-0.00803	0.00046	-0.00046	0.01805	-0.05177	
-1.05	0.00671	3.09107	0.01440	-0.04763	0.00954	-0.01931	0.00596	-0.00628	0.01250	-0.01245	0.00046	-0.00046	0.02214	-0.05326	
-0.84	-0.01461	-0.72043	0.00138	-0.00457	0.00354	-0.00717	0.00836	-0.00564	0.00582	-0.00579	0.00046	-0.00046	0.00879	-0.01175	
-0.63	0.00297	4.97509	0.06650	-0.02010	0.00666	-0.01348	0.02180	-0.02297	0.02915	-0.02902	0.00046	-0.00046	0.07611	-0.04423	
-0.42	-0.00573	-1.94102	0.07463	-0.02256	0.00699	-0.00345	0.00146	-0.00154	0.01538	-0.01532	0.00046	-0.00046	0.07653	-0.02753	
-0.21	0.05602	0.36784	0.01042	-0.00315	0.00187	-0.00092	0.00101	-0.00096	0.00159	-0.00159	0.00046	-0.00046	0.01076	-0.00380	
-0.00	0.39363	0.10728	0.00162	-0.00049	0.00033	-0.00016	0.00021	-0.00020	0.00023	-0.00023	0.00046	-0.00046	0.00175	-0.00075	
0.21	0.08630	0.28854	0.00676	-0.00204	0.00121	-0.00060	0.00065	-0.00062	0.00104	-0.00103	0.00046	-0.00046	0.00700	-0.00249	
0.42	-0.00106	-11.38521	0.40284	-0.12177	0.03772	-0.01862	0.00788	-0.00830	0.08304	-0.08267	0.00046	-0.00046	0.41311	-0.14859	
0.63	0.00316	5.48553	0.06243	-0.01887	0.00625	-0.01266	0.02046	-0.02156	0.02737	-0.02724	0.00046	-0.00046	0.07145	-0.04152	
0.84	-0.00454	-3.17835	0.00445	-0.01472	0.01140	-0.02310	0.01725	-0.01817	0.01874	-0.01863	0.00046	-0.00046	0.02826	-0.03780	
1.05	-0.00324	-5.64794	0.02981	-0.09862	0.01974	-0.03999	0.01235	-0.0301	0.02589	-0.02577	0.00046	-0.00046	0.04584	-0.11027	
1.26	0.01051	3.76735	0.01487	-0.04918	0.00492	-0.00997	0.00248	-0.00235	0.00792	-0.00788	0.00046	-0.00046	0.01773	-0.05085	
1.47	-0.02883	-0.00000	0.00655	-0.02168	0.00069	-0.00139	0.00267	-0.00254	0.00288	-0.00287	0.00046	-0.00046	0.00769	-0.02207	
1.68	0.03754	1.25757	0.00503	-0.01665	0.00107	-0.00053	0.00205	-0.00195	0.00222	-0.00221	0.00162	-0.00162	0.00618	-0.01700	
1.88	-0.01031	-1.82849	0.01516	-0.05016	0.01017	-0.00502	0.00253	-0.00240	0.00815	-0.00812	0.00162	-0.00162	0.02022	-0.05114	
2.09	0.01050	2.19968	0.00920	-0.03043	0.01234	-0.00609	0.00381	-0.00401	0.00808	-0.00804	0.00162	-0.00162	0.01787	-0.03235	
2.30	0.01933	1.03916	0.00104	-0.00346	0.00542	-0.00268	0.00405	-0.00427	0.00444	-0.00442	0.00162	-0.00162	0.00832	-0.00771	
2.51	0.02680	0.75461	0.00737	-0.00223	0.00149	-0.00074	0.00241	-0.00254	0.00324	-0.00323	0.00162	-0.00162	0.00869	-0.00500	
2.72	0.02039	0.79274	0.02097	-0.00634	0.00097	-0.00196	0.00041	-0.00043	0.00431	-0.00429	0.00162	-0.00162	0.02149	-0.00808	
2.93	0.13079	0.23552	0.00446	-0.00135	0.00040	-0.00080	0.00043	-0.00041	0.00068	-0.00067	0.00162	-0.00162	0.00483	-0.00239	
3.14	0.12013	0.23605	0.00532	-0.00161	0.00053	-0.00108	0.00070	-0.00067	0.00074	-0.00074	0.00162	-0.00162	0.00568	-0.00271	
3.35	0.07044	0.35514	0.00829	-0.00251	0.00073	-0.00149	0.00080	-0.00076	0.00126	-0.00123	0.00162	-0.00162	0.00861	-0.00364	
3.56	0.02663	0.69867	0.01606	-0.00485	0.00074	-0.00150	0.00031	-0.00033	0.00330	-0.00328	0.00162	-0.00162	0.01649	-0.00627	
3.77	0.01814	1.10831	0.01089	-0.00329	0.00221	-0.00109	0.00357	-0.00376	0.00479	-0.00477	0.00162	-0.00162	0.01272	-0.00718	
3.98	0.00502	3.10590	0.00403	-0.01332	0.02090	-0.01032	0.01560	-0.01644	0.01711	-0.01703	0.00162	-0.00162	0.03149	-0.02910	
4.19	-0.01696	-0.73511	0.00570	-0.01884	0.00764	-0.00377	0.00236	-0.00249	0.00500	-0.00498	0.00162	-0.00162	0.01114	-0.02007	
4.40	-0.01307	-1.22996	0.01196	-0.03955	0.00802	-0.00396	0.00199	-0.00189	0.00643	-0.00640	0.00162	-0.00162	0.01597	-0.04034	
4.61	-0.02893	-0.00000	0.00653	-0.02161	0.00138	-0.00068	0.00266	-0.00253	0.00288	-0.00287	0.00162	-0.00162	0.00791	-0.02201	

Table 58: 20–40%, 12.0–15.0 \otimes 5.0–7.0 GeV/c Jet Function

ϕ	per trig yield	σ_{stat}/y	systematic errors											
			$+\sigma_{f2}/y$	$-\sigma_{f2}/y$	$+\sigma_{f3}/y$	$-\sigma_{f3}/y$	$+\sigma_{f4}/y$	$-\sigma_{f4}/y$	$+\sigma_{\xi}/y$	$-\sigma_{\xi}/y$	$+\sigma_{\pi^0}/y$	$-\sigma_{\pi^0}/y$	$+\sigma_{total}/y$	$-\sigma_{total}/y$
-1.47	-0.00329	-0.00000	0.00553	0.01655	0.00097	-0.00086	0.00176	-0.00297	0.00446	-0.00476	0.00301	-0.00301	0.00797	-0.01776
-1.26	-0.00330	-0.00000	0.00456	-0.01366	0.00254	-0.00224	0.00059	-0.00100	0.00446	-0.00476	0.00301	-0.00301	0.00752	-0.01498
-1.05	0.00421	1.80835	0.00221	-0.00661	0.00246	-0.00217	0.00127	-0.00075	0.00352	-0.00375	0.00301	-0.00301	0.00583	-0.00849
-0.84	-0.00336	-0.00000	0.00058	-0.00174	0.00249	-0.00220	0.00313	-0.00185	0.00446	-0.00476	0.00301	-0.00301	0.00673	-0.00656
-0.63	-0.00340	-0.00000	0.00507	-0.00169	0.00094	-0.00083	0.00255	-0.00151	0.00446	-0.00476	0.00301	-0.00301	0.00788	-0.00613
-0.42	0.01031	0.77514	0.00362	-0.00121	0.00027	-0.00031	0.00011	-0.00006	0.00149	-0.00159	0.00301	-0.00301	0.00495	-0.00363
-0.21	0.01188	0.65088	0.00429	-0.00143	0.00062	-0.00070	0.00036	-0.00060	0.00130	-0.00139	0.00301	-0.00301	0.00545	-0.00373
-0.00	0.17154	0.16838	0.00033	-0.00011	0.00005	-0.00006	0.00004	-0.00006	0.00009	-0.00010	0.00301	-0.00301	0.00303	-0.00302
0.21	0.02080	0.53190	0.00245	-0.00082	0.00036	-0.00040	0.00020	-0.00035	0.00075	-0.00079	0.00301	-0.00301	0.00397	-0.00326
0.42	0.01080	0.76649	0.00345	-0.00115	0.00026	-0.00030	0.00010	-0.00006	0.00142	-0.00152	0.00301	-0.00301	0.00481	-0.00358
0.63	0.00919	0.97448	0.00188	-0.00063	0.00035	-0.00031	0.00094	-0.00056	0.00165	-0.00176	0.00301	-0.00301	0.00404	-0.00360
0.84	-0.00336	-0.00000	0.00058	-0.00174	0.00249	-0.00220	0.00313	-0.00185	0.00446	-0.00476	0.00301	-0.00301	0.00673	-0.00656
1.05	-0.00332	-0.00000	0.00280	-0.00839	0.00312	-0.00275	0.00161	-0.00095	0.00446	-0.00476	0.00301	-0.00301	0.00701	-0.01052
1.26	-0.00330	-0.00000	0.00456	-0.01366	0.00254	-0.00224	0.00059	-0.00100	0.00446	-0.00476	0.00301	-0.00301	0.00752	-0.01498
1.47	-0.00329	-0.00000	0.00553	-0.01655	0.00097	-0.00086	0.00176	-0.00297	0.00446	-0.00476	0.00301	-0.00301	0.00797	-0.01776
1.68	-0.00330	-0.00000	0.00552	-0.01652	0.00085	-0.00097	0.00175	-0.00297	0.00446	-0.00476	0.00134	-0.00134	0.00748	-0.01752
1.88	-0.00332	-0.00000	0.00454	-0.01360	0.00223	-0.00252	0.00059	-0.00100	0.00446	-0.00476	0.00134	-0.00134	0.00690	-0.01472
2.09	-0.00334	-0.00000	0.00279	-0.00834	0.00273	-0.00310	0.00160	-0.00095	0.00446	-0.00476	0.00134	-0.00134	0.00628	-0.01022
2.30	-0.00337	-0.00000	0.00058	-0.00173	0.00219	-0.00248	0.00311	-0.00184	0.00446	-0.00476	0.00134	-0.00134	0.00604	-0.00608
2.51	0.01594	0.70711	0.00108	-0.00036	0.00018	-0.00020	0.00054	-0.00032	0.00095	-0.00102	0.00134	-0.00134	0.00205	-0.00176
2.72	0.00594	1.12146	0.00629	-0.00210	0.00054	-0.00048	0.00019	-0.00011	0.00258	-0.00275	0.00134	-0.00134	0.00695	-0.00374
2.93	0.03944	0.39242	0.00129	-0.00043	0.00021	-0.00019	0.00011	-0.00018	0.00039	-0.00042	0.00134	-0.00134	0.00191	-0.00149
3.14	0.06089	0.27179	0.00092	-0.00031	0.00017	-0.00015	0.00010	-0.00018	0.00025	-0.00027	0.00134	-0.00134	0.00165	-0.00142
3.35	0.02382	0.60671	0.00214	-0.00071	0.00035	-0.00031	0.00018	-0.00030	0.00065	-0.00069	0.00134	-0.00134	0.00263	-0.00172
3.56	0.01293	0.63779	0.00289	-0.00096	0.00025	-0.00022	0.00009	-0.00005	0.00119	-0.00126	0.00134	-0.00134	0.00340	-0.00209
3.77	0.00257	2.33248	0.00671	-0.00224	0.00110	-0.00124	0.00338	-0.00200	0.00591	-0.00631	0.00134	-0.00134	0.00971	-0.00722
3.98	0.01045	1.35012	0.00019	-0.00056	0.00071	-0.00080	0.00100	-0.00059	0.00144	-0.00154	0.00134	-0.00134	0.00233	-0.00234
4.19	-0.00334	-0.00000	0.00279	-0.00834	0.00273	-0.00310	0.00160	-0.00095	0.00446	-0.00476	0.00134	-0.00134	0.00628	-0.01022
4.40	-0.00332	-0.00000	0.00454	-0.01360	0.00223	-0.00252	0.00059	-0.00100	0.00446	-0.00476	0.00134	-0.00134	0.00690	-0.01472
4.61	-0.00330	-0.00000	0.00552	-0.01652	0.00085	-0.00097	0.00175	-0.00297	0.00446	-0.00476	0.00134	-0.00134	0.00748	-0.01752

F Data Tables: Jet Width

Table 59: 0–20%, Near side Width

trig p_T 4–5 GeV/c												
assoc p_T (GeV/c)	width	σ_{stat}/w	$+\sigma_{f2}/w$	$-\sigma_{f2}/w$	$+\sigma_{f3}/w$	$-\sigma_{f3}/w$	$+\sigma_{f4}/w$	$-\sigma_{f4}/w$	$+\sigma_\xi/w$	$-\sigma_\xi/w$	$+\sigma_{total}/w$	$-\sigma_{total}/w$
0.5–1.0	0.30466	0.12434	0.01722	-0.02139	0.01445	-0.01212	0.02951	-0.02332	0.15149	-0.15283	0.15597	-0.15654
1.0–2.0	0.33982	0.03941	0.00467	-0.00613	0.01188	-0.01031	0.02086	-0.01709	0.02320	-0.02430	0.03371	-0.03204
2.0–3.0	0.23463	0.00000	0.00480	-0.00499	0.00030	-0.00032	0.00443	-0.00377	0.00683	-0.00677	0.00945	-0.00922
3.0–5.0	0.15258	0.02180	0.00153	-0.00157	0.00081	-0.00085	0.00048	-0.00052	0.00129	-0.00127	0.00221	-0.00225
5.0–7.0	0.12328	0.03487	0.00110	-0.00114	0.00146	-0.00162	0.00109	-0.00129	0.00130	-0.00126	0.00249	-0.00268
trig p_T 5–7 GeV/c												
assoc p_T (GeV/c)	width	σ_{stat}/w	$+\sigma_{f2}/w$	$-\sigma_{f2}/w$	$+\sigma_{f3}/w$	$-\sigma_{f3}/w$	$+\sigma_{f4}/w$	$-\sigma_{f4}/w$	$+\sigma_\xi/w$	$-\sigma_\xi/w$	$+\sigma_{total}/w$	$-\sigma_{total}/w$
0.5–1.0	0.24777	0.12723	0.03175	-0.03833	0.00232	-0.00189	0.01237	-0.00906	0.07981	-0.08156	0.08681	-0.09060
1.0–2.0	0.28060	0.04422	0.01243	-0.01527	0.00650	-0.00532	0.01284	-0.00953	0.01595	-0.01640	0.02483	-0.02493
2.0–3.0	0.22607	0.02915	0.00491	-0.00524	0.00045	-0.00060	0.00253	-0.00206	0.00341	-0.00343	0.00651	-0.00662
3.0–5.0	0.14905	0.01691	0.00117	-0.00122	0.00058	-0.00064	0.00025	-0.00032	0.00053	-0.00052	0.00143	-0.00151
5.0–7.0	0.11322	0.01996	0.00054	-0.00059	0.00054	-0.00066	0.00037	-0.00050	0.00036	-0.00038	0.00092	-0.00108
trig p_T 7–9 GeV/c												
assoc p_T (GeV/c)	width	σ_{stat}/w	$+\sigma_{f2}/w$	$-\sigma_{f2}/w$	$+\sigma_{f3}/w$	$-\sigma_{f3}/w$	$+\sigma_{f4}/w$	$-\sigma_{f4}/w$	$+\sigma_\xi/w$	$-\sigma_\xi/w$	$+\sigma_{total}/w$	$-\sigma_{total}/w$
0.5–1.0	0.31910	0.27844	0.01771	-0.01765	0.01368	-0.01392	0.01479	-0.01183	0.05122	-0.05128	0.05782	-0.05723
1.0–2.0	0.22380	0.09988	0.02230	-0.01737	0.00202	-0.00197	0.00491	-0.00398	0.01365	-0.01341	0.02668	-0.02239
2.0–3.0	0.20131	0.04735	0.00520	-0.00399	0.00118	-0.00100	0.00072	-0.00062	0.00168	-0.00166	0.00564	-0.00448
3.0–5.0	0.14775	0.02939	0.00120	-0.00093	0.00052	-0.00047	0.00015	-0.00017	0.00029	-0.00030	0.00135	-0.00109
5.0–7.0	0.09867	0.02901	0.00043	-0.00037	0.00027	-0.00034	0.00016	-0.00024	0.00018	-0.00020	0.00056	-0.00059
trig p_T 9–12 GeV/c												
assoc p_T (GeV/c)	width	σ_{stat}/w	$+\sigma_{f2}/w$	$-\sigma_{f2}/w$	$+\sigma_{f3}/w$	$-\sigma_{f3}/w$	$+\sigma_{f4}/w$	$-\sigma_{f4}/w$	$+\sigma_\xi/w$	$-\sigma_\xi/w$	$+\sigma_{total}/w$	$-\sigma_{total}/w$
0.5–1.0	0.16667	0.22620	0.04119	-0.02750	0.00587	-0.00466	0.00130	-0.00156	0.01356	-0.01617	0.04378	-0.03228
1.0–2.0	0.25396	0.17488	0.02970	-0.01917	0.00194	-0.00231	0.01005	-0.00819	0.01528	-0.01478	0.03493	-0.02566
2.0–3.0	0.15696	0.07461	0.00839	-0.00519	0.00306	-0.00230	0.00062	-0.00069	0.00146	-0.00146	0.00907	-0.00590
3.0–5.0	0.12955	0.03931	0.00124	-0.00079	0.00057	-0.00044	0.00022	-0.00024	0.00019	-0.00019	0.00140	-0.00096
5.0–7.0	0.09558	0.04528	0.00052	-0.00037	0.00025	-0.00031	0.00012	-0.00021	0.00016	-0.00017	0.00061	-0.00055
trig p_T 12–15 GeV/c												
assoc p_T (GeV/c)	width	σ_{stat}/w	$+\sigma_{f2}/w$	$-\sigma_{f2}/w$	$+\sigma_{f3}/w$	$-\sigma_{f3}/w$	$+\sigma_{f4}/w$	$-\sigma_{f4}/w$	$+\sigma_\xi/w$	$-\sigma_\xi/w$	$+\sigma_{total}/w$	$-\sigma_{total}/w$
0.5–1.0	0.12753	0.42713	0.07592	-0.02909	0.01758	-0.00939	0.00392	-0.00346	0.02913	-0.02831	0.08328	-0.04181
1.0–2.0	0.29270	0.24931	0.02274	-0.00958	0.00562	-0.00983	0.01007	-0.01082	0.01231	-0.01232	0.02831	-0.02138
2.0–3.0	0.17054	0.12291	0.00819	-0.00302	0.00226	-0.00109	0.00013	-0.00009	0.00103	-0.00098	0.00856	-0.00336
3.0–5.0	0.11009	0.06538	0.00151	-0.00061	0.00068	-0.00036	0.00027	-0.00018	0.00015	-0.00016	0.00168	-0.00075
5.0–7.0	0.09638	0.12548	0.00102	-0.00044	0.00044	-0.00035	0.00020	-0.00026	0.00025	-0.00020	0.00115	-0.00065

Table 60: 0–20%, Away side Width

trig p_T 4–5 GeV/c												
assoc p_T (GeV/c)	width	σ_{stat}/w	$+\sigma_{f2}/w$	$-\sigma_{f2}/w$	$+\sigma_{f3}/w$	$-\sigma_{f3}/w$	$+\sigma_{f4}/w$	$-\sigma_{f4}/w$	$+\sigma_\xi/w$	$-\sigma_\xi/w$	$+\sigma_{total}/w$	$-\sigma_{total}/w$
0.5–1.0	0.73712	0.07675	0.04492	-0.03834	0.01861	-0.02082	0.01434	-0.01299	0.08908	-0.08257	0.10249	-0.09429
1.0–2.0	0.84649	0.09288	0.06000	-0.04966	0.02749	-0.03270	0.02861	-0.02639	0.05560	-0.05171	0.09092	-0.08310
2.0–3.0	0.76476	0.20713	0.01559	-0.01726	0.00244	-0.00256	0.01740	-0.01660	0.04352	-0.04453	0.04945	-0.05063
3.0–5.0	0.51793	0.29849	0.02841	-0.02375	0.04516	-0.04684	0.06654	-0.06665	0.02841	-0.02927	0.08989	-0.08976
5.0–7.0	0.24884	0.35142	0.00683	-0.00721	0.00107	-0.00118	0.01776	-0.01332	0.01497	-0.01405	0.02423	-0.02069
trig p_T 5–7 GeV/c												
assoc p_T (GeV/c)	width	σ_{stat}/w	$+\sigma_{f2}/w$	$-\sigma_{f2}/w$	$+\sigma_{f3}/w$	$-\sigma_{f3}/w$	$+\sigma_{f4}/w$	$-\sigma_{f4}/w$	$+\sigma_\xi/w$	$-\sigma_\xi/w$	$+\sigma_{total}/w$	$-\sigma_{total}/w$
0.5–1.0	0.79608	0.09283	0.06143	-0.05281	0.01759	-0.02155	0.01242	-0.00995	0.06332	-0.05871	0.09081	-0.08246
1.0–2.0	0.87764	0.10358	0.08437	-0.06761	0.02461	-0.03249	0.02783	-0.02213	0.04015	-0.03744	0.10055	-0.08671
2.0–3.0	0.64810	0.14832	0.06618	-0.04415	0.06599	-0.06143	0.07377	-0.05210	0.02315	-0.02194	0.12129	-0.09444
3.0–5.0	0.50666	0.16810	0.01436	-0.01209	0.02330	-0.02366	0.02981	-0.02316	0.00863	-0.00827	0.04138	-0.03620
5.0–7.0	0.18732	0.20373	0.00680	-0.00729	0.00449	-0.00373	0.00150	-0.00103	0.00603	-0.00615	0.01025	-0.01029
trig p_T 7–9 GeV/c												
assoc p_T (GeV/c)	width	σ_{stat}/w	$+\sigma_{f2}/w$	$-\sigma_{f2}/w$	$+\sigma_{f3}/w$	$-\sigma_{f3}/w$	$+\sigma_{f4}/w$	$-\sigma_{f4}/w$	$+\sigma_\xi/w$	$-\sigma_\xi/w$	$+\sigma_{total}/w$	$-\sigma_{total}/w$
0.5–1.0	0.77079	0.16466	0.05307	-0.05957	0.01909	-0.01815	0.00808	-0.00682	0.03715	-0.03602	0.06802	-0.07226
1.0–2.0	0.66601	0.15013	0.04150	-0.04545	0.03287	-0.02957	0.01774	-0.01522	0.01694	-0.01644	0.05834	-0.05867
2.0–3.0	0.42423	0.21353	0.00732	-0.00831	0.02726	-0.02086	0.02429	-0.02069	0.00853	-0.00836	0.03820	-0.03166
3.0–5.0	0.30485	0.20854	0.00476	-0.00394	0.00497	-0.00412	0.00914	-0.00790	0.00358	-0.00366	0.01199	-0.01041
5.0–7.0	0.20199	0.16265	0.00229	-0.00189	0.00065	-0.00052	0.00076	-0.00048	0.00137	-0.00150	0.00285	-0.00251
trig p_T 9–12 GeV/c												
assoc p_T (GeV/c)	width	σ_{stat}/w	$+\sigma_{f2}/w$	$-\sigma_{f2}/w$	$+\sigma_{f3}/w$	$-\sigma_{f3}/w$	$+\sigma_{f4}/w$	$-\sigma_{f4}/w$	$+\sigma_\xi/w$	$-\sigma_\xi/w$	$+\sigma_{total}/w$	$-\sigma_{total}/w$
0.5–1.0	0.97212	0.25340	0.07394	-0.13935	0.01510	-0.01387	0.00900	-0.00778	0.07739	-0.08050	0.10847	-0.16172
1.0–2.0	0.47837	0.20646	0.01601	-0.02142	0.03296	-0.02278	0.01898	-0.01611	0.01277	-0.01250	0.04320	-0.03733
2.0–3.0	0.37942	0.19757	0.00074	-0.00117	0.01319	-0.00927	0.01118	-0.01035	0.00386	-0.00381	0.01773	-0.01446
3.0–5.0	0.21388	0.15086	0.00613	-0.00396	0.00066	-0.00083	0.00143	-0.00130	0.00141	-0.00136	0.00648	-0.00446
5.0–7.0	0.22854	0.13274	0.00119	-0.00087	0.00001	-0.00001	0.00068	-0.00039	0.00066	-0.00069	0.00152	-0.00117
trig p_T 12–15 GeV/c												
assoc p_T (GeV/c)	width	σ_{stat}/w	$+\sigma_{f2}/w$	$-\sigma_{f2}/w$	$+\sigma_{f3}/w$	$-\sigma_{f3}/w$	$+\sigma_{f4}/w$	$-\sigma_{f4}/w$	$+\sigma_\xi/w$	$-\sigma_\xi/w$	$+\sigma_{total}/w$	$-\sigma_{total}/w$
0.5–1.0	0.64212	0.35054	0.02239	-0.04757	0.02181	-0.01134	0.00523	-0.00554	0.01898	-0.01808	0.03694	-0.05243
1.0–2.0	0.36229	0.39009	0.00225	-0.00099	0.02647	-0.01299	0.01515	-0.01648	0.01329	-0.01355	0.03334	-0.02500
2.0–3.0	0.30156	0.22597	0.00594	-0.00231	0.00459	-0.00237	0.00410	-0.00497	0.00213	-0.00217	0.00881	-0.00635
3.0–5.0	0.14430	0.18134	0.00407	-0.00167	0.00072	-0.00161	0.00031	-0.00042	0.00039	-0.00054	0.00417	-0.00242
5.0–7.0	0.11838	0.23229	0.00140	-0.00072	0.00049	-0.00061	0.00010	-0.00038	0.00034	-0.00039	0.00153	-0.00109

Table 61: 20–40%, Near side Width

trig p_T 4–5 GeV/c												
assoc p_T (GeV/c)	width	σ_{stat}/w	$+\sigma_{f2}/w$	$-\sigma_{f2}/w$	$+\sigma_{f3}/w$	$-\sigma_{f3}/w$	$+\sigma_{f4}/w$	$-\sigma_{f4}/w$	$+\sigma_\xi/w$	$-\sigma_\xi/w$	$+\sigma_{total}/w$	$-\sigma_{total}/w$
0.5–1.0	0.36285	0.09323	0.00442	-0.00693	0.02088	-0.01740	0.05423	-0.03930	0.18144	-0.19407	0.19057	-0.19889
1.0–2.0	0.35426	0.03613	0.01078	-0.01470	0.01548	-0.01278	0.02944	-0.02198	0.02950	-0.03684	0.04575	-0.04711
2.0–3.0	0.23814	0.00000	0.00431	-0.00444	0.00006	-0.00006	0.00629	-0.00489	0.01255	-0.01229	0.01468	-0.01395
3.0–5.0	0.16492	0.02167	0.00143	-0.00146	0.00059	-0.00064	0.00019	-0.00025	0.00281	-0.00280	0.00322	-0.00323
5.0–7.0	0.12349	0.03084	0.00074	-0.00076	0.00095	-0.00106	0.00076	-0.00096	0.00174	-0.00161	0.00225	-0.00228
trig p_T 5–7 GeV/c												
assoc p_T (GeV/c)	width	σ_{stat}/w	$+\sigma_{f2}/w$	$-\sigma_{f2}/w$	$+\sigma_{f3}/w$	$-\sigma_{f3}/w$	$+\sigma_{f4}/w$	$-\sigma_{f4}/w$	$+\sigma_\xi/w$	$-\sigma_\xi/w$	$+\sigma_{total}/w$	$-\sigma_{total}/w$
0.5–1.0	0.28821	0.09384	0.01631	-0.01896	0.00588	-0.00503	0.02267	-0.01621	0.14717	-0.14114	0.14991	-0.14342
1.0–2.0	0.29153	0.03519	0.01015	-0.01358	0.00559	-0.00480	0.01331	-0.00997	0.03020	-0.03416	0.03498	-0.03839
2.0–3.0	0.21283	0.02418	0.00384	-0.00393	0.00052	-0.00056	0.00196	-0.00150	0.00777	-0.00764	0.00890	-0.00874
3.0–5.0	0.15380	0.01695	0.00089	-0.00091	0.00030	-0.00033	0.00014	-0.00020	0.00134	-0.00133	0.00164	-0.00166
5.0–7.0	0.11401	0.02008	0.00033	-0.00036	0.00033	-0.00039	0.00024	-0.00034	0.00065	-0.00067	0.00084	-0.00091
trig p_T 7–9 GeV/c												
assoc p_T (GeV/c)	width	σ_{stat}/w	$+\sigma_{f2}/w$	$-\sigma_{f2}/w$	$+\sigma_{f3}/w$	$-\sigma_{f3}/w$	$+\sigma_{f4}/w$	$-\sigma_{f4}/w$	$+\sigma_\xi/w$	$-\sigma_\xi/w$	$+\sigma_{total}/w$	$-\sigma_{total}/w$
0.5–1.0	0.29173	0.22814	0.02428	-0.03671	0.00741	-0.00522	0.01738	-0.01030	0.12202	-0.11711	0.12584	-0.12327
1.0–2.0	0.24687	0.07049	0.01324	-0.01891	0.00091	-0.00076	0.00559	-0.00351	0.02562	-0.02601	0.02939	-0.03236
2.0–3.0	0.19629	0.04574	0.00441	-0.00537	0.00054	-0.00074	0.00069	-0.00043	0.00512	-0.00506	0.00681	-0.00743
3.0–5.0	0.14185	0.02750	0.00075	-0.00091	0.00017	-0.00023	0.00009	-0.00014	0.00066	-0.00066	0.00102	-0.00116
5.0–7.0	0.10208	0.02793	0.00020	-0.00025	0.00011	-0.00015	0.00007	-0.00012	0.00029	-0.00027	0.00037	-0.00041
trig p_T 9–12 GeV/c												
assoc p_T (GeV/c)	width	σ_{stat}/w	$+\sigma_{f2}/w$	$-\sigma_{f2}/w$	$+\sigma_{f3}/w$	$-\sigma_{f3}/w$	$+\sigma_{f4}/w$	$-\sigma_{f4}/w$	$+\sigma_\xi/w$	$-\sigma_\xi/w$	$+\sigma_{total}/w$	$-\sigma_{total}/w$
0.5–1.0	0.20884	0.28173	0.05219	-0.03474	0.00249	-0.00221	0.00268	-0.00188	0.07116	-0.06684	0.08832	-0.07538
1.0–2.0	0.26286	0.09954	0.01715	-0.01126	0.00114	-0.00126	0.00493	-0.00365	0.01881	-0.01839	0.02595	-0.02191
2.0–3.0	0.17933	0.06250	0.00753	-0.00474	0.00086	-0.00077	0.00012	-0.00013	0.00351	-0.00347	0.00836	-0.00592
3.0–5.0	0.14441	0.04251	0.00144	-0.00090	0.00023	-0.00019	0.00008	-0.00008	0.00054	-0.00054	0.00156	-0.00108
5.0–7.0	0.10043	0.04313	0.00033	-0.00021	0.00008	-0.00010	0.00005	-0.00008	0.00021	-0.00019	0.00040	-0.00031
trig p_T 12–15 GeV/c												
assoc p_T (GeV/c)	width	σ_{stat}/w	$+\sigma_{f2}/w$	$-\sigma_{f2}/w$	$+\sigma_{f3}/w$	$-\sigma_{f3}/w$	$+\sigma_{f4}/w$	$-\sigma_{f4}/w$	$+\sigma_\xi/w$	$-\sigma_\xi/w$	$+\sigma_{total}/w$	$-\sigma_{total}/w$
0.5–1.0	0.41147	0.49395	0.00737	-0.01843	0.00933	-0.01682	0.01190	-0.01140	0.06030	-0.05319	0.06261	-0.05985
1.0–2.0	0.26246	0.20851	0.04455	-0.02034	0.00221	-0.00380	0.00340	-0.00352	0.01270	-0.01439	0.04651	-0.02544
2.0–3.0	0.20922	0.13137	0.01198	-0.00369	0.00052	-0.00030	0.00070	-0.00073	0.00311	-0.00309	0.01240	-0.00488
3.0–5.0	0.11175	0.07243	0.00210	-0.00064	0.00035	-0.00014	0.00018	-0.00016	0.00037	-0.00034	0.00217	-0.00076
5.0–7.0	0.09467	0.09393	0.00067	-0.00019	0.00011	-0.00011	0.00007	-0.00007	0.00022	-0.00019	0.00072	-0.00030

Table 62: 20–40%, Away side Width

trig p_T 4–5 GeV/c												
assoc p_T (GeV/c)	width	σ_{stat}/w	$+\sigma_{f2}/w$	$-\sigma_{f2}/w$	$+\sigma_{f3}/w$	$-\sigma_{f3}/w$	$+\sigma_{f4}/w$	$-\sigma_{f4}/w$	$+\sigma_\xi/w$	$-\sigma_\xi/w$	$+\sigma_{total}/w$	$-\sigma_{total}/w$
0.5–1.0	0.75702	0.06764	0.05204	-0.04401	0.01814	-0.02056	0.02334	-0.02043	0.14368	-0.13294	0.15564	-0.14300
1.0–2.0	1.00596	0.07512	0.07731	-0.06609	0.01649	-0.02103	0.02569	-0.02330	0.08845	-0.08873	0.12138	-0.11500
2.0–3.0	0.85036	0.12713	0.03463	-0.02992	0.04203	-0.04039	0.11506	-0.07513	0.02423	-0.02511	0.12959	-0.09382
3.0–5.0	0.46548	0.13779	0.00718	-0.00648	0.01485	-0.01496	0.04351	-0.03317	0.02402	-0.02319	0.05237	-0.04364
5.0–7.0	0.34344	0.22208	0.00131	-0.00145	0.01447	-0.01426	0.03929	-0.02614	0.02778	-0.02444	0.05027	-0.03855
trig p_T 5–7 GeV/c												
assoc p_T (GeV/c)	width	σ_{stat}/w	$+\sigma_{f2}/w$	$-\sigma_{f2}/w$	$+\sigma_{f3}/w$	$-\sigma_{f3}/w$	$+\sigma_{f4}/w$	$-\sigma_{f4}/w$	$+\sigma_\xi/w$	$-\sigma_\xi/w$	$+\sigma_{total}/w$	$-\sigma_{total}/w$
0.5–1.0	0.72944	0.06736	0.04324	-0.03641	0.01264	-0.01427	0.01539	-0.01240	0.10950	-0.09262	0.11940	-0.10130
1.0–2.0	0.84924	0.08185	0.08698	-0.06468	0.02239	-0.02721	0.03114	-0.02484	0.10435	-0.08368	0.14115	-0.11200
2.0–3.0	0.51192	0.06774	0.01042	-0.00932	0.01354	-0.01429	0.03225	-0.02464	0.02498	-0.02472	0.04422	-0.03885
3.0–5.0	0.34649	0.08876	0.00085	-0.00088	0.00368	-0.00393	0.01414	-0.01064	0.01158	-0.01140	0.01866	-0.01610
5.0–7.0	0.23775	0.10181	0.00188	-0.00187	0.00002	-0.00000	0.00319	-0.00224	0.00634	-0.00616	0.00734	-0.00681
trig p_T 7–9 GeV/c												
assoc p_T (GeV/c)	width	σ_{stat}/w	$+\sigma_{f2}/w$	$-\sigma_{f2}/w$	$+\sigma_{f3}/w$	$-\sigma_{f3}/w$	$+\sigma_{f4}/w$	$-\sigma_{f4}/w$	$+\sigma_\xi/w$	$-\sigma_\xi/w$	$+\sigma_{total}/w$	$-\sigma_{total}/w$
0.5–1.0	0.78505	0.15262	0.07905	-0.05735	0.00988	-0.01383	0.01080	-0.00704	0.09279	-0.08909	0.12277	-0.10708
1.0–2.0	0.74037	0.16493	0.13333	-0.07683	0.02566	-0.03602	0.02912	-0.01905	0.08702	-0.07339	0.16388	-0.11380
2.0–3.0	0.37904	0.11480	0.00106	-0.00081	0.00464	-0.00593	0.01199	-0.00747	0.01278	-0.01263	0.01816	-0.01585
3.0–5.0	0.30572	0.09162	0.00118	-0.00148	0.00082	-0.00107	0.00330	-0.00214	0.00363	-0.00362	0.00511	-0.00458
5.0–7.0	0.21256	0.09034	0.00070	-0.00085	0.00006	-0.00004	0.00051	-0.00030	0.00168	-0.00156	0.00189	-0.00180
trig p_T 9–12 GeV/c												
assoc p_T (GeV/c)	width	σ_{stat}/w	$+\sigma_{f2}/w$	$-\sigma_{f2}/w$	$+\sigma_{f3}/w$	$-\sigma_{f3}/w$	$+\sigma_{f4}/w$	$-\sigma_{f4}/w$	$+\sigma_\xi/w$	$-\sigma_\xi/w$	$+\sigma_{total}/w$	$-\sigma_{total}/w$
0.5–1.0	0.69335	0.17608	0.04323	-0.05875	0.01084	-0.00934	0.00676	-0.00506	0.04863	-0.04595	0.06631	-0.07533
1.0–2.0	0.60548	0.18047	0.05210	-0.06629	0.02427	-0.02168	0.01763	-0.01401	0.03726	-0.03786	0.07073	-0.08059
2.0–3.0	0.33318	0.17358	0.00494	-0.00325	0.00516	-0.00413	0.00948	-0.00699	0.01171	-0.01153	0.01668	-0.01447
3.0–5.0	0.23596	0.10558	0.00348	-0.00218	0.00006	-0.00004	0.00103	-0.00078	0.00205	-0.00204	0.00417	-0.00309
5.0–7.0	0.19918	0.14695	0.00150	-0.00104	0.00018	-0.00013	0.00028	-0.00015	0.00149	-0.00138	0.00214	-0.00174
trig p_T 12–15 GeV/c												
assoc p_T (GeV/c)	width	σ_{stat}/w	$+\sigma_{f2}/w$	$-\sigma_{f2}/w$	$+\sigma_{f3}/w$	$-\sigma_{f3}/w$	$+\sigma_{f4}/w$	$-\sigma_{f4}/w$	$+\sigma_\xi/w$	$-\sigma_\xi/w$	$+\sigma_{total}/w$	$-\sigma_{total}/w$
0.5–1.0	0.60557	0.32028	0.03342	-0.07504	0.01931	-0.00940	0.00763	-0.00775	0.04336	-0.03956	0.05855	-0.08570
1.0–2.0	0.88153	0.69439	0.10715	-0.25426	0.02654	-0.01688	0.01787	-0.01888	0.06122	-0.05794	0.12748	-0.26200
2.0–3.0	0.25551	0.22460	0.01458	-0.00462	0.00093	-0.00043	0.00252	-0.00259	0.00530	-0.00536	0.01574	-0.00755
3.0–5.0	0.25013	0.17732	0.00431	-0.00126	0.00022	-0.00012	0.00072	-0.00081	0.00134	-0.00135	0.00458	-0.00202
5.0–7.0	0.21822	0.20446	0.00133	-0.00040	0.00007	-0.00001	0.00024	-0.00011	0.00069	-0.00063	0.00152	-0.00076

G Data Tables: Per Trigger Yield

Table 63: Near side yield, 0–20%

trig p_T 4–5 GeV/c														
assoc p_T (GeV/c)	yield	σ_{stat}/Y	+ σ_{f_2}/Y	- σ_{f_2}/Y	+ σ_{f_3}/Y	- σ_{f_3}/Y	+ σ_{f_4}/Y	- σ_{f_4}/Y	+ σ_ξ/Y	- σ_ξ/Y	σ_{π^0}	- σ_{π^0}	+ σ_{total}/Y	- σ_{total}/Y
0.5–1.0	0.17498	0.19957	0.07352	-0.07589	0.01044	-0.00978	0.02426	-0.02121	0.56019	-0.56017	0.11751	-0.11751	0.57769	-0.57784
1.0–2.0	0.18953	0.04303	0.01470	-0.01509	0.00343	-0.00321	0.00985	-0.00862	0.06213	-0.06213	0.06037	-0.06037	0.08848	-0.08841
2.0–3.0	0.07224	0.03028	0.00495	-0.00510	0.00115	-0.00108	0.00348	-0.00308	0.01121	-0.01122	0.02562	-0.02562	0.02863	-0.02861
3.0–5.0	0.01278	0.03199	0.00219	-0.00227	0.00050	-0.00047	0.00172	-0.00152	0.00437	-0.00434	0.08208	-0.08208	0.08225	-0.08225
5.0–7.0	0.00202	0.07622	0.00238	-0.00249	0.00120	-0.00109	0.00325	-0.00278	0.00743	-0.00724	0.08179	-0.08179	0.08223	-0.08220
trig p_T 5–7 GeV/c														
assoc p_T (GeV/c)	yield	σ_{stat}/Y	+ σ_{f_2}/Y	- σ_{f_2}/Y	+ σ_{f_3}/Y	- σ_{f_3}/Y	+ σ_{f_4}/Y	- σ_{f_4}/Y	+ σ_ξ/Y	- σ_ξ/Y	σ_{π^0}	- σ_{π^0}	+ σ_{total}/Y	- σ_{total}/Y
0.5–1.0	0.13861	0.33267	0.13708	-0.14398	0.01802	-0.01612	0.03195	-0.02510	0.54119	-0.54111	0.02194	-0.02194	0.55992	-0.56117
1.0–2.0	0.19874	0.05419	0.02277	-0.02363	0.00449	-0.00402	0.00988	-0.00778	0.04689	-0.04690	0.01759	-0.01759	0.05608	-0.05607
2.0–3.0	0.08459	0.03430	0.00657	-0.00686	0.00142	-0.00128	0.00333	-0.00269	0.00778	-0.00779	0.01037	-0.01037	0.01498	-0.01497
3.0–5.0	0.02001	0.02766	0.00205	-0.00216	0.00046	-0.00041	0.00122	-0.00098	0.00223	-0.00219	0.02879	-0.02879	0.02898	-0.02898
5.0–7.0	0.00519	0.04173	0.00114	-0.00123	0.00046	-0.00037	0.00113	-0.00083	0.00207	-0.00215	0.13197	-0.13197	0.13199	-0.13199
trig p_T 7–9 GeV/c														
assoc p_T (GeV/c)	yield	σ_{stat}/Y	+ σ_{f_2}/Y	- σ_{f_2}/Y	+ σ_{f_3}/Y	- σ_{f_3}/Y	+ σ_{f_4}/Y	- σ_{f_4}/Y	+ σ_ξ/Y	- σ_ξ/Y	σ_{π^0}	- σ_{π^0}	+ σ_{total}/Y	- σ_{total}/Y
0.5–1.0	0.14081	0.90025	0.24018	-0.18865	0.02142	-0.02406	0.03076	-0.02573	0.50498	-0.50505	0.11756	-0.11756	0.57264	-0.55292
1.0–2.0	0.20535	0.14424	0.04185	-0.03174	0.00526	-0.00593	0.00940	-0.00792	0.04372	-0.04372	0.01925	-0.01925	0.06442	-0.05820
2.0–3.0	0.11462	0.07013	0.00893	-0.00688	0.00130	-0.00150	0.00253	-0.00228	0.00554	-0.00552	0.00044	-0.00044	0.01089	-0.00925
3.0–5.0	0.03456	0.04593	0.00210	-0.00166	0.00033	-0.00038	0.00073	-0.00065	0.00121	-0.00125	0.00446	-0.00446	0.00514	-0.00498
5.0–7.0	0.01289	0.05573	0.00070	-0.00060	0.00018	-0.00014	0.00039	-0.00025	0.00081	-0.00090	0.06571	-0.06571	0.06572	-0.06572
trig p_T 9–12 GeV/c														
assoc p_T (GeV/c)	yield	σ_{stat}/Y	+ σ_{f_2}/Y	- σ_{f_2}/Y	+ σ_{f_3}/Y	- σ_{f_3}/Y	+ σ_{f_4}/Y	- σ_{f_4}/Y	+ σ_ξ/Y	- σ_ξ/Y	σ_{π^0}	- σ_{π^0}	+ σ_{total}/Y	- σ_{total}/Y
0.5–1.0	0.67007	0.36299	0.07984	-0.05097	0.00566	-0.00730	0.00751	-0.00652	0.11417	-0.11417	0.02823	-0.02823	0.14246	-0.12856
1.0–2.0	0.27996	0.20254	0.04961	-0.03045	0.00486	-0.00628	0.00803	-0.00705	0.03393	-0.03392	0.01091	-0.01091	0.06180	-0.04782
2.0–3.0	0.13506	0.11325	0.01213	-0.00758	0.00140	-0.00187	0.00255	-0.00244	0.00498	-0.00498	0.00299	-0.00299	0.01376	-0.01003
3.0–5.0	0.05179	0.06337	0.00221	-0.00142	0.00028	-0.00037	0.00057	-0.00055	0.00088	-0.00087	0.00058	-0.00058	0.00253	-0.00188
5.0–7.0	0.01733	0.08358	0.00078	-0.00055	0.00015	-0.00012	0.00031	-0.00018	0.00067	-0.00069	0.01835	-0.01835	0.01838	-0.01838
trig p_T 12–15 GeV/c														
assoc p_T (GeV/c)	yield	σ_{stat}/Y	+ σ_{f_2}/Y	- σ_{f_2}/Y	+ σ_{f_3}/Y	- σ_{f_3}/Y	+ σ_{f_4}/Y	- σ_{f_4}/Y	+ σ_ξ/Y	- σ_ξ/Y	σ_{π^0}	- σ_{π^0}	+ σ_{total}/Y	- σ_{total}/Y
0.5–1.0	0.49722	1.18960	0.18144	-0.07130	0.00789	-0.01480	0.01040	-0.01139	0.18598	-0.18599	0.12758	-0.12758	0.28976	-0.23728
1.0–2.0	0.50603	0.27503	0.04682	-0.01750	0.00278	-0.00523	0.00456	-0.00506	0.02191	-0.02191	0.05022	-0.05022	0.07227	-0.05798
2.0–3.0	0.14781	0.24955	0.01878	-0.00718	0.00133	-0.00258	0.00240	-0.00296	0.00524	-0.00524	0.00064	-0.00064	0.01970	-0.00974
3.0–5.0	0.05506	0.14188	0.00348	-0.00138	0.00027	-0.00052	0.00055	-0.00068	0.00094	-0.00094	0.00848	-0.00848	0.00923	-0.00868
5.0–7.0	0.01215	0.25647	0.00179	-0.00081	0.00021	-0.00022	0.00045	-0.00028	0.00117	-0.00111	0.01662	-0.01662	0.01676	-0.01668

Table 64: Away side yield, 0–20%

trig p_T 4–5 GeV/c														
assoc p_T (GeV/c)	yield	σ_{stat}/Y	+ σ_{f2}/Y	- σ_{f2}/Y	+ σ_{f3}/Y	- σ_{f3}/Y	+ σ_{f4}/Y	- σ_{f4}/Y	+ σ_ξ/Y	- σ_ξ/Y	σ_{π^0}	- σ_{π^0}	+ σ_{total}/Y	- σ_{total}/Y
0.5–1.0	0.70861	0.07006	0.00000	-0.00000	0.00781	-0.00834	0.00000	-0.00000	0.18837	-0.18837	0.01466	-0.01466	0.18911	-0.18912
1.0–2.0	0.14998	0.07925	0.00000	-0.00000	0.01313	-0.01402	0.00000	-0.00000	0.10686	-0.10686	0.00231	-0.00231	0.10768	-0.10780
2.0–3.0	0.01528	0.20695	0.00000	-0.00000	0.01653	-0.01756	0.00000	-0.00000	0.07210	-0.07216	0.09434	-0.09434	0.11988	-0.12007
3.0–5.0	0.00256	0.22489	0.00000	-0.00000	0.00759	-0.00807	0.00000	-0.00000	0.02973	-0.02951	0.10132	-0.10132	0.10586	-0.10583
5.0–7.0	0.00012	1.69569	0.00000	-0.00000	0.05746	-0.06313	0.00000	-0.00000	0.16444	-0.16040	0.46073	-0.46073	0.49256	-0.49193
trig p_T 5–7 GeV/c														
assoc p_T (GeV/c)	yield	σ_{stat}/Y	+ σ_{f2}/Y	- σ_{f2}/Y	+ σ_{f3}/Y	- σ_{f3}/Y	+ σ_{f4}/Y	- σ_{f4}/Y	+ σ_ξ/Y	- σ_ξ/Y	σ_{π^0}	- σ_{π^0}	+ σ_{total}/Y	- σ_{total}/Y
0.5–1.0	0.78940	0.08328	0.00000	-0.00000	0.00916	-0.01024	0.00000	-0.00000	0.12943	-0.12941	0.01414	-0.01414	0.13052	-0.13058
1.0–2.0	0.18672	0.08452	0.00000	-0.00000	0.01386	-0.01548	0.00000	-0.00000	0.06794	-0.06795	0.00648	-0.00648	0.06964	-0.06999
2.0–3.0	0.02773	0.15203	0.00000	-0.00000	0.01266	-0.01400	0.00000	-0.00000	0.03232	-0.03235	0.03138	-0.03138	0.04679	-0.04719
3.0–5.0	0.00648	0.12134	0.00000	-0.00000	0.00413	-0.00457	0.00000	-0.00000	0.00939	-0.00923	0.05403	-0.05403	0.05500	-0.05501
5.0–7.0	0.00111	0.26564	0.00000	-0.00000	0.00568	-0.00692	0.00000	-0.00000	0.01323	-0.01373	0.01380	-0.01380	0.01994	-0.02066
trig p_T 7–9 GeV/c														
assoc p_T (GeV/c)	yield	σ_{stat}/Y	+ σ_{f2}/Y	- σ_{f2}/Y	+ σ_{f3}/Y	- σ_{f3}/Y	+ σ_{f4}/Y	- σ_{f4}/Y	+ σ_ξ/Y	- σ_ξ/Y	σ_{π^0}	- σ_{π^0}	+ σ_{total}/Y	- σ_{total}/Y
0.5–1.0	1.15019	0.15703	0.00000	-0.00000	0.00953	-0.00849	0.00000	-0.00000	0.08421	-0.08422	0.01564	-0.01564	0.08618	-0.08608
1.0–2.0	0.22924	0.18854	0.00000	-0.00000	0.01718	-0.01526	0.00000	-0.00000	0.05332	-0.05332	0.01420	-0.01420	0.05779	-0.05725
2.0–3.0	0.05150	0.22765	0.00000	-0.00000	0.01081	-0.00936	0.00000	-0.00000	0.01676	-0.01672	0.04201	-0.04201	0.04650	-0.04617
3.0–5.0	0.00731	0.28576	0.00000	-0.00000	0.00577	-0.00502	0.00000	-0.00000	0.00781	-0.00803	0.02469	-0.02469	0.02653	-0.02644
5.0–7.0	0.00244	0.33011	0.00000	-0.00000	0.00246	-0.00302	0.00000	-0.00000	0.00581	-0.00645	0.01148	-0.01148	0.01310	-0.01351
trig p_T 9–12 GeV/c														
assoc p_T (GeV/c)	yield	σ_{stat}/Y	+ σ_{f2}/Y	- σ_{f2}/Y	+ σ_{f3}/Y	- σ_{f3}/Y	+ σ_{f4}/Y	- σ_{f4}/Y	+ σ_ξ/Y	- σ_ξ/Y	σ_{π^0}	- σ_{π^0}	+ σ_{total}/Y	- σ_{total}/Y
0.5–1.0	1.39248	0.24792	0.00000	-0.00000	0.01136	-0.00881	0.00000	-0.00000	0.07484	-0.07484	0.00809	-0.00809	0.07613	-0.07579
1.0–2.0	0.18756	0.43934	0.00000	-0.00000	0.03034	-0.02346	0.00000	-0.00000	0.06894	-0.06894	0.05916	-0.05916	0.09578	-0.09382
2.0–3.0	0.10249	0.22274	0.00000	-0.00000	0.00796	-0.00598	0.00000	-0.00000	0.00893	-0.00893	0.01296	-0.01296	0.01763	-0.01683
3.0–5.0	0.02320	0.17634	0.00000	-0.00000	0.00266	-0.00200	0.00000	-0.00000	0.00267	-0.00264	0.00120	-0.00120	0.00395	-0.00353
5.0–7.0	0.01090	0.17667	0.00000	-0.00000	0.00063	-0.00075	0.00000	-0.00000	0.00144	-0.00149	0.01280	-0.01280	0.01289	-0.01291
trig p_T 12–15 GeV/c														
assoc p_T (GeV/c)	yield	σ_{stat}/Y	+ σ_{f2}/Y	- σ_{f2}/Y	+ σ_{f3}/Y	- σ_{f3}/Y	+ σ_{f4}/Y	- σ_{f4}/Y	+ σ_ξ/Y	- σ_ξ/Y	σ_{π^0}	- σ_{π^0}	+ σ_{total}/Y	- σ_{total}/Y
0.5–1.0	1.93225	0.43769	0.00000	-0.00000	0.01232	-0.00657	0.00000	-0.00000	0.06519	-0.06520	0.04569	-0.04569	0.08056	-0.07989
1.0–2.0	0.21273	0.95102	0.00000	-0.00000	0.04024	-0.02140	0.00000	-0.00000	0.07097	-0.07096	0.06319	-0.06319	0.10319	-0.09740
2.0–3.0	0.16328	0.34195	0.00000	-0.00000	0.00757	-0.00388	0.00000	-0.00000	0.00646	-0.00646	0.02212	-0.02212	0.02425	-0.02337
3.0–5.0	0.02444	0.42893	0.00000	-0.00000	0.00380	-0.00196	0.00000	-0.00000	0.00290	-0.00294	0.01727	-0.01727	0.01792	-0.01763
5.0–7.0	0.01185	0.36048	0.00000	-0.00000	0.00073	-0.00070	0.00000	-0.00000	0.00164	-0.00155	0.04180	-0.04180	0.04184	-0.04184

Table 65: Near side yield, 20–40%

trig p_T 4–5 GeV/c														
assoc p_T (GeV/c)	yield	σ_{stat}/Y	$+\sigma_{f2}/Y$	$-\sigma_{f2}/Y$	$+\sigma_{f3}/Y$	$-\sigma_{f3}/Y$	$+\sigma_{f4}/Y$	$-\sigma_{f4}/Y$	$+\sigma_\xi/Y$	$-\sigma_\xi/Y$	σ_{π^0}	$-\sigma_{\pi^0}$	$+\sigma_{total}/Y$	$-\sigma_{total}/Y$
0.5–1.0	0.23393	0.11661	0.05070	-0.05165	0.00658	-0.00608	0.02807	-0.02286	0.58953	-0.58953	0.04024	-0.04024	0.59378	-0.59363
1.0–2.0	0.20205	0.03236	0.01461	-0.01488	0.00296	-0.00272	0.01161	-0.00950	0.09872	-0.09872	0.01238	-0.01238	0.10128	-0.10108
2.0–3.0	0.06295	0.02880	0.00583	-0.00595	0.00111	-0.00103	0.00576	-0.00472	0.02581	-0.02581	0.01539	-0.01539	0.03117	-0.03101
3.0–5.0	0.01271	0.02774	0.00187	-0.00190	0.00040	-0.00037	0.00233	-0.00183	0.00794	-0.00797	0.01580	-0.01580	0.01792	-0.01790
5.0–7.0	0.00204	0.05780	0.00154	-0.00157	0.00075	-0.00068	0.00242	-0.00189	0.00922	-0.00864	0.02260	-0.02260	0.02459	-0.02433
trig p_T 5–7 GeV/c														
assoc p_T (GeV/c)	yield	σ_{stat}/Y	$+\sigma_{f2}/Y$	$-\sigma_{f2}/Y$	$+\sigma_{f3}/Y$	$-\sigma_{f3}/Y$	$+\sigma_{f4}/Y$	$-\sigma_{f4}/Y$	$+\sigma_\xi/Y$	$-\sigma_\xi/Y$	σ_{π^0}	$-\sigma_{\pi^0}$	$+\sigma_{total}/Y$	$-\sigma_{total}/Y$
0.5–1.0	0.24795	0.13944	0.05361	-0.05490	0.00543	-0.00492	0.01968	-0.01546	0.49898	-0.49901	0.01211	-0.01211	0.50241	-0.50243
1.0–2.0	0.23941	0.03469	0.01396	-0.01428	0.00215	-0.00194	0.00731	-0.00577	0.07497	-0.07498	0.00376	-0.00376	0.07673	-0.07666
2.0–3.0	0.08471	0.02757	0.00480	-0.00492	0.00073	-0.00066	0.00319	-0.00252	0.01723	-0.01723	0.00299	-0.00299	0.01843	-0.01835
3.0–5.0	0.02039	0.02317	0.00131	-0.00134	0.00022	-0.00020	0.00104	-0.00082	0.00444	-0.00444	0.00847	-0.00847	0.00972	-0.00970
5.0–7.0	0.00468	0.03622	0.00068	-0.00071	0.00026	-0.00022	0.00076	-0.00056	0.00350	-0.00350	0.02662	-0.02662	0.02687	-0.02686
trig p_T 7–9 GeV/c														
assoc p_T (GeV/c)	yield	σ_{stat}/Y	$+\sigma_{f2}/Y$	$-\sigma_{f2}/Y$	$+\sigma_{f3}/Y$	$-\sigma_{f3}/Y$	$+\sigma_{f4}/Y$	$-\sigma_{f4}/Y$	$+\sigma_\xi/Y$	$-\sigma_\xi/Y$	σ_{π^0}	$-\sigma_{\pi^0}$	$+\sigma_{total}/Y$	$-\sigma_{total}/Y$
0.5–1.0	0.25285	0.37381	0.08507	-0.10336	0.00653	-0.00493	0.01687	-0.01072	0.48376	-0.48375	0.00572	-0.00572	0.49155	-0.49485
1.0–2.0	0.28137	0.08090	0.01952	-0.02372	0.00215	-0.00162	0.00550	-0.00352	0.06265	-0.06265	0.00095	-0.00095	0.06589	-0.06711
2.0–3.0	0.11477	0.05590	0.00565	-0.00686	0.00067	-0.00050	0.00208	-0.00133	0.01258	-0.01257	0.00200	-0.00200	0.01410	-0.01453
3.0–5.0	0.03506	0.04004	0.00125	-0.00152	0.00016	-0.00012	0.00054	-0.00034	0.00256	-0.00255	0.00131	-0.00131	0.00319	-0.00326
5.0–7.0	0.01231	0.04909	0.00036	-0.00044	0.00009	-0.00006	0.00022	-0.00013	0.00139	-0.00130	0.01223	-0.01223	0.01231	-0.01230
trig p_T 9–12 GeV/c														
assoc p_T (GeV/c)	yield	σ_{stat}/Y	$+\sigma_{f2}/Y$	$-\sigma_{f2}/Y$	$+\sigma_{f3}/Y$	$-\sigma_{f3}/Y$	$+\sigma_{f4}/Y$	$-\sigma_{f4}/Y$	$+\sigma_\xi/Y$	$-\sigma_\xi/Y$	σ_{π^0}	$-\sigma_{\pi^0}$	$+\sigma_{total}/Y$	$-\sigma_{total}/Y$
0.5–1.0	0.05855	3.10283	0.92293	-0.57767	0.03279	-0.03841	0.07649	-0.05719	2.23016	-2.23010	0.00689	-0.00689	2.41503	-2.30475
1.0–2.0	0.26954	0.16229	0.05166	-0.03216	0.00259	-0.00293	0.00606	-0.00464	0.06980	-0.06980	0.00050	-0.00050	0.08709	-0.07705
2.0–3.0	0.15973	0.07997	0.01010	-0.00636	0.00056	-0.00066	0.00158	-0.00121	0.00963	-0.00964	0.00059	-0.00059	0.01407	-0.01164
3.0–5.0	0.05314	0.05701	0.00208	-0.00130	0.00012	-0.00014	0.00038	-0.00029	0.00179	-0.00180	0.00035	-0.00035	0.00280	-0.00227
5.0–7.0	0.01813	0.07380	0.00056	-0.00038	0.00006	-0.00004	0.00015	-0.00008	0.00099	-0.00092	0.00273	-0.00273	0.00296	-0.00290
trig p_T 12–15 GeV/c														
assoc p_T (GeV/c)	yield	σ_{stat}/Y	$+\sigma_{f2}/Y$	$-\sigma_{f2}/Y$	$+\sigma_{f3}/Y$	$-\sigma_{f3}/Y$	$+\sigma_{f4}/Y$	$-\sigma_{f4}/Y$	$+\sigma_\xi/Y$	$-\sigma_\xi/Y$	σ_{π^0}	$-\sigma_{\pi^0}$	$+\sigma_{total}/Y$	$-\sigma_{total}/Y$
0.5–1.0	0.76356	0.60310	0.15200	-0.04614	0.00259	-0.00516	0.00599	-0.00601	0.17605	-0.17604	0.00490	-0.00490	0.23273	-0.18223
1.0–2.0	0.46837	0.23922	0.06402	-0.01929	0.00153	-0.00290	0.00356	-0.00371	0.04195	-0.04195	0.00126	-0.00126	0.07665	-0.04643
2.0–3.0	0.16810	0.18960	0.02049	-0.00628	0.00055	-0.00111	0.00153	-0.00159	0.00941	-0.00941	0.00195	-0.00195	0.02269	-0.01164
3.0–5.0	0.05441	0.13194	0.00440	-0.00133	0.00012	-0.00025	0.00038	-0.00040	0.00184	-0.00183	0.00046	-0.00046	0.00480	-0.00236
5.0–7.0	0.02359	0.15924	0.00088	-0.00030	0.00005	-0.00004	0.00012	-0.00007	0.00074	-0.00079	0.00301	-0.00301	0.00323	-0.00313

Table 66: Away side yield, 20–40%

trig p_T 4–5 GeV/c														
assoc p_T (GeV/c)	yield	σ_{stat}/Y	+ σ_{f_2}/Y	- σ_{f_2}/Y	+ σ_{f_3}/Y	- σ_{f_3}/Y	+ σ_{f_4}/Y	- σ_{f_4}/Y	+ σ_ξ/Y	- σ_ξ/Y	σ_{π^0}	- σ_{π^0}	+ σ_{total}/Y	- σ_{total}/Y
0.5–1.0	0.65833	0.05832	0.00000	-0.00000	0.00700	-0.00756	0.00000	-0.00000	0.28381	-0.28381	0.01849	-0.01849	0.28450	-0.28451
1.0–2.0	0.18417	0.05089	0.00000	-0.00000	0.00967	-0.01050	0.00000	-0.00000	0.14615	-0.14614	0.01337	-0.01337	0.14708	-0.14712
2.0–3.0	0.03099	0.08272	0.00000	-0.00000	0.00677	-0.00732	0.00000	-0.00000	0.07053	-0.07053	0.00122	-0.00122	0.07086	-0.07091
3.0–5.0	0.00387	0.12246	0.00000	-0.00000	0.00390	-0.00422	0.00000	-0.00000	0.03511	-0.03527	0.01286	-0.01286	0.03760	-0.03778
5.0–7.0	0.00089	0.17427	0.00000	-0.00000	0.00502	-0.00557	0.00000	-0.00000	0.02840	-0.02664	0.00021	-0.00021	0.02884	-0.02721
trig p_T 5–7 GeV/c														
assoc p_T (GeV/c)	yield	σ_{stat}/Y	+ σ_{f_2}/Y	- σ_{f_2}/Y	+ σ_{f_3}/Y	- σ_{f_3}/Y	+ σ_{f_4}/Y	- σ_{f_4}/Y	+ σ_ξ/Y	- σ_ξ/Y	σ_{π^0}	- σ_{π^0}	+ σ_{total}/Y	- σ_{total}/Y
0.5–1.0	0.73821	0.06617	0.00000	-0.00000	0.00535	-0.00590	0.00000	-0.00000	0.22729	-0.22730	0.00703	-0.00703	0.22746	-0.22748
1.0–2.0	0.21360	0.05592	0.00000	-0.00000	0.00703	-0.00781	0.00000	-0.00000	0.11355	-0.11356	0.00556	-0.00556	0.11391	-0.11397
2.0–3.0	0.03807	0.08587	0.00000	-0.00000	0.00475	-0.00523	0.00000	-0.00000	0.05166	-0.05166	0.00478	-0.00478	0.05210	-0.05215
3.0–5.0	0.00713	0.08668	0.00000	-0.00000	0.00183	-0.00201	0.00000	-0.00000	0.01714	-0.01714	0.00697	-0.00697	0.01859	-0.01861
5.0–7.0	0.00153	0.13565	0.00000	-0.00000	0.00223	-0.00256	0.00000	-0.00000	0.01452	-0.01452	0.00599	-0.00599	0.01586	-0.01591
trig p_T 7–9 GeV/c														
assoc p_T (GeV/c)	yield	σ_{stat}/Y	+ σ_{f_2}/Y	- σ_{f_2}/Y	+ σ_{f_3}/Y	- σ_{f_3}/Y	+ σ_{f_4}/Y	- σ_{f_4}/Y	+ σ_ξ/Y	- σ_ξ/Y	σ_{π^0}	- σ_{π^0}	+ σ_{total}/Y	- σ_{total}/Y
0.5–1.0	1.19158	0.11275	0.00000	-0.00000	0.00339	-0.00448	0.00000	-0.00000	0.13937	-0.13937	0.00227	-0.00227	0.13943	-0.13946
1.0–2.0	0.35263	0.09352	0.00000	-0.00000	0.00419	-0.00556	0.00000	-0.00000	0.06768	-0.06768	0.00334	-0.00334	0.06789	-0.06799
2.0–3.0	0.05368	0.16672	0.00000	-0.00000	0.00349	-0.00461	0.00000	-0.00000	0.03631	-0.03629	0.00719	-0.00719	0.03718	-0.03729
3.0–5.0	0.01606	0.11068	0.00000	-0.00000	0.00084	-0.00111	0.00000	-0.00000	0.00755	-0.00752	0.00065	-0.00065	0.00763	-0.00763
5.0–7.0	0.00448	0.14881	0.00000	-0.00000	0.00055	-0.00076	0.00000	-0.00000	0.00517	-0.00482	0.00730	-0.00730	0.00896	-0.00878
trig p_T 9–12 GeV/c														
assoc p_T (GeV/c)	yield	σ_{stat}/Y	+ σ_{f_2}/Y	- σ_{f_2}/Y	+ σ_{f_3}/Y	- σ_{f_3}/Y	+ σ_{f_4}/Y	- σ_{f_4}/Y	+ σ_ξ/Y	- σ_ξ/Y	σ_{π^0}	- σ_{π^0}	+ σ_{total}/Y	- σ_{total}/Y
0.5–1.0	1.15761	0.22334	0.00000	-0.00000	0.00629	-0.00537	0.00000	-0.00000	0.15319	-0.15319	0.00118	-0.00118	0.15333	-0.15329
1.0–2.0	0.43925	0.14522	0.00000	-0.00000	0.00582	-0.00514	0.00000	-0.00000	0.05802	-0.05802	0.00070	-0.00070	0.05831	-0.05825
2.0–3.0	0.07024	0.24960	0.00000	-0.00000	0.00487	-0.00412	0.00000	-0.00000	0.02958	-0.02961	0.00093	-0.00093	0.02999	-0.02991
3.0–5.0	0.02181	0.15762	0.00000	-0.00000	0.00114	-0.00096	0.00000	-0.00000	0.00590	-0.00592	0.00218	-0.00218	0.00639	-0.00638
5.0–7.0	0.00679	0.17912	0.00000	-0.00000	0.00038	-0.00051	0.00000	-0.00000	0.00356	-0.00333	0.00484	-0.00484	0.00602	-0.00590
trig p_T 12–15 GeV/c														
assoc p_T (GeV/c)	yield	σ_{stat}/Y	+ σ_{f_2}/Y	- σ_{f_2}/Y	+ σ_{f_3}/Y	- σ_{f_3}/Y	+ σ_{f_4}/Y	- σ_{f_4}/Y	+ σ_ξ/Y	- σ_ξ/Y	σ_{π^0}	- σ_{π^0}	+ σ_{total}/Y	- σ_{total}/Y
0.5–1.0	1.90091	0.34490	0.00000	-0.00000	0.00671	-0.00337	0.00000	-0.00000	0.09604	-0.09604	0.00088	-0.00088	0.09628	-0.09610
1.0–2.0	0.79665	0.21265	0.00000	-0.00000	0.00552	-0.00292	0.00000	-0.00000	0.03341	-0.03341	0.00183	-0.00183	0.03391	-0.03358
2.0–3.0	0.09465	0.46139	0.00000	-0.00000	0.00635	-0.00315	0.00000	-0.00000	0.02259	-0.02259	0.00335	-0.00335	0.02370	-0.02305
3.0–5.0	0.04361	0.21446	0.00000	-0.00000	0.00101	-0.00050	0.00000	-0.00000	0.00310	-0.00309	0.00162	-0.00162	0.00364	-0.00352
5.0–7.0	0.01557	0.23265	0.00000	-0.00000	0.00020	-0.00023	0.00000	-0.00000	0.00152	-0.00162	0.00134	-0.00134	0.00204	-0.00212

H Data Tables: $I_{AA}(p_T)$
Table 67: 0–20%, Away-side $I_{AA}(p_T)$

trig p_T 4–5 GeV/c					
assoc	p_T	$I_{AA}(p_T)$	σ_{stat}/I	systematic error	
(GeV/c)				$+\sigma_{total}/I$	$-\sigma_{total}/I$
0.5–1.0	2.18588	0.07367	0.25324	-0.25382	
1.0–2.0	1.32846	0.08394	0.14776	-0.14870	
2.0–3.0	0.51972	0.22109	0.16365	-0.16483	
3.0–5.0	0.36227	0.23782	0.09370	-0.09432	
5.0–7.0	0.06542	2.83269	0.76104	-0.77363	
trig p_T 5–7 GeV/c					
assoc	p_T	$I_{AA}(p_T)$	σ_{stat}/I	systematic error	
(GeV/c)				$+\sigma_{total}/I$	$-\sigma_{total}/I$
0.5–1.0	1.99065	0.08523	0.19671	-0.19758	
1.0–2.0	1.22291	0.08666	0.10256	-0.10443	
2.0–3.0	0.59565	0.15496	0.05575	-0.05943	
3.0–5.0	0.53503	0.12482	0.05896	-0.05670	
5.0–7.0	0.41405	0.27955	0.08131	-0.06947	
trig p_T 7–9 GeV/c					
assoc	p_T	$I_{AA}(p_T)$	σ_{stat}/I	systematic error	
(GeV/c)				$+\sigma_{total}/I$	$-\sigma_{total}/I$
0.5–1.0	2.32541	0.15953	0.13564	-0.13058	
1.0–2.0	1.06843	0.19200	0.10945	-0.08448	
2.0–3.0	0.62898	0.23215	0.07659	-0.06588	
3.0–5.0	0.29163	0.29266	0.06978	-0.06387	
5.0–7.0	0.36200	0.35801	0.10750	-0.10694	
trig p_T 9–12 GeV/c					
assoc	p_T	$I_{AA}(p_T)$	σ_{stat}/I	systematic error	
(GeV/c)				$+\sigma_{total}/I$	$-\sigma_{total}/I$
0.5–1.0	2.22876	0.25378	0.12462	-0.12497	
1.0–2.0	0.61656	0.45034	0.15156	-0.12551	
2.0–3.0	1.00361	0.23277	0.07400	-0.08135	
3.0–5.0	0.60891	0.19398	0.07586	-0.08032	
5.0–7.0	0.83814	0.32279	0.15260	-0.18733	

Table 68: 20–40%, Away-side $I_{AA}(p_T)$

trig p_T 4–5 GeV/c					
assoc	p_T	$I_{AA}(p_T)$	σ_{stat}/I	systematic error	
(GeV/c)				$+\sigma_{total}/I$	$-\sigma_{total}/I$
0.5–1.0	1.95737	0.05945	0.28693	-0.28734	
1.0–2.0	1.59178	0.05189	0.15147	-0.15221	
2.0–3.0	1.04215	0.08419	0.08169	-0.08358	
3.0–5.0	0.53583	0.12406	0.06156	-0.06025	
5.0–7.0	0.72720	0.18105	0.08487	-0.07563	
trig p_T 5–7 GeV/c					
assoc	p_T	$I_{AA}(p_T)$	σ_{stat}/I	systematic error	
(GeV/c)				$+\sigma_{total}/I$	$-\sigma_{total}/I$
0.5–1.0	1.74256	0.06771	0.23013	-0.23057	
1.0–2.0	1.31878	0.05715	0.11856	-0.11928	
2.0–3.0	0.76867	0.08758	0.06369	-0.06543	
3.0–5.0	0.55266	0.08965	0.05018	-0.04704	
5.0–7.0	0.54611	0.14602	0.07911	-0.06675	
trig p_T 7–9 GeV/c					
assoc	p_T	$I_{AA}(p_T)$	σ_{stat}/I	systematic error	
(GeV/c)				$+\sigma_{total}/I$	$-\sigma_{total}/I$
0.5–1.0	2.22725	0.11700	0.14818	-0.15020	
1.0–2.0	1.54012	0.09675	0.08119	-0.08374	
2.0–3.0	0.61310	0.17046	0.06206	-0.06658	
3.0–5.0	0.60067	0.12101	0.06117	-0.06134	
5.0–7.0	0.62563	0.19646	0.10664	-0.10687	
trig p_T 9–12 GeV/c					
assoc	p_T	$I_{AA}(p_T)$	σ_{stat}/I	systematic error	
(GeV/c)				$+\sigma_{total}/I$	$-\sigma_{total}/I$
0.5–1.0	1.72568	0.22885	0.16697	-0.17118	
1.0–2.0	1.36811	0.15056	0.08049	-0.08536	
2.0–3.0	0.64204	0.25747	0.07554	-0.08587	
3.0–5.0	0.53300	0.17650	0.07531	-0.08029	
5.0–7.0	0.48624	0.32385	0.15257	-0.18732	

I Data Tables: $I_{AA}(\Delta\phi)$

Table 69: 0–20%, trigger p_T 4.0–5.0 Away-side $I_{AA}(\Delta\phi)$

associate p_T 0.5–1.0 GeV/c														
ϕ	$I_{AA}(\Delta\phi)$	σ_{stat}/I	systematic errors											
			$+\sigma_{f_2}/I$	$-\sigma_{f_2}/I$	$+\sigma_{f_3}/I$	$-\sigma_{f_3}/I$	$+\sigma_{f_4}/I$	$-\sigma_{f_4}/I$	$+\sigma_\varepsilon/I$	$-\sigma_\varepsilon/I$	$+\sigma_{\pi^0}/I$	$-\sigma_{\pi^0}/I$	$+\sigma_{pp}/I$	$-\sigma_{pp}/I$
1.68	6.37423	0.79282	0.14705	-0.14245	0.02139	-0.02285	0.05609	-0.06418	0.35807	-0.35805	0.39188	-0.39149	0.08934	-0.07579
1.88	3.40801	0.53232	0.09637	-0.09335	0.04437	-0.04739	0.01503	-0.01720	0.28419	-0.28417	0.30381	-0.30343	0.04832	-0.04406
2.09	2.54704	0.32321	0.04355	-0.04219	0.04011	-0.04283	0.02035	-0.01779	0.20819	-0.20818	0.21754	-0.21756	0.03522	-0.03302
2.30	2.64778	0.16644	0.00549	-0.00532	0.01956	-0.02089	0.02400	-0.02098	0.12575	-0.12574	0.12985	-0.12952	0.02962	-0.02796
2.51	2.09524	0.12970	0.01365	-0.01409	0.00649	-0.00693	0.01724	-0.01507	0.10942	-0.10942	0.11208	-0.11184	0.02661	-0.02531
2.72	1.78988	0.10637	0.02638	-0.02723	0.00618	-0.00579	0.00199	-0.00174	0.09780	-0.09780	0.10179	-0.10198	0.02509	-0.02393
2.93	1.84563	0.08526	0.03007	-0.03104	0.01352	-0.01266	0.00929	-0.01062	0.08173	-0.08173	0.08895	-0.08930	0.02433	-0.02334
3.14	1.54197	0.09352	0.03625	-0.03742	0.01840	-0.01723	0.01528	-0.01749	0.09006	-0.09005	0.10027	-0.10085	0.02466	-0.02288
associate p_T 1.0–2.0 GeV/c														
ϕ	$I_{AA}(\Delta\phi)$	σ_{stat}/I	systematic errors											
			$+\sigma_{f_2}/I$	$-\sigma_{f_2}/I$	$+\sigma_{f_3}/I$	$-\sigma_{f_3}/I$	$+\sigma_{f_4}/I$	$-\sigma_{f_4}/I$	$+\sigma_\varepsilon/I$	$-\sigma_\varepsilon/I$	$+\sigma_{\pi^0}/I$	$-\sigma_{\pi^0}/I$	$+\sigma_{pp}/I$	$-\sigma_{pp}/I$
1.68	8.39428	1.67672	0.24840	-0.24193	0.05967	-0.06369	0.19363	-0.22139	0.33582	-0.33582	0.46427	-0.47370	0.27577	-0.17776
1.88	2.42710	1.27513	0.20700	-0.20160	0.15739	-0.16800	0.06599	-0.07545	0.33945	-0.33945	0.43267	-0.43565	0.08344	-0.07158
2.09	2.30952	0.30286	0.03712	-0.03615	0.05644	-0.06025	0.03542	-0.03098	0.09878	-0.09878	0.12481	-0.12512	0.03680	-0.03447
2.30	2.48027	0.16290	0.00488	-0.00475	0.02870	-0.03063	0.04355	-0.03809	0.06226	-0.06226	0.08137	-0.07930	0.03139	-0.02954
2.51	1.55048	0.11837	0.01183	-0.01215	0.00924	-0.00986	0.03035	-0.02654	0.05260	-0.05260	0.06257	-0.06097	0.02610	-0.02473
2.72	1.13361	0.10539	0.02493	-0.02560	0.00959	-0.00899	0.00382	-0.00334	0.05134	-0.05134	0.05801	-0.05817	0.02442	-0.02323
2.93	0.88680	0.10014	0.03333	-0.03423	0.02460	-0.02305	0.02092	-0.02392	0.05039	-0.05039	0.06852	-0.06940	0.02340	-0.02231
3.14	0.71338	0.11574	0.04238	-0.04351	0.03532	-0.03309	0.03632	-0.04153	0.05858	-0.05858	0.08829	-0.09025	0.02319	-0.02216
associate p_T 2.0–3.0 GeV/c														
ϕ	$I_{AA}(\Delta\phi)$	σ_{stat}/I	systematic errors											
			$+\sigma_{f_2}/I$	$-\sigma_{f_2}/I$	$+\sigma_{f_3}/I$	$-\sigma_{f_3}/I$	$+\sigma_{f_4}/I$	$-\sigma_{f_4}/I$	$+\sigma_\varepsilon/I$	$-\sigma_\varepsilon/I$	$+\sigma_{\pi^0}/I$	$-\sigma_{\pi^0}/I$	$+\sigma_{pp}/I$	$-\sigma_{pp}/I$
1.68	4.43563	6.21451	0.46395	-0.45057	0.11100	-0.11791	0.38185	-0.43231	0.33370	-0.33401	0.69876	-0.72035	0.36000	-1.28572
1.88	4.98436	1.34490	0.10199	-0.09903	0.07724	-0.08205	0.03433	-0.03887	0.08912	-0.08920	0.17647	-0.17794	0.24053	-0.16236
2.09	3.76371	0.38147	0.02083	-0.02023	0.03156	-0.03352	0.02079	-0.01836	0.02956	-0.02959	0.07359	-0.07365	0.06733	-0.05948
2.30	0.59033	0.80892	0.01265	-0.01228	0.07412	-0.07874	0.11806	-0.10428	0.08609	-0.08617	0.17235	-0.16538	0.04131	-0.03809
2.51	0.75761	0.30391	0.01467	-0.01510	0.01144	-0.01215	0.03945	-0.03485	0.03492	-0.03495	0.07476	-0.07266	0.03096	-0.02909
2.72	0.35451	0.32270	0.03910	-0.04026	0.01496	-0.01408	0.00627	-0.00554	0.04316	-0.04320	0.07887	-0.07926	0.02624	-0.02513
2.93	0.28648	0.28894	0.04620	-0.04757	0.03389	-0.03190	0.03070	-0.03476	0.03748	-0.03752	0.09094	-0.09239	0.02453	-0.02338
3.14	0.25153	0.25160	0.04652	-0.04790	0.03854	-0.03627	0.04221	-0.04779	0.03453	-0.03456	0.09500	-0.09742	0.02381	-0.02249
associate p_T 3.0–5.0 GeV/c														
ϕ	$I_{AA}(\Delta\phi)$	σ_{stat}/I	systematic errors											
			$+\sigma_{f_2}/I$	$-\sigma_{f_2}/I$	$+\sigma_{f_3}/I$	$-\sigma_{f_3}/I$	$+\sigma_{f_4}/I$	$-\sigma_{f_4}/I$	$+\sigma_\varepsilon/I$	$-\sigma_\varepsilon/I$	$+\sigma_{\pi^0}/I$	$-\sigma_{\pi^0}/I$	$+\sigma_{pp}/I$	$-\sigma_{pp}/I$
1.68	40.69336	6.35921	0.05005	-0.04844	0.01171	-0.01245	0.04583	-0.05194	0.03164	-0.03140	0.10113	-0.10330	0.67348	-1.94323
1.88	-22.04266	2.13767	0.03088	-0.02988	0.02287	-0.02432	0.01156	-0.01310	0.02371	-0.02353	0.07037	-0.07064	0.45089	-4.45675
2.09	0.38285	2.53815	0.06454	-0.06247	0.09562	-0.10166	0.07172	-0.06329	0.08041	-0.07981	0.22386	-0.22318	0.07473	-0.06895
2.30	1.25551	0.34731	0.00226	-0.00219	0.01298	-0.01380	0.02354	-0.02077	0.01352	-0.01342	0.06743	-0.06665	0.04924	-0.04898
2.51	0.35420	0.64455	0.01346	-0.01391	0.01030	-0.01096	0.04047	-0.03571	0.02821	-0.02800	0.09375	-0.09187	0.03710	-0.03865
2.72	0.25000	0.37540	0.01981	-0.02047	0.00744	-0.00700	0.00355	-0.00314	0.01926	-0.01912	0.06002	-0.06012	0.02822	-0.03100
2.93	0.27134	0.20831	0.01394	-0.01440	0.01004	-0.00945	0.01034	-0.01172	0.00997	-0.00989	0.05771	-0.05798	0.02469	-0.02776
3.14	0.30042	0.14138	0.01093	-0.01129	0.00889	-0.00837	0.01107	-0.01255	0.00715	-0.00710	0.05606	-0.05635	0.02334	-0.02731
associate p_T 5.0–7.0 GeV/c														
ϕ	$I_{AA}(\Delta\phi)$	σ_{stat}/I	systematic errors											
			$+\sigma_{f_2}/I$	$-\sigma_{f_2}/I$	$+\sigma_{f_3}/I$	$-\sigma_{f_3}/I$	$+\sigma_{f_4}/I$	$-\sigma_{f_4}/I$	$+\sigma_\varepsilon/I$	$-\sigma_\varepsilon/I$	$+\sigma_{\pi^0}/I$	$-\sigma_{\pi^0}/I$	$+\sigma_{pp}/I$	$-\sigma_{pp}/I$
1.68	10.27797	1.73635	0.02058	-0.01974	0.01020	-0.01121	0.03147	-0.03677	0.02019	-0.01969	0.29180	-0.29237	0.31400	-0.80945
1.88	-2.11201	5.30665	0.09239	-0.08863	0.14499	-0.15929	0.05779	-0.06754	0.10994	-0.10723	0.66108	-0.66433	0.33833	-0.98800
2.09	-11.20743	6.10832	0.04332	-0.04155	0.13595	-0.14936	0.08290	-0.07093	0.08361	-0.08155	0.52348	-0.52490	1.86305	-0.68492
2.30	-0.84148	1.54136	0.00492	-0.00472	0.05974	-0.06564	0.08809	-0.07537	0.04553	-0.04441	0.70239	-0.70136	0.11982	-0.10853
2.51	0.28543	2.83197	0.02740	-0.02856	0.04482	-0.04924	0.14309	-0.12244	0.08972	-0.08752	0.30912	-0.30027	0.08444	-0.08483
2.72	0.05912	3.64597	0.08996	-0.09378	0.07466	-0.06796	0.02803	-0.02399	0.13655	-0.13319	0.70133	-0.70035	0.03978	-0.05042
2.93	0.28760	0.35773	0.01073	-0.01119	0.01708	-0.01555	0.01342	-0.01568	0.01197	-0.01168	0.26357	-0.26361	0.02857	-0.04080
3.14	0.22061	0.39651	0.01392	-0.01451	0.02501	-0.02277	0.02376	-0.02777	0.01420	-0.01385	0.24262	-0.24284	0.02767	-0.04002

Table 70: 0–20%, trigger p_T 5.0–7.0 Away-side $I_{AA}(\Delta\phi)$

associate p_T 0.5–1.0 GeV/c																
ϕ	$I_{AA}(\Delta\phi)$	σ_{stat}/I	$+ \sigma_{f2}/I$	$- \sigma_{f2}/I$	$+ \sigma_{f3}/I$	$- \sigma_{f3}/I$	$+ \sigma_{f4}/I$	$- \sigma_{f4}/I$	$+ \sigma_\xi/I$	$- \sigma_\xi/I$	$+ \sigma_{\pi^0}/I$	$- \sigma_{\pi^0}/I$	$+ \sigma_{pp}/I$	$- \sigma_{pp}/I$	$+ \sigma_{total}/I$	$- \sigma_{total}/I$
1.68	9.64426	0.73880	0.13662	-0.13007	0.01728	-0.01931	0.03252	-0.04139	0.16955	-0.16952	0.22104	-0.21871	0.11976	-0.09622	0.25147	-0.23901
1.88	3.16082	0.58191	0.11861	-0.11293	0.04748	-0.05307	0.01155	-0.01476	0.17823	-0.17820	0.21976	-0.21821	0.04963	-0.04515	0.22536	-0.22289
2.09	3.61272	0.33280	0.04950	-0.04713	0.03963	-0.04430	0.01606	-0.01262	0.12054	-0.12052	0.13743	-0.13765	0.04195	-0.03857	0.14378	-0.14304
2.30	2.33320	0.21100	0.00792	-0.00754	0.02453	-0.02743	0.02404	-0.01889	0.09240	-0.09239	0.09929	-0.09889	0.02892	-0.02740	0.10354	-0.10274
2.51	2.00736	0.14418	0.01692	-0.01778	0.00712	-0.00795	0.01510	-0.01186	0.07027	-0.07026	0.07476	-0.07445	0.02459	-0.02343	0.07889	-0.07825
2.72	1.42476	0.13623	0.03795	-0.03986	0.00824	-0.00737	0.00202	-0.00159	0.07288	-0.07287	0.08307	-0.08386	0.02246	-0.02150	0.08620	-0.08672
2.93	1.33030	0.11683	0.04651	-0.04885	0.01936	-0.01732	0.00912	-0.01161	0.06548	-0.06548	0.08357	-0.08475	0.02154	-0.02039	0.08645	-0.08732
3.14	1.25891	0.11131	0.04849	-0.05093	0.02279	-0.02039	0.01298	-0.01652	0.06239	-0.06239	0.08371	-0.08514	0.02112	-0.02026	0.08648	-0.08767
associate p_T 1.0–2.0 GeV/c																
ϕ	$I_{AA}(\Delta\phi)$	σ_{stat}/I	$+ \sigma_{f2}/I$	$- \sigma_{f2}/I$	$+ \sigma_{f3}/I$	$- \sigma_{f3}/I$	$+ \sigma_{f4}/I$	$- \sigma_{f4}/I$	$+ \sigma_\xi/I$	$- \sigma_\xi/I$	$+ \sigma_{\pi^0}/I$	$- \sigma_{\pi^0}/I$	$+ \sigma_{pp}/I$	$- \sigma_{pp}/I$	$+ \sigma_{total}/I$	$- \sigma_{total}/I$
1.68	-129.34773	11.43866	0.23458	-0.22608	0.04510	-0.05037	0.10544	-0.13387	0.15307	-0.15310	0.30270	-0.30826	0.73622	-1.55706	0.79602	-1.58729
1.88	9.40828	0.72366	0.11353	-0.10941	0.06909	-0.07716	0.02087	-0.02650	0.08981	-0.08983	0.16182	-0.16345	0.15750	-0.11973	0.22583	-0.20263
2.09	3.04485	0.33102	0.04907	-0.04729	0.05973	-0.06670	0.02998	-0.02362	0.06298	-0.06299	0.10422	-0.10598	0.04532	-0.04133	0.11368	-0.11379
2.30	2.33836	0.17065	0.00628	-0.00606	0.02960	-0.03306	0.03593	-0.02830	0.03868	-0.03869	0.06100	-0.05869	0.02989	-0.02810	0.06797	-0.06511
2.51	1.24111	0.15258	0.01885	-0.01956	0.01191	-0.01330	0.03129	-0.02465	0.04084	-0.04085	0.05621	-0.05340	0.02392	-0.02289	0.06114	-0.05814
2.72	0.96352	0.11475	0.03342	-0.03468	0.01088	-0.00975	0.00331	-0.00261	0.03532	-0.03532	0.04884	-0.04944	0.02122	-0.02036	0.05330	-0.05351
2.93	0.63640	0.12124	0.04995	-0.05183	0.03120	-0.02794	0.01827	-0.02320	0.03676	-0.03677	0.07190	-0.07330	0.01996	-0.01919	0.07466	-0.07581
3.14	0.62112	0.11085	0.04991	-0.05179	0.03520	-0.03152	0.02492	-0.03165	0.03538	-0.03358	0.07412	-0.07629	0.01987	-0.01862	0.07678	-0.07857
associate p_T 2.0–3.0 GeV/c																
ϕ	$I_{AA}(\Delta\phi)$	σ_{stat}/I	$+ \sigma_{f2}/I$	$- \sigma_{f2}/I$	$+ \sigma_{f3}/I$	$- \sigma_{f3}/I$	$+ \sigma_{f4}/I$	$- \sigma_{f4}/I$	$+ \sigma_\xi/I$	$- \sigma_\xi/I$	$+ \sigma_{\pi^0}/I$	$- \sigma_{\pi^0}/I$	$+ \sigma_{pp}/I$	$- \sigma_{pp}/I$	$+ \sigma_{total}/I$	$- \sigma_{total}/I$
1.68	142.52138	94.24173	0.63191	-0.60543	0.13350	-0.14759	0.33803	-0.41921	0.23518	-0.23545	0.77043	-0.79143	0.96575	-1.03673	1.23637	-1.30520
1.88	16.74550	1.54534	0.07362	-0.07054	0.04923	-0.05443	0.01611	-0.01997	0.03327	-0.03330	0.09786	-0.09906	0.93336	-0.32582	0.93855	-0.34073
2.09	1.98546	0.72615	0.04951	-0.04744	0.06622	-0.07321	0.03517	-0.02836	0.03632	-0.03636	0.10153	-0.10321	0.08298	-0.07117	0.13233	-0.12663
2.30	1.43820	0.29660	0.00529	-0.00507	0.02737	-0.03025	0.03514	-0.02834	0.01861	-0.01863	0.05224	-0.04962	0.04016	-0.03709	0.06686	-0.06298
2.51	0.69571	0.29929	0.01697	-0.01772	0.01185	-0.01310	0.03295	-0.02657	0.02117	-0.02119	0.04876	-0.04534	0.02942	-0.02754	0.05821	-0.05440
2.72	0.61823	0.15945	0.02219	-0.02316	0.00791	-0.00715	0.00257	-0.00207	0.01282	-0.01284	0.03505	-0.03531	0.02332	-0.02228	0.04199	-0.04179
2.93	0.20956	0.28025	0.05287	-0.05519	0.03613	-0.03268	0.02315	-0.02871	0.02245	-0.02247	0.07439	-0.07639	0.02051	-0.01986	0.07804	-0.07979
3.14	0.40937	0.12130	0.02568	-0.02681	0.01982	-0.01793	0.01535	-0.01904	0.00997	-0.00998	0.04187	-0.04322	0.02008	-0.01917	0.04778	-0.04860
associate p_T 3.0–5.0 GeV/c																
ϕ	$I_{AA}(\Delta\phi)$	σ_{stat}/I	$+ \sigma_{f2}/I$	$- \sigma_{f2}/I$	$+ \sigma_{f3}/I$	$- \sigma_{f3}/I$	$+ \sigma_{f4}/I$	$- \sigma_{f4}/I$	$+ \sigma_\xi/I$	$- \sigma_\xi/I$	$+ \sigma_{\pi^0}/I$	$- \sigma_{\pi^0}/I$	$+ \sigma_{pp}/I$	$- \sigma_{pp}/I$	$+ \sigma_{total}/I$	$- \sigma_{total}/I$
1.68	-12.17936	0.88683	0.01861	-0.01769	0.00402	-0.00445	0.01160	-0.01441	0.00632	-0.00621	0.04047	-0.04099	0.22332	-0.39320	0.22781	-0.39581
1.88	-12.13652	0.87094	0.01899	-0.01805	0.01299	-0.01439	0.00484	-0.00602	0.00783	-0.00769	0.04171	-0.04188	0.26324	-0.54317	0.26726	-0.54514
2.09	0.08695	30.54601	0.88884	-0.84501	1.21631	-1.34680	0.73719	-0.59308	0.59464	-0.58425	2.03724	-2.05057	0.28044	-0.18319	2.13791	-2.14010
2.30	0.99822	0.46304	0.00338	-0.00322	0.01792	-0.01985	0.02627	-0.02113	0.01086	-0.01067	0.05065	-0.04888	0.06241	-0.05998	0.08340	-0.08051
2.51	0.82654	0.27078	0.00591	-0.00621	0.00425	-0.00471	0.01349	-0.01086	0.00677	-0.00665	0.03731	-0.03653	0.03960	-0.04157	0.05785	-0.05872
2.72	0.36949	0.19237	0.01080	-0.01136	0.00398	-0.00359	0.00147	-0.00118	0.00574	-0.00564	0.03683	-0.03694	0.02482	-0.02906	0.04884	-0.05120
2.93	0.27137	0.14526	0.01040	-0.01093	0.00734	-0.00663	0.00534	-0.00664	0.00406	-0.00399	0.03593	-0.03616	0.02085	-0.02513	0.04585	-0.04812
3.14	0.30476	0.09796	0.00787	-0.00827	0.00627	-0.00566	0.00552	-0.00686	0.00281	-0.00276	0.03497	-0.03520	0.02008	-0.02412	0.04475	-0.04687
associate p_T 5.0–7.0 GeV/c																
ϕ	$I_{AA}(\Delta\phi)$	σ_{stat}/I	$+ \sigma_{f2}/I$	$- \sigma_{f2}/I$	$+ \sigma_{f3}/I$	$- \sigma_{f3}/I$	$+ \sigma_{f4}/I$	$- \sigma_{f4}/I$	$+ \sigma_\xi/I$	$- \sigma_\xi/I$	$+ \sigma_{\pi^0}/I$	$- \sigma_{\pi^0}/I$	$+ \sigma_{pp}/I$	$- \sigma_{pp}/I$	$+ \sigma_{total}/I$	$- \sigma_{total}/I$
1.68	3.16795	1.44874	0.01671	-0.01550	0.00574	-0.00699	0.01535	-0.02089	0.00925	-0.00960	0.02729	-0.03048	0.29916	-0.19916	0.30046	-0.20157
1.88	-3.58900	1.32471	0.01752	-0.01625	0.01904	-0.02321	0.00658	-0.00896	0.01176	-0.01220	0.03037	-0.03321	0.47680	-0.25381	0.47780	-0.25602
2.09	3.89830	2.47771	0.02468	-0.02288	0.005362	-0.006356	0.03303	-0.02427	0.02687	-0.02788	0.07366	-0.07932	3.43900	-0.44175	3.43980	-0.44887
2.30	1.48347	0.61275	0.00161	-0.00149	0.01354	-0.01651	0.02017	-0.01482	0.00841	-0.00872	0.02806	-0.02635	0.11904	-0.10937	0.12248	-0.11269
2.51	0.27633	1.37924	0.01241	-0.01339	0.01455	-0.01773	0.04691	-0.03448	0.02371	-0.02461	0.05737	-0.04950	0.06788	-0.07387	0.08919	-0.08924
2.72	0.22530	0.62035	0.01377	-0.01485	0.00908	-0.00745	0.00310	-0.00228	0.01218	-0.01264	0.02490	-0.02512	0.03748	-0.05000	0.04573	-0.05654
2.93	0.31019	0.24539	0.00636	-0.00686	0.00805	-0.00661	0.00495	-0.00673	0.00414	-0.00429	0.01486	-0.01512	0.02611	-0.04014	0.03047	-0.04319
3.14	0.44754	0.13379	0.00333	-0.00359	0.00476	-0.00391	0.00354	-0.00481	0.00198	-0.00205	0.01099	-0.01123	0.02312	-0.03752	0.02608	-0.03948

Table 71: 0–20%, trigger p_T 7.0–9.0 Away-side $I_{AA}(\Delta\phi)$

associate p_T 0.5–1.0 GeV/c																
ϕ	$I_{AA}(\Delta\phi)$	σ_{stat}/I	systematic errors													
			$+\sigma_{f_2}/I$	$-\sigma_{f_2}/I$	$+\sigma_{f_3}/I$	$-\sigma_{f_3}/I$	$+\sigma_{f_4}/I$	$-\sigma_{f_4}/I$	$+\sigma_\xi/I$	$-\sigma_\xi/I$	$+\sigma_{\pi^0}/I$	$-\sigma_{\pi^0}/I$	$+\sigma_{pp}/I$	$-\sigma_{pp}/I$		
1.68	-8.24314	40.76106	3.89699	-4.96139	0.56121	-0.49973	0.72562	-0.86764	3.44749	-3.44794	5.28933	-6.12944	1.28044	-0.82036	5.44279	-6.18469
1.88	4.10342	1.59331	0.15522	-0.19761	0.07075	-0.06300	0.01182	-0.01413	0.16621	-0.16623	0.23924	-0.26688	0.14420	-0.11175	0.27942	-0.28941
2.09	6.10640	0.58941	0.03962	-0.05045	0.03612	-0.03217	0.00945	-0.00790	0.06875	-0.06876	0.08834	-0.09210	0.09173	-0.07728	0.12740	-0.12028
2.30	4.87883	0.27263	0.00460	-0.00585	0.01622	-0.01445	0.01026	-0.00858	0.03822	-0.03822	0.04430	-0.04348	0.04893	-0.04462	0.06611	-0.06241
2.51	2.37248	0.30960	0.02329	-0.01829	0.00834	-0.00742	0.01142	-0.00955	0.05150	-0.05150	0.05953	-0.05729	0.03781	-0.03512	0.07064	-0.06733
2.72	1.28454	0.31375	0.05664	-0.04449	0.00834	-0.00937	0.00166	-0.00139	0.05791	-0.05791	0.08218	-0.07445	0.02949	-0.02807	0.08739	-0.07966
2.93	1.42474	0.21072	0.05380	-0.04226	0.01519	-0.01706	0.00617	-0.00738	0.04032	-0.04033	0.06999	-0.06219	0.02691	-0.02537	0.07507	-0.06726
3.14	1.75554	0.14836	0.04087	-0.03210	0.01303	-0.01463	0.00640	-0.00765	0.02799	-0.02800	0.05267	-0.04687	0.02541	-0.02418	0.05859	-0.05286
associate p_T 1.0–2.0 GeV/c																
ϕ	$I_{AA}(\Delta\phi)$	σ_{stat}/I	systematic errors													
			$+\sigma_{f_2}/I$	$-\sigma_{f_2}/I$	$+\sigma_{f_3}/I$	$-\sigma_{f_3}/I$	$+\sigma_{f_4}/I$	$-\sigma_{f_4}/I$	$+\sigma_\xi/I$	$-\sigma_\xi/I$	$+\sigma_{\pi^0}/I$	$-\sigma_{\pi^0}/I$	$+\sigma_{pp}/I$	$-\sigma_{pp}/I$		
1.68	11.10296	1.57196	0.12874	-0.16977	0.02714	-0.02411	0.04389	-0.05205	0.05840	-0.05840	0.15080	-0.18872	0.20612	-0.35068	0.25541	-0.39824
1.88	-8.18110	1.70218	0.14261	-0.18806	0.09518	-0.08454	0.01988	-0.02358	0.07840	-0.07839	0.18992	-0.22214	0.40880	-0.22489	0.45078	-0.31613
2.09	3.87447	0.66607	0.04840	-0.06382	0.06460	-0.05738	0.02095	-0.01766	0.04315	-0.04314	0.09455	-0.09830	0.09635	-0.08097	0.13505	-0.12741
2.30	3.13684	0.30701	0.00551	-0.00726	0.02844	-0.02526	0.02231	-0.01881	0.02354	-0.02353	0.04454	-0.04113	0.05080	-0.04603	0.06765	-0.06182
2.51	1.19266	0.35476	0.03024	-0.02293	0.01530	-0.01359	0.02599	-0.02191	0.03323	-0.03323	0.05494	-0.04884	0.03493	-0.03260	0.06519	-0.05881
2.72	1.22892	0.17464	0.03433	-0.02603	0.00713	-0.00802	0.00176	-0.00148	0.01746	-0.01746	0.04036	-0.03378	0.02652	-0.02544	0.04841	-0.04241
2.93	0.69710	0.19962	0.05624	-0.04265	0.02239	-0.02521	0.01140	-0.01352	0.02098	-0.02098	0.06586	-0.05639	0.02353	-0.02265	0.07002	-0.06087
3.14	0.71592	0.17537	0.05379	-0.04079	0.02418	-0.02722	0.01489	-0.01766	0.01834	-0.01834	0.06424	-0.05607	0.02299	-0.02198	0.06830	-0.06031
associate p_T 2.0–3.0 GeV/c																
ϕ	$I_{AA}(\Delta\phi)$	σ_{stat}/I	systematic errors													
			$+\sigma_{f_2}/I$	$-\sigma_{f_2}/I$	$+\sigma_{f_3}/I$	$-\sigma_{f_3}/I$	$+\sigma_{f_4}/I$	$-\sigma_{f_4}/I$	$+\sigma_\xi/I$	$-\sigma_\xi/I$	$+\sigma_{\pi^0}/I$	$-\sigma_{\pi^0}/I$	$+\sigma_{pp}/I$	$-\sigma_{pp}/I$		
1.68	-29.87148	2.46940	0.03409	-0.04424	0.00839	-0.00726	0.01541	-0.01707	0.00900	-0.00898	0.04964	-0.05740	0.43244	-3.19680	0.43540	-3.19733
1.88	8.74485	2.66152	0.08971	-0.11641	0.06990	-0.06051	0.01658	-0.01837	0.02873	-0.02866	0.12502	-0.14130	0.287640	-0.42594	2.87915	-0.44898
2.09	0.66844	10.12072	0.35606	-0.46203	0.55491	-0.48033	0.19091	-0.17229	0.18507	-0.18461	0.73638	-0.73810	0.59595	-0.27190	0.94959	-0.78932
2.30	0.44270	2.06789	0.01902	-0.02468	0.11470	-0.09928	0.09542	-0.08611	0.04742	-0.04730	0.16136	-0.14589	0.08379	-0.07180	0.18219	-0.16302
2.51	0.48558	0.81870	0.03129	-0.02411	0.01879	-0.01626	0.03385	-0.03055	0.02040	-0.02035	0.06152	-0.05554	0.04764	-0.04317	0.07848	-0.07108
2.72	0.76724	0.22934	0.02042	-0.01574	0.00490	-0.00566	0.00132	-0.00119	0.00617	-0.00615	0.03802	-0.03583	0.03152	-0.02949	0.05051	-0.04760
2.93	0.32382	0.29535	0.03649	-0.02812	0.01680	-0.01941	0.00997	-0.01104	0.00809	-0.00807	0.05071	-0.04634	0.02501	-0.02386	0.05735	-0.05300
3.14	0.38878	0.14956	0.01993	-0.01536	0.01036	-0.01197	0.00743	-0.00824	0.00404	-0.00403	0.03696	-0.03540	0.02141	-0.02108	0.04378	-0.04231
associate p_T 3.0–5.0 GeV/c																
ϕ	$I_{AA}(\Delta\phi)$	σ_{stat}/I	systematic errors													
			$+\sigma_{f_2}/I$	$-\sigma_{f_2}/I$	$+\sigma_{f_3}/I$	$-\sigma_{f_3}/I$	$+\sigma_{f_4}/I$	$-\sigma_{f_4}/I$	$+\sigma_\xi/I$	$-\sigma_\xi/I$	$+\sigma_{\pi^0}/I$	$-\sigma_{\pi^0}/I$	$+\sigma_{pp}/I$	$-\sigma_{pp}/I$		
1.68	-3.38532	2.03090	0.03012	-0.03820	0.00774	-0.00673	0.01615	-0.01801	0.00725	-0.00745	0.04036	-0.04725	0.67956	-0.29049	0.68079	-0.29438
1.88	-0.97769	2.86542	0.05762	-0.07308	0.04689	-0.04074	0.01263	-0.01409	0.01682	-0.01728	0.11775	-0.12410	0.19460	-0.30956	0.22947	-0.33489
2.09	10.70203	3.56700	0.02222	-0.02818	0.03616	-0.03142	0.01422	-0.01276	0.01052	-0.01081	0.05062	-0.05009	0.63615	-2.34431	0.63820	-2.34486
2.30	0.82678	0.80638	0.00282	-0.00357	0.01775	-0.01542	0.01688	-0.01514	0.00640	-0.00658	0.03054	-0.02840	0.11084	-0.09487	0.11512	-0.09920
2.51	0.50142	0.77074	0.01110	-0.00875	0.00712	-0.00619	0.01467	-0.01316	0.00675	-0.00693	0.02670	-0.02478	0.07494	-0.06961	0.07976	-0.07411
2.72	0.27180	0.41141	0.01465	-0.01155	0.00377	-0.00434	0.00115	-0.00104	0.00412	-0.00424	0.02300	-0.02129	0.03556	-0.03804	0.04273	-0.04397
2.93	0.28602	0.19798	0.00826	-0.00652	0.00408	-0.00470	0.00274	-0.00305	0.00171	-0.00175	0.01931	-0.01883	0.02516	-0.02883	0.03223	-0.03490
3.14	0.25218	0.15020	0.00683	-0.00538	0.00381	-0.00438	0.00309	-0.00345	0.00129	-0.00133	0.01858	-0.01830	0.02250	-0.02643	0.02972	-0.03264
associate p_T 5.0–7.0 GeV/c																
ϕ	$I_{AA}(\Delta\phi)$	σ_{stat}/I	systematic errors													
			$+\sigma_{f_2}/I$	$-\sigma_{f_2}/I$	$+\sigma_{f_3}/I$	$-\sigma_{f_3}/I$	$+\sigma_{f_4}/I$	$-\sigma_{f_4}/I$	$+\sigma_\xi/I$	$-\sigma_\xi/I$	$+\sigma_{\pi^0}/I$	$-\sigma_{\pi^0}/I$	$+\sigma_{pp}/I$	$-\sigma_{pp}/I$		
1.68	2.85235	2.62924	0.01314	-0.01530	0.00354	-0.00434	0.00746	-0.01162	0.00579	-0.00643	0.01919	-0.02288	1.67600	-0.39208	1.67611	-0.39276
2.09	-4.29369	1.48789	0.00473	-0.00551	0.00806	-0.00989	0.00448	-0.00288	0.00409	-0.00455	0.01714	-0.01807	1.95712	-0.40407	1.95720	-0.40450
2.30	-1.01295	2.00628	0.00253	-0.00295	0.01671	-0.02050	0.02244	-0.01441	0.01051	-0.01168	0.03300	-0.03102	0.68576	-0.29720	0.68657	-0.29885
2.51	0.12505	5.84689	0.02999	-0.02575	0.02194	-0.02692	0.06382	-0.04098	0.03623	-0.04025	0.08669	-0.07373	0.22330	-0.16561	0.23972	-0.18152
2.72	0.18805	1.00276	0.01190	-0.01022	0.00493	-0.00402	0.00151	-0.00097	0.00665	-0.00739	0.01774	-0.01669	0.06708	-0.07353	0.06947	-0.07548
2.93	0.44657	0.28660	0.00259	-0.00222	0.00206	-0.00168	0.00099	-0.00154	0.00106	-0.00118	0.00892	-0.00884	0.03540	-0.04822	0.03662	-0.04911
3.14	0.36371	0.21260	0.00183	-0.00157	0.00164	-0.00134	0.00096	-0.00149	0.00069	-0.00076	0.00815	-0.00813	0.02660	-0.04047	0.02	

Table 72: 0–20%, trigger p_T 9.0–12.0 Away–side $I_{AA}(\Delta\phi)$

associate p_T 0.5–1.0 GeV/c																
ϕ	$I_{AA}(\Delta\phi)$	σ_{stat}/I	systematic errors													
			$+\sigma_{f2}/I$	$-\sigma_{f2}/I$	$+\sigma_{f3}/I$	$-\sigma_{f3}/I$	$+\sigma_{f4}/I$	$-\sigma_{f4}/I$	$+\sigma_\xi/I$	$-\sigma_\xi/I$	$+\sigma_{\pi^0}/I$	$-\sigma_{\pi^0}/I$	$+\sigma_{pp}/I$	$-\sigma_{pp}/I$		
1.68	-38.48066	7.45816	0.20125	-0.31523	0.03253	-0.02522	0.03516	-0.04050	0.14900	-0.14902	0.25562	-0.35241	0.62676	-2.47230	0.67688	-2.49729
1.88	72.57661	5.80353	0.07508	-0.11760	0.03842	-0.02979	0.00536	-0.00618	0.06728	-0.06729	0.10840	-0.13916	3.15541	-0.59442	3.15728	-0.61049
2.09	5.82178	0.63085	0.02842	-0.04451	0.02908	-0.02255	0.00612	-0.00532	0.04126	-0.04126	0.05857	-0.06525	0.09726	-0.08136	0.11354	-0.10429
2.30	3.37414	0.58875	0.00699	-0.01095	0.02769	-0.02147	0.01410	-0.01224	0.04862	-0.04863	0.05841	-0.05593	0.07075	-0.06198	0.09175	-0.08349
2.51	0.75245	1.09399	0.07050	-0.04501	0.02303	-0.01785	0.02539	-0.02204	0.10601	-0.10602	0.13201	-0.11881	0.04314	-0.03948	0.13888	-0.12520
2.72	1.80633	0.37360	0.05482	-0.03500	0.00641	-0.00827	0.00118	-0.00102	0.03811	-0.03811	0.06735	-0.05276	0.03961	-0.03670	0.07813	-0.06427
2.93	1.32163	0.35404	0.07470	-0.04769	0.01676	-0.02161	0.00653	-0.00753	0.03807	-0.03807	0.08595	-0.06544	0.03361	-0.03135	0.09229	-0.07256
3.14	1.22061	0.34745	0.08061	-0.05146	0.02042	-0.02633	0.00963	-0.01109	0.03754	-0.03754	0.09192	-0.07005	0.03211	-0.03043	0.09737	-0.07638
associate p_T 1.0–2.0 GeV/c																
ϕ	$I_{AA}(\Delta\phi)$	σ_{stat}/I	systematic errors													
			$+\sigma_{f2}/I$	$-\sigma_{f2}/I$	$+\sigma_{f3}/I$	$-\sigma_{f3}/I$	$+\sigma_{f4}/I$	$-\sigma_{f4}/I$	$+\sigma_\xi/I$	$-\sigma_\xi/I$	$+\sigma_{\pi^0}/I$	$-\sigma_{\pi^0}/I$	$+\sigma_{pp}/I$	$-\sigma_{pp}/I$		
1.68	-1.17882	20.62431	1.50727	-2.45518	0.35105	-0.27140	0.47622	-0.54273	0.55315	-0.55311	1.73448	-2.60435	1.32262	-0.36307	2.18123	-2.62954
1.88	-4.93575	1.75903	0.11272	-0.18360	0.08310	-0.06424	0.01456	-0.01660	0.05012	-0.05012	0.19389	-0.23640	0.29189	-0.18449	0.35042	-0.29987
2.09	-3.41156	1.41897	0.07255	-0.11818	0.10697	-0.08270	0.02797	-0.02454	0.05232	-0.05231	0.14827	-0.16094	0.20132	-0.14368	0.25003	-0.21575
2.30	-0.61947	2.43878	0.03260	-0.05311	0.18603	-0.14382	0.11763	-0.10321	0.11271	-0.11270	0.26918	-0.23897	0.08316	-0.07145	0.28174	-0.24943
2.51	1.37700	0.45525	0.03233	-0.01985	0.01463	-0.01131	0.02004	-0.01758	0.02326	-0.02326	0.07051	-0.06435	0.04651	-0.04262	0.08447	-0.07719
2.72	1.10147	0.25845	0.04256	-0.02613	0.00688	-0.00890	0.00157	-0.00138	0.01417	-0.01417	0.06174	-0.05210	0.03156	-0.02987	0.06934	-0.06006
2.93	0.66692	0.30325	0.07192	-0.04415	0.02229	-0.02883	0.01094	-0.01247	0.01756	-0.01756	0.08859	-0.07068	0.02825	-0.02660	0.09299	-0.07552
3.14	0.57155	0.26983	0.06987	-0.04289	0.02445	-0.03162	0.01451	-0.01654	0.01559	-0.01559	0.08765	-0.07146	0.02584	-0.02436	0.09138	-0.07550
associate p_T 2.0–3.0 GeV/c																
ϕ	$I_{AA}(\Delta\phi)$	σ_{stat}/I	systematic errors													
			$+\sigma_{f2}/I$	$-\sigma_{f2}/I$	$+\sigma_{f3}/I$	$-\sigma_{f3}/I$	$+\sigma_{f4}/I$	$-\sigma_{f4}/I$	$+\sigma_\xi/I$	$-\sigma_\xi/I$	$+\sigma_{\pi^0}/I$	$-\sigma_{\pi^0}/I$	$+\sigma_{pp}/I$	$-\sigma_{pp}/I$		
1.68	-39.78379	1.68653	0.01188	-0.01901	0.00330	-0.00248	0.00522	-0.00546	0.00256	-0.00256	0.01643	-0.02210	0.37188	-1.45120	0.37224	-1.45136
1.88	-3.37136	1.22071	0.03870	-0.06192	0.03405	-0.02558	0.00696	-0.00728	0.01012	-0.01012	0.05394	-0.06889	0.15646	-0.22781	0.16550	-0.23800
2.09	94.70158	30.51050	0.05159	-0.08254	0.09079	-0.06819	0.02539	-0.02427	0.02189	-0.02189	0.11161	-0.11385	0.92482	-1.08848	0.93153	-1.09442
2.30	-1.72973	1.52274	0.00901	-0.01442	0.06137	-0.04610	0.04151	-0.03968	0.01834	-0.01834	0.08289	-0.07216	0.25884	-0.17051	0.27179	-0.18515
2.51	0.35119	0.57401	0.01679	-0.01049	0.00923	-0.00693	0.01352	-0.01293	0.00724	-0.00724	0.02667	-0.02206	0.08230	-0.07056	0.08651	-0.07393
2.72	0.91244	0.33940	0.02415	-0.01509	0.00461	-0.00613	0.00116	-0.00111	0.00483	-0.00483	0.02676	-0.01941	0.04562	-0.04180	0.05288	-0.04609
2.93	0.47488	0.25614	0.02453	-0.01533	0.00897	-0.01194	0.00528	-0.00553	0.00360	-0.00360	0.02847	-0.02255	0.02876	-0.02692	0.04047	-0.03512
3.14	0.49635	0.20080	0.02127	-0.01329	0.00879	-0.01170	0.00626	-0.00654	0.00285	-0.00285	0.02571	-0.02118	0.02674	-0.02539	0.03710	-0.03306
associate p_T 3.0–5.0 GeV/c																
ϕ	$I_{AA}(\Delta\phi)$	σ_{stat}/I	systematic errors													
			$+\sigma_{f2}/I$	$-\sigma_{f2}/I$	$+\sigma_{f3}/I$	$-\sigma_{f3}/I$	$+\sigma_{f4}/I$	$-\sigma_{f4}/I$	$+\sigma_\xi/I$	$-\sigma_\xi/I$	$+\sigma_{\pi^0}/I$	$-\sigma_{\pi^0}/I$	$+\sigma_{pp}/I$	$-\sigma_{pp}/I$		
2.09	6.03766	1.63287	0.00830	-0.01294	0.01539	-0.01161	0.00492	-0.00467	0.00332	-0.00329	0.01855	-0.01839	0.204483	-0.40359	2.04491	-0.40401
2.30	1.42298	0.86772	0.00183	-0.00286	0.01315	-0.00992	0.01017	-0.00965	0.00352	-0.00349	0.01712	-0.01459	0.22016	-0.15640	0.22083	-0.15708
2.51	0.49235	1.03272	0.01198	-0.00769	0.00713	-0.00538	0.01193	-0.01132	0.00501	-0.00496	0.01908	-0.01558	0.10818	-0.09295	0.10985	-0.09425
2.72	0.40982	0.36948	0.00949	-0.00609	0.00197	-0.00261	0.00056	-0.00054	0.00184	-0.00182	0.00992	-0.00695	0.04390	-0.04481	0.04501	-0.04535
2.93	0.49455	0.20650	0.00524	-0.00336	0.00208	-0.00276	0.00139	-0.00146	0.00074	-0.00074	0.00592	-0.00472	0.03044	-0.03340	0.03101	-0.03373
3.14	0.62151	0.13562	0.00269	-0.00173	0.00121	-0.00160	0.00097	-0.00102	0.00035	-0.00035	0.00324	-0.00273	0.02525	-0.02871	0.02546	-0.02883
associate p_T 5.0–7.0 GeV/c																
ϕ	$I_{AA}(\Delta\phi)$	σ_{stat}/I	systematic errors													
			$+\sigma_{f2}/I$	$-\sigma_{f2}/I$	$+\sigma_{f3}/I$	$-\sigma_{f3}/I$	$+\sigma_{f4}/I$	$-\sigma_{f4}/I$	$+\sigma_\xi/I$	$-\sigma_\xi/I$	$+\sigma_{\pi^0}/I$	$-\sigma_{\pi^0}/I$	$+\sigma_{pp}/I$	$-\sigma_{pp}/I$		
1.88	0.68062	2.38057	0.00764	-0.01076	0.00602	-0.00721	0.00140	-0.00241	0.00368	-0.00381	0.01411	-0.01664	0.46006	-0.24926	0.46028	-0.24981
2.09	2.00745	2.54325	0.00594	-0.00837	0.00937	-0.01121	0.00491	-0.00286	0.00464	-0.00481	0.01645	-0.01814	9.32861	-0.53181	9.32862	-0.53212
2.51	0.32306	1.62468	0.00566	-0.00402	0.00317	-0.00379	0.00869	-0.00506	0.00510	-0.00528	0.01650	-0.01458	0.26861	-0.18540	0.26911	-0.18598
2.72	0.64516	0.55345	0.00337	-0.00240	0.00104	-0.00087	0.00031	-0.00018	0.00141	-0.00146	0.01011	-0.00982	0.14231	-0.12300	0.14267	-0.12339
2.93	1.10250	0.36053	0.00124	-0.00088	0.00073	-0.00061	0.00031	-0.00053	0.00038	-0.00039	0.00954	-0.00950	0.07129	-0.07606	0.07193	-0.07665
3.14	0.41005	0.35536	0.00091	-0.00064	0.00061	-0.00051	0.00031	-0.00053	0.00025	-0.00026	0.00912	-0.00910	0.03078	-0.04358	0.03211	-0.04452

Table 73: 20–40%, trigger p_T 4.0–5.0 Away-side $I_{AA}(\Delta\phi)$

associate p_T 0.5–1.0 GeV/c																
ϕ	$I_{AA}(\Delta\phi)$	σ_{stat}/I	systematic errors													
			$+\sigma_{f_2}/I$	$-\sigma_{f_2}/I$	$+\sigma_{f_3}/I$	$-\sigma_{f_3}/I$	$+\sigma_{f_4}/I$	$-\sigma_{f_4}/I$	$+\sigma_\xi/I$	$-\sigma_\xi/I$	$+\sigma_{\pi^0}/I$	$-\sigma_{\pi^0}/I$	$+\sigma_{pp}/I$	$-\sigma_{pp}/I$		
1.68	2.39379	1.51697	0.35627	-0.34968	0.04739	-0.05123	0.21524	-0.26430	1.31296	-1.31294	1.37822	-1.38518	0.08934	-0.07579	1.38113	-1.38726
1.88	2.13735	0.64364	0.13980	-0.13722	0.05887	-0.06364	0.03454	-0.04242	0.62585	-0.62584	0.64514	-0.64550	0.04832	-0.04406	0.64701	-0.64707
2.09	4.05907	0.16506	0.02486	-0.02440	0.02094	-0.02264	0.01975	-0.01608	0.18133	-0.18133	0.18565	-0.18543	0.03522	-0.03302	0.18905	-0.18844
2.30	2.21564	0.15572	0.00597	-0.00586	0.01945	-0.02103	0.04436	-0.03613	0.20990	-0.20989	0.21583	-0.21443	0.02962	-0.02796	0.21794	-0.21633
2.51	1.75444	0.12233	0.01503	-0.01531	0.00645	-0.00697	0.03185	-0.02594	0.18378	-0.18378	0.18760	-0.18673	0.02661	-0.02531	0.18957	-0.18853
2.72	1.79242	0.08483	0.02429	-0.02474	0.00520	-0.00481	0.00307	-0.00250	0.13821	-0.13821	0.14094	-0.14099	0.02509	-0.02393	0.14328	-0.14313
2.93	1.71098	0.07340	0.02990	-0.03046	0.01228	-0.01136	0.01443	-0.01772	0.12532	-0.12531	0.13074	-0.13119	0.02433	-0.02334	0.13312	-0.13339
3.14	1.50584	0.07648	0.03422	-0.03486	0.01587	-0.01468	0.02255	-0.02769	0.13128	-0.13128	0.13893	-0.13988	0.02466	-0.02288	0.14122	-0.14187
associate p_T 1.0–2.0 GeV/c																
ϕ	$I_{AA}(\Delta\phi)$	σ_{stat}/I	systematic errors													
			$+\sigma_{f_2}/I$	$-\sigma_{f_2}/I$	$+\sigma_{f_3}/I$	$-\sigma_{f_3}/I$	$+\sigma_{f_4}/I$	$-\sigma_{f_4}/I$	$+\sigma_\xi/I$	$-\sigma_\xi/I$	$+\sigma_{\pi^0}/I$	$-\sigma_{\pi^0}/I$	$+\sigma_{pp}/I$	$-\sigma_{pp}/I$	$+\sigma_{total}/I$	$-\sigma_{total}/I$
1.68	16.38205	1.03054	0.13373	-0.13134	0.02766	-0.03002	0.11664	-0.14254	0.28110	-0.28107	0.33373	-0.34290	0.27577	-0.17776	0.43296	-0.38627
1.88	5.61907	0.48020	0.09394	-0.09226	0.06150	-0.06676	0.03351	-0.04095	0.24073	-0.24071	0.26787	-0.26955	0.08344	-0.07158	0.28060	-0.27893
2.09	4.10134	0.14559	0.02196	-0.02157	0.02875	-0.03121	0.02506	-0.02051	0.09208	-0.09207	0.10241	-0.10202	0.03680	-0.03447	0.10890	-0.10778
2.30	2.81232	0.11825	0.00452	-0.00444	0.02290	-0.02485	0.04826	-0.03949	0.09186	-0.09185	0.10669	-0.10346	0.03139	-0.02954	0.11130	-0.10768
2.51	1.57671	0.09497	0.01232	-0.01255	0.00822	-0.00892	0.03749	-0.03068	0.08756	-0.08755	0.09676	-0.09442	0.02610	-0.02473	0.10032	-0.09770
2.72	1.21801	0.08051	0.02458	-0.02503	0.00821	-0.00757	0.00446	-0.00365	0.08174	-0.08173	0.08628	-0.08630	0.02442	-0.02323	0.08977	-0.08948
2.93	0.93724	0.07782	0.03342	-0.03403	0.02141	-0.01973	0.02327	-0.02844	0.08218	-0.08217	0.09456	-0.09581	0.02340	-0.02231	0.09751	-0.09847
3.14	0.96820	0.07037	0.03308	-0.03369	0.02394	-0.02205	0.03146	-0.03844	0.07459	-0.07458	0.09106	-0.09345	0.02319	-0.02216	0.09406	-0.09614
associate p_T 2.0–3.0 GeV/c																
ϕ	$I_{AA}(\Delta\phi)$	σ_{stat}/I	systematic errors													
			$+\sigma_{f_2}/I$	$-\sigma_{f_2}/I$	$+\sigma_{f_3}/I$	$-\sigma_{f_3}/I$	$+\sigma_{f_4}/I$	$-\sigma_{f_4}/I$	$+\sigma_\xi/I$	$-\sigma_\xi/I$	$+\sigma_{\pi^0}/I$	$-\sigma_{\pi^0}/I$	$+\sigma_{pp}/I$	$-\sigma_{pp}/I$	$+\sigma_{total}/I$	$-\sigma_{total}/I$
1.68	-6.19413	3.94074	0.33764	-0.33114	0.06603	-0.07131	0.36532	-0.44652	0.45637	-0.45637	0.67830	-0.72277	0.36000	-1.28572	0.76791	-1.47495
1.88	7.92390	0.83397	0.06520	-0.06394	0.04036	-0.04359	0.02885	-0.03526	0.10779	-0.10779	0.13539	-0.13730	0.24053	-0.16236	0.27602	-0.21263
2.09	3.71664	0.32352	0.02144	-0.02103	0.02655	-0.02867	0.03036	-0.02484	0.05820	-0.05820	0.07398	-0.07259	0.06733	-0.05948	0.10004	-0.09385
2.30	2.42622	0.17800	0.00313	-0.00307	0.01498	-0.01618	0.04143	-0.03390	0.04131	-0.04131	0.06048	-0.05593	0.04131	-0.03809	0.07325	-0.06767
2.51	1.20674	0.16298	0.00945	-0.00964	0.00597	-0.00644	0.03573	-0.02923	0.04393	-0.04393	0.05772	-0.05403	0.03096	-0.02909	0.06550	-0.06136
2.72	0.92369	0.10881	0.01540	-0.01570	0.00485	-0.00449	0.00347	-0.00284	0.03368	-0.03368	0.03752	-0.03755	0.02624	-0.02513	0.04579	-0.04518
2.93	0.60446	0.11824	0.02247	-0.02291	0.01356	-0.01256	0.01944	-0.02376	0.03650	-0.03650	0.04899	-0.05080	0.02453	-0.02338	0.05479	-0.05592
3.14	0.55127	0.10005	0.02178	-0.02221	0.01485	-0.01375	0.02573	-0.03145	0.03249	-0.03249	0.04913	-0.05223	0.02381	-0.02249	0.05459	-0.05687
associate p_T 3.0–5.0 GeV/c																
ϕ	$I_{AA}(\Delta\phi)$	σ_{stat}/I	systematic errors													
			$+\sigma_{f_2}/I$	$-\sigma_{f_2}/I$	$+\sigma_{f_3}/I$	$-\sigma_{f_3}/I$	$+\sigma_{f_4}/I$	$-\sigma_{f_4}/I$	$+\sigma_\xi/I$	$-\sigma_\xi/I$	$+\sigma_{\pi^0}/I$	$-\sigma_{\pi^0}/I$	$+\sigma_{pp}/I$	$-\sigma_{pp}/I$	$+\sigma_{total}/I$	$-\sigma_{total}/I$
1.68	1.45954	33.23831	1.16586	-1.14477	0.25392	-0.27416	1.53193	-1.86866	1.51682	-1.52383	2.48085	-2.69869	0.67348	-1.94323	2.57491	-3.32882
1.88	-34.20620	2.01544	0.01662	-0.01632	0.01146	-0.01237	0.00893	-0.01090	0.02644	-0.02657	0.03570	-0.03649	0.45089	-4.45675	0.45233	-4.45690
2.09	1.14458	0.70960	0.01804	-0.01771	0.02487	-0.02685	0.03093	-0.02538	0.04707	-0.04729	0.06477	-0.06319	0.07473	-0.06895	0.09900	-0.09363
2.30	0.39360	0.86864	0.00603	-0.00592	0.03219	-0.03475	0.09688	-0.07942	0.07660	-0.07695	0.12817	-0.11651	0.04924	-0.04898	0.13741	-0.12650
2.51	0.69519	0.28472	0.00581	-0.00592	0.00408	-0.00441	0.02660	-0.02181	0.02594	-0.02606	0.03876	-0.03578	0.03710	-0.03865	0.05383	-0.05285
2.72	0.50900	0.16491	0.00825	-0.00840	0.00289	-0.00267	0.00225	-0.00185	0.01733	-0.01741	0.02115	-0.02121	0.02822	-0.03100	0.03551	-0.03779
2.93	0.39510	0.12783	0.00811	-0.00826	0.00545	-0.00505	0.00852	-0.01039	0.01268	-0.01273	0.01991	-0.02077	0.02469	-0.02776	0.03200	-0.03492
3.14	0.38991	0.09809	0.00714	-0.00727	0.00541	-0.00501	0.01023	-0.01248	0.01024	-0.01029	0.01885	-0.02012	0.02334	-0.02731	0.03029	-0.03417
associate p_T 5.0–7.0 GeV/c																
ϕ	$I_{AA}(\Delta\phi)$	σ_{stat}/I	systematic errors													
			$+\sigma_{f_2}/I$	$-\sigma_{f_2}/I$	$+\sigma_{f_3}/I$	$-\sigma_{f_3}/I$	$+\sigma_{f_4}/I$	$-\sigma_{f_4}/I$	$+\sigma_\xi/I$	$-\sigma_\xi/I$	$+\sigma_{\pi^0}/I$	$-\sigma_{\pi^0}/I$	$+\sigma_{pp}/I$	$-\sigma_{pp}/I$	$+\sigma_{total}/I$	$-\sigma_{total}/I$
1.68	5.38890	1.99917	0.02504	-0.02444	0.01218	-0.01351	0.04095	-0.05245	0.04629	-0.04341	0.06778	-0.07359	0.31400	-0.80945	0.32123	-0.81279
1.88	-3.74114	2.37023	0.03329	-0.03249	0.05125	-0.05686	0.02226	-0.02851	0.07497	-0.07031	0.09925	-0.10023	0.33839	-0.98800	0.35265	-0.99307
2.09	76.87860	4.95179	0.00403	-0.00393	0.01241	-0.01377	0.00904	-0.00706	0.01485	-0.01393	0.02174	-0.02118	1.86305	-0.68492	1.86317	-0.68525
2.30	1.46036	0.72806	0.00181	-0.00177	0.02156	-0.02391	0.03796	-0.02963	0.03233	-0.03033	0.05435	-0.04871	0.11982	-0.10853	0.13157	-0.11896
2.51	1.09863	0.58381	0.00462	-0.00474	0.00729	-0.00809	0.02780	-0.02170	0.02910	-0.02730	0.04116	-0.03611	0.08444	-0.08483	0.09394	-0.09220
2.72	0.57114	0.31140	0.00605	-0.00620	0.00489	-0.00441	0.00217	-0.00169	0.01786	-0.01675	0.01960	-0.01848	0.03978	-0.05042	0.04435	-0.05370
2.93	0.46256	0.19078	0.00433	-0.00444	0.006											

Table 74: 20–40%, trigger p_T 5.0–7.0 Away-side $I_{AA}(\Delta\phi)$

associate p_T 0.5–1.0 GeV/c																
ϕ	$I_{AA}(\Delta\phi)$	σ_{stat}/I	$+ \sigma_{f_2}/I$	$- \sigma_{f_2}/I$	$+ \sigma_{f_3}/I$	$- \sigma_{f_3}/I$	$+ \sigma_{f_4}/I$	$- \sigma_{f_4}/I$	$+ \sigma_\xi/I$	$- \sigma_\xi/I$	$+ \sigma_{\pi^0}/I$	$- \sigma_{\pi^0}/I$	$+ \sigma_{pp}/I$	$- \sigma_{pp}/I$	$+ \sigma_{total}/I$	$- \sigma_{total}/I$
1.68	-3.33555	1.34397	0.26944	-0.26309	0.02727	-0.03010	0.10356	-0.13189	0.79425	-0.79429	0.84554	-0.84761	0.11976	-0.09622	0.85398	-0.85306
1.88	1.01748	1.29708	0.25133	-0.24541	0.08051	-0.08887	0.03951	-0.05031	0.89925	-0.89930	0.93809	-0.93783	0.04963	-0.04515	0.93941	-0.93893
2.09	2.57415	0.34407	0.04738	-0.04627	0.03036	-0.03351	0.02483	-0.01950	0.27590	-0.27592	0.28272	-0.28248	0.04195	-0.03857	0.28582	-0.28511
2.30	2.68652	0.14218	0.00469	-0.00458	0.01163	-0.01284	0.02301	-0.01807	0.13157	-0.13157	0.13423	-0.13359	0.02892	-0.02740	0.13733	-0.13638
2.51	2.11307	0.10606	0.01125	-0.01152	0.00369	-0.00407	0.01580	-0.01241	0.11007	-0.11007	0.11192	-0.11154	0.02459	-0.02343	0.11461	-0.11399
2.72	1.70080	0.08863	0.02224	-0.02278	0.00372	-0.00337	0.00186	-0.00146	0.10117	-0.10118	0.10378	-0.10388	0.02246	-0.02150	0.10620	-0.10610
2.93	1.75551	0.06951	0.02466	-0.02525	0.00791	-0.00716	0.00761	-0.00969	0.08252	-0.08253	0.08695	-0.08727	0.02154	-0.02039	0.08960	-0.08964
3.14	1.07137	0.09999	0.03986	-0.04082	0.01443	-0.01308	0.01680	-0.02140	0.12208	-0.12209	0.13040	-0.13123	0.02112	-0.02026	0.13211	-0.13280
associate p_T 1.0–2.0 GeV/c																
ϕ	$I_{AA}(\Delta\phi)$	σ_{stat}/I	$+ \sigma_{f_2}/I$	$- \sigma_{f_2}/I$	$+ \sigma_{f_3}/I$	$- \sigma_{f_3}/I$	$+ \sigma_{f_4}/I$	$- \sigma_{f_4}/I$	$+ \sigma_\xi/I$	$- \sigma_\xi/I$	$+ \sigma_{\pi^0}/I$	$- \sigma_{\pi^0}/I$	$+ \sigma_{pp}/I$	$- \sigma_{pp}/I$	$+ \sigma_{total}/I$	$- \sigma_{total}/I$
1.68	80.50249	11.46080	0.27446	-0.26828	0.04208	-0.04671	0.15137	-0.19173	0.45959	-0.45963	0.55790	-0.56762	0.73622	-1.55706	0.92373	-1.65730
1.88	7.95580	0.67312	0.09776	-0.09556	0.04744	-0.05266	0.02205	-0.02793	0.19931	-0.19932	0.22810	-0.22897	0.15750	-0.11973	0.27720	-0.25839
2.09	4.24474	0.19795	0.02563	-0.02505	0.02488	-0.02761	0.01917	-0.01514	0.08537	-0.08538	0.09457	-0.09445	0.04532	-0.04133	0.10488	-0.10311
2.30	2.62601	0.12190	0.00407	-0.00398	0.01530	-0.01699	0.02852	-0.02252	0.06567	-0.06567	0.07342	-0.07168	0.02989	-0.02810	0.07928	-0.07700
2.51	1.49073	0.10101	0.01159	-0.01186	0.00576	-0.00639	0.02322	-0.01834	0.06544	-0.06545	0.07074	-0.06939	0.02392	-0.02289	0.07468	-0.07308
2.72	1.02991	0.08491	0.02309	-0.02363	0.00588	-0.00529	0.00276	-0.00218	0.06088	-0.06088	0.06554	-0.06566	0.02122	-0.02036	0.06890	-0.06876
2.93	0.89650	0.06897	0.02619	-0.02679	0.01278	-0.01151	0.01159	-0.01468	0.05097	-0.05097	0.05996	-0.06065	0.01996	-0.01919	0.06321	-0.06363
3.14	0.91455	0.06067	0.02504	-0.02561	0.01380	-0.01243	0.01512	-0.01916	0.04464	-0.04464	0.05524	-0.05643	0.01987	-0.01862	0.05873	-0.05944
associate p_T 2.0–3.0 GeV/c																
ϕ	$I_{AA}(\Delta\phi)$	σ_{stat}/I	$+ \sigma_{f_2}/I$	$- \sigma_{f_2}/I$	$+ \sigma_{f_3}/I$	$- \sigma_{f_3}/I$	$+ \sigma_{f_4}/I$	$- \sigma_{f_4}/I$	$+ \sigma_\xi/I$	$- \sigma_\xi/I$	$+ \sigma_{\pi^0}/I$	$- \sigma_{\pi^0}/I$	$+ \sigma_{pp}/I$	$- \sigma_{pp}/I$	$+ \sigma_{total}/I$	$- \sigma_{total}/I$
1.68	-577.70532	94.00619	0.11213	-0.10936	0.01696	-0.01869	0.07832	-0.09922	0.12339	-0.12339	0.18508	-0.19342	0.96575	-1.03673	0.98333	-1.05462
1.88	4.60214	2.44617	0.19268	-0.18791	0.09224	-0.10166	0.05504	-0.06973	0.25888	-0.25888	0.34014	-0.34284	0.93336	-0.32582	0.99341	-0.47297
2.09	0.50976	2.09711	0.13870	-0.13527	0.13280	-0.14636	0.13141	-0.10373	0.30540	-0.30540	0.38397	-0.37917	0.08298	-0.07117	0.39284	-0.38580
2.30	1.48852	0.23167	0.00367	-0.00358	0.01361	-0.01500	0.03258	-0.02572	0.03929	-0.03929	0.05305	-0.04953	0.04016	-0.03709	0.06655	-0.06189
2.51	1.20436	0.14644	0.00718	-0.00736	0.00352	-0.00388	0.01826	-0.01441	0.02707	-0.02707	0.03376	-0.03193	0.02942	-0.02754	0.04480	-0.04219
2.72	0.64035	0.12632	0.01569	-0.01608	0.00392	-0.00356	0.00238	-0.00188	0.02774	-0.02774	0.03235	-0.03247	0.02332	-0.02228	0.03990	-0.03940
2.93	0.56853	0.08897	0.01427	-0.01463	0.00684	-0.00620	0.00801	-0.01015	0.01869	-0.01869	0.02596	-0.02674	0.02051	-0.01986	0.03311	-0.03333
3.14	0.62605	0.06878	0.01230	-0.01261	0.00665	-0.00604	0.00943	-0.01195	0.01478	-0.01478	0.02264	-0.02380	0.02008	-0.01917	0.03029	-0.03059
associate p_T 3.0–5.0 GeV/c																
ϕ	$I_{AA}(\Delta\phi)$	σ_{stat}/I	$+ \sigma_{f_2}/I$	$- \sigma_{f_2}/I$	$+ \sigma_{f_3}/I$	$- \sigma_{f_3}/I$	$+ \sigma_{f_4}/I$	$- \sigma_{f_4}/I$	$+ \sigma_\xi/I$	$- \sigma_\xi/I$	$+ \sigma_{\pi^0}/I$	$- \sigma_{\pi^0}/I$	$+ \sigma_{pp}/I$	$- \sigma_{pp}/I$	$+ \sigma_{total}/I$	$- \sigma_{total}/I$
1.68	-0.67466	6.92437	0.21347	-0.20858	0.03538	-0.03898	0.17838	-0.22545	0.22199	-0.22199	0.35775	-0.38105	0.22332	-0.39320	0.42175	-0.54755
1.88	-12.06386	0.82265	0.01214	-0.01186	0.00637	-0.00702	0.00415	-0.00524	0.01541	-0.01541	0.02165	-0.02193	0.26324	-0.54317	0.26414	-0.54362
2.09	0.22272	9.27578	0.22053	-0.21548	0.23139	-0.25492	0.24937	-0.19731	0.45855	-0.45855	0.61478	-0.60327	0.28044	-0.18319	0.67609	-0.63086
2.30	1.13809	0.33970	0.00189	-0.00184	0.00766	-0.00844	0.01996	-0.01579	0.01905	-0.01905	0.02913	-0.02668	0.06241	-0.05998	0.06890	-0.06567
2.51	0.71115	0.25597	0.00448	-0.00459	0.00241	-0.00265	0.01359	-0.01075	0.01594	-0.01594	0.02204	-0.02047	0.03960	-0.04157	0.04536	-0.04637
2.72	0.40031	0.15147	0.00651	-0.00666	0.00178	-0.00161	0.00118	-0.00093	0.01086	-0.01086	0.01365	-0.01368	0.02482	-0.02906	0.02838	-0.03217
2.93	0.45716	0.08219	0.00403	-0.00413	0.00211	-0.00192	0.00270	-0.00342	0.00498	-0.00498	0.00860	-0.00885	0.02085	-0.02513	0.02263	-0.02670
3.14	0.44470	0.06533	0.00352	-0.00360	0.00208	-0.00189	0.00322	-0.00408	0.00399	-0.00399	0.00801	-0.00838	0.02008	-0.02412	0.02169	-0.02560
associate p_T 5.0–7.0 GeV/c																
ϕ	$I_{AA}(\Delta\phi)$	σ_{stat}/I	$+ \sigma_{f_2}/I$	$- \sigma_{f_2}/I$	$+ \sigma_{f_3}/I$	$- \sigma_{f_3}/I$	$+ \sigma_{f_4}/I$	$- \sigma_{f_4}/I$	$+ \sigma_\xi/I$	$- \sigma_\xi/I$	$+ \sigma_{\pi^0}/I$	$- \sigma_{\pi^0}/I$	$+ \sigma_{pp}/I$	$- \sigma_{pp}/I$	$+ \sigma_{total}/I$	$- \sigma_{total}/I$
1.68	-2.51950	1.24366	0.01085	-0.01049	0.00390	-0.00448	0.01785	-0.01587	0.01714	-0.01714	0.02423	-0.02638	0.29916	-0.19916	0.30014	-0.20090
1.88	1.52152	1.91220	0.02135	-0.02064	0.02429	-0.02790	0.00953	-0.01276	0.04105	-0.04105	0.05405	-0.05615	0.47680	-0.25381	0.47987	-0.25997
2.09	6.82581	1.44773	0.00728	-0.00704	0.01656	-0.01902	0.01139	-0.00851	0.02286	-0.02286	0.03192	-0.03234	3.43900	-0.44175	3.43915	-0.44294
2.30	0.89426	0.67435	0.00138	-0.00133	0.01215	-0.01396	0.02021	-0.01509	0.02099	-0.02099	0.03216	-0.03001	0.11904	-0.10937	0.12333	-0.11344
2.51	0.75793	0.41358	0.00244	-0.00252	0.00287	-0.00329	0.01033	-0.00771	0.01315	-0.01315	0.01767	-0.01637	0.06788	-0.07387	0.07016	-0.07568
2.72	0.32831	0.33262	0.00509	-0.00526	0.00318	-0.00276	0.00129	-0.00096	0.01284	-0.01284	0.01492	-0.01487	0.03748	-0.05000	0.04038	-0.05220
2.93	0.57566	0.13796	0.00185	-0.00191	0.00221	-0.00192	0.00164	-0.00219	0.00345	-0.00345	0.00622	-0.00631	0.02611	-0.04014	0.02688	-0.04066
3.14	0.57636	0.10752	0.00139	-0.00144	0.00188	-0.00164	0.00169	-0.00226	0.00238	-0.00238	0.00544	-0.00558	0.02312	-0.03752	0.02380	-0.03796

Table 75: 20–40%, trigger p_T 7.0–9.0 Away-side $I_{AA}(\Delta\phi)$

associate p_T 0.5–1.0 GeV/c																
ϕ	$I_{AA}(\Delta\phi)$	σ_{stat}/I	systematic errors													
			$+\sigma_{f2}/I$	$-\sigma_{f2}/I$	$+\sigma_{f3}/I$	$-\sigma_{f3}/I$	$+\sigma_{f4}/I$	$-\sigma_{f4}/I$	$+\sigma_\xi/I$	$-\sigma_\xi/I$	$+\sigma_{\pi^0}/I$	$-\sigma_{\pi^0}/I$	$+\sigma_{pp}/I$	$-\sigma_{pp}/I$		
1.68	186.28232	20.09104	0.16967	-0.13965	0.00914	-0.01210	0.02403	-0.03781	0.25888	-0.25887	0.31064	-0.29685	1.28044	-0.82036	1.31758	-0.87242
1.88	12.36636	0.61078	0.05067	-0.04171	0.00864	-0.01144	0.00294	-0.00462	0.09377	-0.09376	0.10698	-0.10337	0.14420	-0.11175	0.17955	-0.15223
2.09	6.84158	0.43728	0.03480	-0.02864	0.01187	-0.01570	0.00830	-0.00528	0.10465	-0.10465	0.11124	-0.10977	0.09173	-0.07728	0.14419	-0.13424
2.30	2.00130	0.46454	0.01103	-0.00908	0.01456	-0.01926	0.02463	-0.01565	0.15956	-0.15955	0.16248	-0.16173	0.04893	-0.04462	0.16969	-0.16778
2.51	2.00739	0.27836	0.01751	-0.02127	0.00363	-0.00480	0.01329	-0.00844	0.10468	-0.10468	0.10703	-0.10727	0.03781	-0.03512	0.11352	-0.11287
2.72	1.66812	0.18774	0.02774	-0.03370	0.00351	-0.00265	0.00126	-0.00080	0.07699	-0.07699	0.08193	-0.08410	0.02949	-0.02807	0.08708	-0.08866
2.93	1.61452	0.14417	0.03020	-0.03669	0.00733	-0.00554	0.00408	-0.00641	0.06160	-0.06160	0.06913	-0.07221	0.02691	-0.02537	0.07419	-0.07654
3.14	1.15093	0.16946	0.03965	-0.04818	0.01087	-0.00821	0.00731	-0.01150	0.07398	-0.07398	0.08497	-0.08942	0.02541	-0.02418	0.08869	-0.09264
associate p_T 1.0–2.0 GeV/c																
ϕ	$I_{AA}(\Delta\phi)$	σ_{stat}/I	systematic errors													
			$+\sigma_{f2}/I$	$-\sigma_{f2}/I$	$+\sigma_{f3}/I$	$-\sigma_{f3}/I$	$+\sigma_{f4}/I$	$-\sigma_{f4}/I$	$+\sigma_\xi/I$	$-\sigma_\xi/I$	$+\sigma_{\pi^0}/I$	$-\sigma_{\pi^0}/I$	$+\sigma_{pp}/I$	$-\sigma_{pp}/I$		
1.68	-17.18300	1.17795	0.08517	-0.07010	0.00657	-0.00874	0.01725	-0.02698	0.07239	-0.07240	0.11332	-0.10471	0.20612	-0.35068	0.23521	-0.36598
1.88	16.29810	1.12856	0.07330	-0.06032	0.01791	-0.02381	0.00607	-0.00950	0.07573	-0.07574	0.10710	-0.10019	0.40880	-0.22489	0.42260	-0.24620
2.09	4.70553	0.45813	0.04080	-0.03358	0.01994	-0.02650	0.01384	-0.00885	0.06874	-0.06874	0.08357	-0.08148	0.09635	-0.08097	0.12755	-0.11487
2.30	2.42876	0.30465	0.00728	-0.05599	0.01377	-0.01830	0.02311	-0.01478	0.05922	-0.05923	0.06550	-0.06405	0.05080	-0.04603	0.08289	-0.07888
2.51	1.24275	0.26658	0.01854	-0.02253	0.00550	-0.00732	0.02001	-0.01279	0.06259	-0.06259	0.06854	-0.06818	0.03493	-0.03260	0.07693	-0.07558
2.72	1.25033	0.13678	0.02156	-0.02620	0.00393	-0.00296	0.00139	-0.00089	0.03390	-0.03390	0.04045	-0.04301	0.02652	-0.02544	0.04838	-0.04998
2.93	0.97067	0.11573	0.02581	-0.03136	0.00902	-0.00679	0.00498	-0.00779	0.02990	-0.02990	0.04088	-0.04461	0.02353	-0.02265	0.04718	-0.05003
3.14	0.95950	0.10577	0.02565	-0.03116	0.01012	-0.00761	0.00676	-0.01057	0.02720	-0.02720	0.03938	-0.04343	0.02299	-0.02198	0.04561	-0.04868
associate p_T 2.0–3.0 GeV/c																
ϕ	$I_{AA}(\Delta\phi)$	σ_{stat}/I	systematic errors													
			$+\sigma_{f2}/I$	$-\sigma_{f2}/I$	$+\sigma_{f3}/I$	$-\sigma_{f3}/I$	$+\sigma_{f4}/I$	$-\sigma_{f4}/I$	$+\sigma_\xi/I$	$-\sigma_\xi/I$	$+\sigma_{\pi^0}/I$	$-\sigma_{\pi^0}/I$	$+\sigma_{pp}/I$	$-\sigma_{pp}/I$		
1.68	-13.63576	2.65567	0.07454	-0.06134	0.00618	-0.00818	0.01976	-0.03092	0.04345	-0.04343	0.08914	-0.08212	0.43244	-3.19680	0.44153	-3.19785
1.88	-13.83171	2.08859	0.05661	-0.04658	0.01487	-0.01966	0.00614	-0.00960	0.04020	-0.04018	0.07148	-0.06552	0.287640	-0.42594	2.87729	-0.43096
2.09	-0.68320	7.59951	0.34770	-0.28613	0.18263	-0.24146	0.15441	-0.09870	0.40371	-0.40351	0.58407	-0.55928	0.59595	-0.27190	0.83445	-0.62187
2.30	0.57478	1.25758	0.01462	-0.01203	0.02972	-0.03929	0.06076	-0.03884	0.08221	-0.08217	0.10764	-0.09994	0.08379	-0.07180	0.13642	-0.12307
2.51	0.77833	0.42092	0.01236	-0.01501	0.00394	-0.00521	0.01746	-0.01116	0.02893	-0.02892	0.03657	-0.03523	0.04764	-0.04317	0.06008	-0.05574
2.72	0.72931	0.19875	0.01360	-0.01653	0.00265	-0.00200	0.00115	-0.00073	0.01488	-0.01488	0.02095	-0.02287	0.03152	-0.02949	0.03788	-0.03735
2.93	0.70045	0.12629	0.01068	-0.01298	0.00399	-0.00302	0.00270	-0.00422	0.00863	-0.00863	0.01537	-0.01715	0.02501	-0.02386	0.02939	-0.02942
3.14	0.43228	0.11585	0.01135	-0.01379	0.00479	-0.00362	0.00391	-0.00612	0.00841	-0.00840	0.01618	-0.01831	0.02141	-0.02108	0.02687	-0.02795
associate p_T 3.0–5.0 GeV/c																
ϕ	$I_{AA}(\Delta\phi)$	σ_{stat}/I	systematic errors													
			$+\sigma_{f2}/I$	$-\sigma_{f2}/I$	$+\sigma_{f3}/I$	$-\sigma_{f3}/I$	$+\sigma_{f4}/I$	$-\sigma_{f4}/I$	$+\sigma_\xi/I$	$-\sigma_\xi/I$	$+\sigma_{\pi^0}/I$	$-\sigma_{\pi^0}/I$	$+\sigma_{pp}/I$	$-\sigma_{pp}/I$		
1.68	0.29653	15.12067	0.31946	-0.26286	0.02831	-0.03743	0.09910	-0.15464	0.17150	-0.17067	0.37701	-0.35155	0.67956	-0.29049	0.77714	-0.45604
1.88	-3.50673	0.71015	0.01492	-0.01228	0.00419	-0.00553	0.00189	-0.00295	0.00976	-0.00971	0.01842	-0.01687	0.19460	-0.30956	0.19547	-0.31002
2.09	-3.35379	5.04158	0.06588	-0.05421	0.03696	-0.04886	0.03414	-0.02188	0.07043	-0.07009	0.10882	-0.10356	0.63615	-2.34431	0.64539	-2.34660
2.30	0.64076	0.82992	0.00338	-0.00278	0.00733	-0.00970	0.01638	-0.01050	0.01749	-0.01740	0.02529	-0.02269	0.11084	-0.09487	0.11369	-0.09755
2.51	0.71184	0.47710	0.00471	-0.00573	0.00161	-0.00212	0.00777	-0.00498	0.01017	-0.01012	0.01374	-0.01283	0.07494	-0.06961	0.07619	-0.07079
2.72	0.62872	0.18544	0.00382	-0.00464	0.00079	-0.00060	0.00008	-0.00024	0.00385	-0.00383	0.00551	-0.00607	0.03556	-0.03804	0.03598	-0.03852
2.93	0.49945	0.12571	0.00285	-0.00347	0.00114	-0.00086	0.00084	-0.00132	0.00212	-0.00211	0.00385	-0.00438	0.02516	-0.02883	0.02546	-0.02916
3.14	0.51825	0.09595	0.00200	-0.00243	0.00090	-0.00068	0.00081	-0.00137	0.00136	-0.00137	0.00275	-0.00317	0.02250	-0.02643	0.02267	-0.02662
associate p_T 5.0–7.0 GeV/c																
ϕ	$I_{AA}(\Delta\phi)$	σ_{stat}/I	systematic errors													
			$+\sigma_{f2}/I$	$-\sigma_{f2}/I$	$+\sigma_{f3}/I$	$-\sigma_{f3}/I$	$+\sigma_{f4}/I$	$-\sigma_{f4}/I$	$+\sigma_\xi/I$	$-\sigma_\xi/I$	$+\sigma_{\pi^0}/I$	$-\sigma_{\pi^0}/I$	$+\sigma_{pp}/I$	$-\sigma_{pp}/I$		
1.68	4.30529	1.96059	0.00606	-0.00499	0.00096	-0.00133	0.00249	-0.00419	0.00617	-0.00575	0.01152	-0.01132	1.67600	-0.39208	1.67604	-0.39225
1.88	-0.39159	6.85404	0.03613	-0.02972	0.03622	-0.05006	0.02674	-0.01590	0.07281	-0.06788	0.09651	-0.09449	1.95712	-0.40407	1.95951	-0.41504
2.09	-1.04950	1.39450	0.00170	-0.00140	0.00661	-0.00914	0.01180	-0.00701	0.01659	-0.01546	0.02234	-0.02029	0.68576	-0.29720	0.68612	-0.29790
2.30	-0.42064	1.19574	0.00439	-0.00533	0.00267	-0.00369	0.01033	-0.00614	0.01775	-0.01655	0.02175	-0.01945	0.22330	-0.16561	0.22436	-0.16676
2.51	0.62596	0.35885	0.00176	-0.00214	0.00068	-0.00049	0.00025	-0.00015	0.00332	-0.00309	0.00687	-0.00686	0.06708	-0.07353	0.06745	-0.07387
2.72	0.68454	0.24612	0.00083	-0.00101	0.00062	-0.00045	0.00033	-0.00055	0.00116	-0.00108	0.00532	-0.00534	0.03540	-0.04822	0.03583	-0.04854
2.93	0.63026	0.18625	0.00052	-0.00063	0.00044	-0.00032	0.00028	-0.00047	0.00066	-0.00062	0.00507	-0.00508	0.02660	-0.04047	0.02712	-0.04081

Table 76: 20–40%, trigger p_T 9.0–12.0 Away-side $I_{AA}(\Delta\phi)$

associate p_T 0.5–1.0 GeV/c																
ϕ	$I_{AA}(\Delta\phi)$	σ_{stat}/I	systematic errors													
			$+\sigma_{f2}/I$	$-\sigma_{f2}/I$	$+\sigma_{f3}/I$	$-\sigma_{f3}/I$	$+\sigma_{f4}/I$	$-\sigma_{f4}/I$	$+\sigma_\xi/I$	$-\sigma_\xi/I$	$+\sigma_{\pi^0}/I$	$-\sigma_{\pi^0}/I$	$+\sigma_{pp}/I$	$-\sigma_{pp}/I$		
1.68	91.78193	6.99336	0.08356	-0.13349	0.00627	-0.00536	0.01129	-0.01511	0.10530	-0.10530	0.13505	-0.17078	0.62676	-2.47230	0.64114	-2.47819
1.88	-11.63846	7.60190	0.46364	-0.74075	0.11018	-0.09407	0.02563	-0.03428	0.70842	-0.70841	0.85418	-1.02984	3.15541	-0.59442	3.26899	-1.18908
2.09	3.14176	0.82842	0.05214	-0.08331	0.02478	-0.02116	0.01009	-0.00755	0.12946	-0.12946	0.14212	-0.15558	0.09726	-0.08136	0.17221	-0.17557
2.30	4.68955	0.35913	0.00498	-0.00796	0.00916	-0.00782	0.00902	-0.00675	0.05947	-0.05947	0.06103	-0.06089	0.07075	-0.06198	0.09345	-0.08688
2.51	2.07592	0.32160	0.02581	-0.01615	0.00384	-0.00328	0.00819	-0.00612	0.06558	-0.06558	0.07106	-0.06790	0.04314	-0.03948	0.08313	-0.07854
2.72	1.24563	0.41033	0.08029	-0.05026	0.00471	-0.00552	0.00152	-0.00114	0.09466	-0.09465	0.12423	-0.10732	0.03961	-0.03670	0.13039	-0.11342
2.93	1.78800	0.20935	0.05577	-0.03491	0.00627	-0.00735	0.00370	-0.00495	0.04832	-0.04831	0.07415	-0.06027	0.03361	-0.03135	0.08141	-0.06793
3.14	1.33963	0.24671	0.07419	-0.04644	0.00942	-0.01103	0.00672	-0.00899	0.05878	-0.05878	0.09536	-0.07625	0.03211	-0.03043	0.10062	-0.08210
associate p_T 1.0–2.0 GeV/c																
ϕ	$I_{AA}(\Delta\phi)$	σ_{stat}/I	systematic errors													
			$+\sigma_{f2}/I$	$-\sigma_{f2}/I$	$+\sigma_{f3}/I$	$-\sigma_{f3}/I$	$+\sigma_{f4}/I$	$-\sigma_{f4}/I$	$+\sigma_\xi/I$	$-\sigma_\xi/I$	$+\sigma_{\pi^0}/I$	$-\sigma_{\pi^0}/I$	$+\sigma_{pp}/I$	$-\sigma_{pp}/I$		
1.68	6.81379	3.44372	0.26514	-0.42588	0.02728	-0.02409	0.05222	-0.06825	0.18555	-0.18555	0.32893	-0.47015	1.32262	-0.36307	1.36291	-0.59402
1.88	8.43361	1.04023	0.06707	-0.10774	0.02184	-0.01929	0.00540	-0.00706	0.05704	-0.05704	0.09088	-0.12363	0.29189	-0.18449	0.30571	-0.22208
2.09	2.17489	1.69530	0.11571	-0.18587	0.07537	-0.06657	0.03189	-0.02440	0.16037	-0.16037	0.21403	-0.25553	0.20132	-0.14368	0.29384	-0.29315
2.30	3.75093	0.37938	0.00547	-0.00879	0.01380	-0.01219	0.01412	-0.01080	0.03661	-0.03661	0.04196	-0.04103	0.08316	-0.07145	0.09315	-0.08239
2.51	1.86035	0.28047	0.02400	-0.01494	0.00487	-0.00430	0.01078	-0.00825	0.03410	-0.03410	0.04334	-0.03837	0.04651	-0.04262	0.06357	-0.05735
2.72	0.62865	0.34619	0.07477	-0.04655	0.00618	-0.00700	0.00200	-0.00153	0.04945	-0.04945	0.08988	-0.06829	0.03156	-0.02987	0.09526	-0.07454
2.93	1.11691	0.15457	0.04306	-0.02681	0.00683	-0.00773	0.00414	-0.00541	0.02098	-0.02098	0.04856	-0.03532	0.02825	-0.02660	0.05618	-0.04422
3.14	0.98498	0.13463	0.04065	-0.02531	0.00728	-0.00824	0.00534	-0.00698	0.01813	-0.01813	0.04542	-0.03295	0.02584	-0.02436	0.05225	-0.04098
associate p_T 2.0–3.0 GeV/c																
ϕ	$I_{AA}(\Delta\phi)$	σ_{stat}/I	systematic errors													
			$+\sigma_{f2}/I$	$-\sigma_{f2}/I$	$+\sigma_{f3}/I$	$-\sigma_{f3}/I$	$+\sigma_{f4}/I$	$-\sigma_{f4}/I$	$+\sigma_\xi/I$	$-\sigma_\xi/I$	$+\sigma_{\pi^0}/I$	$-\sigma_{\pi^0}/I$	$+\sigma_{pp}/I$	$-\sigma_{pp}/I$		
1.68	0.73594	15.99676	0.63765	-1.01200	0.07492	-0.06333	0.16527	-0.21624	0.30760	-0.30793	0.73086	-1.01855	0.37188	-1.45120	0.82003	-1.80989
1.88	1.31677	2.27635	0.09835	-0.15609	0.03658	-0.03092	0.01043	-0.01364	0.05777	-0.05783	0.12025	-0.16987	0.15646	-0.22781	0.19734	-0.28417
2.09	124.82930	30.46105	0.03885	-0.06166	0.02890	-0.02443	0.01411	-0.01078	0.03729	-0.03733	0.06272	-0.07687	0.92482	-1.08848	0.92695	-1.09119
2.30	4.00811	0.74863	0.00386	-0.00613	0.01111	-0.00939	0.01312	-0.01003	0.01793	-0.01795	0.02515	-0.02343	0.25884	-0.17051	0.26006	-0.17211
2.51	0.28213	1.98939	0.07916	-0.04988	0.01858	-0.01568	0.04742	-0.03624	0.07933	-0.07941	0.12310	-0.10176	0.08230	-0.07056	0.14807	-0.12383
2.72	0.96134	0.27867	0.02257	-0.01422	0.00206	-0.00244	0.00081	-0.00062	0.01056	-0.01057	0.02502	-0.01791	0.04562	-0.04180	0.05203	-0.04548
2.93	0.52981	0.20413	0.02165	-0.01364	0.00380	-0.00449	0.00277	-0.00363	0.00748	-0.00748	0.02339	-0.01661	0.02876	-0.02699	0.03707	-0.03163
3.14	0.65441	0.14705	0.01589	-0.01001	0.00315	-0.00372	0.00278	-0.00363	0.00503	-0.00503	0.01719	-0.01237	0.02674	-0.02539	0.03179	-0.02824
associate p_T 3.0–5.0 GeV/c																
ϕ	$I_{AA}(\Delta\phi)$	σ_{stat}/I	systematic errors													
			$+\sigma_{f2}/I$	$-\sigma_{f2}/I$	$+\sigma_{f3}/I$	$-\sigma_{f3}/I$	$+\sigma_{f4}/I$	$-\sigma_{f4}/I$	$+\sigma_\xi/I$	$-\sigma_\xi/I$	$+\sigma_{\pi^0}/I$	$-\sigma_{\pi^0}/I$	$+\sigma_{pp}/I$	$-\sigma_{pp}/I$		
2.09	0.20790	19.94598	0.22667	-0.36316	0.17960	-0.15156	0.09575	-0.07389	0.19825	-0.19899	0.36362	-0.44725	2.04483	-0.40359	2.07691	-0.60243
2.30	-0.30720	2.60229	0.00798	-0.01279	0.02447	-0.02065	0.03155	-0.02435	0.03378	-0.03391	0.05311	-0.04852	0.22016	-0.15640	0.22648	-0.16376
2.51	0.62731	0.72288	0.00909	-0.00567	0.00225	-0.00190	0.00627	-0.00484	0.00822	-0.00825	0.01405	-0.01140	0.10818	-0.09295	0.10909	-0.09365
2.72	0.44352	0.31755	0.00848	-0.00529	0.00082	-0.00097	0.00035	-0.00027	0.00358	-0.00359	0.00942	-0.00673	0.04390	-0.04481	0.04491	-0.04532
2.93	0.62658	0.18247	0.00400	-0.00250	0.00074	-0.00088	0.00060	-0.00077	0.00125	-0.00125	0.00456	-0.00339	0.03044	-0.03340	0.03078	-0.03357
3.14	0.57748	0.13835	0.00280	-0.00175	0.00058	-0.00069	0.00057	-0.00074	0.00080	-0.00080	0.00266	-0.002525	-0.02871	0.02548	-0.02883	
associate p_T 5.0–7.0 GeV/c																
ϕ	$I_{AA}(\Delta\phi)$	σ_{stat}/I	systematic errors													
			$+\sigma_{f2}/I$	$-\sigma_{f2}/I$	$+\sigma_{f3}/I$	$-\sigma_{f3}/I$	$+\sigma_{f4}/I$	$-\sigma_{f4}/I$	$+\sigma_\xi/I$	$-\sigma_\xi/I$	$+\sigma_{\pi^0}/I$	$-\sigma_{\pi^0}/I$	$+\sigma_{pp}/I$	$-\sigma_{pp}/I$		
1.88	0.33672	3.11011	0.01099	-0.01644	0.00461	-0.00624	0.00137	-0.00248	0.01129	-0.01056	0.01802	-0.02191	0.46006	-0.24926	0.46042	-0.25022
2.09	-1.88480	1.83661	0.00450	-0.00674	0.00378	-0.00511	0.00266	-0.00147	0.00754	-0.00705	0.01144	-0.01248	9.32861	-0.53195	9.32861	-0.53195
2.51	0.60225	0.91284	0.00229	-0.00153	0.00064	-0.00087	0.00237	-0.00131	0.00424	-0.00396	0.00638	-0.00566	0.26861	-0.18540	0.26868	-0.18549
2.72	0.48125	0.57688	0.00342	-0.00228	0.00060	-0.00044	0.00021	-0.00012	0.00294	-0.00275	0.00623	-0.00557	0.14231	-0.12300	0.14245	-0.12312
2.93	0.87789	0.37438	0.00117	-0.00078	0.00039	-0.00029	0.00019	-0.00034	0.00074	-0.00070	0.00397	-0.00386	0.07129	-0.07606	0.07140	-0.07616
3.14	0.35444	0.35985	0.00079	-0.00053	0.00030	-0.00022	0.00017	-0.00031	0.00046	-0.00043	0.00352	-0.00347	0.03078	-0.04358	0.03099	-0.04372

J Good Run List: Run14

405863 405864 405868 405869 405964 405966 405971 405972 405973 405977 405981 405982 405984
 405990 405995 405996 406088 406089 406090 406093 406094 406095 406099 406180 406182 406183
 406190 406259 406265 406266 406268 406539 406540 406543 406544 406549 406555 406579 406582
 406584 406661 406662 406663 406666 406671 406674 406675 406676 406677 406696 406697 406698
 406700 406745 406746 406747 406748 406753 406754 406759 406760 406761 406762 406764 406766
 406767 406769 406772 406773 406831 406832 406833 406848 406849 406850 406851 406853 406857
 406858 406859 406861 406869 406870 406871 406872 406881 406882 406889 406891 406893 406898
 406902 406905 406920 406921 407086 407143 407144 407145 407146 407147 407175 407176 407195
 407196 407197 407199 407200 407269 407270 407271 407272 407276 407362 407367 407368 407369
 407370 407371 407372 407375 407376 407377 407378 407379 407380 407381 407445 407447 407448
 407454 407455 407456 407457 407523 407524 407526 407608 407611 407614 407618 407620 407621
 407660 407661 407662 407664 407666 407669 407671 407672 407673 407675 407676 407711 407712
 407790 407792 407796 407797 407798 407799 407800 407802 407842 407944 407945 407946 407947
 407948 407950 407951 407953 407959 407960 407963 407964 407965 407966 408070 408071 408073
 408074 408075 408076 408077 408078 408175 408176 408176 408181 408182 408183 408184 408217 408218
 408219 408220 408224 408225 408226 408227 408229 408321 408322 408323 408324 408325 408328
 408329 408330 408332 408333 408334 408335 408336 408404 408405 408406 408408 408432 408433
 408434 408435 408436 408437 408438 408440 408567 408572 408574 408575 408577 408579 408580
 408582 408583 408584 408585 408586 408587 408588 408589 408641 408642 408643 408644 408645
 408646 408648 408649 408650 408670 408671 408672 408673 408674 408675 408798 408799 408801
 408802 408803 408804 408805 408857 408858 408859 408860 408881 408882 408883 408885 408886
 408887 408888 408889 408920 408921 408923 408924 408925 408994 408995 408996 408997 408998
 408999 409004 409009 409010 409011 409012 409014 409082 409084 409086 409087 409088 409089
 409092 409115 409116 409118 409120 409121 409125 409147 409149 409151 409152 409153 409154
 409200 409222 409223 409224 409225 409226 409227 409228 409229 409230 409231 409232 409233
 409235 409236 409237 409239 409241 409243 409295 409297 409298 409299 409300 409303 409304
 409305 409306 409307 409308 409310 409311 409312 409429 409431 409433 409435 409436 409437
 409438 409439 409440 409442 409454 409456 409457 409458 409465 409467 409611 409612 409613
 409614 409616 409617 409619 409620 409637 409638 409639 409640 409641 409644 409647 409678
 409680 409681 409682 409683 409684 409687 409688 409696 409699 409703 409705 409706 409707
 409709 409716 409718 409720 409723 409825 409826 409827 409828 409829 409830 409831 409832
 409833 409835 409836 409837 409838 409839 409840 409841 409842 409885 409887 409889 409890
 409891 409892 409893 409894 409897 409900 409902 409968 409971 409972 409973 409974 409975
 409977 410009 410010 410011 410012 410013 410014 410015 410066 410104 410105 410106 410107
 410108 410110 410111 410112 410118 410119 410120 410122 410156 410158 410166 410167 410168
 410169 410185 410221 410222 410224 410225 410226 410227 410228 410230 410231 410261 410262
 410263 410265 410266 410267 410653 410654 410655 410656 410659 410670 410675 410677 410678
 410679 410680 410681 410682 410685 410718 410721 410722 410723 410724 410725 410726 410728
 410729 410748 410749 410750 410752 410753 410796 410797 410800 410802 410803 410808 410810
 410835 410836 410837 410838 410839 410840 410841 410842 410843 410920 410921 410922 410923
 410924 410929 410937 410938 410939 410940 410942 410943 410944 411008 411009 411010 411011
 411012 411013 411014 411015 411018 411019 411020 411022 411024 411025 411139 411154 411155
 411156 411158 411159 411173 411266 411267 411268 411269 411270 411271 411272 411273 411274

411275 411276 411277 411349 411350 411351 411352 411353 411354 411356 411404 411408 411411
411422 411423 411425 411456 411458 411459 411460 411461 411462 411497 411500 411501 411502
411503 411504 411506 411507 411508 411509 411540 411541 411543 411545 411551 411553 411554
411555 411556 411557 411558 411559 411561 411596 411597 411598 411599 411600 411601 411602
411635 411636 411637 411638 411639 411640 411643 411644 411645 411649 411651 411652 411763
411764 411767 411817 411818 411819 411823 411825 411826 411912 411913 411914 411915 411916
411921 411922 411924 411926 411991 411993 411994 411995 412067 412068 412069 412092 412093
412097 412098 412099 412101 412102 412148 412150 412214 412215 412216 412317 412318 412319
412320 412321 412322 412324 412328 412412 412413 412415 412416 412417 412424 412426 412427
412428 412429 412430 412431 412433 412484 412485 412486 412487 412488 412489 412490 412491
412512 412514 412515 412516 412517 412518 412519 412520 412521 412523 412646 412647 412648
412706 412707 412708 412709 412742 412745 412804 412805 412806 412807 412836 412841 412842
412843 412847 412848 412849 412850 412851 412878 412879 412881 412882 412883 412884 412932
412933 412934 412979 412984 412985 412986 412987 412988 412990 412993 413074 413075 413076
413077 413078 413079 413080 413081 413086 413087 413088 413089 413090 413092 413142 413143
413144 413146 413148 413149 413151 413154 413155 413157 413158 413160 413162 413163 413164
413165 413183 413187 413240 413241 413242 413243 413264 413265 413267 413268 413382 413383
413384 413392 413435 413440 413508 413511 413512 413513 413514 413539 413540 413541 413542
413543 413544 413549 413551 413552 413553 413556 413560 413561 413562 413563 413564 413604
413605 413607 413608 413609 413610 413611 413612 413631 413633 413634 413636 413637 413638
413639 413642 413643 413662 413663 413664 413667 413669 413672 413708 413709 413712 413715
413716 413717 413721 413722 413723 413724 413747 413748 413749 413750 413751 413752 413753
413755 413756 413843 413844 413924 413926 413927 413931 413932 413933 413934 413936 413940
414049 414050 414051 414052 414053 414059 414060 414061 414071 414072 414073 414074 414075
414076 414077 414078 414079 414132 414133 414134 414135 414136 414140 414148 414149 414150
414151 414152 414153 414154 414157 414158 414186 414187 414191 414195 414196 414197 414198
414201 414203 414204 414205 414206 414207 414284 414285 414424 414425 414427 414428 414430
414431 414432 414434 414499 414505 414507 414511 414512 414515 414517 414518 414519 414520
414557 414559 414560 414562 414563 414564 414565 414599 414604 414605 414606 414607 414608
414609 414610 414626 414627 414629 414631 414632 414633 414634 414635 414636 414702 414703
414704 414705 414706 414707 414726 414728 414729 414731 414732 414824 414825 414826 414827
414828 414829 414830 414832 414847 414848 414849 414851 414852 414853 414854 414855 414856
414857 414884 414885 414886 414887 414888 414889 414890 414893 414899 414976 414978 414979
414980 414981 414982 414985 414986 414987 414988